Ground Vehicle Engineering Series

Design and Simulation of Heavy Haul Locomotives and Trains

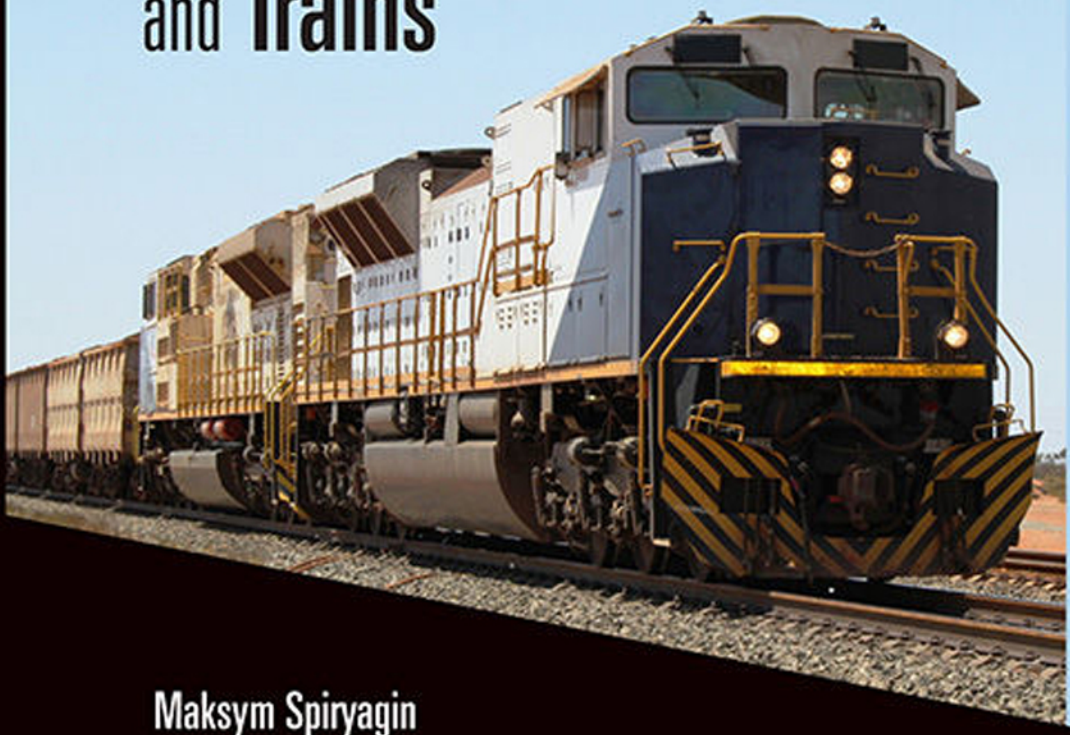

Maksym Spiryagin
Peter Wolfs
Colin Cole
Valentyn Spiryagin
Yan Quan Sun
Tim McSweeney

CRC Press
Taylor & Francis Group

Design and Simulation of Heavy Haul Locomotives and Trains

Ground Vehicle Engineering Series

Series Editor:
Dr. Vladimir V. Vantsevich
Professor and Director
Program of Master of Science in Mechatronic Systems Engineering
Lawrence Technological University, Michigan

Design and Simulation of Heavy Haul Locomotives and Trains
Maksym Spiryagin, Peter Wolfs, Colin Cole, Valentyn Spiryagin, Yan Quan Sun, and Tim McSweeney

Design and Simulation of Rail Vehicles
Maksym Spiryagin, Colin Cole, Yan Quan Sun, Mitchell McClanachan, Valentyn Spiryagin, and Tim McSweeney

Automotive Accident Reconstruction: Practices and Principles
Donald E. Struble

Dynamics of Wheel–Soil Systems: A Soil Stress and Deformation-Based Approach
Jaroslaw A. Pytka

Road Vehicle Dynamics: Fundamentals and Modeling
Georg Rill

Driveline Systems of Ground Vehicles: Theory and Design
Alexandr F. Andreev, Viachaslau Kabanau, and Vladimir Vantsevich

Design and Simulation of Heavy Haul Locomotives and Trains

Maksym Spiryagin
Centre for Railway Engineering, Central Queensland University, Rockhampton, Australia

Peter Wolfs
Centre for Railway Engineering, Central Queensland University, Rockhampton, Australia

Colin Cole
Centre for Railway Engineering, Central Queensland University, Rockhampton, Australia

Valentyn Spiryagin
ZhelDorRemMash OJSC, Yaroslavl, Russia

Yan Quan Sun
Centre for Railway Engineering, Central Queensland University, Rockhampton, Australia

Tim McSweeney
Centre for Railway Engineering, Central Queensland University, Rockhampton, Australia

CRC Press
Taylor & Francis Group
Boca Raton London New York

CRC Press is an imprint of the
Taylor & Francis Group, an **informa** business

CRC Press
Taylor & Francis Group
6000 Broken Sound Parkway NW, Suite 300
Boca Raton, FL 33487-2742

Printed on acid-free paper
Version Date: 20160622

International Standard Book Number-13: 978-1-4987-3352-6 (Hardback)

Library of Congress Cataloging-in-Publication Data

Names: Spiryagin, Maksym, author.
Title: Design and simulation of heavy haul locomotives and trains / Maksym Spiryagin [and five others]
Description: Boca Raton : CRC Press, 2017. | Series: Ground vehicle engineering ; 6 | Includes bibliographical references and index.
Identifiers: LCCN 2016012106 | ISBN 9781498733526
Subjects: LCSH: Locomotives--Design and construction. | Railroad trains--Dynamics. | Railroad trains--Computer simulation.
Classification: LCC TJ635 .S66 2017 | DDC 625.26/62--dc23
LC record available at https://lccn.loc.gov/2016012106

Visit the Taylor & Francis Web site at
http://www.taylorandfrancis.com

and the CRC Press Web site at
http://www.crcpress.com

Contents

Preface xiii
Acknowledgements xv
Authors xvii

Chapter 1 Introduction 1

1.1 The Origin of Railways 1
1.2 Heavy Haul Freight 2
1.2.1 Classification of Heavy Haul Railways 3
1.2.2 Operation and Maintenance of Heavy Haul Lines 4
1.3 Review of Existing Heavy Haul Railway Operations 5
1.3.1 Australia 6
1.3.2 Brazil 8
1.3.3 Canada 8
1.3.4 China 9
1.3.5 India 10
1.3.6 Nordic Countries 10
1.3.7 Russia 11
1.3.8 South Africa 11
1.3.9 United States of America 12
References 13

Chapter 2 Heavy Haul Locomotives and Their Design 15

2.1 Introduction 15
2.2 Types of Locomotives and Their Classification 16
2.3 Motive Power Energy Principles 23
2.4 Main Parameters of Locomotives 25
2.4.1 Axle Load 25
2.4.2 Locomotive Tractive Effort 27
2.4.3 Maximum Adhesion/Traction Coefficient 27
2.4.4 Locomotive Power Output 27
2.4.5 Maximum Locomotive Speed 28
2.5 Power Generation Systems 29
2.5.1 Diesel Engine and Its Systems 29
2.5.2 Electric Power Systems 34
2.6 Tractive Effort and Dynamic Braking Characteristics 37
2.6.1 Tractive Effort Characteristics 37
2.6.2 Dynamic Braking Characteristics 39

2.7 Locomotive Auxiliary Systems and Equipment....40
2.7.1 Forced Air Systems....40
2.7.2 Air Brake Systems....41
2.8 Modern Heavy Haul Locomotive Design Layouts and Characteristics....42
2.8.1 Diesel-Electric Locomotives....43
2.8.1.1 Diesel-Electric Locomotives with a DC Traction System....43
2.8.1.2 Diesel-Electric Locomotives with an AC Traction System....46
2.8.2 Electric Locomotives....57
2.8.2.1 Electric Locomotives with a DC Traction System....57
2.8.2.2 Electric Locomotives with an AC Traction System....60
References....70

Chapter 3 Design of Mechanical Systems of Locomotives....73

3.1 Classification of Main Components....73
3.1.1 Locomotive Bodies....75
3.1.2 Locomotive Frames....81
3.2 Bogies....82
3.2.1 Classification of Bogies....83
3.2.2 Bogie Frames....86
3.2.3 Wheelsets....90
3.2.4 Journal Housings....92
3.3 Suspension....93
3.3.1 Classification of Suspension Designs and Associated Elements....94
3.3.1.1 Leaf Springs....96
3.3.1.2 Helical (Coil) Springs....97
3.3.1.3 Air Springs....97
3.3.1.4 Rubber and Elastomer Springs....98
3.3.1.5 Dampers....98
3.3.2 Primary Suspension....100
3.3.3 Secondary Suspension....101
3.4 Design Components for Transmission of Traction and Braking Forces between a Locomotive Frame and Bogies....104
3.4.1 Pivot Assemblies....104
3.4.2 Traction Rods....106
3.5 Electric Traction Drives....106
3.6 Bogie Subsystems....108

3.6.1 Brake Subsystem and Associated Devices 109
3.6.1.1 Components of Air Brake Systems 109
3.6.1.2 Parking Brakes 110
3.6.2 Sanding Subsystem 110
3.6.3 Wheel Flange Lubrication Subsystem 111
References 112

Chapter 4 Design of Locomotive Power Electronics Systems and Electrical Machines 113

4.1 Classification of Locomotive Electrical Transmissions 113
4.1.1 DC Traction 114
4.1.2 AC Traction 115
4.2 Transformers 115
4.3 Traction Generators and Alternators 116
4.4 Traction Motor Operating Principles 117
4.4.1 Single Conductor Model 117
4.4.2 Coupled Circuit Model 120
4.4.3 AC Traction Motors 122
4.4.4 DC Traction Motors 123
4.5 Control of Traction Motors 124
4.5.1 DC Traction Motors and Control Strategies 124
4.5.2 AC Traction Motors and Control Strategies 126
4.5.3 Synchronous Traction Motors and Control Strategies 134
4.5.4 Induction Traction Motors and Control Strategies 137
4.5.4.1 Scalar Control 141
4.5.4.2 Vector Control 146
References 154

Chapter 5 Longitudinal Train Dynamics 157

5.1 Introduction 157
5.2 Modelling Longitudinal Train Dynamics 158
5.2.1 Train Models 158
5.2.2 Modelling Vehicle Inputs 161
5.2.2.1 Locomotive Traction and Dynamic Braking 162
5.2.2.2 Propulsion Resistance 167
5.2.2.3 Curving Resistance 170
5.2.2.4 Gravitational Components 170
5.2.2.5 Pneumatic Brake Models 171
5.2.3 Rail Vehicle Connection Models 175

5.2.3.1 Conventional Auto-Couplers and Draft Gear Packages 175
5.2.3.2 Slackless Packages 181
5.2.3.3 Drawbars 182
5.2.4 Train Configurations 182
5.2.5 Train Dynamics Model Development and Simulation 183
5.3 Interaction of Longitudinal Train and Lateral/Vertical Rail Vehicle Dynamics 193
5.3.1 Wheel Unloading, Wheel Climb and Rollover on Curves due to Lateral Components of Coupler Forces 193
5.3.2 Rail Vehicle Body and Bogie Pitch due to Coupler Impact Forces 199
5.3.3 Rail Vehicle Lift-Off due to Vertical Components of Coupler Forces 207
5.4 Energy Considerations 209
5.5 Train Control Management and Driving Practices 210
5.6 Heavy Haul System Design Considerations 213
5.6.1 Starting the Train (Traction) 216
5.6.2 Stopping the Train (Braking) 217
5.6.3 Topography Issues 217
5.6.4 Traction Pinch Points 217
5.6.5 Cycle Time 218
5.7 Distributed Power 219
5.7.1 Head–Tail Configuration 222
5.7.2 Head–Mid Configuration 223
5.7.3 Head–Mid–Tail Configuration 223
5.8 Concluding Remarks 224
References 224

Chapter 6 Traction/Adhesion Control Systems and Their Modelling 227

6.1 Classification of Traction/Adhesion Control Systems 229
6.1.1 Adhesion Control Strategies 229
6.1.2 Adhesion/Creep Control Algorithms 230
6.1.3 Design Configurations 233
6.2 Simplified Modelling Approach 235
6.2.1 Power Plant 235
6.2.2 Mechanical Subsystem 237
6.2.2.1 Wheelset Dynamics 238
6.2.2.2 Adhesion Force Modelling 239
6.2.2.3 Train Dynamics 240
6.2.2.4 Modelling of Traction Control Subsystem 241

6.3 Simplified Traction Control Study 242
6.3.1 Train, Locomotive and Wagon Parameters 242
6.3.2 Simulation Scenarios 243
6.3.3 Case 1: Constant Speed Mode 244
6.3.3.1 Implementation of the Model in Simulink 244
6.3.3.2 Simulation Results 249
6.3.4 Case 2: Acceleration Mode 251
6.3.4.1 Implementation of the Model in Simulink 251
6.3.4.2 Simulation Results 257
6.3.5 Uncertainties in Applying Simplified Modelling for Locomotive Dynamics Studies 259
References 260

Chapter 7 Modelling of Locomotives 263

7.1 Introduction to Modelling Approaches 263
7.1.1 Newton–Euler Equations 264
7.1.2 D'Alembert's Principle and Generalised Forces 264
7.1.3 Lagrange's Equation 265
7.1.4 Dynamic Equations 266
7.2 Numerical Integrators 268
7.3 How to Model a Locomotive 270
7.3.1 Equations of Dynamic Equilibrium: Locomotive Car Body 271
7.3.1.1 Longitudinal Dynamic Equilibrium Equation 272
7.3.1.2 Lateral Dynamic Equilibrium Equation 272
7.3.1.3 Vertical Dynamic Equilibrium Equation 273
7.3.1.4 Roll Rotational Dynamic Equilibrium Equation 273
7.3.1.5 Pitch Rotational Dynamic Equilibrium Equation 273
7.3.1.6 Yaw Rotational Dynamic Equilibrium Equation 274
7.3.2 Equations of Dynamic Equilibrium: Bogie Frame 274
7.3.2.1 Longitudinal Dynamic Equilibrium Equation 274
7.3.2.2 Lateral Dynamic Equilibrium Equation 276
7.3.2.3 Vertical Dynamic Equilibrium Equation 276
7.3.2.4 Roll Rotational Dynamic Equilibrium Equation 277

7.3.2.5 Pitch Rotational Dynamic Equilibrium Equation 277
7.3.2.6 Yaw Rotational Dynamic Equilibrium Equation 278
7.3.3 Secondary Suspension Forces 278
7.3.4 Traction Motor Assembly with Wheelset 279
7.3.4.1 Equations of Dynamic Equilibrium – Wheelset 279
7.3.4.2 Equations of Dynamic Equilibrium – Traction Motor System 280
7.3.5 Primary Suspension Forces 281
7.3.6 Couplers: Draft Gear Modelling 282
7.4 Track Modelling 285
7.4.1 Rail 285
7.4.2 Pads, Fasteners, and Sleepers 288
7.4.3 Ballast and Sub-Ballast 289
7.4.4 Dynamics of Complete Locomotive-Track System 291
7.5 Contact Modelling at the Wheel-Rail Interface 292
7.5.1 Wheel-Rail Contact – The Normal Problem 292
7.5.1.1 Normal Contact (Hertz) Theory 292
7.5.2 Wheel-Rail Tangential Contact Modelling 294
7.5.2.1 Kalker Linear Theory 295
7.5.2.2 Kalker Simplified Theory 296
7.5.2.3 Creep Force Law of Shen–Hedrick–Elkins 299
7.5.2.4 Polach Approach 301
7.5.2.5 Comparison of Kalker Simplified, Shen–Hedrick–Elkins and Polach Approaches 302
7.5.3 Friction and Adhesion Coefficients 304
7.5.4 Tangential Forces, Including Variable Friction Coefficient 306
7.6 Multibody Dynamics Software Packages for Rail Vehicle-Track Interaction Simulation 308
7.6.1 NUCARS® 310
7.6.2 GENSYS® 311
7.6.3 VAMPIRE® 314
7.6.4 VI-RAIL® 315
7.6.5 SIMPACK® 317
7.6.6 Universal Mechanism 322
7.7 Locomotive Model Acceptance Procedure 326
7.7.1 Locomotive Modelling 326
7.7.2 Methodology in LMAP 329
7.7.2.1 Stage 1: Basic Locomotive Model Checking/Debugging 331

7.7.2.2 Stage 2: Tests Currently Included in Standards 332
7.7.2.3 Stage 3: Tests Not Included in Standards (Traction and Braking) 335
7.7.3 Simulated Case Studies for Locomotive Model Validation 336
7.8 Examples of Heavy Haul Locomotive Dynamic Behaviour Studies in GENSYS 339
7.8.1 Application of Adjustable Air Suspension under Traction Control 340
7.8.1.1 Secondary Suspension Design and Its Modelling Approach 340
7.8.1.2 Locomotive Modelling in GENSYS 341
7.8.1.3 Control Systems 342
7.8.1.4 Simulation and Results 343
7.8.2 Optimisation of Primary Suspension Characteristics for Heavy Haul Locomotives 346
7.8.2.1 Locomotive Mechanical Model 349
7.8.2.2 Simulation and Results 350
7.8.3 Heavy Haul Locomotive Dynamic Inverse Modelling 353
7.8.3.1 Locomotive Dynamics Inverse Modelling 353
7.8.3.2 Bogie Frame 353
7.8.3.3 Wheelset 355
7.8.3.4 Wheel-Rail Contact Forces 355
7.8.3.5 Locomotive Dynamics Modelling Using GENSYS 356
7.8.3.6 Case Study 357
References 361

Chapter 8 Locomotive Power Systems Modelling 367

8.1 Introduction 367
8.2 Diesel Engine Modelling 367
8.3 Transformer Modelling 371
8.4 Inverter Modelling 373
8.5 Traction Motor Modelling 380
8.6 Power System Modelling for Heavy Haul Locomotives in Simulink 382
8.6.1 Case Study 1: AC Electric Locomotive 382
8.6.2 Case Study 2: AC Diesel-Electric Locomotive 387
8.7 Conclusions 394
References 394

Chapter 9 Advanced Simulation Methodology 397

9.1 Co-Simulation and Its Application 399
9.1.1 Development of the Co-Simulation Client Interface 399
9.1.2 Case Studies 415
9.1.2.1 Multibody Model of a Heavy Haul Locomotive in GENSYS 415
9.1.2.2 Simulation Scenario 417
9.1.2.3 Case Study 1: Simplified Approach: Multibody Model and Traction Control System 420
9.1.2.4 Case Study 2: Full Locomotive Model 420
9.1.2.5 Simulation Results 423
9.2 Longitudinal Train Dynamics in Heavy Haul Locomotive Dynamics Behaviour Studies 428
9.2.1 Simulation Scenario Task 429
9.2.2 Longitudinal Train Dynamics Simulation 429
9.2.3 Locomotive Dynamics Simulation 432
References 435

Chapter 10 Conclusion 437

Glossary 439

Index 447

Preface

Understanding critical vehicle–track interaction issues and the associated dynamic responses is fundamental to ensuring safe and cost-effective operations of modern railways. With increasing demands for safer freight trains operating at higher speeds with higher loads, it is also necessary to implement more innovative methods for controlling longer and heavier trains. This requires a comprehensive understanding of the factors that affect all aspects of their dynamic performance. Advanced simulation techniques allow proposed innovations to be examined in detail and optimised before the costly process of introducing them into the operational railway environment is contemplated.

Coverage is given to the various types of locomotives used with heavy haul freight trains, along with the various possible configurations of those trains. This book is intended both as an introductory text for graduate or senior undergraduate students and as a reference for engineers practicing in the field of heavy haul rail network design, as well as for those undertaking research into performance issues related to these types of railway operations. The information provided progresses from basic concepts and terminology to the detailed explanations and techniques that provide a comprehensive understanding of the subject matter.

The following text summarises the content covered in each chapter:

Chapter 1: This chapter introduces heavy haul railway transport, encompassing the history and evolution of these hugely successful railway networks that run our longest and heaviest trains. Coverage is given to the classification of heavy haul railways, plus various operational and engineering issues that distinguish them from other freight railways. This chapter concludes with a review of existing heavy haul railway networks around the world.

Chapter 2: An introduction to both electric and diesel–electric heavy haul locomotive design is provided in this chapter. The main components of these locomotives and their elements are described in detail. The functions and design of primary systems for generating power and applying traction and braking are explained, and the basic processes of their operation and control are overviewed. Various auxiliary systems and equipment are also described in detail.

Chapter 3: The mechanical systems of locomotives, including the main load-bearing components and the structure for housing the equipment, are discussed in detail. The various types of bogies and their components are described, along with suspension designs, the mechanical components of locomotive drives and the braking and sanding systems.

Chapter 4: This chapter covers the design of locomotive electric transmission systems, the need for on-board transformers in some designs and on-board generators/alternators in others. Detailed coverage of the operation of the various types of traction motors and their associated control strategies is provided.

Chapter 5: Longitudinal train dynamics and approaches for its modelling are described in detail in this chapter. Focus is given to alternate train configurations and rail vehicle connection models. Information on modelling

of traction and dynamic braking systems, pneumatic braking, gravitational effects plus propulsion and curving resistance is included. The need for modelling driver control actions on the stability of long heavy haul trains is discussed. This chapter includes examples of heavy haul train modelling.

Chapter 6: The classification and modelling of traction control systems are described in this chapter. Modelling of wheel dynamics, train dynamics, adhesion and traction control systems are discussed, and an example of a simulation in Simulink® for a single wheelset under traction is provided.

Chapter 7: This chapter discusses how to simulate the dynamic interaction of a locomotive on virtually any track. First, it introduces the fundamentals of multi-body dynamics required to understand the concepts, and then discusses some numerical integration methods necessary to solve the equations. The process for modelling of locomotives as well as the various elements required to construct a locomotive model are described. Discussion of a comprehensive track model and the detailed non-linear modelling of wheel–rail interaction are included. A locomotive model acceptance procedure incorporating best practices from international standards applicable to locomotive dynamic behaviour is described, and an example of the modelling of a heavy haul locomotive using GENSYS multi-body software is provided.

Chapter 8: This chapter covers power system modelling for electric and diesel–electric locomotives. Diesel engine, transformer, inverter and traction motor modelling are explained in detail. This chapter concludes with two case studies with high-level task complexity, using real simulation examples in order to find typical solutions.

Chapter 9: The principles of an advanced simulation methodology applicable for traction studies are described in this chapter, and two simulation cases are performed to demonstrate the process. The first one presents a comparison of simplified and detailed approaches for modelling of locomotive traction systems based on the application of a co-simulation interface. The design concept of the co-simulation interface between GENSYS and Simulink used there is described in detail. Then a detailed methodology is described, and a worked example for utilising longitudinal train dynamics modelling and multi-body software together to deliver results combining traction dynamics and in-train forces is provided.

Acknowledgements

The authors thank their colleagues and friends for their assistance with the preparation of this book. Particular mention must be made of

- Oldrich Polach from Bombardier Transportation, Switzerland, for his significant and very valuable contribution in the development of creep force modelling under traction and ongoing consultation regarding bogie design for heavy haul locomotives.
- Frank Szanto from Downer Rail, Australia, for his always helpful consultation on locomotive modelling and studies for various Australian heavy haul routes.
- Gerald Grabner from Siemens, Austria, for information on the design of Australian heavy haul locomotive bogies and drawings for this book, and Eric Graph, for providing information on the wide spectrum of bogies produced by Siemens.
- Qing Wu from the Centre for Railway Engineering and Shihui Luo from Southwest Jiaotong University, for their help in gathering information on Chinese heavy haul locomotives and Chinese research in this field.
- Karl Heinz Buchholz, Imke Koch and Katherine Pirkle from Bombardier Transportation, Germany, for arranging and providing information on heavy haul locomotives used in Sweden.

We also thank the following people involved in the development of specialised rail vehicle dynamics software products and multi-body models:

- Ingemar Persson from ABDesolver, Sweden, for his great support of our research developments and innovations, and for the implementation of his and our ideas in the GENSYS rail vehicle dynamics software.
- Scott Simson from Bradken, Australia, for his significant contribution in Australian heavy haul locomotive studies and model development.
- Christoph Weidemann from Dassault Systèmes, Germany, for providing detailed information on the SIMPACK modelling software package, its functionality and features for the modelling of rail vehicles.
- Erik Pfleger from Siemens, Germany, for assistance with examples of locomotive bogie and traction drive modelling in SIMPACK.
- Roman Kovalev, Alexey Sakalo and Dmitry Pogorelov from Universal Mechanism, Russia, for providing relevant information on their multi-body modelling software package.

We thank Igor Spiryagin for his long-term support and significant contribution in the development of content on locomotive design, dynamic behaviour and engineering solutions related to locomotive applications.

Our sincere thanks also go to the team at CRC Press who worked on this book, particularly Jonathan Plant, executive editor; Laurie Oknowsky and Ashley Weinstein, project coordinators; Richard Tressider, project editor; Dr. Vladimir Vantsevich, series editor; and Arlene Kopeloff, executive assistant. Their acceptance of our proposal followed by ongoing support and encouragement during the writing process made the project much easier to complete.

Our humble apologies if we have forgotten to mention anyone. Without doubt, there are also others we are not aware of who have helped with our project behind the scenes. Our thanks go to all those involved.

Finally, we thank our families for their support during the writing of this book.

Authors

Maksym Spiryagin is the deputy director of the Centre for Railway Engineering at Central Queensland University (CQU). His research interests include locomotive traction, rail vehicle dynamics, contact mechanics, mechatronics, acoustics and real-time and software-enabled control systems. He earned his PhD in the field of railway transport in 2004 at the East Ukrainian National University. He has published four books and has more than 100 other scientific publications and 20 patents as one of the inventors.

Peter Wolfs is a professor of electrical engineering at CQU. He is a fellow of Engineers Australia, a senior member of IEEE and an associate member of the Centre for Railway Engineering. His areas of expertise include electrical power distribution, power quality and harmonics, railway traction power supply, renewable energy supply, solar and hybrid electric vehicles and intelligent systems applications in power systems and railways. He earned his PhD in the field of high frequency link power conversion in 1992 at the University of Queensland. He has more than 230 scientific publications, 4 book chapters and 5 patents as an inventor.

Colin Cole is the director of the Centre for Railway Engineering at CQU. He has worked in the Australian rail industry since 1984, starting with 6 years in mechanised track maintenance for Queensland Railways. Since then, he has focused on a research and consulting career involving work on track maintenance, train and wagon dynamics, train control technologies and the development of on-board devices. He has been extensively engaged with the industry in the past through nationally funded Rail Cooperative Research Centre (CRC) programs, and is continuing involvement with the Australian Centre for Rail Innovation and the new Rail Manufacturing CRC. His PhD was based on longitudinal train dynamics modelling. He has authored and co-authored more than 120 technical papers, a book chapter, a book, numerous commercial research and consulting reports, and has developed 2 patents related to in-cabin locomotive technologies.

Valentyn Spiryagin earned his PhD in the field of railway transport in 2004 at the East Ukrainian National University, Lugansk, Ukraine. His research activities include rail vehicle dynamics, multi-body simulation and control systems. Currently, he works as the diesel–electric locomotive lead expert for ZhelDorRemMash OJSC, a subsidiary of Locomotive Technologies LLC, at its Engineering Centre in Yaroslavl, Russia, on rail vehicle design and dynamics, mechatronic suspension systems for locomotives, locomotive traction control systems and associated field and laboratory testing. He has more than 60 scientific papers, 2 books and 28 patents as one of the inventors.

Yan Quan Sun works as a senior research engineer at the Centre for Railway Engineering at CQU. His current research interests include rail vehicle dynamics, longitudinal train dynamics, rail vehicle–track interaction dynamics, and rail-track

and bridge dynamics. He came to Australia in 1998 and earned his PhD in dynamics modelling of heavy haul railway transportation in 2002 at CQU. He has published more than 100 scientific and academic papers and a book.

Tim McSweeney has more than 40 years experience in the field of railway infrastructure asset management, specialising in track engineering in the heavy-haul environment. He was the senior infrastructure manager overseeing the Bowen Basin export coal network for Queensland Rail from 1991 until 2001 when he joined the Centre for Railway Engineering at CQU to follow his interest in railway research. He retired in 2007, but has continued his involvement with the Centre for Railway Engineering as an adjunct research fellow and was awarded an honorary Master of Engineering degree by CQU in 2011. He is a member of the Railway Technical Society of Australasia and a fellow of the Permanent Way Institution.

1 Introduction

1.1 THE ORIGIN OF RAILWAYS

The predecessors of conventional railways as we know them today are considered to be early 'trackways' or 'wagonways' that provided the means for guiding a wheeled vehicle along a defined path. The earliest known example of such a system is the Diolkos, a 7 km long stone-paved portage trackway constructed in the sixth century BC near Corinth in ancient Greece. It enabled boats to be moved overland across the Isthmus of Corinth on a trolley hauled by manpower along a curved route that avoided steeper gradients [1]. This innovation replaced a 900 km circumnavigation by sea of the Peloponnese peninsula and continued in use until the first century AD. Horse-drawn wagonways using cut-stone tracks also first appeared in ancient Greece, and others can be found on Malta and in various parts of the Roman Empire.

Similar wagonways are well documented in the late Middle Ages, primarily associated with underground mining activity in various parts of Europe where tubs or carts were pushed by hand on unflanged wooden rollers to move ore. Guide pins attached to the carts and running in a groove in the trackbed to provide steering were sometimes used. Wooden rails to guide horse-drawn wagons with flanged wheels were also certainly in use in similar mining applications by the sixteenth century. Above ground wagonways were documented in the early seventeenth century in England, with the first overland precursor railway thought to be the Wollarton Wagonway in Nottingham, which is known to have carried coal in wagons with flanged wheels running on wooden rails over several kilometres, operating for about 10 years from 1604. Some operators eventually plated the wooden rails with iron to reduce both friction and wear, which inevitably led to increased wear of the wooden wheels/rollers, resulting in the introduction of iron wheels towards the middle of the eighteenth century.

It is no surprise that the Industrial Revolution, commencing in Great Britain about that same time and quickly spreading to Western Europe and the United States, saw an increasingly rapid evolution of these relatively primitive wagonways towards the conventional railways, which have been in common use for the past 200 years. Developments in metallurgy and steam power enabled the innovations that were necessary for railway tracks to carry steam locomotives hauling loads of many times their own weight through realising significant tractive effort from the friction between smooth flanged wheels and smooth rails. The end of the nineteenth century saw a world railway network of various gauges, totalling more than 800,000 km served by steam locomotives. Train operations were also becoming safer with the progressive introduction of the Westinghouse air brake which was patented in 1873.

The second quarter of the twentieth century saw the parallel development of diesel traction and electrical traction locomotives, the latter becoming the main form of propulsion in Europe after World War II. Meanwhile, the main concentration of diesel traction was to occur in railways in industrialised countries such as the

United States, Canada, Australia, Russia, China, India, Brazil and South Africa. The world currently has approximately 1.4 million route km of railways, of which only some 300,000 km is electrified [2].

1.2 HEAVY HAUL FREIGHT

As evidenced by the range of track gauges currently in use worldwide as shown in Table 1.1, there are a multitude of options available with which to attempt to optimise the concept of flanged wheels running on parallel steel rails resting on some form of support structure. The logical progression to longer trains hauling heavier wagons was evident throughout the second half of the twentieth century, particularly once bulk commodities such as coal, grain and iron ore began to be primarily transported in 'unit' or 'block' trains consisting of a single type of wagon carrying the product from origin to destination without being separated en route. The increase in axle loads has been gradual but steady for the many decades since, with the main aim of providing more efficient and cost-effective transportation of bulk freight. This has resulted in the use of the 'heavy haul' designation for railways that operate long unit trains with high axle loads. One critical limitation that remains is that the maximum speed of these heavy haul trains is rarely above 80 km/h, primarily to minimise the rate of deterioration of the track structure and the likely extent of damage in the event of a derailment.

Research undertaken over many decades has been critical to providing the necessary technological innovations that allow heavy haul railways to operate safely and economically [3], but there are still opportunities for further improvements with significant challenges and a variety of risks to overcome (see a typical example in Figure 1.1).

TABLE 1.1
Current Operational Railway Track Gauges

Description	Metric	Imperial	Operational Track (km and % of total)
Narrow Gauges			
Two-foot gauge	600 mm	1 ft 11 5/8 in.	2,124 km (0.2%)
Bosnian gauge	760 mm	2 ft 5 15/16 in.	2,067 km (0.2%)
Three-foot gauge	914 mm	3 ft	3,568 km (0.3%)
Italian metre gauge	950 mm	3 ft 1 3/8 in.	1,595 km (0.1%)
Metre gauge	1,000 mm	3 ft 3 3/8 in.	77,760 km (5.7%)
Cape Colony gauge	1,067 mm	3 ft 6 in.	106,395 km (7.8%)
Standard Gauge	1,435 mm	4 ft 8 1/2 in.	896,962 km (65.5%)
Broad Gauges			
Russian gauge	1,520 mm	4 ft 11 27/32 in.	154,228 km (11.3%)
Irish gauge	1,600 mm	5 ft 3 in.	11,724 km (0.8%)
Iberian gauge	1,668 mm	5 ft 5 21/32 in.	14,311 km (1.0%)
Indian gauge	1,676 mm	5 ft 6 in.	97,900 km (7.1%)

FIGURE 1.1 Heavy haul railways can have 'expensive' accidents.

1.2.1 Classification of Heavy Haul Railways

The International Heavy Haul Association (IHHA) is a worldwide non-governmental scientific and technological association of heavy haul railways and their advocates. Its members comprise national, state and private railways and railway organisations dedicated to the pursuit of excellence in heavy haul railway operating and maintenance practices and the improvement of rail technology. A heavy haul railroad is defined by the IHHA as one that meets at least two of these requirements [4]:

- Operates unit or combined trains of at least 5000 gross tonnes
- Hauls at least 22 million gross tonnes (MGT) per year of freight over a railway corridor of at least 150 km in length
- Regularly operates rolling stock with axle loadings of 27.5 tonnes or more

There are many railways across the globe that can now lay claim to meeting this definition. However, there is a unique event on record that demonstrates just how much further the achievement of the ultimate 'heavy haul' status could be pushed in the future. On 21 June 2001, the BHP Billiton-owned Mount Newman railway broke the world record for both the heaviest train and the longest train when a 7.3 km long train of 682 wagons and 99,734 tonnes gross weight ran for 275 km between Yandi and Port Hedland. The train carried 82,000 tonnes of wet iron ore and was hauled by eight 6000 hp diesel locomotives that were distributed through the train as three pairs and two single units, linked by Locotrol radio communications and controlled by a single driver. Although this is unlikely to ever be considered for the routine operation of a heavy haul railway, the trial of this massive train was 'an opportunity to push the technology to the maximum' with the reasoning that 'you have to keep trying different things – if you don't, you don't know what you can do' [5].

1.2.2 Operation and Maintenance of Heavy Haul Lines

Because of the complexity of the various interactions involved, many of the engineering parameters of a heavy haul railway can only be 'optimised' by using an integrated 'systems' approach. It is critical that operators do not change individual aspects of their particular network or corridor without examining the potential impacts on all the other parts. For example, increasing the maximum axle load may minimise the size and cost of the requisite wagon fleet, but it can have dramatically adverse effects on the railway subgrade, track and bridge structures. Consideration also needs to be given to horizontal and vertical track alignments; trains use less energy, average speeds are higher and much less stress/wear on equipment occurs when railways can avoid tight curves, steep gradients and undulating terrain.

The wheel-rail interface is commonly considered to be the most critical area of railway operations, requiring ongoing multidisciplinary technical investigation and corridor specific management to minimise damage mechanisms such as wheel flange/tread wear and rolling contact fatigue as operators seek to increase the level of traffic and run heavier and faster trains. Getting control of that small but highly stressed quasi-elliptical contact zone through the development of suitable standards and maintenance procedures provides the opportunity to reduce defect rates, improve safety, extend wheel and rail life, improve vehicle-track interaction and reduce wheel-rail noise. Developing the set of desired wheel-rail profiles for the tangent track as well as various degrees of curvature is essential, as is then maintaining them through wheel turning and rail grinding processes. Effective management of friction at the wheel-rail interface is also essential; it has been claimed that 100% effective friction management can be obtained in heavy haul systems by combining rail gauge face lubrication with top of rail friction modification, resulting in 10-fold reductions in lateral wear of wheels and rails [6].

The performance of any track structure is dominated by the quality of the subgrade foundation on which it is supported, and particularly the drainage of that subgrade. It is critical that a heavy haul railway avoids excessive progressive settlement under repeated cyclic loading, significant volume change with moisture content variation, progressive shear failure under wheel load cycles and subgrade attrition/puncturing from ballast action. Ballast must be kept free of fouling to maintain the resiliency that allows optimal distribution of axle loads over the track structure/subgrade, and to ensure free drainage of the track so as to prevent subgrade damage due to moisture retention.

Heavy haul railways have generally adopted the use of premium track materials (head hardened rail, concrete sleepers, premium turnouts, moveable vees/frogs and the like) combined with proactive preventative maintenance processes and non-destructive testing methods to achieve the proper balance between low life cycle track ownership costs and the necessary levels of safety and operational reliability.

Likewise, the rolling stock area has introduced automatic train inspection technology that allows critical issues on wagons, and more particularly on their bogies, to be reliably and accurately monitored during normal operations by on-board or trackside sensors. Such systems were originally introduced in heavy haul railways so that conditions that exceeded safe limits while in motion could be detected before

catastrophic failures occurred. Subsequently, the development of more sophisticated sensors, data collection systems and communication capabilities have enabled various parameters to be measured and analysed with a view to predicting when maintenance intervention should be scheduled, enhancing the productivity of railway operations. Typical examples include hot bearing, hot/cold wheel and brake detectors, acoustic bearing defect detectors, dragging equipment detectors and wheel impact load detectors [7]. The capability and range of conditions that may be detected and monitored using automated wayside installations continue to expand as new inspection technologies, for example, capture and analysis of high-speed digital imaging, are developed into reliable analytical and/or predictive systems.

The economic imperative to increase train lengths has been constrained by issues such as excessive longitudinal dynamic action, problems with air brake signal propagation, and greater stress and wear on infrastructure and equipment. Distributed power (locomotives distributed at several points along the length of the train as single units or groups which can be synchronised and controlled from the lead locomotive) allows these concerns to be ameliorated through improving train handling over undulating track profiles, reducing drawgear and lateral forces and enabling brake applications to be initiated simultaneously from the location of each locomotive group.

Traditional Westinghouse pneumatic air brakes are initiated from the locomotive and are mechanically applied progressively to one wagon at a time down the length of a train in a domino-like sequence. This results in significant delay in the application of brakes on wagons remote from the locomotive, causing opposing buff and draft forces between wagons during the braking process. Electronically controlled pneumatic (ECP) braking systems use microprocessor and networking technologies to apply the brakes to each wagon in the train simultaneously, resulting in improved braking efficiency that provides shorter stopping distances, reduced fuel consumption and less risk of derailment plus reduced wagon component wear/damage [8].

A significant challenge for most heavy haul operators is that, given their often high traffic volumes, available track maintenance windows are usually short. Two fundamental requirements have to be met when maintaining the track; work must be performed quickly while also producing durable results. This requires high-capacity machines for such routine tasks as levelling/relining track, tamping and dynamically stabilising ballast, replacing sleepers, grinding rail to the appropriate profiles and, on many railways, periodically cleaning fouled ballast.

When it becomes necessary to rehabilitate the track structure, heavy haul railways almost universally use fully automated track renewal machines that remove old ballast, rails, sleepers and fastenings and simultaneously replace them without manual assistance. Such a quality controlled process ensures the track structure's maximum carrying capacity per axle is reliably achieved with optimal material use.

1.3 REVIEW OF EXISTING HEAVY HAUL RAILWAY OPERATIONS

The membership of the IHHA consists of private and public railway systems, and national railway industry trade and advocate groups interested in furthering the exchange of technical information that will benefit the world's heavy haul rail

operations. The remainder of this chapter highlights selected railway operations of interest involving those members.

1.3.1 Australia

Between 1966 and 1969, four heavy haul railways were developed in the Pilbara region in the far north of the state of Western Australia for the haulage of iron ore from several mines to three export ports; there have been substantial rail extensions as old mines have closed and new deposits have been developed. These are all 1435 mm (4 ft 8½ in.) standard gauge railways and originally used American standards for track, locomotives and wagons. They are currently operated by just two companies, Rio Tinto and BHP Billiton, and now service over 20 mines.

The very heavy traffic operated over each of these lines, in excess of 100 MGT per year on the trunk routes, pushed wheel-rail technology to its limits, and finding appropriate solutions to the problems this caused resulted in considerable R&D from the 1970s onwards that has been of value to freight railways worldwide.

In 2008, the Fortescue Metals Group commenced operating a fifth iron ore railway in the Pilbara and is now servicing three mines. Details of each of the Pilbara's existing iron ore railway assets and their routine operating parameters are shown in Table 1.2.

In addition to these long-term Pilbara operations, Hancock Prospecting constructed 344 km of single track railway during 2014–2015 to service the Roy Hill mine and commenced operations in December 2015. Trains of 232 wagons hauled by three 4400 hp GE ES44ACi locomotives each carry a payload of 32,100 tonnes.

Aurizon (formerly the state government-owned QR National) is a privatised railway operator that manages Australia's largest heavy haul export coal rail system, the Central Queensland Coal Network. This is a 1067 mm (3 ft 6 in.) Cape Colony narrow

TABLE 1.2
Operational Parameters of Pilbara Iron Ore Railways

	Fortescue Metals Group (FMG)	Rio Tinto		BHP Billiton	
		Robe River	Hamersley	Newman	Goldsworthy
Railway length (route km)	420	252	867	526	209
Train size (wagons and km)	250 and 2.7	163 and 1.6	236 and 2.4	312 and 3.3	90 and 1.0
Train payload (tonnes)	35,000	18,000	29,500	37,440	7,650
Axle load (tonnes)	42	36	36	37.5	32
Maximum speed (km/h)	80	70	75	75	60
Ore railed (MGT/year)	150	255 total over both railways		215 total over both railways	

gauge network on the eastern coast of Australia comprising four major coal systems (Moura, Blackwater, Goonyella and Newlands), totalling almost 1800 route km. These heavy haul lines were built beginning in 1968 to link export coal mines to several nearby ports. Electrification of the majority of the Blackwater and Goonyella systems was undertaken in 1986 and 1987, providing a 25 kV/50 Hz AC overhead traction supply system to allow more powerful and lower maintenance electric locomotives to replace the original diesel electric traction. Around 450 route km have bi-directionally signalled duplicated tracks to cope with the density of traffic (see Figure 1.2). The Blackwater system services mines at the southern end of the Bowen Basin and the Moura system services mines in the Dawson and Callide Valleys; both these systems ship coal through the port of Gladstone.

The Goonyella and Newlands systems transport northern Bowen Basin coal to export ports at Hay Point/Dalrymple Bay and Abbot Point. All four of these systems carry trains with axle loads of 26.5 tonnes at a maximum operating speed of 80 km/h. The maximum train length of 2.1 km operates on the Goonyella system, with 124 wagons carrying a payload of 9970 tonnes hauled by two head-end 5360 hp electric locomotives with one similar Locotrol managed locomotive in the middle of the train. This Goonyella system alone shipped 114 MGT of coal in 2014, with the full Central Queensland Coal Network carrying 214 MGT [9].

The Hunter Valley heavy haul railway system in the Australian state of New South Wales comprises some 540 route km of standard gauge track, allowing 1.5 km long trains to operate with 30 tonnes axle loads at a maximum speed of 60 km/h and 25 tonnes axle loads at 80 km/h [10]. It is an important part of the supply chain that exported 159 MGT of coal through the port of Newcastle in 2014. The railway network consists of 125 route km of a dedicated double track coal line between the port

FIGURE 1.2 Duplicated track section on the Goonyella coal railway system.

and Muswellbrook (with some sections having a third track), and two single tracks with passing loops shared with other traffic branching off to the north and west of Mussellbrook for a further 260 and 155 km, respectively.

1.3.2 Brazil

Carajas Railway (Estrada de Ferro Carajs or EFC) is part of an integrated mine/railway/port iron ore operation controlled by the Brazilian logistics company Vale (formerly Companhia Vale do Rio Doce). This railway has provided freight and passenger transportation services in the north of Brazil since 1985. It operates 892 route km of 1600 mm (5 ft 3 in.) Irish broad gauge railway mainly hauling around 110 MGT per year of iron ore from Carajas to the Ponta da Madeira terminal at the port of Sao Luis [11]. The typical iron ore train comprises 4 locomotives and 330 wagons (3.2 km length and 33,330 tonnes payload/41,838 gross tonnes) with an axle load of 30.5 tonnes and a maximum operating speed of 80 km/h. EFC also carried 308,000 passengers in 2013. Premium hardwood sleepers were originally used, but extensions and double tracking are now being constructed with concrete sleepers.

The Vitoria–Minas Railway (Estrada de Ferro Vitoria a Minas or EFVM), also operated by Vale, links mines in the Iron Quadrangle region of the Brazilian state of Minas Gerais to the Port of Tubarao at Vitoria. EFVM consists of 905 route km of 1000 mm (3 ft 3⅜ in.) metre narrow gauge railway, with duplicated track extending for 601 km of the corridor and single track over the rest. EFVM transported 120 MGT of iron ore in 2013, and also carried significant quantities of general freight plus 890,000 passengers. The maximum allowable axle load is 30 tonnes with a maximum operating speed of 70 km/h. The typical iron ore train consists of 4 distributed power locomotives hauling 320 wagons (3.1 km in length and carrying 32,000 tonnes of payload/40,100 gross tonnes).

MRS Logística S.A. (MRS) operates 1643 route km of Irish broad gauge railway in the southeast of Brazil [12]. The main commodities hauled are iron ore, steel products, cement, bauxite, coal, agricultural products, coke and containers. Iron ore represents about 75% of the hauled tonnage and is transported by trains consisting of 2 head-end locomotives and 134 gondola wagons (1.2 km length and 13,330 tonnes payload/16,730 gross tonnes) running from mines in the mountains of Minas Gerais to export ports at Guaíba and Sepetiba in Rio de Janeiro state. Iron ore is also supplied to a steel mill at Cubatão near the port of Santos in São Paulo state. In 2014, the MRS railway system carried a total of 164 MGT of cargo, including 121 MGT of iron ore. The maximum allowable axle load is 32.5 tonnes with a maximum operating speed of 50 km/h.

1.3.3 Canada

The standard gauge Canadian Pacific Railway (CPR) transports more than 25 MGT of metallurgical coal per year from the mines of south-eastern British Columbia to the port of Vancouver. This involves significant challenges to negotiate a route of 1207 km over two mountain ranges. Coal trains of 2.2 km in length powered by three

4400 hp AC traction diesel locomotives haul up to 152 wagons with maximum axle loads of 33 tonnes carrying payloads of 13,250 tonnes (17,000 gross tonnes). The route is predominantly single track and, for over half the trip (Golden to Vancouver), the coal traffic runs over the primary east–west mainline, which carries a total of approximately 80 MGT per year.

On the other side of the country, iron ore from mines in Labrador and Quebec is transported to ports on the St. Lawrence Seaway over several standard gauge single track railways. The remaining 414 route km of a longer line opened in 1954, the Quebec North Shore and Labrador Railway now runs distributed power trains 2.5 km in length with three locomotives and 265 wagons, transporting up to 24,000 tonnes of ore (33,000 gross tonnes). The Cartier Railway opened in 1960 and carries around 25 MGT of iron ore per year, and two head-end locomotives haul trains of 160 wagons (1.5 km length and 14,900 tonnes payload/17,330 gross tonnes) over 418 route km of single track with maximum axle loads of 27 tonnes [13].

1.3.4 China

The initial heavy haul railway in China was the Daqin Railway, opened to traffic in several phases between 1988 and 1992 to transport coal produced in Shaanxi Province and Inner Mongolia from the western terminus of Datong to the east coast port of Qinhuangdao. This is a standard gauge duplicated track system with a route length of 653 km operated by the state-owned China Railway Corporation [14]. Distributed power coal trains of 210 wagons hauled by two 8-axle articulated 25 kV/50 Hz AC twin-unit HXD1 electric locomotives are 2.7 km long with a gross mass of 21,400 tonnes. Maximum axle load is 25 tonnes with a maximum operating speed of 90 km/h and the trains are fitted with ECP brakes [15]. This railway transported approximately 440 MGT of coal in 2011. In mid-2014, China Railway Corporation and China Academy of Railway Sciences undertook trials with 33,000 tonnes trains on this line. These trains, almost 4 km long, hauled 320 wagons with 4 HXD1 electric locomotives [16].

A second electrified heavy haul line dedicated to hauling coal from the Shanxi Province coalfields to the east coast of China was provided by the commissioning between 1997 and 2000 of the Shuohuang Railway, 594 route km of electrified and duplicated standard gauge track built and operated by the Shenhua Group, a state-owned mining and energy company [14]. It carried 234 MGT of coal to the port of Huanghua in 2012. At that time, the railway was operating trains of 116 wagons at axle loads of 21–25 tonnes with a maximum gross mass of 12,000 tonnes [17]. However, following extensive research and field tests of an innovative distributed power control system, longer trains of 25,500 gross tonnes began operating in late 2014. Hauled by a head-end 12-axle articulated locomotive and a remote 8-axle articulated locomotive, the 1.6 km long trains convey 210 wagons of 30 tonnes axle load. The aim of the bigger trains is to increase the capacity to 350 MGT per year on this corridor. Shenhua Group now operates a network with a total length approaching 1900 route km supplying rail transport demand between the east and west of China, and is busily constructing new corridors and upgrading existing railways to cater for the ongoing growth of coal traffic.

Moreover, China now has the world's longest dedicated heavy haul line with the commissioning at the end of 2014 of the 1269 km Shanxi South Central Railway, operated by China Railway Corporation to connect the coalfields in the western part of Shanxi province to the port of Rizhao. It is an electrified and duplicated standard gauge track, has a design capacity of 200 MGT a year and is capable of carrying axle loads of 30 tonnes.

1.3.5 India

Although traffic volumes over the state-owned Indian Railways network continue to increase year by year, rail's market share of freight transport has gone down steadily over the past 50 years from around 90% to just 30%. Key reasons for this included the saturation of key freight routes with huge passenger traffic flows, and insufficient government emphasis on creating additional capacity over existing and new corridors [18].

Given the fast expansion of the Indian economy since 1990, the booming transport needs led to the national government committing to the construction of two dedicated multi-modal heavy haul freight corridors to world class standards with state-of-the-art technology. These 1676 mm (5 ft 6 in.) Indian broad gauge railways are currently being constructed to carry axle loads of 25 tonnes. Bridges are designed to a standard that will allow axle loads to eventually be increased to 32.5 tonnes. Trains of 1.5 km in length will haul payloads of up to 15,000 tonnes at a maximum speed of 100 km/h. Since the origin and destinations of traffic do not necessarily fall on these new corridors, a number of interconnections have been planned to transfer traffic to and from the existing Indian Railway network [19].

The Eastern Dedicated Freight Corridor will have a route length of 1839 km, made up of a 25 kV/50 Hz AC electrified duplicated track segment of 1392 km between Kolkata (Calcutta) on the east coast and New Delhi, then an electrified single track segment of 447 km on to Ludhiana in the north-western Punjab State. The total traffic over the corridor is projected to be around 265 MGT per year by 2040, primarily coal and various minerals.

The Western Dedicated Freight Corridor will consist of 1534 route km of a duplicated track electrified railway from Jawaharlal Nehru Port at Mumbai (Bombay) to New Delhi where it will connect with the Eastern Corridor. Traffic on the Western Corridor is projected to be around 280 MGT per year by 2040, comprising ISO containers, fertilisers, grains, salt, coal, iron/steel and cement. Both railways are due for commissioning in 2020 [20].

1.3.6 Nordic Countries

The combined Malmbanan/Ofotbanen line, Europe's only true heavy haul railway corridor [21], extends from the Swedish port of Lulea via iron ore mines around Gällivare and Kiruna to the Norwegian port of Narvik. This standard gauge single line railway, much of it above the Arctic Circle, was constructed through rugged terrain between 1898 and 1902 over a route of 473 km; unlike modern heavy haul

railways, it is consequently characterised by sharp radii curves and steep gradients. It was electrified at 15 kV/16⅔ Hz AC between 1915 and 1922. The track structure was progressively upgraded between 1998 and 2008 to allow an axle load increase from 25 to 30 tonnes; two Bombardier IORE 7200 hp head-end locomotives now haul 68 wagons in 750 m long trains of 8520 gross tonnes, which can operate at maximum speeds of 60 km/h loaded and 70 km/h empty [22,23]. The northern Kiruna to Narvik section of the corridor carries over 30 MGT per year. Increasing the maximum axle load to 32.5 tonnes is being investigated; wagons purchased since 2005 already have this capacity.

1.3.7 Russia

Russian Railways (RZD) does not currently have lines dedicated specifically for heavy haul operations. However, they do have two corridors that carry significant mixed traffic over long distances: the Trans-Siberian Railway and the Baikal–Amur Mainline (BAM). Siberian oil, coal and ores move to domestic and overseas consumers in trains of 6300 gross tonnes in the easterly direction, and 9000 tonnes in the westerly direction; large numbers of shipping containers transit in both directions. In accordance with the 'Development Strategy for Rail Transport in the Russian Federation until 2030', it is planned that the Trans-Siberian will concentrate on container and passenger transportation, and the BAM will be upgraded and used for heavy freight traffic [24].

The Trans-Siberian Railway was built from Moscow to the Pacific Ocean port of Vladivostok between 1891 and 1916. It has since been progressively double tracked and electrified throughout its 9288 route km. The line is 1520 mm (4 ft 11$^{27}/_{32}$ in.) Russian broad gauge, electrified at 3 kV DC over the western quarter of the route and at 25 kV AC for the rest. 2012 saw the railway carry some 33 MGT of general freight plus the equivalent of 238,000 twenty foot shipping containers.

The BAM is a 1520 mm Russian broad gauge railway that connects eastern Siberia and the port of Sovetskaya Gavan over a route of 4324 km. It is a single-track corridor except for its western end, which is double tracked for 722 km from Tayshet (where it links to the Trans-Siberian Railway) to Ust'-Kut. It was constructed sporadically between 1938 and 1984, being repeatedly halted for long periods for various reasons including war, a lack of labour/resources and engineering difficulties associated with permafrost and tunnelling in earthquake zones. The western 1484 km from Tayshet to Taksimo is now electrified at 25 kV AC, but diesel traction is used on the remainder where typical train gross mass is 5600 tonnes. The original design standard was 23.5 tonnes per axle, however, new or reconstructed track built over the past decade has been to a standard to allow 30 tonnes [25].

1.3.8 South Africa

Two significant Cape Colony narrow gauge heavy haul railways were constructed in the mid-1970s in South Africa. The Richards Bay Coal Railway (CoalLink) commenced operation in 1974, and now hauls coal from over 40 mines in the Mpumalanga

TABLE 1.3
Operational Parameters of South African Heavy Haul Railways

	Richards Bay Railway	Sishen – Saldanha Railway
Railway length (route km)	588	861
Train size (wagons and km)	200 and 2.2 (8 locos)	342 and 4.1 (6 × 5 MW locos)
Train payload (tonnes)	16,800 (20,800 gross)	34,200 (41,200 gross)
Axle load (tonnes)	26	30
Maximum speed (km/h)	80	60 (70 when empty)
Product railed (MGT/year)	70 coal + 10 general freight	56 iron ore + 1 general freight

province through rural KwaZulu-Natal and terminates at the export port of Richards Bay. This railway is electrified at 3 kV DC north of Ermelo, and with 25 kV/50 Hz AC from Ermelo to the port [26].

The Sishen–Saldanha Iron Ore Railway (OREX) opened in 1976 as an 861 km single track diesel electric locomotive system with 10 passing loops. It links the mines of the Northern Cape Province of South Africa to the port at Saldanha Bay on the west coast. The railway now has 19 passing loops at around 40 km spacing and is electrified at 50 kV/50 Hz AC instead of the usual 25 kV in order to allow a larger distance between transformers. Since 2007, three electric and seven diesel locomotives have been mixed together in a unique distributed power Locotrol controlled system to haul 342 wagon trains [24]. However, the introduction of 5 MW class 15 E electric locomotives now allows an all-electric operation as set out in Table 1.3 which provides details of South Africa's heavy haul railway routine operating parameters [27].

1.3.9 United States of America

After the Association of American Railroads undertook significant investigations under their Heavy Axle Load (HAL) Research Program, the rail industry in the United States accepted the introduction of wagons with axle loads of 32.4 tonnes in 1991. By 2010, almost all coal traffic and one-third of general freight was being carried in wagons of this heavy haul capacity [28].

The Powder River Basin in Wyoming and Montana provides around 40% of coal used for electricity generation throughout the United States. Two of the world's largest privately owned railways, the BNSF Railway and the Union Pacific Railroad, operate unit coal trains over the 166 route km of their primarily triple track Joint Line corridor in Wyoming. This corridor is the core of the Powder River Basin railway network through which over 400 million tonnes per year of coal is shipped around the United States. The Joint Line is the busiest and highest density freight railway in the world, carrying over 130 loaded and empty coal trains each day. Loaded trains vary in size up to 135 wagons (2.1 km long and 16,700 gross tonnes) and are hauled at a maximum operational speed of 80 km/h by distributed power locomotives at the head-end and tail [29].

REFERENCES

1. M.J.T. Lewis, Railways in the Greek and Roman world. In *Early Railways: A Selection of Papers from the First International Early Railways Conference*, A. Guy, J. Rees (eds.), Newcomen Society, London, UK, 2001, pp. 8–19.
2. M. Spiryagin, C. Cole, Y.Q. Sun, M. McClanachan, V. Spiryagin, T. McSweeney, *Design and Simulation of Rail Vehicles*, CRC Press, Boca Raton, FL, 2014.
3. M. Darby, Technology for profit. In *Proceedings of the 7th International Heavy Haul Conference: Confronting the Barriers of Heavy Haul Rail Technology*, IHHA, Brisbane, Australia, 10–14 June 2001, pp. 3–6.
4. International Heavy Haul Association, *Guidelines to Best Practices for Heavy Haul Railway Operations: Wheel and Rail Interface Issues*, IHHA, Virginia Beach, VA, 2001.
5. BHP breaks its own 'heaviest train' record, *Railway Gazette International*, Volume 157, Number 8, Sutton, UK, August 2001, p. 508.
6. International Heavy Haul Association, *Guidelines to Best Practices for Heavy Haul Railway Operations: Infrastructure Construction and Maintenance Issues*, IHHA, Virginia Beach, VA, 2009.
7. J. Lundgren, Enhancing railway safety and productivity with automated inspection technologies: The art and science of watching and listening to your trains. In *Proceedings of the International Heavy Haul Association Specialist Technical Session: High Tech in Heavy Haul*, IHHA, Kiruna, Sweden, 11–13 June 2007, pp. 507–516.
8. R.C. Kull, ECP braking and PTC for increasing heavy haul railway capacity. In *Proceedings of the 9th International Heavy Haul Conference: Heavy Haul and Innovation Development*, IHHA, Shanghai, China, 22–25 June 2009, pp. 551–557.
9. Aurizon Network Pty Ltd, 2014 Network development plan, Brisbane, Australia, November 2014.
10. Australian Rail Track Corporation, *Heavy Haul Infrastructure Guidelines: Track, Civil and Structures*, Sydney, Australia, 2013.
11. International Railway Journal, Vale pushes the limits, Volume 49, Issue 6, New York, NY, June 2009, pp. 45–49.
12. C. Jorge, C. Rodrigues, W. Vidon, Proactive track maintenance applying high technologies – MRS heavy haul experience. In *Proceedings of the International Heavy Haul Association Specialist Technical Session: High Tech in Heavy Haul*, IHHA, Kiruna, Sweden, 11–13 June 2007, pp. 339–347.
13. E. Magel, P. Sroba, Managing the wheel-rail interface: The Canadian experience. In *Wheel-Rail Interface Handbook*, R. Lewis, U. Olofsson (eds.), Woodhead Publishing, Cambridge, UK, 2009, pp. 669–685.
14. R. Bullock, J. Sondhi, P. Amos, Tracks from the past, transport for the future: China's railway industry 1990–2008 and its future plans and possibilities, Report No. 56415 to Transport Coordinator, World Bank, Beijing, China, 2009.
15. G. Zhixiu, *Heavy-Haul Transportation Technologies on Datong – Qinhuangdao Railway*, China Railway Publishing House, Beijing, China, 2009.
16. China South Locomotive & Rolling Stock Corporation Limited News & Media, Success traction tests on 30,000-ton combined trains with CSR ZELC locomotives, 8 April 2014. See http://www.csrgc.com.cn/g981/s2780/t248208.aspx.
17. International Railway Journal, Meeting China's burning desire for coal, Volume 53, Issue 8, New York, NY, August 2013, pp. 24–28.
18. R. Gupta, H. Mehta, T. Netzer, *Building India: Transforming the Nation's Logistics Infrastructure*, McKinsey & Company, Mumbai, India, September 2010.
19. Japan International Cooperation Agency, Feasibility study on the development of dedicated freight corridor for Delhi – Mumbai and Ludhiana – Sonnagar in India: Final Report - Volume 3: Main Report (Task 2), New Delhi, India, October 2007.

20. Work advances on dedicated freight corridors, *International Railway Journal*, Volume 55, Issue 4, New York, NY, April 2015, pp. 26–29.
21. F. Delooz, B. Paulsson, Heavy haul trains in Europe: State of the art and perspectives. In *Proceedings of the 9th International Heavy Haul Conference: Heavy Haul and Innovation Development*, IHHA, Shanghai, China, 22–25 June 2009, pp. 927–932.
22. P.O. Larsson-Kraik, Managing the wheel-rail interface: Railway infrastructure maintenance in a severe environment: The Swedish experience. In *Wheel-Rail Interface Handbook*, R. Lewis, U. Olofsson (eds.), Woodhead Publishing, Cambridge, UK, 2009, pp. 633–652.
23. W. Schöch, A. Frick, Development of the grinding practice at Malmbanan. In *Proceedings of the International Heavy Haul Association Specialist Technical Session: High Tech in Heavy Haul*, IHHA, Kiruna, Sweden, 11–13 June 2007, pp. 245–254.
24. M. Keyno, D. van der Meulen, Differences and similarities: Learning from heavy haul in cold and heat. In *Proceedings of the International Heavy Haul Association Specialist Technical Session: Railroading in Extreme Conditions*, Calgary, Canada, 19–22 June 2011, CD-ROM.
25. S.M. Zakharov, V. Bogdanov, I.A. Zharov, Wheel and rail profiles optimization: Problems and possible solutions for heavy haul lines in the Russian railways. In *Proceedings of the International Heavy Haul Association Specialist Technical Session: High Tech in Heavy Haul*, IHHA, Kiruna, Sweden, 11–13 June 2007, pp. 289–294.
26. H. Tournay, Heavy haul in South Africa: Three sides to a coin. In *Proceedings of the 7th International Heavy Haul Conference: Confronting the Barriers of Heavy Haul Rail Technology*, IHHA, Brisbane, Australia, 10–14 June 2001, pp. 13–18.
27. P.J. Grabe, D. Jacobs, J.F. Bester, J. Meyer, Determining the neutral temperature of continuous welded rail: New insights and observations. In *Proceedings of the 11th International Heavy Haul Association Conference: Operational Excellence*, IHHA, Perth, Australia, 21–24 June 2015, pp. 571–576.
28. C.D. Martland, Introduction of heavy axle loads by the North American rail industry, *Journal of the Transportation Research Forum*, 52(2), 2013, 103–125.
29. B. Solomon, P. Yough, *Coal Trains: The History of Railroading and Coal in the United States*, Voyageur Press, Minneapolis, MN, 2009.

2 Heavy Haul Locomotives and Their Design

2.1 INTRODUCTION

The transport of cargo with the application of powered propulsion systems on a railway was implemented in 1814 by the British inventor George Stephenson, when he built the first practical freight locomotive (then called a 'travelling engine') for hauling coal at the Killingworth Colliery. This locomotive, named Blücher, was a traction vehicle with flanged wheels and equipped with a steam engine that was able to haul a load of 30 tonnes, comprising eight wagons loaded with coal, up to a gradient of 1 in 450 at a speed of 6.4 km/h relying only on adhesion between rails and wheels. Figure 2.1 shows an improved version of that first freight locomotive; the sketch is believed to have been drawn by George Stevenson circa 1815. The success achieved by Stephenson's first series of locomotives provided the stimulus for the further development of rail freight traffic. For more than 150 years, steam locomotives were the main means of traction on the railways for the transportation of goods and freight, and in the mid-twentieth century, they were gradually replaced by diesel and electric powered locomotives that evolved into the modern machines now working on the railways throughout the world.

The world's first public railway, the Stockton and Darlington Railway, opened in 1825. The first train to run was hauled by a George Stephenson-built steam engine and carried a load of 80 tonnes of coal and flour 15 km in 2 h, reaching a top speed of 40 km/h. That vehicle was named 'Locomotion' and that name became the generic term 'locomotive' that we use at the present time. This word comes from the combination of two Latin words 'loco' and 'motivus', which mean 'from a place' and 'causing motion', respectively. In modern terminology, the definition of 'locomotive' corresponds to the railway-powered propulsion machine designed for the movement of trains on the tracks.

Freight or heavy haul locomotives are used to haul freight trains, the latter being specifically designated for hauling the much longer unit trains used to carry very large payloads of bulk products such as coal and iron ore. Unlike passenger locomotives, which are designed to reach their maximum permissible speed very quickly, the main characteristics expected of modern freight locomotives are to achieve and to sustain the maximum tractive efforts for as long as necessary, and keeping to the desired speed. Tractive efforts occur as a consequence of the implementation of the torque generated by traction motors from energy supplied by the power plant, and are realised due to the adhesion process between wheelsets and rails.

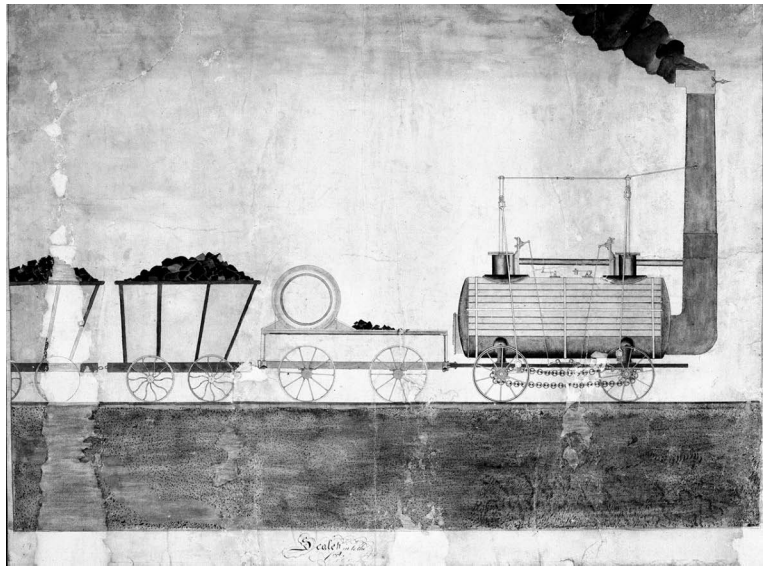

FIGURE 2.1 Earliest known drawing of a steam locomotive prototype invented by George Stephenson. (From National Railway Museum/Science & Society Picture Library, York, UK. With permission.)

2.2 TYPES OF LOCOMOTIVES AND THEIR CLASSIFICATION

Modern freight locomotives are divided into four subgroups based on the type of power supply:

- Electric
- Diesel
- Gas turbine
- Hybrid locomotives

An electric locomotive is a non-autonomous rail vehicle that receives electricity from an external source to power its movement. The external source in this case is a power station. The electrical power generated by the station is transmitted to traction substations by means of high-voltage distribution lines. The traction substations perform the transformation of that transmitted supply to the parameters (voltage, current type and frequency) necessary for powering the equipment on the electric locomotives. The power is supplied through overhead line equipment to the pantograph(s) of each electric locomotive. Closed loop railways are equipped with return feeders back to the traction substations. The basic principle of electric locomotive power supply is shown in Figure 2.2 [1], and an example of the layout scheme of an alternating current (AC) electric locomotive is shown in Figure 2.3. The advantages of the operation of electric locomotives are more power and greater reliability, plus lower costs of maintenance and repairs. The main disadvantages in comparison to other types

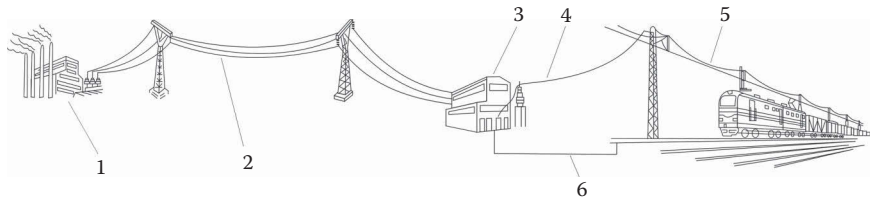

FIGURE 2.2 Basic operational principle for power supply in electrified railway systems. 1 – power station; 2 – distribution power lines; 3 – electrical traction substation; 4 – feeder power line; 5 – overhead line equipment; 6 – return feeder. (From Spiryagin, M. et al., *Design and Simulation of Rail Vehicles, Ground Vehicle Engineering Series*, CRC Press, Boca Raton, FL, 2014.)

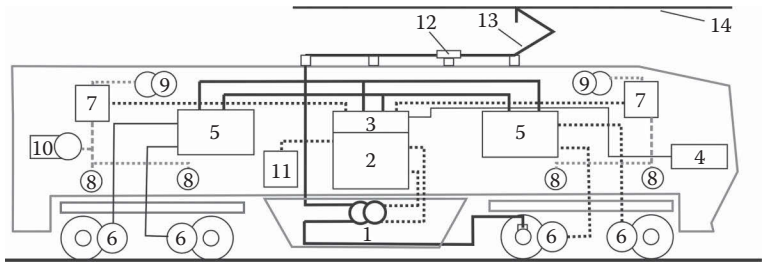

FIGURE 2.3 Overview of basic components of an AC electric locomotive. 1 – traction transformer; 2 – main rectifier; 3 – traction control; 4 – train control and monitoring system; 5 – traction converters; 6 – traction motors; 7 – auxiliary converters; 8 – motor blowers; 9 – cooling fans; 10 – air compressor; 11 – battery equipment; 12 – circuit breaker; 13 – pantograph; 14 – overhead line equipment.

of locomotives are the high cost of electrified network infrastructure and the cost of its maintenance, and also the lack of autonomous operation because the locomotive cannot move onto tracks not fitted with overhead line equipment.

In contrast to an electric locomotive, a diesel-powered locomotive is the most common autonomous traction vehicle running on the track. The power plant of such a locomotive is an internal combustion engine, typically operating on diesel fuel. Engines running on petrol (gasoline) are not generally utilised by railways because of high operating costs. The last few years have seen the application of dual-fuel diesel locomotives, allowing the locomotive to run on either diesel or liquefied natural gas. In this case, an additional tank for storing liquefied natural gas on a separate wagon can be attached to the locomotive or mounted on the extended frame of the locomotive. An example of the layout scheme of the diesel-fuelled locomotive is shown in Figure 2.4. The main advantages of diesel power are that the locomotives are self-contained, are capable of performing operations in any climate zone and can be designed to produce sufficient power and traction to efficiently undertake particular operations on a specific railway network. The main disadvantages include the harmful effects on the environment due to the emission of products of combustion and the higher cost of maintenance and repair.

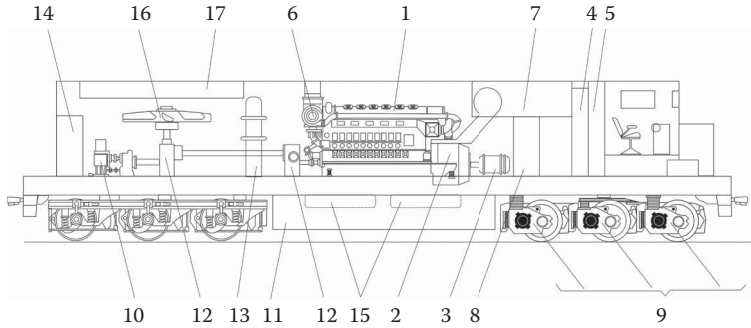

FIGURE 2.4 General equipment layout of a diesel-electric locomotive. 1 – diesel engine; 2 – main alternator; 3 – auxiliary generator; 4 – high voltage chamber; 5 – electronic control equipment; 6 – turbocharger; 7 – centralised air intake system; 8 – motor-fans; 9 – traction motors; 10 – brake compressor; 11 – fuel tank; 12 – gear boxes; 13 – water-oil heat exchanger; 14 – sand box; 15 – air reservoirs; 16 – cooling fan; 17 – radiator.

Like diesel locomotives, gas turbine locomotives are also autonomous, but they are equipped with a gas turbine as a power plant. Gas turbine locomotives have not found wide application in heavy haul operations, but R&D works on their further improvement are still in progress because such a design solution has potentially significant advantages in power density and the cost of fuel, as well as providing a significantly simpler design in comparison with diesel locomotives. Disadvantages include low values of energy conversion efficiency, large variation in this efficiency across the notch position operating range, high consumption of fuel at idle notch position and increased aerodynamic noise from the operation of the turbine engine. Taking into account the high fuel consumption, most operational scenarios would require the locomotive to be connected with tank wagons for storing fuel oil, liquefied natural gas, pulverised coal or peat to allow increasing the operating range of the locomotive. However, it can also provide some undesirable effects on longitudinal train dynamics because such fuel wagons reduce the train payload. An example of the layout scheme of a gas turbine locomotive is shown in Figure 2.5 [1].

Hybrid locomotives are also similar in design to diesel locomotives. The significant difference lies in the fact that, along with the power plant, they also use other energy storage sources (electric batteries, supercapacitors or flywheels). Charging of the energy storage source occurs during operation of the diesel generator or gas turbine in an idling mode and during the conversion of kinetic energy from braking (locomotive and train) into electrical energy, thereby reducing the requirement for electric power produced by the power plant. In order to realise the maximum tractive effort, the electrical energy from the generator/alternator and the energy supplied from energy storage can be used simultaneously. Further transformation and transfer of energy to the wheels of the locomotive is carried out in exactly the same way as for a diesel or gas-turbine locomotive with electric transmission. An example of the conceptual design of a hybrid locomotive is shown in Figure 2.6. The implementation of such designs is complicated by the difficulty of achieving the required

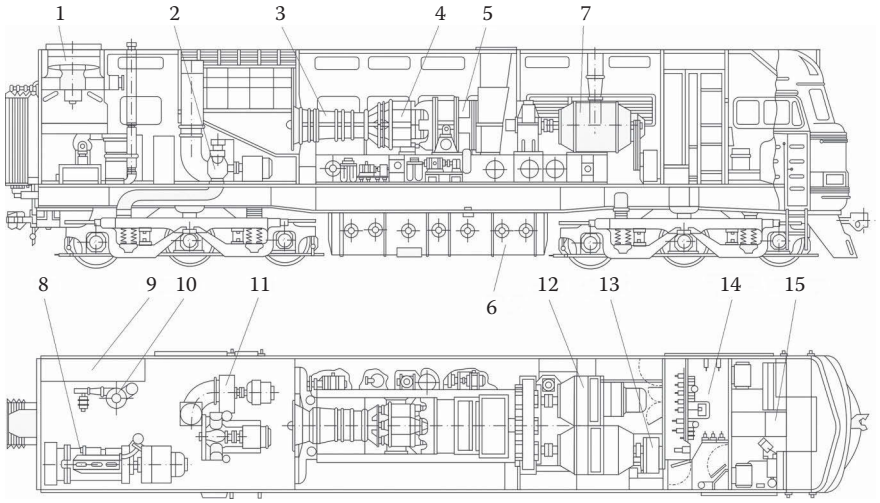

FIGURE 2.5 Overview of basic components of a gas turbine-electric locomotive (Manufactured by Kolomensky Zavod, Kolomna, Russia). 1 – cooling compartment; 2 – air compressor; 3 – turbine compressor; 4 – turbine combustion chamber; 5 – turbine; 6 – heavy fuel tank; 7 – traction generator; 8 – auxiliary diesel generator plant; 9 – diesel fuel tank; 10 – boiler-heater; 11 – cooling fan for rear bogie traction motors; 12 – exciter; 13 – cooling fan for front bogie traction motors; 14 – high voltage chamber; 15 – driver's compartment (cab). (From Spiryagin, M. et al., *Design and Simulation of Rail Vehicles*, CRC Press, Boca Raton, FL, 2014.)

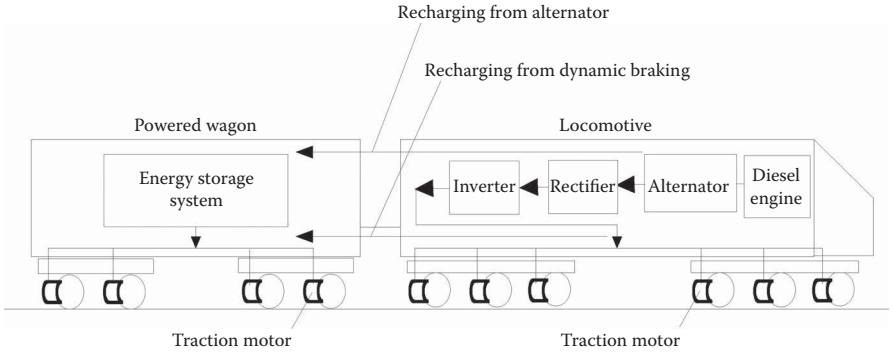

FIGURE 2.6 Conceptual design for a hybrid-powered locomotive. (From Spiryagin, M. et al., *Design and Simulation of Rail Vehicles*, CRC Press, Boca Raton, FL, 2014.)

performance for the electrical energy storage components, but work in this direction continues. The advantages of the use of hybrid traction locomotives are the reduction of both energy costs and emissions of air pollutants compared to conventionally powered locomotives. The disadvantages include the significant rising cost of hybrid vehicles and additional operating costs related to the servicing of energy storage devices.

According to the International Union of Railways (UIC) classification of locomotive axle arrangements, the axles within the same bogie (truck) are classified starting from the front end of the locomotive by alphabetical symbols for the number of consecutive motorised axles (A for one, B for two, C for three etc.), and numerals for the number of consecutive non-motorised (idle) axles between motorised axles. The use of a lower case 'o' as a suffix after the letter indicates that those motorised axles are individually driven by separate traction motors. A prime sign indicates axles that are mounted in a bogie; alternatively, brackets can be used to group letters and numbers describing a particular bogie. For example, Co'Co' means a locomotive with two independent three-axle bogies which have all individually motorised axles/wheelsets [2]. According to the system developed by the Association of American Railroads (AAR), a 'minus' sign is used to indicate the separation (non-articulation) of bogies used in one locomotive and a 'plus' sign indicates articulated connections between bogies of a locomotive or between locomotive units in a locomotive set. Moreover, the suffix 'o' indicating individual drive axles in the UIC classification is not used. That is, the simplified classification used in the AAR system does not distinguish between drive axles that are individually driven and those that are mechanically linked. For example, a locomotive with two independent three-axle bogies that have all individually motorised axles/wheelsets is written as C-C [3].

In addition, the general classification of heavy haul locomotives can be carried out as follows:

- *By gauge of the track*: To carry his first steam locomotive, George Stephenson initially chose a gauge of 4 ft 8 in. between the inner rail faces (soon eased to 4 ft 8½ in. or 1435 mm to reduce wheelset binding on curves); the latter is now called the 'standard gauge' because it has become the main gauge of the railways in many countries (approximately 60% of global railway track length and gradually increasing with new construction and gauge conversion to increase interoperability). At the same time, many other railway gauges were built and operated as described in Chapter 1.
- *By an envelope (usually specified as dimensions above top of rail and from track centreline) that represents a limiting outline*: The outer contours of the rail vehicle should always remain inside of the envelope, either inside a static envelope when not moving or inside a kinematic envelope when a locomotive is running on the track. The envelopes must also take into account wear processes for locomotive components. The existing envelopes of the rolling stock for different countries and railways may differ significantly from each other. Examples of static and kinematic envelopes are shown in Figures 2.7 and 2.8. In Figure 2.7, the solid light line represents the outline of the vehicle in maximum static height condition, the dotted line represents the vehicle in minimum static height condition, and the solid dark line represents the reference static envelope. In Figure 2.8, the solid light line represents the reference swept kinematic envelope, the solid dark line represents the reference static envelope and the dashed line represents the reference basic kinematic envelope.

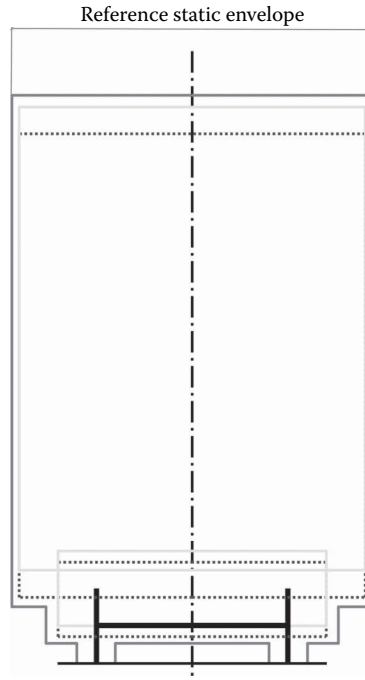

FIGURE 2.7 Example of a static envelope for a locomotive.

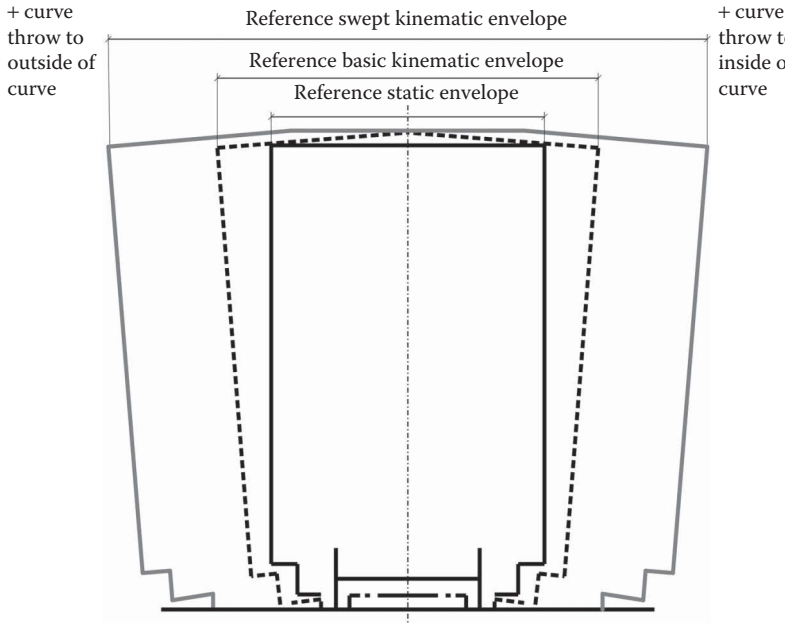

FIGURE 2.8 Example of a kinematic envelope for a locomotive.

- *By the vertical wheelset/axle loads*: The difference in the maximum permissible loads on the rails are determined by the structure of the rail networks, which can potentially use rails with a variety of load-bearing capacity, different types of sleepers, various track substructure designs (types of ballast and subgrade material) and the bearing capacity of bridges and other engineering structures.
- *By maximum power of the locomotive*: Generally, the maximum power of the autonomous locomotive means the effective maximum capacity of the power plant. Heavy diesel-electric locomotives typically produce 3–5 MW or up to 6000 hp, and non-autonomous locomotives such as electric locomotives typically have a peak power output of 5 or 6 MW and are rated by their power at the wheel. In the case of diesel-electric locomotives, the total power at the wheels is slightly lower than the power plant power. As a result of this difference, an additional characteristic is used in some countries to indicate the available traction force that is applied to the rails tangentially to the rim of the driven axle wheels of all types of locomotives.
- According to the type of car body – the cab unit or the hood unit (Figure 2.9).
- By the number of driving cabs – one cab or two-cab designs (Figure 2.10).
- According to the number of units in a locomotive set – one, two, … , multi unit(s) (Figure 2.11). In some locomotive designs, a booster unit is also present that does not have a driving cab and is remotely controlled from other locomotive driving cabs included in a locomotive set. A driving cab unit is usually defined as an A unit; a booster unit is defined as a B unit.

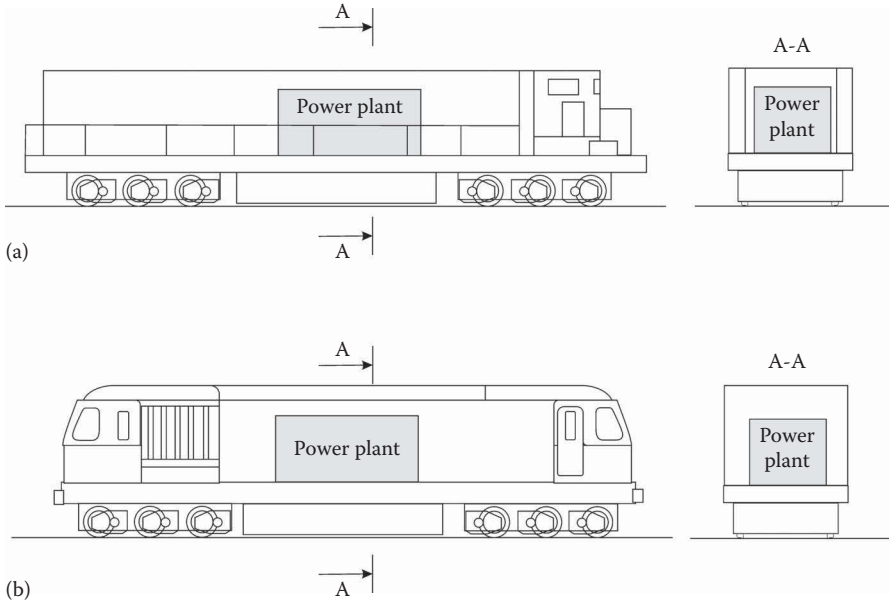

FIGURE 2.9 Types of car body: (a) cab unit and (b) hood unit.

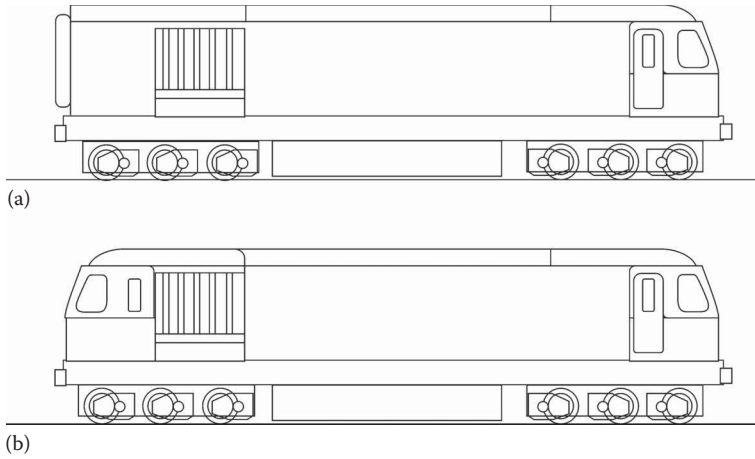

FIGURE 2.10 Types of locomotive by number of driving cabs: (a) locomotive with one driving cab and (b) locomotive with two driving cabs.

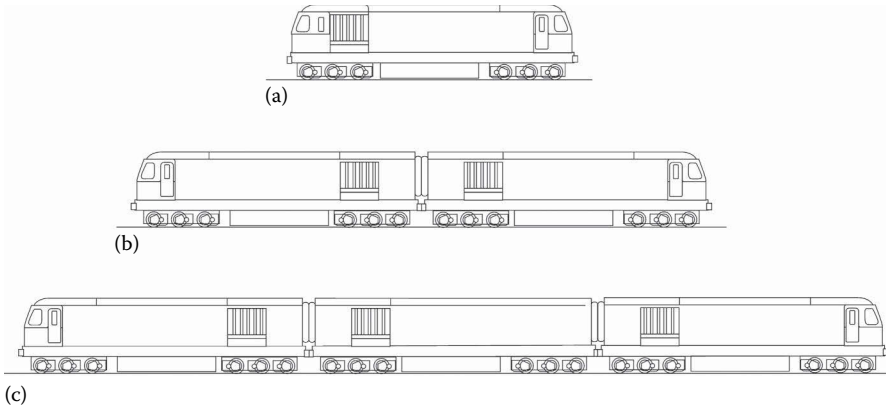

FIGURE 2.11 Types of locomotive/locomotive sets: (a) one unit locomotive, (b) two unit locomotive, and (c) three unit locomotive.

2.3 MOTIVE POWER ENERGY PRINCIPLES

The locomotives used on heavy haul lines are universally equipped with electric transmission, which allows achieving an optimal dependence between the tractive effort of a locomotive and its operational speed. It also facilitates rapid and accurate control of multiple locomotives, which can be distributed in various ways at the front, middle and/or end of the train configuration (distributed power). This is commonly done for the implementation of the high motive power required for hauling longer and heavier trains along designated routes.

A schematic of the power generation principles for diesel-electric locomotives is shown in Figure 2.12. Thermal energy from the combustion of fuel in the diesel engine/s is converted into the mechanical energy of rotation of the crankshaft, which is then converted in the main generator into electrical energy, either AC or direct current (DC). The generated current is passed through special electrical and electronic

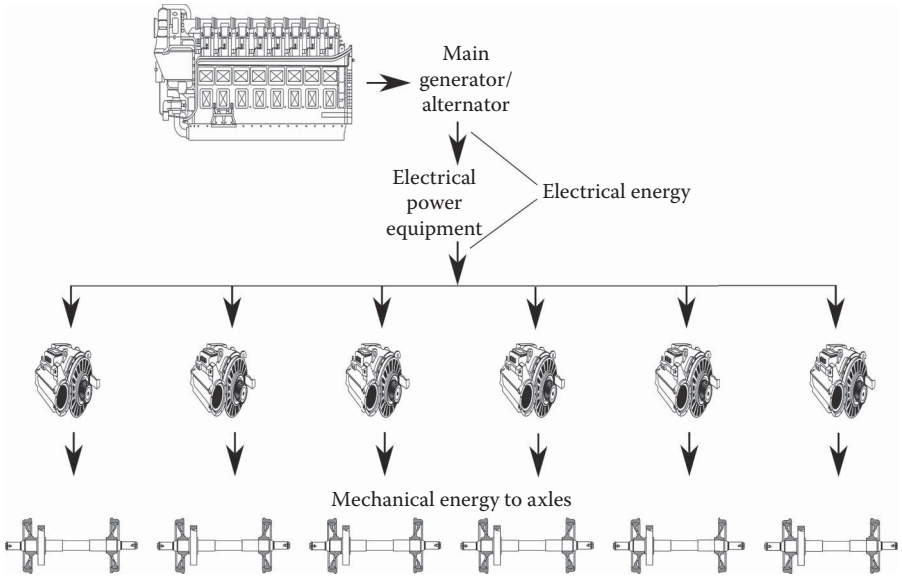

FIGURE 2.12 Energy transformation principles for a six-axle diesel-electric locomotive.

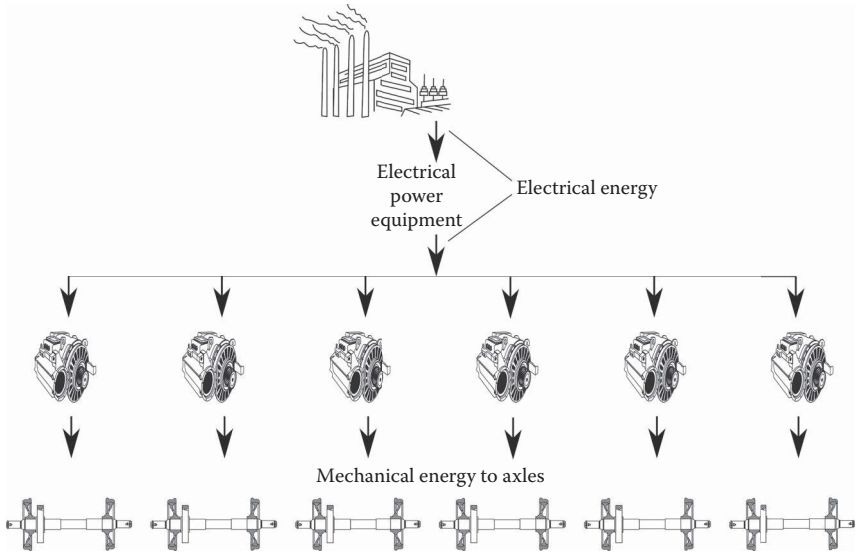

FIGURE 2.13 Energy transformation principles for a six-axle electric locomotive.

equipment, regulating its parameters before being further distributed through the cable connections to the traction motors where electrical energy is converted into rotational mechanical energy of the rotors of the traction motors which, through the gear boxes, rotate the axles/wheelsets of a heavy haul locomotive.

A schematic of energy transformation in an electric locomotive, shown in Figure 2.13, is basically a simplified version of the scheme for a diesel-electric locomotive, because the electric locomotive is not equipped with any diesel generator units, and electric energy comes from an electric power station through the overhead line equipment to the locomotive as shown in Figure 2.2.

2.4 MAIN PARAMETERS OF LOCOMOTIVES

The main parameters of the diesel or electric locomotive that determine traction performance are as follows:

- Axle load
- Tractive effort
- Maximum adhesion/traction coefficient achieved
- Power output
- Maximum speed

2.4.1 Axle Load

Axle loads can be specified in two ways. The first method is indicative, with the mass of the locomotive considered to be carried equally by each axle, giving an average mass per axle, m_{axle}, and a corresponding axle load, F_{axle}, determined by the following formulas:

$$m_{axle} = \frac{m_{tot}}{n} \tag{2.1}$$

$$F_{axle} = m_{axle} \times g = \frac{m_{tot} \times g}{n} \tag{2.2}$$

where:

m_{tot} is the total locomotive mass (kg)
g is gravitational acceleration, equal to 9.81 m/s^2
n is the number of axles in the locomotive

The second method is a more detailed one to determine the variation in load on each individual wheel (and hence on each axle). As an example, let us consider a six-axle heavy haul locomotive. The layout of running gear and the position of the centre of mass for the locomotive car body structure are shown in Figure 2.14. In this case, assume that the mass of the car body is bearing on four secondary suspension points for each bogie and that the sprung mass of the car body and bogies is equally distributed on the bogie wheels. Knowing the position of the centre of mass for a locomotive

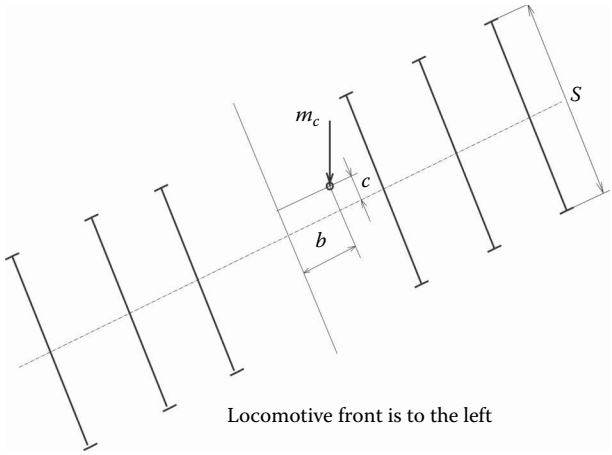

FIGURE 2.14 Calculation scheme for the determination of axle loads in a six-axle locomotive.

car body for the defined axis coordinate system, as shown by the offsets b and c from the dotted line geometrical centreline axes in Figure 2.14, the mass of the locomotive attributed to each wheel can be determined according to the formula:

$$m_{\text{wheel } j} = \frac{m_c}{12} \pm \frac{m_c \times c}{6 \times S} \pm \frac{m_c \times b}{6 \times S} + \frac{m_{\text{bs}}}{6} + m_{\text{bwu } j} \tag{2.3}$$

where:

j is an index for right or left wheel
m_c is total mass of the car body (kg)
b and c are coordinates of the centre of mass for the locomotive car body (m)
S is the distance between nominal rolling radii of left and right wheels of the same axle/wheelset (m)
m_{bs} is the sprung mass of a bogie (kg)
m_{bwu} is the unsprung mass of a bogie attributed to each wheel (kg)

The signs '+' and '–' are used in cases when the centre of mass either loads or unloads a wheel of the wheelset, respectively, relative to the axis of symmetry. In this example, if c is positive, then the second component in Equation 2.3 should be taken as positive for a right wheel and negative for a left wheel. If b is negative, then the third component in Equation 2.4 should be taken as positive for wheelsets situated between the front of the locomotive and the car body centre of mass, and negative for wheelsets situated behind the car body centre of mass.

Thus, knowing the mass of the locomotive attributable to each wheel, the mass of the locomotive attributable to each axle can be determined by:

$$m_{\text{axle}} = m_{\text{wheel left}} + m_{\text{wheel right}} \tag{2.4}$$

Finally, each axle load can be calculated using Equation 2.2.

2.4.2 Locomotive Tractive Effort

The tractive effort exerted by a locomotive, F_{TE}, is necessary to move its train along the track.

The maximum possible tractive effort, $F_{TE\,max}$, is limited by the adhesion between wheels and rails, μ, and is defined by

$$F_{TE\,max} = \mu \times m_{tot} \times g \tag{2.5}$$

Then, the tractive effort able to be realised by a locomotive, F_{TE}, obeys the following law:

$$F_{TE} \leq \mu \times m_{tot} \times g \tag{2.6}$$

In practice, two characteristics are often used in the description of locomotive tractive effort: starting and continuous. Starting tractive effort is needed to determine how much train weight may be set into motion by a locomotive. Starting traction is mainly limited by the locomotive weight and the achievable adhesion/traction coefficient between wheels and rails as shown in Equation 2.6. Continuous mode tractive effort allows for the possibility of an indefinite period of train operation. In other words, the continuous tractive effort is designed to determine the train weight that can be moved over very long periods of locomotive traction operation. This effort is limited by the power and dynamic performance of the traction electric transmission of a locomotive.

2.4.3 Maximum Adhesion/Traction Coefficient

The value of the maximum adhesion/traction coefficient able to be achieved by a locomotive can be defined as

$$\mu_{max} = \frac{F_{TE\,max}}{m_{tot} \times g} \tag{2.7}$$

A maximum realised traction coefficient of more than 40% can be achieved only on a dry track with ideal conditions and optimised traction control algorithms managing the power traction transmission system of a heavy haul locomotive.

2.4.4 Locomotive Power Output

The power output of locomotives is usually defined in units of watts or horsepower. The tangent locomotive power in kilowatts, which is applied to the rail, can be calculated as

$$P_{rail} = \frac{F_{TE} \times V}{3.6} \tag{2.8}$$

where V is the locomotive speed (km/h).

TABLE 2.1
Comparison of Energy Efficiencies for Diesel-Electric and Electric Locomotives

Diesel-Electric Locomotive		Electric Locomotive	
Component	**Efficiency**	**Component**	**Efficiency**
Power plant – diesel engine	0.40	Power plant – electric power station	0.38–0.44
Main generator/alternator	0.92	Power distribution network	0.90
Inverter	0.97	Inverter	0.97
Traction electric motors	0.90	Traction electric motors	0.90
Gear box	0.97	Gear box	0.97
Total energy efficiency	0.31	Total energy efficiency	0.28–0.34

To calculate the horsepower (hp), the ratio of 1 kW = 1.3596 metric hp should be used in Equation 2.8, giving locomotive power in hp as

$$P_{\text{rail hp}} = \frac{1.3596 \times F_{\text{TE}} \times V}{3.6} \tag{2.9}$$

Effective power of a locomotive in kilowatts, which equals the power of the power plant for a diesel-electric locomotive or the power consumed from the external power supply for an electric locomotive, can then be defined as

$$P_e = \frac{P_{\text{rail}}}{\eta_t \times \eta_a} \tag{2.10}$$

where:

η_t is the efficiency of the locomotive traction transmission
η_a is a coefficient that takes into account the auxiliary equipment power needs

The energy efficiency of the traction transmission of a locomotive, η_t, can be defined as

$$\eta_t = \frac{P_{\text{rail}}}{P_e - P_a} \tag{2.11}$$

where P_a is the total power required for auxiliary equipment (kW).

The comparison of overall energy efficiencies for diesel-electric and electric locomotives with full power utilisation is presented in Table 2.1.

2.4.5 Maximum Locomotive Speed

The maximum locomotive speed, $V_{\max}$ (km/h), is commonly limited by a speed characteristic of the traction electric motor that can be determined by the following formula:

$$V_{\max} = \frac{1.8 \times d_{\text{wheel}} \times \omega_{\text{m max}}}{i} = \frac{0.18849 \times d_{\text{wheel}} \times n_{\text{m max}}}{i} \tag{2.12}$$

where:

d_{wheel} is the locomotive wheel diameter (m)
$\omega_{\text{m max}}$ is the maximum angular velocity of rotor/shaft of the traction motor (rad/s)
$n_{\text{m max}}$ is the maximum rotor/shaft speed of the traction motor (rev/min)
i is the gear box ratio, which is equal to the number of teeth of the gears mounted on the wheelset divided by the number of teeth of the gears mounted on the rotor/shaft of the traction motor

However, it should be noted that the maximum speed can also be further limited by the technical solutions or design of the running gear of a locomotive.

2.5 POWER GENERATION SYSTEMS

As described in Sections 2.2 and 2.3, the main components that produce or transmit energy to power transmissions are either the combination of a diesel engine and an electric power system in the case of diesel-electric locomotives, or just an electric power system in the case of electric locomotives. We consider and describe these components in more detail in the following Sections 2.5.1 and 2.5.2.

2.5.1 Diesel Engine and Its Systems

In modern diesel-electric heavy haul locomotives, the diesel engine usually has the following configuration: V-type engine, 4 strokes per cycle, one or two turbochargers and an intercooler. The number of cylinders can vary from 12 to 20. The power output of these diesel engines usually ranges from 3000 to 6500 hp.

The example of a diesel engine installed on the General Electric Transportation Evolution Series locomotives is shown in Figure 2.15. This particular engine model is the GEVO16, and it can be classified as a 4-stroke V-type diesel engine with 16 cylinders, equipped with double turbochargers. Such a design can provide a nominal crankshaft speed of 1050 rpm and a nominal power of 4660 kW (6250 hp). In addition, it has a cylinder bore of 250 mm and a piston stroke of 320 mm. The other characteristics include a compression ratio of 16.8:1, a displacement volume of 251.3 L and a weight of 24,857 kg, with approximate engine dimensions of 5,105 mm length × 1,771 mm width × 2,603 mm height.

Another example of a locomotive power plant, which includes a diesel engine and a main generator, is shown in Figure 2.16. This diesel engine can be classified as a 4-stroke V-type with 16 cylinders, turbocharged and equipped with an intercooler, with a nominal crankshaft speed of 1000 rpm and a nominal power of 2650 kW (3604 hp).

The auxiliary systems of the diesel engine include the following:

- Air system
- Fuel system
- Oil system

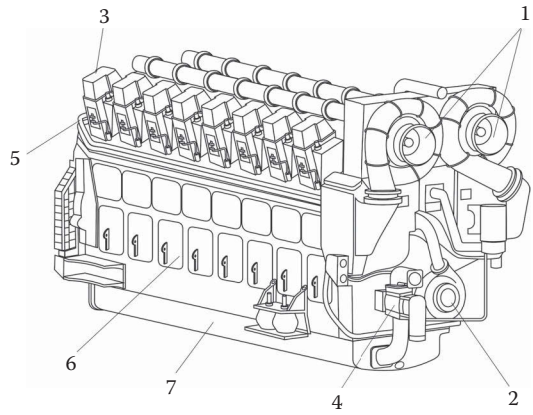

FIGURE 2.15 Example of diesel engine of heavy haul locomotive (Manufactured by GE Transportation, Erie, PA). 1 – turbocharger; 2 – water pump; 3 – cylinder head; 4 – lube oil pump; 5 – fuel pipes; 6 – crankcase inspection cover; 7 – lube oil pan.

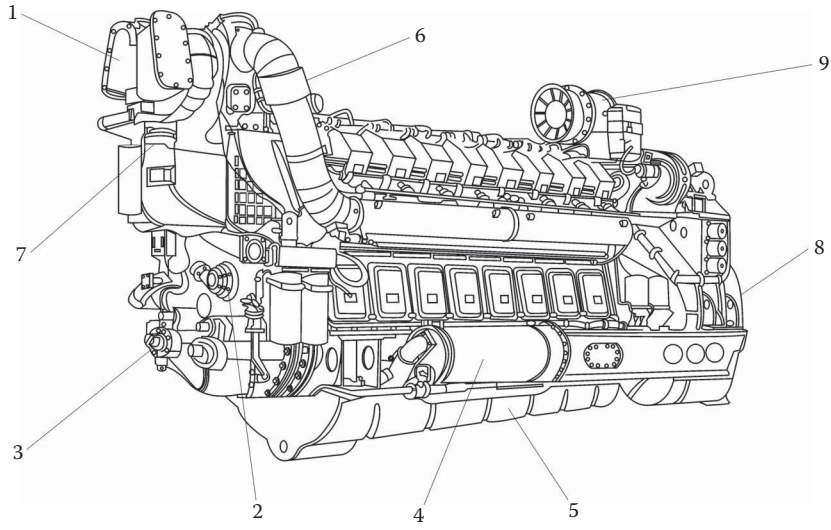

FIGURE 2.16 Typical power plant of heavy haul locomotive (Manufactured by Kolomensky Zavod, Kolomna, Russia). 1 – turbocharger; 2 – water pump; 3 – lube oil pump; 4 – oil cooler; 5 – lube oil pan; 6 – muffler; 7 – intercooler; 8 – main alternator; 9 – main alternator cooler.

- Cooling water system
- Exhaust system
- Engine monitoring and control system/governor

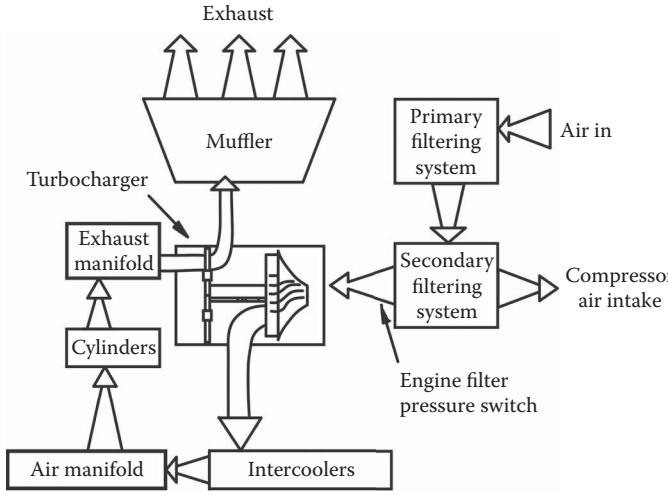

FIGURE 2.17 Typical air system of a heavy haul locomotive.

The air system is needed for the proper working of a diesel engine to provide air flow into the cylinders in the formation of a combustible mixture. The air supplied is called the combustion air for the diesel engine. The working principle is based on a standard scheme where air is taken from outside the locomotive and passed through the filtering system (passive and inertial), then redirected to the air intake on the engine and again passed through the engine air filter. The purified air is supplied to the turbocharger. In the process of charging, the air is heated. The temperature of the charge air of a diesel engine has a significant impact on its efficiency and reliability, so the charge air in locomotives is cooled in intercoolers. Then, the air is supplied into the cylinder through the intake manifolds for combustion. An example of such a system is shown in Figure 2.17.

The fuel system is designed to provide an uninterrupted supply of fuel into the cylinders of the diesel engine under all possible modes of operation. This system includes fuel tanks, pipes, a fuel pump, a fuel filter system and a fuel preheater if the locomotive is to be used in extreme winter conditions. A typical example of such a system is shown in Figure 2.18.

The oil lubrication (lube) system of the locomotive is designed for lubrication of the contacting surfaces of the component parts of the diesel engine. The main tasks of this system are heat removal and the storage, filtration and cooling of the engine oil. For winter operational scenarios, locomotives can be equipped with additional devices that allow oil heating. There are internal and external subsystems of the oil system. The internal subsystem includes pipes and channels that supply oil to the contacting surfaces to minimise friction. The external oil subsystem includes filters, a lube oil cooler, heat exchangers, pumps, valves, piping, oil tanks and sensors to monitor the working of the whole system. An example of such a system is shown in Figure 2.19.

The cooling system is designed to circulate through and collect the heat from the heated parts of the diesel engine (cylinder liners and heads). Water or another coolant

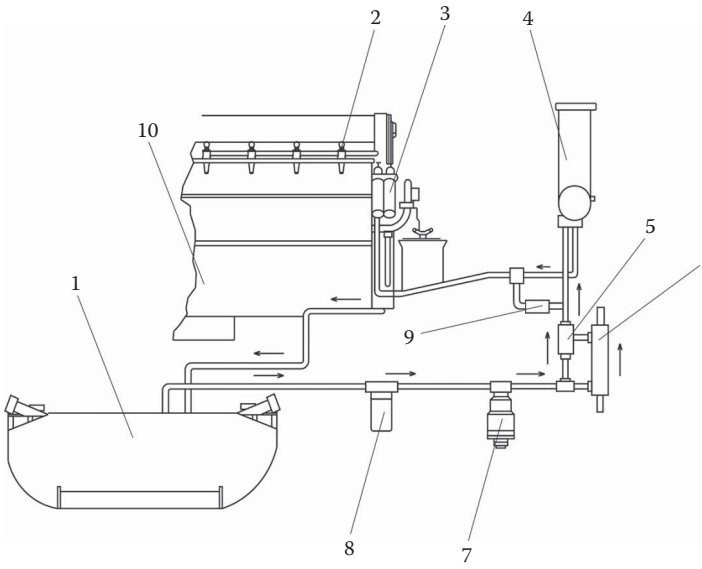

FIGURE 2.18 Typical diesel engine fuel system (Manufactured by Electro-Motive Diesel, McCook, IL). 1 – fuel tank; 2 – fuel injector; 3 – secondary fuel filter; 4 – primary fuel filter; 5 – thermostatic mixing valve; 6 – fuel preheater; 7 – fuel pump; 8 – suction strainer; 9 – bypass valve; 10 – diesel engine.

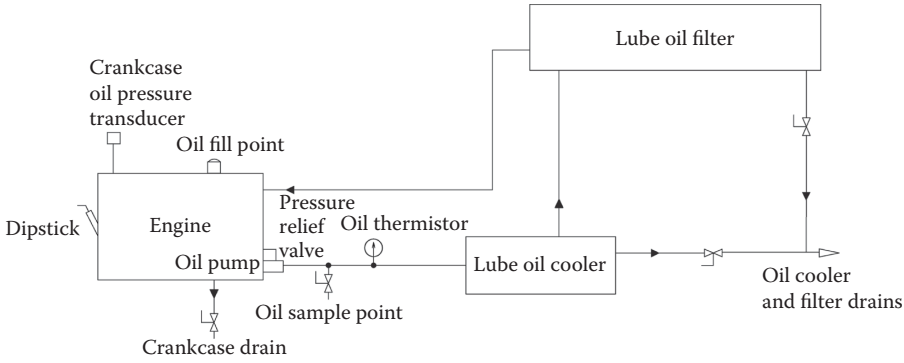

FIGURE 2.19 Typical lube oil system of a heavy haul locomotive (Manufactured by Goninan, Newcastle, Australia).

transfers heat to the air-cooled heat exchanger, also called a radiator, where it is dissipated into the atmosphere. In modern heavy haul locomotives, the water cooling system is normally a closed loop and often has multiple cooling loops and radiators. It includes water pumps, an expansion tank, radiators, fans, valves, piping and a lube oil cooler. A typical example of a cooling water system is shown in Figure 2.20.

The exhaust system is designed for removal of exhaust gases produced by the diesel engine and its main elements consist of the exhaust manifolds and mufflers.

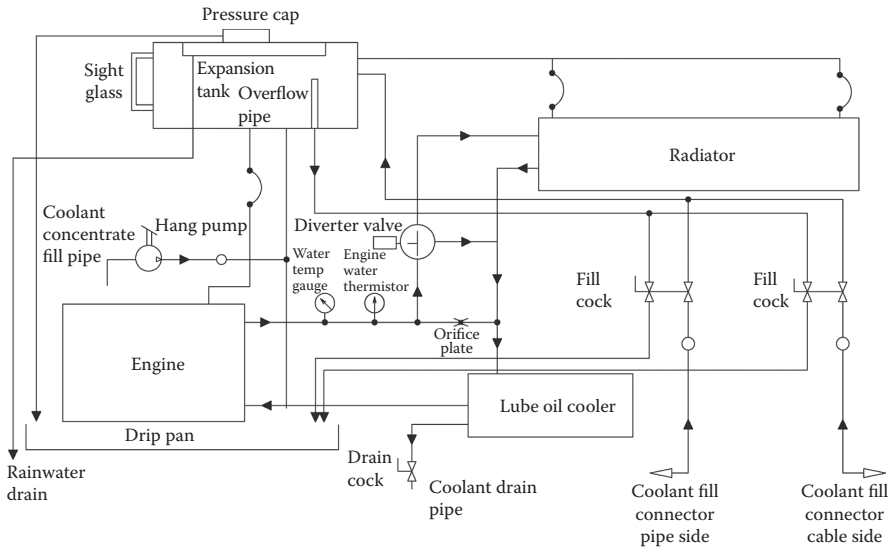

FIGURE 2.20 Typical cooling water system of a heavy haul locomotive (Manufactured by Goninan, Newcastle, Australia).

The exhaust gases from the cylinders of a diesel engine are discharged to the turbocharger by means of the exhaust manifolds. The engine on heavy haul locomotives is normally equipped with a common exhaust manifold for all the cylinders that allows the gas pressure to be normalised, and the turbocharger operates at constant pressure. Exhaust manifolds are usually cooled by water or another coolant.

The muffler is used for reducing gas combustion noise produced by a diesel engine. The classical muffler design comprises an inlet pipe with perforated ducting inside the resonator chamber, absorbent materials in that chamber, and perforated ducting leading to an exhaust pipe. The perforated inlet ducting is used to split the main gas stream into multiple streams to pass through the absorbent materials in many different directions, followed by exhausting the gases to the atmosphere; sound waves are also attenuated when passing through the absorbent materials.

In addition, the system may include diesel oxidation catalyst treatment technologies that reduce emissions to meet regulatory requirements.

Presently, the engine monitoring and control systems of diesel engines are commonly electronic and regulate the speed of the diesel engine and its power output. However, in some locomotives, the engine control governor is still an electrohydraulic device. In modern heavy haul locomotives, the engine monitoring and control systems are fully computerised, allowing precise control and monitoring of such factors as the timing of the valve response and the operating temperature. Such computerised systems can instantly process the data received from the sensors and respond quickly to changes in the working conditions of the locomotive to immediately implement appropriate adjustments. As a result of such control approaches, it is possible to obtain the necessary power output and to achieve an optimal balance between exhaust emissions and fuel efficiency.

2.5.2 Electric Power Systems

Four types of topologies for electric traction are currently in use on heavy haul locomotives:

- DC–DC topology
- AC–DC topology
- AC–AC topology
- DC–AC topology

For diesel-electric locomotives, DC traction has a significant drawback of large overall dimensions of the main generator, and this is the reason why that topology has largely been replaced by an alternator (a synchronous AC generator), which is significantly smaller in size. For the same reason, locomotives commonly use AC–DC or AC–AC traction topologies.

For electric locomotives running on a DC electrification system, locomotives can utilise a DC–AC topology with variable voltage and variable frequency drives, or a DC–DC topology with pulse width control.

For both types of heavy haul locomotives (diesel and electric), it is common to classify them as either AC or DC locomotives based on the type of electricity that is supplied to their traction motors. However, this does not really indicate what other components of the traction system are installed in a locomotive.

To summarise the information on the power traction transmission systems of locomotives that are currently in use on heavy haul routes, it is possible to present the following classification descriptions:

- *Diesel-electric locomotives with an AC–DC topology*: These types of locomotives are equipped with the following main components of the power traction transmission system: main and auxiliary alternators, rectifier and traction motors. An example of such a topology is shown in Figure 2.21.

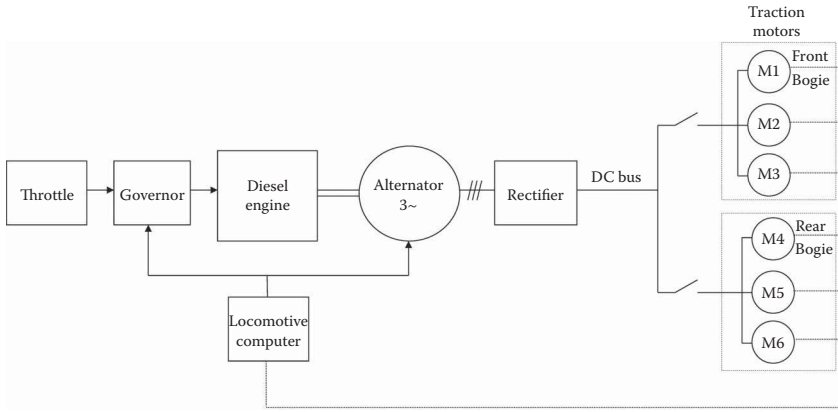

FIGURE 2.21 Example of an electric traction scheme for a diesel-electric locomotive with an AC–DC topology.

- *Diesel-electric locomotives with an AC–DC–AC topology*: These types of locomotives are equipped with the following main components of the power traction transmission system: main and auxiliary alternators, rectifier, traction inverters and traction motors. Two types of traction system configurations are commonly in use: one inverter per bogie or one inverter per wheelset. A typical scheme of electrical traction with such a topology for a diesel-electric locomotive with one inverter per bogie is shown in Figure 2.22.
- *Electric locomotives with a DC–DC topology*: These types of locomotives commonly have the following main components: pantograph, choppers or thyristor convertor and control equipment and traction motors. An example of such a topology is shown in Figure 2.23.

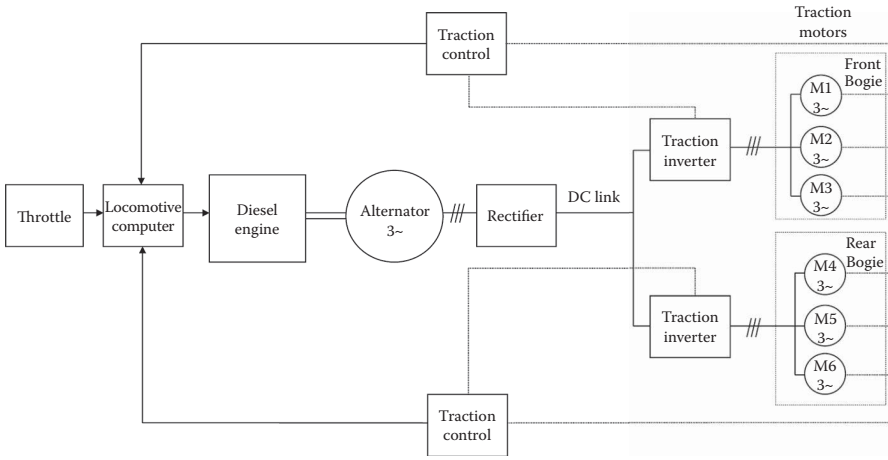

FIGURE 2.22 Example of an electric traction scheme for a diesel-electric locomotive with an AC–DC–AC topology.

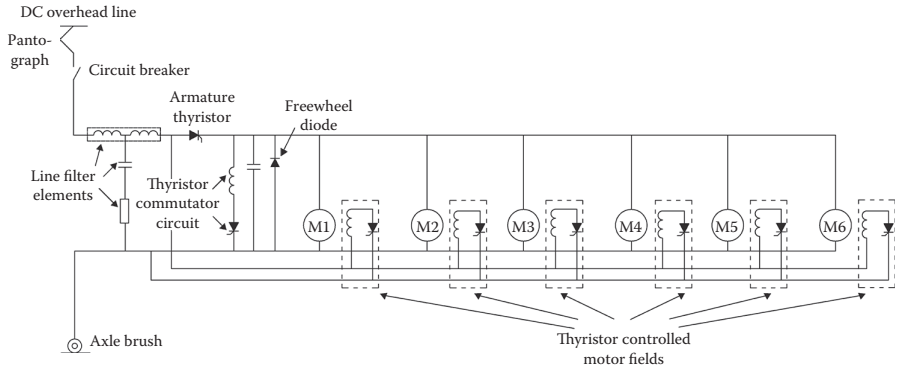

FIGURE 2.23 Example of an electric traction scheme for an electric locomotive with a DC–DC topology.

- *Electric locomotives with an AC–DC topology*: These types of locomotive commonly use AC power from an overhead network, but they are equipped with DC traction motors. The locomotives have the following main components: pantograph, transformer, rectifiers and traction motors. An example of such a topology is shown in Figure 2.24.

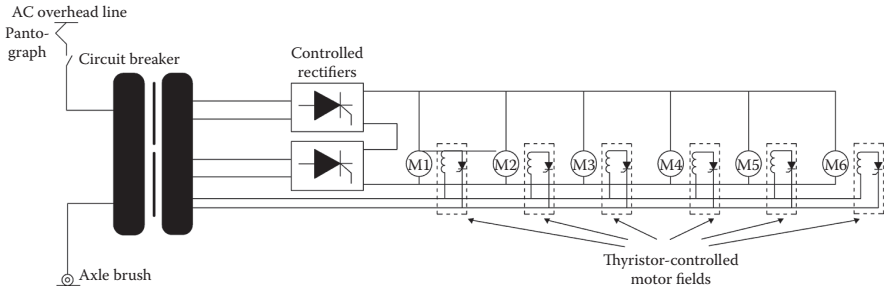

FIGURE 2.24 Example of an electric traction scheme for an electric locomotive with an AC–DC topology.

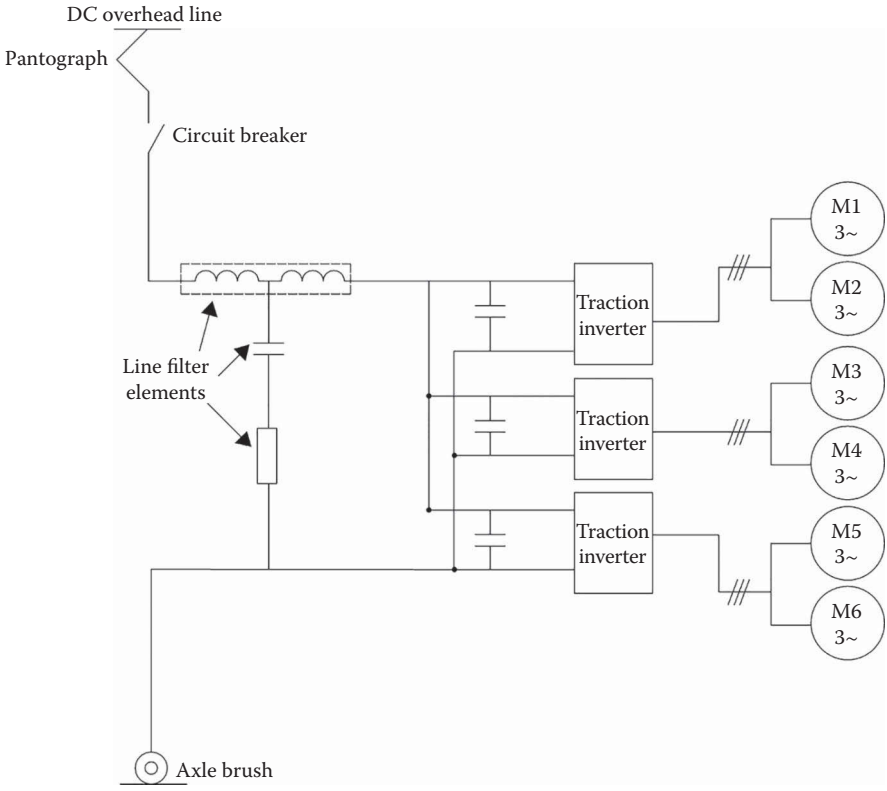

FIGURE 2.25 Example of an electric traction scheme for an electric locomotive with a DC–AC topology.

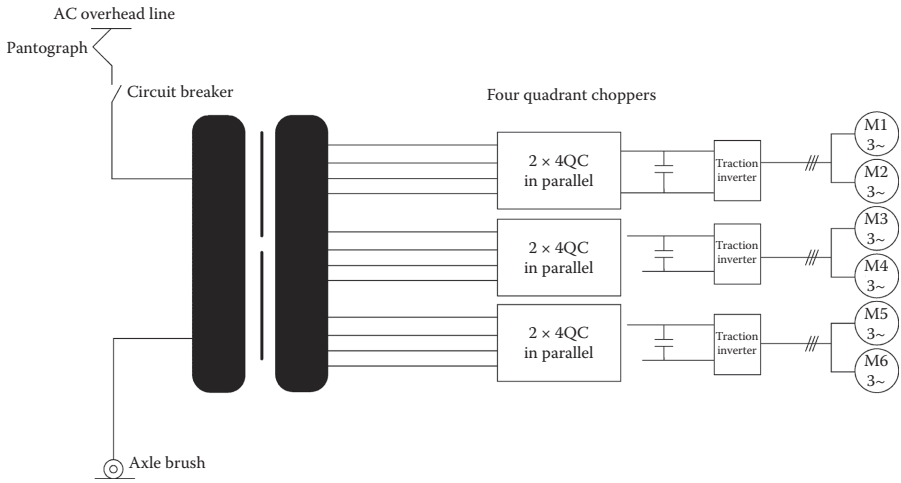

FIGURE 2.26 Example of an electric traction scheme for an electric locomotive with an AC–DC–AC topology.

- *Electric locomotives with a DC–AC topology:* These types of locomotive commonly use DC power from an overhead network, but they are equipped with AC traction motors. The locomotives have the following main components: pantograph, traction inverters and traction motors. An example of such a topology is shown in Figure 2.25.
- *Electric locomotives with an AC–DC–AC topology*: These types of locomotives commonly have the following main components: pantograph, transformer, rectifier, traction inverters and traction motors. An example of such a topology is shown in Figure 2.26.

More detailed descriptions of locomotive power traction systems can be found in Chapter 4.

2.6 TRACTIVE EFFORT AND DYNAMIC BRAKING CHARACTERISTICS

The main performance descriptors for heavy haul locomotives are generally based on the characteristics of their power plant or power supply and on their electro-traction transmission characteristics, and thus describe the tractive and braking capabilities of a rail vehicle that are also dependent on the train speed and the load being hauled.

2.6.1 Tractive Effort Characteristics

Locomotive tractive effort characteristics are usually specified using a graph of dependence between the tangential tractive effort and the speed at a given engine power.

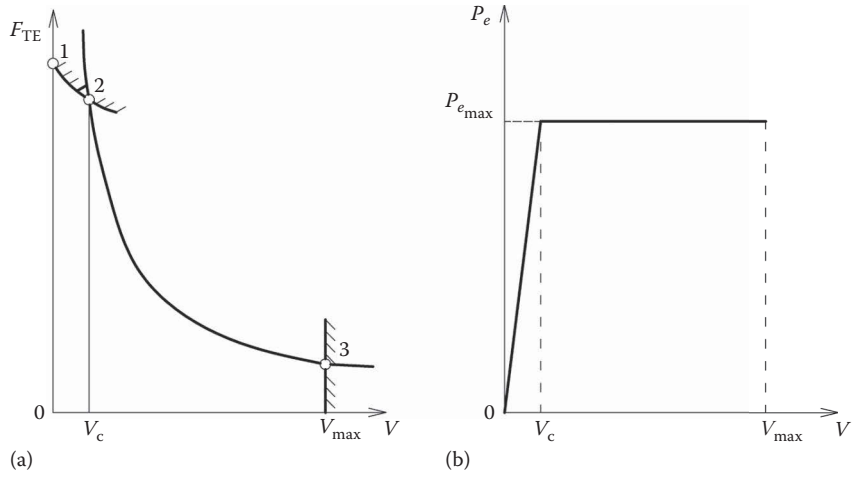

FIGURE 2.27 Ideal tractive effort and power characteristics of a diesel-electric locomotive: (a) tractive effort versus train speed and (b) effective power versus train speed.

Diesel locomotives are designed in such a way that, when the locomotive is running at the required design speed on a steep track gradient, its continuous tractive effort should equal the value of the maximum achievable tractive effort, which is limited by the adhesion conditions between the wheels and rails. For realising maximum efficiency, it is advisable to keep the power produced by the locomotive power plant constant, and this should be maintained for all possible operational speeds of the train. Given this requirement, the tractive effort in the range of speeds from zero to the design maximum speed, V_{max}, will vary along a curve in the shape of a hyperbola. Examples of ideal tractive effort characteristics as well as effective power characteristics are shown in Figure 2.27. However, the tractive effort characteristic shown in Figure 2.27a also contains a line 1–2 that constitutes a restriction on the tractive effort due to the effect of an adhesion coefficient between wheels and rails at speeds below the continuous tractive effort speed, V_c. The line 2–3 in Figure 2.27a represents the limit on the tractive effort set by the power plant in the range of velocities from V_c to V_{max}. As shown in Figure 2.27b, the constancy of the effective power delivered by the locomotive can be observed over the same speed range, making this the working range for the locomotive. In the ideal case, providing the characteristics of the electrical equipment (e.g. thermal time constants of traction motors or the commutation limit of motors) are not taken into account, the continuous tractive effort speed, also called the continuous speed, will be characterised by point 2. Otherwise, this point of the hyperbolic curve will be shifted slightly to the right in the horizontal direction.

Tractive effort characteristics of electric locomotives are different from those of diesel-electric locomotives in that the shape for the former is parabolic. Examples of tractive effort characteristics of DC and AC current electric locomotives are shown in Figure 2.28a and b, respectively.

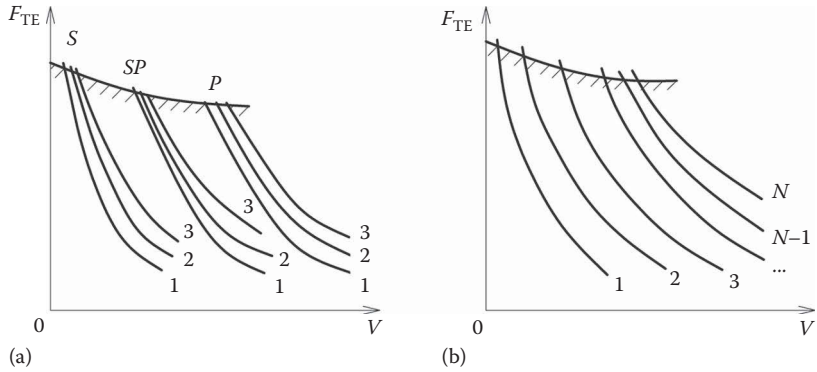

FIGURE 2.28 Examples of tractive effort characteristics of electric locomotives: (a) tractive effort versus speed for DC locomotive and (b) tractive effort versus speed for AC locomotive.

Figure 2.28a presents tractive effort characteristics for DC electric locomotives with three different types of connection configurations for the traction motors:

- Series (S) connection when all the traction motors are connected in series, resulting in the voltage drop at the motor terminals being directly proportional to the number of motors used to operate at slow speeds.
- Parallel (P) connection when the traction motors are directly connected to the power supply source in parallel with each other – this scheme is used to obtain the maximum voltage at the terminals of the traction motors and, therefore, to achieve the maximum speed.
- Series to parallel (SP) connection when traction motors are connected in series to form a group – there are commonly two or more groups per locomotive and these groups are connected in parallel to the power supply source.

In addition, Figure 2.28a contains examples of curves for three operational scenarios (1 – full field, 2 – intermediate field and 3 – weak field), which represent different loads for motors and those three curves are shown for each type of connection configuration of the electric traction motors. Figure 2.28b presents the tractive effort characteristics for an electric locomotive equipped with an AC traction propulsion system, and the numbering 1 to N on this figure represent curves for different notch positions of the throttle which can be set by the locomotive driver.

More detailed descriptions of the tractive effort characteristics used on actual locomotives can be found in Chapter 5.

2.6.2 Dynamic Braking Characteristics

In dynamic or regenerative braking modes, the traction motors mounted on the bogies of a heavy haul locomotive operate as a generating device instead of a power device. During dynamic braking, the traction motors convert the kinetic energy of

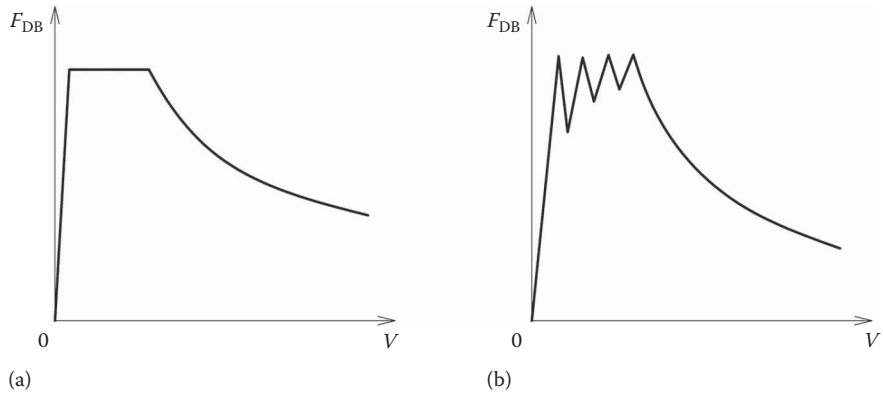

FIGURE 2.29 Examples of dynamic braking characteristics of diesel-electric locomotives: (a) DC traction and (b) AC traction.

the train into electrical energy, which in most cases is then converted into thermal energy on the brake grids (specific resistor unit) mounted in the body of the locomotive, and then dissipates into the atmosphere. In the case of non-autonomous locomotives, this electrical energy may be returned to the power supply contact system by regenerative braking. Examples of dynamic braking characteristics are shown in Figure 2.29. Commonly, at speeds approximately less than 5–10 km/h, the traction motors cannot provide the required braking effort because of insufficient terminal voltages. The dynamic or regenerative braking on modern freight locomotives is normally used as an additional brake to supplement the air brakes.

More detailed descriptions of the dynamic braking characteristics used on actual locomotives can be found in Chapter 5.

2.7 LOCOMOTIVE AUXILIARY SYSTEMS AND EQUIPMENT

2.7.1 Forced Air Systems

During the operation of the traction electrical machinery and equipment, some of the electrical energy supplied to them is converted into thermal energy, which leads to an increase in their operating temperature and the possibility of their overheating and malfunctioning.

It is therefore common to equip locomotives with forced air systems that allow air cooling of the traction and auxiliary generators (for diesel locomotives), or of the input filter (for electric locomotives), plus the traction motors, traction inverter equipment and electrical cabinets.

Air intake takes place outside the car body and passes through the primary filters (passive and inertial). For the further purification of air, additional filters can be used. Centralised, individual and mixed air forced systems can be used on locomotives. The most common applications found on diesel locomotives are mixed air forced systems, which usually include an individual air cooling system for the generator and two air cooling group systems for the traction motors.

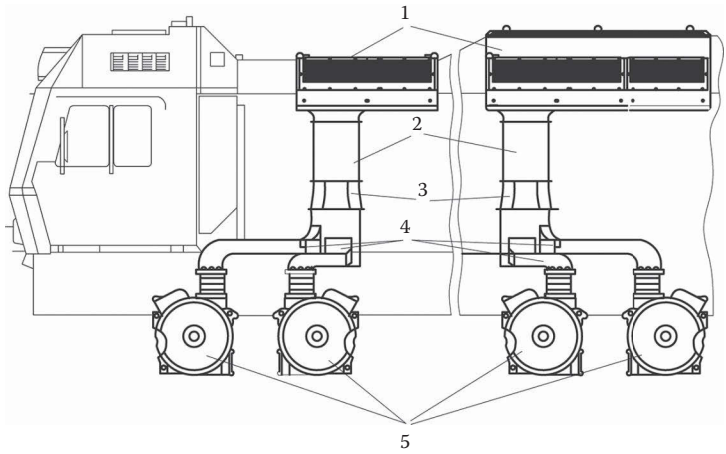

FIGURE 2.30 Example of a forced air system of an electric locomotive (Manufactured by Ural Locomotives, Yekaterinburg, Russia). 1 – filters; 2 – air channels; 3 – fans; 4 – injection air channels; 5 – traction motors.

The group cooling systems of traction motors are basically the same for all types of locomotives. An example of the forced air system for traction motors designed for an electric locomotive is shown in Figure 2.30. The outside air goes through the air filter in the roof of the locomotive car body, then through the suction channel to the fans, and subsequently through injection channels distributed over the traction motors, and is finally released into the atmosphere.

2.7.2 Air Brake Systems

The main task of the brake system is the creation of an artificially controlled resistance force by a locomotive or train in order to control the speed or bring its movement to a full stop, and the creation of the forces which allow keeping the locomotive or train from inadvertent movement when it is fully stopped or parked on inclined sections of the track.

On heavy haul locomotives, the standard brake system is a pneumatic air system with brake blocks (brake shoes). This system may work in conjunction with dynamic or regenerative braking described in Section 2.6.2. The standard brake system of a heavy haul locomotive also includes a manual parking brake.

The air braking system is commonly connected with a sand supply system, which also requires an air supply for its operation. An example of such a system is shown in Figure 2.31.

A typical air brake system includes the following main components:

- Feeding and supply components, including an air compressor and feeding pipes and equipment
- Energy storage components, including main and auxiliary air reservoirs

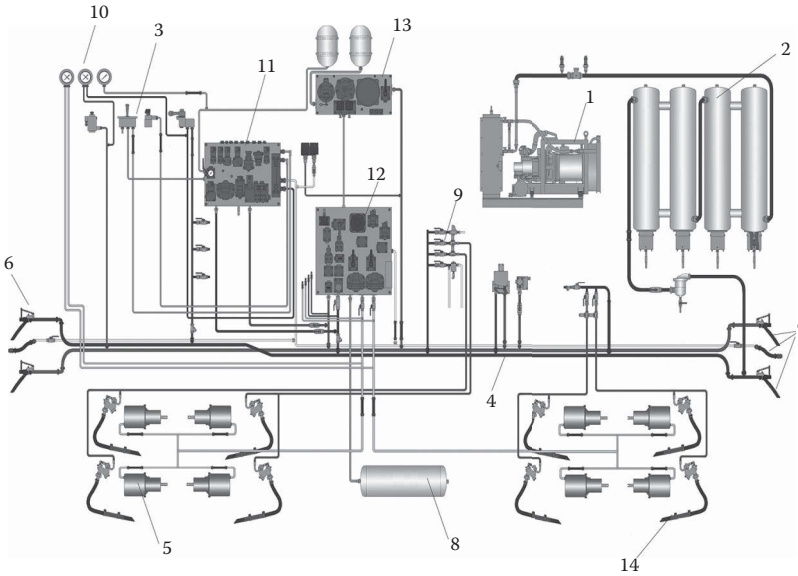

FIGURE 2.31 Example of an air pneumatic system of an electric locomotive (Manufactured by Ural Locomotives, Yekaterinburg, Russia). 1 – main air compressor; 2 – main air reservoirs; 3 – brake valve control panel; 4 – main reservoir pipeline; 5 – brake cylinders; 6 – angle cocks; 7 – hoses; 8 – auxiliary air reservoir; 9 – block of auxiliary pneumatic devices; 10 – gauge panel; 11 – block of electric pneumatic devices; 12 – block of pneumatic braking equipment; 13 – air distribution block; 14 – sand nozzles.

- Acting components or actuators, including brake cylinders that are connected to the mechanical systems used for transferring braking efforts to brake blocks
- Control devices and instrumentation such as the driver's brake valve, emergency stop valves and the like
- Distribution elements, including pipes, hoses and so on, which transport air to actuator devices or between locomotive units or to wagons
- An electronic control system that is designed to check system integrity and to perform automatic braking and automatic control

2.8 MODERN HEAVY HAUL LOCOMOTIVE DESIGN LAYOUTS AND CHARACTERISTICS

This section presents descriptions of the design of electric and diesel-electric heavy haul locomotives. The main manufacturers of freight locomotives are provided in Table 2.2.

In North America, electric locomotives are generally not used by heavy haul railways, and this explains the lack of manufacturers of electric locomotives in this large market. In other countries, production of electric locomotives is well developed along with the production of diesel-electric locomotives. The demand for locomotives in the international markets for 2010–2015 is estimated to be about 5000 electric locomotive units per year and about 5500 diesel-electric locomotive units per year.

TABLE 2.2
Main Manufacturers of Electric and Diesel-Electric Heavy Haul Locomotives

Electric Locomotives		Diesel-Electric Locomotives	
Manufacturer	**Country**	**Manufacturer**	**Country**
Bombardier Transportation	Germany	GE Transportation	United States
Siemens AG	Germany	Electro-Motive Diesel	United States
Toshiba	Japan	Transmashholding	Russia
Transmashholding	Russia	CRRC Corporation	China
Sinara Group	Russia		
CRRC Corporation	China		
Alstom Transport	France		

It should be noted that a great number of locomotives in production at the present time are either designed under cooperative agreements between companies in, for example, North America, Australia, China, Russia and India, or technology transfer schemes are used for their design solutions. Some examples of such locomotives will be described in the following sections of this chapter.

2.8.1 Diesel-Electric Locomotives

2.8.1.1 Diesel-Electric Locomotives with a DC Traction System

2.8.1.1.1 GE Transportation ES44DC

Evolution Series locomotives are the main family of DC freight/heavy haul locomotives produced by GE Transportation and delivered to many countries around the world. In addition, the technology for the production of these locomotives has been transferred to countries such as Australia, China and Kazakhstan. The basis for this series is the application of modular technology in the assembly, allowing quick configuration of the locomotive to the specific needs of consumers. The ES44DC locomotive variant shown in Figure 2.32 is representative of this approach, and this example is built with the implementation of AC–DC topology, which is the main difference from other locomotives manufactured in this series that are mostly designed with the AC–DC–AC topology. It is mainly used in North America, although an extended international version is used in Western Australia (a modification designated ES44DCi, the distinctive feature of this model being the extended radiator section to cope with the sub-tropical climate).

The designation ES44DC used for this locomotive indicates

ES – Evolution Series locomotive
44 – That locomotive traction power is 4400 hp (3280 kW)
DC – That DC traction motors are used in the locomotive's traction system

This type of the locomotive is powered by the GE GEVO engine. This combustion engine is a 4-stroke V-type diesel engine with 12 cylinders, equipped with a turbocharger.

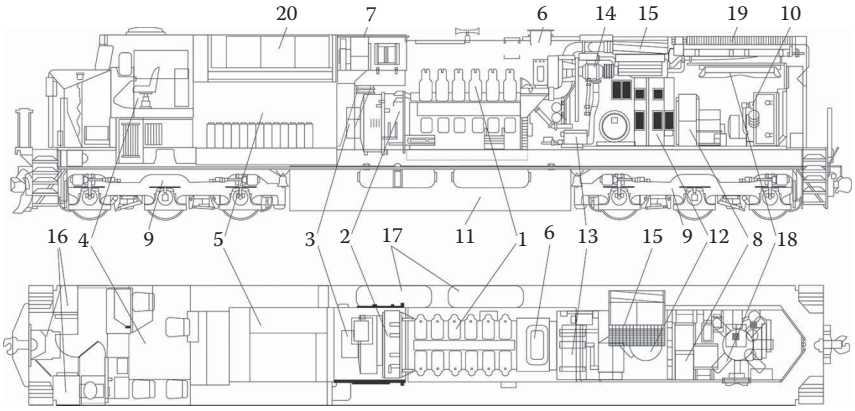

FIGURE 2.32 General arrangement of equipment on the ES44DC locomotive (Manufactured by GE Transportation, Erie, PA). 1 – diesel engine; 2 – main alternator; 3 – auxiliary generator; 4 – driver's compartment (cab); 5 – area of electric power and electronic control equipment; 6 – engine muffler; 7 – alternator blower; 8 – traction motor blower; 9 – bogies; 10 – air compressor; 11 – fuel tank; 12 – engine water tank; 13 – oil cooler; 14 – water to air intercooler; 15 – air to air intercooler; 16 – sand box; 17 – air reservoirs; 18 – cooling fan; 19 – radiator; 20 – dynamic braking grid blowers.

It provides a nominal crankshaft speed of 1050 rpm and a nominal power of 4500 hp. It has a cylinder bore of 250 mm and a piston stroke of 320 mm, with a compression ratio of 16.8:1 and a displacement volume of 251.3 L. The locomotive car body is placed on two standard Hi-AD bogies, each of which is equipped with three traction motors. Technical characteristics of the ES44DC locomotive are summarised in Table 2.3.

2.8.1.1.2 Transmashholding 2TE116U

TE116 series locomotives are the main DC locomotives with AC–DC topology manufactured by Transmashholding at its Lugansk Diesel Locomotive Plant in Ukraine. Presently, locomotives of this series are available in several variants. The latest modification of the locomotive with an improved type of diesel engine is designated 2TE116U and is shown in Figure 2.33. This locomotive is used throughout the former Soviet Union countries. In addition, there is a special modification for Mongolia which is designated 2TE116UM (this version is equipped with additional radiator sections for operation in high altitude, high temperatures and dusty environments). Modification 2TE116UD differs from the basic model, using GEVO V12 diesel engines (3350 kW or 4560 hp) produced by GE Transportation, and the main generator is A723MU2 (produced by Electrotyazhmash, Ukraine), with the power of the diesel engine on this diesel locomotive limited to 3100 kW (4200 hp). There is also a modification designated 3TE116U, which differs from the 2TE116U locomotive in that it has a booster unit in the middle in order to increase the power of the locomotive. The designation 2TE116U indicates

2 – Two unit locomotive set
T – Diesel locomotive
E – That this locomotive is equipped with an electric traction system

TABLE 2.3
Main Characteristics of the ES44DC Locomotive

General Information	
Manufacturer	GE Transportation
Power type	Diesel-electric
Wheel arrangement (UIC/AAR)	C_o-C_o/C-C
Gauge (mm)	1,435
Dimensions (approximately):	
• Length (mm)	22,300
• Width (mm)	3,022
• Height (mm)	4,699
Locomotive weight (tonnes)	189.6
Axle load (tonnes/kN)	31.6/310
Type of car body	Hood unit
Topology of electric power transmission system	AC–DC
Brake system	Air and dynamic
Wheel diameter (mm)	1,067
Power Plant and Traction Equipment Data	
Engine model	GEVO
Engine type	4-stroke V12 diesel
Power output (gross) (hp)	4,500
Traction alternator	5GMG206A
Traction motor (number of motors/type)	6 DC motors/GE 5GEB752AH
Gear ratio	4.15 (83/20)
Performance Figures	
Traction power (hp)	4,390
Locomotive speed:	
• Maximum speed (km/h)	121
• Minimum continuous speed (km/h)	21
Tractive effort:	
• Maximum starting traction effort (kN)	631.64
• Maximum continuous traction effort (kN)	470.08
Maximum dynamic braking effort (kN) (from 42 to 14.5 km/h)	332.17

116 – A freight locomotive of the 116 series
U – ‘Improved’

As shown in Figure 2.32, the 18–9 DG power plant is mounted to a subframe in the middle part of the locomotive frame. The power plant consists of a combustion engine and a main generator. The combustion engine is a 4-stroke V-type diesel engine with 16 cylinders. It can provide a nominal crankshaft speed of 1000 rpm and a rated power of 2650 kW (3604 hp). It has a cylinder bore of 260 mm, a piston stroke of 260 mm and the diesel engine is equipped with a turbocharger and an intercooler.

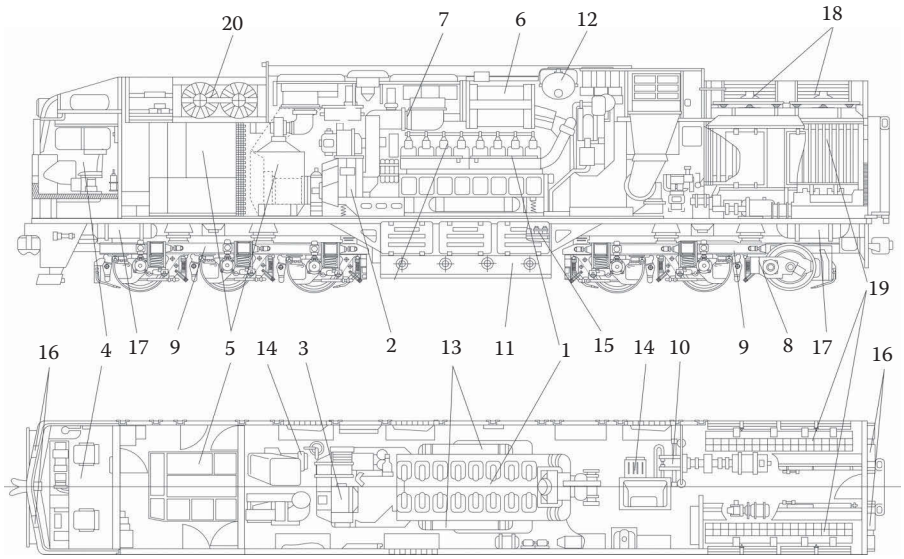

FIGURE 2.33 General arrangement of equipment on the TE116 series locomotive (Manufactured by Lugansk Diesel Locomotive Plant, Lugansk, Ukraine). 1 – diesel engine; 2 – main alternator; 3 – auxiliary generator; 4 – driver's compartment (cab); 5 – area of electric power and electronic control equipment; 6 – engine muffler; 7 – alternator blower; 8 – traction motor; 9 – bogies; 10 – air compressor; 11 – fuel tank; 12 – engine water tank; 13 – oil cooler; 14 – traction motor blower; 15 – battery; 16 – sand box; 17 – air reservoirs; 18 – cooling fans; 19 – radiators; 20 – dynamic braking grid blowers.

The locomotive car body is supported by two standard conventional bogies, each of which is equipped with three DC traction motors. Technical characteristics of the 2TE116U locomotive are summarised in Table 2.4.

2.8.1.2 Diesel-Electric Locomotives with an AC Traction System

2.8.1.2.1 Downer EDI Rail GT46C-ACe and Variants

The GT46C-ACe locomotive, shown in Figure 2.34, was developed by Downer EDI Rail (Downer Rail, Australia) [4] for use in Australia and based on technology transfer and components supplied by Electro-Motive Diesel (EMD, USA). This locomotive uses an AC–DC–AC topology and has been designed to replace its predecessor GT46C that had an AC–DC topology. Therefore, the design of this locomotive can be considered as a smaller version of the EMD SD70ACe and its engineering solutions are based on the standard-gauge GT46C locomotive, and on the narrow-gauge locomotive GT42CU AC, produced by Downer under a licence scheme from Electro-Motive Diesel. In addition, another modification of this locomotive, called GT46MAC, has been manufactured and operated by Indian Railways. The latest modification for Australia, called GT46C-ACe GEN II, has been developed by Electro-Motive Diesel with improved traction performance as well as with two weight configurations of 134 and 180 tonnes.

TABLE 2.4
Main Characteristics of the 2TE116U Locomotive

General Information	
Manufacturer	Lugansk Diesel Locomotive Plant
Power type	Diesel-electric
Wheel arrangement (UIC/AAR)	C_o-C_o/C-C
Gauge (mm)	1,520
Dimensions (approximately):	
• Length (mm)	18,700
• Width (mm)	3,080
• Height (mm)	5,105
Locomotive weight (tonnes)	139
Axle load (tonnes/kN)	23.1/227
Type of car body	Cab unit
Topology of electric power transmission system	AC–DC
Brake system	Air and dynamic
Wheel diameter (mm)	1,050
Power Plant and Traction Equipment Data	
Power plant model	18–9DG (Kolomensky Zavod)
Engine type	5D49 4-stroke V16 diesel
Power output (gross) (hp)	3,604
Traction alternator	GS-501AU2
Rectifier	M-TPP-3600DL-U2
Rectifier's power output (kW)	3,600 (6 channels)
Traction motor (number of motors/type)	6 DC motors/ED-133UHL1
Gear ratio	4.41 (75/17)
Performance Figures	
Locomotive speed	
• Maximum speed (km/h)	100
• Minimum continuous speed (km/h)	22.7
Tractive effort	
• Maximum starting traction effort (kN)	403.5
• Maximum continuous traction effort (kN)	323.62
Maximum dynamic braking power (kW)	2,700

The designation GT46C-ACe used for this locomotive indicates

G – EMD export locomotive series and it also means one cab, by default
T – Turbocharged
46 – A 16 Cylinder 710 engine
C – Six motors
AC – AC technology

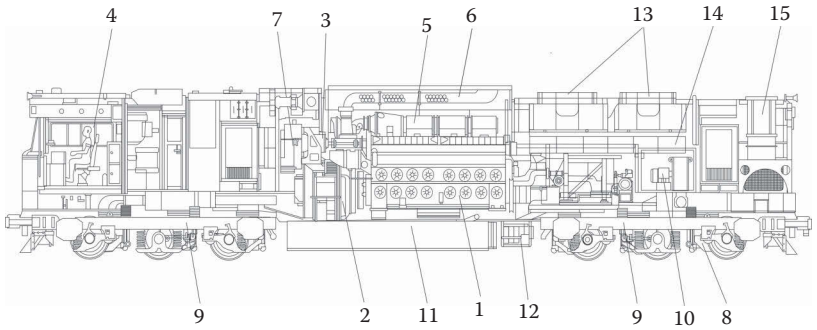

FIGURE 2.34 General arrangement of equipment on the GT46C-ACe locomotive (Manufactured by Downer EDI Rail, Newcastle, Australia). 1 – diesel engine; 2 – main alternator; 3 – auxiliary generator; 4 – driver's compartment (cab); 5 – engine exhaust manifold; 6 – engine muffler; 7 – alternator blower; 8 – traction motor; 9 – bogies; 10 – air compressor; 11 – fuel tank; 12 – battery box; 13 – cooling fans; 14 – radiators; 15 – dynamic brake grid.

e – 'Enhanced', which applies to this second generation of AC technology using insulated gate bipolar transistors (IGBTs) rather than gate turn-off (GTO) thyristors.

All types of these locomotives are powered by the EMD 710 engine. This combustion engine is a 2-stroke V-type diesel engine with 16 cylinders, equipped with a turbocharger. It can provide a nominal crankshaft speed of 900 rpm and a maximum power of 4500 hp with a compression ratio of 16:1.

Two semi-steering radial bogies are used on this locomotive. Each of the bogies is equipped with three traction motors operated by one inverter. Technical characteristics of this locomotive are summarised in Table 2.5.

2.8.1.2.2 Transmashholding TE25 and Its Variants

The 2TE25A locomotive was built on the basis of the 2TE25K locomotive, the latter being equipped with a DC traction system (AC–DC topology and commutator motors). The 2TE25A locomotive is manufactured by the Bryansk Engineering Works, which is one of the enterprises owned by Transmashholding. This AC locomotive uses an AC–DC–AC topology and has been designed to work with two or three units in a locomotive set. The modification of this locomotive, designated 2TE25AM, differs from the original locomotive by using a diesel generator on the basis of the 20V4000R43 engine produced by MTU, Germany (2×2700 kW). All these locomotives are designed to operate on Russian railways. One such locomotive unit is shown in Figure 2.35.

The designation 2TE25A indicates

2 – Two unit locomotive set
T – Diesel locomotive
E – Equipped with an electric traction system
25 – A freight locomotive of the 25 series
A – Equipped with AC traction motors

TABLE 2.5
Main Characteristics of the GT46C-ACe Locomotive

General Information	
Manufacturer	Downer EDI Rail EMD
Power type	Diesel-electric
Wheel arrangement (UIC/AAR)	C_o-C_o/C-C
Gauge (mm)	1,435
Dimensions (approximately)	
• Length (mm)	21,200
• Width (mm)	2,950
• Height (mm)	4,245
Locomotive weight (tonnes)	136.2
Axle load (tonnes/kN)	22.7/222.6
Type of car body	Hood unit
Topology of electric power transmission system	AC–DC–AC
Brake system	Air and dynamic
Wheel diameter (mm)	1,066
Power Plant and Traction Equipment Data	
Engine model	EMD 16–710G3C-ES2
Engine type	2-stroke V16 diesel
Power output (gross) (hp)	4,500
Traction alternator	EMD TA17-CA9E
Traction motor (number of motors/type)	6 AC motors/Siemens ITB 2630
Gear ratio	4.61 (83/18)
Performance Figures	
Traction power (hp)	4,300
Locomotive speed	
• Maximum speed (km/h)	130
• Minimum continuous speed (km/h)	19.6
Tractive effort	
• Maximum starting traction effort (kN)	600
• Maximum continuous traction effort (kN)	520
Maximum dynamic braking power (kW)	3,600
Maximum dynamic braking effort (kN) (from 45 to near zero km/h)	325

The 2TE25A locomotive is powered by the 21–26DG-01 power plant, which consists of a combustion engine and a main generator. This combustion engine is a 4-stroke V-type diesel engine with 16 cylinders, equipped with a turbocharger. It can provide a maximum crankshaft speed of 1000 rpm and a maximum power of 3400 hp (2500 kW) with a cylinder bore of 260 mm and a piston stroke of 260 mm.

Two radial steering bogies are installed on this locomotive. Each of the bogies is equipped with three traction motors. Technical characteristics of this locomotive are summarised in Table 2.6.

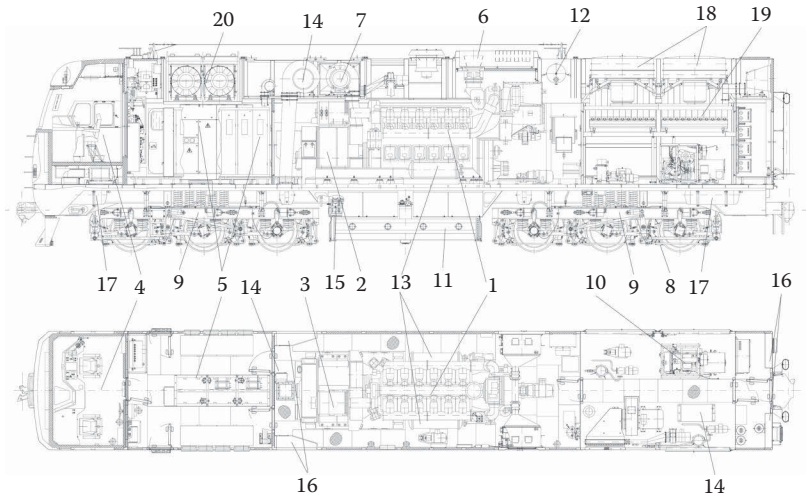

FIGURE 2.35 General arrangement of equipment on one unit of the 2TE25A locomotive. (Manufactured by Bryansk Engineering Works, Bryansk, Russia). 1 – diesel engine; 2 – main alternator; 3 – auxiliary generator; 4 – driver's compartment (cab); 5 – area of electric power and electronic control equipment; 6 – engine muffler; 7 – alternator blower; 8 – traction motor; 9 – bogies; 10 – air compressor; 11 – fuel tank; 12 – engine water tank; 13 – oil cooler; 14 – traction motor blower; 15 – battery; 16 – sand box; 17 – air reservoirs; 18 – cooling fans; 19 – radiators; 20 – dynamic braking grid blowers.

2.8.1.2.3 GE Transportation/CRRC Corporation HXN5

This AC locomotive was designed by GE Transportation for China Railway Corporation. The first two locomotives of this series were built by GE at Erie, Pennsylvania in 2008 and were designated ES59ACi according to GE Transportation's existing system, indicating that the locomotive belongs to the Evolution Series. The first five bogies of this locomotive series were produced by UGL Rail in Australia, a technology partner of GE Transportation. The technology of construction of the locomotive was subsequently transferred to the CRRC Qishuyan Locomotive Company in China, where the locomotives of this series were designated HXN5 (see a typical example shown in Figure 2.36). This locomotive has an AC–DC–AC topology.

The designation HXN5 indicates

HX – One of the 'Harmony' series ('HéXié' in Chinese) because these locomotive series are based on technology transfer arrangements from overseas
N – Equipped with a combustion engine
5 – The series number

This locomotive type is powered by the GE GEVO engine. This combustion engine is a 4-stroke V-type diesel engine with 16 cylinders and can provide a nominal crankshaft speed of 1050 rpm. It is equipped with a turbocharger, which allows achieving a nominal power of 4500 hp. It has a cylinder bore of 250 mm and a piston stroke of 320 mm, a compression ratio of 16.8:1 and a displacement volume of 251.3 L.

TABLE 2.6
Main Characteristics of the 2TE25A Locomotive

General Information	
Manufacturer	Bryansk Engineering Works
Power type	Diesel-electric
Wheel arrangement (UIC/AAR)	C_o-C_o/C-C
Gauge (mm)	1,520
Dimensions (approximately)	
• Length (mm)	20,000
• Width (mm)	3,120
• Height (mm)	5,010
Locomotive weight (tonnes)	144
Axle load (tonnes/kN)	24/235.4
Type of car body	Cab unit
Topology of electric power transmission system	AC–DC–AC
Brake system	Air and dynamic
Wheel diameter (mm)	1,050
Power Plant and Traction Equipment Data	
Engine model	12CHN26/26 (Kolomensky Zavod)
Engine type	4-stroke V12 diesel
Power output (gross) (hp)	3,400
Traction alternator	ASTG2 2800/400–1000 (Electrotyazhmash – Privod)
Traction motor (number of motors/type)	6 AC motors/DAT-470
Gear ratio	4.41 (75/17)
Performance Figures	
Traction power (hp)	2,720
Locomotive speed:	
• Maximum speed (km/h)	120
• Minimum continuous speed (km/h)	18.5
Tractive effort:	
• Maximum starting traction effort (kN)	441.5
• Maximum continuous traction effort (kN)	390
Maximum dynamic braking power (kW)	2,400

The locomotive car body is supported by two standard pedestal bogies, each of which is equipped with three traction motors. Technical characteristics of the HXN5 locomotive are summarised in Table 2.7.

2.8.1.2.4 Electro-Motive Diesel SD70 and SD90 Series

Production of SD70 series locomotives began in 1992, and this series is one of the most successful locomotive types produced by Electro-Motive Diesel for the heavy haul market. Initially, the locomotives of this series were equipped with 2-stroke

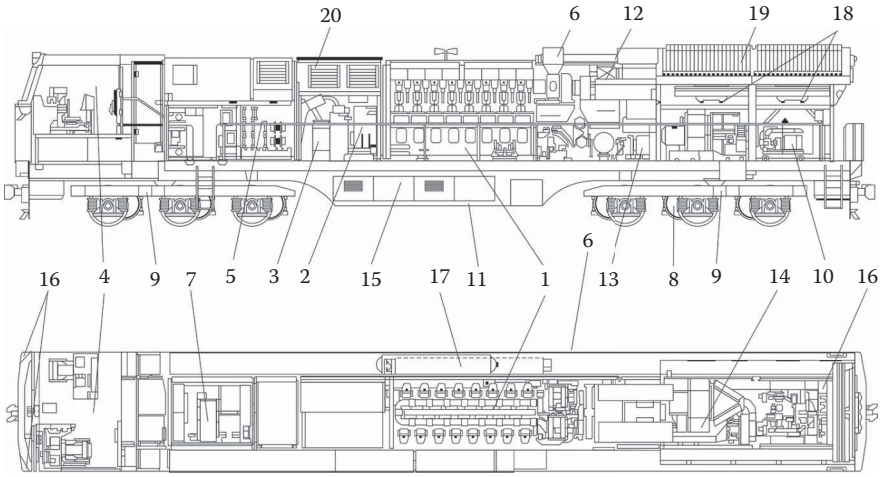

FIGURE 2.36 General arrangement of equipment on the HXN5 locomotive (Manufactured by CRRC Qishuyan Locomotive Company, Changzhou, China). 1 – diesel engine; 2 – main alternator; 3 – auxiliary generator; 4 – driver's compartment (cab); 5 – area of electric power and electronic control equipment; 6 – engine muffler; 7 – alternator blower; 8 – traction motor; 9 – bogies; 10 – air compressor; 11 – fuel tank; 12 – engine water tank; 13 – oil cooler; 14 – traction motor blower; 15 – battery box; 16 – sand box; 17 – air reservoirs; 18 – cooling fans; 19 – radiators; 20 – dynamic brake grid.

engines and DC traction motors. Later, the company moved to the release of AC locomotives with AC–DC–AC topology, resulting in the SD70MAS and SD90MAC locomotives. These were the first locomotives of the SD series equipped with traction equipment produced by Siemens and three-axle bogies with radial installation wheelsets designed by EMD. The SD90MAC locomotive, shown in Figure 2.37, is the most powerful locomotive produced by EMD and works in North America and Australia. The designation SD90MAC indicates

SD – Special duty series
90 – The series number
M – Wide nose and safety cab
AC – Alternating-current drive system

The locomotive car body is supported by two HTC-II radial self-steering bogies. The locomotive is equipped with six traction motor (three in parallel per bogie). The technical specifications of this locomotive are summarised in Table 2.8.

On the SD90MAC locomotives, the diesel engine installed is an EMD H-engine. This 4-stroke diesel engine is a V-type (at 45°) with 16 cylinders, turbocharged and with a maximum engine speed of 1000 rpm, and a maximum power of 6300 hp. It has a cylinder bore of 260 mm and a piston stroke of 300 mm, giving a displacement volume of 264 L. This diesel engine is also used on HXN3 locomotives (EMD classification – JT56ACe) assembled by the CRRC Dalian Locomotive and Rolling Stock

TABLE 2.7
Main Characteristics of the HXN5 Locomotive

General Information	
Manufacturer	GE Transportation & CRRC Qishuyan Locomotive Company
Power type	Diesel-electric
Wheel arrangement (UIC/AAR)	C_o-C_o/C-C
Gauge (mm)	1,435
Dimensions (approximately)	
• Length (mm)	22,295
• Width (mm)	3,119
• Height (mm)	4,775
Locomotive weight (tonnes)	150
Axle load (tonnes/kN)	25/245.2
Type of car body	Hood unit
Topology of electric power transmission system	AC–DC
Brake system	Air and dynamic
Wheel diameter (mm)	1,050
Power Plant and Traction Equipment Data	
Power plant model	GEVO
Engine type	4-stroke V16 diesel
Power output (gross) (hp)	6,250
Traction alternator	5GM201E1
Traction alternator's active power (kW)	5,572
Traction inverter	17KG530E2 (6 inverters)
Traction motor (number of motors/type)	6 AC motors/GE 5GEB32
Gear ratio	5.31 (85/16)
Performance Figures	
Traction power	4,155
Locomotive speed	
• Maximum speed (km/h)	120
• Minimum continuous speed (km/h)	22/3
Tractive effort	
• Maximum starting traction effort (kN)	620
• Maximum continuous traction effort (kN)	565
Maximum dynamic braking power (kW)	4,004
Maximum dynamic braking effort (kN)	352

Company in China. In connection with the tightening of locomotive emission regulations in the United States, EMD found it necessary to develop a new model of locomotive designated the SD70ACe as shown in Figure 2.38, which is currently EMD's base model. At present, only export versions of this locomotive (SD70ACe and SD70ACe/lc) are produced outside of the United States. The next version for the U.S. market, the

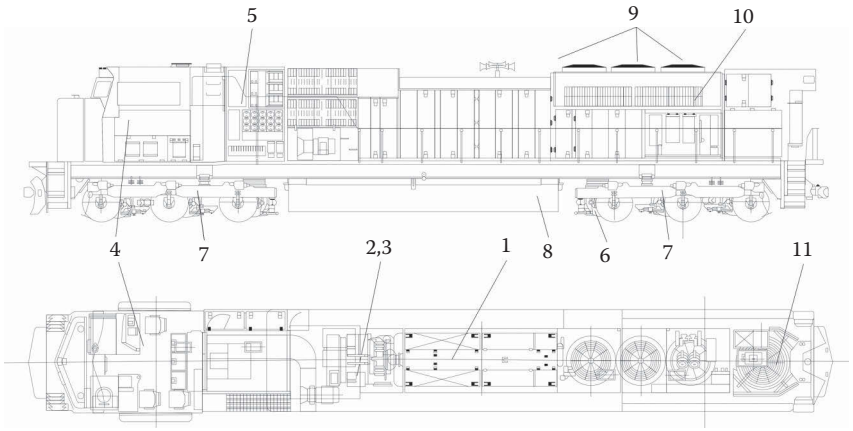

FIGURE 2.37 General arrangement of equipment on the SD90MAC locomotive (Manufactured by Electro-Motive Diesel, McCook, IL). 1 – diesel engine compartment; 2 – main alternator; 3 – rectifier; 4 – driver's compartment (cab); 5 – area of electric power and electronic control equipment; 6 – traction motor; 7 – bogies; 8– fuel tank; 9 – cooling fans; 10 – radiators; 11 – dynamic brake grid.

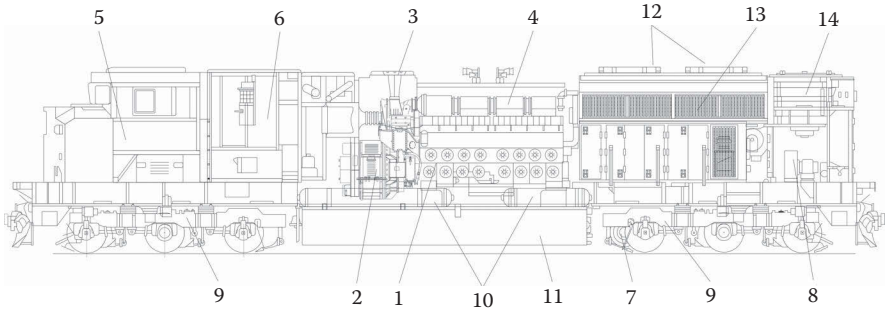

FIGURE 2.38 General arrangement of equipment on the SD70ACe locomotive (Manufactured by Electro-Motive Diesel, McCook, IL). 1 – diesel engine; 2 – main alternator; 3 – exhaust stack; 4 – engine exhaust manifold; 5 – driver's compartment (cab); 6 – area of electric power and electronic control equipment; 7 – traction motor; 8 – traction motor blower (rear); 9 – bogies; 10 – air reservoirs; 11 – fuel tank; 12 – cooling fans; 13 – radiators; 14 – dynamic brake grid.

SD70ACe-T4, which complies with the U.S. Environmental Protection Agency's Tier 4 locomotive emission standard, was presented in mid-2015, with production planned to begin in 2017. The SD70ACe locomotive is in operation in many countries around the world. The designation SD70ACe/lc, used for one model of the SD70 series specifically designed for use in heavy haul mining routes in Australia, indicates

SD – Special duty series
70 – The series number
AC – Alternating-current drive system

TABLE 2.8
Main Characteristics of the SD90MAC Locomotive

General Information	
Manufacturer	Electro-Motive Diesel
Power type	Diesel-electric
Wheel arrangement (UIC/AAR)	C_o-C_o/C-C
Gauge (mm)	1,435
Dimensions (approximately)	
• Length (mm)	24,434
• Width (mm)	3,127
• Height (mm)	4,775
Locomotive weight (tonnes)	189.6
Axle load (tonnes/kN)	31.6/310
Type of car body	Hood unit
Topology of electric power transmission system	AC–DC–AC
Brake system	Air and dynamic
Wheel diameter (mm)	1,118
Power Plant and Traction Equipment Data	
Engine model	EMD 16–265H
Engine type	4-stroke V16 diesel
Power output (gross) (hp)	6,000
Traction alternator	TA22–9MBFH
Traction motor (number of motors/type)	6 DC motors/Siemens ITB 2830 AC
Gear ratio	5.19 (83/16)
Performance Figures	
Maximum locomotive speed (km/h)	128
Tractive effort	
• Maximum starting traction effort (kN)	890
• Maximum continuous traction effort (kN)	734
Maximum dynamic braking effort (kN)	510

e – 'Enhanced', which applies to the second generation of AC with IGBTs rather than GTOs
lc – stands for 'low clearance'

All the SD70 series of locomotives are powered by EMD's 710 engine as is also the case for the GT46C-ACe locomotives. This combustion engine is a 2-stroke V-type diesel engine with 16 cylinders, equipped with a turbocharger. It can provide a nominal crankshaft speed of 950 rpm and a maximum power of 4300 hp (3207 kW) with a cylinder bore of 230 mm and a piston stroke of 279 mm.

Conventional or optional radial bogies are in use for this locomotive series. Each of the bogies is equipped with three traction motors operated by one inverter. Technical characteristics of this locomotive are summarised in Table 2.9.

TABLE 2.9
Main Characteristics of the SD70ACe Locomotive

General Information	
Manufacturer	GE Transportation
Power type	Diesel-electric
Wheel arrangement (UIC/AAR)	C_o-C_o/C-C
Gauge (mm)	1,435
Dimensions (approximately)	
• Length (mm)	22,630
• Width (mm)	3,170
• Height (mm)	4,850
Locomotive weight (tonnes)	195
Axle load (tonnes/kN)	32.5/318.8
Type of car body	Hood unit
Topology of electric power transmission system	AC–DC–AC
Brake system	Air and dynamic
Wheel diameter (mm)	1,067
Power Plant and Traction Equipment Data	
Engine model	EMD 16–710G3C-T2
Engine type	4-stroke V12 diesel
Power output (gross) (hp)	4,300
Traction alternator	TA17/CA9
Traction motor (number of motors/type)	6 DC motors/EMD A3432
Gear ratio	5.19 (83/16)
Performance Figures	
Locomotive speed	
• Maximum speed (km/h)	113
• Minimum continuous speed (km/h)	14.16
Tractive effort	
• Maximum starting traction effort (kN)	850
• Maximum continuous traction effort (kN)	698
Maximum dynamic braking effort (kN)	472

Currently, one more modification of the SD70ACe series is also produced by GE Transportation, the distinguishing feature of which is the implementation of four bogies with two axles per bogie. This eight axle locomotive, which is designated the SD70ACe-BB, has an axle load of 24.5 tonnes, a traction power of 3420 kW, a maximum speed of 80 km/h and a starting tractive effort of 724 kN. It has been designed for operation on Brazilian railways, but modification of the bogie design would allow this locomotive to run on track with various gauges in the range between 1000 and 1600 mm (Figure 2.39).

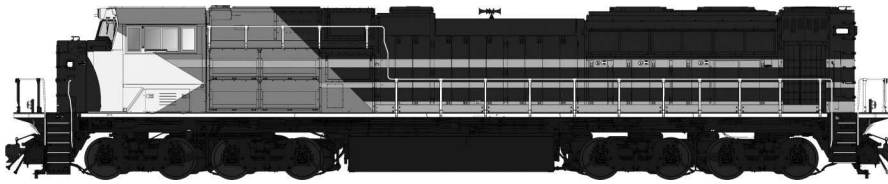

FIGURE 2.39 Eight axle heavy haul locomotive – SD70Ace-BB (Manufactured by Electro-Motive Diesel, McCook, IL).

2.8.2 Electric Locomotives

2.8.2.1 Electric Locomotives with a DC Traction System

2.8.2.1.1 Electric Locomotives with a DC–DC Topology

An example of a locomotive with DC–DC topology is the 2ES6 electric locomotive which has been produced in Russia since 2006 by Ural Locomotives (a joint venture between Sinara Group and Siemens AG). The 2ES6 electric locomotives are designed for Russian conditions to haul heavy trains on a track gauge of 1520 mm and an overhead traction supply voltage of 3 kV DC. The design of electrical systems and equipment allows operation as a multiple-unit locomotive set as well as autonomous operation of each individual electric locomotive unit. In order to improve traction performance to allow hauling heavy trains, the 2ES6 locomotives may be configured as three to four units locomotive sets, where one or two booster units are used in the middle of a locomotive configuration. Such configurations are designated 3ES6 or 4ES6, respectively. Three or four head units can also be configured, but this restricts the possibility of an internal passage through from the front to rear units. The A unit locomotive is shown in Figure 2.40, and the booster (B unit) in Figure 2.41.

The designation 2ES6 used for such electric locomotives indicates

2 – Two unit locomotive set
E – Electrical traction
S – Can work as multiple-unit locomotive
6 – The series number

The locomotive car body is supported by two standard conventional bogies, each of which is equipped with two DC traction motors. The traction equipment allows the setting of the optimal connection configuration between motors (series, series to parallel or parallel connections) in order to improve the locomotive traction performance. Technical characteristics of the 2ES6 locomotives are summarised in Table 2.10.

2.8.2.1.2 Electric Locomotives with an AC–DC Topology

The E5K or ES5K locomotive series are produced by Novocherkassk Electric Locomotive Plant, one of the enterprises of Transmashholding, Russia. The ES5K series are classified as freight locomotives for use on Russian railways with a track

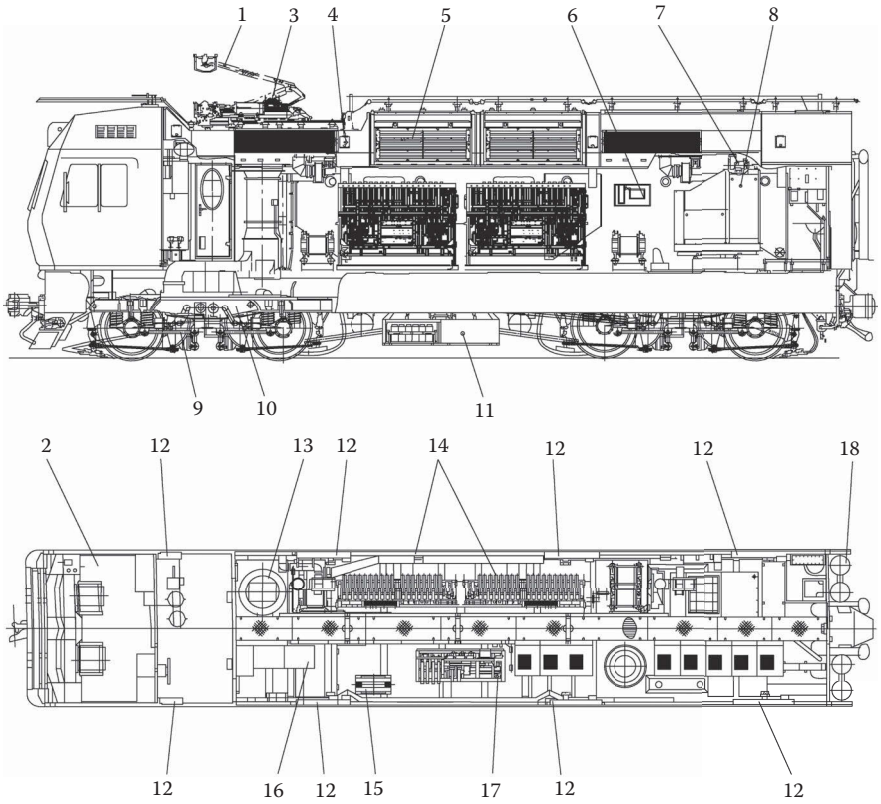

FIGURE 2.40 General equipment layout on an A unit of the 2ES6 locomotive set (Manufactured by Ural Locomotives, Yekaterinburg, Russia). 1 – pantograph; 2 – driver's compartment (cab); 3 – line filter element; 4 – dynamic brake grid; 5 – circuit breaker; 6 – air dryer; 7 – auxiliary compressor; 8 – main compressor; 9 – traction motor; 10 – bogie; 11 – battery box; 12 – sand boxes; 13 – traction motor blower; 14 – traction blocks 1 and 2; 15 – high speed circuit breaker block; 16 – locomotive microprocessor and monitor system; 17 – traction block 3; 18 – brake pneumatic system main reservoirs.

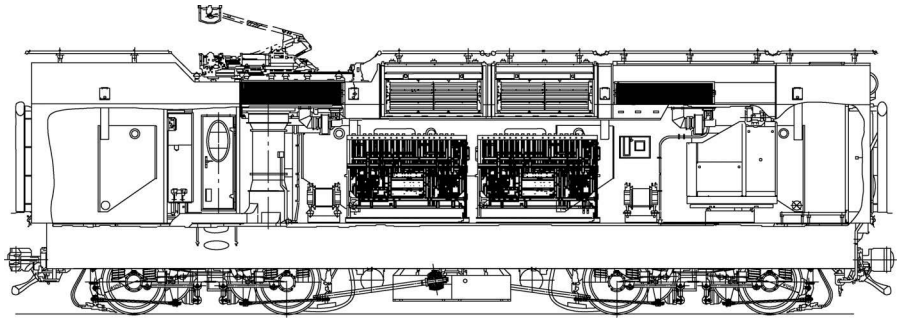

FIGURE 2.41 General equipment layout on a B-unit of the 3ES6 or 4ES6 locomotive set (Manufactured by Ural Locomotives, Yekaterinburg, Russia).

TABLE 2.10
Main Characteristics of a Single Unit of the 2ES6 Locomotives

General Information	
Manufacturer	Ural Locomotives
Power type	Electric, 3 kV DC
Wheel arrangement (UIC/AAR)	B_o-B_o/B-B
Gauge (mm)	1,520
Dimensions (approximately)	
• Length (mm)	17,000
• Width (w/o handrails and mirrors) (mm)	3,128
• Height (with the folded pantograph) (mm)	5,100
Locomotive weight (tonnes)	100
Axle load (tonnes/kN)	25/245
Type of car body	Cab unit
Topology of electric power transmission system	DC–DC
Brake system	Air and recuperative
Wheel diameter (mm)	1,250
Traction Equipment Data	
Traction motor (number of motors/type)	4 DC motors/EDP-810
Gear ratio	3.44 (86/25)
Performance Figures	
One-hour traction power at 49.2 km/h (kW)	3,220
Locomotive speed	
• Maximum speed (km/h)	120
• Continuous speed (km/h)	51
Tractive effort	
• Starting tractive effort ($\mu = 0.28$) (kN)	340
• One hour tractive effort (kN)	232
• Continuous tractive effort (kN)	209
Maximum recuperative braking power (kW)	3,200
Maximum dynamic braking power (kW)	2,750

gauge of 1520 mm, and electrified with a rated voltage of 25 kV AC at a frequency of 50 Hz, and are assembled in two- and three-unit locomotive configurations, designated 2ES5K and 3ES5K, respectively. For the 3ES5K configuration, a booster unit is used as the middle unit. The A unit of this locomotive is shown in Figure 2.42.

The designation 2ES5K used for such electric locomotives indicates

2 – Two unit locomotive set
E – Electrical traction
S – Can work as multiple-unit locomotive
5 – The series number
K – Equipped with DC traction motors

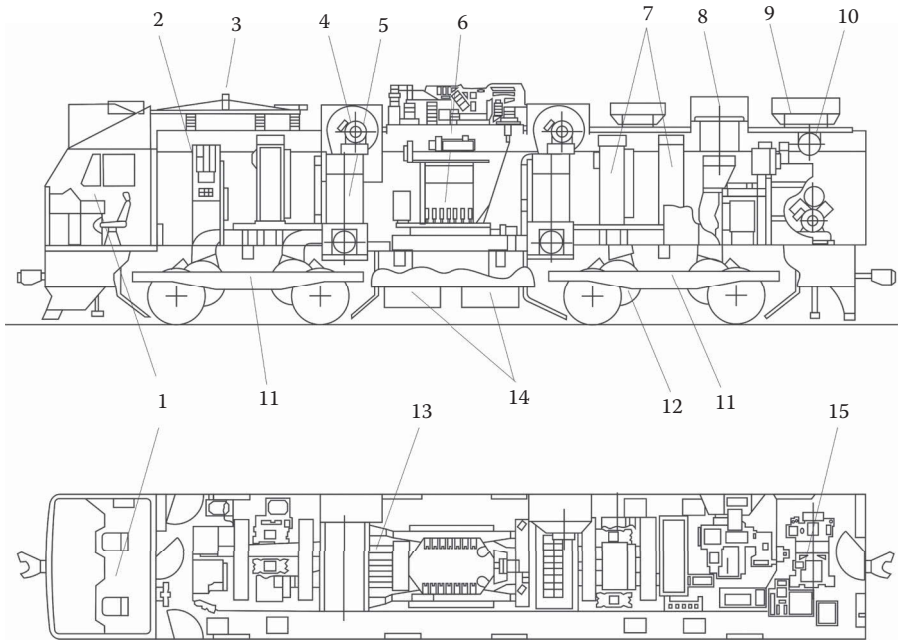

FIGURE 2.42 General equipment layout on the A-unit of the 2ES5K locomotive set (Manufactured by Novocherkassk Electric Locomotive Plant, Novocherkassk, Russia). 1 – driver's compartment; 2 – electrical equipment and microprocessor control system cabinet; 3 – pantograph; 4 – traction motor blower; 5 – inverter; 6 – main transformer; 7 – traction cabinets; 8 – dynamic brake grid; 9 – brake pneumatic system main reservoir; 10 – brake pneumatic system auxiliary reservoir; 11 – bogies; 12 – traction motor; 13 – capacitor block; 14 – batteries; 15 – air compressor.

Each locomotive unit is equipped with two standard two-axle bogies, and each of the bogies has two DC traction motors. The technical specifications of this locomotive are summarised in Table 2.11.

2.8.2.2 Electric Locomotives with an AC Traction System

2.8.2.2.1 Electric Locomotive with a DC–AC Topology

An example of a locomotive with a DC–AC topology is the 2ES10 electric locomotive, which has been produced since 2010 by Ural Locomotives (a joint venture between Sinara Group, and Siemens AG). 2ES10 electric locomotives are designed for hauling freight trains on Russian railways with a track gauge of 1520 mm and a voltage of 3 kV DC. The design of the traction electric transmission is based on technologies developed and provided by Siemens, particularly the traction equipment, such as traction inverters, asynchronous traction motors and so on. The designation 2ES10 used for such electric locomotives indicates

2 – Two unit locomotive set
E – Electrical traction

TABLE 2.11
Main Characteristics of the A-Unit of the 2ES5K Locomotives

General Information	
Manufacturer	Novocherkassk Electric Locomotive Plant
Power type	Electric, 25 kV AC, 50 Hz
Wheel arrangement (UIC/AAR)	B_o-B_o/B-B
Gauge (mm)	1,520
Dimensions (approximately)	
• Length (mm)	17,502
• Width (with mirrors) (mm)	3,560
• Height (with the folded pantograph) (mm)	5,050
Locomotive weight (tonnes)	100
Axle load (tonnes/kN)	24/235
Type of car body	Cab unit
Topology of electric power transmission system	AC–DC
Brake system	Air, dynamic and recuperative
Wheel diameter (mm)	1,250
Traction Equipment Data	
Traction motor (number of motors/type)	4 DC motors/NB-514B or NB-514E
Gear ratio	4.19 (88/21)
Performance Figures	
One-hour traction power at 49.9 km/h (kW)	3,160
Locomotive speed	
• Maximum speed (km/h)	110
• Continuous speed (km/h)	51
Tractive effort	
• Starting tractive effort (kN)	360
• One hour tractive effort (kN)	232
• Continuous tractive effort (kN)	211.5
Maximum recuperative braking effort at 45.9 km/h (kN)	225

S – Can work as multiple-unit locomotive
10 – The series number

To haul heavier trains, an additional booster unit can be added to the 2ES10 electric locomotive set. Unlike electric locomotive configurations described previously, this locomotive configuration is just called '2ES10 with booster unit'. The A-unit of this locomotive set is shown in Figure 2.43.

The locomotive is equipped with two two-axle bogies that support the locomotive car body. Each of the bogies is equipped with two AC traction motors. The technical specifications of this locomotive type are summarised in Table 2.12.

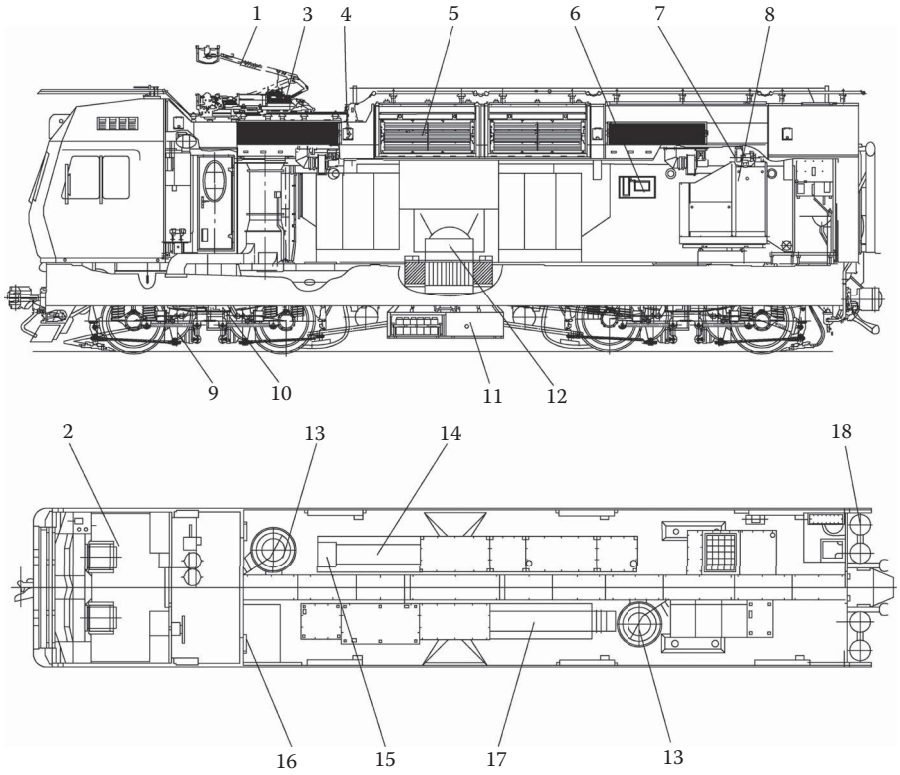

FIGURE 2.43 General equipment layout on the A-unit of 2ES10 locomotives set (Manufactured by Ural Locomotives, Yekaterinburg, Russia). 1 – pantograph; 2 – driver's compartment (cab); 3 – line filter element; 4 – dynamic brake grid; 5 – circuit breaker; 6 – air dryer; 7 – auxiliary compressor; 8 – main compressor; 9 – traction motor; 10 – bogie; 11 – battery box; 12 – reactor; 13 – traction motor blower; 14 – traction block for the front bogie; 15 – high speed circuit breaker block; 16 – locomotive microprocessor and monitor system; 17 – traction block for the rear bogie; 18 – brake pneumatic system main reservoirs.

2.8.2.2.2 Electric Locomotives with an AC–DC–AC Topology

2.8.2.2.2.1 Siemens E40 Series This series of heavy haul locomotives has been designed for operations on coal lines in Queensland, Australia. Siemens uses the designation E40AC for this type of locomotive, but in Australia, they are known as Class 3800 locomotives in Aurizon and Class 7100 locomotives in Pacific National (both companies are among the largest railway operators in Australia). The locomotive is designed to operate on narrow gauge track and is based on the Queensland Railways Class 3700 locomotive design, which is a product of the locomotive modernisation project performed by UGL Limited, Australia, with the usage of Siemens technologies and components for an AC–DC–AC topology. Side and top views of the E40AC locomotive are shown in Figure 2.44.

TABLE 2.12
Main Characteristics of the A-Unit of the 2ES10 Locomotives

General Information	
Manufacturer	Ural Locomotives
Power type	Electric, 3kV DC
Wheel arrangement (UIC/AAR)	B_o-B_o/B-B
Gauge (mm)	1,520
Dimensions (approximately)	
• Length (mm)	17,000
• Width (with mirrors) (mm)	3,128
• Height (with the folded pantograph) (mm)	5,288
Locomotive weight (tonnes)	100
Axle load (tonnes/kN)	25/245
Type of car body	Cab unit
Topology of electric power transmission system	DC–AC
Brake system	Air, dynamic and recuperative
Wheel diameter (mm)	1,250
Traction Equipment Data	
Traction motor (number of motors/type)	4 AC motors/Siemens ITB 2822
Gear ratio	3.44 (86/25)
Performance Figures	
Traction power (kW)	4,400
Locomotive speed	
• Maximum speed (km/h)	120
• Continuous speed (km/h)	57
Tractive effort	
• Starting tractive effort (kN)	376
• Continuous tractive effort (kN)	240
• Maximum tractive effort at 120 km/h (kN)	108
Maximum dynamic/recuperative braking effort (kN)	250
Maximum recuperative braking power (kW)	4,400
Maximum dynamic braking power (kW)	2,800

The locomotive is equipped with three SF8 bogies that support the locomotive car body. Each of the bogies is equipped with two AC traction motors connected in parallel. Technical characteristics of this locomotive are summarised in Table 2.13.

2.8.2.2.2.2 CRRC Corporation HXD1 Series The HXD1 series are a two unit electric locomotive set built in China by CRRC Zhuzhou Locomotive Company from 2006. This locomotive has been designed with technology provided by Siemens which is used for the Eurosprinter series, that is, this locomotive has an AC–DC–AC topology. The locomotives of this series are operated on the Chinese heavy haul

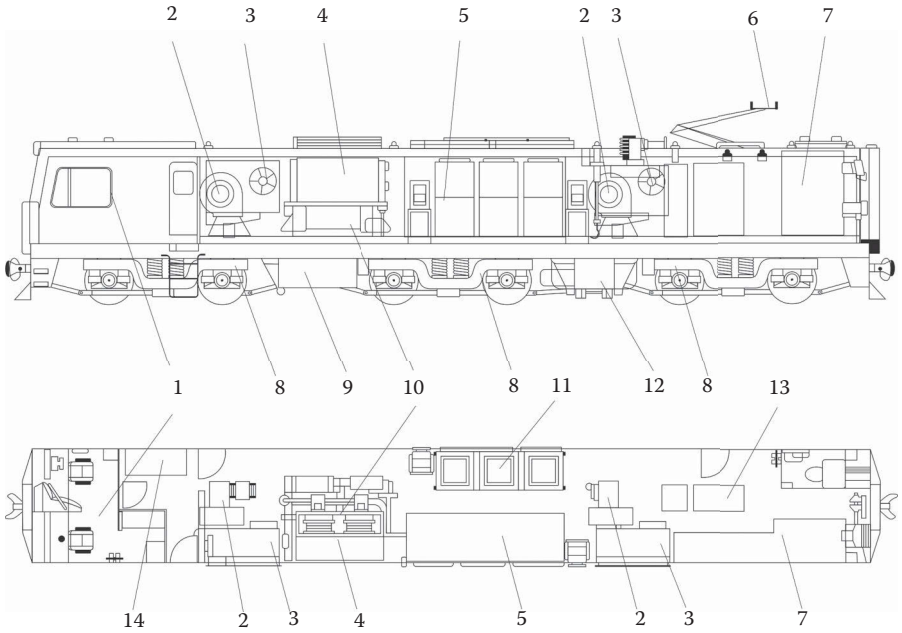

FIGURE 2.44 General equipment layout on the E40AC locomotive (Manufactured by Siemens AG, Kassel, Germany). 1 – driver's compartment (cab); 2 – traction motor blower; 3 – inertial air filter boxes; 4 – cooling rack; 5 – main converter; 6 – pantograph; 7 – auxiliary switchgear compartment; 8 – bogie; 9 – battery box; 10 – main transformer; 11 – brake resistors; 12 – air compressor; 13 – brake rack; 14 – air conditioning unit.

(coal) line between Datong and Qinhuangdao. This series also has two variants with a single-unit elongated two cab locomotive equipped with two three-axle bogies, designated as HXD1B (9600 kW) and HXD1C (7200 kW). Two side views and a top view of a single unit HXD1 locomotive are shown in Figure 2.45. This locomotive can be produced with an axle load of 23 or 25 tonnes. The designation HXD1 indicates

HX – The 'Harmony' series ('HéXié' in Chinese) because these locomotive series are based on technology transfer arrangements from overseas
D – Electric locomotive
1 – The series number

Each unit of this locomotive is equipped with two two-axle locomotive bogies that support the locomotive car body. Each of the bogies is equipped with two AC traction motors connected in parallel. Technical characteristics of this locomotive are summarised in Table 2.14.

2.8.2.2.2.3 CRRC Corporation HXD3 Series The HXD3 electric locomotive is a two-cab heavy haul locomotive built in China by CRRC Dalian Locomotive & Rolling Stock Company in co-operation with Toshiba, Japan, commencing in 2004. The

TABLE 2.13
Main Characteristics of the E40AC Locomotive

General Information	
Manufacturer	Siemens AG
Power type	Electric, 25 kV AC, 50 Hz
Wheel arrangement (UIC/AAR)	B_o-B_o-B_o/B-B-B
Gauge (mm)	1,065/1,067
Dimensions (approximately)	
• Length (mm)	20,400
• Width (including mirrors) (mm)	3,103
• Height (without pantograph) (mm)	3,890
Locomotive weight (tonnes)	132
Axle load (tonnes/kN)	22/215.82
Type of car body	Cab unit
Topology of electric power transmission system	AC–DC–AC
Brake system	Air, dynamic and recuperative
Wheel diameter (mm)	1,092
Traction Equipment Data	
Traction motor (number of motors/type)	6 AC motors/Siemens ITB 2KF2821–2EA10
Gear ratio	5.41
Performance Figures	
Rated power (kW)	4,000
Locomotive speed	
• Maximum speed (km/h)	80
• Design speed (km/h)	100
Tractive effort	
• Starting tractive effort ($\mu = 0.4$) (kN)	525
• Continuous tractive effort (kN)	450
Maximum dynamic/recuperative braking effort (kN)	450
Maximum recuperative braking power (kW)	4,000
Maximum dynamic braking power (kW)	4,000

other locomotive variant in this series, designated HXD3B, was built commencing in 2009 in co-operation between Dalian Locomotives and Bombardier Transportation, Germany. This electric locomotive is equipped with an improved traction control system which uses technologies from the IORE heavy haul locomotives produced by Adtranz (now Bombardier Transportation) for the Swedish mining company, LKAB. Both HXD3 series locomotives have an AC–DC–AC topology. The axle load of the HXD3 locomotive varies from 23 to 25 tonnes. The HXD3B locomotive has an extended length in comparison with the HXD3 (22,900 versus 20,846 mm).

The designation of the HXD3B locomotive, shown in Figure 2.46, indicates

HX – The 'Harmony' series ('HéXié' in Chinese) because these locomotive series are based on technology transfer arrangements from overseas

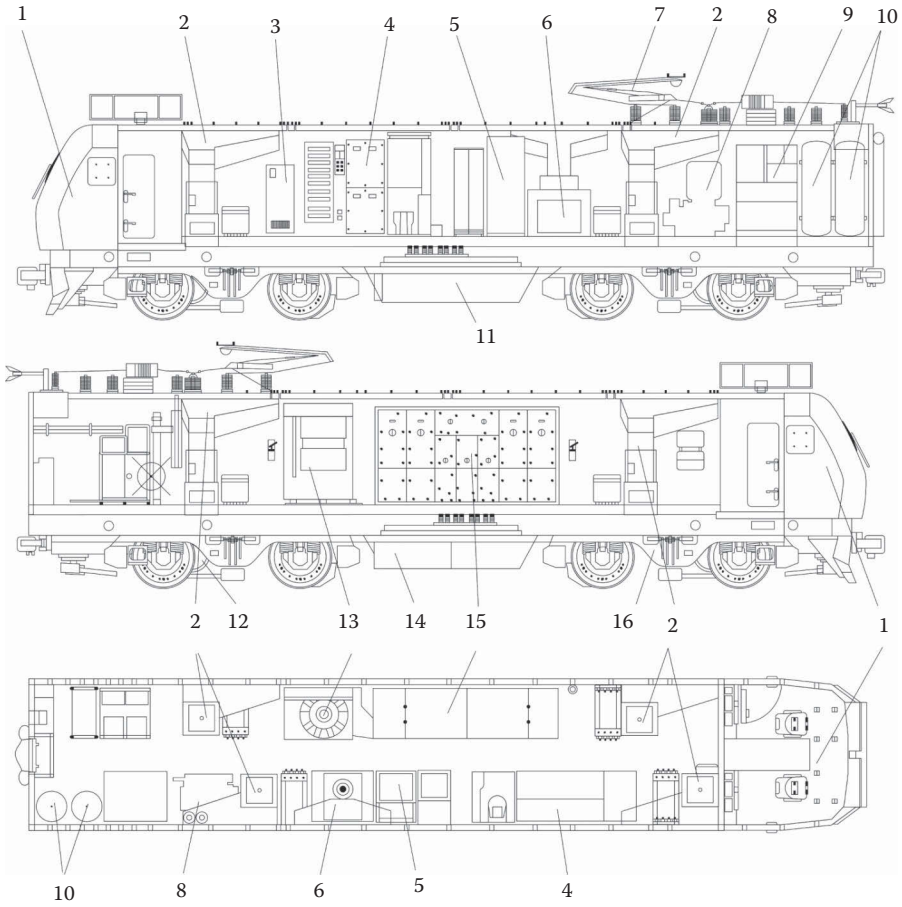

FIGURE 2.45 General equipment layout on the HXD1 locomotive (Manufactured by Zhuzhou Locomotive Company, Zhuzhou, China). 1 – driver's compartment (cab); 2 – traction motor blower; 3 – battery charger; 4 – low voltage control equipment; 5 – signal equipment; 6 – auxiliary transformer; 7 – pantograph; 8 – air dryer and compressor; 9 – brake rack; 10 – main reservoirs; 11 – main transformer; 12 – traction motor; 13 – oil cooling tower; 14 – battery box; 15 – main converter; 16 – bogie.

D – Electric locomotive
3 – The series number
B – Modification

The HXD3 locomotive is equipped with two conventional three-axle bogies. Each of the bogies has three AC traction motors with individual axle traction control. In the case of the HXD3B, the locomotive has two MITRAC TC 3300 AC traction converters and a different bogie design belonging to the Flexifloat bogie family of Bombardier Transportation. Technical characteristics of the HXD3B are summarised in Table 2.15.

TABLE 2.14
Main Characteristics of a Single Unit of the HXD1 Locomotive

General Information	
Manufacturer	CRRC Zhuzhou Locomotive Company
Power type	Electric, 25 kV AC, 50 Hz
Wheel arrangement (UIC/AAR)	B_o-B_o/B-B
Gauge (mm)	1,435
Dimensions (approximately)	
• Length (mm)	17,611
• Width (at handrail) (mm)	3,100
• Height (roof) (mm)	4,020
Locomotive weight (tonnes)	100
Axle load (tonnes/kN)	25/245
Type of car body	Cab unit
Topology of electric power transmission system	DC–AC
Brake system	Air and recuperative
Wheel diameter (mm)	1,250
Traction Equipment Data	
Traction motor (number of motors/type)	4 AC motors/Siemens ITB 2624
Gear ratio	6.24 (106/17)
Performance Figures	
Traction power (kW)	4,800
Locomotive speed	
• Maximum speed (km/h)	120
• Continuous speed (km/h)	65
Tractive effort	
• Starting tractive effort (kN)	380
• Continuous tractive effort (kN)	266
Maximum electric braking effort (kN)	461
Maximum electric braking power (kW)	4,800

2.8.2.2.2.4 Indian Railways WAG9 The WAG9 electric locomotive is a two-cab heavy haul locomotive designed by Adtranz (now Bombardier Transportation) in 1996 as heavy haul locomotives for Indian railways. The first six locomotives were assembled in Switzerland and the others were subsequently manufactured in India by Chittaranjan Locomotive Works. The WAG9 locomotive is still in production and several variants (WAG-9i, WAG-9H, WAG-9Hi) can be found in operation, having different axle loads (20.5 or 22.5 tonnes) and some modified versions of their traction components.

The designation for the WAG9 locomotive, shown in Figure 2.47, indicates

W – Wide gauge
A – Electric locomotive with AC traction

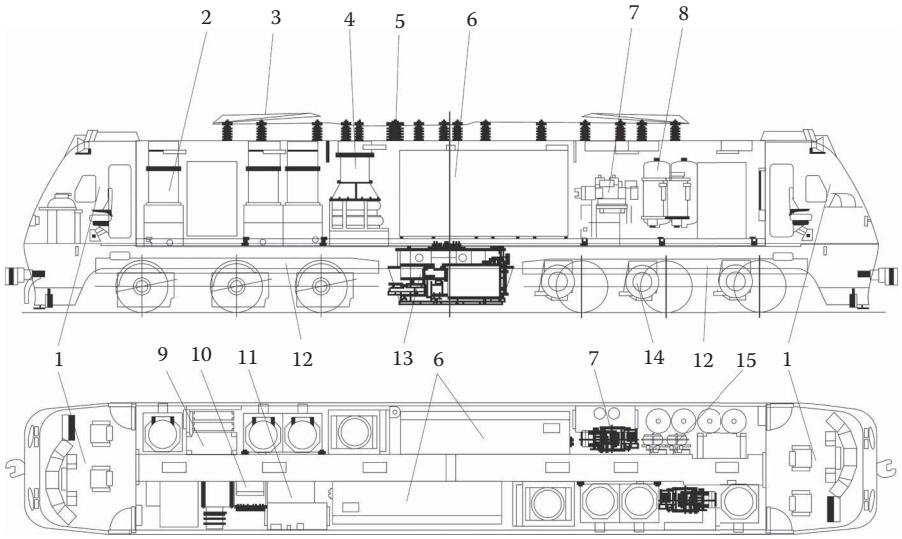

FIGURE 2.46 General equipment layout on the HXD3B locomotive (Manufactured by CRRC Dalian Locomotive & Rolling Stock Company, Dalian, China). 1 – driver's compartment (cab); 2 – traction motor blower; 3 – pantograph; 4 – oil cooling tower; 5 – circuit breaker; 6 – traction converter; 7 – air compressor; 8 – main reservoirs; 9 – battery charger; 10 – microprocessor control and diagnostics system; 11 – control apparatus cabinet; 12 – bogies; 13 – main transformer; 14 – traction motor; 15 – air drier.

TABLE 2.15
Main Characteristics of the HXD3B Locomotive

General Information	
Manufacturer	Dalian Locomotive & Rolling Stock
Power type	Electric, 25 kV AC, 50 Hz
Wheel arrangement (UIC/AAR)	C_o-C_o/C-C
Gauge (mm)	1,435
Dimensions (approximately)	
• Length (mm)	22,900
• Width (mm)	2,950
• Height (mm)	4,250
Locomotive weight (tonnes)	150
Axle load (tonnes/kN)	25/245
Type of car body	Cab unit
Topology of electric power transmission system	AC–DC–AC
Brake system	Air and recuperative
Wheel diameter (mm)	1,250

(*Continued*)

TABLE 2.15 (*Continued*)
Main Characteristics of the HXD3B Locomotive

Traction Equipment Data	
Traction motor (number of motors/type)	6 AC motors/MITRAC DR 3800N
Gear ratio	4.95
Performance Figures	
Traction power (kW)	9,600
Maximum locomotive speed (km/h)	120
Tractive effort	68.2
• Starting tractive effort (kN)	570
• Tractive effort at 68.2 km/h (kN)	506
• Tractive effort at 120 km/h (kN)	300
Maximum electric braking effort (from 73 to 4 km/h) (kN)	480
Maximum electric braking power (kW)	9,600

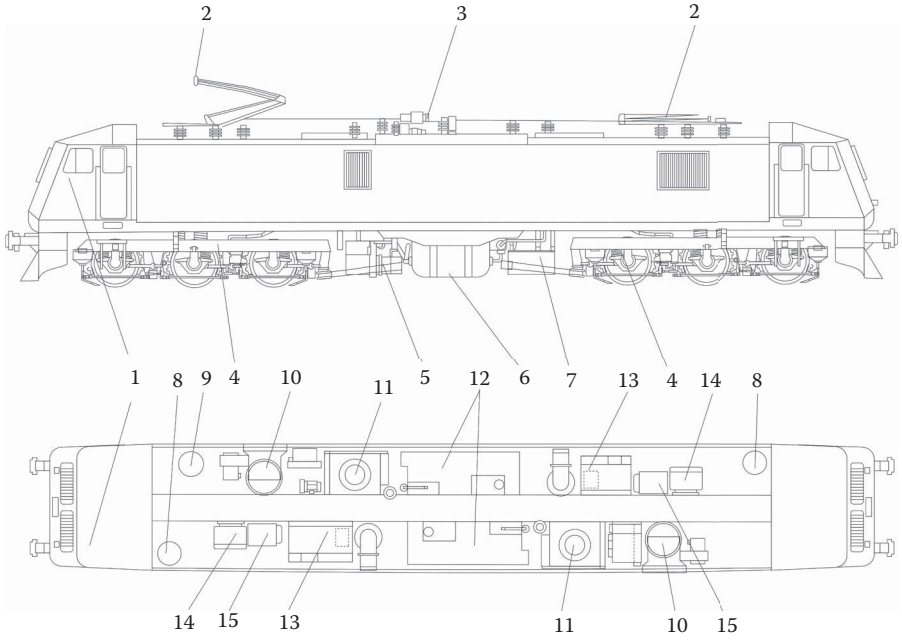

FIGURE 2.47 General equipment layout on the WAG9 locomotive (Manufactured by Chittaranjan Locomotive Works, Asansol, India). 1 – driver's compartment (cab); 2 – pantograph; 3 – circuit breaker; 4 – bogies; 5 – air compressor; 6 – main transformer; 7 – battery box; 8 – main reservoirs; 9 – auxiliary reservoir; 10 – traction motor blower; 11 – oil cooling tower; 12 – traction converters; 13 – auxiliary converters; 14 – microprocessor control and diagnostics system; 15 – auxiliary circuit cabinet.

TABLE 2.16
Main Characteristics of the WAG9 Locomotive

General Information	
Manufacturer	Chittaranjan Locomotive Works
Power type	Electric, 25 kV AC, 50 Hz
Wheel arrangement (UIC/AAR)	C_o-C_o/C-C
Gauge (mm)	1,676
Dimensions (approximately)	
• Length (mm)	20,562
• Width (mm)	3,152
• Height (with folded pantograph) (mm)	4,255
Locomotive weight (tonnes)	132
Axle load (tonnes/kN)	22/215.82
Type of car body	Cab unit
Topology of electric power transmission system	AC–DC–AC
Brake system	Air and recuperative
Wheel diameter (mm)	1,092
Traction Equipment Data	
Traction motor (number of motors/type)	6 AC motors/ABB 6FRA 6068
Gear ratio	5.10 (107/21)
Performance Figures	
Traction power (kW)	4,500
Maximum locomotive speed (km/h)	100
Tractive effort	68.2
• Starting tractive effort (kN)	460
• Continuous tractive effort (kN)	325
Maximum electric braking effort (kN)	460

G – For hauling goods, that is, freight locomotive
9 – The series number

Two three-axle Adtranz Flexicoil IV bogies support the entire weight of the locomotive car body, with each of the bogies having three AC traction motors. Technical characteristics of the WAG-9 are summarised in Table 2.16.

The details contained in Tables 2.3 through 2.16 were obtained from promotional material, performance specifications, technical papers and maintenance manuals published by the manufacturers or operators of the various locomotives.

REFERENCES

1. M. Spiryagin, C. Cole, Y.Q. Sun, M. McClanachan, V. Spiryagin, T. McSweeney, *Design and Simulation of Rail Vehicles*, CRC Press, Boca Raton, FL, 2014.
2. UIC Leaflet 650, *Standard Designation of Axle Arrangement on Locomotives and Multiple-Unit Sets*, 5th Edition, International Union of Railways, Paris, France, 1983.

3. Association of American Railroads, *Manual of Standards and Recommended Practices, Section M – Locomotives and Locomotive Interchange Equipment: RP-5523 Axle Nomenclature Arrangement – Locomotives*, Association of American Railroads, Washington, DC, 2008.
4. N. Ramsey, F. Szanto, P. Hewison, Introducing the next generation locomotive to the Australian rail network. In *Conference on Railway Engineering*, Perth, Australia, 7–10 September 2008.

3 Design of Mechanical Systems of Locomotives

3.1 CLASSIFICATION OF MAIN COMPONENTS

From the standpoint of modern locomotives, their mechanical systems can be seen as a set of unified design elements consisting of the following main assemblies and components:

- The locomotive car body with a main structural frame that transmits traction and dynamic forces, and on which are located the main power plant units and various units that undertake the overall monitoring and management of the locomotive's performance and movement. These include the traction transmission control, braking, cooling, ventilation, oil, water and fire protection systems, plus auxiliary equipment and safety devices. This leads to the division of the body and underbody spaces into the relevant areas and compartments needed for the protection of the equipment and the locomotive crew from the effects of various hazards arising from the operation of the locomotive. The layout is designed to create a safe and comfortable working environment for the crew and locomotive maintainers.
- Bogies (referred to as trucks in North America) which, for a locomotive, are an assembly comprising wheelsets, bearings, a frame, a bolster or transom, brake rigging, springs and connecting components used to support the locomotive and capable of rotation in the horizontal plane to provide guidance along the track. Modern locomotive bogies are designed to improve curving performance by means of the reduction of dynamic interaction between the running gear and track. Early locomotives and wagons were designed without any bogies, with all wheelsets fixed in a rigid frame or directly attached to the car body. The development of large railway transport networks with massively increased freight volumes required rail vehicle manufacturers to increase the capacity of locomotive power plants and improve their traction performance, inevitably seeing an increase in the weight of locomotives. This subsequently resulted in locomotives that reached and exceeded the permissible limit of the vertical load that could safely be supported on the track structure. As a result, the number of wheelsets carrying locomotives had to be increased, along with locomotive dimensions, causing difficulties with stability of locomotives when traversing tightly curved track sections and problems with the force interactions between locomotives and track. One of the solutions to address these problems was the separation of the rigid rail vehicle superstructure and those parts that provide guidance along the track, which led to the creation of the modern design of a railway

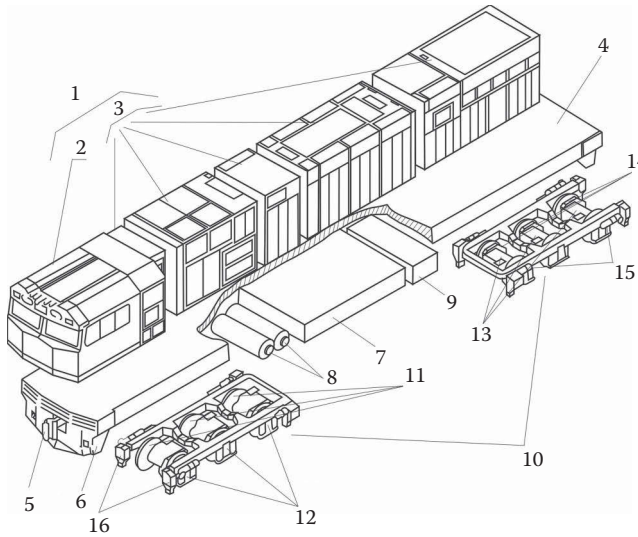

FIGURE 3.1 Main components of a heavy haul locomotive (a hood unit). 1 – car body; 2 – driver's compartment (cab); 3 – equipment compartments; 4 – main frame; 5 – coupling device; 6 – pilot (cowcatcher); 7 – fuel tank; 8 – air reservoirs; 9 – battery compartment; 10 – bogies; 11 – wheelsets; 12 – journal housings (axle boxes); 13 – traction motors; 14 – gear boxes; 15 – brake cylinders; 16 – sand boxes.

vehicle, where the body and the main structural frame are supported via elastic elements based on small frames containing the necessary running gear with sprung wheelsets. These latter frames with wheelsets are now called bogies (trucks). A typical example of the setup of the main components of a conventional design solution for a heavy haul locomotive is shown in Figure 3.1.

Each bogie includes

- Wheelsets that comprise a pair of wheels semi-permanently mounted on an axle and designed for transmitting traction and braking torque to the wheels via traction gear and brake devices. Bogies may hold one, two or more wheelsets and support the superstructure of a locomotive through the journal bearing housings and provide the means of transfer of traction and braking effort to the vehicle that allows it to move along the track in a controlled way due to the rolling of its powered (driven) wheelsets on the rails.
- Journal bearings that provide the load bearing and wheelset rotation capabilities at the ends of each axle of a rail vehicle bogie (truck). Vertical loads are transferred through each of the journal housings (axle boxes) to the bogie frame through a device known as a roller bearing adapter that fits between the bearing outer ring and the frame pedestal. Journal housings serve to support the bogie frame via elastic-damping elements and are connected to the wheelsets by means of the bearings. Journal bearings enable

the rotation of the wheelsets, with their housings providing the necessary lateral clearances for the realisation of the vehicle's movement along the track, particularly crucial when traversing curves.

- Suspension components that provide elastic-damping connections between journal housings and the bogie frame (primary suspension) and between the bogie frame and the locomotive car body (secondary suspension) in order to transmit traction and braking forces. These bear the vertical forces from the weight of the suspended parts, and redistribute their weight among the elements of the running gear, absorb the dynamic forces arising during the movement of the locomotive on track that contains irregularities and the impact of external surrounding forces and other natural phenomena associated with train operations, enabling the locomotive to achieve the required power and safe dynamic interaction with the track. This also allows achievement of the necessary ride comfort standards in order to reduce dynamic loads transferred to the locomotive driver, as well as maintaining the operational conditions required for stable functioning of the locomotive equipment.
- Traction drives, where the main task is to transmit the traction torque of the traction motors to the wheelsets of the locomotive.
- Braking equipment that is used to exert braking force(s) on the wheels, which then transfer to the contact patches between the running rails and the wheels in order to maintain or reduce the operational speed, or bring the locomotive to a full stop whether operating as an independent unit or as a traction vehicle in a train configuration. Braking equipment also allows retaining the locomotive in a fixed (locked) state when parked on any track in order to avoid inadvertent movement. In this latter case, the mechanism of the brake system being utilised is called a parking brake.
- Sanding system elements designed to improve adhesion conditions between wheels and rails to enable an increased tractive or braking effort to be realised by a locomotive in cases when wheel skidding or sliding occurs due to the poor friction conditions at the wheel–rail interface. Sanding systems are normally designed to work automatically when in notch position 3 or less, or when the traction control system cannot overcome skidding and sliding with its traction algorithms.

3.1.1 Locomotive Bodies

Locomotive bodies (car bodies) can be built in two primary design variations: a monocoque body design (Figure 3.2) [1] and various body-on-frame designs (Figures 3.3 and 3.4). In the first design approach, all elements of the monocoque body are rigidly connected such that the body shell and wall sheeting assist the main frame to carry all the loads and stresses associated with the process of movement of the locomotive, as well as loads acting from the equipment installed in it. It also handles all traction and braking forces, transferring them to the train, and receiving longitudinal dynamic loads from the train. Monocoque construction has advantages of high rigidity and low weight.

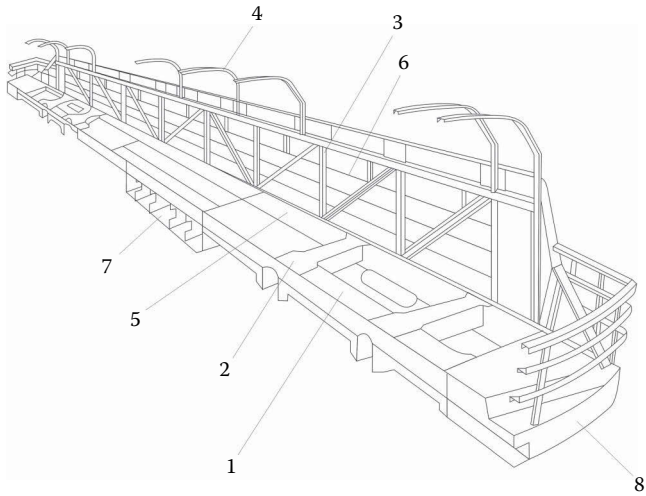

FIGURE 3.2 Monocoque locomotive car body design (Manufactured by Kolomensky Zavod, Kolomna, Russia). 1 – longitudinal sill; 2 – cross beam; 3 – vertical beam; 4 – arc for fixing the roof elements; 5 – metal packaging strip; 6 – strap for fixation of skin elements; 7 – frame for installation of fuel tanks; 8 – coupling box. (From Spiryagin, M. et al., *Design and Simulation of Rail Vehicles, Ground Vehicle Engineering Series*, CRC Press, Boca Raton, FL, 2014. With permission.)

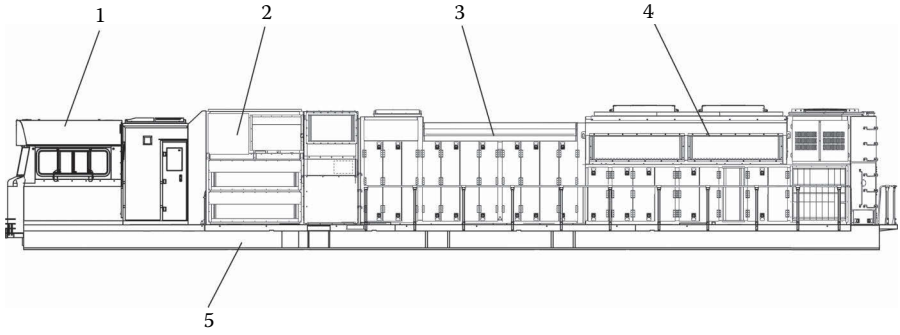

FIGURE 3.3 Example of a locomotive with a body-on-frame hood unit design (Manufactured by Electro-Motive Diesel, McCook, IL). 1 – driver's compartment (cab); 2 – auxiliary compartment; 3 – power plant (engine) compartment; 4 – radiator compartment; 5 – main frame.

Under the second design approach, a structural main frame (underframe) is the primary load-bearing component, and all the traction and braking forces and dynamic and impact loads are received, carried or borne by its strong longitudinal design. Other elements of the body, such as the side and end walls, the roof and the cab/s, are supported on the main frame and only carry loads from equipment fixed on these elements and provide protection from adverse factors arising from the operation of the locomotive equipment and comfortable working conditions for locomotive drivers in all weather and environmental conditions.

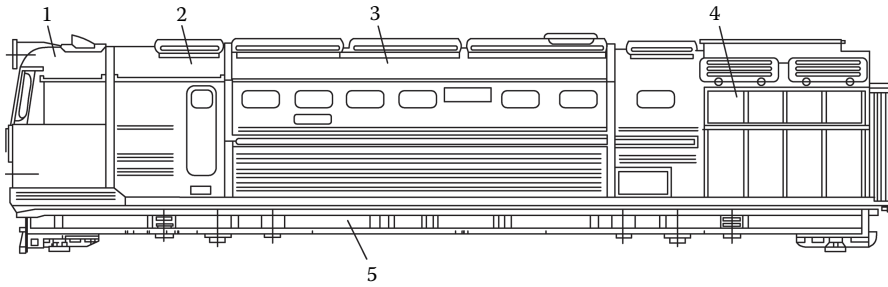

FIGURE 3.4 Example of a locomotive with a body-on-frame cowl unit design (Manufactured by Lugansk Diesel Locomotive Plant, Lugansk, Ukraine). 1 – driver's compartment (cab); 2 – auxiliary compartment; 3 – power plant (engine) compartment; 4 – radiator compartment; 5 – main frame.

Based on the physical layout of the car body, heavy haul locomotives may be produced with either hood unit (Figure 3.3) or cowl unit (Figure 3.4) design styles. In the case of a hood unit design, equipment is located in compartments built on the main frame and covered with side walls and a roof that can easily be opened when required for maintenance. In addition, for easy access to the locomotive's equipment, this design is usually equipped with a special external service platform (walkway) encircling these compartments. In car bodies with such designs, the driver can be located above or on the same level as the equipment compartments. The advantage of this design is better visibility in both directions of operation and easy access to the equipment for repair and service jobs. However, disadvantages are worse aerodynamics in comparison with cowl unit designs and some trackside safety concerns and environmental hazards for drivers and/or technical staff from natural phenomena such as rain or snow, wind, low and high temperatures, and dust pollution when equipment needs to be serviced or repaired in the open during the operation of the locomotive.

Cowl unit locomotives have a full-width car body for the complete length of the locomotive, the size and shape of which is only restricted by the existing loading gauge. Such a design has service walkways inside the car body to access the equipment when necessary. The installation or replacement of the equipment inside the body is usually done through removable roof hatches. This type of car body is preferred for high-speed operations because of good aerodynamics; although this is generally not an important issue for heavy haul operations, such locomotives provide better working conditions when operated in very cold or hot climates.

Car bodies are divided into two main zones: (1) a zone for technological equipment and (2) a zone for the location of the driver/s and the equipment that is needed to control the operation of the locomotive. This latter zone is called a driver's compartment or cab.

The classification of car bodies can be further distinguished by the number and positioning of cabs, and by the design approach of the cabs.

Using the number of cabs, the car bodies are classified in a similar fashion to the many locomotive descriptions provided in Chapter 2, that is, one cab or two-cab designs. In the case of cowl unit designs, the main disadvantage of only having one cab is the low visibility for the driver past the other end of the locomotive.

According to the location of the cab/s, car bodies can be classified as

- End cab, located on the extreme end/s of the car body.
- Central cab, that is, centrally located in the length of the rail vehicle (this is very rare for heavy haul locomotives).
- Off centre cab, when the cab is shifted away from the central position in the longitudinal direction, but does not take the extreme end position, and the locomotive's technological compartments and equipment are placed behind the cab.

The cabs themselves can also be divided into two types based on their structural design parameters:

- Cockpit type design, where the cab is constructed as an integral part of the car body (e.g., a monocoque car body design).
- Capsular type design, as shown in Figure 3.5, where the cab frame is executed in the form of a protective capsule that is mounted in the car body or on the main frame, and may have additional elastic-damping and noise-insulating elements to provide a safe and ergonomically comfortable

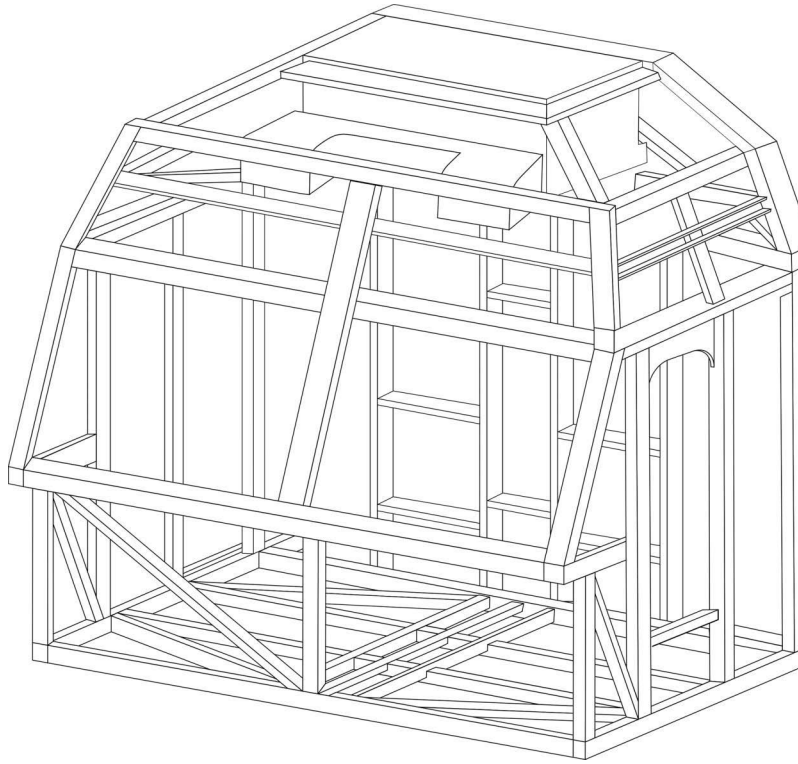

FIGURE 3.5 Modular cab of a heavy haul locomotive (Manufactured by Electro-Motive Diesel, McCook, IL).

working environment for drivers with reduced vibro-dynamics and noise impacts. Such a design is typically applied for locomotives based on a modular construction approach.

Locomotive car bodies can be divided into two types based on the structural design of the frames used to create the body side profile:

- Truss framework design, as shown in Figure 3.6, which consists of a mix of straight and inclined beams in the car body's structure.
- Stressed skin (monocoque) design, as shown in Figure 3.7, which uses only horizontal and vertical beams in the car body's structure.

The stressed skin design type has a greater carrying capacity in comparison with the truss framework design, but the latter is more practically feasible to manufacture, particularly in regard to the skin elements of the body shell such as the wall covering sheets.

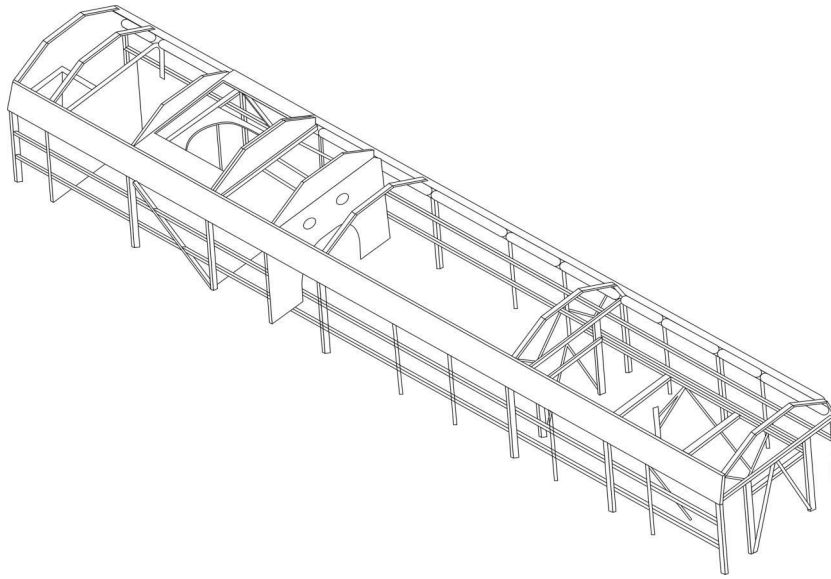

FIGURE 3.6 Body-on-frame car body structure with truss framework design (Manufactured by Electro-Motive Diesel, McCook, IL).

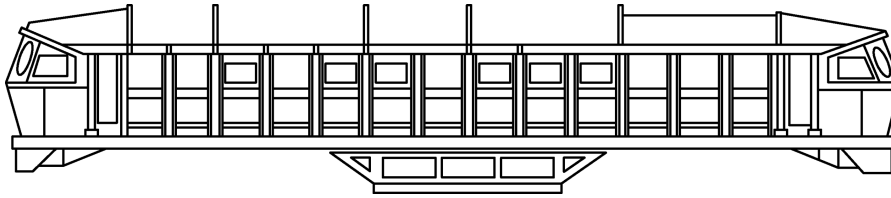

FIGURE 3.7 Monocoque car body structure with stressed skin design (Manufactured by Lugansk Diesel Locomotive Plant, Lugansk, Ukraine).

Descriptions of monocoque car bodies can also include the type of materials used for skin elements of the body shell such as the wall-covering sheets that can be manufactured from the following materials:

- Metal (ferrous metals, alloys, non-ferrous metals or a combination)
- Composite materials
- Combined, indicating combinations of different materials used as skin elements of a locomotive car body in order to optimise the weight and size ratio parameters while providing the required load-bearing capacity

Skin elements of the body shell, commonly produced from metallic wall covering sheets or composite materials, may consist of one or two sheet/s or sandwich panels with various fireproof insulation materials providing a reduction of vibration and noise transmission. Such skin elements may be designed to be either load carrying or non-load carrying.

Finally, the process of manufacturing can be part of the car body description, namely,

- Welded
- Riveted
- Glued
- Welded and riveted
- Combinations of these

Locomotive car bodies usually have multiple compartments and spaces to accommodate the locomotive equipment. The main technological compartments of the diesel–electric locomotive are as follows:

- Diesel engine compartment
- Electrical and power equipment compartment/s
- Radiator compartment
- Fuel tank/s
- Battery compartment/s

In the case of electric locomotives, the car body can be divided into compartments for the following:

- A main transformer or inductor
- Traction control equipment and other power and brake equipment
- Cooling and ventilation systems for processing main transformer oil and heat generated by other equipment
- Battery box or boxes

In addition, the boxes housing couplings with absorbing devices (draft gear) or buffers, mounted on the front and rear ends, are considered as parts of a car body when utilising a monocoque design approach (see Figure 3.2).

3.1.2 Locomotive Frames

For locomotives designed with a main frame (underframe), all the loads from the weight of installed equipment as well as traction and braking forces and dynamic and impact loads are received, carried or borne by the strong structural design of the main frame. Such locomotives are relatively easy to manufacture and repair, but they have a much greater consumption of materials, the extra weight of which must be considered in the design so far as the axle load is concerned. In addition, the main frame must be constructed with a longitudinal camber, so that the frame does not sag when all of the equipment and body is placed onto the frame. An example of a typical main frame design for a heavy haul locomotive with two cabs is shown in Figure 3.8.

Locomotive frames can be divided into three groups according to the structural design of the main bearing elements (beams) of the frame:

- Centre beam design where loads and stresses are primarily carried by several centrally placed longitudinal beams running the full length of the locomotive
- Contour beam design where loads and stresses are primarily carried by external beams fully encompassing the frame's perimeter or outer contour
- Combined

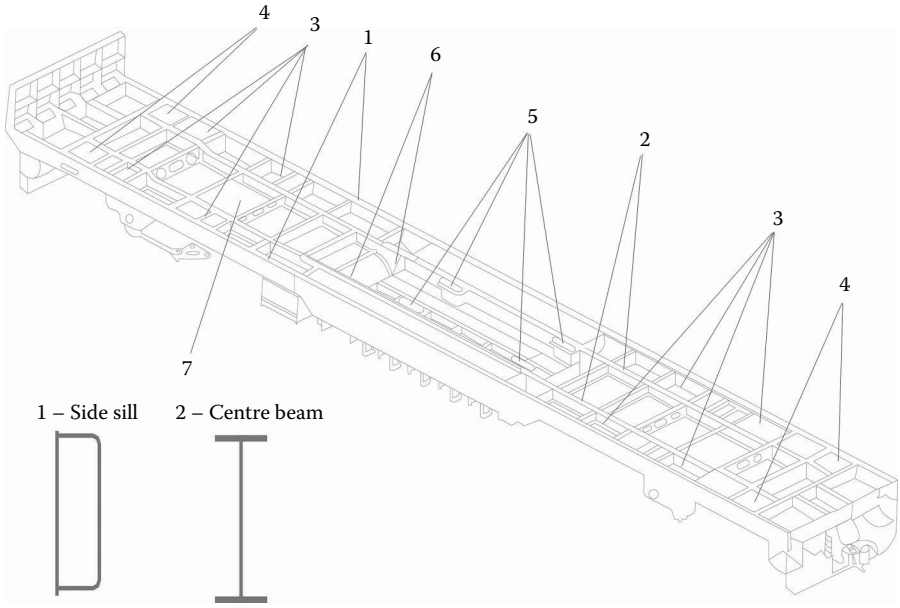

FIGURE 3.8 Example of a heavy haul locomotive main frame design (Manufactured by Electro-Motive Diesel, McCook, IL). 1 – side sills; 2 – centre beams; 3 – positions for secondary suspension springs; 4 – points for mounting cab isolators; 5 – engine mounting points; 6 – alternator mounting points; 7 – bottom plate of the main frame.

In the centre beam design, the main longitudinal beams, which react with all traction and braking loads, are located towards the centreline of the frame. In modern locomotives, it is common to use beams with T, I, rectangular or channel cross-sectional shapes, interconnected by transverse cross beams and bulkheads. At the ends of the main beams are the coupling boxes that contain the shock-absorbing devices of the automatic couplers. Centrally placed between the main beams, and longitudinally equidistant from the lateral centreline of the frame, are mounted pivot assemblies to support the frame on the bogies. Side sills are placed along opposite sides of the frame at both ends of the lateral beams. These are a lighter profile than the main beams, do not react longitudinal dynamic forces, and only provide support to the locomotive bodywork. In addition, the entire structure is fitted with top and/or bottom plates or sheets that have openings to allow technological equipment and ventilation ducts to pass through.

In the contour beam design approach, all traction and braking loads are reacted by external beams (primary beams) of the main frame. This design is very similar to a ladder-frame design, but with structural headstocks at each end of the locomotive providing the frame with a fully enclosed outer contour. Transverse beams (also called secondary beams) placed along the length of the frame are designed to be attachment points for the fixation of pivots, secondary suspension elements such as springs, or side bearings with return devices. Such frames are also covered with top and/or bottom plates as for the centre beam design.

In combined frames, loads and stresses are distributed to be taken by the outer and inner beams. In all three main frame types, cable conduits (channelling) can be installed internally along the main beams or other parts of the frame in order to accommodate the mounting of electric cables and wires, as well as piping lines for pneumatic air brake or hydraulic systems of the locomotive.

3.2 BOGIES

The bogie is one of main components of a heavy haul locomotive and usually consists of a frame that supports the locomotive car body through elastic dissipative ties or couplings (spring suspension elements; damping elements; stroke stops or bumpstops, which limit travel of the bogie frame with respect to the locomotive car body or frame; side bearings with roller return devices or other elastic-damping side bearing elements) as shown in Figure 3.9. The bogie frame is supported by journal housings (axle boxes) via elastic-damping elements, with the complete locomotive supported on the running rails through wheelsets connected to the journal housings by means of the bearings. The main purpose of the bogie is to improve the locomotive's dynamic interaction in the curved sections of track, to ensure the locomotive remains within its prescribed dynamic envelope, to maintain permissible dynamic forces between wheelsets and track, and to implement technical and economic specifications incorporated into the locomotive design during all real-world operational service scenarios.

The bogie frame also bears the loads from traction motors, traction gear mechanisms (suspended joints, drive shafts and gear boxes) and braking mechanisms. As a result, the choice of appropriate design characteristics for a bogie is a complex engineering task because it includes the selection of structural materials, work on

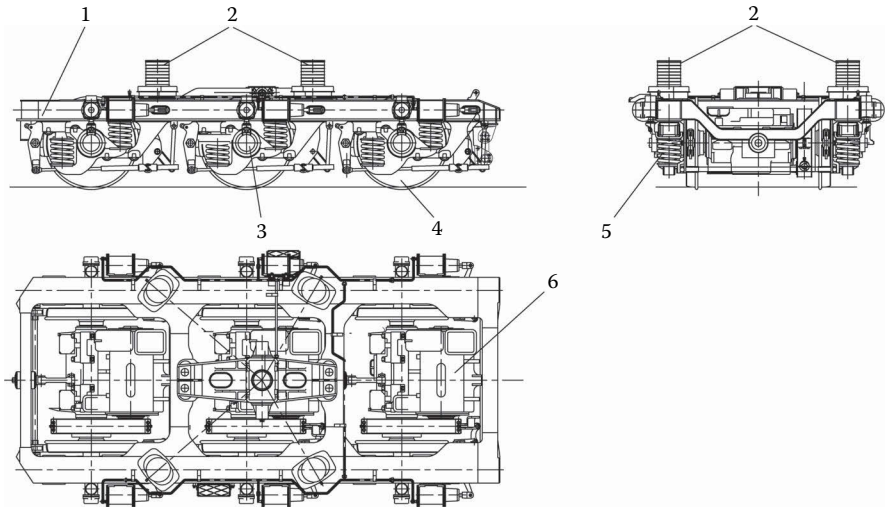

FIGURE 3.9 Three-axle bogie of a heavy haul diesel-electric locomotive (Manufactured by Lugansk Diesel Locomotive Plant, Lugansk, Ukraine). 1 – bogie frame; 2 – sideframe; 3 – journal housing; 4 – wheelset; 5 – coil spring; 6 – traction motor.

the layout of components, the calculation of the strength and load-bearing characteristics of the frame and the like.

The qualitatively and optimally designed bogie is based on correctly selected characteristics of spring suspension and traction drives, which are critically important parameters of the performance potential of a heavy haul locomotive.

The main indicators of the locomotive dynamic interaction with track, as well as implementation of traction and braking forces, are directly connected with proper and high-quality design of the mechanical parts of running gear. All the other locomotive systems only assist in achieving the specified design features when operating close to the extremes set by the design of the mechanical parts of the running gear. Therefore, engineers who design heavy haul locomotive running gear have to pay special attention to the quality of mechanical design solutions as these are the primary drivers of the ultimate performance of the bogie design.

3.2.1 Classification of Bogies

Bogies can be classified according to several criteria:

- By the number of wheel pairs enclosed in a frame. According to the UIC classification of locomotive axle arrangements, the axles within the same bogie (truck) are classified starting from the front end of the locomotive by alphabetical symbols for the number of consecutive driven axles (A for one, B for two, C for three etc.). Refer to Section 2.2 for more details. The three-axle and two-axle bogie designs shown in Figures 3.9 and 3.10 are the most common arrangements in use for heavy haul locomotives.

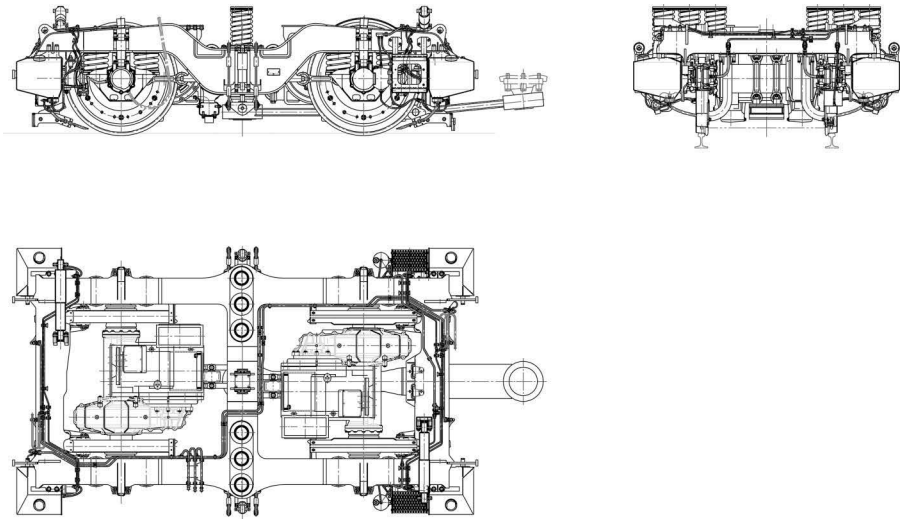

FIGURE 3.10 Two-axle bogie of a heavy haul electric locomotive (Manufactured by CRRC Zhuzhou Locomotive Company, Zhuzhou, China).

- According to the number of suspension stages used in the bogie:
  - Single-stage suspension, when the bogie frame and wheelset are connected with only one link (e.g., elastic-dissipative coupling) for each wheel
  - Double or two-stage suspension, when two levels of links are provided for each wheel
  - More stages are not usual with heavy haul locomotives
  - It is also necessary under this classification to consider the spatial orientation of these links; these usually are in the longitudinal (along the track in the direction of travel), lateral and vertical directions
- By the type of connection between an axle and a bogie frame:
  - Individual suspension, where each axle is connected to the bogie frame by its own set of elastic-damping elements. Figures 3.9 and 3.10 show bogies with individual suspension design
  - Balanced suspension, a design commonly used on older types of heavy haul locomotive, where the set of elastic-damping elements are grouped together using levers and balance beams
- By the type of suspension elements used in the bogie design:
  - Passive suspension, where uncontrolled elements such as leaf springs, coil springs, conical springs, elastic rubber elements, pneumatic or electromagnetic elements are used in the suspension design
  - Active suspension, where suspension elements have controlled characteristics, which may include several types of elastic elements and actuators that convert source (electrical, hydraulic etc.) energy into mechanical energy for providing the desired characteristics of the suspension element
- By the function of the axles in the bogie design:
  - Motorised axle, when driven by a traction motor

- Non-motorised axle, when the axle is used only to support the weight of a locomotive

- By the traction drive design:
  - Individual drive design, where the traction torque from the motor acts through a gear box on each axle. According to the UIC classification of locomotive axle arrangements, the use of a lower case 'o' as a suffix after the letter indicates that those motorised axles are individually driven by separate traction motors. However, this suffix is not used in the system for locomotive axle arrangements developed by the Association of American Railroads (AAR). Figures 3.9 and 3.10 show bogies with individual drive designs
  - Grouped drive design, where the traction torque from the motor or an output shaft of transmission is shared between multiple axles. This type of design is uncommon for heavy haul locomotives
- By the interconnection or separation of bogies used in a locomotive:
  - Articulated design, where a locomotive has articulated connections between two bogie frames in its bogie design; an example is shown in Figure 3.11. According to the system for locomotive axle arrangements developed by the AAR, a 'plus' sign indicates articulated connections being present in a locomotive design
  - Non-articulated design, where no articulated connection exists between bogies. This type of design is commonly in use for heavy haul locomotives. According to the system for locomotive axle arrangements developed by the AAR, a 'minus' sign is used to indicate the separation (non-articulation) of bogies

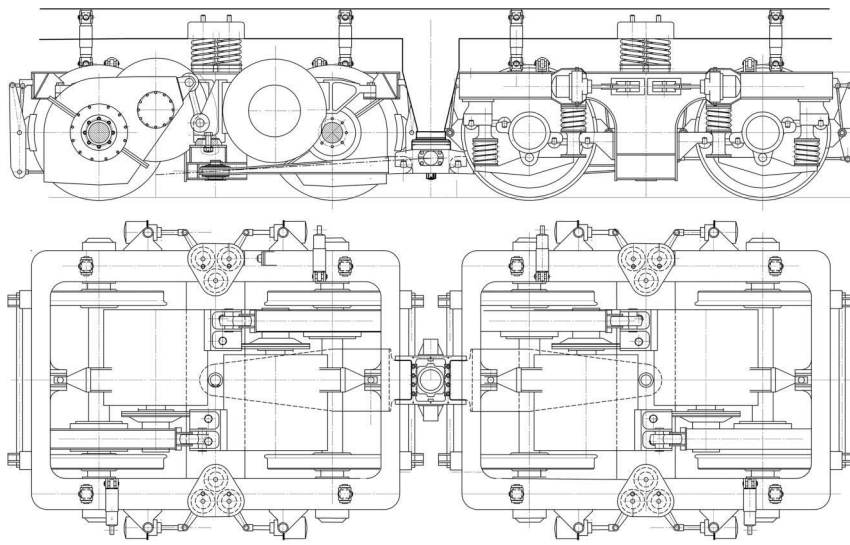

FIGURE 3.11 Four-axle bogie of a heavy haul diesel-electric locomotive (Manufactured by Lugansk Diesel Locomotive Plant, Lugansk, Ukraine).

- By the method of traction and braking force transmission from the bogie to the locomotive car body:
  - Through the pivot point
  - Through the traction rod(s)
- By the application of return mechanisms, which allows the return of the locomotive car body and the bogies to their central (original) position during operation on tangent track, and car body inclination and bogie rotation on curved sections of track
- By connection types between journal housings (axle boxes) and a bogie frame:
  - Connection with pedestal legs (also called a jaw connection)
  - Connection with cylindrical guides and a link arm (also called a traction rod)
  - Connection with radius links
- By traction motor mounting support designs:
  - Nose-suspended traction motor
  - Bogie-frame mounted traction motor
  - Axle hung suspended traction drive, which is uncommon for heavy haul locomotives, but was used on some freight electric locomotives
  - Body mounted traction motor which is uncommon for heavy haul locomotives
- By radial steering of wheelsets [2–4]:
  - Rigid bogie design
  - Semi-steering (yaw relaxation) bogie design
  - Self-steering bogie design
  - Forced steering bogie design

More detailed information and explanations on classification aspects is provided in Sections 3.2.2 through 3.2.4 which review and describe bogie design solutions and the major components used in such designs.

3.2.2 Bogie Frames

The bogie frame is the primary structural component of a bogie and must be designed to receive and transmit the forces of the weight of the car body and its installed equipment, the dynamic and impact loads from wheelsets resulting from interaction between wheels and track, and the forces from implementation of traction or braking efforts through elastic-damping suspension elements. To perform their function, the bogie frame and associated load-bearing elements must possess the necessary strength and durability to ensure that the geometric, deformation and deflection characteristics are able to be maintained as designed under all operational loading scenarios. An example of a typical bogie frame is shown in Figure 3.12.

The bogie frame commonly consists of two longitudinal beams interconnected by transverse cross beam(s). Common design variants for the positioning of transverse cross beam(s) for heavy haul locomotives are as follows:

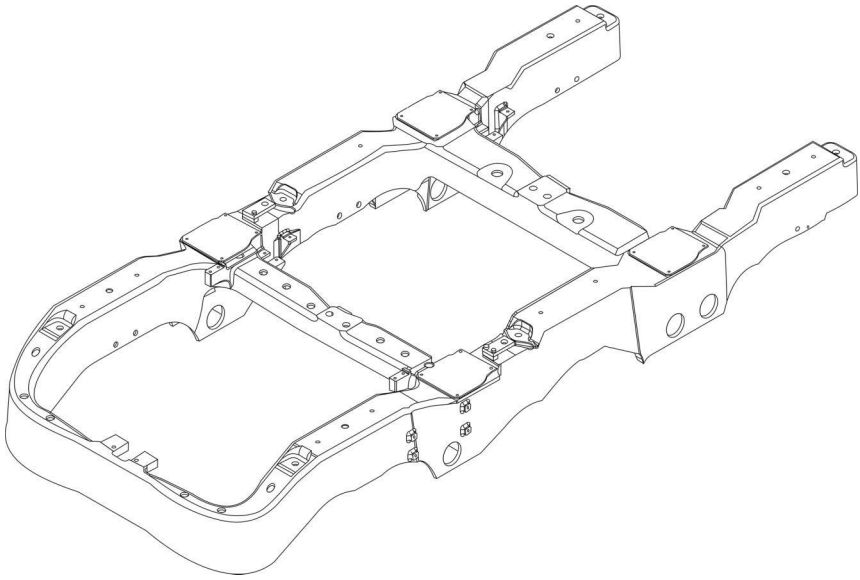

FIGURE 3.12 Bogie frame (Manufactured by Electro-Motive Diesel, McCook, IL).

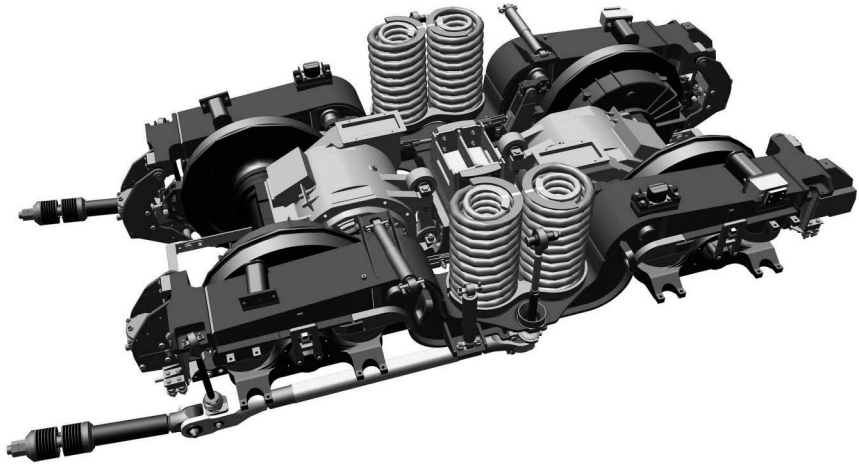

FIGURE 3.13 Two-axle bogie of an electric locomotive. (From © Siemens, AG, Graz, Austria. With permission.)

- One beam in the centre of a bogie frame. This type of design is also called an H-type bogie frame, and it is commonly used on two-axle bogies. An example of a bogie with such frame design is shown in Figure 3.13.
- One beam at the front and one or two in the middle of a bogie frame. Such a bogie frame, shown in Figure 3.12, is commonly used for two-axle or three-axle bogies. This type of design is also called a U-type bogie frame. Examples of bogies with such a bogie frame design are shown in Figures 3.14 and 3.15.

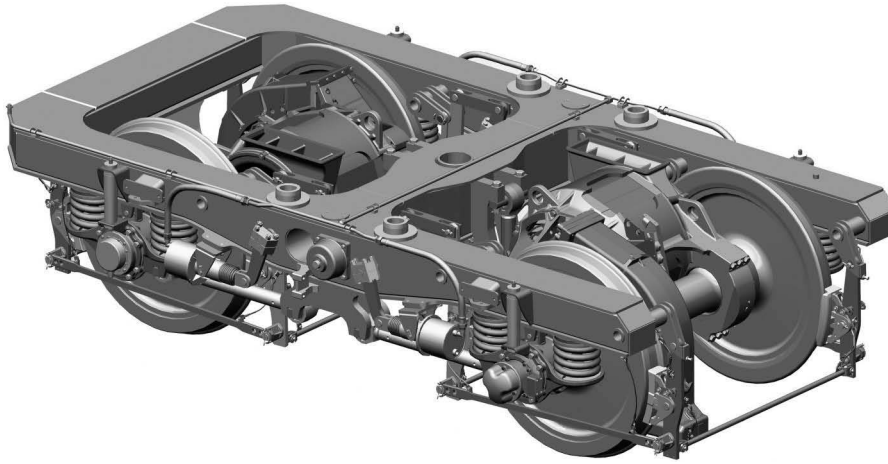

FIGURE 3.14 Two-axle bogie of an electric locomotive (Manufactured by Ural Locomotives, Yekaterinburg, Russia).

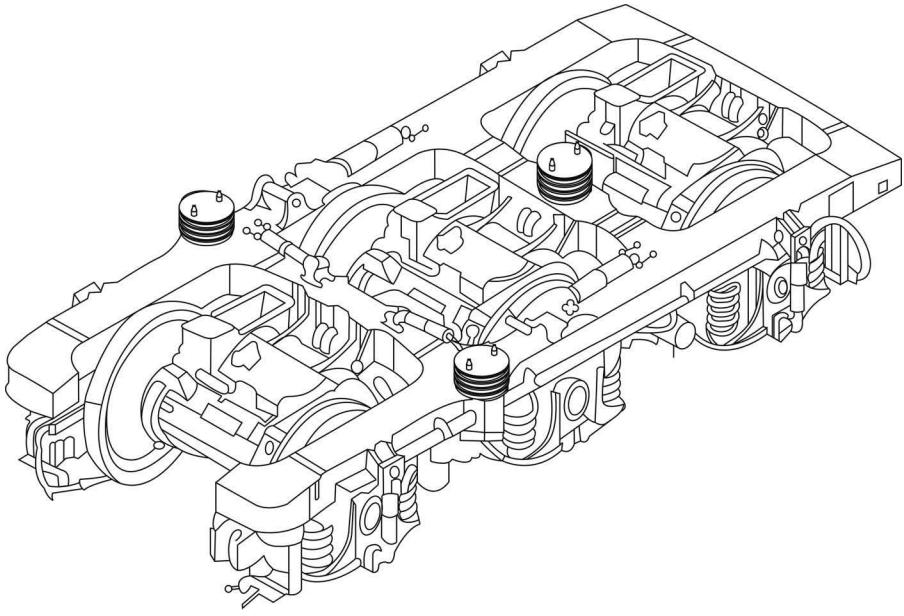

FIGURE 3.15 Three-axle bogie of a diesel-electric locomotive (Manufactured by United Group Limited, Newcastle, Australia).

- One beam at the front, one beam at the rear and one or two in the middle of a bogie frame. Such a bogie frame is commonly used for two-axle and three-axle bogies. Such a design is also called an O-type bogie frame design, and it can also be used for articulated bogies as shown in Figure 3.11. Examples of bogies with such a bogie frame design are shown in Figures 3.16 and 3.17.

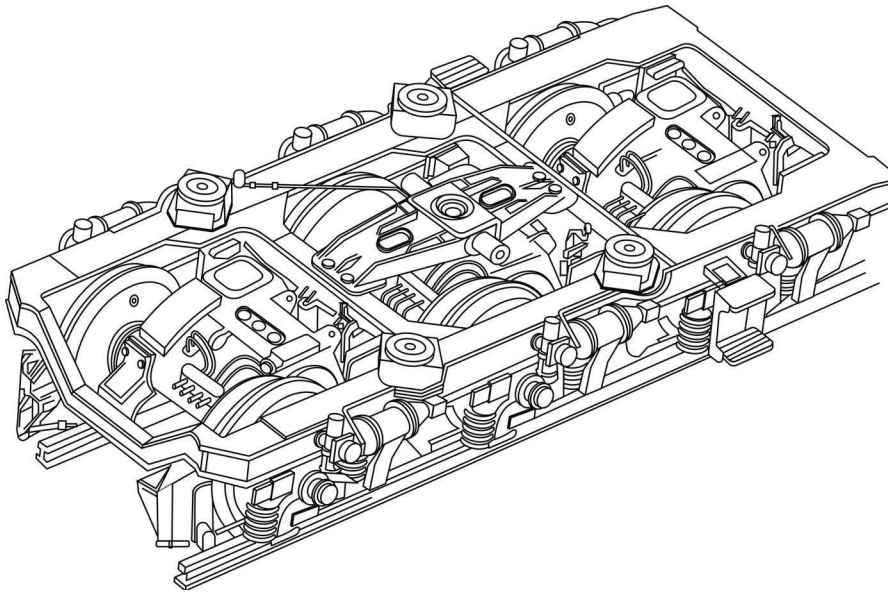

FIGURE 3.16 Three-axle bogie of a diesel-electric locomotive (Manufactured by Lugansk Diesel Locomotive Plant, Lugansk, Ukraine).

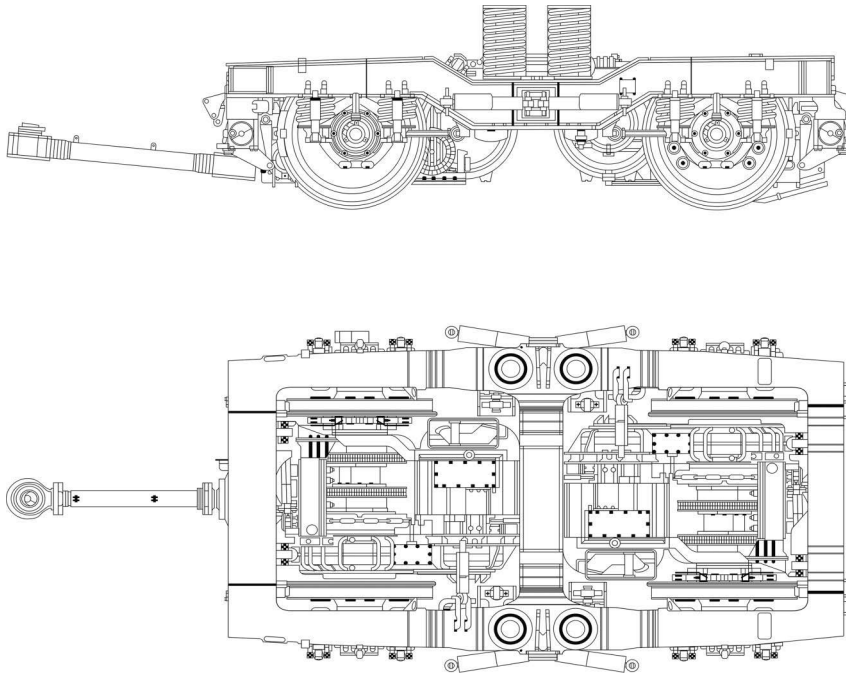

FIGURE 3.17 Two-axle bogie of an electric locomotive (Manufactured by Bombardier, Kassel, Germany).

Transverse cross beams are used to bear points of suspension for traction motors and gearboxes, as well as mounting pivot mechanisms and pivot beams.

Bogie frames can be manufactured using either a cast frame or a fabricated frame (welding of elements). Materials typically used for the construction of bogie frames are steels or alloys.

3.2.3 Wheelsets

The wheelsets are key elements of a bogie. The main functions of locomotive wheelsets are:

- Guidance of the locomotive along the track within the permissible kinematic envelope
- Transmission of traction and braking forces to the rails that allows the controlled acceleration or deceleration of the locomotive

An example of a typical locomotive wheelset is shown in Figure 3.18. Despite the variety of wheelset designs used on rail vehicles, the wheelset of a heavy haul locomotive bogie commonly consists of the following main components:

- Axle
- Two wheels
- Gear wheel

Locomotive axles are made from special high-quality steels that must meet the specified internal grain structure and density requirements since the axles operate under high rotary and torsional bending loads. There are special requirements for the machining of axle surfaces. In particular, the transitions between differing diameters of the axle required at the positions of journal bearing, gear wheel and wheel seats should be designed so as to minimise levels of stress concentration under the various forces acting on the axle. Axles also have centre holes at the ends as shown in Figure 3.18 to

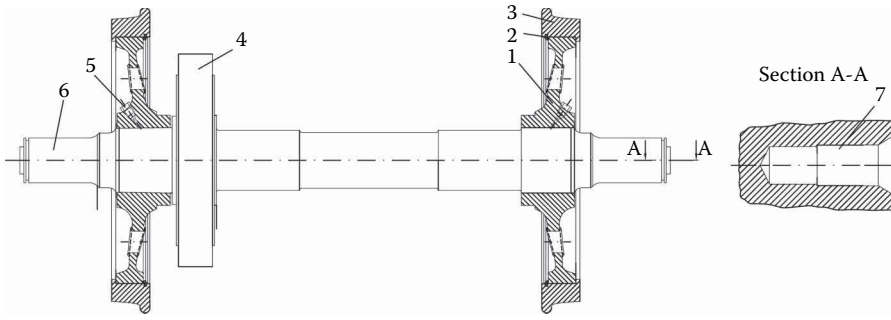

FIGURE 3.18 Example of a locomotive wheelset with tyre wheels. 1 – wheel disc; 2 – tyre ring; 3 – tyre; 4 – gear wheel; 5 – oil injection hole for assisting wheel press mounting and removal; 6 – axle; 7 – centre hole.

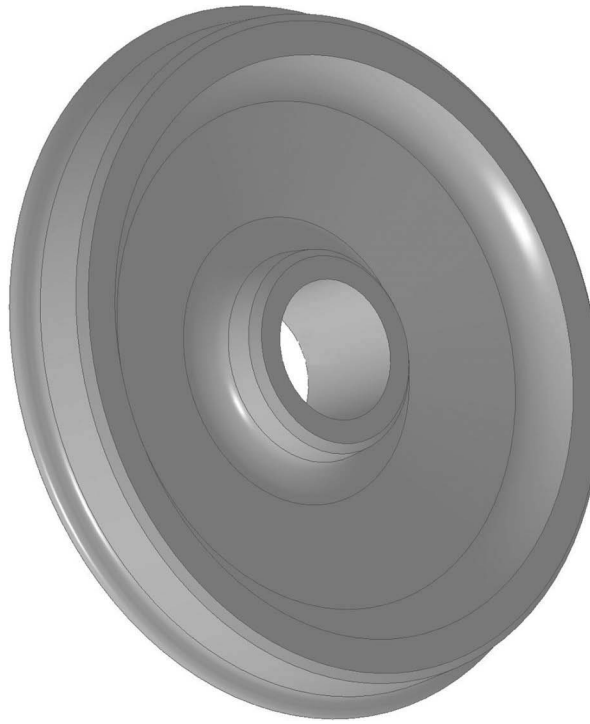

FIGURE 3.19 Example of a locomotive solid wheel.

facilitate manufacturing and maintenance operations (wheel press fitting, axle bearing installation and removal, re-establishment of wheel profiles in a lathe etc.).

Wheels are very critical components of the running gear and must provide exact geometrical and mechanical properties in order to minimise dynamic action and avoid derailments. During wheelset assembly, railway wheels are press-fitted onto the axle wheel seats. Two types of wheels are generally applied for heavy haul locomotives: tyre wheels (see Figure 3.18) and solid wheels (see Figure 3.19). In some cases, tyre wheels can incorporate a layer of low elasticity material in order to reduce wheel–rail interaction forces. However, this design is uncommon for heavy haul applications. All wheels can have different types of wheel tyres/discs in order to achieve desired construction and operational properties. Different profiles can be machined on wheel tread and flange surfaces in order to improve dynamic behaviour and interaction at the wheel–rail interface. Solid locomotive wheels can be classified according to the manufacturing methods as either wrought (forged) steel wheels or cast steel wheels.

Gear wheels are also press-fitted onto the axle wheel seats. Gear wheels are designed for the transmission of a traction torque received from the pinion of a traction motor to the axle. Various designs of spur gears can be used on heavy haul locomotives.

3.2.4 Journal Housings

Journal housings (axle boxes) are connected to the wheelsets by means of the bearings which enable the rotation of the wheelsets, and make possible the transfer of traction and braking efforts as well as vertical and lateral forces to the bogie frame via elastic-damping connections. In addition, the journal housings should provide for the reciprocating movements of the wheelset in the lateral direction of the horizontal plane (so-called free run), which are needed for optimal dynamics of the locomotive in curved sections of the track and the reduction of the dynamic interaction forces between wheels and rails.

Three types of journal housings are currently in use for heavy haul locomotives. These are classified by the design of their connection to the bogie frame using:

- Pedestal legs as shown in Figure 3.20
- A cylindrical guide and a link arm as shown in Figure 3.21
- Radius links as shown in Figure 3.22

The second and third designs are commonly used for the development of radial steering bogies which reduce the lateral forces in the curved sections. For wheelset

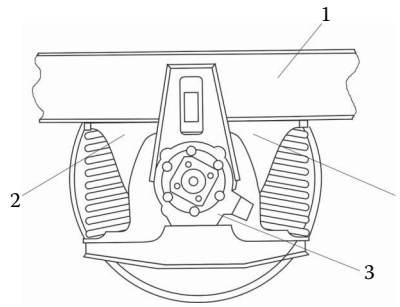

FIGURE 3.20 Journal housing with pedestal leg connection design (Manufactured by Goninan, Newcastle, Australia). 1 – bogie frame; 2 – pedestal legs; 3 – journal housing body.

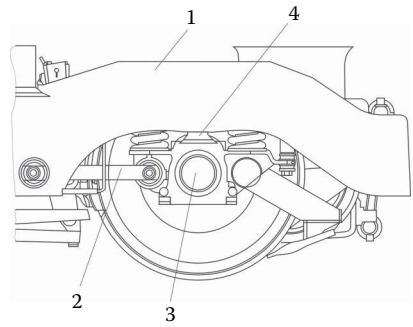

FIGURE 3.21 Journal housing connection with the usage of a cylindrical guide and a link arm (Manufactured by Electro-Motive Diesel, McCook, IL). 1 – bogie frame; 2 – link arm; 3 – journal housing body; 4 – cylindrical guide.

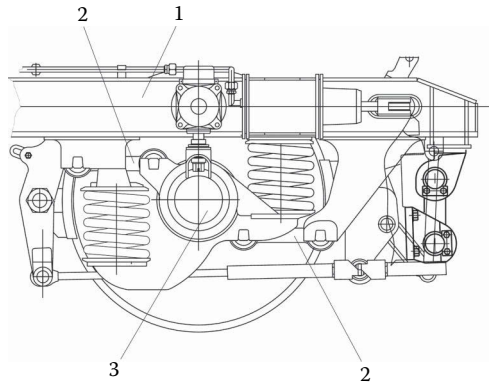

FIGURE 3.22 Journal housing connection with the usage of radius links (Manufactured by Lugansk Diesel Locomotive Plant, Lugansk, Ukraine). 1 – bogie frame; 2 – radius links; 3 – journal housing body.

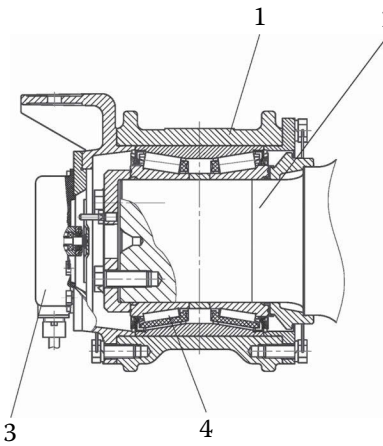

FIGURE 3.23 Journal bearing assembly (Manufactured by Ural Locomotives, Yekaterinburg, Russia). 1 – journal housing body; 2 – axle; 3 – tachometer; 4 – journal bearing assembly.

guidance in the longitudinal direction, the arms or links are fitted with rubber bushes that provide cushioning of the longitudinal thrust between journal housing and bogie frame.

Journal bearings on locomotives can be equipped with either cylindrical or conical roller type bearings. An example of a journal housing equipped with a bearing assembly is shown in Figure 3.23.

3.3 SUSPENSION

The need for the application of spring suspension on rail vehicles arises from the fact that the running rails and the track are not perfectly smooth and the rolling

wheels are also not perfect (tread surface irregularities, wheels not perfectly round, imbalance of mass and inertial forces etc.). Such irregularities lead to the resulting disturbing forces being transferred to locomotives.

In principle, if an ideal wheel rolling surface and an ideal track without any irregularities existed, the need for rail vehicles to be fitted with spring suspension would be eliminated due to the absence of perturbing forces acting on the running gear. However, there are no engineering and scientific solutions for the creation of the perfect track and the perfect wheel. Therefore, the design of locomotives went in the direction of the creation of spring suspension systems that can compensate or reduce the impact arising from the rolling of an imperfect wheel on an imperfect rail track. The aim of these systems is to provide optimal performance by achieving values of ride quality and other parameters as close as possible to the locomotive design solutions. These parameters concern equalising the distribution of weight loads between the wheels, minimising the dynamic forces caused by the interaction between wheels and rails, realising the maximum possible tractive and brake efforts for the locomotive/s to haul and control the largest possible train, and also minimise and damp the dynamic forces and natural oscillations received from the train under traction and braking. In addition, the suspension design should create safe and comfortable working conditions for the locomotive crew and minimise adverse impacts on the equipment placed on the locomotive.

3.3.1 Classification of Suspension Designs and Associated Elements

Heavy haul locomotive suspension is commonly designed to perform in one or two stages (primary and secondary), and acting in the horizontal, vertical and transverse planes.

The primary suspension is usually located at the connection points of journal housings with their bogie frame, but it can also be located inside the wheelset or the wheels (so-called elastic or resilient wheels). The latter design is uncommon for existing heavy haul locomotives, but was studied for some experimental prototypes. The secondary suspension is commonly located at the connection points of bogie frames with the locomotive car body, but it may also be incorporated between various elements of the bogie itself.

Suspension systems of rail vehicles can include the following:

- Elastic elements that have stiffness, with their deformation being dependent on the external force applied, and their task being to allow controlled reciprocating movement of elements of running gear under the force loads and under oscillations arising therefrom.
- Damping elements and shock-absorbing devices have damping properties and are used to absorb vibration energy and reciprocating movement of elements of running gear.
- Elastic-damping elements have combined properties of elastic and damping elements.

The main characteristics of the suspension system are the deflection and damping values for each of the stages and planes as defined by:

- Displacements of elements:
  - Static displacement under the action of the static weight of the vehicle
  - Maximum displacement, which is limited by the maximum mutual displacement of suspension elements and by the need to remain clear of the railway structure gauge (which allows a safe amount of clearance outside the locomotive swept envelope as discussed in Section 2.2) under static or dynamic loading conditions
- Damping coefficients for each of the stages which show the rate of damping of oscillations of the elements of running gear.

If the set of elastic-damping elements are connected to each axle or journal housing of a bogie individually, such a suspension is called an individual suspension. An example of such a suspension system is shown in Figure 3.24. If the sets of elastic-damping elements for two or more axles are grouped together using levers and balance beams or joint leaf springs, the suspension is said to be a balanced suspension. An example of such a suspension system is shown in Figure 3.25. To ensure uniform redistribution of loads between locomotive axles and wheels, a combination of the elastic elements in groups is widely used. In this case, one group can be considered a point of suspension. Therefore, it is possible to add one more characteristic to suspension classification, this being the number of 'points of suspension'. Although the balanced suspension is not in use for modern locomotives, it is present in some older heavy haul locomotives that are still in operational service.

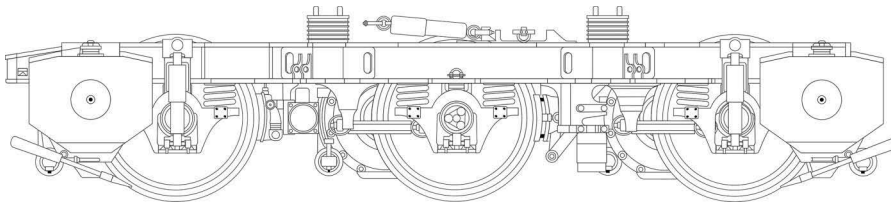

FIGURE 3.24 Three-axle bogie with individual suspension (Manufactured by United Group Limited, Newcastle, Australia).

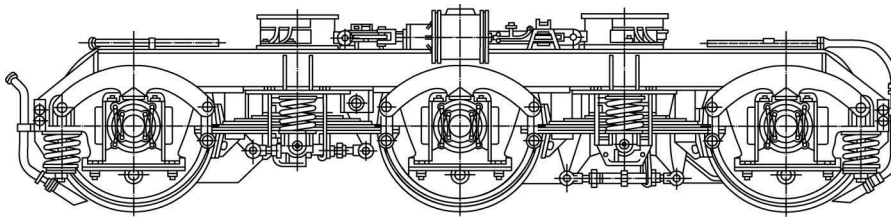

FIGURE 3.25 Three-axle bogie with balanced suspension (Manufactured by Lugansk Diesel Locomotive Plant, Lugansk, Ukraine).

The main elements supporting the locomotive car body and bogie frames are leaf springs, coil springs, rubber and rubber-metallic elements, elastomers, pneumatic elements and hydraulic cylinders. Each of these elements has different elastic-damping properties, but all have a load characteristic (dependence of the deformation of the element on the external force applied). In addition, the elastic suspension elements have damping properties defined by a characteristic shape of the applied force versus deformation curves for load and unload cycles. In some cases, when the load is removed from these elastic-damping suspension elements, the element may not return to its original size or state, resulting in permanent deformation, which is also characteristic of elastic-damping elements. One more important characteristic of elastic-damping elements is the potential need for changing the values of stiffness and damping properties under different ambient temperatures, operating time periods or number of loading cycles. All locomotives with passive suspension are equipped with these suspension elements, which are also called conventional suspension elements.

Any suspension system equipped with a control system is called an active suspension. For such a system, the suspension not only includes conventional elements, but also special devices (actuators) that generate control efforts. Actuators can be classified by their principles of work as follows:

- Hydraulic
- Mechanical
- Pneumatic
- Electric and electro-dynamic
- Magnetic and magneto-dynamic
- Complex or combined

In modern heavy haul locomotives, such actuators might be used for wheelset steering purposes or to facilitate re-distribution of wheel loads. The next Sections 3.3.1.1 through 3.3.1.5 discuss the conventional elements used in the design of heavy haul locomotive suspensions.

3.3.1.1 Leaf Springs

Leaf springs are one of the common elements of the suspension of rail vehicles and have both stiffness and damping properties. An example of a bogie with leaf springs in its primary suspension is shown in Figure 3.25. Stiffness characteristics of leaf springs provide resistance forces from metal leaves, and spring flexibility is dependent on the number and thickness of the leaves and their length. All leaves in the spring are covered with spring clamps that limit the relative movement between the leaves in the transverse direction. Disadvantages of leaf springs are their large specific gravity in comparison with other elastic elements, complicated manufacturing process and their poor repairability, as well as inconsistent damping characteristics due to variation in the friction force between the leaves. Leaf suspension designs were commonly in use on older types of locomotives, but are not used on modern heavy haul locomotives.

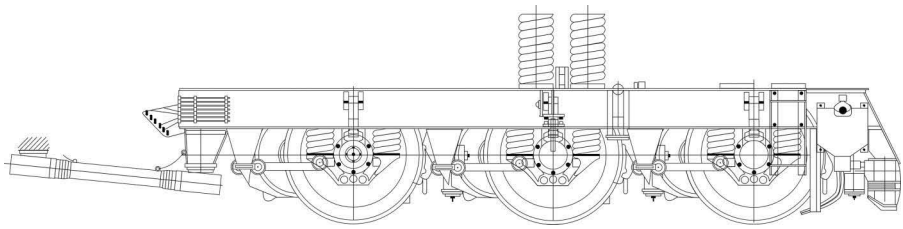

FIGURE 3.26 Helical spring suspension design of a heavy haul locomotive (Manufactured by Bombardier, Kassel, Germany).

3.3.1.2 Helical (Coil) Springs

Suspensions on helical springs, also known as coil springs, have currently found wide application because of their light weight and their ability to work as a vertical spring as well as in the transverse plane. It is common practice to use such springs in locomotive primary suspensions. However, the property of these springs to act in the transverse plane is often used in the secondary suspension. Such suspension is also called 'flexi-coil suspension'. An example of the usage of helical springs in both stages of a locomotive suspension is shown in Figure 3.26.

In order to increase the stiffness of helical springs, they can be combined into sets. Obtaining non-linear stiffness characteristics is also possible through the use of steel wire with variable cross-sectional diameters along the length, as well as varying the diameter and shape of the spring.

3.3.1.3 Air Springs

Air (pneumatic) spring suspension is currently one of the sought-after elements of suspension systems because its elastic characteristics can be adjusted under certain loads and operating conditions, along with the ability for load transfer between the elements of the running gear. A typical air spring suspension system consists of the following elements: air springs, connecting pipes, the levelling valve, an additional reservoir, differential pressure and safety valve. An additional elastic element is installed inside the air spring in order to prevent suspension collapse and allow the vehicle to reach a place of repair in cases of failure of the rubber-shell or air feed line.

Changes of the stiffness characteristics are performed by the adjustment of air pressure and temperature parameters. Damping characteristics can be changed by adjusting the size of the additional reservoir and the flow capacity of the pressure valve. Typically, air suspension is used in the secondary suspension because it is more effective in absorbing low-frequency oscillations.

Air suspension can have several air springs connected in the loop and several additional air reservoirs. Air springs can also operate in pairs without the application of an additional reservoir.

The advantages of air suspension are the possibility of varying the stiffness and damping characteristics as well as low weight. The disadvantages are the additional energy costs for feeding air to them and filtering the air, and more expensive maintenance and increased cost in comparison with coil and leaf springs.

It is uncommon to use air springs in suspension designs of heavy haul locomotives, but it has a potential major benefit in terms of controlling axle load distributions that may improve the dynamic performance. An example of the investigation of air springs in the secondary suspension of a heavy haul locomotive is presented in Section 7.8.

3.3.1.4 Rubber and Elastomer Springs

The application of rubber and elastomer materials to create elastic-damping suspension elements in modern locomotives is a quite common design solution. Polymer and rubber materials have high absorption properties for damping of vibration energy, and they can also provide high cushioning characteristics by means of their enhanced properties of elasticity. However, because of low strength characteristics and poor thermal conductivity, these materials have to be reinforced with metal or carbon fibre components. Another disadvantage of these elements is their change in stiffness and plastic properties under varying temperature conditions found in operational service, and the loss of their ability to maintain their original form (permanent plastic deformation). However, these problems may be resolved as the modern chemical industry is constantly improving the manufacturing techniques and the chemical composition of rubber and polymeric materials. Additionally, there are some difficulties in terms of the large variations of stiffness parameters that require a detailed selection of such spring elements for a locomotive in order to provide the required level of deviation characteristics in the running gear design, which results in the need for additional testing of each element during the manufacturing process.

However, all of the above shortcomings are more than compensated for by the low manufacturing and operating costs for rubber and polymer elements, their low weight characteristics and the positive effects on damping and vibration. An example of the usage of rubber conical springs in a locomotive primary suspension is shown in Figure 3.27. An example of the application of rubber springs in a secondary suspension is shown in Figure 3.28.

3.3.1.5 Dampers

Damping and absorbing devices are classified by the type of working fluid used in them or by the physical process that creates an absorbing effort.

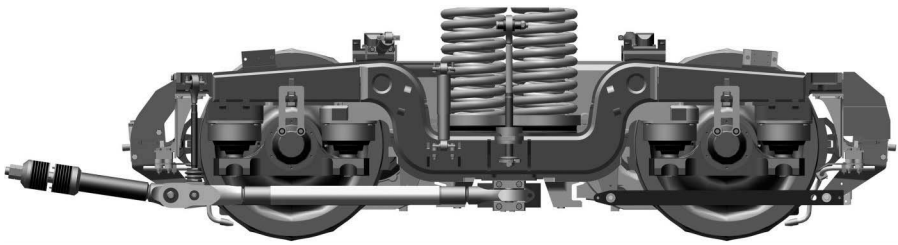

FIGURE 3.27 Two-axle bogie of an electric locomotive with rubber conical spring in primary suspension. (From © Siemens, AG, Graz, Austria. With permission.)

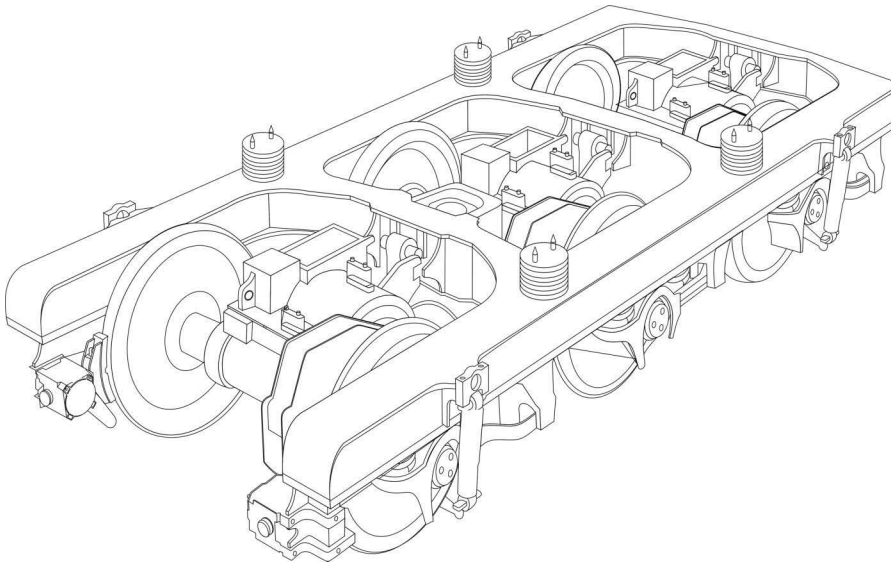

FIGURE 3.28 Three-axle bogie with rubber elements in secondary suspension (Manufactured by United Group Limited, Newcastle, Australia).

Dry friction dampers may be designed with a translational characteristic in which a damping force is generated due to a friction process between the piston and the cylinder (their mutual displacement), or be of a torsional type where the damping force is created by the friction between two or more disks, one of which has a rotational motion associated with a torsion arm actuated by motion of movable elements of the running gear. To ensure constancy of the friction process in such dampers, compensation has to be made for wear; special mechanisms are used which usually consist of spring elements and tensioners.

These types of dampers are sometimes used in the primary suspension, but can give problems due to the inconsistency of their characteristics and the initial force required for displacement, which can lead to locking of the spring suspension. During servicing of such rail vehicles, it is necessary to monitor the tightness of the friction elements. The advantages are the simplicity of design and the low cost of manufacturing.

Hydraulic dampers (shock absorbers) for damping and absorbing of vibration use the viscous properties of liquids. They usually consist of a cylinder in which a rod, with a piston that has holes drilled in it, is inserted. This makes it possible for the fluid to flow from one chamber of the cylinder to another. Flow can also be carried out through channels in the cylinder walls. These dampers have stable damping characteristics for low-frequency vibrations, but they are very sensitive to high frequencies because the latter is associated with liquid cavitation processes and hydraulic impact. The performance of these dampers is significantly affected by the ambient temperature and the temperature of their fluid. This type of damper is often installed in secondary suspensions.

Gas shock absorbers are filled with gas under high pressure and work on the same principle as hydraulic dampers. However, they do not have the disadvantages associated with the liquid flow process, and can therefore be used in primary suspensions.

Rubber dampers or rubber-absorbing elements act based on the damping properties of rubber. To increase the stiffness and strength characteristics of the rubber elements, they are covered and reinforced with metal or composite materials, fabrics and fibres. They can be used in primary and secondary suspensions.

Combined dampers integrate several types of dampers mentioned above. Among them, for example, are gas-hydraulic dampers that find wide application. Such dampers are also used in primary suspensions.

3.3.2 Primary Suspension

The main objective of the primary suspension is the damping of high-frequency oscillations arising due to force interaction between the rolling wheels and the rails, preventing their transfer to the locomotive car body and the bogie frame, as well as damping of vibration of the car body itself and reducing its impact on the force interaction between wheel and rail. In addition, the elements of the primary suspension may balance and redistribute the load between the wheels or wheelsets in the bogie. Typically, the static deflection of the primary suspension is 30%–40% of the total suspension deflection of a locomotive. Given these high frequency and low deflection characteristics, primary suspensions are able to utilise elastic elements such as coil springs, leaf springs or rubber elements. For this purpose, the dampers have inserts made from rubber or polymeric materials because these materials have high energy-absorption capacity. The low-frequency part of the oscillation spectrum is absorbed by hydraulic or friction dampers.

An example of the usage of coil springs and hydraulic dampers in the primary suspension of a two-axle bogie is shown in Figure 3.29. An example of the usage of coil springs and a friction damper is shown in Figure 3.22.

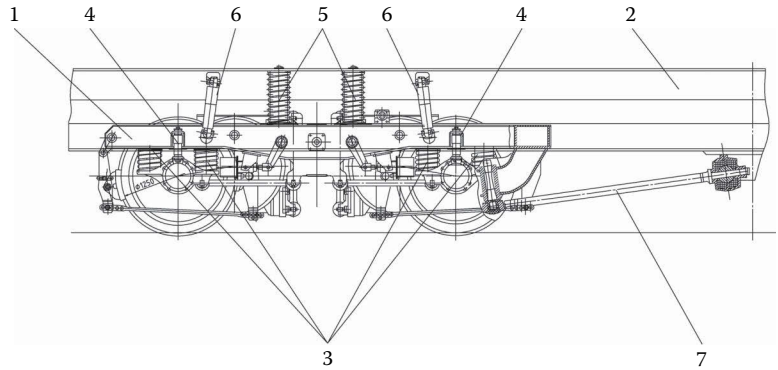

FIGURE 3.29 Suspension system of a two-axle bogie and its connection to locomotive frame (Manufactured by Ural Locomotives, Yekaterinburg, Russia). 1 – bogie frame; 2 – locomotive main frame; 3 – primary suspension coil springs; 4 – primary suspension dampers; 5 – secondary suspension 'flexi-coil' springs; 6 – secondary suspension dampers; 7 – traction rod.

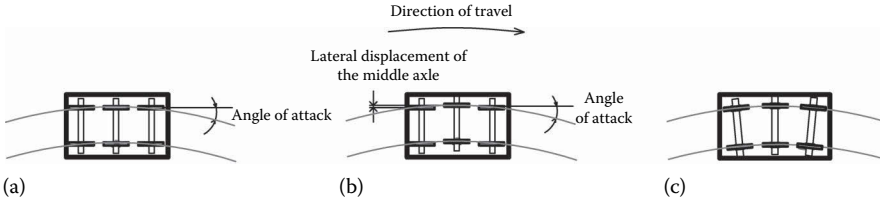

FIGURE 3.30 Conventional and steering bogies during curving: (a) conventional bogie, (b) conventional bogie with floating middle axle, and (c) steering bogie.

The conventional bogie, which is also called a rigid bogie, has some clearances provided in its primary suspension design in order to improve dynamic interaction between wheels and rails that allows small displacements of wheelsets, resulting in reduced cornering forces. However, for better dynamic performance and significant wear reduction, it is desirable to reduce wheelset angles of attack in curved sections of track as shown in Figure 3.30. For this purpose, steering of the wheelsets within a bogie is a good solution. Presently, four typical bogie designs can be used on heavy haul locomotives [2,3]:

- Rigid frame
- Semi-steering or yaw relaxation
- Self-steering
- Forced steering

The control methods, which allow for provision of steering, can be divided into three main groups [4]:

- Acting by means of wheel-rail contact forces
- Acting by means of centrifugal forces
- Acting by means of application of external forces

The semi-steering and self-steering designs are generally achieved by applying elastomeric bushes or by modifying kinematical mechanisms in the primary suspension design that allows elements to work in several planes and makes the primary suspension more flexible and adjustable under the action of wheel-rail contact or centrifugal forces. By contrast, the forced steering designs only work under the application of external forces. Some attempts have been made to implement the latter design in prototypes, but it is still uncommon in routine heavy haul operations. Examples of the orientation of wheelsets of various types of three-axle bogie designs during curving are shown in Figure 3.31.

3.3.3 Secondary Suspension

The secondary suspension is located between a locomotive's main frame and its bogies and is designed for supporting the locomotive car body on the bogie frames and absorbing the vertical deflection. Typically, the static deflection of the secondary suspension is 60%–70% of the total suspension deflection of a locomotive. In addition,

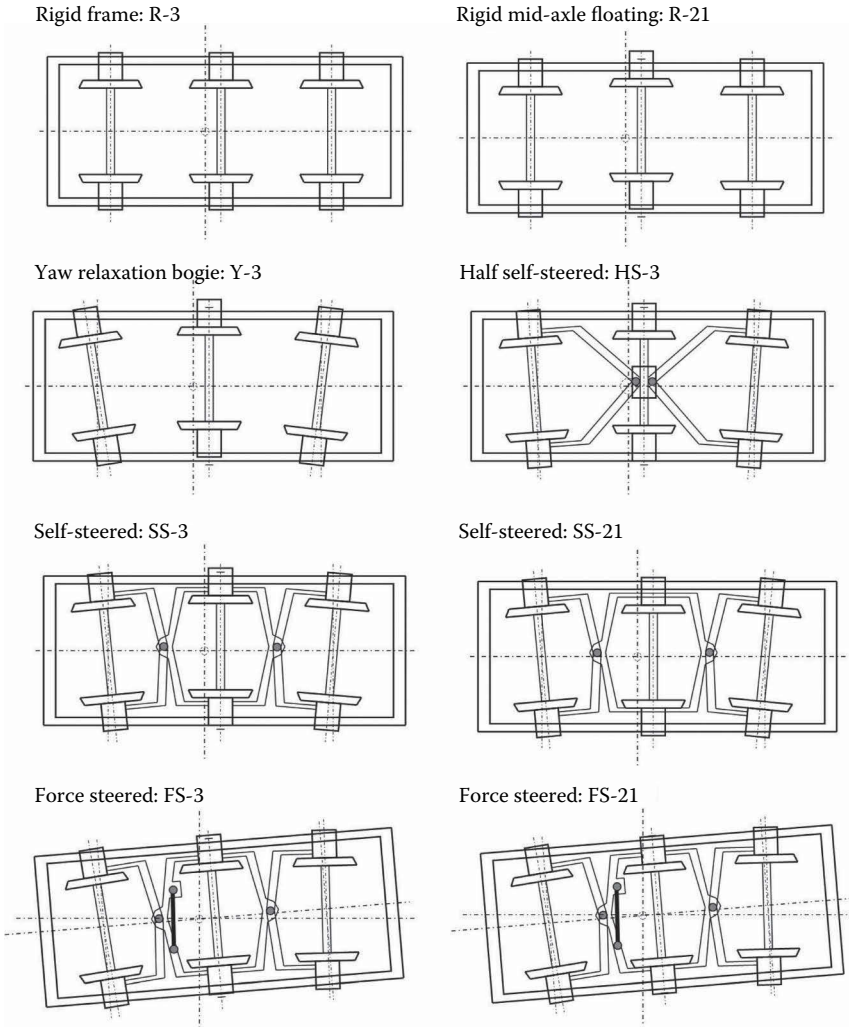

FIGURE 3.31 Examples of wheelset orientation of various three-axle bogie designs during curving. (From Simson, S., Three axle locomotive bogie steering, simulation of powered curving performance: Passive and active steering bogies, PhD Thesis, Central Queensland University, Rockhampton, Queensland, Australia, 2009. With permission.)

the elements of secondary suspension make possible rotations and displacements of bogies relative to the car body within the prescribed limits and their return to the initial position. The secondary suspension elements include

- Springs
- Side bearers
- Dampers
- Actuators

Any of the spring elements described earlier in Sections 3.3.1.2 and 3.3.1.3 can be used in the secondary suspension. However, by analysing existing designs with an application of such elements, it is possible to state that 'flexi-coil' suspensions have found the most widespread application in designs of modern heavy haul locomotives. An example of such a suspension design is shown in Figure 3.29.

Side bearers are designated to transfer vertical loads from the car body onto the bogie frames. In addition, they should provide the ability for bogies to rotate relative to the car body and allow movements in all planes within the prescribed limits. In addition, the side bearers can generate return moments and reduce hunting oscillations of bogies, as well as provide a tilting motion of the car body when the locomotive operates in the curved sections of the track.

At the present time, commonly used types of side bearers are [1]

- *Side bearer pads (rubber springs)* – an example of their application is shown in Figure 3.32, where metal plates are present inside the rubber springs to separate the rubber layers, and the edges of the metal plates are covered in rubber to avoid corrosion.
- *Side bearers with return devices* – an example is depicted in Figure 3.33, the concept being that the side bearer can have rubber or coil spring(s) and even an air spring at the top, while it has rollers which operate in their nest with a lubricant at the bottom, the advantages being low coefficients of friction and the ability to get different values of return moments.

The dampers used in the secondary suspension designs are commonly hydraulic dampers, as described in Section 3.3.1.5, which are generally needed to damp

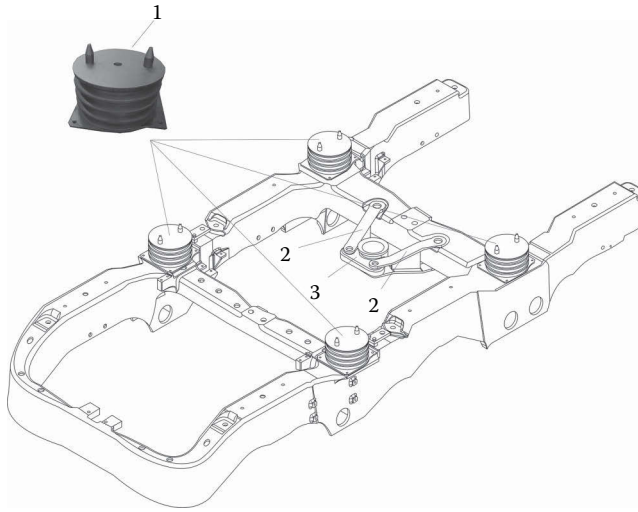

FIGURE 3.32 Secondary suspension and traction transfer elements mounted on the bogie frame (Manufactured by Electro-Motive Diesel, McCook, IL). 1 – side bearing; 2 – yoke; 3 – traction rod.

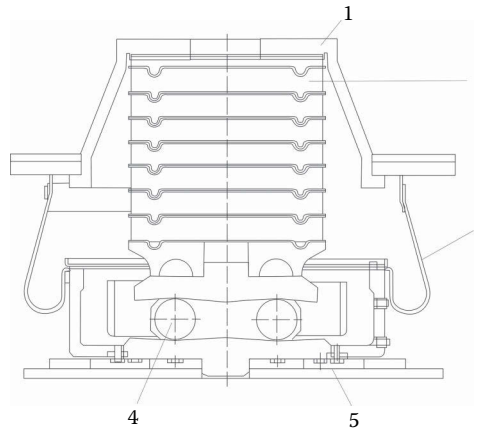

FIGURE 3.33 Side bearer with roller return device (Manufactured by Lugansk Diesel Locomotive Plant, Lugansk, Ukraine). 1 – top plate connected to an underframe; 2 – rubber elements; 3 – dust cover; 4 – roller; 5 – base plate connected to a bogie frame. (From Spiryagin, M. et al., *Design and Simulation of Rail Vehicles, Ground Vehicle Engineering Series*, CRC Press, Boca Raton, FL, 2014.)

vertical and lateral movements. The dampers working in the vertical direction are applied to achieve the required ride comfort. Meanwhile, the dampers for the lateral direction are needed to improve stability and guidance at higher operational speeds.

Actuators can be used in secondary suspension designs for the improvement of weight distribution/utilisation by a heavy haul locomotive in order to realise maximum possible tractive efforts. Mechanical optimisation of the secondary suspension is not a very attractive option in such cases because it can only be optimised for some specific tasks when travelling over tracks with specific characteristics. In order to get more universal results, it seems very reasonable to work on the characteristics of the secondary suspension and to use an active spring suspension instead of a conventional design. This means that hydraulic or air actuators can be mounted between the main frame and bogies, either to act in conjunction with other suspension elements (e.g., springs or side bearings) or singly (adjustable air springs). However, at the present time, this direction requires further research for progressing future design solutions.

3.4 DESIGN COMPONENTS FOR TRANSMISSION OF TRACTION AND BRAKING FORCES BETWEEN A LOCOMOTIVE FRAME AND BOGIES

On heavy haul locomotives, these components include pivot assemblies and traction rods.

3.4.1 Pivot Assemblies

Such assemblies are used to transmit traction and braking forces from the bogie to the car body or the main frame of the locomotive. The pivot assembly is also the

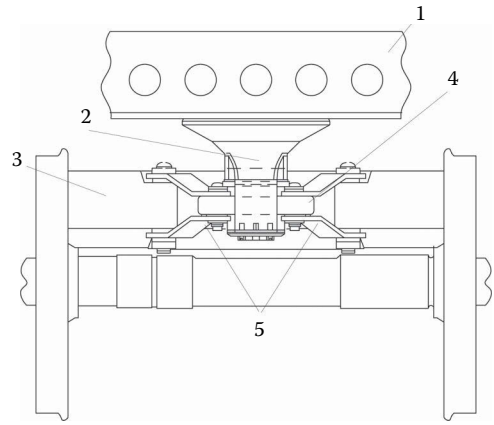

FIGURE 3.34 Example of pivot assembly (Manufactured by Electro-Motive Diesel, McCook, IL). 1 – main frame; 2 – pivot pin; 3 – bogie frame; 4 – yoke; 5 – traction rod.

point about which a bogie undergoes rotational movement in the horizontal plane relative to the car body. An example of a pivot assembly is shown in Figure 3.34.

Pivot assemblies can be divided into two types characterised by their position relative to the centre of the wheelset axles in the horizontal plane:

- *High location of the pivot point* – in this case, the force transmitted from the bogie to the car body is at a point that is located higher than the centre of the wheelset axles in the horizontal plane. Examples of such a design solution for bogies are shown in Figures 3.9 and 3.14.
- *Low location of the pivot point* – in this case, the force transmitted from the bogie to the car body is at a point which is located below the centre of the wheelset axles in the horizontal plane. An example of such a design solution for an articulated bogie is shown in Figure 3.11.

A higher value of tractive and brake efforts can be achieved by a locomotive that has pivot assemblies with low pivot point locations in comparison with a locomotive which has the same design and configuration, but with high pivot points.

Pivot assemblies of locomotives can have a rigid design when the bogie can perform a translational motion in the vertical plane and a rotation in the horizontal plane. In addition, pivot assemblies can be designed with additional gaps that allow some small motion in the horizontal plane transverse to the longitudinal axis of the locomotive.

Pivot assemblies with spherical joints allow the bogie to carry out rotational movement within specified limits with respect to all planes. In addition, these can have movement in the vertical plane and partial displacement in the horizontal plane.

From the design point of view, the pivot assembly can consist of a pin rigidly fixed to the main frame or car body of the locomotive on one end, while, on the other end, a pin is inserted in the pivot yoke which is fixed to the frame of the bogie (Figure 3.14) or the bolster (Figure 3.16).

The advantages of rigid pivot assemblies are the simplicity of their design and low cost of manufacturing. Pivot assemblies, which allow lateral motions, have better dynamics in comparison with rigid joints. Furthermore, pivot assemblies with spherical joints can provide improved dynamic behaviour for a locomotive in comparison to other existing designs.

3.4.2 Traction Rods

Traction rods are used to transfer traction and braking efforts. Examples of the usage of traction rods for the connection of the pivot assembly are shown in Figures 3.32 and 3.34. When a powered rail vehicle is not equipped with pivot assemblies, as shown in Figure 3.29, then traction rods can directly connect a locomotive car body and a bogie.

For damping of oscillations caused by traction and braking forces, traction rods can be equipped with absorbing devices; most often in such cases, rubber and rubber-metal elements or bushings have found wide application.

3.5 ELECTRIC TRACTION DRIVES

Electric traction drives are designated for transferring kinematic power from the traction motors to the wheelsets of a heavy haul locomotive. Such drives are usually represented as a part of the wheelset assemblies, which include the following components:

- Traction motor
- Gear box
- Wheelset

The design and parameters of traction drives are often dependent on the installation designs of traction motors and associated gearing. As mentioned earlier in the discussion of bogie classification (see Section 3.2.1), two design variants are common for heavy haul locomotives:

- With a nose-suspended traction motor
- With a bogie frame-mounted traction motor

The nose-suspended traction motor design is most commonly used for heavy haul locomotives. Torque from the motor is transmitted to the gear box, from the pinion mounted at the end of the rotor to the driven gear wheel which is seated firmly on the axle. This enables the effective transfer of high tractive effort. However, about 60% of the weight of the traction motor and the traction drive account for unsprung mass with the nose suspended design; this causes increased dynamic effects of the locomotive on the track. This drive is the most simple in terms of design concept and service, but has poor dynamic performance in view of the large weight distributed as unsprung mass.

The design with a bogie frame-mounted traction motor can also be used for heavy haul locomotives. The traction motor is directly connected to the bogie frame. The traction drive has one side mounted on the axle and the other side commonly uses a nose-suspended suspension approach. The axle receives a torque through mobile and flexible connection elements that provide the necessary freedom of movement of the wheelset or the wheels relative to the traction motor. In this case, unsprung weight is sharply reduced and this improves the dynamic performance of locomotives. However, such a design may have an adverse effect on the rotor life of the traction motor.

An example of a nose-suspended traction motor design is shown in Figure 3.35, and an example of the application of a flexible coupling in a traction drive with a bogie frame-mounted traction motor is shown in Figure 3.36.

The design of traction drives can also be classified by the number of gear boxes installed in the system. This can be one (as shown in Figure 3.35) or two gear coupling used per one traction motor and per axle. The example of a two gear box design is shown in Figure 3.37.

One of the main characteristics of gear boxes is the gear ratio, which also a main characteristic in locomotives as described in Chapter 2.

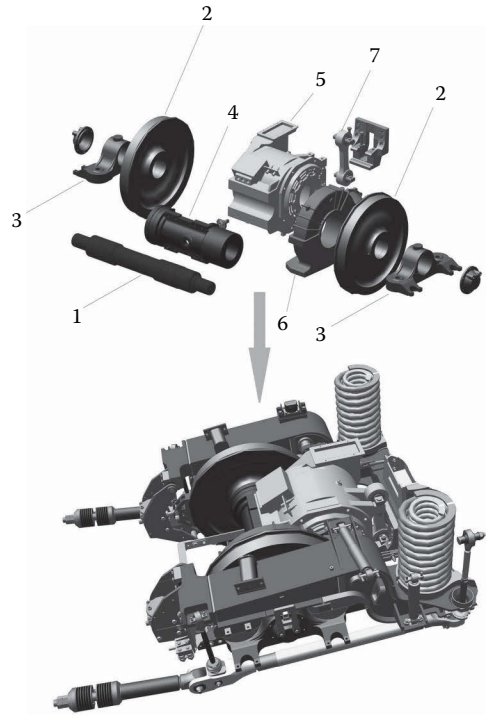

FIGURE 3.35 Example of a nose suspended traction motor design. 1 – axle; 2 – wheels; 3 – journal housing; 4 – tube assembly; 5 – traction motor; 6 – gearbox assembly; 7 – dog bone. (From © Siemens AG, Graz, Austria. With permission.)

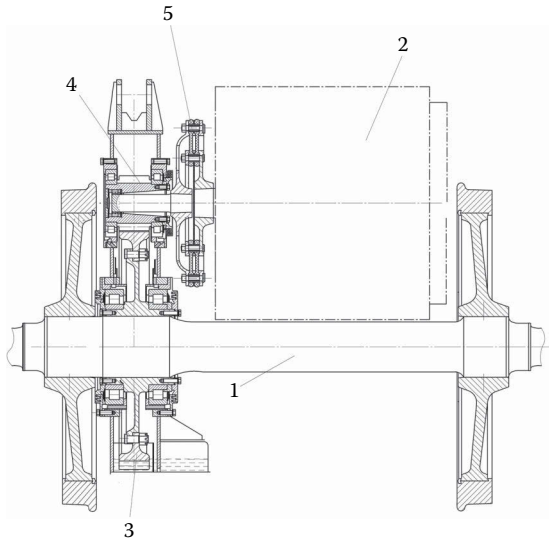

FIGURE 3.36 Example of a bogie frame-mounted traction motor design (Manufactured by Lugansk Diesel Locomotive Plant, Lugansk, Ukraine). 1 – axle; 2 – traction motor; 3 – gear wheel; 4 – pinion; 5 – flexible coupling.

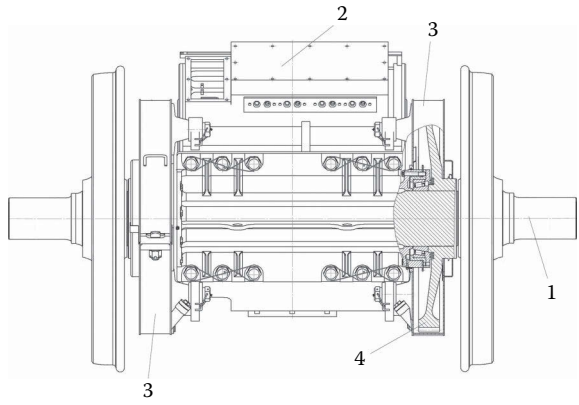

FIGURE 3.37 Example of a traction drive with two gear boxes (Manufactured by Ural Locomotives, Yekaterinburg, Russia). 1 – wheelset; 2 – traction motor; 3 – gear housing; 4 – gear wheel.

3.6 BOGIE SUBSYSTEMS

The bogie is equipped with other subsystems that are also important components of running gear. In this section, we will examine brake, sanding and wheel flange lubricating subsystems installed on the bogie. The latter subsystem is optional and can be replaced by a wayside lubrication process on heavy haul routes.

3.6.1 Brake Subsystem and Associated Devices

As described in Section 2.7.2, the standard brake subsystems used on bogies of heavy haul locomotives are the air brake and parking brake.

3.6.1.1 Components of Air Brake Systems

The following elements of the pneumatic system are usually located on the bogie frame: air pipes used to supply brake cylinders, brake rigging with connected brake shoes and the brake cylinders. The number of brake cylinders shows what type of mechanism is in use: if one cylinder is acting on several brake shoes located on different wheelsets, then such a mechanism is called a grouped scheme; if each wheelset uses its own cylinder, then it is called an individual scheme.

If only one brake shoe is used to produce the braking force on each wheel, as shown in Figure 3.38, such a design is called a single-shoe brake system. When the braking force is applied from both sides of the wheel by means of two brake shoes, as shown in Figures 3.39 and 3.40, such a design is called a double-shoe braking system.

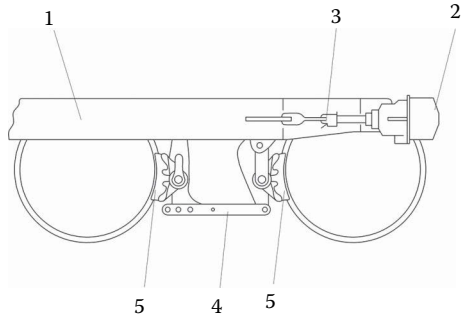

FIGURE 3.38 Example of a single-shoe braking system.

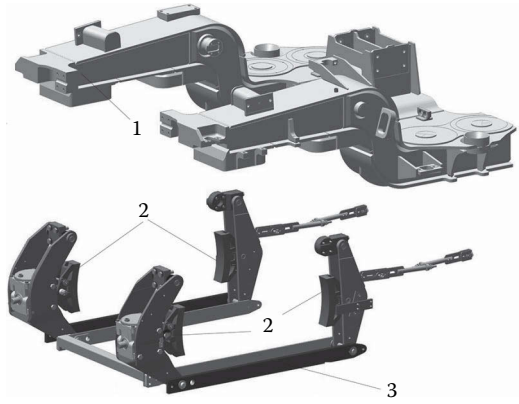

FIGURE 3.39 Example of a double-shoe braking system. 1 – bogie frame; 2 – brake shoes; 3 – brake rigging. (From © Siemens AG, Graz, Austria. With permission.)

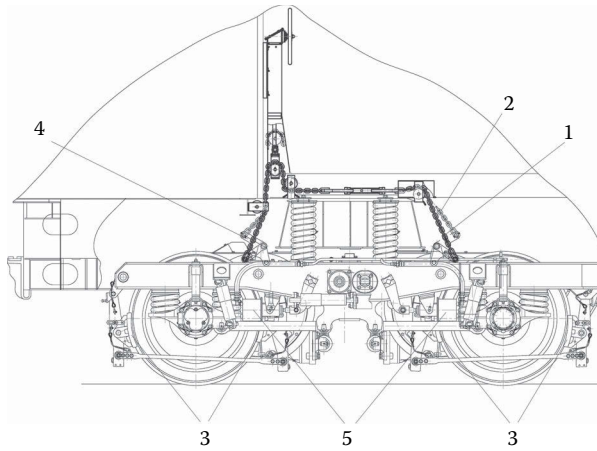

FIGURE 3.40 Example of parking brake system (Manufactured by Ural Locomotives, Yekaterinburg, Russia). 1 – chain, when brake released; 2 – chain, when brake applied; 3 – brake shoes; 4 – brake rigging; 5 – brake cylinders.

The braking system needs regular adjustment of brake shoe position, which is commonly performed with a special mechanical or automatic slack adjuster connected directly to the rod of the brake cylinder, or by means of brake rigging systems that have resetting latches, plates or rods.

The brake blocks used on heavy haul locomotives these days are commonly equipped with cast iron or composite shoes.

3.6.1.2 Parking Brakes

The parking brake is used to prevent inadvertent movement of the locomotive and the train during periods when the train is stopped on the main line or stabled in a siding.

The control with which to activate the parking brake can sometimes be located in the driver cab, but more often is inside the locomotive body or mounted on the main frame. A wheel or lever is generally used to actuate a gear or brake rigging. An example of the actuation with a chain mechanism is shown in Figure 3.40. The system creates a tension of the chain and the brake rigging sets the brake shoes in the applied state to press the brake blocks against the wheels, thereby preventing the wheels from rotating. When the parking brake is not applied, the chain is not under tension and the wheels are released.

3.6.2 Sanding Subsystem

Locomotive sanding systems serve to enhance the adhesion coefficient between wheels and running rails when locomotives operate in modes of traction and braking under conditions of insufficient friction which limits the implementation of the necessary tractive and braking efforts. This can be attributed to the presence of some surface contaminants at the wheel-rail interface, caused by either natural or man-made factors or events. The main components of such a system are shown in Figure 3.41.

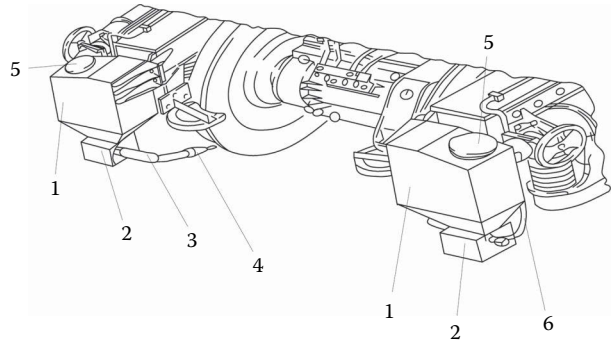

FIGURE 3.41 Example of a bogie-mounted sanding subsystem installation (Manufactured by Goninan, Newcastle, Australia). 1 – sand box; 2 – sand trap; 3 – sanding pipe; 4 – sanding nozzle; 5 – sand box filler; 6 – air pipe.

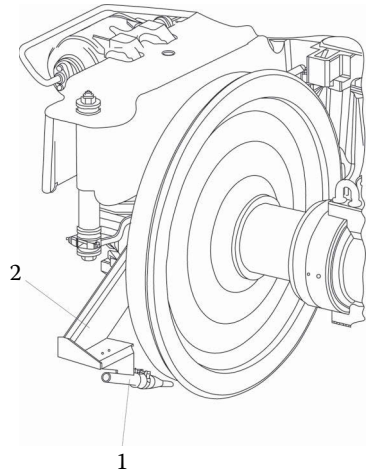

FIGURE 3.42 Example of car body-mounted sanding subsystem installation (Manufactured by Electro-Motive Diesel, McCook, IL). 1 – sanding nozzle (pipework not shown); 2 – mounting bracket.

Sand boxes and the sand traps can be installed on the bogie, as shown in Figure 3.41, or on the locomotive car body. In the latter case, the bogie is equipped with sanding nozzles only, as shown in Figure 3.42, and flexible pipework is used in order to supply sand to them.

3.6.3 Wheel Flange Lubrication Subsystem

Flange lubrication systems are often used for the improvement of dynamic interaction and the reduction of wear processes at the wheel–rail interface when locomotives operate on curved sections of the track. An example of a locomotive wheel flange lubrication system is shown in Figure 3.43. Similar to sand systems, the lube

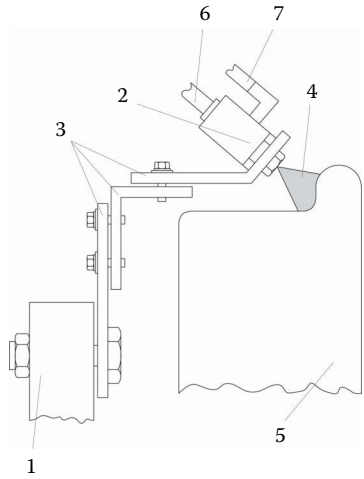

FIGURE 3.43 Example of wheel flange lubrication installation (Manufactured by Electro-Motive Diesel, McCook, IL). 1 – journal housing or bogie frame; 2 – nozzle assembly; 3 – adjustable brackets; 4 – lubricant; 5 – wheel; 6 – pipe to lube system; 7 – pipe to air control system.

tanks and other pieces of equipment can be installed on the bogie or on the locomotive car body. Solid lubricant can also be applied to the wheel flange by direct contact instead of spraying liquid lubricant.

REFERENCES

1. M. Spiryagin, C. Cole, Y.Q. Sun, M. McClanachan, V. Spiryagin, T. McSweeney, *Design and Simulation of Rail Vehicles, Ground Vehicle Engineering Series*, CRC Press, Boca Raton, FL, 2014.
2. C.A. Swenson, R.T. Scott, The effect of locomotive radial steering bogies on wheel and rail wear. In *Proceedings of the ASME/IEEE Joint Railroad Conference*, IEEE, Oakbrook, IL, 30 April–2 May 1996, pp. 91–100.
3. S. Simson, Three axle locomotive bogie steering, simulation of powered curving performance: Passive and active steering bogies, PhD Thesis, Central Queensland University, Rockhampton, Queensland, Australia, 2009.
4. V. Spiryagin, Improvement of dynamic interaction between the locomotive and railway track, PhD Thesis, East Ukrainian National University, Lugansk, Ukraine, 2004.

4 Design of Locomotive Power Electronics Systems and Electrical Machines

4.1 CLASSIFICATION OF LOCOMOTIVE ELECTRICAL TRANSMISSIONS

The locomotive electric power train consists of the following elements:

- A source of electrical energy – either an electrical overhead power system or an on-board generator;
- Power conditioning equipment; and
- The traction motors.

The possible combinations and topologies have been described in Chapter 2. The electrical source is normally the most significant choice and the one that is usually imposed by the track infrastructure owner. An electrical overhead system offers a clear operational cost advantage but with high initial capital costs. Once a decision is made as to the power source, the remaining choices relate to the traction motors and their supporting power conditioning. The AC machines, and generally squirrel-cage induction machines, are the dominant technology choice for modern designs. The AC machine is cheaper and much more robust than the DC machine. The existence of affordable high-performance inverters and inverter control strategies allows an AC machine to be controlled as easily as a DC machine. Induction machines, driven by gate-turn-off–based inverters, were reported in railway applications from 1984 onwards [1]. Since that time, the DC traction motors have been steadily displaced; however, significant numbers of DC traction motors are still in service in legacy fleets.

Traction motors have several distinguishing features when compared to stationary machines found in general industry. These include the following:

- A wide speed range, which include operation from zero speed;
- Higher torque and power-to-volume ratios;
- Higher temperature insulation systems and intensive cooling, normally by forced air;
- Designed for a high external contamination environment; and

- Designed for a high mechanical shock environment, especially where the motor is totally or partially unsprung weight.

The consequences for the AC and DC motors are now discussed.

4.1.1 DC Traction

The DC traction machines best suited for heavy haul applications are separately excited machines. These have independent control of the armature and field windings. The field circuit is controlled to maintain the highest reasonable value of magnetising flux, as this maximises the motor torque production for each ampere of armature current. There are two clearly identifiable operating regions [2]:

- The low-speed or torque-limited region, which applies from standstill to approximately one-third of the vehicle's maximum operational speed; and
- The constant power, field weakening or high-speed region.

In the torque-limited region, the field is maintained at its rated value and the motor torque is limited by the permissible armature current. The armature voltage is dependent upon the vehicle speed and the field winding magnetising flux. At higher speeds, the field strength must reduce to limit the armature voltage. A consequence of the necessary reduction in field strength is the reduction in the achievable torque.

The armature circuit is current controlled, and this is the primary mechanism for controlling the motor torque and tractive effort. In a diesel-electric locomotive, as shown in Figure 2.21, the armature current is easily controlled by adjusting the generator voltage through the control of the generator field winding or exciter winding. In this case, the generator rectifier is an uncontrolled diode rectifier. The dynamic response of this system is relatively slow, with small signal response times of approximately 1 s, as the control loop includes the dynamics of the generator exciter. Large-scale variations in tractive effort are limited to tens of seconds by the power ramp rate limitations of the diesel prime mover. In the DC–DC topology electric locomotive shown in Figure 2.23, the armature circuit current is controlled by a chopper. In the AC–DC topology electric locomotive shown in Figure 2.24, the armature circuit current is set by a phase-controlled rectifier. Both these electric locomotive systems are dynamically much faster than the diesel-electric system using alternator excitation control. The armature circuit current can be significantly changed in 100 ms.

A traction motor will have a rating of several hundred kilowatts. Motors of this size have compensation windings or interpole windings to counteract the armature reaction and to maintain the best operating conditions for the commutator. A compensation winding is constructed by embedding current-carrying conductors in the face of the field pole. An interpole is an additional magnetic pole and winding located between the main field poles. Both types of winding are connected in series with the armature, as they are intended to counteract the impact of the armature current upon the commutation process.

The existence of the commutator imposes a number of design constraints on the traction motor. The commutator diameter increases with voltage and, in a traction motor, the armature voltage is limited to approximately 1000 V.

4.1.2 AC Traction

The AC machine most favoured for modern heavy haul designs is the induction machine [3]. The preferred machines are squirrel-cage induction machines with four or six poles. These have no electrical connection to the rotor and no slip rings or commutators. The motors are controlled by inverters that provide variable-frequency AC power. The speed of the motor is nearly directly proportional to frequency. Modern AC traction systems utilise field-oriented control (FOC) or direct torque control (DTC) methods which provide precise control of the induction motor torque. These control methods are dynamically highly responsive, but the overall locomotive response is still strongly influenced by the power source. The AC–DC–AC topology, as shown in Figure 2.22, is representative of most modern diesel-electric locomotives. The main generator provides power to a DC link, or DC bus, that supplies the inverters. The inverters can quickly control the traction motors. However, a rapid change in the mechanical power at the wheel-rail interface is immediately visible as a change in the electrical demand at the DC link. The DC link has capacitors that provide very limited energy storage. It is normal practice to impose a torque rate limit upon the AC drive so that the diesel and generator are able to follow the changing demands in electrical power. For those locomotives that derive their power from an overhead system, such as the examples shown in Figures 2.25 and 2.26, rapid changes in tractive effort are possible.

Synchronous machines appear in some high-power rail applications such as high-speed passenger rail and could be applied in heavy haul applications. The synchronous machine can use a permanent magnet rotor or a directly excited rotor. The permanent magnet machines are well established at powers up to, perhaps, 100 kW. These are brushless machines and offer advantages with respect to power and torque density. However, the current permanent magnet technology is more applicable to lighter electric road vehicles and light rail.

The directly excited synchronous machine has a clear advantage at very high powers. These are popular for multimegawatt drives that may be found in ship propulsion. In the early history of inverter development, a synchronous machine could be designed to run with a load commutated inverter (LCI). This helped to avoid some of the power device limitations at that time.

4.2 TRANSFORMERS

Railway traction transformers are a specialised form of the well-established industry transformer technology. Some of the special characteristics, relative to a general-purpose industrial transformer, are as follows:

- Higher power density with respect to volume and weight;
- Higher impedances – by up to 20%, especially with DC traction motors;

- Higher harmonic current loadings and higher harmonic current or *k* factors;
- Multiple secondary windings to accommodate several traction converters and a multiplicity of bushings;
- Much harsher mechanical vibration and shock design requirements; and
- Low profile construction and, with DC traction motors, sharing of the oil volume with armature circuit inductors.

The higher power density is primarily achieved through intensive cooling. The core and winding mass in a traction transformer are roughly half of that found in a conventional transformer [4]. The core losses are similar, but the winding losses are roughly 4 times higher [4]. Many industrial transformers utilise natural convection, but traction transformers use forced oil cooling (OF) to circulate the internal oil through winding ducts to extract heat. A traction transformer may use forced air cooling (AF) to remove heat from its external surfaces or radiators. In some applications, an oil-to-water heat exchanger and then a water-to-air radiator may be used.

The traction transformer, a heavy item, is most commonly slung under the locomotive floor to help maintain a low centre of gravity. This forces a low-profile construction. A few attempts have been made to produce lightweight transformers, either through the use of superconductors [5] or through the use of power electronics and high-frequency ferrite transformer cores [4]. These efforts have produced full-scale prototypes, but, as yet, the advantages are not sufficient to drive commercial applications.

4.3 TRACTION GENERATORS AND ALTERNATORS

A generator converts mechanical power, most commonly from a diesel prime mover, into DC power. Modern traction generators are normally implemented as three-phase synchronous alternators, which produce AC power, and diode rectifiers to convert the AC output from the alternator into DC. The alternator output is adjusted by controlling the alternator field current provided to the rotor. The rotor can be connected to its exciter with slip rings, or a rotating exciter can be applied. The modern generator is never implemented as a DC machine. This would introduce a commutator, which brings additional maintenance and cost.

The alternator is normally three phase, with four or six poles, and the full-power operational speed ranges from 600 to 1800 rpm. At low load, the rotational speed might be reduced to as low as 200 rpm. The speed range is tailored to suit the characteristics of diesel machines. This arrangement results in a maximum alternator frequency of 25–60 Hz, and this is tailored to suit the electrical properties of readily available electrical steels for the alternator stator. The conversion efficiency for modern alternators is high. For example, the ABB WGX500–560 family generators are 1200 V, 600–1800 rpm, 6-pole alternators, in the 1–3.3 MW range. These claim a 96.9% peak efficiency [6].

A traction alternator will operate over a moderate speed range to allow the diesel prime mover operations to be optimised with respect to fuel efficiency and exhaust emissions. At low powers, a diesel will operate at, or just above, a minimum idle

speed. A diesel will operate at higher speeds when higher powers are required. The speed range from idle to full power may be more than two to one.

The generator output voltage can vary considerably. In a locomotive with AC traction, the alternator voltage may change by a range of five to one to provide an optimal voltage for the traction inverters. The inverters require the higher voltages at the higher train speeds. In a locomotive with a DC traction system, the alternator may directly supply the armatures of the traction motors. In this case, the alternator voltage may be required to drop to nearly zero when the locomotive is operating at very low speeds.

To accommodate simultaneous variations in the diesel prime mover mechanical speed and generator output voltage, the alternator excitation currents could vary over a range of more than ten to one.

It is possible to supply the excitation current directly to the alternator rotor by using slip rings. An alternative, which avoids the slip rings and brushes, is brushless excitation. This uses a 'rotating exciter' with a small alternator and rectifier, which are physically on the rotor shaft, to supply the rotor current. The rotating exciter is controlled by a stationary DC winding. A rotating exciter introduces some additional control delay. As the required field current response time is in the order of hundreds of milliseconds, this delay is tolerable.

If the main alternator has to accommodate a wide range of output voltages, there may be a second alternator to provide a fixed voltage supply to power auxiliary equipment such as compressors and blowers.

4.4 TRACTION MOTOR OPERATING PRINCIPLES

As with any electrical machine, the torque production relies upon either the Lorentz force or reluctance forces. The Lorentz force, the force on electric charges moving in electric and magnetic fields, dominates in most traction motors. In these machines, the torque is produced by the interaction of currents in two windings, that is, the currents in the field winding and armature in a DC machine or the currents in the stator and the rotor in the induction machine.

A purely reluctance torque-based machine has a single winding and a magnetic path where the magnetic flux varies with the rotation of the machine. The torque is a consequence of the variation in the magnetic field energy with the rotor position. An example is the switched reluctance machine (SRM). Although use of SRMs in rail application is uncommon, these machines are used in some heavy vehicles [7].

To illustrate some of the key principles that are common to both AC and DC traction motors, two models of machine operation are presented. The first model is based on a single conductor mounted on a rotor positioned in a uniform magnetic field. The second model is based on the coupled circuit approach that is widely used in machine modelling.

4.4.1 Single Conductor Model

Figure 4.1 shows a single conductor of length l fixed on a cylindrical rotor or armature of radius r in a uniform magnetic field with a flux density B. The cylinder is free

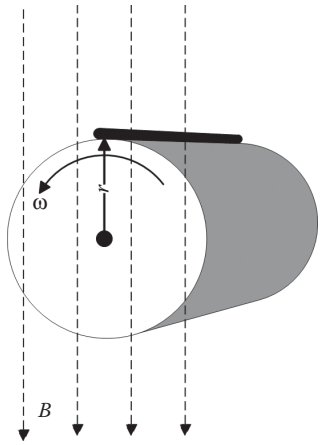

FIGURE 4.1 A current-carrying conductor on a rotor in a uniform magnetic field.

to rotate. This forms an elemental electrical machine which can be used to illustrate some of the key operational limitations for both AC and DC machines.

The Lorentz force is

$$F = q\left[E + (v \times B)\right] \tag{4.1}$$

where:

F is the Lorentz force
q is the electronic charge
E is the electric field strength
v is the velocity
B is the magnetic field strength
$\times$ is the vector cross-product

In traction motors, the electric fields do not produce appreciable forces and the current flows occur in the conductors of the windings. The mechanical design of the machine generally seeks to maintain the flux and conductors in orthogonal orientations. In this case, the scalar equation for force on a current-carrying conductor is

$$F = Bil \tag{4.2}$$

where:

F is the Lorentz force
B is the magnetic field strength
i is the current
l is the conductor length

For both AC and DC traction motors, the force production is proportional to the machine length, the air-gap flux density and the total current flowing in the conductors

on the surface of the rotor or armature. The tangential components of these forces are translated into torques by multiplying by the armature or rotor radius. The air-gap flux strength is referred to as the level of machine excitation or magnetisation. At higher excitation levels, more torque can be produced for the same level of armature or rotor current. A given torque can be achieved with the lowest current in a fully excited or fully magnetised machine. This is operationally desirable as it results in the lowest conduction losses.

The Lorentz equation also imposes a limit on the machine torque. The magnetic field strength is determined by the magnetic properties of the machine's magnetic materials. The saturation level of steel laminations is typically 1.7 Tesla. All machines have current limits that are largely imposed by the lifetime of the electrical insulation. For continuous operation, the cooling methods employed determine the maximum allowable losses. Higher currents are possible for short time durations. For short-term operation, the specific heat of the motor materials determines the rate of temperature rise. In combination, the magnetic field strength and current limits impose a torque limitation. All electric drives have a characteristic low-speed region, where the machine torque is adjustable within the limits set by the rated maximum field and rated maximum currents. In this region, the machine is operated in a fully excited state and the torque-producing current is controlled to adjust the machine torque. The low-speed region is also termed the constant-torque region.

As the number of the conductors on the surface of a rotor or armature is proportional to the circumference or radius, the machine torque varies with the square of radius and the rotor armature length. Torque is proportional to the machine volume. The mechanical power is the product of the machine torque and rotational velocity. The power rating is then proportional to the machine volume and the rated speed. In a traction application, a gearbox will allow a higher speed traction machine with a lower volume to achieve the same mechanical power.

Another key equation that determines the behaviour of electrical traction machines is the generator equation. For an orthogonal arrangement of conductors and flux, a scalar expression for the voltage induced on a conductor moving in a magnetic field is

$$E = Blv \tag{4.3}$$

where:

E is the induced voltage
v is the velocity
B is the magnetic field strength
l is the conductor length

In an electric machine, the conductor velocity is proportional to the armature/rotor radius and the rotational speed. In any traction application, the allowable machine voltage is limited by the voltage rating of the insulation system, the voltage rating of the traction converters and the available voltage from the overhead power system or from the on-board alternator. If the machine is fully excited, there will be a particular rotational speed, ω_{rated}, or frequency, f_{rated}, at which the voltage limit is reached.

Beyond this, the machine flux density must be reduced either to limit the machine voltages or to maintain the current flows within the machine. Above this speed, the machine enters the field-weakening mode. Above the threshold field-weakening speed, ω_{rated}, the flux and the available machine torque fall inversely with speed. The machine power, which is the product of speed and torque, is constant. This region is also termed the constant-power region or the high-speed region.

Finally, Equations 4.2 and 4.3 can be considered together to illustrate the equality of electrical and mechanical power in an ideal machine. Noting that the torque, T, is the product of the radius, r, and the tangential force, Bil, the mechanical power delivered by a conductor on an armature or rotor rotating at w_{mech} is

$$P_{mech} = w_{mech}T = w_{mech}rBil \tag{4.4}$$

This is equal to the electrical power:

$$P_{elec} = iE = iBlv = iBlw_{mech}r = w_{mech}rBil \tag{4.5}$$

For both AC and DC traction motors, and their electronic controls, the mechanical to electrical efficiencies are high. In models where fast dynamics are not significant, simple models can be developed based on the equality of the input and output powers and constraints on torque and power in the low-speed, constant-torque region and the high-speed, constant-power operational region.

4.4.2 Coupled Circuit Model

The elemental single-conductor model can be extended by the addition of multiple conductors to model complex real machine cases. A much more compact machine model makes use of the coupled-circuit approach, where the aggregated behaviours of many elemental conductors can be described using the concepts of self and mutual inductance. This approach is extensively used to model the behaviour of both DC and AC machines. Consider an elementary two-pole generalised machine with a uniform air gap, as shown in Figure 4.2.

The elementary machine has a winding 's' on the stationary stator or field and a winding 'r' on the rotating rotor or armature. The machine is assumed to have a smooth air gap, so the self-inductance of the windings is not dependent on the rotor angle within the stator. The mutual inductance between windings 's' and 'r' is a positive maximum when the angle $\theta = 0$ and a negative maximum when the angle $\theta = \pi$. The mutual inductance is zero when $\theta = \pm\pi/2$. On the assumption that the windings are distributed to give a sinusoidal air gap flux, the mutual inductance, as viewed from the stator winding, can be written as

$$L_{sr}(\theta) = L_{sr}\cos\theta \tag{4.6}$$

where:

θ is the electrical angle

L_{sr} is the mutual inductance, referred to the stator, for the fully aligned case, $\theta = 0$

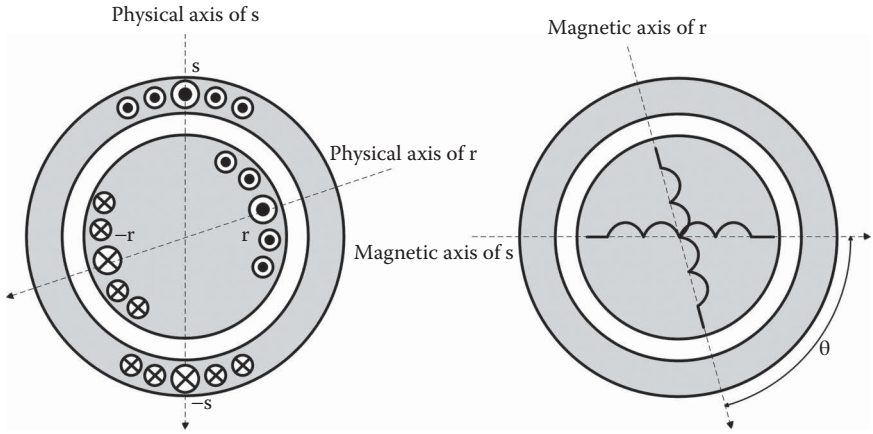

FIGURE 4.2 Elementary two-pole machine.

The stator and rotor flux linkages are

$$\begin{bmatrix} \lambda_s \\ \lambda_r \end{bmatrix} = \begin{bmatrix} L_s & L_{sr}(\theta) \\ L_{rs}(\theta) & L_r \end{bmatrix} \begin{bmatrix} i_s \\ i_r \end{bmatrix} \tag{4.7}$$

where:

$L_{rs}(\theta)$ is the mutual inductance, referred to the rotor
L_s and L_r are the stator and rotor self-inductances
i_s and i_r are the stator and rotor currents

The winding terminal voltages are

$$\begin{bmatrix} v_s \\ v_r \end{bmatrix} = \begin{bmatrix} r_s & 0 \\ 0 & r_r \end{bmatrix} \begin{bmatrix} i_s \\ i_r \end{bmatrix} + \begin{bmatrix} p & 0 \\ 0 & p \end{bmatrix} \begin{bmatrix} \lambda_s \\ \lambda_r \end{bmatrix} \tag{4.8}$$

where:

r_s and r_r are the stator and rotor resistances
p is the time derivative d/dt

The electromagnetic torque can be found from the change of the magnetic field coenergy with respect to the electrical alignment angle θ. Coenergy is directly related to the magnetic field energy, and these quantities are equal in a linear system. The coenergy is

$$W' = \frac{1}{2} L_s i_s^2 + \frac{1}{2} L_r i_r^2 + L_{sr} i_s i_r \cos\theta \tag{4.9}$$

The electromagnetic torque is the derivative of the coenergy with respect to θ. This is

$$T = L_{sr} i_s i_r \sin\theta \tag{4.10}$$

The physical interpretation of this equation is that torque depends on the two winding currents and the electrical alignment angle θ. In both AC and DC machines, one current is primarily responsible for the establishment of the machine's magnetic field. This is the field current in a DC machine and the one component of the stator current (the magnetising current) in an induction machine. The second current is the torque-producing current. This is the armature current in the DC machine and the rotor current in an induction machine. The torque will be maximised if the alignment angle can be kept close to $\pm\pi/2$. In the DC machine, this is achieved by the action of the commutator. In an induction machine, especially one with an FOC scheme, this is actively achieved by controlling the phase angle of the stator current.

4.4.3 AC Traction Motors

Induction machines are the dominant motor type applied in modern heavy haul locomotives [2]. Table 4.1 gives several examples. Synchronous machines can be applied, but their applications in rail seen thus far have been in high-speed passenger rail, as seen in Table 4.2. Both types of AC machines are best analysed using the coupled circuit concepts described in the previous section. These concepts will be expanded to explain the most popular AC machine control methods in the following sections.

TABLE 4.1
Summary of Induction Machine Motors in Locomotives

Vehicle	Motors: Type and Rating	Vehicle	Motors: Type and Rating
German DB-Railion 189 electrical freight locomotive; maximum speed 140 km/h; in operation since 2003 [7]	4 × 1600 kW induction machines made by Siemens AG [7]	German DB 152 electrical locomotive; maximum speed 170 km/h; in operation since 2001 [7]	4 × 1600 kW induction machines made by Siemens AG [7]
Indian electric freight locomotive WAG-9; maximum speed 100 km/h; in operation since 1996 [7,8]	6 × 850 kW induction Motors, FRA6068, made by ABB [7,8]	Chinese Railways DJ4 electrical locomotive; maximum speed 120 km/h; in operation since 2006 [7]	8 × 1200 kW induction machines made by Siemens AG and Zhuzhou Electric Locomotives Works [7]
Swiss Railways SBB FLIRT RABe 521/523; maximum speed 160 km/h; in operation since 2004 [7]	4 × 500 kW induction motors made by TSA Traktionssysteme [7]	Swiss SBB Re 460 electrical locomotive; maximum speed 230 km/h; in operation since 1992 [7]	4 × 1525 kW induction machines made by ABB [7]

TABLE 4.2
Summary of Synchronous Machine Motors in Rail Vehicles and Locomotives

Vehicle	Motors: Type and Rating	Vehicle	Motors: Type and Rating
Korean KTX high-speed train; operational speed 300 km/h; in operation since 2004 [7]	12×1130 kW self-commutated synchronous machines (later replaced by induction machines) [7]	Alstom AGV very-high-speed train [7,9]	760 kW enclosed self-ventilated Alstom 4500 rpm [7,9]

4.4.4 DC Traction Motors

The DC machine was the mainstay of railway traction before the development of the AC machine as an effective alternative once the inverter and control methods became feasible [1]. The DC traction machine operation can be readily explained in terms of the elemental machine shown in Figure 4.1. The current-carrying conductors are mounted on the armature. The Lorentz force is tangential and causes the armature to rotate. As the armature rotates, the switching – or commutation – action of the commutator maintains the current flow in the conductors directly under the field poles. This maintains the orthogonal relationship between the conductor and the magnetising flux and maximises the torque production.

In heavy haul applications, the precise torque control of the machine is important if the maximum adhesion is to be achieved. A separately excited machine has the best control flexibility and is preferred. Both series and shunt DC machines impose operational constraints. A series machine forces the armature and field currents to be equal, whereas the shunt machine forces equality on the armature and field voltages. The previous discussion has shown that the torque capability of a machine depends on the machine volume, and the mechanical power depends on the product of volume and mechanical speed. Series and shunt machines, in comparison with the separately excited machine, offer no special advantages with respect to the ultimately achievable power or torque. The separately excited machine requires two independent converters to control the armature and field circuits. This is a small price in comparison with the control precision gained.

For a traction motor of a few hundred kilowatts, the armature voltage is limited to approximately 1000 V and the resulting armature current must be a few hundred amperes. This must be transferred to the armature via the brushes and the commutator. The commutator is subject to wear and requires maintenance. The voltage limitation imposed by the commutator results from the limited voltage that can be sustained between the adjacent armature segments. A high-voltage machine needs more commutator segments, and this increases the commutator diameter. The armature of the DC machine is a wound armature and has a far higher requirement for insulation, both between the turns and from the turns to the armature slot, than an induction machine.

4.5 CONTROL OF TRACTION MOTORS

In heavy haul locomotive applications, the primary goal is to provide a well-controlled and sustained tractive effort. The tractive effort may be required for extended periods, often tens of minutes. This might suggest that the dynamic response of the drive system can be quite slow. There are specific instances, such as adhesion control, where changes in the friction conditions at the wheel-rail interface require a fast dynamic response to prevent wheel slip and consequent wheel and rail damage. As the tractive effort is directly determined by the traction motor torque, a well-controlled and dynamic control of the tractive effort requires a well-controlled and dynamic control of the machine torque. The strategies for achieving this in AC and DC machines are now considered.

4.5.1 DC Traction Motors and Control Strategies

The torque equation for a separately excited DC machine is

$$T_{\text{mech}}(t) = k_T \psi_f(t) i_a(t) \tag{4.11}$$

where:

$i_a(t)$ is the armature current
$\psi_f(t)$ is the magnetising flux
k_T is the torque constant

If the magnetising flux is constant, then the torque can be directly controlled by controlling the machine armature current. Figure 4.3 shows the equivalent circuit for a separately excited DC machine, where the armature circuit is to be controlled by adjusting the armature voltage, $v_a(t)$. The armature resistance and inductance are r_a and L_a, respectively. The equation for the armature voltage induced by the magnetising field and the rotation of the armature is

$$e_a(t) = k_T \psi_f(t) \omega_m(t) \tag{4.12}$$

where:

$e_a(t)$ is the armature back electromagnetic force (EMF)
$\omega_m(t)$ is the rotational velocity
k_T is the torque constant

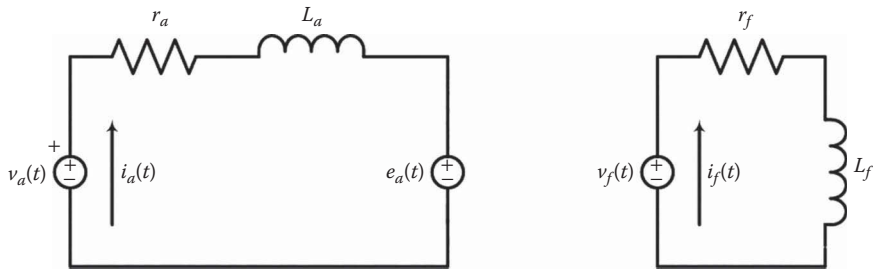

FIGURE 4.3 Separately excited DC machine.

The magnetising flux is a function of the field current. In Figure 4.3, the field resistance is r_f, the field inductance is L_f and a linear relationship is implied for the magnetising flux, as:

$$\psi_f(t) = L_f i_f(t) \tag{4.13}$$

To control the DC machine current, the magnitude of the armature terminal voltage must be adjustable and able to exceed the back EMF voltage. If the back EMF voltage exceeds the available terminal voltage, it becomes impossible to force current into the armature, and torque cannot be developed. Once the machine speed exceeds a rated speed, the field flux must be reduced so that armature current control can be maintained. Above this rated speed, the machine operates in the field-weakening mode. Below rated speed, the full field is applied. If the rated armature current is supplied, then the machine can develop its rated torque.

A torque control strategy is shown in Figure 4.4 for an AC–DC topology. The machine flux is determined with respect to the mechanical speed from a lookup table. A target flux level or field current level is produced by a controllable field rectifier supply. Once the field flux is established, the required current to produce the desired torque can be calculated using the torque constant. The required armature current is produced by a current-controlled rectifier. The armature controller is rated at the full power rating of the machine. The field controller is much smaller and is typically only a few percent of the machine rating.

In the other locomotive topology cases, the torque control strategy still requires two controlled converters. In a DC–DC topology, an armature circuit chopper and a field circuit chopper are required. In a diesel-electric topology, the armature circuit may be controlled by controlling the exciter of the main alternator. In this case, the field converter would be powered from an auxiliary alternator supply so that the full excitation would be available across the locomotive speed range.

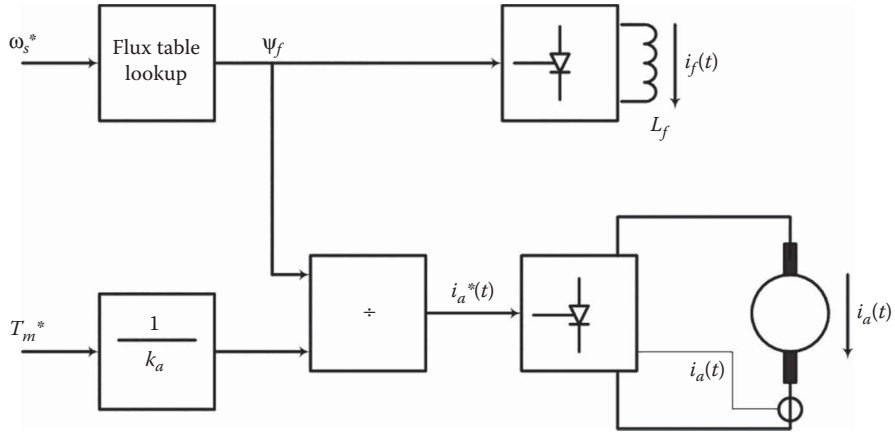

FIGURE 4.4 Torque control for a separately excited machine.

4.5.2 AC Traction Motors and Control Strategies

AC traction motors of the induction and synchronous types are most frequently controlled through the use of inverters that produce variable-frequency electric power. The mechanical speed of these machines is determined directly by the electrical frequency. Inverters rely on power electronic switching devices. Switching power conversion is a theoretically lossless power conversion method, and the practical power conversion efficiencies are typically more than 97%. The combination of inverters and AC machines offers exceptional operational advantages, and this technology pairing dominates heavy haul locomotive designs. Inverter technology will be discussed in Chapter 8. For the purposes of this chapter, it is sufficient to assume that inverters can provide a source of variable frequency power which is readily dynamically adjustable for the purposes of motor control.

The AC traction motors, such as the synchronous and induction motors, develop torque through the interaction of an exciting magnetic field and a torque-producing current. These motors are nearly always three-phase machines in traction applications even though other phase numbers, such as five, are possible and occasionally found in other vehicle applications. The number of phases is immaterial in one aspect. The machine responds to the sum of the magnetic fluxes produced by the phase windings and these can be resolved into two key components – a magnetising component and a torque-producing component. The analysis of AC machines can be undertaken using a vectorial representation of the aggregation of the winding currents. This approach is termed the space-phasor modelling method.

Consider a machine with a smooth air gap and three-phase windings, A, B and C, distributed upon a stator as shown in Figure 4.5. A stationary reference frame is attached to the stator with two axes designated as a real axis (Re) and an imaginary axis (Im). The real axis is aligned with the magnetic axis of the A phase winding.

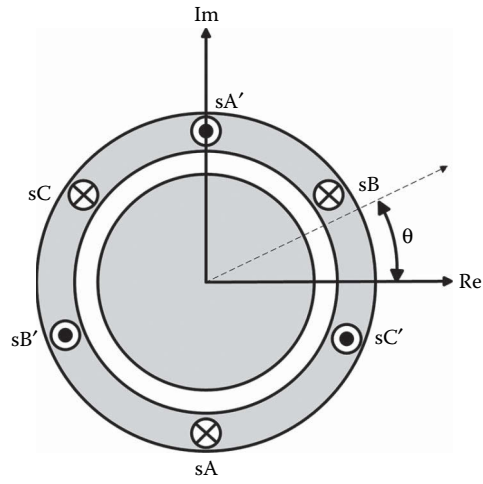

FIGURE 4.5 A stator with three-phase windings.

The real axis is also termed the direct axis of the stator (sD) and the imaginary axis is also termed the quadrature axis of the stator (sQ).

The stator windings can be supplied with a system of three-phase currents and can be connected in star or delta configurations. If a star connection is used, the normal practice is not to connect the neutral point, so there cannot be any zero sequence phase currents. The magnetomotive force (MMF) distribution in the air gap as a function of time and the angle θ is [10]:

$$f_s(t,\theta) = N_{se}\left[i_{sA}(t)\cos(\theta) + i_{sB}(t)\cos\left(\theta - \frac{2\pi}{3}\right) + i_{sC}(t)\cos\left(\theta + \frac{2\pi}{3}\right)\right] \quad (4.14)$$

where:

N_{se} is the effective number of turns, the product of the physical number of turns and a winding distribution factor

θ is the air gap angle measured from the direct axis

$i_{sA}(t)$, $i_{sB}(t)$ and $i_{sC}(t)$ are the phase currents

This equation may be rewritten as [10]:

$$f_s(\mathrm{t},\theta) = \frac{3}{2}N_{se}\mathrm{Re}\left\{\frac{2}{3}\left[i_{sA}(t) + a i_{sB}(t) + a^2 i_{sC}(t)\right] e^{j\theta}\right\} \quad (4.15)$$

where $a = e^{j2\pi/3}$.

The stator current space phasor is given by

$$\overline{\imath}_s(t) = \frac{2}{3}\left[i_{sA}(t) + a i_{sB}(t) + a^2 i_{sC}(t)\right] = |\overline{\imath}_s| e^{j\alpha_s} \quad (4.16)$$

The physical interpretation of the space phasor components is that α_s is the angular location relative to the stator reference frame, and $|\overline{\imath}_s|$ is the magnitude of the peak of the sinusoidal MMF generated in the air gap by the combined actions of the three-phase windings. The space phasor of the air gap MMF due to the stator windings is

$$\overline{f}_s(t) = N_{se}\overline{\imath}_s(t) \quad (4.17)$$

If a three-phase sinusoidal current set is applied to the windings, a rotating magnetic field is established. Consider the balanced positive sequence current set:

$$i_{sA}(t) = I_s \cos(\omega t - \theta_s) \quad (4.18)$$

$$i_{sB}(t) = I_s \cos\left(\omega t - \theta_s - \frac{2\pi}{3}\right) \quad (4.19)$$

$$i_{sC}(t) = I_s \cos\left(\omega t - \theta_s + \frac{2\pi}{3}\right) \quad (4.20)$$

Substitution into Equation 4.16 gives [10]:

$$\overline{\imath}_s(t) = I_s e^{j(\omega t - \emptyset_s)} \tag{4.21}$$

Physically, the three-phase currents produce a fixed-length current phasor that rotates at a constant angular velocity, ω. This results in a rotating air gap MMF and a rotating magnetic flux. The rotating magnetic field travels at synchronous speed, N_s, where:

$$N_s = \frac{2\omega}{P} \text{ rad s}^{-1} \tag{4.22}$$

$$N_s = \frac{120\, f}{P} \text{ rpm} \tag{4.23}$$

where:

P is the number of poles

f is the electrical frequency, given by $f = \dfrac{\omega}{2\pi}$

The variable speed operation of AC traction motors of the induction and synchronous types is achieved by the application of electric currents with variable frequency. These are produced by inverters, and the control of these will be discussed shortly. The rotating current phasors can be resolved into their projections on the direct and quadrature axes:

$$\overline{\imath}_s(t) = i_{sD}(t) + j\, i_{sQ}(t) \tag{4.24}$$

The direct and quadrature currents are related to the currents in the physical phases by the Clarke Transformation relationship:

$$\begin{bmatrix} i_{sD} \\ i_{sQ} \end{bmatrix} = \frac{2}{3} \begin{bmatrix} 1 & -\frac{1}{2} & -\frac{1}{2} \\ 0 & \frac{\sqrt{3}}{2} & -\frac{\sqrt{3}}{2} \end{bmatrix} \begin{bmatrix} i_{sA} \\ i_{sB} \\ i_{sC} \end{bmatrix} \tag{4.25}$$

In the power electronics literature, the terms sα and sβ are sometimes used in place of sD and sQ [10]. For a machine that utilises the Lorenz force for torque production, a second winding is required. Consider Figure 4.6 where a three-phase winding has been added to the rotor of the elementary machine. The physical centre of phase 'ra' of the rotor winding is displaced by an angle of θ_r from the physical centre of the stator phase 'sA'. The rotor current space phasor can be determined using the same approach as used for the stator. The MMF in the air gap, as a function of the angle Θ from the rotor direct axis rD, due solely to the action of the rotor is [10]:

$$f_s(t, \Theta) = \frac{3}{2} N_{se} \text{Re}\left\{ \frac{2}{3} \left[i_{ra}(t) + a i_{rb}(t) + a^2 i_{rc}(t) \right] e^{j\Theta} \right\} \tag{4.26}$$

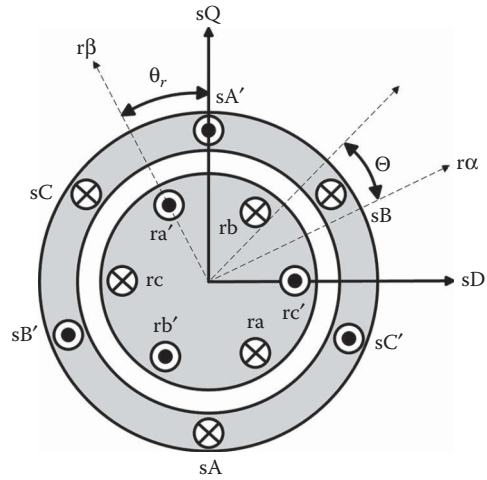

FIGURE 4.6 An elemental machine with stator and rotor three-phase windings.

where:

N_{re} is the effective number of rotor turns, the product of the physical number of turns and a winding distribution factor

Θ is the air gap angle measured from the rotor direct axis

$i_{ra}(t)$, $i_{rb}(t)$ and $i_{rc}(t)$ are the rotor phase currents

The rotor space phasor, relative to the reference frame attached to the rotor, is [10]:

$$\overline{\imath}_r(t) = \frac{2}{3}\left[i_{ra}(t) + a i_{rb}(t) + a^2 i_{rc}(t)\right] = \left|\overline{\imath}_r\right| e^{j\alpha_r} \tag{4.27}$$

The physical interpretation of the space phasor components is that α_r is the angular location relative to the rotor reference frame and $\left|\overline{\imath}_r\right|$ is the magnitude of the peak of the sinusoidal MMF generated in the air gap by the combined actions of the three rotor phase windings. Naturally, the rotor currents can be represented using two-axis theory. The rotor current can be expressed as

$$\overline{\imath}_r(t) = i_{r\alpha}(t) + j\, i_{r\beta}(t) \tag{4.28}$$

and

$$\begin{bmatrix} i_{r\alpha} \\ i_{r\beta} \end{bmatrix} = \frac{2}{3}\begin{bmatrix} 1 & -\frac{1}{2} & -\frac{1}{2} \\ 0 & \frac{\sqrt{3}}{2} & -\frac{\sqrt{3}}{2} \end{bmatrix}\begin{bmatrix} i_{ra} \\ i_{rb} \\ i_{rc} \end{bmatrix} \tag{4.29}$$

The rotor space phasor has thus far been defined relative to a reference frame fixed to the rotor. The space vector can also be expressed in a reference frame attached

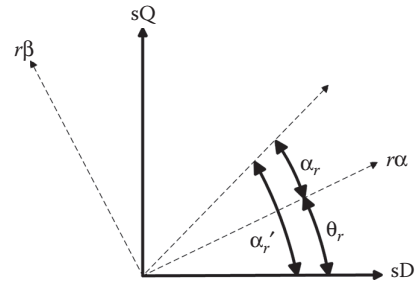

FIGURE 4.7 The relationship between the stator and rotor reference frames.

to the stator. Figure 4.7 shows that the space phasor angle of the rotor current in the stator frame is $\alpha_r' = \alpha_r + \theta_r$.

The rotor space phasor in the stator frame is [10]:

$$\overline{\imath}_r'(t) = \left|\overline{\imath}_r\right| e^{j\alpha_{r'}} = \left|\overline{\imath}_r\right| e^{j(\alpha_r+\theta_r)} \tag{4.30}$$

This space phasor can be represented as its projections on the stator reference frame as

$$\overline{\imath}_r'(t) = i_{rd}(t) + j i_{rq}(t) \tag{4.31}$$

The relationship between the rotor frame currents $i_{r\alpha}$ and $i_{r\beta}$ and the stator frame currents i_{rd} and i_{rq} can be expressed by a rotational transformation matrix [10]:

$$\begin{bmatrix} i_{rd} \\ i_{rq} \end{bmatrix} = \begin{bmatrix} \cos(\theta_r) & -\sin(\theta_r) \\ \sin(\theta_r) & \cos(\theta_r) \end{bmatrix} \begin{bmatrix} i_{r\alpha} \\ i_{r\beta} \end{bmatrix} \tag{4.32}$$

If currents simultaneously flow in both the stator and rotor windings, then the combined MMF will drive the air gap flux. The sum of the winding current MMFs is the magnetising current. If this is expressed as an equivalent stator current, the magnetising space vector is [10]:

$$\overline{\imath}_m(t) = \overline{\imath}_s(t) + \left(\frac{N_{re}}{N_{se}}\right)\overline{\imath}_r'(t) \tag{4.33}$$

In a similar way as applied to define current phasors, it is possible to define flux phasors in terms of the flux linkage $\psi(t)$ in each phase [10].

$$\overline{\psi_s}(t) = \frac{2}{3}\left[i\psi_{sA}(t) + a\psi_{sB}(t) + a^2\psi_{sC}(t)\right] = \left|\overline{\psi_s}\right| e^{j\alpha_s} \tag{4.34}$$

The flux linkage in each phase is a function of the phase current and its self-inductance and the currents and mutual inductances in the other two stator phases and the three rotor phases [10]:

$$\overline{\psi_{sA}}(t) = \acute{L}_s\, i_{sA} + \acute{M}_s\, i_{sB} + \acute{M}_s\, i_{sC} + \acute{M}_{sr}\cos(\theta_r) i_{ra} + \acute{M}_{sr}\cos\left(\theta_r + \frac{2\pi}{3}\right) i_{rb} + \acute{M}_{sr}\cos\left(\theta_r + \frac{4\pi}{3}\right) i_{rc} \tag{4.35}$$

$$\overline{\psi_{sB}}(t) = \acute{L}_s\, i_{sB} + \acute{M}_s\, i_{sA} + \acute{M}_s\, i_{sC} + \acute{M}_{sr}\cos\left(\theta_r + \frac{4\pi}{3}\right) i_{ra} + \acute{M}_{sr}\cos(\theta_r) i_{rb} + \acute{M}_{sr}\cos\left(\theta_r + \frac{2\pi}{3}\right) i_{rc} \tag{4.36}$$

$$\overline{\psi_{sC}}(t) = \acute{L}_s\, i_{sC} + \acute{M}_s\, i_{sB} + \acute{M}_s\, i_{sA} + \acute{M}_{sr}\cos\left(\theta_r + \frac{2\pi}{3}\right) i_{ra} + \acute{M}_{sr}\cos\left(\theta_r + \frac{4\pi}{3}\right) i_{rb} + \acute{M}_{sr}\cos(\theta_r) i_{rc} \tag{4.37}$$

where:

$\acute{L}_s$ is the self-inductance of a stator phase winding
$\acute{M}_s$ is the mutual inductance between the stator phase windings
$\acute{M}_{sr}$ is the peak value of mutual inductance between a stator phase and rotor phase winding

Substitution of Equations 4.35 through 4.37 into Equation 4.34 will result, after much simplification [10], in the following expression for the stator flux linkage:

$$\overline{\psi_s}(t) = L_s\overline{i_s}(t) + L_m\overline{i_r}'(t) = L_s\overline{i_s}(t) + L_m\overline{i_r}(t)e^{j\theta_r} \tag{4.38}$$

where:

$L_s = \acute{L}_s - \acute{M}_s$ is the total inductance of a stator phase winding
$L_m = 2/3\,\acute{M}_s$ is the magnetising inductance

The stator flux can be expressed as its projections on the D and Q axes as

$$\overline{\psi_s}(t) = \overline{\psi_{sD}}(t) + j\overline{\psi_{sQ}}(t) \tag{4.39}$$

From Equation 4.35, it can be shown [10]:

$$\overline{\psi_{sD}}(t) = L_s\overline{i_{sD}}(t) + L_m\overline{i_{rd}}(t) \tag{4.40}$$

$$\overline{\psi_{sQ}}(t) = L_s\overline{i_{sQ}}(t) + L_m\overline{i_{rq}}(t) \tag{4.41}$$

Similar expressions can be found for the rotor fluxes in the rotor reference frame. Space phasors can also be defined for the winding voltages. The stator space vector in the stator reference frame is defined as [10]

$$\overline{v}_s(t) = \frac{2}{3}\left[v_{sA}(t) + a v_{sB}(t) + a^2 v_{sC}(t) \right] = \left|\overline{v}_s\right| e^{j\alpha_s} = \overline{v_{sD}}(t) + j\overline{v_{sQ}}(t) \tag{4.42}$$

Similarly, the rotor voltages in the rotor reference frame are [10]

$$\overline{v}_r(t) = \frac{2}{3}\left[v_{ra}(t) + a v_{rb}(t) + a^2 v_{rc}(t) \right] = \left|\overline{v}_r\right| e^{j\alpha_r} = \overline{v_{r\alpha}}(t) + j\overline{v_{r\beta}}(t) \tag{4.43}$$

The stator and winding terminal voltages are a function of the winding currents, resistance and the rate of change of their flux linkage. The stator terminal voltages can be expressed in their phase variable form as

$$v_{sA}(t) = r_s i_{sA}(t) + \frac{d\psi_{sA}(t)}{dt} \tag{4.44}$$

$$v_{sB}(t) = r_s i_{sB}(t) + \frac{d\psi_{sB}(t)}{dt} \tag{4.45}$$

$$v_{sC}(t) = r_s i_{sC}(t) + \frac{d\psi_{sC}(t)}{dt} \tag{4.46}$$

The space vector form of this equation in the stator frame is

$$\overline{v}_s(t) = r_s \overline{i}_s(t) + \frac{d\overline{\psi}_s(t)}{dt} \tag{4.47}$$

The rotor terminal voltages can be expressed in their phase variable forms in the rotor frame as

$$v_{ra}(t) = r_r i_{ra}(t) + \frac{d\psi_{ra}(t)}{dt} \tag{4.48}$$

$$v_{rb}(t) = r_r i_{rb}(t) + \frac{d\psi_{rb}(t)}{dt} \tag{4.49}$$

$$v_{rc}(t) = r_r i_{rc}(t) + \frac{d\psi_{rc}(t)}{dt} \tag{4.50}$$

The space vector form of the rotor frame equation is

$$\overline{v}_r(t) = r_r \overline{i}_r(t) + \frac{d\overline{\psi}_r(t)}{dt} \tag{4.51}$$

The rotor voltage can also be expressed in the stator reference frame as

$$\overline{v}_r'(t) = r_r \overline{i}_r'(t) + \frac{d\,\overline{\psi}_r'(t)}{dt} - j\omega_r\,\overline{\psi}_r'(t) \tag{4.52}$$

The winding voltage equations can be expressed in terms of currents and inductances rather than flux linkages. If the stator flux is expressed in terms of machine inductance and winding currents, then Equation 4.52 becomes

$$\overline{v}_s(t) = r_s \overline{i}_s(t) + L_s \frac{d\,\overline{i}_s(t)}{dt} + L_m \frac{d\,\overline{i}_r'(t)}{dt} \tag{4.53}$$

Similarly, the rotor voltage equation becomes

$$\overline{v_r'}(t) = r_r \overline{i}_r'(t) + L_r \frac{di_r'(t)}{dt} + L_m \frac{d\,\overline{i}_s(t)}{dt} - j\omega\left(L_r \overline{i}_r'(t) + L_m \overline{i}_s(t)\right) \tag{4.54}$$

The combined stator and rotor voltages may be expressed in a compact matrix form as

$$\begin{bmatrix} \overline{v}_s(t) \\ \overline{v_r'}(t) \end{bmatrix} = \begin{bmatrix} r_s & 0 \\ 0 & r_r \end{bmatrix} \begin{bmatrix} \overline{i}_s(t) \\ \overline{i_r'}(t) \end{bmatrix} + \frac{d}{dt} \begin{bmatrix} L_s & L_m \\ L_m & L_r \end{bmatrix} \begin{bmatrix} \overline{i}_s(t) \\ \overline{i_r'}(t) \end{bmatrix} - j\omega_r \begin{bmatrix} 0 & 0 \\ L_m & L_r \end{bmatrix} \begin{bmatrix} \overline{i}_s(t) \\ \overline{i_r'}(t) \end{bmatrix} \tag{4.55}$$

The torque production in this elemental machine from the change in the magnetic field energy with changes in the rotor angle can be found to be [10]

$$t_e(t) = -\frac{3}{2}\,\overline{\psi_r'}(t) \times \overline{i_r'}(t) \tag{4.56}$$

This torque equation is in the stationary frame. Torque is invariant with the reference frame, so the following is valid [10]

$$t_e(t) = -\frac{3}{2}\,\overline{\psi_r}(t) \times \overline{i_r}(t) \tag{4.57}$$

Equation 4.57 can be rewritten using the expression for the rotor flux, as

$$t_e(t) = -\frac{3}{2}\left(L_r \overline{i}_r'(t) + L_m \overline{i}_s(t)\right) \times \overline{i}_r'(t) \tag{4.58}$$

Recognising that the cross-product of a vector with itself is zero, an alternative torque equation is

$$t_e(t) = -\frac{3}{2}\,L_m\,\overline{i}_s(t) \times \overline{i}_r'(t) \tag{4.59}$$

This can be expanded as [10]

$$t_e(t) = -\frac{3L_m}{2L_s}\left(L_m \overline{\imath}_r'(t) + L_s \overline{\imath}_s(t)\right) \times \overline{\imath}_r'(t) \tag{4.60}$$

The bracketed term is the stator flux linkage, which includes a product of the stator inductance and current and the mutual flux of the rotor. Further equivalent expressions for the electromagnetic torque are [10]

$$t_e(t) = -\frac{3L_m}{2L_s}\overline{\psi_s}(t) \times \overline{\imath}_r'(t) \tag{4.61}$$

$$t_e(t) = -\frac{3L_m}{2L_s L_r}\overline{\psi_s}(t) \times \overline{\psi_r}'(t) \tag{4.62}$$

Equation 4.10 gave an expression for torque for a two-coil machine, where torque was the product of the current magnitudes and the sine of the angle between the two winding sets. Equation 4.62 is structurally similar, where the torque is determined by the magnitudes of the current space vectors and the sine of the angle separating these. Equation 4.61 shows that torque is a cross-product of the stator flux phasor and the rotor current phasor. The elemental machine of Figure 4.1 showed the same dependencies. In the case where the machine has more than two poles, the torque equations become

$$t_e(t) = -\frac{3}{2}\frac{P}{2}L_m \overline{\imath}_s(t) \times \overline{\imath}_r'(t) \tag{4.63}$$

$$t_e(t) = -\frac{3L_m}{2L_s}\frac{P}{2}\overline{\psi_s}(t) \times \overline{\imath}_r'(t) \tag{4.64}$$

where P is the number of poles.

These equations show that an AC traction motor can be torque controlled by the application of controlled stator and rotor currents. The stator is normally connected to an inverter that has a direct influence on the stator current. In some machines, notably synchronous machines and doubly fed induction machines, the rotor is directly controlled. More often, the rotor circuit is isolated and the rotor currents are indirectly controlled from the stator side.

4.5.3 Synchronous Traction Motors and Control Strategies

Synchronous traction motors have

- A rotor that carries either a DC field winding or permanent magnets; and
- A three-phase stator winding, which may be called an armature.

The use of permanent magnets for traction machines has thus far been limited to lower power applications and is not seen in heavy haul applications [7]. Permanent

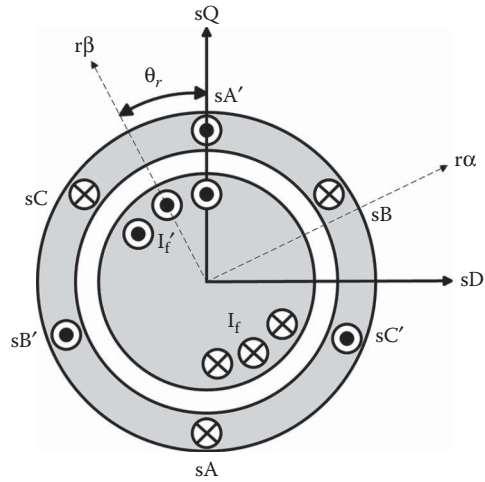

FIGURE 4.8 Synchronous machine.

magnet machines achieve high power-to-weight ratios, but the magnets themselves have a degree of mechanical and electrical fragility. The range of operating temperatures can be limited, and the materials may be demagnetised in certain conditions. The eventual application of permanent magnets for heavy haul applications cannot be completely discounted, given a steady advance in magnet technology.

The synchronous machine, as shown in Figure 4.8, can be considered as a special case of the elemental machine shown in Figure 4.6. The stator carries a three-phase winding that produces a rotating stator MMF phasor, $\overline{\psi}_s(t)$. The rotor is simplified and has only one winding, that is, the field winding. This winding carries a DC current and the rotor produces a DC MMF. The field MMF distribution around the air gap is a function of θ_r, the angle relative to the physical axis of the field winding. This distribution is approximately sinusoidal, but for a machine intended for an inverter drive application, this distribution can deviate considerably. In Figure 4.8, the rotor axis is physically displaced from the stator reference frame by θ_r. The rotor MMF is at its maximal value along the direct axis, or the α axis of the rotor as shown in Figure 4.8. The MMF falls to zero along the quadrature axis, or the β axis, which is displaced 90 electrical degrees. If the rotor rotates at synchronous speed, then the rotor MMF phasor, $\overline{\psi}_r'(t)$, also moves at synchronous speed. The machine develops a torque that is proportional to the cross-product of the stator and rotor MMFs. For constant torque production, the relative angle between the stator and rotor must remain constant and the rotor must move at synchronous speed.

The general form of the torque equation is as seen in Equation 4.62. The constants will change in recognition of the replacement of the three-winding rotor with a single-winding rotor. A very popular control method for a synchronous machine, the rotor FOC method [10], is as follows:

- Adjust the rotor current, $i_f(t)$, to maintain the highest flux level that is consistent with the field rating, the operating speed and the available stator voltage;

- Physically measure the rotor position, as this determines the rotor MMF phasor angle that is on the α axis;
- Set the stator MMF phasor angle $\theta_s = \theta_r \pm \pi/2$ for maximum torque production in traction or braking, as required;
- Set the phasor current magnitude according to the required torque;
- Calculate the physical phase currents from the required stator MMF; and
- Impress those currents with a current-controlled inverter.

In this method, the stator current phasor phase angle, and hence the stator frequency, is completely determined by the speed of the mechanical machine. The drive can start from standstill, and in this case, the stator currents are DC but their magnitudes are such that the MMF of the stator is orthogonal to the rotor flux from maximum torque. As the rotor begins to rotate, the stator MMF advances to maintain the torque-producing angle.

The synchronous machine generates an internal voltage owing to the motion of the rotor and to the resultant cutting of the stator conductors by rotor MMF. The equivalent circuit of the synchronous machine is shown in Figure 4.9. The internal voltage, $e_a(t)$, is termed the air gap voltage. The reactance, L_s, termed the synchronous reactance, determines the peak torque capability of the machine. The field circuit is included and is modelled by a reactance and the field winding resistance. The field is normally supplied via slip rings and a secondary converter that can supply sufficient current and voltage. If the drive is required to have fast dynamics, the field may need to change relatively quickly and a significant driving voltage may be required to overcome the field inductance. In a drive application, a brushless exciter would generally be avoided as this introduces additional dynamics into the field current control which is undesirable from a bandwidth perspective.

The synchronous machine drive exhibits the familiar low-speed or constant-torque region and the high-speed or field-weakening regimes. At a certain rated speed, ω_{rated}, or frequency, f_{rated}, the induced air gap voltage would exceed the capability of the drive inverter, and control of the stator current would be lost unless the field current was reduced. The inverter voltage is the vector sum of the air gap voltage and the voltage drop across the synchronous reactance. In a traction operation with rotor FOC, the inverter voltage must be higher than the air gap voltage to drive current into the stator. A reduction in the rotor flux to accommodate the

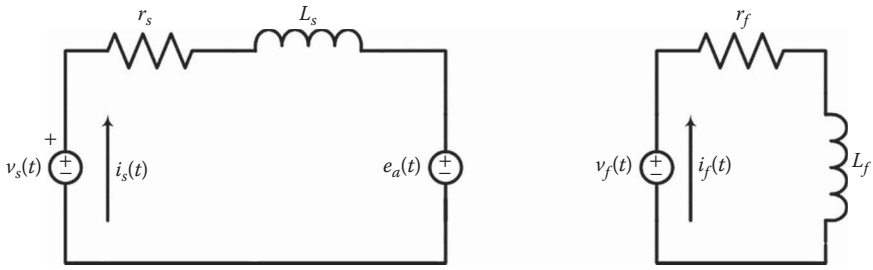

FIGURE 4.9 Synchronous machine equivalent circuit.

inverter voltage limit reduces the torque capability. All DC and AC drives share this inherent characteristic.

The rotor FOC method is not suited to synchronous machines using the LCI approach [10]. The LCI drive uses the internal air gap voltage of the machine to commutate thyristor switches in the drive inverter. Very large drives, tens of megawatts, can be produced in this way, and in the early history of power electronics, this was an advantage. Although at least one LCI application has been seen in high-speed rail [7], for a modern locomotive, the LCI approach is no longer technically necessary as adequate-power semiconductors are available. The LCI has poor performance at low speed because the commutation effect is reduced by a low air gap voltage, and this is a disadvantage in heavy haul applications.

4.5.4 Induction Traction Motors and Control Strategies

The induction machine most commonly applied in heavy haul applications is the squirrel-cage machine. The rotor winding is constructed by die casting the rotor bars directly into a prepared stack of rotor laminations. The winding is short circuited by diecast end rings. These are diecast onto the end of the rotor lamination stack, normally as part of the rotor bar die casting operation. The rotor that has an uninsulated construction is extremely robust. The material most frequently used is aluminium, but in heavy haul, traction copper can be applied [11]. Copper has a lower electrical resistivity on a volume basis relative to aluminium, and therefore, in a space- and cooling-constrained motor design, the losses will be lower. Copper has a higher specific thermal mass and melting point, which allows higher short-term overloads relative to an aluminium cage.

The electrical operations of the squirrel-cage machine can be represented by Equation 4.55 with a zero rotor voltage term, as follows:

$$\begin{bmatrix} \overline{v}_s(t) \\ 0 \end{bmatrix} = \begin{bmatrix} r_s & 0 \\ 0 & r_r \end{bmatrix} \begin{bmatrix} \overline{\imath}_s(t) \\ \overline{\imath}_r'(t) \end{bmatrix} + \frac{d}{dt} \begin{bmatrix} L_s & L_m \\ L_m & L_r \end{bmatrix} \begin{bmatrix} \overline{\imath}_s(t) \\ \overline{\imath}_r'(t) \end{bmatrix} - j\omega_r \begin{bmatrix} 0 & 0 \\ L_m & L_r \end{bmatrix} \begin{bmatrix} \overline{\imath}_s(t) \\ \overline{\imath}_r'(t) \end{bmatrix} \tag{4.65}$$

These equations can be represented as an equivalent circuit diagram, as shown in Figure 4.10. The stator circuit contains the applied stator space vector, $\overline{v}_s(t)$, the stator resistance and two inductances. The magnetising inductance is L_m and the stator leakage inductance is $L_{sl} = L_s - L_m$. The rotor circuit contains the rotor resistance, r_r, and two inductances. The magnetising inductance is L_m and the rotor leakage inductance is $L_{rl} = L_r - L_m$. The voltage source is a rotor speed-dependent term. The electrical power transferred to this source is the mechanical power delivered to the rotor. This voltage is

$$-j\omega_r \left(L_m \overline{\imath}_s(t) + L_r \overline{\imath}_r'(t) \right) = -j\omega_r \overline{\psi}_r(t) \tag{4.66}$$

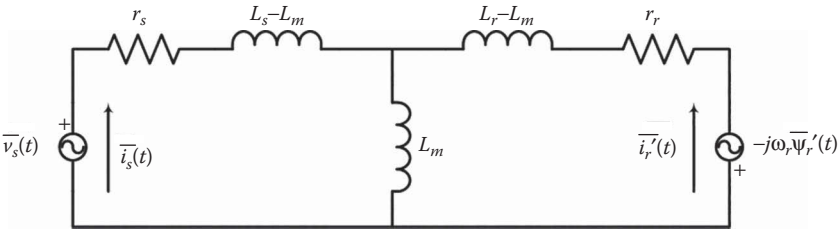

FIGURE 4.10 Equivalent circuit representation in phasor form.

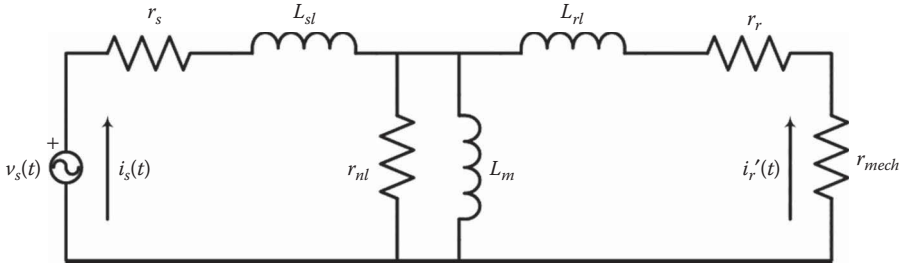

FIGURE 4.11 Equivalent circuit representation in phase variables.

The power delivered to this voltage source by the passage of the rotor current is the product of the voltage phasor with the conjugate of the current phasor and is presented in [10] as:

$$P_m = \frac{3}{2}\mathrm{Re}\left(-j\omega_r \overline{\psi_r}(t)\,\overline{i_r}'(t)^*\right) = \omega_r\left[-\frac{3}{2}\overline{\psi_r}(t)\times\overline{i_r}'(t)\right] = \omega_r T_e \tag{4.67}$$

The phasor form of the equivalent circuit can be readily redrawn in terms of the phase variables, that is, the phase voltages and currents, as shown in Figure 4.11. Here, the circuit components have been replaced with the winding resistances, winding leakage reactances and the magnetising inductance that can be physically measured in no-load and blocked rotor tests. The mechanical power element has been replaced by an equivalent load resistor. An additional resistor has been placed in parallel with the magnetising inductance. This 'no-load loss' resistor is included to capture:

- Magnetic losses in the stator and rotor due to eddy currents and hysteresis; and
- Parasitic mechanical losses due to windage or mechanical bearing losses.

Arguably, these could be split into two loss resistors, but it is not possible to resolve the no-load loss into an electrical component and a mechanical component just on the basis of normal no-load test recordings of the stator current, voltage and power factor.

It can be shown that the mechanical load resistance is [12]:

$$r_{\text{mech}} = r_m \left[\frac{1-s}{s} \right] \tag{4.68}$$

where s is the rotor slip, and

$$s = \frac{\omega_r}{\omega_e} \tag{4.69}$$

The machine currents and voltages can be found for any given rotor slip condition by the application of classical circuit theory. Once these are known, it is possible to determine the power in the mechanical load, the resultant mechanical torque, the machine losses, the electrical/mechanical conversion efficiency and the power factor. As an illustrative example, these are found over a slip range from 0% to 20% for a high-quality traction motor, using the parameters as given in Table 4.3 [13]. These machine parameters are derived from blocked rotor and no-load tests. The key results are seen in Figures 4.12 through 4.17. Figure 4.12 shows that the machine rapidly develops torque with increasing slip. There is a clear peak in the torque curve. This peak torque, known as the pull-out torque, is a multiple of the normal operating torque. Induction machines achieve their full-load torque at low slip. This machine achieves 500 kW at 1.83% slip at a shaft speed of 854 rpm and a mechanical torque of 5.59 kN/m. The machine efficiency is 95.5% and the machine losses are 23.3 kW. The stator input power is 523 kW, the apparent power is 585 kVA, the current is 167 A and the power factor is 0.89.

Figure 4.12 shows the motor torque peaks at 16.9 kN/m and a slip of 11.6%. This is 3 times higher than the rated torque, but an inspection of other performance curves

TABLE 4.3
Traction Motor Parameters

Parameter	Value
Real power rating	500 kW
Line-to-line voltage	2027 Vrms
Number of phases	3
Base frequency	29 Hz
Number of poles	4
Stator resistance	132 mΩ
Stator reactance	3.14 mH
Rotor resistance	132 mΩ
Rotor reactance	3.14 mH
Magnetising resistance	1240 Ω
Magnetising reactance	117 mH

Source: Spiryagin, M., *Vehicle Syst. Dyn.*, 53(5), 672–691, 2015.

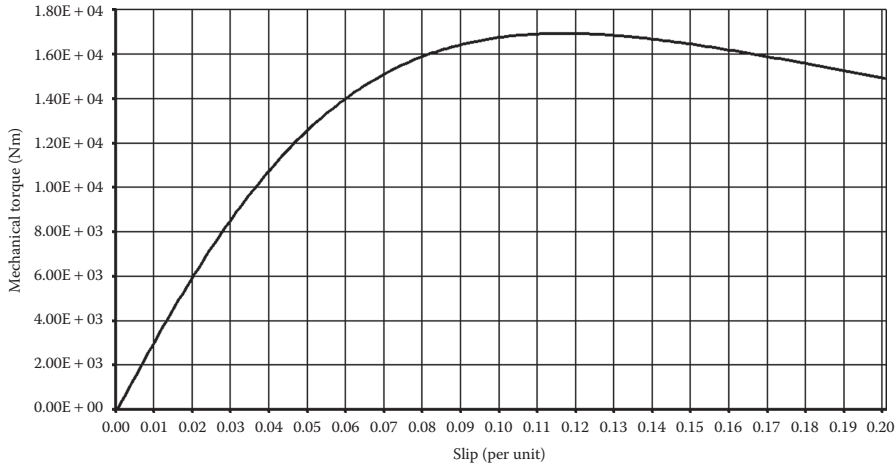

FIGURE 4.12 Mechanical torque (Nm) versus slip (per unit).

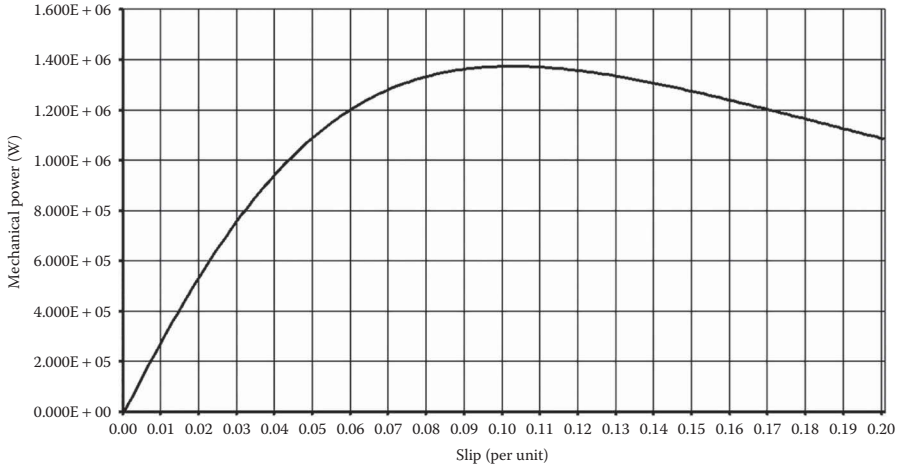

FIGURE 4.13 Mechanical power (W) versus slip (per unit).

shows that this is a very undesirable operating point. The conversion efficiency and power factor have fallen to 79% and 0.71%, respectively. The machine losses are extremely high at 370 kW, and this is more than 15 times the losses at the machine's 500 kW rating. The stator current has also reached 691 A. A three-fold increase in torque has been achieved with a four-fold increase in current, and this imposes additional inverter costs.

All practical induction machine control methods seek to operate the machine in the low-slip region where the efficiencies are high, the machine losses and cooling requirements are low and good torque production is achieved for the magnitude of

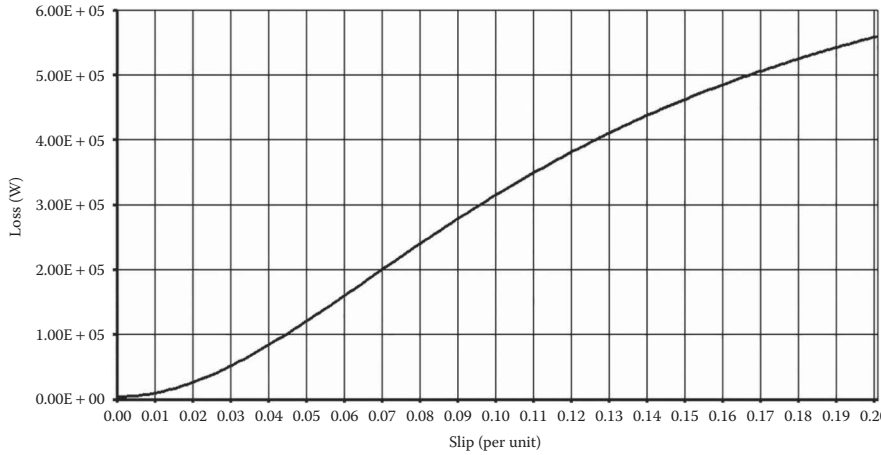

FIGURE 4.14 Machine losses (W) versus slip (per unit).

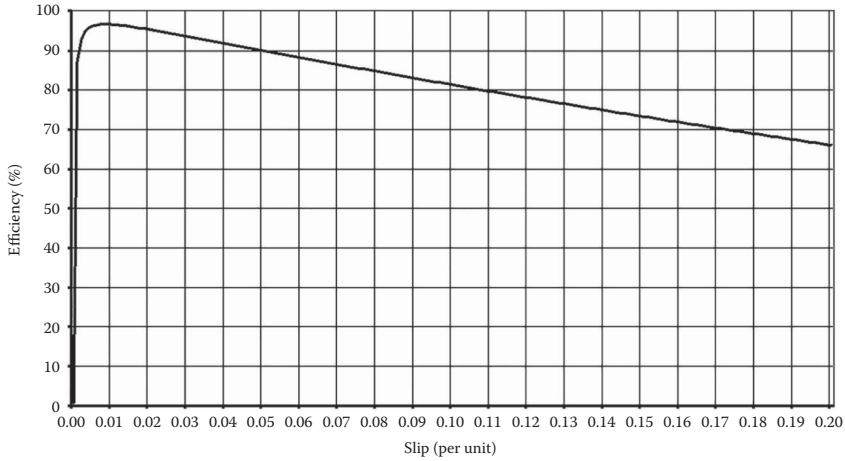

FIGURE 4.15 Conversion efficiency versus slip (per unit).

the applied stator current. This can be achieved by carefully adjusting the stator frequency to purposefully limit the slip to keep the machine in the low-slip, high-torque region. Several control methods are now discussed.

4.5.4.1 Scalar Control

Scalar control is the earliest form of control implemented in AC variable-frequency drives [12]. In comparison with the FOC and DTC methods [14,15], this technique is now considered obsolete. A short discussion is included, as the scalar methods do illustrate some fundamental characteristics and limitations of variable-frequency

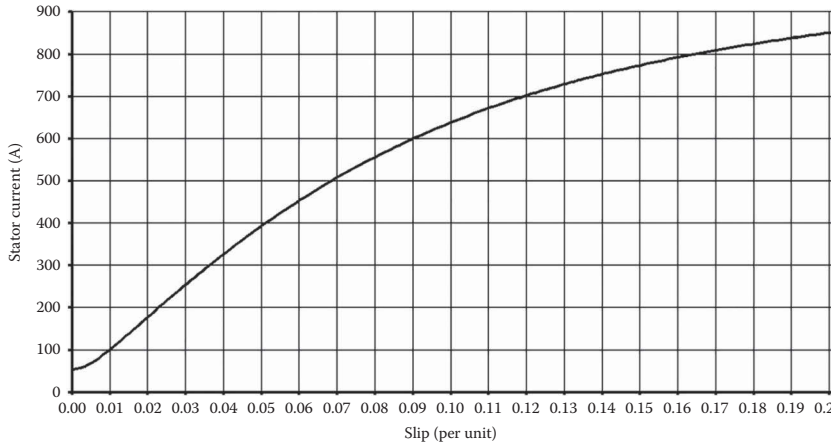

FIGURE 4.16 Stator current (A) versus slip (per unit).

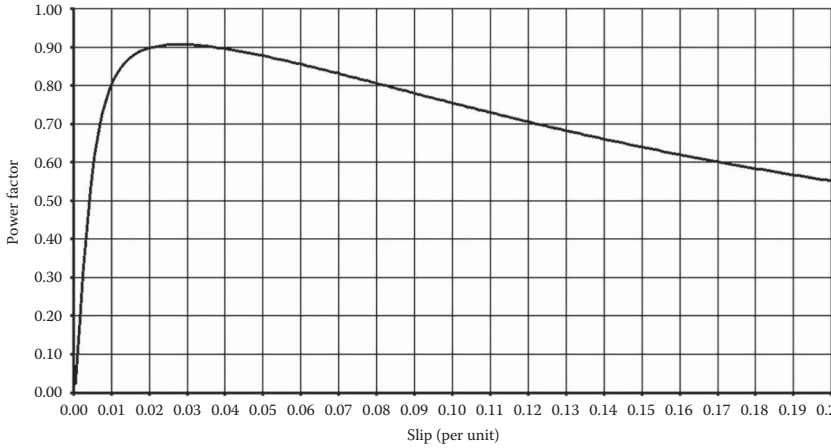

FIGURE 4.17 Power factor (PF) versus slip (per unit).

drives that still appear in the advanced control methods. The scalar drive can achieve a similar steady state performance, but the modern methods have superior dynamic responses.

The equivalent circuit, as seen in Figure 4.11, is the basis of the scalar control techniques. Two observations can be very quickly made:

- The best torque production is achieved in machines that are fully magnetised, and the magnetising current should be maintained at its rated condition. This implies that the stator voltage should be a function frequency.
- Machines work best in the low-slip regime, so the stator frequency needs to be controlled relative to the rotor frequency.

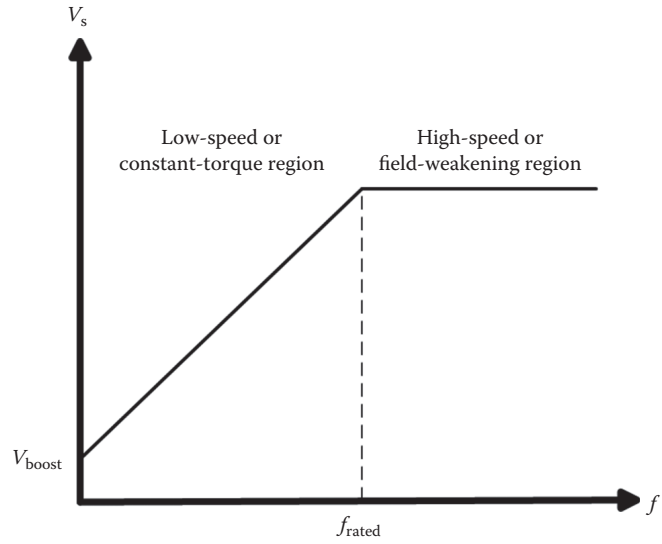

FIGURE 4.18 Constant volts per hertz control with low-frequency voltage boost.

With reference to Figure 4.11, if the voltage drop across the combined stator resistance and leakage inductance is small, then the magnetising flux is

$$\psi_m = \frac{v_s}{2\pi f_s} \tag{4.70}$$

To maintain a constant magnetising flux, the ratio of the stator voltage to the stator frequency should be constant. This is known as the Constant Volts per Hertz (CVH) method [13]. At low stator frequencies, the stator resistance becomes significant and it is a normal practice to boost the voltage, as shown in Figure 4.18. A minimum voltage, V_{s0}, is set for low-frequency operation. The proportionality of voltage and frequency can be maintained only up to the rated frequency, f_{rated}. Above this, the machine voltage is limited by the insulation system or the inverter DC bus voltage. At higher frequencies, the magnetising flux must fall and the machine enters the field-weakening or constant-power mode. Figure 4.19 shows a family of torque-speed curves for the traction motor example from Table 4.3 at various frequencies by using the scalar CVH method. For this motor, the base frequency is 29 Hz and the base voltage is 2027 V. A low-frequency boost voltage equal to 5.5% of the machine voltage is applied to overcome the stator resistance drop at low speeds. The pull-out torque is maintained up to the base speed. Above the base speed, the machine flux reduces linearly with frequency. The steady-state torque falls linearly with frequency. The pull-out torque, which is proportional to the square of the flux, falls much faster.

For this traction motor, the pull-out torque at rated frequency is 3 times the steady-state torque rating. The pull-out torque is a design variable, and the machine designer can influence the pull-out and steady-state torque ratios. A ratio of 3:1 for the pull-out

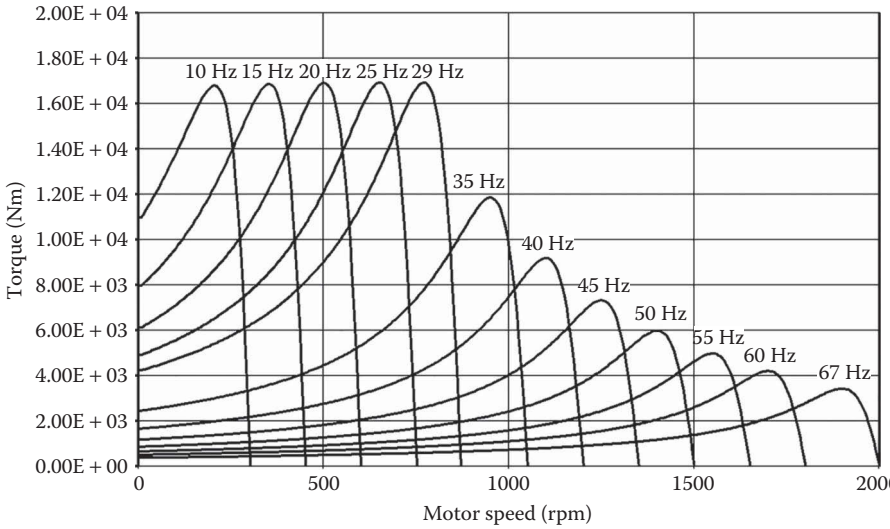

FIGURE 4.19 Torque speed curves for a V/f-controlled four-pole traction motor.

torque and rated torque at base frequency will allow the machine to work up to 3 times the base frequency while retaining its rated power. Consider the following

- At 29 Hz, the base frequency, the machine develops 5.59 kN/m at 89.5 r/s (854 rpm) or 500 kW, and the pull-out torque is 16.9 kN/m; and
- At 87 Hz, 3 times the base frequency, the machine is expected to develop 500 kW or 1.86 kN/m at 268 r/s, and this is equal to its pull-out torque which is one-ninth the pull-out torque at the rated frequency.

This choice of pull-out torque allows the constant horsepower regime to extend to 3 times the rated frequency. If the drive is operated at still higher frequencies, the pull-out torque becomes the operational limitation. An extended constant power region allows the locomotive to reach its top speed with a higher gear box ratio. This translates into higher torque at the wheelset in the low-speed region.

A slip-controlled drive with CVH control is shown in Figure 4.20 for the purposes of explaining the scalar methods in a simple application. This is a speed-controlled drive, where the target mechanical speed is ω_m^*. This is compared with the machine speed to form a speed error, $\Delta\omega_m$. The correction of the speed error requires a machine torque, and this is produced by applying a controlled rotor slip frequency, ω_{sl}^*. The addition of the slip frequency to the mechanical rotor frequency determines a target stator frequency. A lookup table is then used to determine the appropriate stator voltage, v_s^*. The inverter is then controlled to produce three-phase waveforms of the correct voltage and frequency. A speed-controlled drive is not the preferred control for heavy haul traction. For vehicle propulsion systems torque-controlled drives are preferred. A drive that can provide well-controlled torque

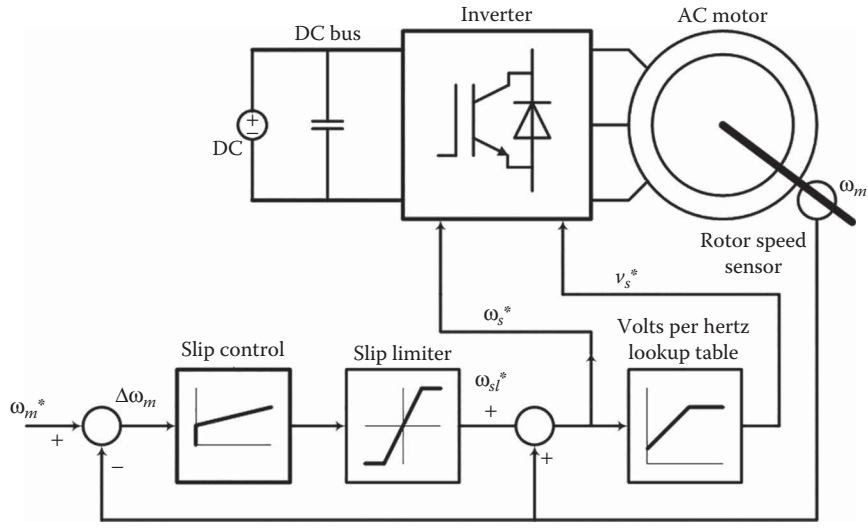

FIGURE 4.20 Speed-controlled scalar drive.

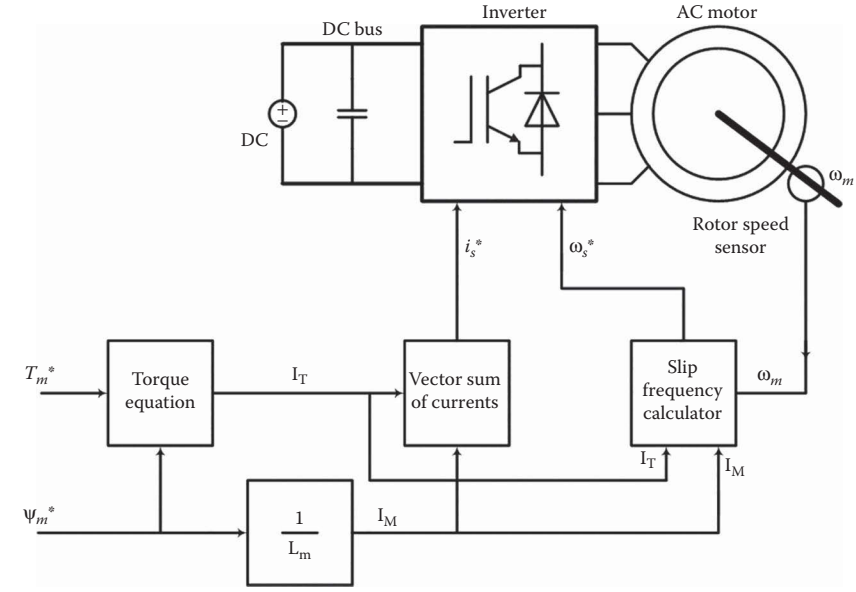

FIGURE 4.21 Scalar torque control.

outputs produces well-controlled traction forces, and this is desirable from a vehicle-handling and maintenance viewpoint. In heavy haul systems in particular, a good traction control system is a prerequisite for a high-quality adhesion control system.

A torque-controlled scalar drive is shown in Figure 4.21. In this case, the inverter is current controlled. At least two of the motor phase currents are fed

back to the inverter controller. The motor current applied by the inverter contains two components – a flux-generating current and a torque-producing current. The flux-generating current is calculated from a reference flux table that is frequency dependent. Full flux is applied below the rated frequency and reduced flux in the field-weakening region. A torque-producing current is calculated from the torque demand signal and the magnetising flux. The two currents are added orthogonally to produce an inverter current magnitude. A slip frequency is calculated from the torque requirement and the available flux, and this is added to the rotor frequency to give a final stator frequency.

The limitations of the scalar methods are rooted in simplified equivalent models used to represent the induction machine behaviour. These models produce good steady state results, but none of the dynamic processes within the machine are captured. As a result, the scalar drives are slow to respond to changes in speed and torque demands. A significant change in torque will typically be achieved over tens of electrical cycles. Modern FOC or DTC drives, which make full use of the phasor models, can achieve full torque reversals within an electrical cycle. These are an order of magnitude more responsive than the scalar models, and this advantage is achieved without any significant additional cost.

4.5.4.2 Vector Control

Traction applications utilise a variety of FOC or vector control to implement AC motor control schemes that yield high-quality dynamic performances. DTC is an example of a related vector-based control scheme that, amongst others, will be discussed in this chapter. DTC offers a simplified implementation relative to the FOC drives, but, given the low cost of control processors, this is a small difference.

For either DTC or FOC control methods, the induction machine is represented using the D–Q axes model. Consider the general AC induction machine, as shown in Figure 4.22. To focus the discussion on the D–Q model, a two-winding representation is used. The stator windings for A, B and C phases are replaced by two-phase windings, D and Q, that would provide an identical MMF if these windings carried currents, as calculated using the Clarke Transformation relationship given in Equation 4.25.

Assume that the direct axis winding D carries a fixed current that produces a magnetising flux ψ_m'. If at $t = t_0$, a current is suddenly injected into the stator Q axis winding, an opposing current is introduced into the mutually coupled rotor

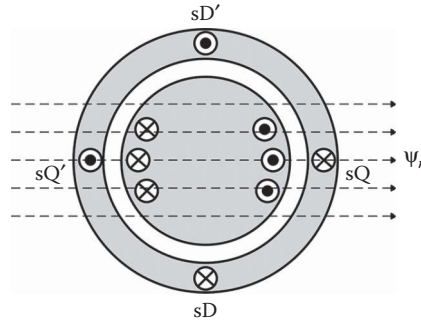

FIGURE 4.22 Two-phase induction machine.

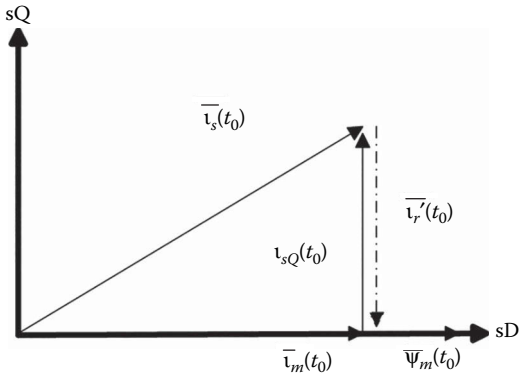

FIGURE 4.23 Rotor current and magnetising flux at $t = t_0$.

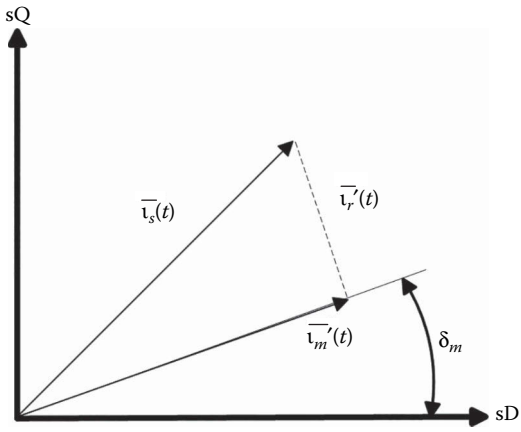

FIGURE 4.24 Realignment via mechanical rotation of the stator.

(Lenz's law). If the equivalent turns ratio is 1:1, then a current phase diagram can be drawn, as shown in Figure 4.23 [10].

The magnetising space phasor, $\overline{\imath_m}(t_0)$, is the sum of the stator space phasor, $\overline{\imath_s}(t_0)$, and the rotor space phasor, $\overline{\imath_r}'(t_0)$. The rotor current and magnetising vectors are orthogonal, and the torque as expressed in Equation 4.61 is maximised. The magnetising flux vector remains aligned with the D axis.

As time passes, the rotor current exponentially decays according to the rotor time constant. As the rotor current is reduced, the orthogonal relationship of the rotor current and the magnetising flux is lost, as shown in Figure 4.24.

This alignment could be re-established by physically rotating the stator through a mechanical angle, δ_m, as shown in Figure 4.24. In a drive system, this mechanical rotation is avoided by adjusting the currents in the D axis and Q axis windings. A new x, y reference frame that rotates at an appropriate mechanical speed, so that the x axis remains aligned with the magnetising current vector, is defined in Figure 4.25.

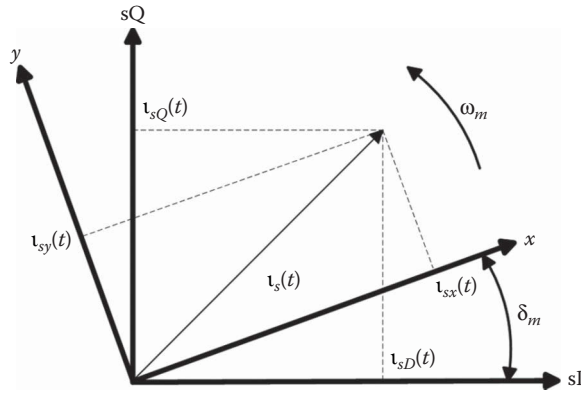

FIGURE 4.25 Rotor flux-aligned reference frame.

The relationship between the stator aligned currents and the currents in the *x*–*y* reference frame is [10]:

$$\begin{bmatrix} i_{sx} \\ i_{sy} \end{bmatrix} = \begin{bmatrix} \cos(\delta_m) & -\sin(\delta_m) \\ \sin(\delta_m) & \cos(\delta_m) \end{bmatrix} \begin{bmatrix} i_{sD} \\ i_{sQ} \end{bmatrix} \tag{4.71}$$

or

$$\overline{\iota_{sm}} = \overline{\iota_s}\, e^{-j\delta_m} \tag{4.72}$$

In the special *x*–*y* reference frame, the magnetising flux is aligned with the *x* axis. The torque equation becomes [10]:

$$t_e(t) = -\frac{3}{2}\frac{P}{2}\,\overline{\psi_{sm}}(t) \times \overline{\iota_{sy}}(t) \tag{4.73}$$

As the magnetising current is aligned to the *x* axis, this may be rewritten as

$$t_e(t) = -\frac{3}{2}\frac{P}{2} L_m\, \overline{\iota_{mx}}(t) \times \overline{\iota_{sy}}(t) \tag{4.74}$$

These equations show that the machine torque is a product of the magnetising flux and the quadrature torque-producing stator current. This is the basis of all the rotor flux FOC or vector-control schemes. The implementation schemes vary considerably, and this variation is driven by the practical requirements of specific implementations.

4.5.4.2.1 Field-Oriented Control

One major practical issue is the need to align the stator current components with the magnetising flux of the rotor. There are two major implementation methods – the direct and indirect methods. The direct method is shown in Figure 4.26. In this

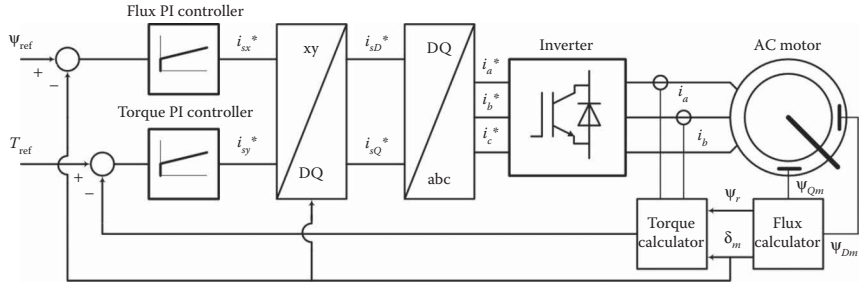

FIGURE 4.26 Direct rotor flux-oriented control.

method, the air gap magnetising flux is directly measured either by flux sensors or by search coils where the coil voltage, the flux derivative, is integrated to produce *D* axis and *Q* axis signals. The rotor flux can be calculated from [13]:

$$\overline{\psi}_r(t) = \frac{L_r}{L_m}\,\overline{\psi}_m(t) - L_{ls}\overline{i}_s(t) \tag{4.75}$$

The rotor flux phasor incorporates information regarding the magnitude of ψ_m, and the angle, δ_m. The rotor flux magnitude is controlled to track a reference flux, ψ_{ref}, which is selected according to the operating frequency. Typically, the machine is operated at rated flux below the rated speed, and field weakening is applied in the high-speed region. The proportional-integral (PI) flux controller adjusts the rotor *x* axis current to maintain the required flux.

The torque calculator has access to the stator current measurements, and hence the stator current phasor. This can be converted into the *x* and *y* components by using the rotor flux angle and Equation 4.71. The electromagnetic torque can then be determined using Equation 4.61. The torque controller compares the torque reference to the electromagnetic torque and adjusts the machine torque by manipulating the *y* axis current. The stator *x* and *y* axis currents are converted first into *D* and *Q* components by utilising the rotor flux angle, and then into *a*, *b* and *c* phase currents. In this implementation, the inverter is current controlled and is able to impress the required currents upon the induction machine.

The obvious difficultly with direct FOC is the presence of the air gap flux sensors. The air gap is a hot, electrically dangerous and an aggressive vibration environment. The sensors therefore present a reliability issue. An alternative is to use a rotor flux estimator that is often based on state estimators or observers.

The indirect or flux feed-forward method avoids the need for the direct measurement of the rotor flux [13]. The magnitude and location of the rotor flux vector are calculated from the stator currents and rotor speed. The method is illustrated in Figure 4.27. The rotor flux angle can be calculated from the mechanical angle of the rotor and the integration of ω_r, the necessary rotor frequency for flux orientation:

$$\delta_m(t) = \theta_r(t) + \int_0^t \omega_r(t)\,dt \tag{4.76}$$

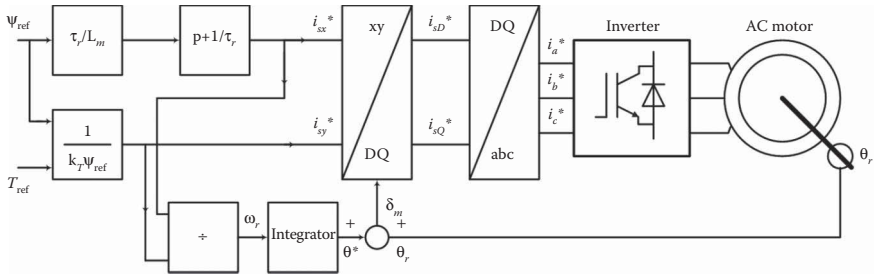

FIGURE 4.27 Indirect rotor flux field-oriented control.

The rotor frequency can be found using the following procedure. The stator frame rotor flux equation can be written as:

$$\overline{i_r'}(t) = \frac{1}{L_r}\left(\overline{\psi_r'}(t) - L_m\overline{i}_s(t)\right) \tag{4.77}$$

This can be substituted into the rotor voltage Equation 4.66 to yield:

$$L_m\overline{i}_s(t) = \overline{\psi_r'}(t) + \tau_r\left(p - j\omega_r\right)\overline{\psi_r'}(t) \tag{4.78}$$

In field orientation, the rotor flux axis, x, is aligned to the stator D axis. The real part gives [13]:

$$L_m i_{sx}(t) = \left(1 + \tau_r p\right)\psi_{rx}(t) \tag{4.79}$$

and the imaginary part gives [13]:

$$L_m i_{sy}(t) = -\tau_r\omega_r\psi_{rx}(t) \tag{4.80}$$

$$L_m i_{sy}(t) = -\tau_r\omega_r L_m i_{rx}(t) \tag{4.81}$$

$$\omega_r = \frac{1}{\tau_r}\frac{i_{sy}(t)}{i_x(t)} \tag{4.82}$$

This term can now be integrated and added to the mechanical rotor angle to determine the rotor flux angle. The y axis current required to produce the necessary flux can be calculated from Equation 4.80. The torque-producing x axis current magnitude can be calculated using the machine torque constant, k_T:

$$i_{sx}(t) = \frac{T_{\text{ref}}}{k_T\psi_{\text{ref}}} \tag{4.83}$$

The computed angle strongly depends on the rotor parameters, especially the rotor time constant. As these change with the operating temperature and saturation, some

form of on-line adaption is normally present. Another practical issue relates to the limitations of the driving power electronics. At higher powers, the switching frequency of inverters is somewhat limited and it is difficult to achieve perfect control of the stator currents. In many instances, the inverter must be treated as a voltage source. There are additional dynamics and cross-couplings between the D and Q axes that need to be compensated for in the inverter control. Even with these limitations, modern drives are capable of producing torque step changes or full reversals equal to the drive rating in a few tens of milliseconds. In practice, such aggressive changes are mechanically undesirable and torque rate limiting will be applied.

4.5.4.2.2 Direct Torque Control

The DTC method [13,15] utilises a space vector representation of the voltages that can be produced by a three-phase inverter. The induction machine is controlled by sequentially selecting a series of inverter output voltage phasors that cause the stator and rotor flux phasors to follow ideal trajectories in the DQ plane. Equation 4.62, which is reprinted below, shows that torque production is maximised if these two fluxes are orthogonal.

$$t_e(t) = -\frac{3L_m}{2L_s L_{sr}} \overline{\psi_s}(t) \times \overline{\psi_r}'(t) \tag{4.84}$$

A six-switch bridge (B6) inverter has three output terminals (a, b and c). These can be switched to connect to either the positive DC bus or the negative DC bus. If the potential at the positive bus is designated as E and that at the negative bus is designated as zero, then Table 4.4 shows the eight possible states that the B6 converter can produce. These phasors are represented diagrammatically in Figure 4.28.

At a particular instant, the stator and rotor fluxes in a machine may be positioned as shown in Figure 4.29. The rotor and stator fluxes are separated by an angle θ_{sr}. The stator flux vector, $\psi_s(t)$, is most directly affected by a short-term application of the stator voltage. The stator flux, neglecting the effect of the stator resistance, is the integration of the stator terminal voltages. The rotor flux vector is somewhat isolated

TABLE 4.4
Voltage Phasor Produced by a B6 Inverter

Conventional State	DTC State	V_a	V_b	V_c	V_D	V_Q
v_0	v_0	0	0	0	0	0
v_1	v_V	0	0	E	–E/3	–E/√3
v_2	v_{III}	0	E	0	–E/3	E/√3
v_3	v_{IV}	0	E	E	–2E/3	0
v_4	v_I	E	0	0	2E/3	0
v_5	v_{VI}	E	0	E	E/3	–E/√3
v_6	v_{II}	E	E	0	E/3	E/√3
v_7	v_{VII}	E	E	E	0	0

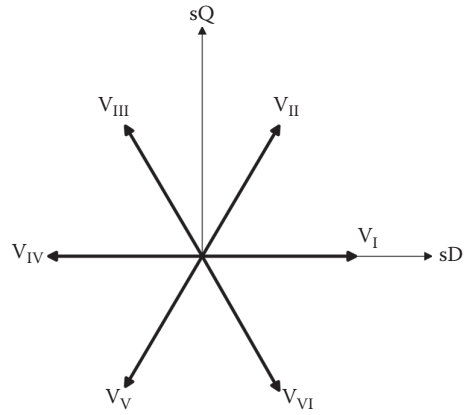

FIGURE 4.28 B6 inverter output voltage phasors.

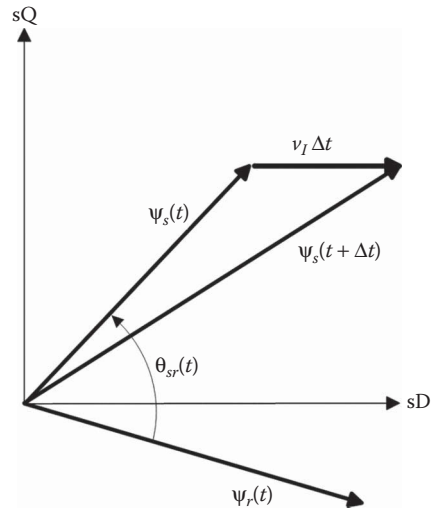

FIGURE 4.29 Influence of state v_I upon the stator flux vector.

from the effect of short-term voltages by the rotor and stator leakage inductances. These provide low-pass filtering, and the rotor flux changes more slowly than the stator flux. The change in the stator flux linkage is proportional to the volt-second product applied. If the voltage vector v_I is applied for Δt seconds, then the new stator flux is $\psi_s(t+\Delta t)$. In this case, the length of the stator flux vector increases and the rotor-stator angle reduces. This voltage vector application increases the machine magnetisation but reduces the torque angle. Each of the six inverter voltage vectors produces a different motion for the stator flux vector. By the appropriate selection of the inverter states, the stator flux vector can be forced to follow a circular trajectory. The radius is proportional to the magnetisation flux. The torque can be adjusted by

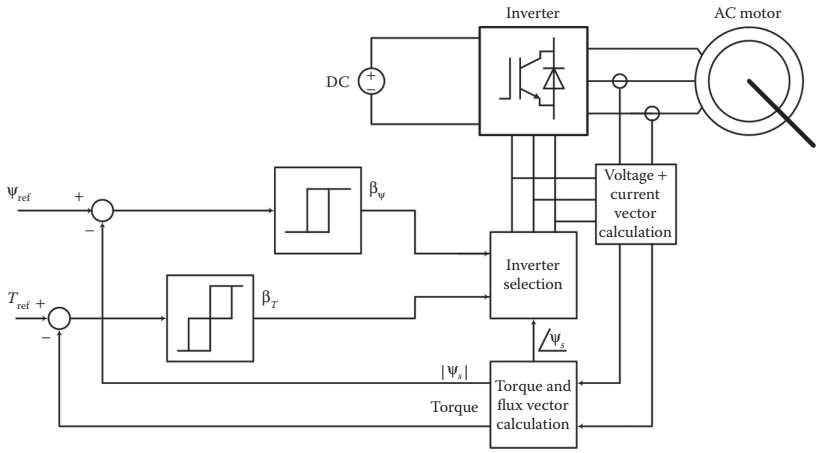

FIGURE 4.30 DTC drive.

TABLE 4.5
Vector Selection for a DTC Drive (Counterclockwise Rotation)

β_ψ	1			0		
β_T	**1**	**0**	**–1**	**1**	**0**	**–1**
Sector 1	6	7	5	2	0	1
Sector 2	2	0	4	3	7	5
Sector 3	3	7	6	1	0	4
Sector 4	1	0	2	5	7	6
Sector 5	5	7	3	4	0	2
Sector 6	4	0	1	6	7	3

Source: Spiryagin, M., *Vehicle Syst. Dyn.*, 53(5), 672–691, 2015.

controlling the angle between the stator and rotor fluxes, that is, by increasing or decreasing the stator frequency.

The block diagram of a DTC-controlled drive is shown in Figure 4.30. The motor voltages and currents are measured and the stator voltage and current phasors are determined. The electromagnetic torque and stator flux vector are determined from these. The stator flux angle determines the operating sector. The calculated torque is compared to the torque reference. The resulting torque error produces a decision variable, β_T, which takes on the value +1, 0 or −1 if the torque is to be raised, held steady or reduced, respectively. The stator flux magnitude is compared to a flux reference. The flux error produces a decision variable, β_ψ, which takes on a Boolean value of +1 if the flux is to be raised or 0 if it is to be reduced. The two decision variables drive the vector selection, which is a lookup table that gives the best state choice for each sector and the value of β_T and β_ψ. The contents of the vector selection table are given in Table 4.5 [13]. The voltage sectors are shown in

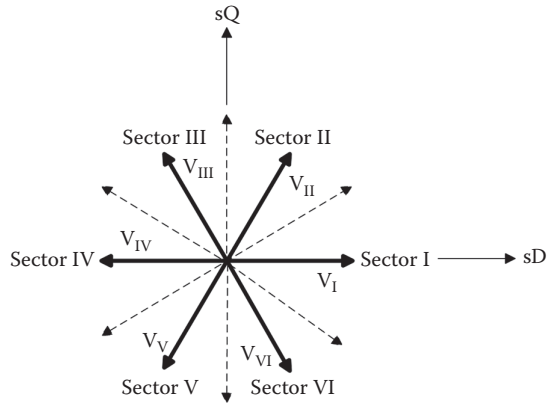

FIGURE 4.31 DQ plane sectors.

Figure 4.31. This is generically known as a 'bang-bang' control. In each decision period, a specific vector is selected and applied. To achieve a smooth operation of the drive, the decision period should be short so that the discrete electrical states are held for periods that are much less than the machine time constants. One state decision can be made for each inverter-switching period. In a modern inverter, switching can occur at a few kilohertz, so the decision period is typically a few hundred microseconds.

REFERENCES

1. M.C. Duffy, *Electric Railways: 1880–1890*, Institution of Engineering and Technology, Stevenage, UK, 2002.
2. R.J. Hill, Electric railway traction: Part 1 – Electric traction and DC traction motor drives, *IET Power Engineering Journal*, 8(1), 1994, 47–56.
3. R.J. Hill, Electric railway traction: Part 2 – Traction drives with three-phase induction motors, *IET Power Engineering Journal*, 8(3), 1994, 143–152.
4. N. Hugo, P. Stefanutti, M. Pellerin, A. Akdag, Power electronics traction transformer. In *IEEE European Conference on Power Electronics and Applications*, 2–5 September 2007, IEEE, Aalborg, Denmark, pp. 1–10.
5. H. Kamijo, H. Hata, H. Fujimoto, A. Inoue, K. Nagashima, K. Ikeda, M. Iwakuma et al., Tests of superconducting traction transformer for railway rolling stock, *IEEE Transactions on Applied Superconductivity*, 17(2), 2007, 1927–1930.
6. ABB Product Note: Rail traction: Synchronous generators for diesel-electric locomotives, 2014. https://library.e.abb.com/public/15b0232323c04e52c1257bbe001adfe8/Product%20note%20Rail%20tractiongeneratorLowRes_170914.pdf.
7. A.M. Refaie, Motors/generators for traction/propulsion applications: A review, *IEEE Vehicular Technology Magazine*, 8(1), 2013, 90–99.
8. SKF Solutions for Traction Motors, 2012. http://www.skf.com/au/system/SearchResult.html?search=traction+motors.
9. Alstom AGV Product Sheet, 2014. http://www.alstom.com/products-services/product-catalogue/rail-systems/trains/products/agv-very-high-speed-train/.
10. P. Vas, *Vector Control of AC Machines*, Oxford Science Publications, Oxford, UK, 1990.

11. ABB Product Note: Frameless induction traction motors, 2011 http://www.abb.com/product/seitp322/3288ca81d72fe139c12574c2004c424d.aspx.
12. A. Trzynadlowski, *Control of Induction Motors*, Academic Press, San Diego, CA, 2001.
13. M. Spiryagin, P. Wolfs, F. Szanto, C. Cole, Simplified and advanced modelling of traction control systems of heavy-haul locomotives, *Vehicle System Dynamics*, 53(5), 2015, 672–691.
14. D. Casadei, F. Profumo, G. Serra, A. Tani, FOC and DTC: Two viable schemes for induction motors torque control, *IEEE Transactions on Power Electronics*, 17(5), 2002, 779–787.
15. G.S. Buja, M.P. Kazmierkowski, Direct torque control of PWM inverter-fed AC motors – A survey, *IEEE Transactions on Industrial Electronics*, 51(4), 2004, 744–757.

5 Longitudinal Train Dynamics

5.1 INTRODUCTION

This chapter has been designed to provide a hands-on guide to both understanding and analysing longitudinal train dynamics. It is specifically focused on the longitudinal dynamics of heavy haul trains and adds new insights to a previous work by one of the co-authors [1].

Longitudinal train dynamics is defined as the motions of rail vehicles in the direction along the track. Therefore, it includes the motion of the train as a whole and any relative motions between the vehicles because of the looseness and travel allowed by spring and damper connections between vehicles. In the railway industry, the term 'slack action' is used for the relative motions of vehicles in a train due to the correct understanding that these motions are primarily allowed by the free slack and deflections existing in wagon connections. Coupling 'free slack' is defined as the free movement allowed by the sum of the clearances in the vehicle connection. In the case of autocouplers, these clearances consist of clearances in the auto-coupler knuckles and draft gear assembly pins. In older rolling stock connection systems, such as drawhooks and buffers, free slack is the clearance between the buffers measured in tension. Note that a system with drawhooks and buffers could be preloaded with the screw link to remove free slack. The occurrence of 'slack action' is further classified in various railways by different terms; in the Australian industry vernacular, the events are referred to as 'run-ins' and 'run-outs'. The case of a 'run-in' describes the situation where vehicles progressively impact each other as the train compresses. The case of a 'run-out' describes the opposite situation, where vehicles reach the extended extreme of the connection free slack as the train stretches. Different terms are used in other countries, for example, impact acceleration, jerk and so forth. Longitudinal train dynamics, therefore, has implications for driver and crew comfort, freight product damage, vehicle stability, rolling stock design and rolling stock metal fatigue [1].

The study and understanding of longitudinal train dynamics were probably initially motivated by the desire to reduce longitudinal vehicle dynamics in passenger trains and, in doing so, to improve the general comfort of passengers. The practice of 'power braking', which is the seemingly strange technique of keeping the locomotive power applied while a minimum air brake application is made, is still widely used in passenger trains. Power braking is also used on partly loaded mixed-freight trains to keep the train stretched during braking and when operating on undulating track. Interest in train dynamics in freight trains increased as trains became longer, particularly for heavy haul trains as evidenced in published technical papers. In the

late 1980s, measurement and simulation of in-train forces on such trains in Australia were reported by Duncan and Webb [2]. The engineering issues associated with moving to trains of double the existing length were reported at the same time, also in Australia, in a paper by Jolly and Sismey [3]. Another paper that focused on train-handling techniques on the Richards Bay line presented the South African experience [4]. The research at this time was driven primarily by the occurrence of fatigue cracking and tensile failures in auto-couplers. From these studies, an understanding of the force magnitudes was developed along with an awareness of the need to limit these forces with appropriate driving strategies [1–4].

More recent research into longitudinal train dynamics was started in the early 1990s, this time motivated, not by equipment failures and fatigue damage, but by derailments. The direction of this research was concerned with the linkage of longitudinal train dynamics to increases in wheel unloading. It stands to reason that, as trains get longer and heavier, in-train forces get larger. As coupler forces become larger, the lateral and vertical components of these forces resulting from coupler angles on horizontal and vertical curves also become larger. At some point, these components will adversely affect vehicle stability. The first known work published that addressed this issue was that of El-Siabie in 1993 [5], which investigated the relationship between lateral coupler force components and wheel unloading. Further modes of interaction were reported and simulated by McClanachan et al. in 1999 [6], who detailed vehicle body and bogie pitch.

Concurrent with this emphasis on the relationship between longitudinal dynamics and vehicle stability is the emphasis on train energy management. The operation of larger trains means that the energy consequences for stopping a train become more significant. Train simulators also now applied to the task of training drivers to reduce energy consumption. Measurements and simulations of the energy consumed by trains normalised per tonne-kilometre hauled have shown that different driving techniques can cause large variances in the energy consumed [7,8].

5.2 MODELLING LONGITUDINAL TRAIN DYNAMICS

5.2.1 Train Models

The longitudinal behaviour of trains is a function of train control inputs from the locomotive, train brake inputs, track topography, track curvature and vehicle connection characteristics.

The longitudinal dynamic behaviour of a train can be described by a system of differential equations. For the purposes of setting up the equations for modelling and simulation, it is usually assumed that there is no lateral or vertical movement of the vehicles. This simplification of the system is employed by all known commercial rail-specific simulation packages and by texts such as that of Dukkipati and Garg [9]. The governing differential equations can be developed by considering the generalised three mass train, as shown in Figure 5.1. It will be noticed that the in-train vehicle, whether locomotive or wagon, can be classified as one of only three connection configuration options, lead (shown as m_1), in-train and tail. All vehicles

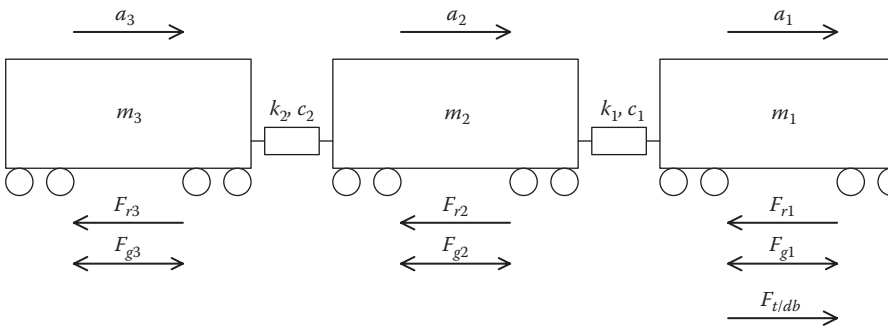

FIGURE 5.1 A three mass train model.

are subject to retardation and grade forces. Traction and dynamic brake forces are added to powered vehicles.

In Figure 5.1, a = vehicle acceleration (m/s^2), c = damping constant (Ns/m), k = spring constant (N/m), m = vehicle mass (kg), v = vehicle velocity (m/s), x = vehicle displacement (m), F_g = gravity force components due to track grade (N), F_r = sum of retardation forces (N) and $F_{t/db}$ = traction and dynamic brake forces from a locomotive unit (N).

It can be noted on the model in Figure 5.1 that the grade force can be in either direction. The sum of the retardation forces, F_r, is made up of rolling resistance, curving resistance or curve drag, air resistance and braking (excluding dynamic braking, which is more conveniently grouped with locomotive traction in the $F_{t/db}$ term). Rolling and air resistances are usually grouped in a term known as propulsion resistance, F_{pr}, resulting in the following equation:

$$F_r = F_{pr} + F_{cr} + F_b$$

where:

F_{pr} is the propulsion resistance
F_{cr} is the curving resistance
F_b is the braking resistance due to pneumatic braking

The three mass train allows three different differential equations to be developed. With linear vehicle connection models, the equations can be written as

$$m_1a_1 + c_1(v_1 - v_2) + x_1(x_1 - x_2) = F_{t/db} - F_{r1} - F_{g1} \tag{5.1}$$

$$m_2a_2 + c_1(v_2 - v_1) + c_2(v_2 - v_3) + k_1(x_2 - x_1) + k_2(x_2 - x_3) = -F_{r2} - F_{g2} \tag{5.2}$$

$$m_3a_3 + c_2(v_3 - v_2) + k_2(x_3 - x_2) = -F_{r3} - F_{g3} \tag{5.3}$$

Note that a positive value of F_g is taken as an upward grade, that is, a retarding force.

Allowing for locomotives to be placed at any train position and extending equation notation for a train of any number of vehicles, a more general set of equations can be written as:

For the lead vehicle:

$$m_1a_1 + c_1(v_1 - v_2) + k_1(x_1 - x_2) = F_{t/db1} - F_{r1} - F_{g1} \tag{5.4}$$

For the *i*th vehicle:

$$m_ia_i + c_{i-1}(v_i - v_{i-1}) + c_i(v_i - v_{i+1}) + k_{i-1}(x_i - x_{i-1}) + k_i(x_i - x_{i+1}) = F_{t/dbi} - F_{ri} - F_{gi} \tag{5.5}$$

For the *n*th or last vehicle:

$$m_na_n + c_{n-1}(v_n - v_{n-1}) + k_{n-1}(x_n - x_{n-1}) = F_{t/dbn} - F_{rn} - F_{gn} \tag{5.6}$$

By including $F_{t/db}$ in each equation, and thus on every vehicle, the equations can be applied to any locomotive placement or system of distributed power. $F_{t/db}$ is set to zero for unpowered vehicles.

For non-linear modelling of the system, the stiffness and damping constants are replaced with functions or more complex non-linear models. In the general case, the model must include dependency on both displacement and velocity (Figure 5.2). The generalised non-linear equations are therefore:

For the lead vehicle:

$$m_1a_1 + f_{wc}(v_1, v_2, x_1, x_2) = F_{t/db1} - F_{r1} - F_{g1} \tag{5.7}$$

For the *i*th vehicle:

$$m_ia_i + f_{wc}(v_i, v_{i-1}, x_i, x_{i-1}) + f_{wc}(v_i, v_{i+1}, x_i, x_{i+1}) = F_{t/dbi} - F_{ri} - F_{gi} \tag{5.8}$$

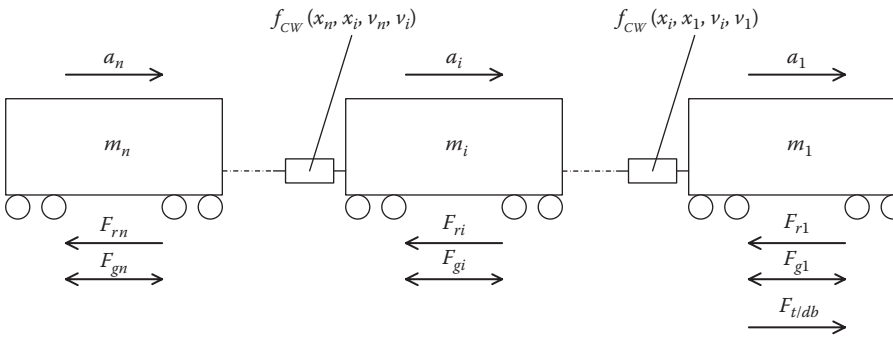

FIGURE 5.2 Generalised train model.

For the *n*th or last vehicle:

$$m_n a_n + f_{wc}(v_n, v_{n-1}, x_n, x_{n-1}) = F_{t/dbn} - F_{rn} - F_{gn} \tag{5.9}$$

where f_{wc} is the non-linear function that describes the full characteristics of the vehicle connection.

Solution and simulation of the above equation set are further complicated by the need to calculate the force inputs to the system, that is, $F_{t/db}$, F_r and F_g. The traction-dynamic brake force term, $F_{t/db}$, must be continually updated for driver control adjustments and any changes to the locomotive speed. The retardation forces, F_r, are dependent on braking settings, vehicle velocity, track curvature and rolling stock design. Gravity force components, F_g, are dependent on track grade and therefore on the position of the vehicle along the track. Approaches to the non-linear modelling of the vehicle connections and modelling of each of the force inputs are included and discussed in the following sections.

5.2.2 Modelling Vehicle Inputs

A simple single-vehicle model is firstly developed, as described by the equation:

$$m_1 a_1 = F_{t/db} - F_{r1} - F_{g1} \tag{5.10}$$

Note that this is just Equation 5.1 with the vehicle connection removed.

The single-vehicle model has a mass of 120 tonnes and is provided with a constant traction input of 10 kN. The only resistive forces in this case are rolling and air resistances. Under this rather hypothetical simulation case, the vehicle reaches 'terminal' velocity after approximately 2500 s, as shown in Figure 5.3.

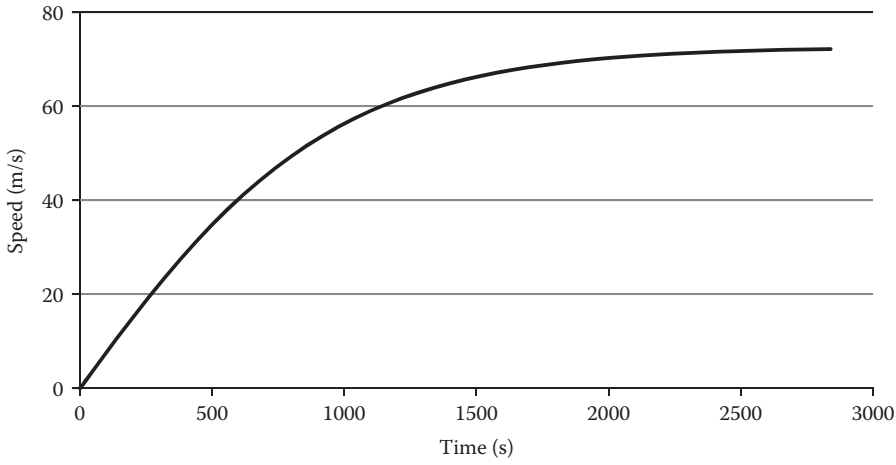

FIGURE 5.3 Simulated speed response of single-vehicle model.

5.2.2.1 Locomotive Traction and Dynamic Braking

Of course, the modelling in this case is oversimplified. Traction, braking and other input forces are not provided as step inputs. Locomotive traction and dynamic braking have evolved over many years, and several systems exist. In diesel locomotives, a tradition of eight notches for the throttle control emerged, based on a three-valve fuel control. More modern locomotives can have different numbers of notches and levels for dynamics braking; however, eight notches remain common for operational reasons. As designs have become complex, it is now usual to base models upon manufacturers' locomotive performance curves. An approximate model for traction, assuming that notch level is linearly proportional to traction motor current, can be derived from the following equations:

$$\text{For} \quad F_{t/db} * v < \left(N^2/64\right) * P_{max}, \quad F_{t/db} = \left(N/8\right) * Te_{max} - k_f * v \tag{5.11}$$

$$\text{Else} \quad F_{t/db} = \left(N^2/64\right) * P_{max}/v \tag{5.12}$$

where:

N is the throttle setting in notches (0–8)
P_{max} is the maximum locomotive traction horsepower (W)
Te_{max} is the maximum locomotive traction force (N)
k_f is the torque reduction (N/[m/s])

Equations 5.11 and 5.12 adequately describe locomotive traction performance, as shown in Figure 5.4.

Although a reasonable fit to the published power curves may be possible with a simple equation of the form $P = F_{t/db} * v$, it may be necessary to modify this model to reflect further control features or to reflect changes in efficiency or thermal effects at different train speeds. It is common for the traction performance characteristic to fall below

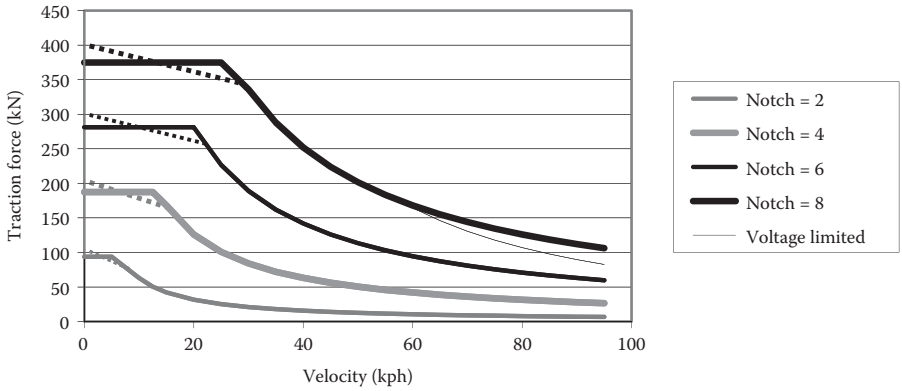

FIGURE 5.4 Typical tractive effort performance curves for diesel-electric locomotive. (From Cole, C., *Handbook of Railway Vehicle Dynamics*, Chapter 9, Taylor & Francis Group, Boca Raton, FL, pp. 239–278, 2006. With permission.)

the power curve $P_{max} = F_{t/db} * v$ at higher speeds because of the limits imposed by the generator maximum voltage (see the voltage limited trace associated with the Notch 8 power curve in Figure 5.4). Enhanced performance closer to the power curve at higher speeds is achieved in some locomotives by adding a motor field-weakening control [10]. It can be seen that accurate modelling of locomotives, even without considering the electrical modelling in detail, can become quite complicated. In all cases, the performance curves should be sourced and as much precise details as possible should be obtained about the control features to ensure that a suitable model is developed.

It is typical for locomotive manufacturers to publish both the maximum tractive effort and the maximum continuous tractive effort. The maximum continuous tractive effort is the traction force delivered at full throttle notch after the traction system has heated to a nominal maximum operating temperature. As the resistivity of the windings increases with temperature, the motor torque decreases because of the lower motor current. As traction motors have considerable mass, considerable time is needed for the locomotive motors to heat, with performance levels progressively dropping to maximum continuous tractive effort. A typical thermal derating curve for a modern locomotive is shown in Figure 5.5.

Manufacturers' data from which performance curves such as those shown in Figure 5.4 are derived can usually be taken as maximum rather than continuous values. If the longitudinal dynamics problem under study has severe grades and the locomotives are delivering large traction forces for long periods, it becomes necessary to modify the simple model, represented in Figure 5.4, to a more advanced model incorporating allowances for the thermal derating effects mentioned in the previous paragraph.

A key parameter in any discussion about tractive effort is wheel-rail adhesion or the coefficient of friction. Before enhancement of motor torque control, a wheel-rail adhesion level of ~0.20 could be expected. Modern locomotive traction control systems deliver higher values of adhesion, reaching ~0.35 in daily operation, with manufacturers claiming the adhesion values of up to 0.52 in published performance curves.

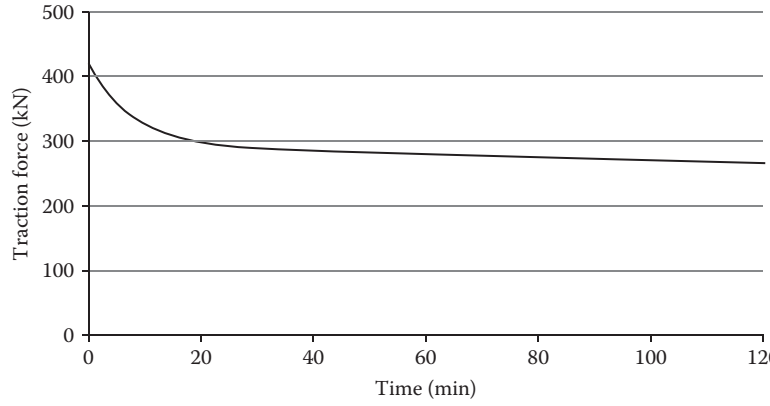

FIGURE 5.5 Tractive effort thermal derating curve. (From Cole, C., *Handbook of Railway Vehicle Dynamics*, Chapter 9, Taylor & Francis Group, Boca Raton, FL, pp. 239–278, 2006. With permission.)

One must remember that a smooth control system can deliver an adhesion level only up to the maximum set by the coefficient of friction for the wheel-rail conditions. Wheel-rail conditions in frost and snow could reduce the adhesion to as low as 0.1. Figure 5.6 superimposes adhesion levels on the curves from Figure 5.4, showing how significant adhesion is as a locomotive performance parameter.

The use of dynamic brake as a means of train deceleration has continued to increase as dynamic brake control systems have improved. As shown in Figure 5.7, early systems gave only a variable retardation force and were not well received by train drivers. As the effectiveness was so dependent on velocity, the use of dynamic brake gave unpredictable results unless a mental note of the locomotive velocity

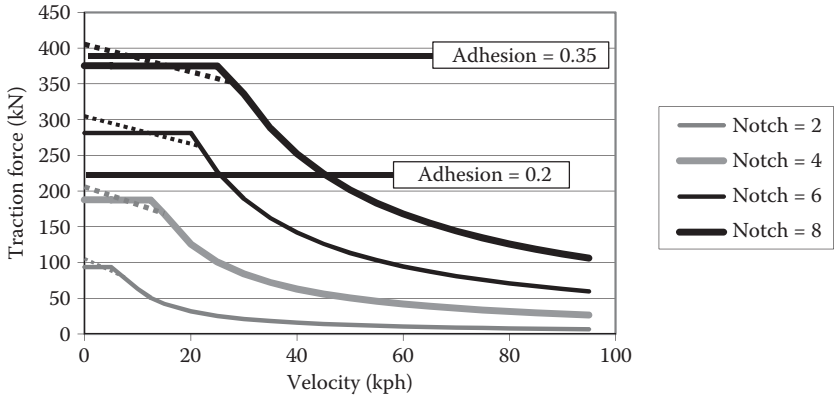

FIGURE 5.6 Tractive effort performance curves showing the effect of adhesion levels. (From Cole, C., *Handbook of Railway Vehicle Dynamics*, Chapter 9, Taylor & Francis Group, Boca Raton, FL, pp. 239–278, 2006. With permission.)

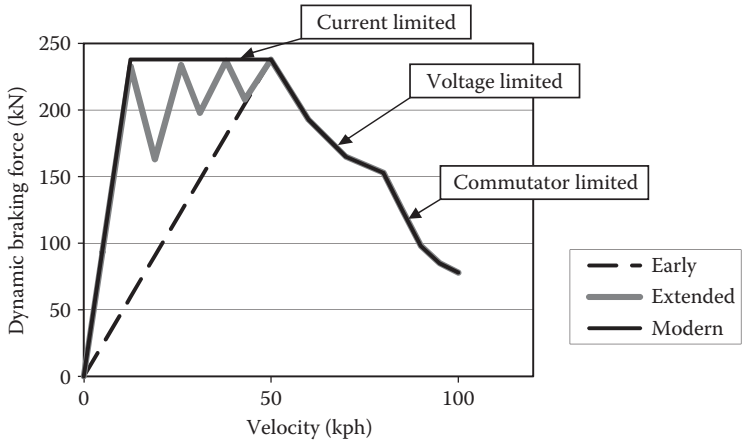

FIGURE 5.7 Dynamic brake characteristics. (From Cole, C., *Handbook of Railway Vehicle Dynamics*, Chapter 9, Taylor & Francis Group, Boca Raton, FL, pp. 239–278, 2006. With permission.)

was made and the driver was aware of what performance to expect. Extended range systems, which involved switching resistor banks, greatly improved the usability of dynamic brakes on diesel-electric locomotives, and more recent locomotive packages have provided large regions of maximum retardation at steady force levels (Figure 5.7). The performance of the dynamic brake is limited at higher speeds by current, voltage and commutator limits, and at lower speeds by the motor field. Designs have continued to extend the full dynamic brake force capability to lower and lower speeds. Recent designs have achieved the retention of maximum dynamic braking force down to 2 km/h. Dynamic brake can be controlled as a continuous level or at discrete control levels, depending on the locomotive design. The way in which the control level affects the braking effort differs for different locomotive traction packages. Four different dynamic brake characteristics have been identified, but further variations are not excluded; see Figures 5.8 and 5.9.

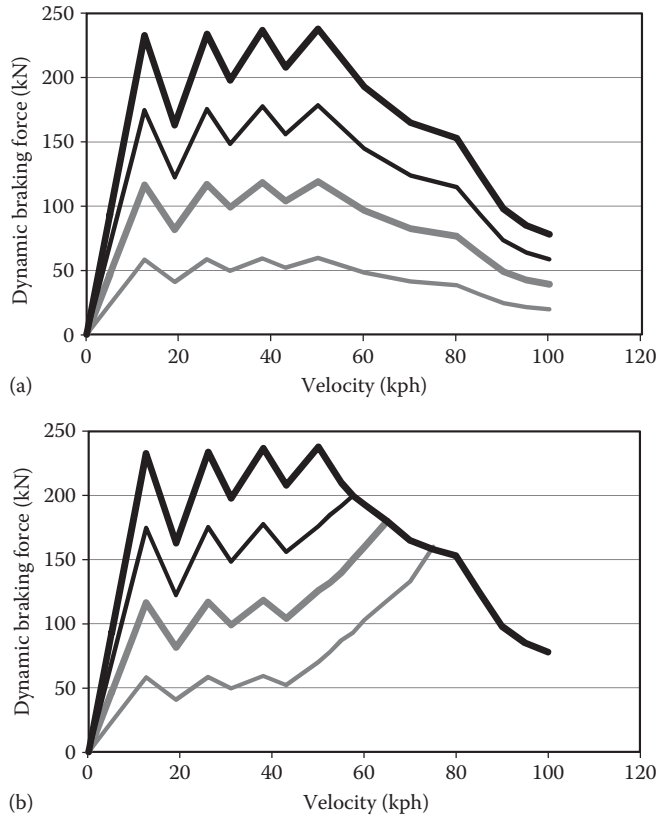

FIGURE 5.8 Examples of dynamic brake characteristics for diesel-electric locomotives: (a) modern locomotive and (b) older type locomotive (graph traces correspond to levels of control - the thickest black line is 100% DB application and levels reduce in 25% steps to 25% for the thin grey line). (From Cole, C., *Handbook of Railway Vehicle Dynamics*, Chapter 9, Taylor & Francis Group, Boca Raton, FL, pp. 239–278, 2006. With permission.)

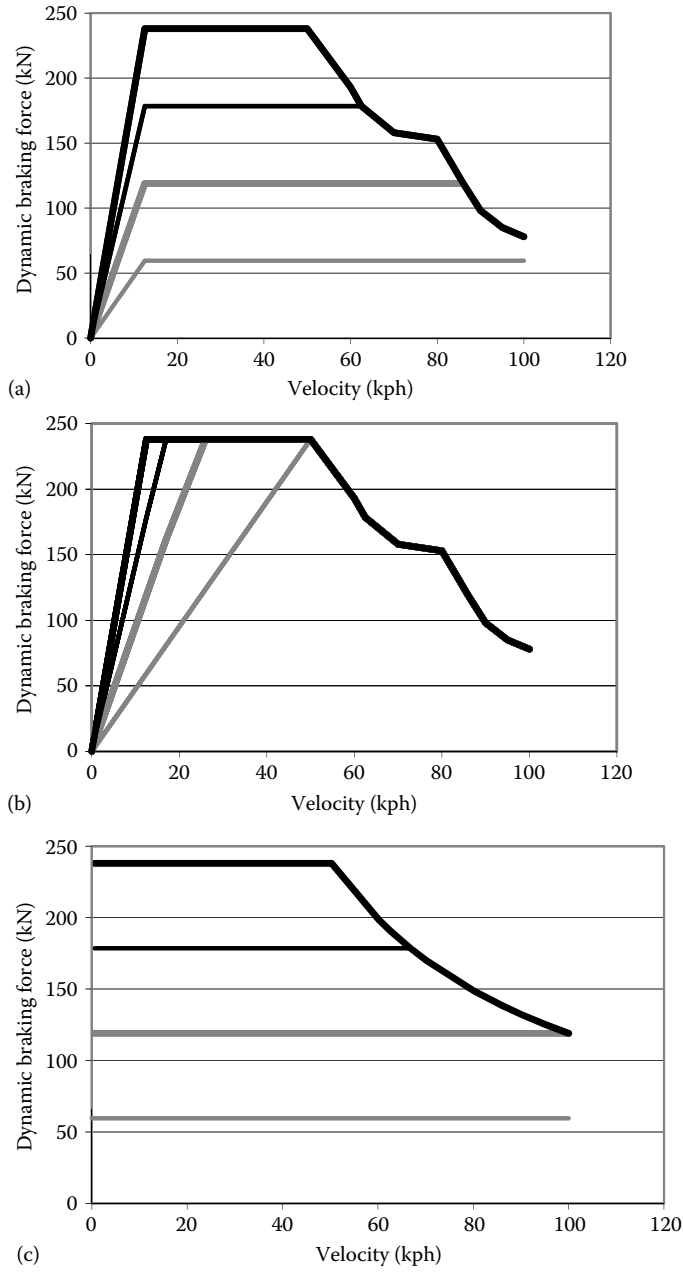

FIGURE 5.9 Dynamic brake characteristics for electric locomotives: (a) modern DC electric locomotive, (b) older type DC electric locomotive, and (c) modern AC diesel-electric or electric locomotive (graph traces correspond to levels of control—the thickest black line is 100% DB application and levels reduce in 25% steps to 25% for the thin grey line). (From Cole, C., *Handbook of Railway Vehicle Dynamics*, Chapter 9, Taylor & Francis Group, Boca Raton, FL, pp. 239–278, 2006. With permission.)

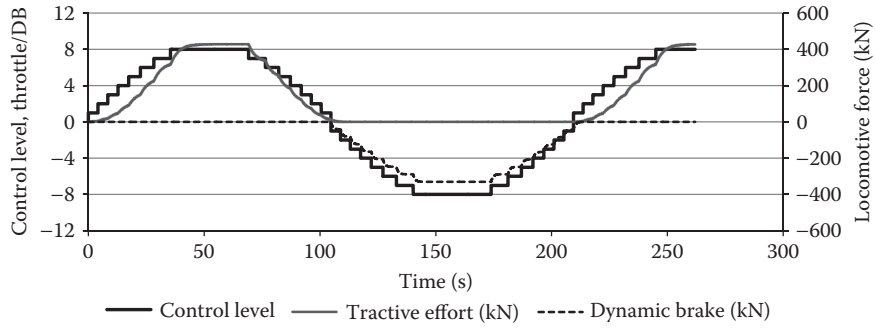

FIGURE 5.10 Locomotive dynamic brake simulation results for speed of 25.2 km/h.

Modern designs, shown in Figure 5.8a and in Figure 5.9a and c, provide larger ranges of speed at which a near-constant braking effort can be applied. Modelling of this characteristic can be achieved by fitting a piecewise linear function to the curve, representing 100% dynamic braking force. The force applied to the simulation can then be scaled linearly in proportion to the control setting. In some configurations, it becomes necessary to truncate the calculated value by different amounts.

Although traction characteristics can sometimes be reduced to a small number of equations, dynamic braking is usually more complicated and requires piecewise functions and/or a lookup table. The results from a simplified locomotive dynamic brake model are shown in Figure 5.10.

To continue the process of building a train model, locomotive traction and dynamic brake control systems are combined with the single-vehicle model to give a locomotive model, the output results of which are shown in Figure 5.11.

5.2.2.2 Propulsion Resistance

Propulsion resistance is usually defined as the sum of rolling resistance and air resistance. In most cases, increased vehicle drag due to track curvature is considered separately. The variable shapes and designs of rolling stock and the complexity of aerodynamic drag mean that the calculation of rolling resistance is still dependent on empirical formulas. Typically, propulsion resistance is expressed in an equation of the form $R = R_1 + R_2V + R_3\,V^2$ where R_1, R_2 and R_3 are coefficients relating to the rolling resistance component dependent only on vehicle weight and bearing type, on flanging resistance and train dynamic losses, and on air resistance, respectively. Hay [11] presented the work of W. J. Davis, which identified the term R_1 as journal resistance dependent on both vehicle mass and the number of axles; an equation of the form $R_1 = ax + b$, giving in imperial units $1.3wn + 29n$, where w is weight per axle and n is the number of axles, is quoted in Ref. [11]. The second term is mainly dependent on flanging friction, and therefore, the coefficient R_2 is usually small (nonexistent in some empirical formulas), and the third term is dependent on air resistance. The forms of propulsion resistance equations used and the empirical factors selected vary between railway systems, reflecting the use of equations that more closely match the different types of rolling stock and running speeds. An instructive collection of propulsion resistance formulas is presented in Table 5.1 based on Ref. [11] and work by

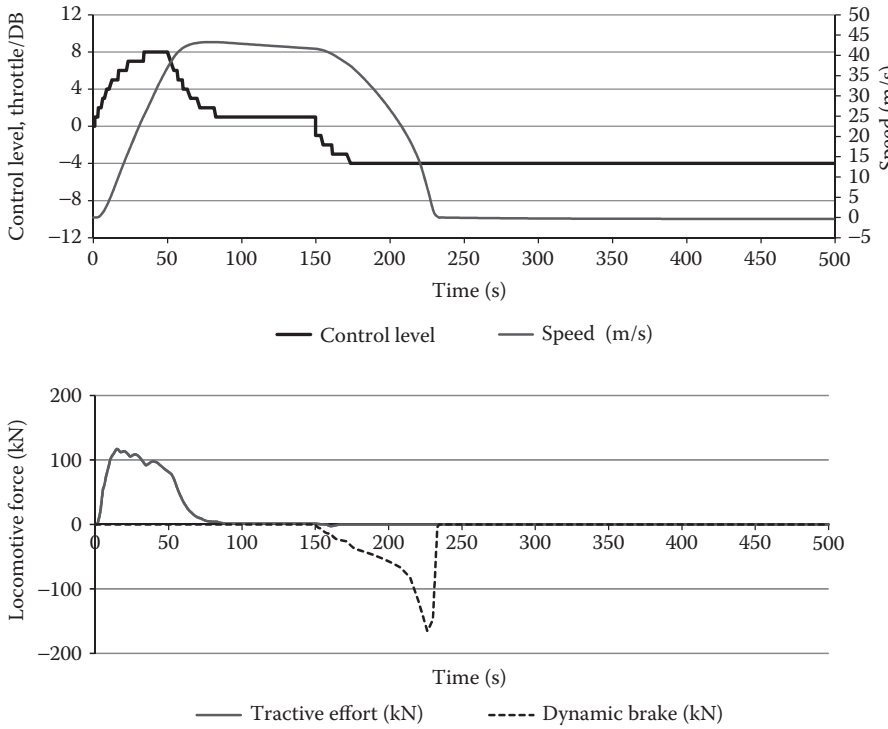

FIGURE 5.11 Single-vehicle simulation results, including locomotive traction and dynamic brake control systems.

TABLE 5.1
Empirical Formulas for Freight Rolling Stock Propulsion Resistance

Description	Equation 5.13
Original Davis equation (USA)	$6.376 + 129.0/m_a + BV + CAV^2/(m_a n)$ A = frontal area in square metres B = 0.091 locomotives, 0.137 freight cars C = 0.044 locomotives, 0.0092 freight cars
Modified Davis equation (USA)	$K_a\,[2.943 + 89/m_a + 0.0305V + 1.718k_{ad}V^2/(m_a n)]$ K_a = 1.0 for pre-1950, 0.85 for post-1950, 0.95 container on flat car, 1.05 trailer on flat car, 1.05 hopper cars, 1.2 empty covered auto-racks, 1.3 loaded covered auto-racks and 1.9 empty uncovered auto-racks k_{ad} = 0.07 for conventional equipment, 0.0935 for containers and 0.16 for trailers on flatcars
French locomotives	$0.65m_a n + 13n + 0.01m_a nV + 0.03V^2$
French standard UIC vehicles	$9.81(1.25 + V^2/6300)$
French express freight	$9.81(1.5 + V^2/(2000\ldots2400))$
French 10t/axle	$9.81(1.5 + V^2/1600)$

(*Continued*)

TABLE 5.1 (*Continued*)

Description	Equation 5.13
French 18t/axle	$9.81(1.2 + V^2/4000)$
German Strahl formula	$25 + k(V + \Delta V)/10$ $k = 0.05$ for mixed freight trains and 0.025 for block trains
Broad gauge (i.e., 1.676 m)	$9.81(0.87 + 0.0103V + 0.000056V^2)$
Broad gauge (i.e., ~1.0 m)	$9.81(2.6 + 0.0003V^2)$

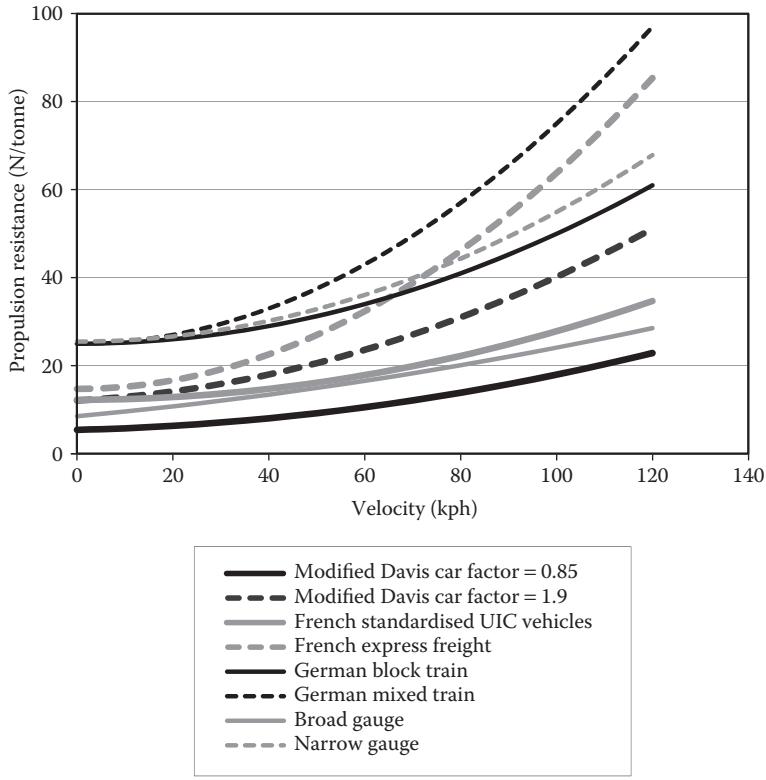

FIGURE 5.12 Comparison of freight rolling stock propulsion resistance equations.

Profillidis [12]. All equations are converted to SI units and expressed as Newtons per tonne mass. There are many variations of propulsion resistance equations, as shown by the Equation 5.13 column in Table 5.1. A graphical representation of their various outcomes is provided in Figure 5.12.

In Table 5.1, K_a is an adjustment factor depending on rolling stock type; k_{ad} is an air drag constant depending on car type; m_a is mass supported per axle in tonnes; n is the number of axles; V is the velocity in km/h; and ΔV is the headwind speed, usually taken as 15 km/h.

Even with the number of factors described in Table 5.1, the effects of many factors are not, and usually cannot be, meaningfully considered. How are the differing rail vehicle frontal and side areas considered? How are headwind, crosswind and tailwind considered? How are the drag forces due to poor bogie steering considered? In the area of air resistance, rail vehicle body design is more variable than suggested by the few adjustment factors presented here. Higher-than-expected aerodynamic drag has been observed from the addition of headwinds with a slight crosswind component for certain types of trains (e.g., open empty hopper wagons). The dynamicist should therefore be aware that considerable differences between calculations and field measurements are probable. Similarly, with regard to bogie steering and drag, the equations do not include centre bowl friction, warp stiffness or wheel rail profile information.

5.2.2.3 Curving Resistance

Curving resistance calculations have similarity to propulsion resistance calculations in that empirical formulas must be used. Vehicle design and condition, cant (superelevation) deficiency, rail profile, rail lubrication and curve radius will all affect the resistance imposed on a vehicle on the curve. As all of these factors can vary significantly, it is usual to estimate curving resistance by a function relating only to curve radius. The equation commonly used, as detailed in Ref. [11], is

$$F_{cr} = 6116/R \tag{5.14}$$

where:

F_{cr} is curving resistance in Newtons per tonne of vehicle mass
R is the curve radius in metres

Rail flange lubrication is thought to be capable of reducing curving resistance by 50%. The curving resistance of a vehicle that is stationary on a curve is thought to be approximately double the value given by Equation 5.14.

5.2.2.4 Gravitational Components

Gravitational components, F_g, are added to longitudinal train models by simply resolving the weight vector into components parallel and at right angles to the vehicle body chassis. The parallel component of the vehicle weight becomes F_g. On a grade, a force will be either added to or subtracted from the longitudinal forces on the vehicle depending on whether the vehicle is travelling down or up the grade; see Figures 5.1 and 5.13.

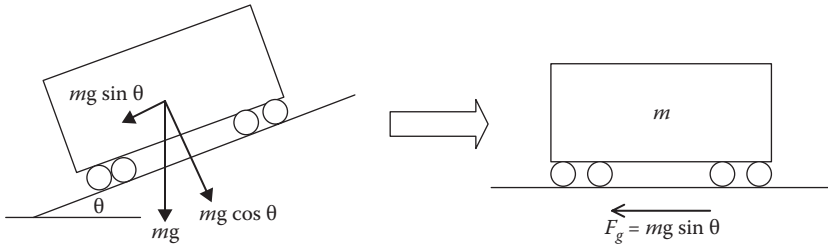

FIGURE 5.13 Modelling gravitational components.

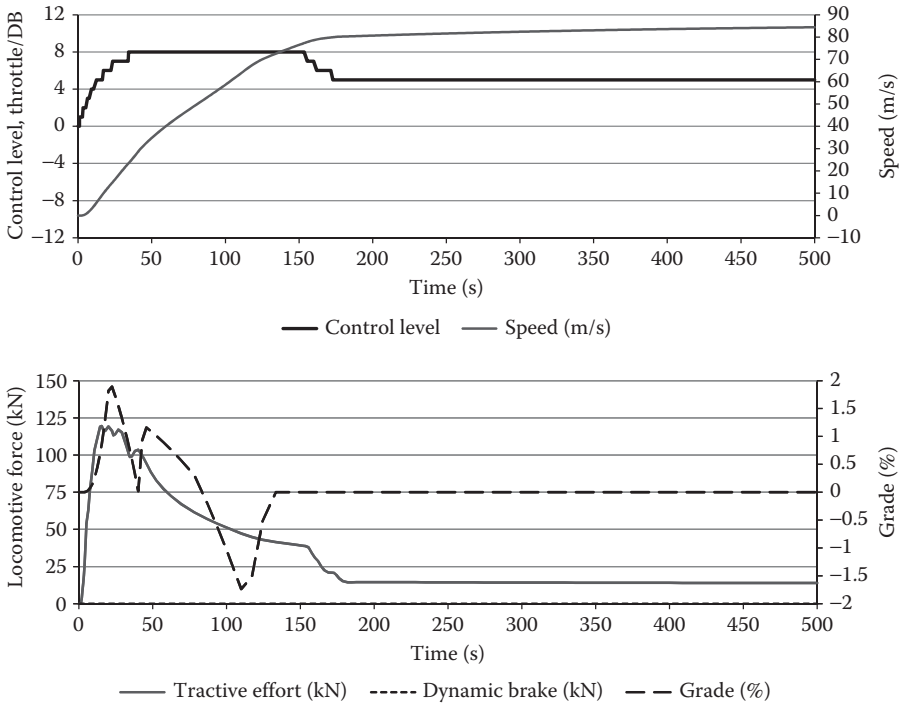

FIGURE 5.14 Simulation results—locomotive traction dynamic brake vehicle model with grades.

The grade also reduces the sum of the reactions of the vehicle downwards on the track. This effect has implications for propulsion resistance equations that are dependent on vehicle weight. However, the effect is small, and owing to the inherent uncertainty in propulsions resistance calculations, it can be safely ignored. For example, a 1 in 50 grade gives a grade angle θ of 1.146°. The cosine of this angle is 0.99979. The reduction in the sum of the normal reactions for a vehicle on a 1 in 50 grade is, therefore, a fraction of 1/5000 or 0.02%. Grades are obtained from track plan and section data. The grade force component must be calculated for each vehicle in the train and updated each time step during simulation to account for train progression along the track section.

Adding track grades to the modelling gives the results in Figure 5.14, and then adding curve drag gives the results in Figure 5.15. It can be noted that the curve drag of the few curves has very little effect on the results.

5.2.2.5 Pneumatic Brake Models

The modelling of the brake system requires the simulation of a fluid dynamic system that must run in parallel with the train simulation. The output from the brake pipe simulation is the brake cylinder force, which is converted by means of rigging factors and shoe friction coefficients into a retardation force that is one term of the sum of the retardation forces F_r.

Modelling of the brake pipe and triple valve systems is a subject in itself and will therefore not be treated in this chapter beyond characterising the forces that

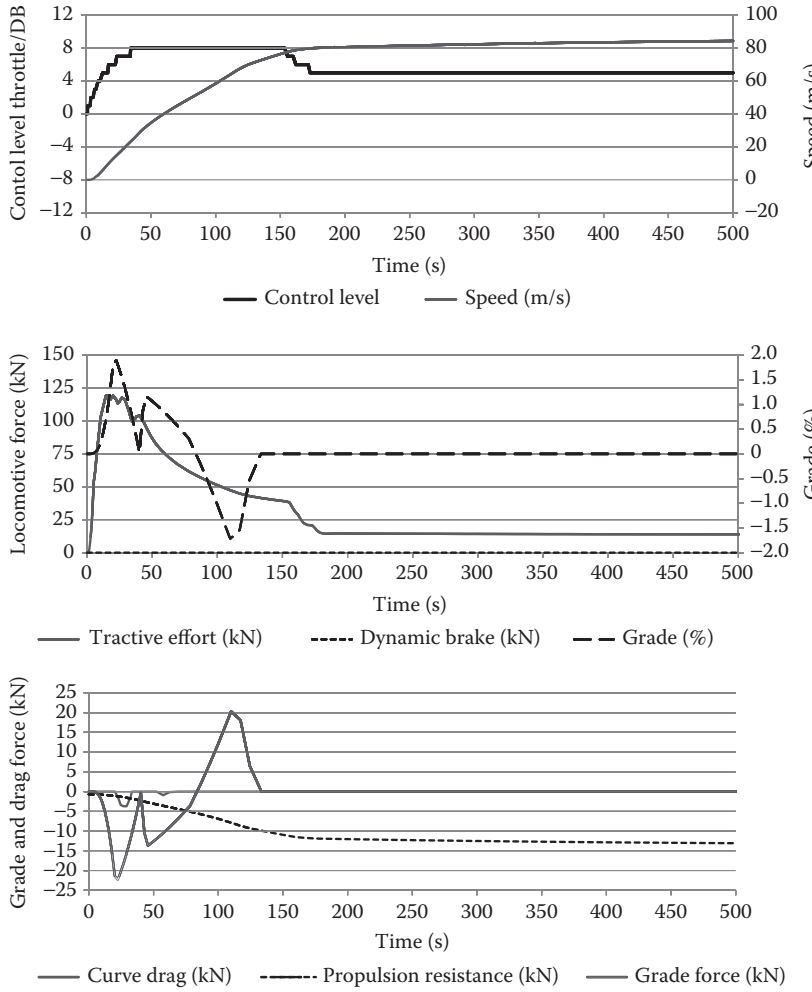

FIGURE 5.15 Simulation results—locomotive traction dynamic brake vehicle model with grades and curves.

can be expected and the effect of these forces on train dynamics. The majority of freight rolling stock still utilises pneumatic control of the brake system. The North American system differs in design from the British/Australian system, but both apply brakes sequentially starting from the points at which the brake pipe is exhausted. Both systems depend on the fail-safe feature whereby the opening of the brake valve in the locomotive or the fracture of the brake pipe, thus allowing loss of the brake pipe pressure, results in application of brakes along the train. The particular valves used on each vehicle to apply the brakes work on the same principle, but vary slightly in function and capabilities. These valves are known as 'triple valves' in the British/Australian system, whereas they are known as 'AB valves' in North America and 'distributor valves' in Europe.

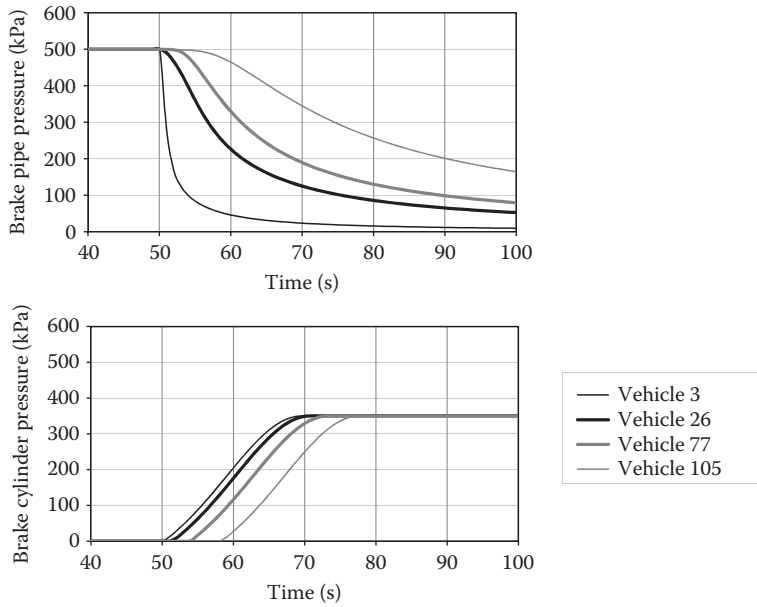

FIGURE 5.16 Simulation results—brake pipe and cylinder responses: emergency application. (From Cole, C., *Handbook of Railway Vehicle Dynamics*, Chapter 9, Taylor & Francis Group, Boca Raton, FL, pp. 239–278, 2006. With permission.)

Irrespective of the particular version of pneumatically controlled brakes, the key issue is that the pneumatic control adjustments made to the brakes via the brake pipe take time to propagate along the train. Since the introduction of the first triple valve systems in the late 1800s, many refinements have been progressively added to ensure or improve brake control propagation. As the control is via a pressure wave, the system is limited to sonic speed, which is 350 m/s for sound in air (noting 318 m/s at −20°C and 349 m/s at 30°C). Allowing for losses in brake equipment, a well-designed system can achieve signal propagation at speeds typically in the range of 250–300 m/s. For short trains of 20 wagons (each 15 m long, ~300 m long train), this gives quite reasonable performance. As trains have increased in length, in particular for heavy haul applications (lengths of 1.6–4.0 km), brake control signal propagation can take several seconds. Some simulated data of a brake system emergency application are given in Figure 5.16.

It is the demand for better braking in these longer trains that is the primary driver for recent adoption of electronically controlled pneumatic (ECP) brakes, which can apply all train brakes almost simultaneously. Using a simplified triple-valve model involving many assumptions, the characteristic curve shown in Figure 5.17 is obtained, which is quite representative of cylinder fill and exhaust parameters.

The simplified model is then used with a simplified brake pipe model to allow it to be implemented in the three-vehicle train model. The simulation results are shown in Figures 5.18 and 5.19. Again, these are not exact models of the actual pipe characteristic, but are useful representations for the purpose of demonstration.

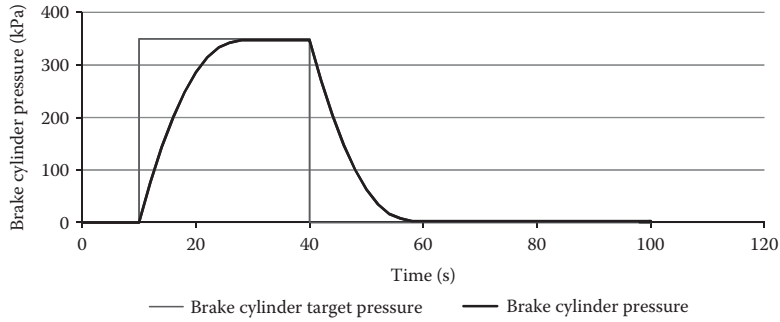

FIGURE 5.17 Simulation results—simplified triple-valve cylinder model.

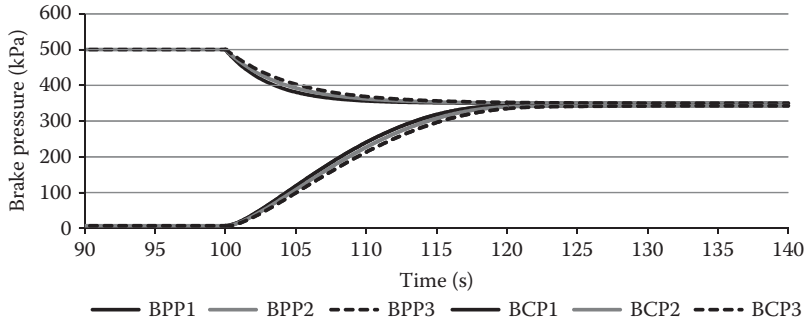

FIGURE 5.18 Simulation results—simplified three-vehicle train air brake model (BPP = brake pipe pressure, BCP = brake cylinder pressure).

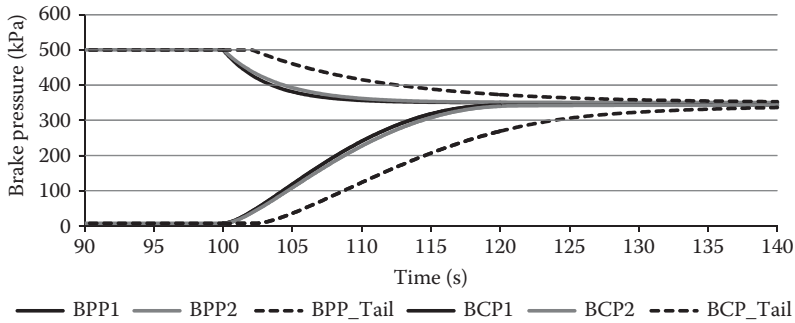

FIGURE 5.19 Simulation results—simplified train air brake model for 750 m brake pipe (BPP = brake pipe pressure, BCP = brake cylinder pressure).

Note that, for a three-vehicle model, delays are minimal, as shown in Figure 5.18. To better illustrate the delay issue, the model is simulated again, assuming that the third vehicle is 750 m away; results are shown in Figure 5.19.

As shown in Figure 5.19, the cylinder fill rates for the brake cylinder at the tail of the train are now limited by the control target provided by the brake pipe, rather

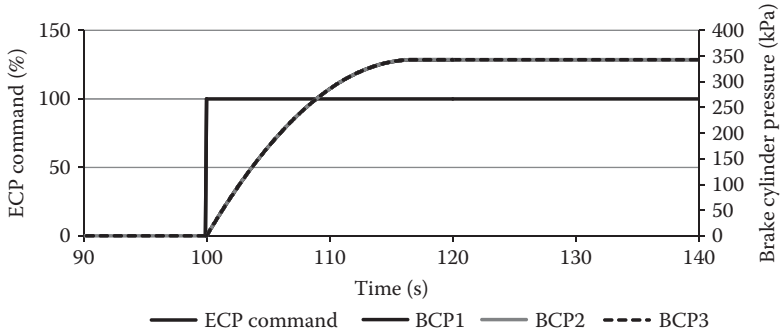

FIGURE 5.20 Simulation results—simplified train ECP brake model for 750 m brake pipe.

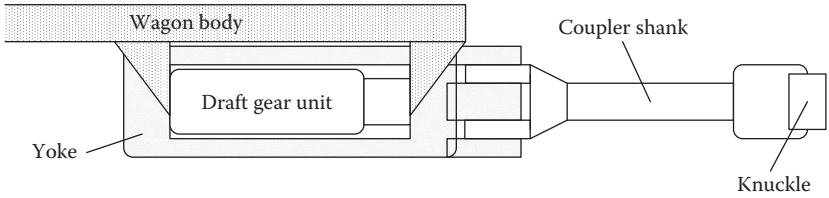

FIGURE 5.21 Conventional auto-coupler assembly.

than by the fill rates allowed by the chokes in the triple-valve systems. This problem tends to limit the maximum length of brake pipe systems and is a significant reason for the interest in ECP braking for long heavy haul trains. An ECP brake system with almost no control delay will give results similar to those shown in Figure 5.20. While control delays are removed, note that brake cylinders still have a fill time as shown in Figure 5.20.

5.2.3 Rail Vehicle Connection Models

Perhaps the most important component in any longitudinal train simulation is the connection element between vehicles. The auto-coupler with friction-type draft gears is the most common connection used in the Australian and North American freight train systems. It also often presents the most challenges for modelling and simulation because of the non-linearities of the air gap (or coupler slack), draft gear spring characteristic (polymer or steel) and stick–slip friction provided by a wedge system. Owing to these complexities, the common auto-coupler-friction-type draft gear connection will be examined first. Other innovations such as slackless packages, drawbars and shared bogies can then be more easily considered.

5.2.3.1 Conventional Auto-Couplers and Draft Gear Packages

A conventional auto-coupler and draft gear package is illustrated in the schematic in Figure 5.21. A schematic of the wedge arrangement of the draft gear unit is included in Figure 5.22. There are also several variations in wedge system designs

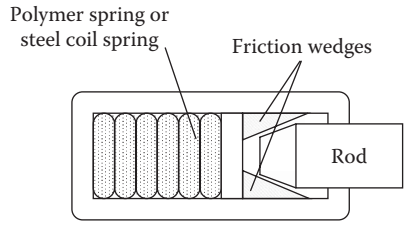

FIGURE 5.22 Friction-type draft gear unit.

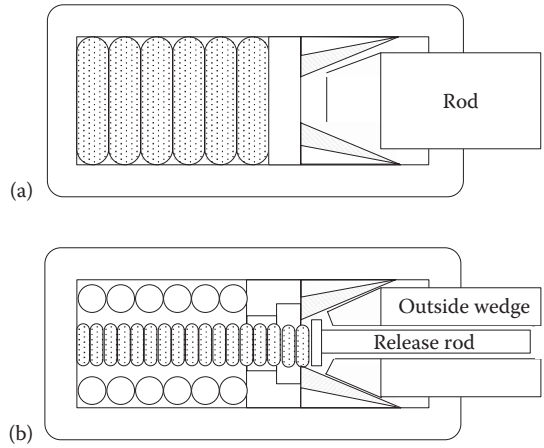

FIGURE 5.23 Variations on friction-type draft gear units: (a) Angled surfaces for increased wedge force and (b) release spring type.

which are more complicated than those illustrated in Figure 5.22; two examples are shown in Figure 5.23.

When considering a rail vehicle connection, two auto-coupler assemblies must be considered along with gap elements and the stiffness elements describing flexure in the vehicle body. A vehicle connection model will, therefore, appear as something similar to the schematic in Figure 5.24. Modelling the coupler slack is straightforward, this being by inserting a simple dead zone. Modelling of the steel components, including body stiffness, can be provided by a single linear stiffness. Work by Duncan and Webb [2], based on the test data measured on long unit trains, identified cases where the draft gear wedges wlocked and slow sinusoidal vibration was observed. The behaviour was observed in distributed power trains when in a single stress state. The trains could be either in a tensile or compressed condition. The stiffness corresponding to the fundamental vibration mode observed was defined as the locked stiffness of the vehicle connections. The locked stiffness for the freight trains tested was nominally a value in the order of 80 MN/m [2]. As the locked stiffness is also the limiting stiffness of the system, it must be incorporated into the vehicle connection model. The limiting stiffness is the equivalent of all the stiffnesses of the

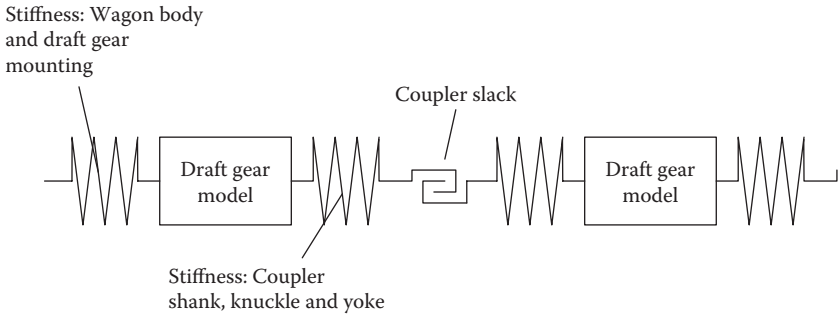

FIGURE 5.24 Rail vehicle connection model components.

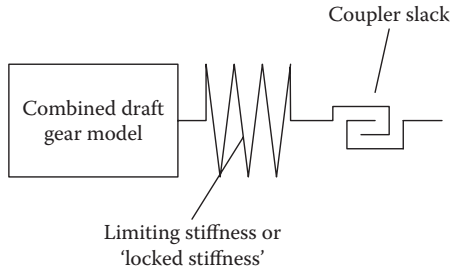

FIGURE 5.25 Simplified rail vehicle connection model.

structural components and connections added in series and includes the components such as the Further shank, knuckle, yoke, draft gear structure and the vehicle body. It also includes any pseudolinear stiffness due to gravity and bogie steering force components, whereby a longitudinal force is resisted by gravity as a vehicle is lifted or forced higher on a curve. The limiting stiffness of a long train may, therefore, vary for different rail vehicle loadings and on-track placement.

Rail vehicle connection modelling can be simplified to a combined draft gear package model equivalent to two draft gear units, and includes one spring element, representing locked or limiting stiffness; see Figure 5.25.

Determination of the mathematical model for the draft gear model has received considerable attention in technical papers. For the purposes of providing a model for train simulation, a piecewise linear model representing the hysteresis in the draft gear friction wedge (or clutch) mechanism is usually used [2,13]. The problem of modelling the draft gear package has been approached in several ways. In early driver training simulators, when computing power was limited, it was a common practice to further reduce the complexity of the dynamic system by lumping vehicle masses together and deriving equivalent connection models. As adequate computational capacities are now available, it is a normal practice to model each vehicle in detail [13,14]. It would seem reasonable in the first instance to base models on the hysteresis data published for the drop hammer tests of draft gear units. Typical draft gear response curves are shown in Figure 5.26.

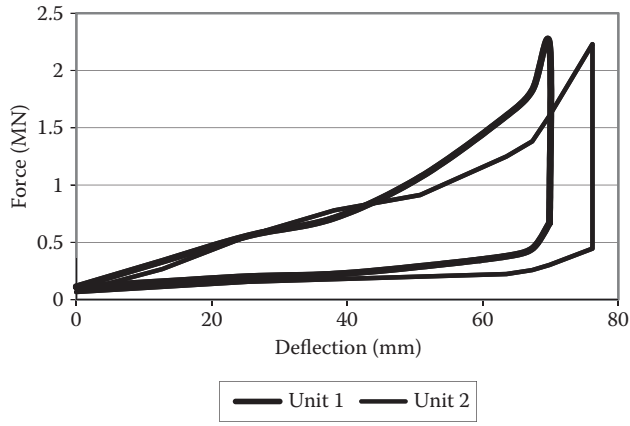

FIGURE 5.26 Typical published draft gear response data—drop hammer tests. (From Cole, C., *Handbook of Railway Vehicle Dynamics*, Chapter 9, Taylor & Francis Group, Boca Raton, FL, pp. 239–278, 2006. With permission.)

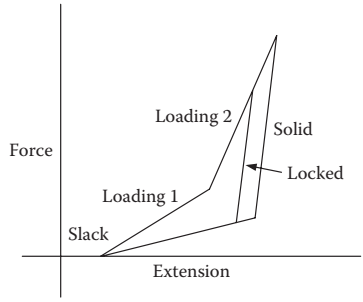

FIGURE 5.27 Piecewise linear vehicle connection model. (From Cole, C., *Handbook of Railway Vehicle Dynamics*, Chapter 9, Taylor & Francis Group, Boca Raton, FL, pp. 239–278, 2006. With permission.)

The first thing to remember is that the published data, as shown in Figure 5.26, represent the operating extreme simulated by a drop hammer test. The drop hammer of 12.27 tonne (27,000 lb) impacts the draft gear at a velocity of 3.3 m/s, thus simulating an intervehicle impact with a relative velocity between vehicles of 6.6 m/s, (23.8 km/h). In normal train operation, it would be hoped that such conditions are quite rare. Data recording of in-train forces of unit trains in both iron ore and coal haulage systems in Australia revealed that draft gear stiffness in normal operation could be very different from that predicted by the data of drop hammer test [2,13]. The approach taken by Duncan and Webb [2] was to fit a model to the experimental data by using piecewise linear functions (see example in Figure 5.27).

It can be noted that the model proposed in Ref. [2] includes the locked stiffness discussed earlier. A significant outcome from the train test data reflected in the

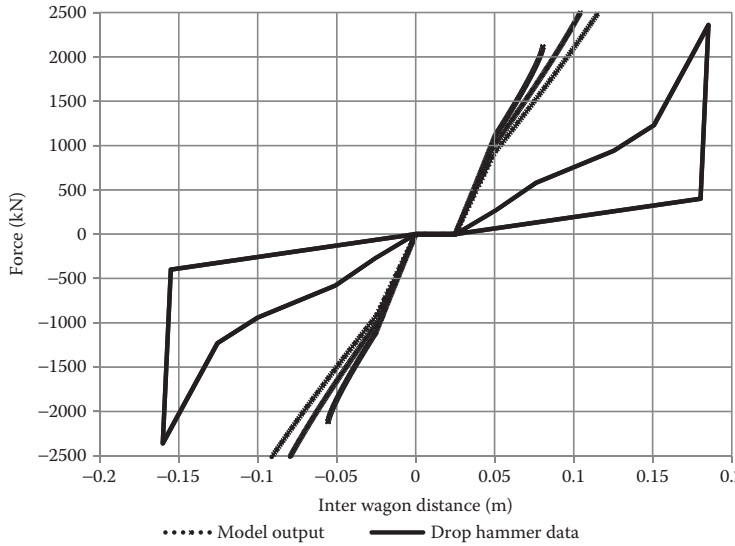

FIGURE 5.28 Vehicle connection model response—slow loading (0.1 Hz). (From Cole, C., *Handbook of Railway Vehicle Dynamics*, Chapter 9, Taylor & Francis Group, Boca Raton, FL, pp. 239–278, 2006; Cole, C., *Proceedings of the Conference on Railway Engineering*, Rockhampton, Australia, September 7–9, pp. 187–194, 1998. With permission.)

model in Figure 5.27 was that unloading and loading could occur along the locked curve whenever the draft gear unit was locked. This cyclic unloading and loading could occur at any extension. Data from this train test program [2] and later work by Cole [13] confirmed that the draft gear unit would remain locked until the force level reduced to a point close to the relaxation or unloading line. Owing to individual friction characteristics, there is considerable uncertainty about where 'unlocking' occurs. In some cases, unlocking was observed below the unloading curve, even sometimes reaching zero force.

Further refinement of rail vehicle connection modelling was proposed in Ref. [13]. The difficulty presented by the work of Duncan and Webb [2] is that draft gear units, and obviously the mathematical models used to represent them, differ depending on the regime of the expected train operation. Clearly, if extreme impacts were expected in simulation due to shunting or hump yard operations, a draft gear model representing drop hammer test data would be appropriate. Conversely, if normal train operations were expected, a vehicle connection model of the type proposed in Figure 5.27 would be appropriate. It was noted in Ref. [13] that the stiffness of the draft gear units for small deflections varied typically by 5–7 times the stiffness indicated by the drop hammer test data shown in Figure 5.26. It is therefore evident that, for mild intervehicle dynamics (i.e., gradual loading of draft gear units), the static friction in the wedge assemblies can sometimes be large enough to keep draft gears locked. A model incorporating the wedge angles and static and dynamic frictions was, therefore, proposed in Ref. [13] and published in detail in Ref. [1]. Results of this modelling approach are shown in Figures 5.28–5.30.

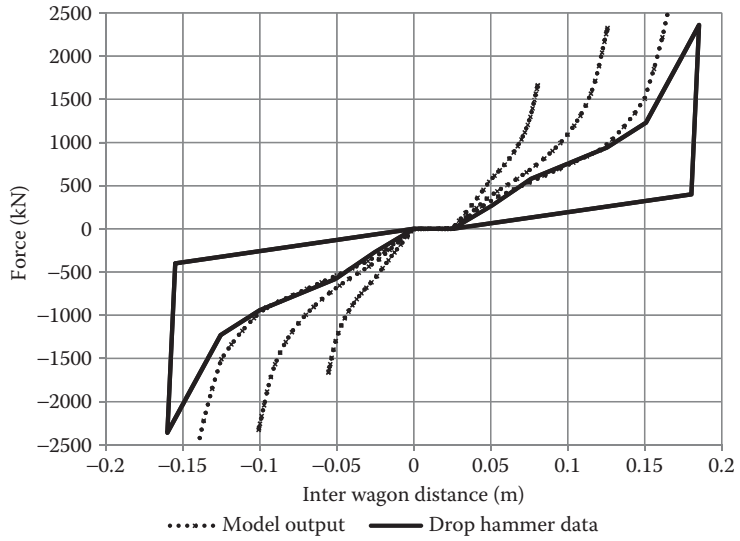

FIGURE 5.29 Wagon connection model response—mild impact loading (1 Hz). (From Cole, C., *Handbook of Railway Vehicle Dynamics*, Chapter 9, Taylor & Francis Group, Boca Raton, FL, pp. 239–278, 2006; Cole, C., *Proceedings of the Conference on Railway Engineering*, Rockhampton, Australia, September 7–9, pp. 187–194, 1998. With permission.)

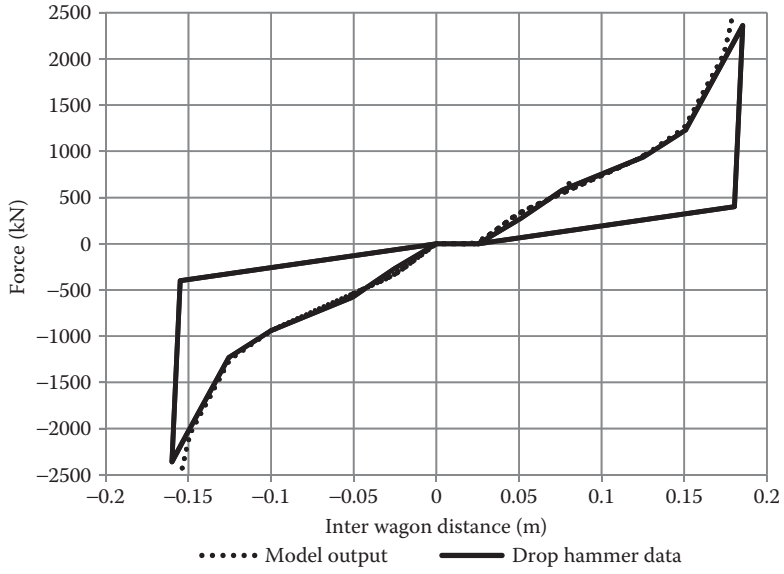

FIGURE 5.30 Wagon connection model response—shunt impact loading (10 Hz). (From Cole, C., *Handbook of Railway Vehicle Dynamics*, Chapter 9, Taylor & Francis Group, Boca Raton, FL, pp. 239–278, 2006; Cole, C., *Proceedings of the Conference on Railway Engineering*, Rockhampton, Australia, September 7–9, pp. 187–194, 1998. With permission.)

Irrespective of the type of draft gear being used, the general principles for modelling are the same. They are generally characterised by a non-linear spring of some kind. Generally, a non-linear mathematical function or piecewise linear model will be required for the basic stiffness. The draft gear unit will have damping. As with many railway applications, damping provided by friction (Coulomb damping) is a popular choice, as it can provide very high forces at slow velocities. Note that such properties are very hard to emulate in fluid- or polymer-based dampers. The damping in most freight draft gears is provided by the hysteresis of both friction and polymer components; however, some gears still utilise coil springs.

5.2.3.2 Slackless Packages

Slackless draft gear packages are sometimes used in bar-coupled wagons or are integrated into shared bogie designs. The design of slackless packages is that the components are arranged to continually compensate for wear to ensure that small connection clearances do not get larger as the draft gear components wear. Slackless packages have been deployed in North American train configurations such as the trough train [15] and bulk product unit trains [16]. The advantage of slackless systems is found in reductions in longitudinal accelerations and impact forces of up to 96% and 86%, respectively, as reported in Ref. [15]. Disadvantages lie in the inflexibility of operating permanently coupled wagons and the reduced numbers of energy-absorbing draft gear units in the train. When using slackless coupled wagon sets, it is usual that the auto-couplers at each end will be equipped with heavier-duty energy-absorbing draft gear units. The reduced capacity of these train configurations to absorb impacts can result in accelerated wagon body fatigue, or even impact related failures during shunting impacts. Modelling slackless couplings is simply a linear spring limited to a maximum stiffness appropriate to the coupling type, vehicle body type and vehicle loading. A linear or friction damper of very small value should be added to approximate small levels of damping available in the connection from friction in pins, movement in bolted or riveted plates and so on. See Figure 5.31 for the typical modelling setup.

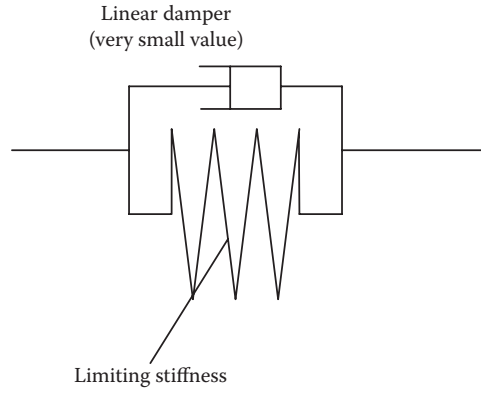

FIGURE 5.31 Slackless vehicle connection model.

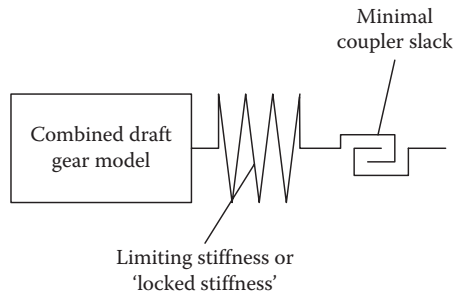

FIGURE 5.32 Drawbar coupled vehicle connection model.

5.2.3.3 Drawbars

Drawbars refer to the use of a single solid link between draft gear packages in place of two auto-couplers. Drawbars can be used with either slackless or energy-absorbing draft gear packages. Early practice seems to favour retention of full-capacity dry-friction-type draft gear packages at the drawbar connections. The most recent practice in Australia is to utilise small short-pack draft gear units at the drawbar connections. These short packs are quite stiff and provide only short compression displacements; they utilise only polymer or elastomer elements (no friction damping). Modelling drawbars with energy-absorbing draft gear units is simply a matter of removing most of the coupler slack from the model, as some slack will remain in pins and pocket components. A drawbar model schematic is shown in Figure 5.32. For cases where short packs are used, a short-pack draft gear model replaces the traditional combined draft gear model.

5.2.4 Train Configurations

Train configurations that are used in freight and heavy haul practice continue to evolve. There are three essential variables:

- Use of distributed power;
- Use of permanently coupled groups of wagons; and
- Selection of brake control.

Several train marshalling and distributed power arrangements are given in Table 5.2. The type of configuration chosen depends on many factors, including the productive capacity required (route cycle times) and the railway's grades and curves. Faster haulage cycles will demand that more locomotives be added, as will steeper ruling grades. Sharper curves have the effect of requiring that in-train forces be limited, favouring smaller locomotive groups and distributed power (see the six distributed power options in Table 5.2). Longer trains gain advantage from using permanently coupled wagon groups. Tandem wagons (permanently coupled pairs) are very common in Australian heavy haul trains, with some use of quad groups (four permanently

TABLE 5.2
Examples of Heavy Haul Train Configurations

Configuration Type	Diagram
Head-end	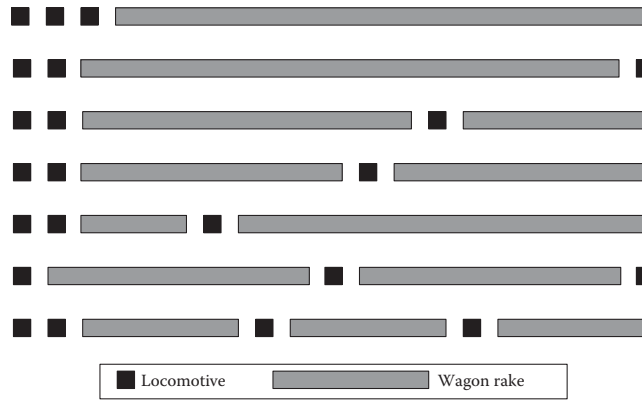
Head–tail	
Remote 2/3	
Remote mid-train	
Lead short rake	
Head–mid–tail	
Remote 1/3, 2/3	

coupled wagons). There are small numbers of groups of five to eight permanently coupled wagons used in freight and heavy haul trains. The advantage of grouped wagons is the improved longitudinal stability resulting from reduced coupling slack. The disadvantage is related to maintenance, as two or more wagons must be removed from the train to rectify a fault on one wagon.

There are also trade-offs in the solution that can be chosen by considering the brake system. If distributed power is not required to limit in-train forces, particularly those at start-up, then electronic braking could be a suitable solution that negates the need for distributed power. There are many cases where distributed power was originally adopted to ensure reliable operation of the brake pipe and not because of traction forces.

5.2.5 Train Dynamics Model Development and Simulation

Combining the modelling from the previous sections allows all the elements of a train to be assembled. The results of a three-vehicle train simulation are shown in Figure 5.33. The simulation has the same grades, curves and modelling as earlier examples. A significant issue in-train dynamics is coupling free slack. Although it adversely affects train dynamics and is the cause of impact forces, train free slack has practical merits. The first and most obvious is that loose coupling systems will always have some slack. Even if slack is small, wear will always increase it. A second practical merit is that slack allows a staged application of force to the train. This has the advantage that relatively simple traction systems can be used. If a large train was tightly coupled, very precise traction control would be required as it would be necessary to move all the wagons at once. Conversely, for a train with slack,

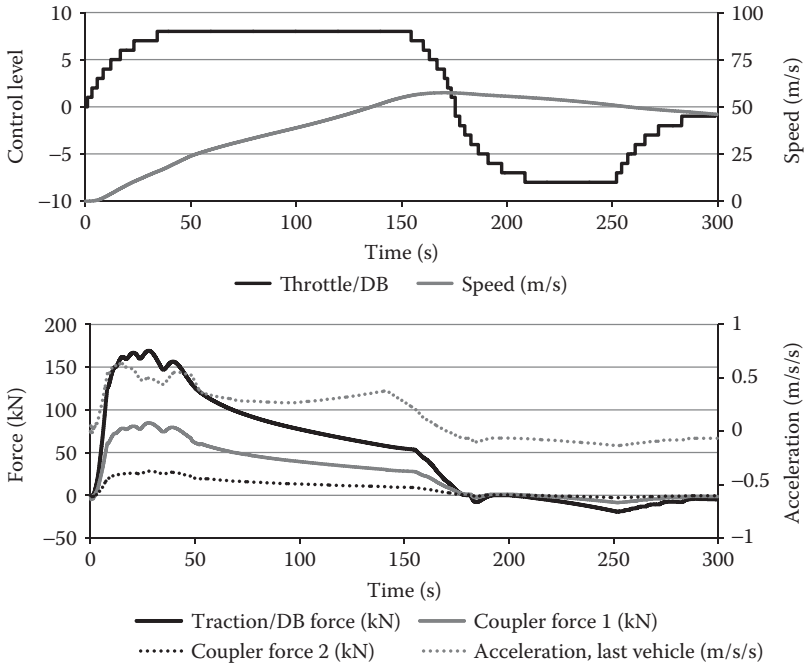

FIGURE 5.33 Simulation results—three-vehicle train model incorporating linear connections with zero coupling slack.

the locomotive firstly moves the first wagon or wagon group. Upon take-up of the second connection gap, the locomotives and the first wagon (or group) have momentum. The second wagon (or group) is then pulled by both adhesion and momentum. It still follows that better train dynamics can be achieved with less slack. The simulation results in Figure 5.34 incorporate 20 mm of slack in the intervehicle connections but are identical in all other respects to the train model used for the results in Figure 5.33. Note that, with the slack added in Figure 5.34, impact force transients and impact accelerations exist at the start-up and at the change from tensile to compressive forces.

Note that the connection model used to produce the results in Figures 5.33 and 5.34 is still a poor approximation of typical couplings, as it has linear stiffness and viscous damping. To illustrate the modelling issues further, a very simple draft gear model is implemented in the train model to give the results shown in Figure 5.35; a cross-plot of the model characteristic is shown in Figure 5.36. It should be noted that this model, though providing hysteresis indicative of Coulomb damping, does not give representative results. In Figure 5.35, it can be noted that the plot of the second coupler force (the third force trace) is now noisy. This is caused by numerical instability in the solver, which is in turn caused by the inadequacy of the model. Note that there is no solution to the question of the force state, as the loading switches

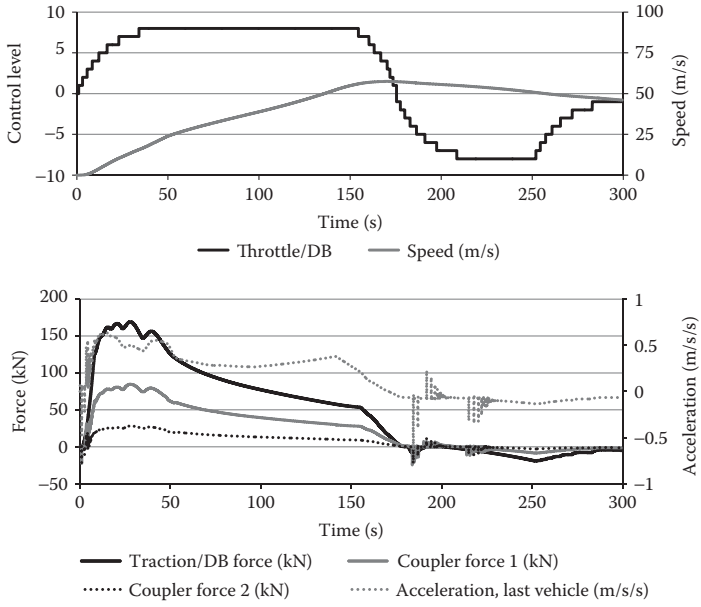

FIGURE 5.34 Simulation results—three vehicle train model incorporating linear connections with 20 mm coupling slack.

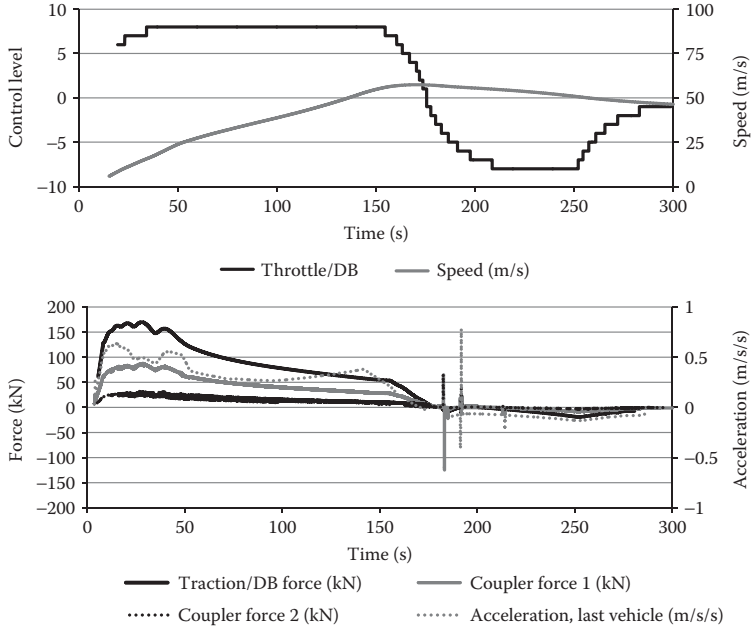

FIGURE 5.35 Simulation results—three-vehicle train model incorporating non-linear connections with friction damping with 20 mm coupling slack.

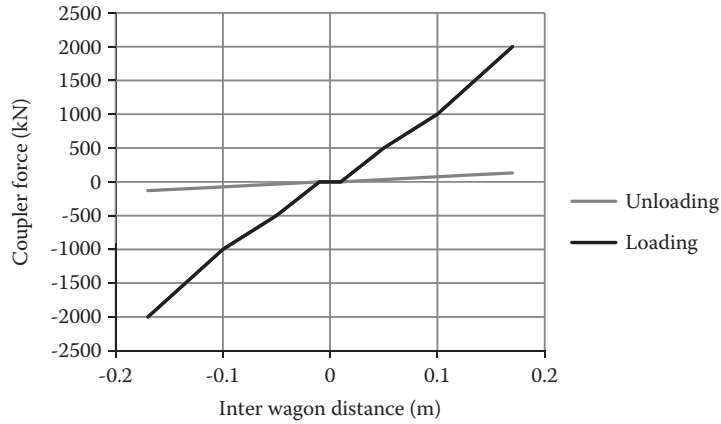

FIGURE 5.36 Wagon connection model response—non-linear connection with estimated non-linear damping and 20 mm coupling slack.

from 'loading' to 'unloading'. The consequence is that, between these curves, there is the impossibility of infinite stiffness. Some minor improvement can be achieved by adding viscous damping, but even if this is made large, there is still the case when an extremely slow velocity exists at the point where switching of direction occurs. The problem, of course, stems from the fact that the limiting stiffness (as discussed in Section 5.2.3) is ignored in the model. It is therefore reasonable to expect a much better result if the model is more representative of reality; infinite stiffness does not exist in reality. In addition, infinite stiffness is problematic to step-wise numerical solvers, and it would be expected that a real model (with a finite maximum stiffness) would be much more easily solved. This, in fact, is what happens. More detailed models, accommodating limit stiffness, are implemented as shown in Figures 5.37 and 5.38. As the effect of limit stiffness can be easily seen only as a fundamental low-vibration mode in a very long train, results from a long train model are shown in Figures 5.39 and 5.40. The effects of coupler slack are indicated by the force transient peaks reaching 3 MN in the first case and 2.4 MN in the second case. Note that both of these correspond to changes in power control. Low-frequency vibration in both examples is then evident by the smooth sinusoids with very low damping, indicating the action of the wagon stiffness (limiting stiffness) rather than draft gear or damper movement.

The simple non-linear model in Figure 5.36 does not include the locked or limiting stiffness discussed earlier. A more complete modelling is shown in Figure 5.37.

The realistic freight train simulations in Figures 5.39 and 5.40 also illustrate the significant effect of train control inputs. As the dynamic system is large, changes to control can have significant effects. Traction control techniques, as shown by the examples in Figures 5.39 (fast throttle application) and 5.40 (longer pauses in the throttle increase), can significantly change the force results, hence the emphasis on specific driver training for various train types. In the case of

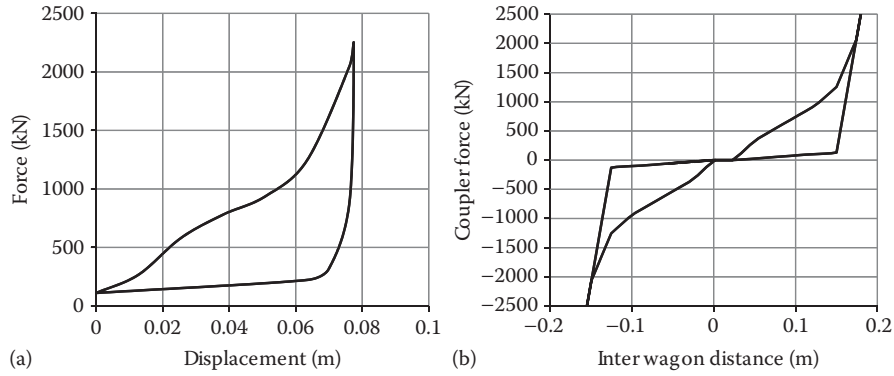

FIGURE 5.37 Wagon connection model response—non-linear connection with non-linear damping based on drop hammer data, limiting stiffness and 20 mm coupling slack: (a) Drop hammer test data and (b) wagon connection model.

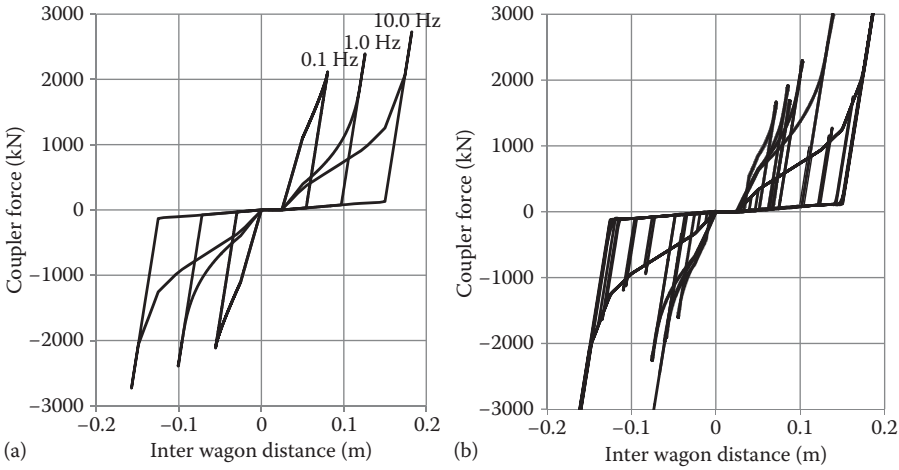

FIGURE 5.38 Wagon connection model response—nonl-inear connection with non-linear damping based on drop hammer data, limiting stiffness, loading rate dependence and 20 mm coupling slack: (a) Wagon connection model response to different loading rates (single sine input) and (b) wagon connection model response to different loading rates (compound sine input).

heavy haul train systems, control strategies are focused on limiting forces to prevent component failure and ensure wagon stability. Note that the example given is for flat track and for a head-end train. There will be different practices for different situations of track topography and different train types. Although power application is one issue, a more complicated issue is braking. There are two types of brakes. The first, known as dynamic brake, is a reverse traction force applied by the locomotive. Dynamic braking examples are shown in Figures 5.33 through 5.35; the data after $t \cong 180$ s shows negative control levels for dynamic brake,

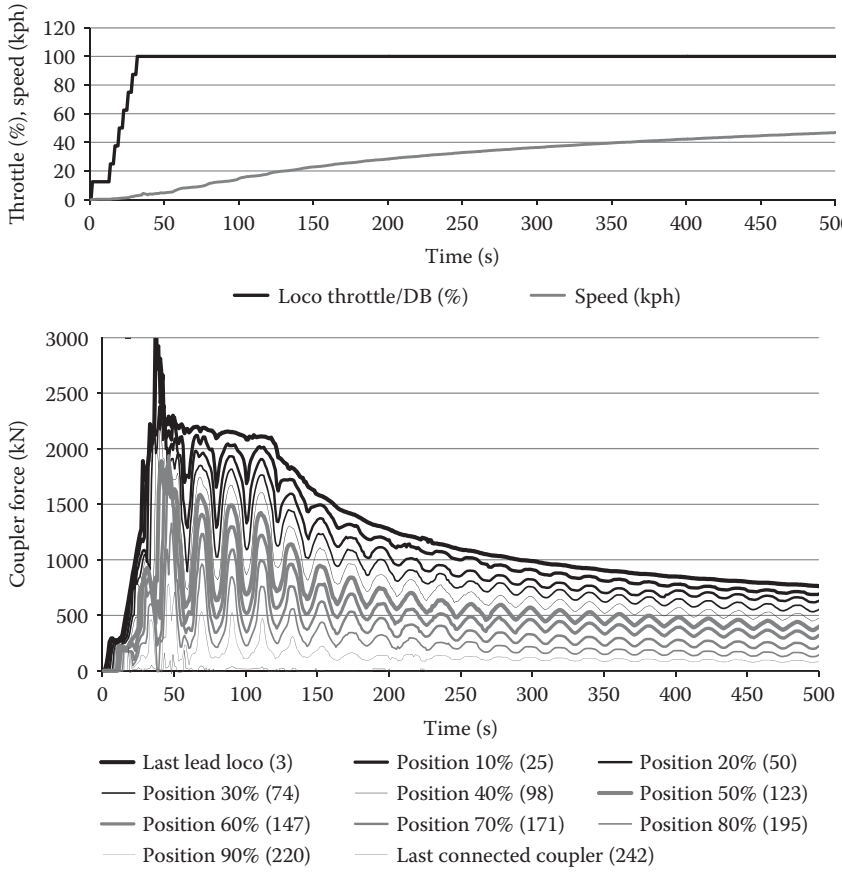

FIGURE 5.39 Simulation results—train start-up, fast throttle application—3 head-end locomotives, 240 wagons—non-linear connection with non-linear damping based on drop hammer data and field data, limiting stiffness, loading rate dependence with 25 mm coupling slack between permanently coupled wagon pairs.

negative acceleration and compressive coupler forces. As can be noted from the examples in Figures 5.6 and 5.7, dynamic braking usually delivers a smaller maximum force than the maximum tractive effort. An important difference is that locomotive systems are generally able to apply this force more quickly than traction can be applied. Another difference is that maximum traction is associated with very slow speeds, whereas maximum dynamic brake is available over a range of speeds, including much higher speeds. The second type of braking is the pneumatic train brake system, introduced earlier in Section 5.2.2.5, with modelling details and simulation results given in Figures 5.17 through 5.20. It is important to realise that adding pneumatic braking to a train simulation results in a cosimulation problem. The brake pipe model is a dynamic system in itself and

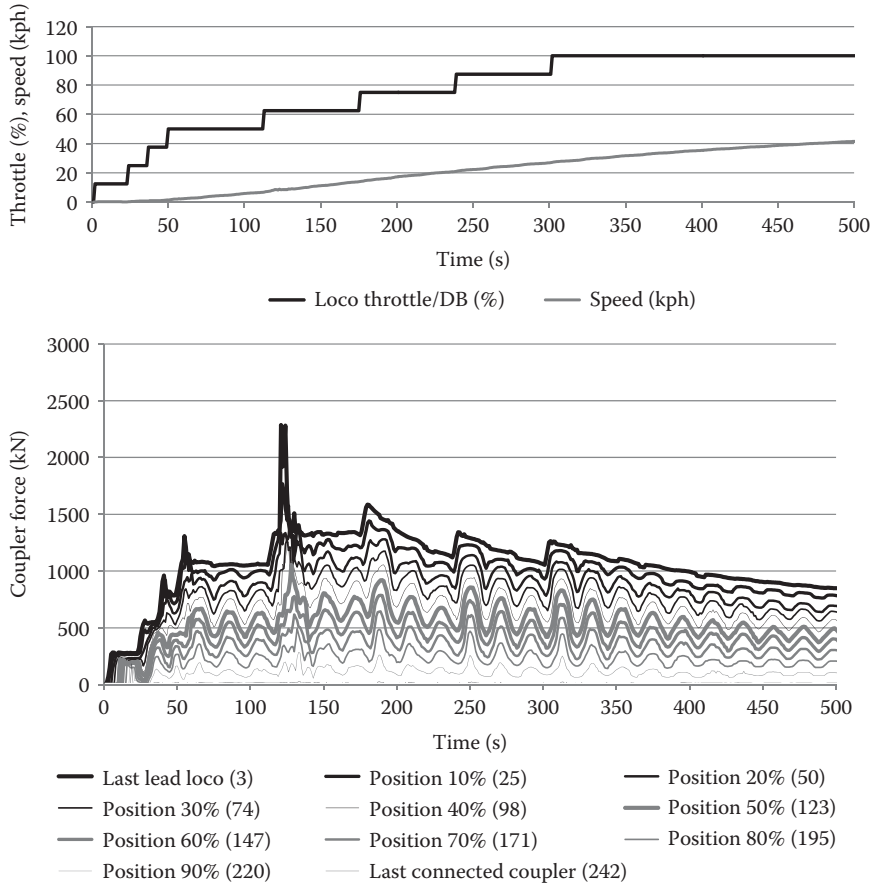

FIGURE 5.40 Simulation results—train start-up—3 head-end locomotives, 240 wagons—non-linear connection with non-linear damping based on drop hammer data and field data, limiting stiffness, loading rate dependence with 25 mm coupling slack between permanently coupled wagon pairs.

often requires a different integrator step size. Computational fluid dynamic models of a pneumatic brake system are generally unworkable with a train simulator because of the very high computational demands. Brake pipe models in practical train simulators are usually partly or totally based on empirical equations. The brake pipe model implemented here uses standard signal-processing blocks to approximate pipe behaviour. Gas laws are then used to model the cylinder fill. This model is implemented with the linear three-vehicle model to give the results in Figure 5.41. As the train is very short, pipe delays are minimal and, given linear connections, the coupler force results are well behaved. A more realistic simulation over a route of 115.3 km of train operation is given in Figures 5.42 and 5.43. It can be noted that dynamic brake and mainly minimum brake pipe applications

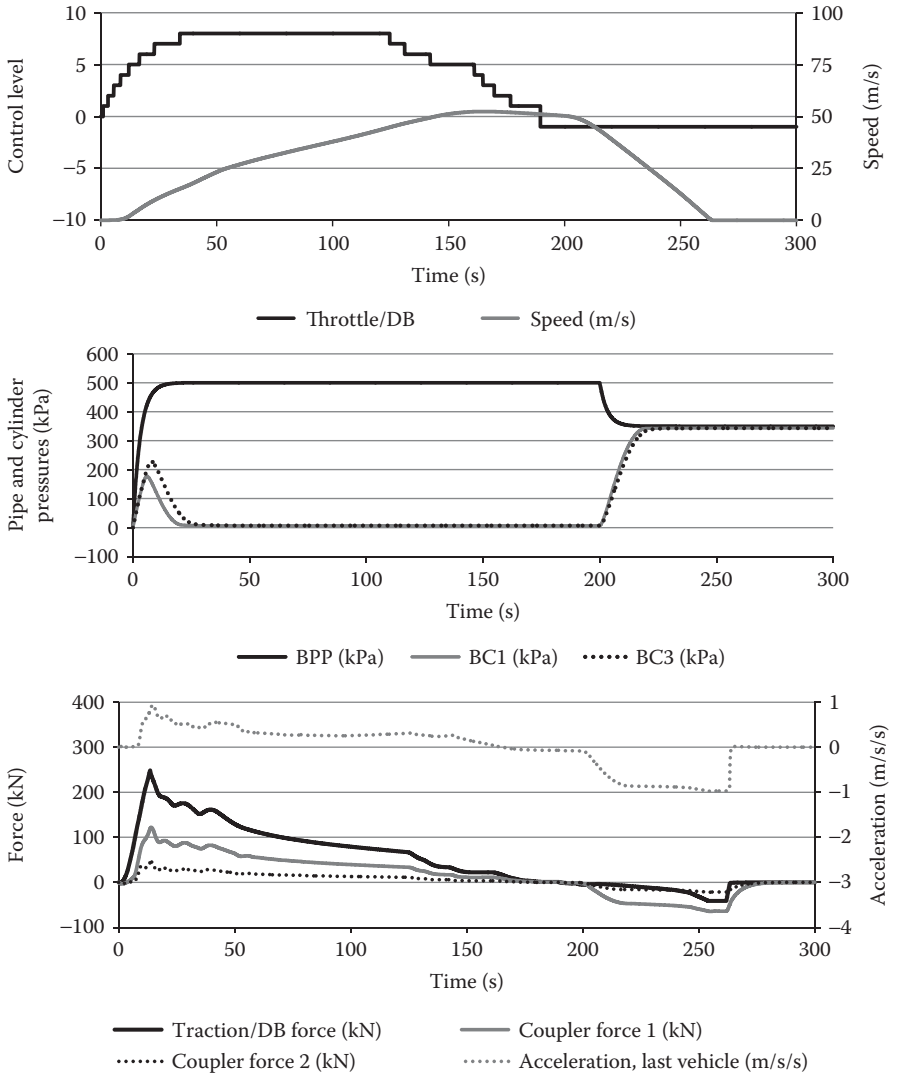

FIGURE 5.41 Simulation results—three-vehicle train model—linear connections with brake application.

(50 kPa drop) are used to control train speed. A zoom in of a braking event is shown in Figure 5.43. Sharper compressive force transients will be noted at t ~3980 s, corresponding to the air brake application, whereas the triangular shape of the compressive force profile corresponds to the dynamic brake application. Note also that the limiting stiffness gives rise to small, low-damped vibrations and that severe accelerations correspond to changes in control and switching from tensile to compressive coupler forces.

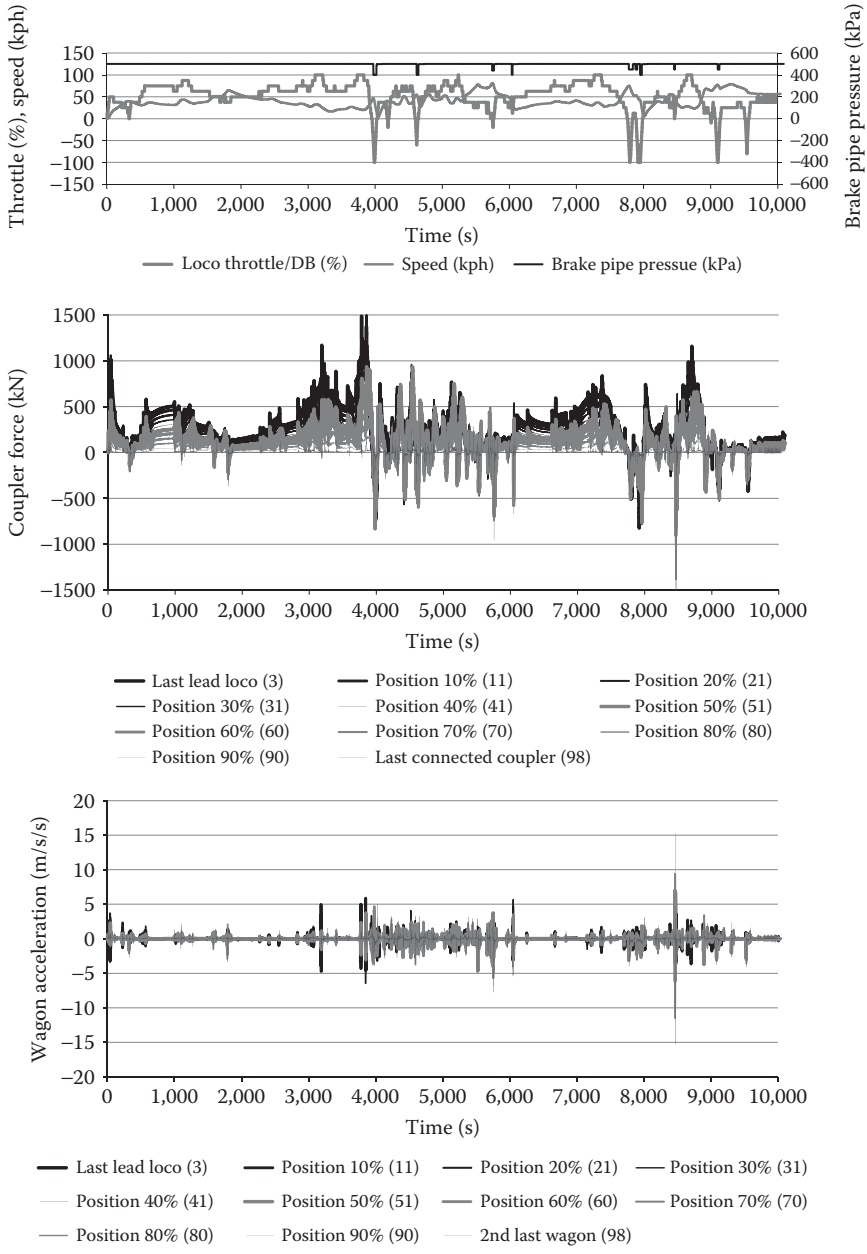

FIGURE 5.42 Overall simulation results—115.3 km train route simulation—3 head-end locomotives, 96 wagons—non-linear connection with non-linear damping based on drop hammer data and field data, limiting stiffness, loading rate dependence with 25 mm coupling slack between permanently coupled wagon pairs.

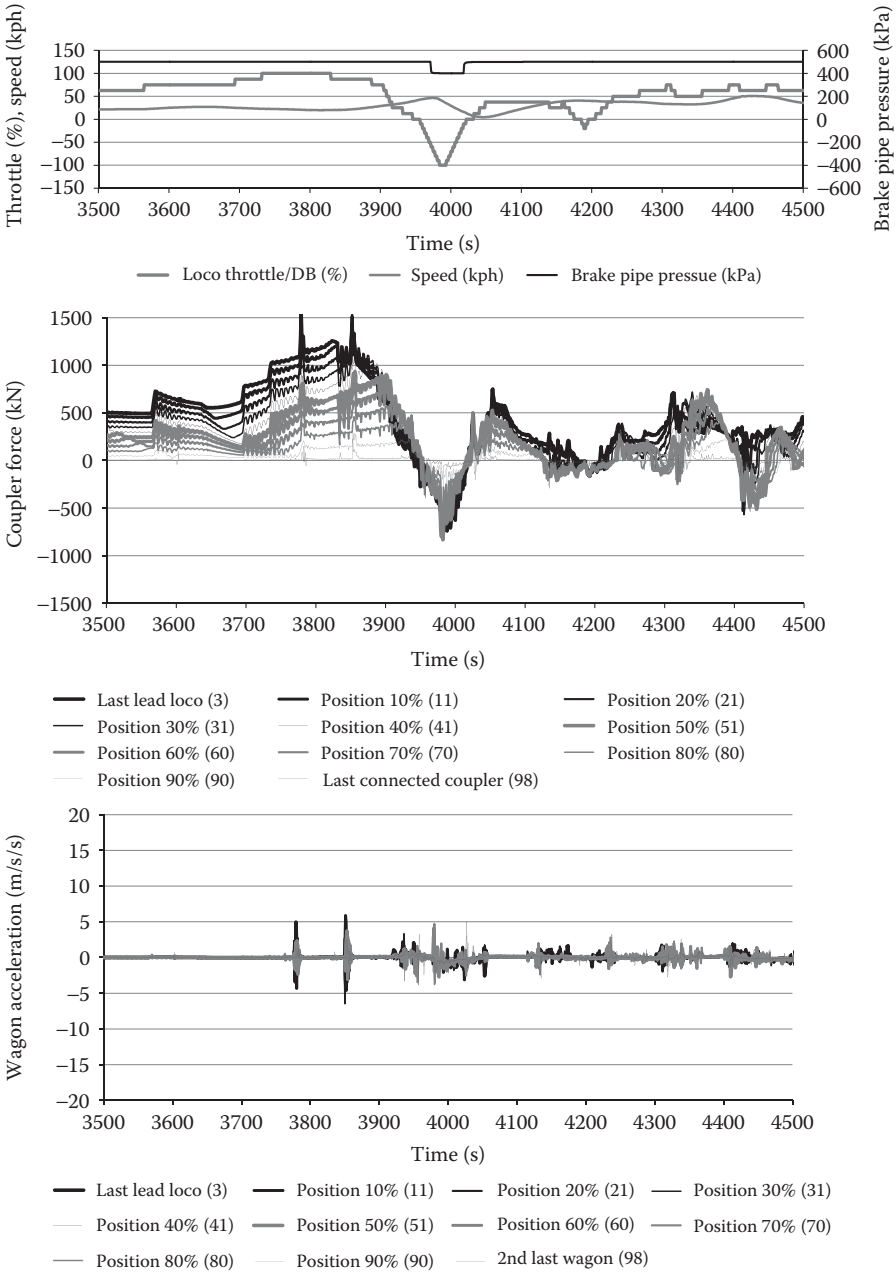

FIGURE 5.43 Overall simulation results—zoom-in of Figure 5.42—115.3 km train route simulation—3 head-end locomotives, 96 wagons—non-linear connection with non-linear damping based on drop hammer data and field data, limiting stiffness, loading rate dependence with 25 mm coupling slack between permanently coupled wagon pairs.

5.3 INTERACTION OF LONGITUDINAL TRAIN AND LATERAL/VERTICAL RAIL VEHICLE DYNAMICS

The long tradition of analysing train dynamics and vehicle dynamics separately is strongly entrenched in both software and standards. Train dynamics tends to be concerned with only longitudinal dynamics, whereas vehicle dynamics tends to focus on just one vehicle (or a small number of vehicles) and on vertical and lateral dynamics. The assumption that coupler angles are so small that the consequential vertical and lateral force components can be ignored does not necessarily hold as trains become heavier and longer and coupler forces become larger. Some possibilities for wagon instabilities were examined in Ref. [17], namely wheel unloading due to the lateral components of coupler forces and wagon lift due to mismatches in coupling height. In both these cases, the most severe events occur when an empty wagon is placed in a loaded train. It is evident that mechanisms of wagon instability can be more complex than just these clearly extreme cases. Furthermore, wheel unloading can be added to by wagon body and bogie pitch induced by both track irregularities and train dynamics. An early paper that explored this issue is [6]. Just as there has been a questionable tradition of separating train and vehicle dynamics, it would also be incorrect to discount the possibility of two or more mechanisms relating to longitudinal dynamics combining unfavourably.

5.3.1 Wheel Unloading, Wheel Climb and Rollover on Curves due to Lateral Components of Coupler Forces

For operating stability and true calculation of the lateral to vertical force L/V ratios that are an indicator of derailment potential, it is important to combine the lateral coupler force components with individual vehicle dynamics; however, before this can be done, the lateral force components for the whole train simulation trip need to be calculated.

Coupler angles can be calculated by the equations provided in the Association of American Railroads (AAR) manual [18] or the technique developed by Simson [19] and utilised in many locomotive traction-steering studies [20,21]. This technique is easier to apply than the AAR method and has no significant error penalty unless used for very sharp curves (error < 0.1% at $R = 100$ m). The method also allows different curvatures to be applied for movement through curve transitions and is easier to implement in a train simulation context. The method uses the same assumptions as the AAR calculation and makes the assumption that the two railway vehicles are coupled and are curving normally together, ignoring any offset tracking and/or suspension misalignment at each bogie. The bogie pivot centre is assumed to be located centrally between the rails. The coupler pins are located at some distance overhanging the bogie centre distance. Figure 5.44a shows the configuration of the two vehicles, with the angles between them being θ and the angle of the coupler with respect to vehicle 1 being ϕ. The angle ϕ of the coupler can be determined from the radius of curvature, the lengths between the adjacent vehicle bogie centres and the overhang distance to the coupler pin and the coupler length. These define the angles

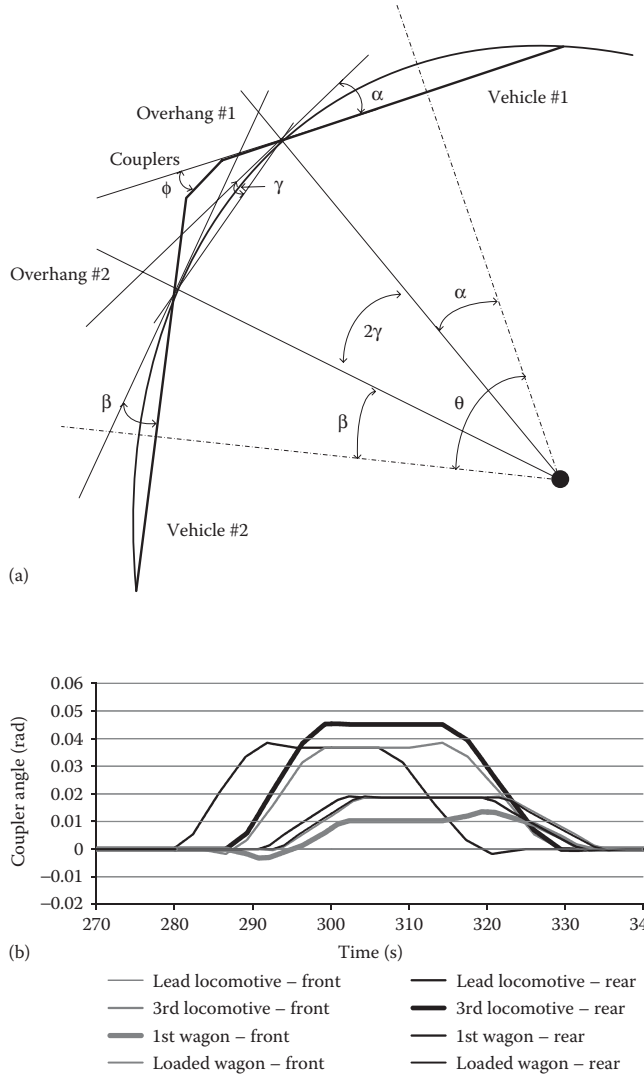

FIGURE 5.44 (a) Vehicle configuration during curving and (b) coupler angles for various vehicle combinations/locations.

α, β and γ, which are the chord angles to the arc for two vehicles and between the adjacent vehicle bogie centres, as shown in Figure 5.44a.

The relationship between θ and the chord arc angles is given by

$$\theta = \alpha + \beta + (2 * \gamma) \tag{5.15}$$

where

$$\alpha = \arcsin(BC_1/R_0); \quad \beta = \arcsin(BC_2/R_0); \quad \gamma = \arcsin(L/2/R_0)$$

where:

BC_i equals the half length between bogie centres of vehicle i
L equals the chord length between the adjacent vehicle bogie centres
R_0 is the radius of the track curve

By taking small angle approximations, the above expressions can be simplified to

$$\alpha = BC_1/R_0; \quad \beta = BC_2/R_0; \quad \gamma = L/2/R_0 \tag{5.16}$$

As the arc of the curve must be common, it is not necessary to restrict this calculation to a single radius R_0; therefore, the approach can be used to evaluate coupler angles in curve transitions as follows:

$$\alpha = BC_1/R_{Veh1}; \quad \beta = BC_2/R_{Veh2}; \quad \gamma = L/2/R_L \tag{5.17}$$

Similarly, L can be approximated by using a small angle assumption as

$$L = Ov_1 + Ov_2 + Cpl_1 + Cpl_2 \tag{5.18}$$

where:

Ov_i equals the overhang length of vehicle i (Ov_i = half the coupler pin centre to centre distance less half the bogie centre to centre distance)
Cpl_i equals the coupler length of vehicle i

The coupler angle ϕ can be approximated by the equation:

$$\phi = (L*(\alpha+\gamma) - Ov_2*\theta)/D \tag{5.19}$$

where D is the combined length of the two couplers, that is, $D = Cpl_1 + Cpl_2$.

Coupler angles will differ for variations in vehicle length, overhang length and coupling length in the train. In heavy haul trains, the dimensions of wagons are more uniform and the dimensions can be standardised to just a few cases. In most heavy haul trains, just two vehicle lengths need to be analysed for locomotives and wagons, as shown in Table 5.3. A few interesting observations can be made from the table:

- Increasing wagon length increases coupler angles;
- Increasing coupler length increases coupler angles; and
- Unequal coupler pin distances from the bogie give large variations in coupler angles in long/short connections, such as locomotive-to-wagon connections.

It is also important to note where these different connection combinations might be positioned in the train. Typical cases on curves (excluding transitions) for a head-end train are as follows:

- *Lead locomotive*: No coupling at the front; no lateral force at the front; equal coupling angle coupling at the rear if there are multiple locomotives; and unequal coupling angles at the rear between the locomotive and the first wagon if there is only one locomotive;

TABLE 5.3
Coupler Angles for Various Vehicle Combinations on a 300 m Radius Curve

	Lead Vehicle			Trailing Vehicle			Vehicle Coupler Angles		
Dimensions [*a*]	B_1	C_1	Cpl_1	B_2	C_2	Cpl_2	**Angle on**	**Radians**	**Degrees**
Datum									
Short wagon–short wagon	8.5	9.6	0.8	8.5	9.6	0.8	Wagon	0.0186	1.06
Locomotive–	16	21	0.8	8.5	9.6	0.8	Locomotive	0.0809	4.64
short wagon	8.5	9.6	0.8	16	21	0.8	Wagon	–0.0247	–1.41
Longer Wagons									
Long wagon–long wagon	10	13.4	0.8	10	13.4	0.8	Wagon	0.0250	1.43
Locomotive–	16	21	0.8	10	13.4	0.8	Locomotive	0.0651	3.73
long wagon	10	13.4	0.8	16	21	0.8	Wagon	–0.0025	–0.14
Longer Couplers									
Short wagon–short wagon	8.5	9.6	1.2	8.5	9.6	1.2	Wagon	0.0199	1.14
Locomotive–	16	21	1.2	8.5	9.6	1.2	Locomotive	0.0678	3.89
short wagon	8.5	9.6	1.2	16	21	0.8	Wagon	–0.0153	–0.88

Note: [*a*] all dimensions in metres; *B* is bogie centre to centre distance; *C* is coupler pin to pin distance; *Cpl* is coupler length.

- *Second and further locomotives*: Equal coupling angles at the front between two locomotives and unequal coupling angles at the rear between the locomotive and the first wagon;
- *First wagon*: Unequal coupling angles at the front between locomotive and wagon and equal coupling angles at the rear between identical wagons; and
- *In-train wagons*: Equal coupling angles front and rear between identical wagons.

For a train with remote-controlled locomotives, the following cases are added:

- *Single-remote locomotive*: Unequal coupling angles at both the front and the rear between the locomotive and the two connecting wagons;
- *Lead locomotive in a remote group*: Unequal coupling angles at the front between the locomotive and the wagon and equal coupling angles at the rear between two locomotives; and
- *Single pusher locomotive in a remote group*: Unequal coupling angles at the front between the locomotive and the wagon; no coupling at the rear; and no lateral force at the rear.

Examples of angles from the various locomotive/wagon combinations are shown in Figure 5.44b. Where couplings are of ‘like’ vehicles, the angles are equal as expected. As angles are calculated as the vehicles move through the curve, a small

overthrow 'kick' can be seen in all curves. When one vehicle has a longer bogie overthrow than another, for example, the last locomotive and the first wagon, larger and smaller angles than those on matching wagons can occur. In many configurations, the largest angle in the train occurs on the locomotive at the connection between the locomotive (or locomotive group) and the wagons. In such cases, the smallest angle occurs on the first connecting wagon. If the mismatch is large enough, the wagon coupling can even be straight or opposite to the direction of the curve. As locomotives almost always have longer bogie overhang than wagons, the maximum coupler angle in the train is usually one of the locomotive-to-wagon connections. As the minimum wagon angle is also at this connection, the maximum lateral force components on wagons (which can often be expected near locomotives) will actually occur at the connection between the first and second wagons in the rake; hence, the second wagon usually has the greatest risk of overturning.

The methodology for the calculation of coupler angles and associated forces is as follows:

- Calculate front and rear coupler angles on all vehicles using curvature data and vehicle dimensions;
- This is completed using the equations above, but with the refinement of allowing changes in the overhang distances Ov_1 and Ov_2 in response to draft gear deflections as measured in the train simulations, and allowing changes in the sum of $Cpl_1 + Cpl_2$ to incorporate the effect of coupling slack;
- Combine these angles with coupler forces to get lateral force components at the coupler pins. This is done simply as

$$F_{\text{lateral}} = F_{\text{coupler}} * \phi \tag{5.20}$$

- Use moments to translate these forces to the bogies, noting that the forces are not equal during transitions. These parameters are designated as lateral forces from couplers:

$$F_{lfb} = \left[F_1 * (C+B) - F_2 * (C-B)\right] / (2B) \tag{5.21}$$

$$F_{lrb} = \left[F_2 * (C+B) - F_2 * (C-B)\right] / (2B) \tag{5.22}$$

where:

F_{lfb} and F_{lrb} are the lateral forces at the front and rear bogies
F_1 is the front lateral coupler force component
F_2 is the rear lateral coupler force component
C is the coupler pin half distance
B is the bogie centre half distance

- Match the sign convention of longitudinal forces, considering lateral forces as:
  - *Positive if associated with tensile forces*: These forces pull the vehicle towards the centre of the curve (stringlining effect); and
  - *Negative if associated with compressive coupler forces*: These forces push the vehicle away from the centre of the curve (buckling effect).

- Add vehicle centripetal forces to the lateral forces, assuming equal distribution of mass between front and rear bogies and using bogie curvature and superelevation. This parameter is designated as total quasistatic bogie lateral force:

$$F_{lfb\_TL} = m_w/2\ (g * \sin(\psi) - V_w{}^2/abs(R) * \cos(\psi)) + F_{lfb} \tag{5.23}$$

$$F_{lrb\_TL} = m_w/2\ (g * \sin(\psi) - V_w{}^2/abs(R) * \cos(\psi)) + F_{lrb} \tag{5.24}$$

where:

F_{lfb_TL} and F_{lrb_TL} are the total quasistatic lateral force at the front and rear bogies
m_w is the vehicle mass
V_w is the vehicle velocity
R is the curve radius
ψ is the track cant angle

- Taking moments about each rail, the total quasistatic bogie lateral force can be used to calculate quasistatic vertical forces on each side of each bogie, again assuming equal distribution of mass between front and rear bogies, and using bogie curvature and superelevation. This parameter is designated as quasistatic bogie vertical force.

$$F_{vflhr\_TV} = m_w/2 * (g * \cos(\psi)/2 - g * \sin(\psi) * H_{cog}/d_c) + m_w/2 * V_w{}^2/abs(R) * (\sin(\psi)/2 + \cos(\psi) * H_{cog}/d_c) - F_{lfb} * h_c/d_c \tag{5.25}$$

$$F_{vflr\_TV} = m_w/2 * (g * \cos(\psi)/+ g * \sin(\psi) * H_{cog}/d_c) + m_w/2 * V_w{}^2/abs(R) * (\sin(\psi)/2 - \cos(\psi) * H_{cog}/d_c) + F_{lfb} * h_c/d_c \tag{5.26}$$

$$F_{vrhr\_TV} = m_w/2 * (g * \cos(\psi)/2 - g * \sin(\psi) * H_{cog}/d_c) + m_w/2 * V_w{}^2/abs(R) * (\sin(\psi)/2 + \cos(\psi) * H_{cog}/d_c) - F_{lrb} * h_c/d_c \tag{5.27}$$

$$F_{vrlr\_TV} = m_w/2 * (g * \cos(\psi)/2 + g * \sin(\psi) * H_{cog}/d_c) + m_w/2 * V_w{}^2/abs(R) * (\sin(\psi)/2 - \cos(\psi) * H_{cog}/d_c) + F_{lrb} * h_c/d_c \tag{5.28}$$

where:

F_{vfhr_TV} and F_{vflr_TV} are the total quasistatic vertical force at the front high and low rails, respectively
F_{vrhr_TV} and F_{vrlr_TV} are the total quasistatic vertical force at the rear high and low rails, respectively
H_{cog} is the height of the vehicle centre of mass above the rail
d_c is the distance between wheel rail contact points (~ track gauge + 0.07 m)
h_c is the height of the vehicle coupler above the rail

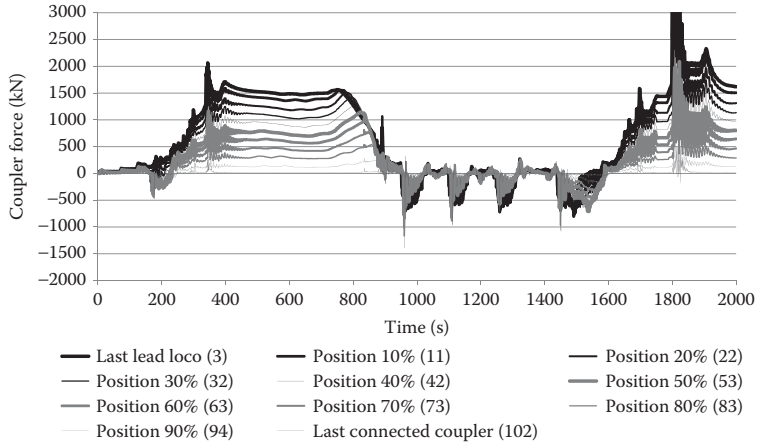

FIGURE 5.45 Simulation results—coupler forces—100 wagons, head-end power.

Having derived the total quasistatic bogie lateral force, it is also possible to calculate quasistatic bogie L/V, but the vertical forces calculated cannot be used to give bogie side L/V because the lateral force components cannot be separated into right and left rail components. To prevent confusion, it is not recommended that this parameter be used as it is very different from other definitions of L/V ratio.

To provide context for an example of the effects of coupler angles, coupler force results from a train simulation are shown in Figure 5.45. Coupler angles, coupler lateral forces and lateral and vertical forces at the bogies are shown in Figures 5.46 through 5.49.

5.3.2 Rail Vehicle Body and Bogie Pitch due to Coupler Impact Forces

Typically, for rail vehicle dynamics studies, modelling is undertaken of single vehicles with a longitudinal constraint as shown in Figure 5.50. The models involve full modelling of the wheel-rail contact patch and of the 11 masses and up to 62 degrees of freedom. For the consideration of vehicle body and bogie pitch, longitudinal forces and accelerations need to be known. A rail vehicle model is also required that is computationally economical, so that it can be undertaken for whole train trip simulations (e.g., >100 km). A simplified model is therefore desirable. The vehicle pitch behaviour is modelled as in Ref. [17], with three pitch motions and three vertical motions; see Figure 5.51a for a dynamic model of a typical wagon.

As only pitch and vertical motions are being modelled, the model can be further simplified by joining the bolster to the car body and modelling the bogie sideframes and wheelsets as one mass. As some of the dynamic parameters are already calculated in the train simulation, the modelling of each vehicle can be reduced to just six equations—three describing vertical motions of the vehicle body and the two bogies and three describing the pitch rotations; see Figure 5.51a. It is also necessary

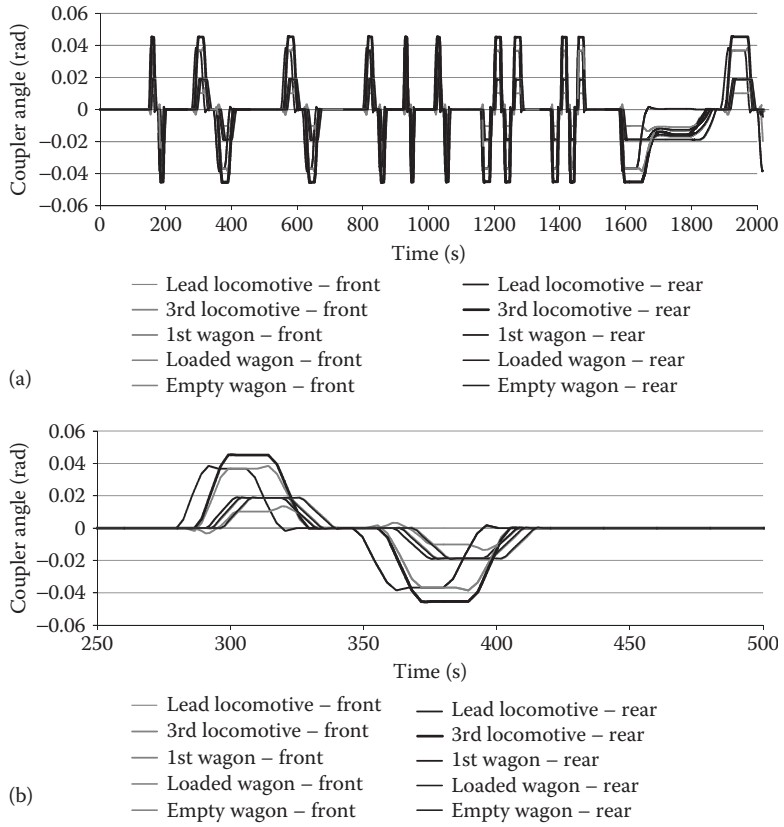

FIGURE 5.46 Simulation results—coupler angles—locomotive and wagon connections: (a) Coupler angles and (b) coupler angles—zoom-in view.

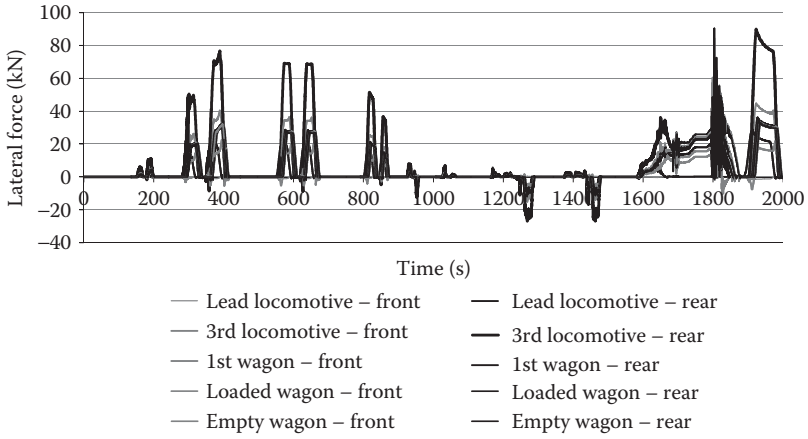

FIGURE 5.47 Simulation results—lateral forces due to couplers—locomotive and wagon connections (positive forces corresponding to tensile coupler stress).

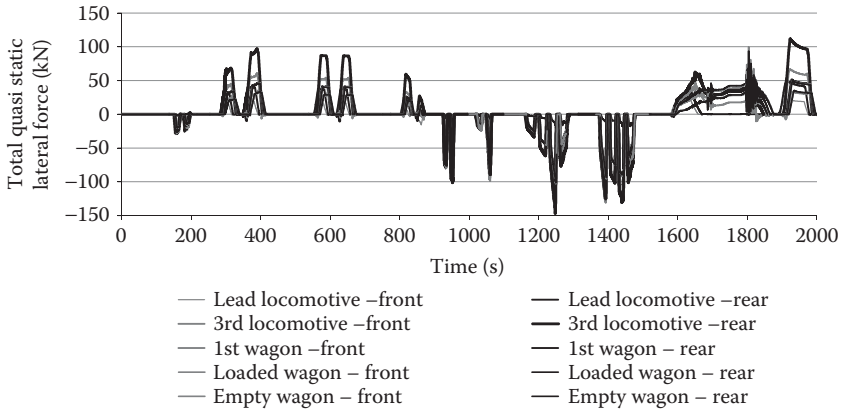

FIGURE 5.48 Simulation results—total quasistatic lateral forces—locomotives, loaded wagons and empty wagons (positive forces corresponding to force towards the low rail).

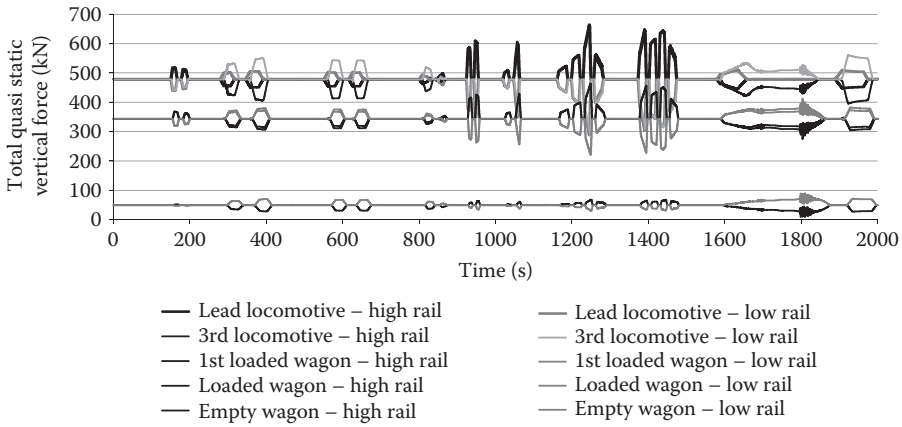

FIGURE 5.49 Simulation results—total quasistatic vertical forces—locomotives, loaded wagons and empty wagons.

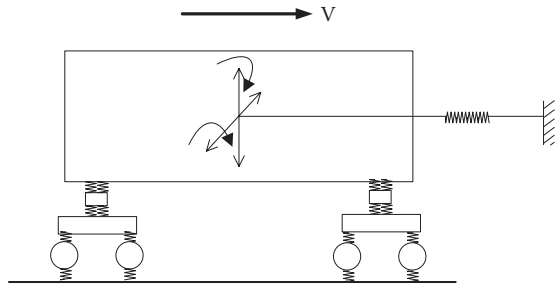

FIGURE 5.50 Schematic of a typical wagon dynamic model.

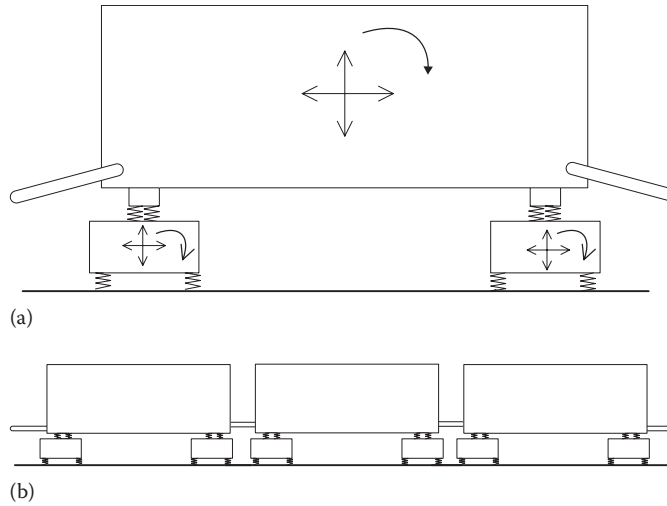

FIGURE 5.51 Simplified rail vehicle pitch model implemented with longitudinal simulation: (a) Simplified rail vehicle pitch model and (b) simplified three-vehicle pitch model.

to consider the effects of coupling heights and vertical force components between vehicles. If vehicles are of the same type and load, these components will be small, but bogie pitch motions will result in angles and vertical components. To ensure that correct interaction occurs at the couplings, three vehicles are included as shown in Figure 5.51b, and only the results from the middle vehicle are used. The connection of the other two vehicles to the rest of the train model assumes that points are at a fixed height above the rail.

The modelling equations for the simplified model are reproduced from Ref. [17]:

$$F_{zwb} = -F_{c1} * (z_{wb} - z_n - C * \sigma_{wb}) / (2C_{pl}) - F_{c2} * (z_{wb} - z_p + C * \sigma_{wb}) / (2C_{pl}) + F_{s1} + F_{s2} + F_{s3} + F_{s4} + F_{d1} + F_{d2} + F_{d3} + F_{d4} - abs(m_{wb} * g \cos(\lambda)) \quad (5.29)$$

$$F_{zfb} = -F_{s1} - F_{s2} - F_{d1} - F_{d2} + F_{wrc1} + F_{wrc2} - m_{fb} * g \quad (5.30)$$

$$F_{zrb} = -F_{s3} - F_{s4} - F_{d3} - F_{d4} + F_{wrc3} + F_{wrc4} - m_{rb} * g \quad (5.31)$$

$$\begin{aligned} M_{wb} = {} & -F_{s1} * (B + l_s) - F_{s2} * (B - l_s) + F_{s3} * (B - l_s) + F_{s4} * (B + l_s) \\ & - F_{d1} * (B + l_d) - F_{d2} * (B - l_d) + F_{d3} * (B - l_d) + F_{d4} * (B + l_d) \\ & + F_{c1} * (z_{wb} - z_n - C * \sigma_{wb}) / (2C_{pl}) * C - F_{c2} * (z_{wb} - z_p + C * \sigma_{wb}) / (2C_{pl}) * C \\ & - F_{c1} * (h_{cg} + C * \sigma_{wb}) + F_{c2} * (h_{cg} - C * \sigma_{wb}) + m_{fb} * h_{cg} * a_w \\ & + m_{rb} * h_{cg} * a_w + h_{cg} * (m_{wb} + m_{fb} + m_{rb}) * g * \sin(\lambda) \end{aligned} \quad (5.32)$$

Note that the moment from the longitudinal reaction at the centre bowl connection is calculated from the bogie inertia term $m_{fb} * h_{cg} * a_w + m_{rb} * h_{cg} * a_w$. This is also done in Equations 5.33 and 5.34:

$$M_{fb} = -F_{wrc1} * A + F_{wrc2} * A - F_{s1} * l_s + F_{s2} * l_s - F_{d1} * l_d + F_{d2} * l_d + m_{fb} * h_b * a_w + F_{brake} / R_w \quad (5.33)$$

$$M_{rb} = -F_{wrc3} * A + F_{wrc4} * A - F_{s3} * l_s + F_{s4} * l_s - F_{d3} * l_d + F_{d4} * l_d + m_{rb} * h_b * a_w + F_{brake} / R_w \quad (5.34)$$

where:

A is the axle centre half length
B is bogie centre half length
C is coupler pin centre half length
Cpl is coupler length
F_{zwb}, F_{zfb} and F_{zrb} are the vertical forces on the vehicle body, front bogie and rear bogie, respectively
F_{c1} and F_{c2} are the front and rear coupler forces, respectively
F_{s1} and F_{s2} are the spring forces from the front and rear halves of the two spring nests in the front bogie, respectively
F_{s3} and F_{s4} are the spring force from the front and rear halves of the two spring nests in the rear bogie, respectively
F_{d1} and F_{d2} are the damper forces from the front and rear wedges in the front bogie, respectively
F_{d3} and F_{d4} are the damper forces from the front and rear wedges in the rear bogie, respectively
F_{wrc1}, F_{wrc2}, F_{wrc3} and F_{wrc4} are the total vertical wheel rail contact forces per axle on wheelsets 1, 2, 3 and 4, respectively
F_{brake} is the bogie braking force
M_{wb}, M_{fb} and M_{rb} are the moments about the pitch axis on the vehicle body, front bogie and rear bogie, respectively
R_w is the wheel radius
a_w is longitudinal acceleration of the vehicle obtained from the train simulation
h_b is height of the coupling line above the bogie centre of gravity (CoG)
h_{cg} is height of vehicle body CoG above coupling line
l_s is distance to force centroid of spring half nest
l_d is distance to line of action of wedge dampers
m_{wb} is mass of the vehicle body
m_{fb} is mass of the front bogie
m_{rb} is mass of the rear bogie
z_{wb} is height of the centre of mass of the vehicle body
z_n is height of the centre of mass of the vehicle body connecting to the front
z_p is height of the centre of mass of the vehicle body connecting to the rear

σ_{wb} is the pitch angle of the vehicle body
λ is the track grade angle

To provide context for an example of wagon body pitch, a train simulation result is shown in Figure 5.52. A hypothetical heavy haul train is simulated with all wagons loaded. To induce wagon body pitch, a minimum brake application is applied. Compressive coupler forces are induced, as shown in Figure 5.53. Details of the coupler forces at the 7th wagon are shown in Figure 5.54, axle forces in Figure 5.55 and 'zoom-in' on axle forces showing body pitch in Figure 5.56.

Similarly, a hypothetical heavy haul train is simulated with all wagons empty. To induce wagon bogie pitch, a minimum brake application is applied. Details of the coupler forces at the 7th wagon are shown in Figure 5.57, axle forces in Figure 5.58 and 'zoom-in' on axle forces showing body pitch in Figure 5.59.

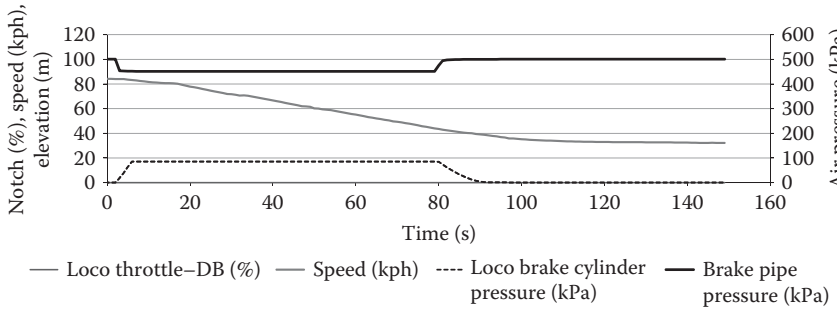

FIGURE 5.52 Simulation results—operational data—loaded train.

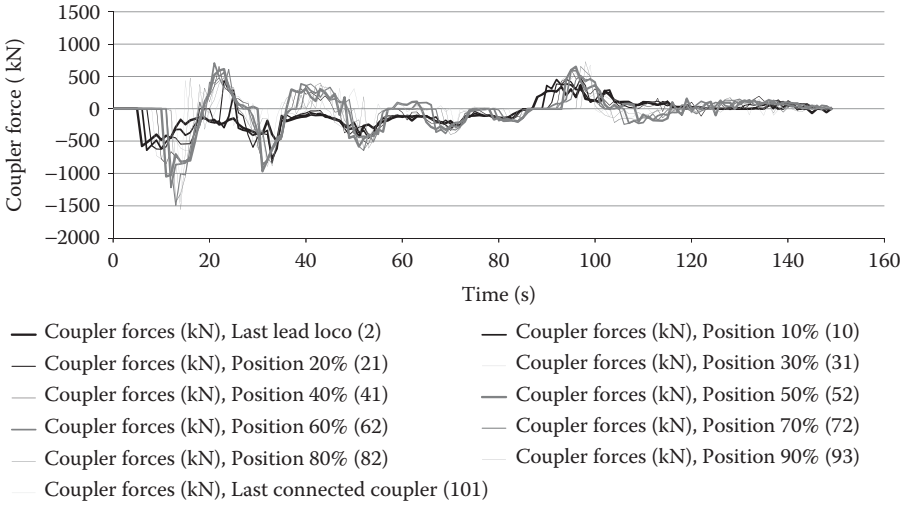

FIGURE 5.53 Simulation results—coupler forces—loaded train.

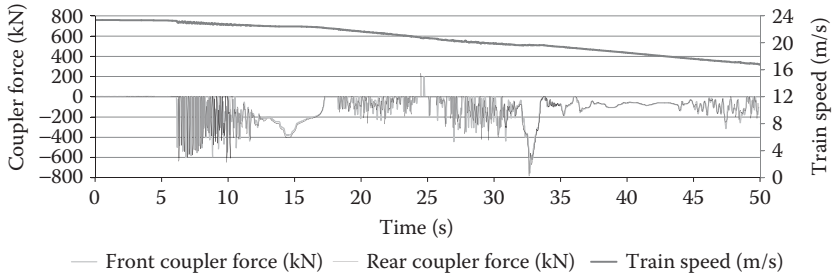

FIGURE 5.54 Simulation results—selected coupler force and operational data, wagon #7—loaded train.

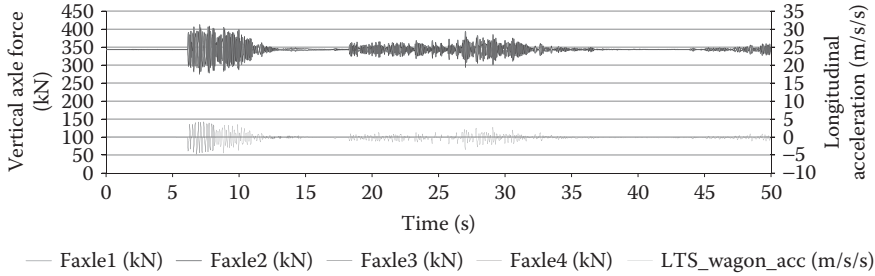

FIGURE 5.55 Simulation results—selected axle force data, wagon #7—loaded train.

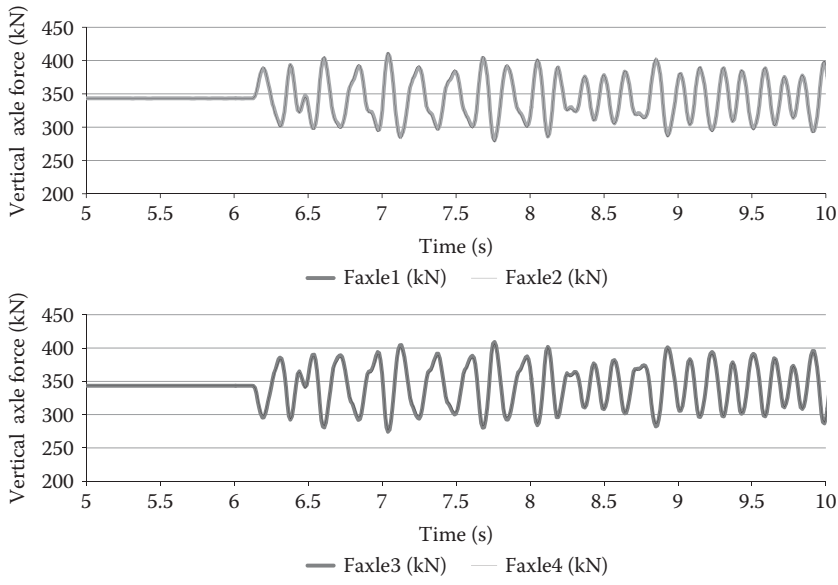

FIGURE 5.56 Simulation results—zoom-in on axle force data, wagon #7—loaded train.

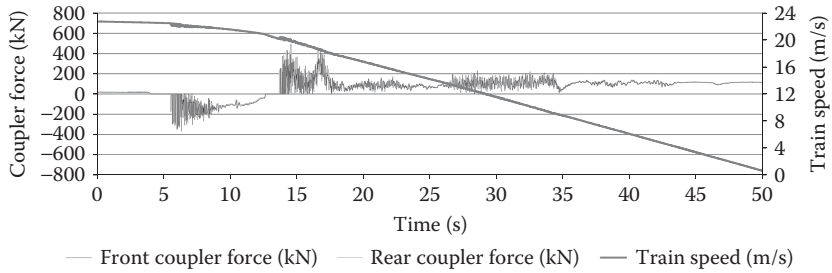

FIGURE 5.57 Simulation results—selected coupler force and operational data, wagon #7—empty train.

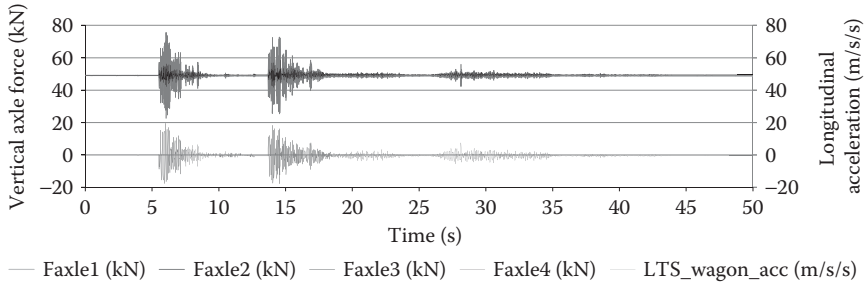

FIGURE 5.58 Simulation results—selected axle force data, wagon #7—empty train.

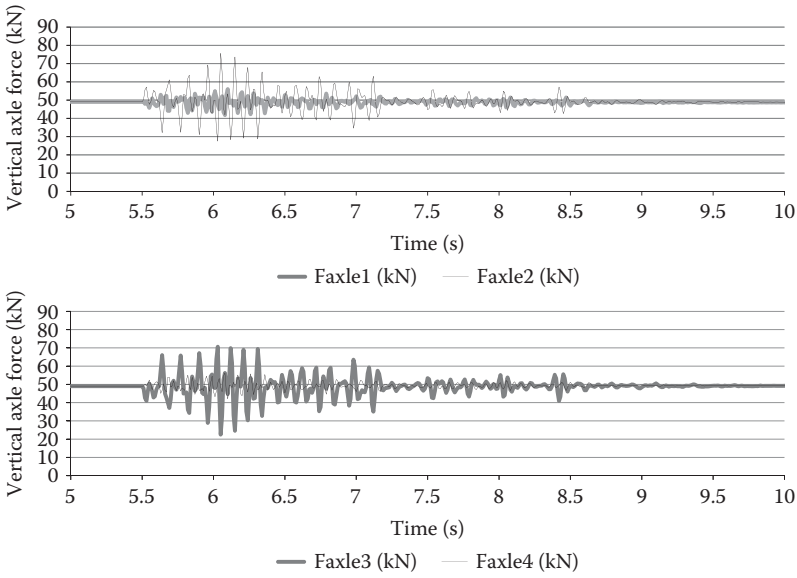

FIGURE 5.59 Simulation results—zoom-in on axle force data, wagon #7—empty train.

5.3.3 Rail Vehicle Lift-Off due to Vertical Components of Coupler Forces

Vehicle lift can more easily occur if there is a mismatch in coupling heights. The more severe case of vertical force components from coupling vehicles with different coupling heights, either empty/loaded combinations or vehicles of different types, can also be handled by the three-vehicle model approach. A schematic of this case is shown in Figure 5.60. It is assumed that the effect of a slight pitch angle on the adjacent vehicles will have no significant effect on the vehicle under study.

To provide context for examples of wagon lift-off instability, train simulation results for coupler forces are shown in Figure 5.61, which involves coupler tension, so the empty wagon is effectively pulled downwards by the couplers, increasing wheel loads as shown in Figure 5.62. This situation increases wagon stability. The second example in Figure 5.63 is the opposite and involves coupler compression. In this case, the wagon is lifted off the track by the couplers, and severe wheel unloading occurs as shown in Figure 5.64. If such events are severe enough, complete wheel lift-off and consequent jack knifing can occur.

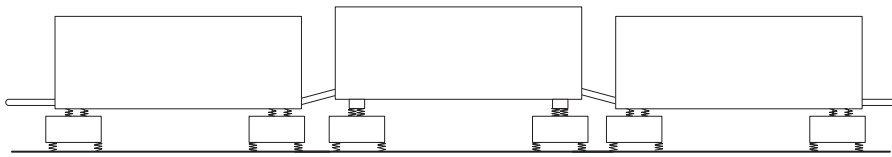

FIGURE 5.60 Simplified vehicle pitch model implemented as a three-vehicle model.

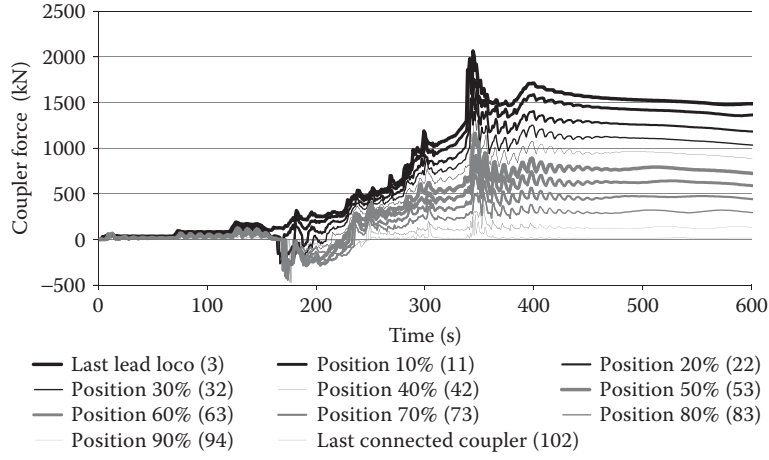

FIGURE 5.61 Simulation results—coupler forces—loaded train, traction case.

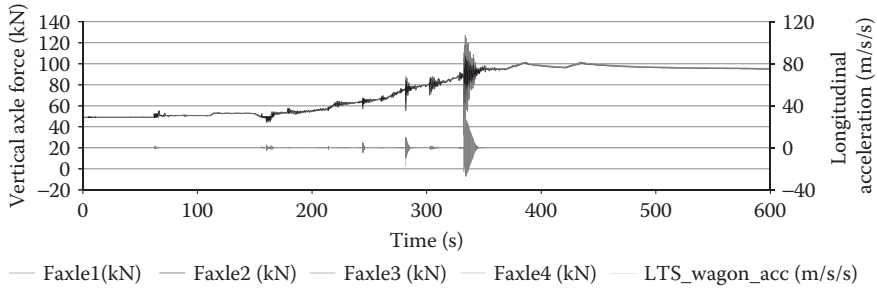

FIGURE 5.62 Simulation results—selected axle force and acceleration data, empty wagon #7—loaded train, traction case.

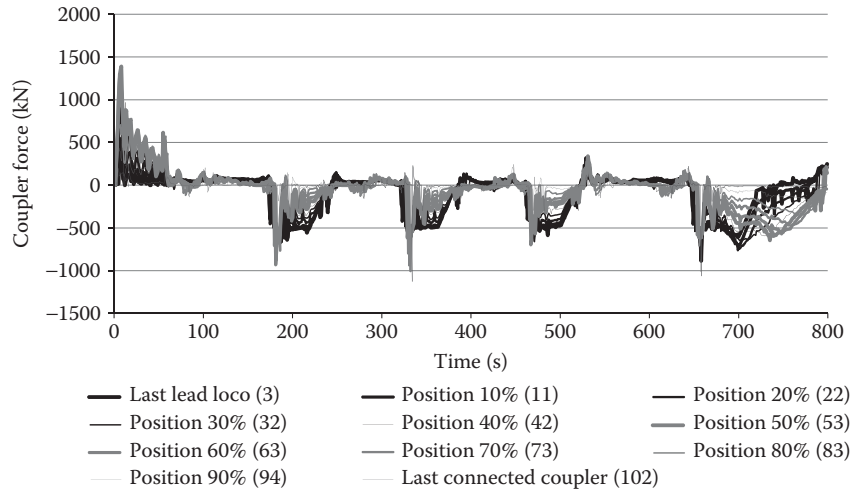

FIGURE 5.63 Simulation results—coupler forces—loaded train, braking case.

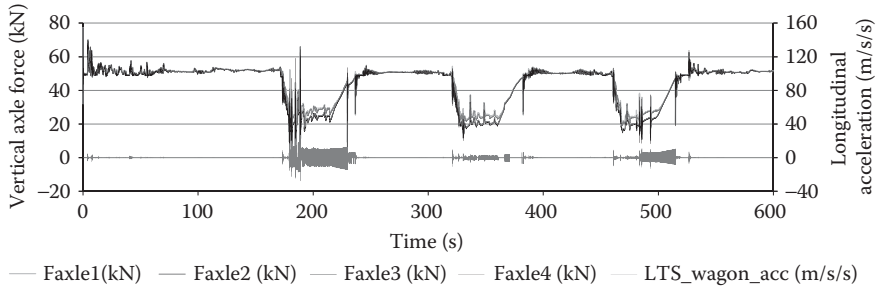

FIGURE 5.64 Simulation results—selected axle force and acceleration data, empty wagon #7—loaded train, braking case.

5.4 ENERGY CONSIDERATIONS

Minimisation of energy usage is often a popular emphasis in-train management. It is helpful to examine the way energy is utilised before innovations or changes to practice are adopted. Air resistance, for example, is often overstated. A breakdown of the Davis equation [1] shows the significance of air resistance compared with curving resistance and rolling resistance factors and grades; see Figure 5.65. It can be noticed that a 1 in 400 grade, or 0.25%, is approximately equal to the propulsion resistance at 80 km/h.

The minimum energy required for a trip can be estimated by assuming an average train speed for the calculation of train propulsion resistance, F_{pr}, and computing the sum of the resistances to motion, and not forgetting the potential energy effects of changes in altitude. The work done to get the train up to the target running speed once must also be added. As the train must stop at least once, this energy is lost at least once. Any further energy consumed will be due to signalling conditions, braking, stop-starts and the design of grades. Minimum trip energy can be estimated as

$$E_{\min} = \frac{1}{2} m_t v^2 + m_t g h + \sum_{i=1}^{q} \left(m_i * \sum_{j=1}^{r} \left[\int_0^{x=lcj} F_{crj}.dx \right] \right) + \sum_{i=1}^{q} \left(m_i * \int_0^{x=L} F_{pri}.dx \right) \quad (5.35)$$

where:

$E_{\min}$ is the minimum energy consumed (J)
g is gravitational acceleration (m/s^2)
h is the net altitude change (m)
L is the track route length (m)
m_i is the individual mass for vehicle i (kg)
m_t is the total train mass (kg)
F_{crj} is the curving resistance for curve j (N)
F_{pri} is the propulsion resistance for vehicle i (N)

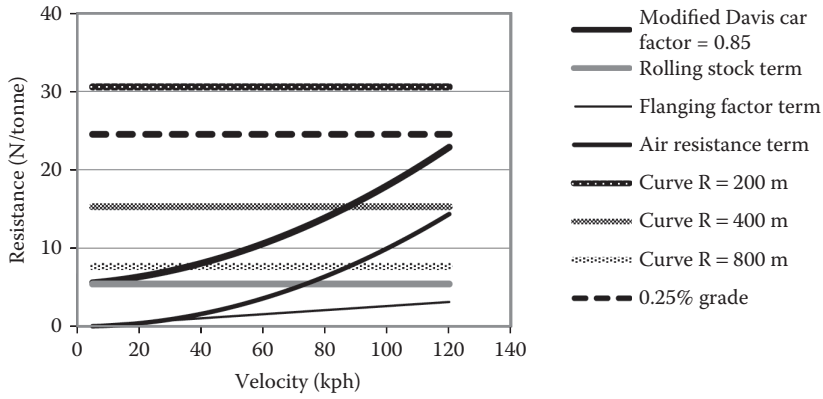

FIGURE 5.65 Comparative effects of resistances to motion. (From Cole, C., *Handbook of Railway Vehicle Dynamics*, Chapter 9, Taylor & Francis Group, Boca Raton, FL, pp. 239–278, 2006. With permission.)

TABLE 5.4
Energy Losses Equivalent to One Train Stop for a Train Running at 80 km/h

Energy Parameter	Equivalent Loss	Units
Gravitational potential energy (2nd term, Equation 5.35)	~25	Metres of altitude
Curving resistance (3rd term, Equation 5.35)	~16	Kilometres of curving resistance on 400 m radius curve
Propulsion resistance (4th term, Equation 5.35)	~18	Kilometres of propulsion resistance
Air resistance (part of propulsion resistance)	~36	Kilometres of air resistance

q is the number of vehicles
r is the number of curves
v is the train target running speed for the trip (m/s)

Unless the track is extremely flat and signalling conditions are particularly favourable, the energy used will be much larger than that given by the above equation. It is, however, a useful equation in determining how much scope exists for improved system design and practice. It is illustrative to consider a simple example of a 2000- tonne train with a running speed of 80 km/h. The work done to bring the train to speed, represented in Equation 5.35 by the kinetic energy term, is lost every time the train must be stopped and partly lost by any brake application. The energy loss per train stop in terms of other parameters in Equation 5.35 is given in Table 5.4.

What can be seen at a glance from Table 5.4 is the very high cost of stops and starts compared with other parameters. Air resistance becomes more significant for higher running speeds. High densities of tight curves can also add considerable costs. It should be noted that this analysis does not include the additional costs in rail wear or speed restriction caused by curves.

In negotiating crests and dips, the driver has the objectives of minimising the power loss in braking and managing in-train forces. In approaching the top of a crest, at some point close to the top (depending on grades, train size, etc.), power should be reduced to allow the upgrade to reduce train speed, the objective being that excess speed requiring severe braking will not occur as the train travels down the next grade. Similarly, when negotiating dips, braking should be reduced at some point while approaching the dip to allow the current falling grade to 'push' the train to reduce the power needed to climb the next rising grade. It can be seen that there is considerable room for variations in judgement and hence variation in energy usage. Work published in Ref. [7] indicated variations in fuel usage of up to 42% due primarily to differences in the way drivers manage the momentum of trains.

5.5 TRAIN CONTROL MANAGEMENT AND DRIVING PRACTICES

Train management and driving practices have received considerable attention in literature dating back several decades. Technology developments such as the transitions from steam to diesel-electric locomotives, improved locomotive traction

control systems, remote control locomotives and operation of very long heavy haul unit trains have ensured that this area continues to evolve. Train management and driving practices differ for different rail operations, and optimum practice depends on the different organisational targets. Train dynamics management has implications for the following parameters:

- Productivity
  - On-time running
  - Tonnes transported
- Energy
- Asset management
  - Safety
    - Speed compliance
    - Failure prevention
    - Rail vehicle stability
- Equipment
    - Failure prevention
    - Fatigue life of components

Heavy haul trains are characterised by longer and heavier trains of a single wagon and payload type. As payloads are usually bulk or hardware commodities, longitudinal accelerations that are a concern in passenger trains are usually not a primary concern in heavy haul trains. The exception would be if a heavy haul train was used to ship more sensitive commodities (i.e., computer equipment, instruments and cars). On-time running is usually a secondary consideration to weekly tonnage targets. As the trains can be large (up to 50,000 tonnes), operations place a high emphasis on controlling train dynamics as railways seek high productivity and safety targets. Note that a derailment of a large heavy haul train can easily cost in excess of $US30 million at the time of writing (2015). This threat must be managed by clearly understanding the risks associated with:

- Coupler and draft gear assembly failure (Section 5.2.3) by reaching yield and ultimate stress;
- Rail vehicle stability (Section 5.3); and
- Failure of components due to fatigue.

As in-train forces in current heavy haul trains in Australian service can easily exceed the tensile yield of couplers of 1.8 MN as designated in the AAR Standard M-211 [22], it is normal practice to use train simulation at both design and implementation stages of heavy haul train projects. Control of in-train forces is then the responsibility of properly developed and implemented train driving practice unless a system of automated train control (driverless trains) is adopted. Safe operation of heavy haul trains is therefore highly dependent on adequate driver training programs and compliance with recommended practices. Wagon stability is a further complication that arises in different ways. When new heavy haul routes are designed and built, wagon stability issues tend to be designed out by keeping the radius of curves adequately large and grades adequately small for the train configuration concerned. When this occurs, quite extraordinary

designs can be achieved; for example, heavy haul train systems have been built with wagon-to-locomotive mass ratios as high as 90. Wagon stability becomes an issue when trains are made larger but are operated on older infrastructure. The situation arises that larger in-train forces are applied on sharper curves. In addition, grade forces are larger. Risks for wagon stability that need to be understood and managed include the following:

- In-train forces at start-up and braking in empty trains on curves (wagon overturning);
- Longitudinal wagon accelerations at start-up and braking in empty trains (wagon pitch);
- The above two scenarios combined; and
- Operation of empty wagons in loaded trains:
  - Lateral instability on curves—overturning and wheel climb; and
  - Wagon lift-off and jack knifing.

A common thread to train dynamics management is the issue of speed control and hence management of train momentum. In general, it is desirable to apply power gradually until in-train slack is taken up. During running, it is desirable to minimise braking and energy wastage, utilising coasting where possible. Route running times limit the amount of time that the train can coast. Longer trains can coast over undulating tracks more easily than shorter trains because of the grade forces being partially balanced within the train length. Stopping is achieved at several different rates. Speed can be reduced by removal of power and utilisation of rolling resistance (slowest), application of dynamic braking, application of minimum pneumatic braking, service application of pneumatic braking and emergency application of pneumatic braking (fastest). The listed braking methods are also in the order of increasing energy wastage and increased maintenance costs. The selection and blending of train braking methods are quite complicated and will often be governed by practice rules. Note that the recent adoption of ECP brakes is expected to simplify and revolutionise braking practice, but traditional train braking, controlled by the brake pipe, will also continue to exist for many years to come. Braking scenarios are listed as follows:

- Locomotive dynamic braking only;
- Locomotive air braking only (usually forbidden);
- Minimum braking with locomotive brakes off (applying a 30% brake application to wagons only);
- Minimum braking with locomotive brakes on (applying a 30% brake application to all vehicles);
- Service braking with locomotive brakes off (applying >30% up to 100% brake application to wagons only);
- Service braking with locomotive brakes on (applying >30% up to 100% brake application to all vehicles);
- Emergency braking (100% brake application to all vehicles, braking at a higher pressure on AAR compliant systems); and
- Penalty braking (100% brake application to all vehicles, braking at a higher pressure on AAR compliant systems).

Policies differ as to whether dynamic braking is allowed during an air braking application or not. Much of braking practice is dependent on the type of train configuration. Heavy haul trains with very long wagon rakes will tend to favour only very mild applications of dynamic brakes and greater use of minimum applications. The use of distributed power (remote locomotives) is often driven by the need to improve brake control, which is achieved by controlling the brake pipe from multiple points and thus reducing application delays and interwagon impacts. The use of ECP brakes is now an option for greatly improving braking, as all wagons in a train can be braked simultaneously. If locomotive brakes are controlled appropriately, ECP braking systems can be tuned so that there are no in-train forces or interwagon impacts at all. In other differences, the ECP systems provide greater selectivity, allowing application in the range of 10%–100% and permitting graduated adjustment during both application (increasing brake forces) and release (reducing braking forces). Note that many traditional braking systems in heavy haul applications do not have 'graduated release'. Graduated release exists in European railways, but not in Australian and North American systems.

5.6 HEAVY HAUL SYSTEM DESIGN CONSIDERATIONS

As shown in this chapter, the study of the longitudinal train dynamics has significant implications for design strength of couplings and draft gear components. Heavy haul trains continue to push the limits of train design in both yield strength and fatigue life. It will be realised that modern locomotives, if marshalled in groups of three, can deliver up to 2.4 MN as a starting force. This can therefore exceed the yield stress of some coupler knuckles, and the AAR standard specifies 1.8 MN (400,000 lb) yield and 2.9 MN (650,000 lb) ultimate for the tensile strength of these components [22]. It is also not correct to assume that in-train forces in a long train will be limited to the maximum traction forces applied. As heavy haul trains can be more than 2 km long, a train on a hill with long steady grades can have significant in-train forces just from the gravity components. A simple example of this is illustrated by the simulation results for the large head-end train shown in Figure 5.66. It can be seen in this figure that the mid-train forces exceed the locomotive group drawbar forces because of the crest of the hill, noting drawbar at ~500 kN and mid train at ~1250 kN in the track region 124–125 km. Note that the graph shows all plots relative to the lead locomotive position, so the high mid-train force corresponds to when the mid-train is near 126 km. The train is ~2.4 km long.

It can therefore be seen that the combination of gravity forces and traction forces can easily exceed component strength. In the case in Figure 5.66, any further increase in tractive effort would add to the mid-train peak force; if the train was going slower, the locomotives could add substantially more than 400 kN.

Long trains have also pushed the limits of traditional train brake systems. Even with excellent performance of signal propagation of 300 m/s, the time delay in an Australian 240-wagon ore train would be 8.8 s (assuming a wagon-coupled length of 11 m). A further issue is that, in longer trains, not all pneumatic air brakes have the same design features and different adjustments are required to get very long rakes of wagons to operate correctly. As the traditional pneumatic brake system has developed into a complex system of volumes, chokes and valve logic, when

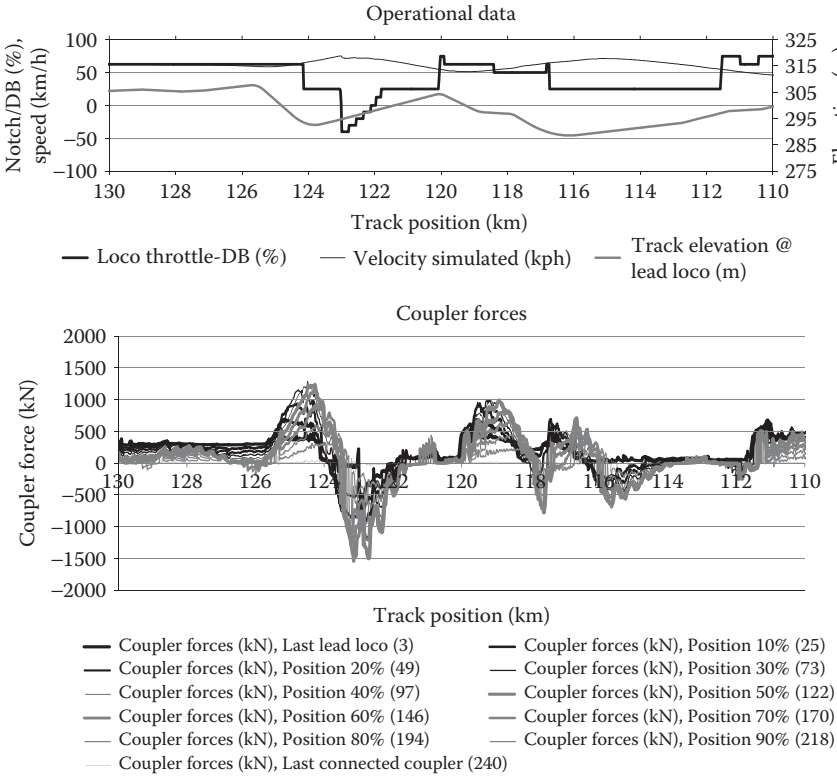

FIGURE 5.66 Operational data—head-end train, 3 locomotives, 238 wagons.

combined in a very large system, every design detail becomes important, including quite simple things like pipe length per wagon, the volumes of branch tees and the like on each wagon. The actual pipe length of the brake system can, in some cases, be significantly longer than the train. Propagation times in heavy haul systems are improved by the use of distributed power (which can give multiple brake pipe exhaust points), end-of-train devices, larger bulb volumes and the use of venting valves on each wagon. The use of venting valves differs in various countries, but it is standard in North America and on Australian Pilbara Iron Ore operations. The alternate British/Australian Westinghouse-type triple-valve system is still dominant on other Australian railways, and these generally have not used vent valves. Some examples of brake propagation are given in the simulations of a head-end train of 100 wagons shown below. It will be noted that, although propagation of the brake pipe still appears to be reasonable, the application rate of the brake cylinders becomes limited by the rate of pressure drop in the pipe; see Figure 5.67. Note that much better results are achieved by the head–tail configuration in Figure 5.68.

The delay in brake force applications results in substantial slack action and decreases the braking effort available until all the brakes are applied.

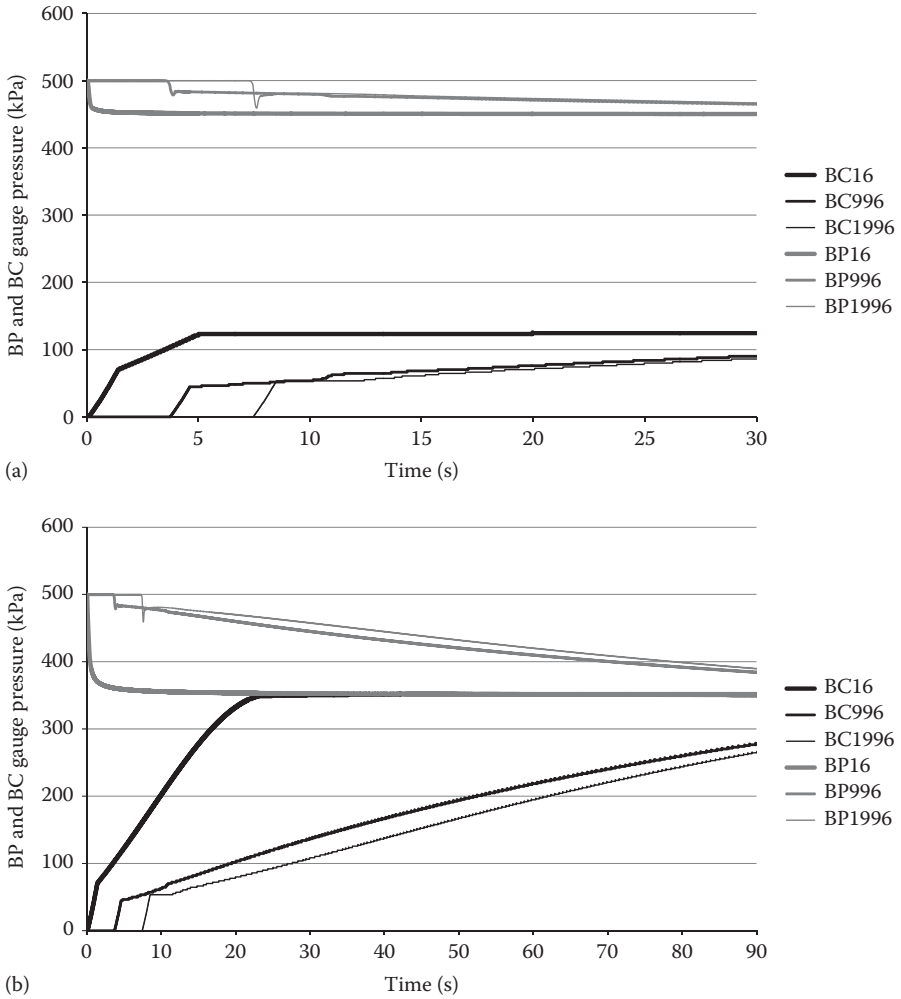

FIGURE 5.67 Operational data—head-end train, 100 wagons, one valve per wagon, pipe length ~2000 m: (a) Minimum application and (b) full-service application.

These problems have been addressed by progressive improvements: distributed power, reduced slack in the train and, more recently, ECP braking. However, it should be noted that track topography can also dictate which heavy haul operational parameters are possible. The typical considerations when designing a heavy haul system are as follows:

- Starting the train (traction);
- Stopping the train (braking);
- Topography issues;
- Traction pinch points; and
- Cycle time.

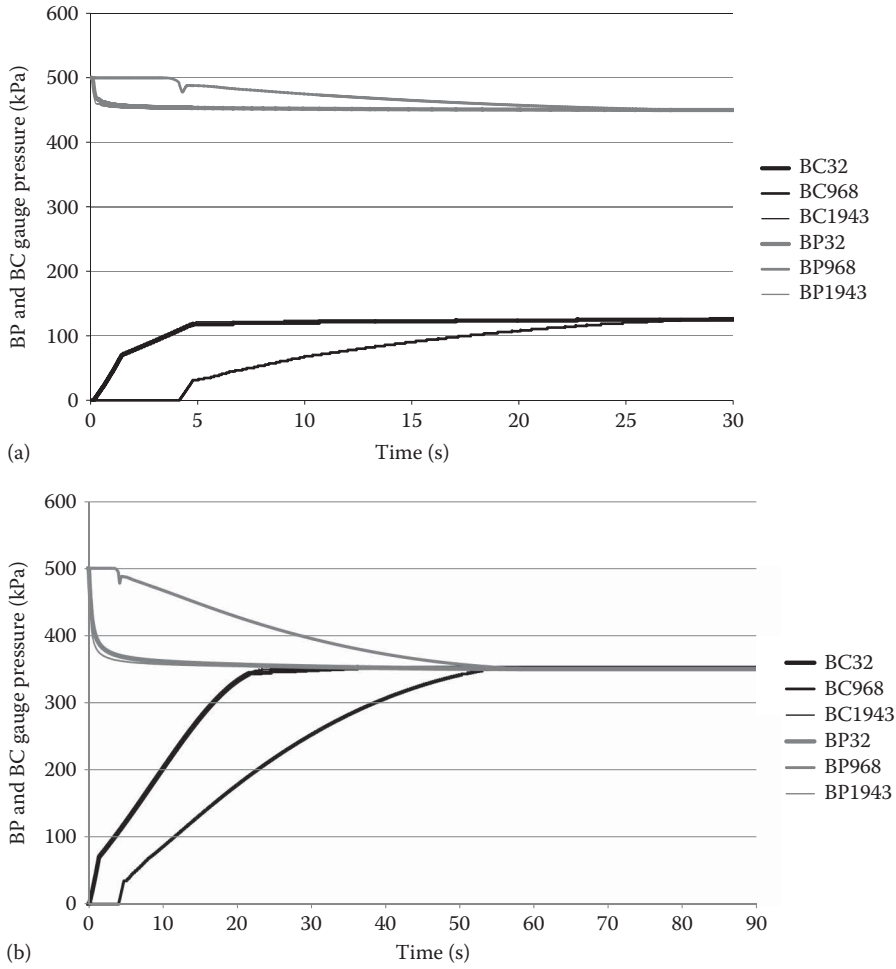

FIGURE 5.68 Operational data—head–tail train, 100 wagons, one valve per tandem wagon pair, pipe length ~2000 m: (a) Minimum application and (b) full-service application.

5.6.1 Starting the Train (Traction)

Traction has been discussed briefly in earlier sections and in some examples given in Figures 5.39 and 5.40. The basic premise is that coupler forces cannot exceed the knuckle strength. Management can be achieved by driver care, as demonstrated in Figure 5.40, or via using distributed power to reduce the drawbar force of each locomotive group. A further consideration is the track topography. A decision needs to be made concerning whether the locomotive(s) can lift the train at every possible track site. In some heavy haul systems, this requirement has been relaxed, acknowledging that a train that stopped at a certain site would need to be backed up to a better site to restart from or would need to be assisted by additional motive power to start. A second and less obvious consideration is the starting of empty trains. Heavy

haul tracks often allow greater grades against the travel direction of the empty train. Combining this with the tighter curves that often exist in sections with steep grades, the combination of high in-train forces while transiting those curves may be enough to increase wheel-climb and roll-over risks.

5.6.2 Stopping the Train (Braking)

Freight trains have traditionally favoured dynamic braking for mild or early braking, as passenger comfort is not a concern and it does not add brake shoe wear costs. As trains get longer and heavier and dynamic brake performance increases (as it has in the modern locomotives), the use of a minimum air brake application as a first stage of braking may be required. This is particularly true in very long head-end trains. It therefore also follows that more use of dynamic brake and less use of air brakes will be possible with distributed power. Dynamic brake can also be used selectively; it is a mild brake at higher speeds, as noted in Figure 5.9.

5.6.3 Topography Issues

Problems with gravitational components were introduced in the general comments when discussing Figure 5.66. Topography issues are a key driver for the use of distributed power. In the case of the head-end train example in Figure 5.66, the only way to control the in-train forces is to reduce the tractive effort as much as possible. If the grade continued or steepened, this would not be possible as the forces would have to increase. Distributed power offers solutions to this problem in two ways. Firstly, the fact that locomotives can be placed mid-train or further back at the tail of the train allows the mid-train tension to be reduced on such sites. Secondly, the controls of the two or more locomotive groups can be made independent. In cases where a hill is being negotiated, the front locomotive group can reduce power, whereas mid-train and pusher locomotives can maintain or increase power. This can give very good results, provided that the locomotives collectively can still lift the train in this reduced-power state; see Figures 5.69 and 5.70.

Another aspect of topography is the crest shape. It can be shown that flat plateau profiles will give fewer force problems than nicely smoothed over-vertical curves. Two examples are given in Figures 5.71 and 5.72.

Surprisingly, the parabolic track profile shown in Figure 5.73 gives higher forces than the trapezoidal approximation. There are two implications: peak forces can be reduced by appropriate civil engineering design (i.e., flat plateaus rather than just joining two log grades) and it is observed that poorly resolved survey data can result in underestimations of in-train forces from simulations.

5.6.4 Traction Pinch Points

The so-called traction pinch points are the locations on track where locomotive traction and power are very close to the limit. An illustration of this is given in Figure 5.74. The train is lugging down to approximately 14 km/h, which is a balance speed limit that is now available on some locomotives. The lead locomotive

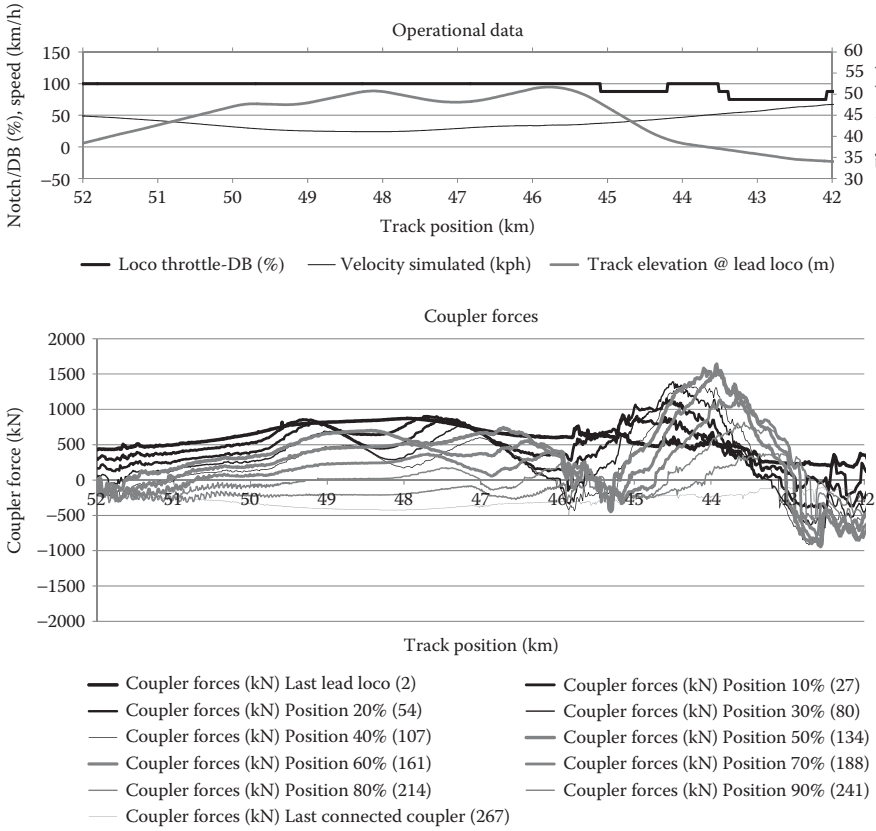

FIGURE 5.69 Operational data and in-train forces—head–mid–tail configuration, 4 locomotives, 264 wagons—synchronised controls.

force is approximately 760 kN in this case and depends on achieving very high adhesion (approaching 40%, which is only feasible in dry conditions). The problem is compounded further in that the effect of traversing the hill results in coupler forces approaching 2 MN and certainly in the region of knuckle yield. An independent locomotive control strategy might be possible, but cutting power might mean that the train would stall. This example would require further study to resolve an appropriate solution.

5.6.5 Cycle Time

Although there is often a push when designing an integrated train-track system to reduce capital expenditure as much as possible by minimising the number of locomotives (as these are expensive assets), the other critical aspect of heavy haul operation is cycle time. It is sometimes quite false economy to have tightly defined (i.e., almost unachievable) peak performance requirements, because the system will almost inevitably suffer longer-than-expected cycle times as conditions vary. A small margin in

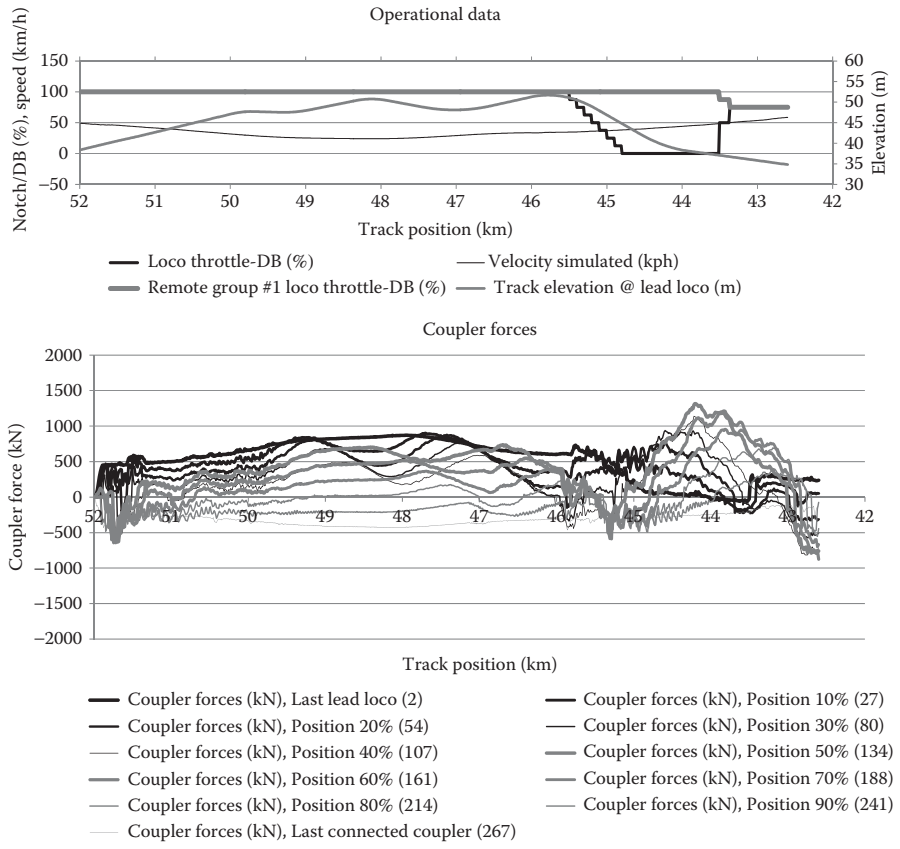

FIGURE 5.70 Operational data and in-train forces—head–mid–tail configuration, 4 locomotives, 264 wagons—independent controls.

improved engineering specifications will result in a more reliable operation under changes in wheel-rail condition, train load, locomotive condition etc., while also giving faster average speed and the desired higher production rates.

5.7 DISTRIBUTED POWER

Considering the previous discussion, it would appear that there are many options and paths to suitable heavy haul designs. The design adopted will be a system balance of needs, costs and the required production rate. At first glance, it might appear that distributed power is the logical solution to all problems of excessive in-train forces. As distributed power technology has improved, it is now possible to have two or more remote locomotive groups. The obvious advantage is that, as trains get longer and heavier, new train designs can keep locomotive groups small. A sensible approach might be to limit the locomotive group to capabilities less than 1.7 MN (corresponding to two large modern AC locomotives and still less than coupler knuckle yield).

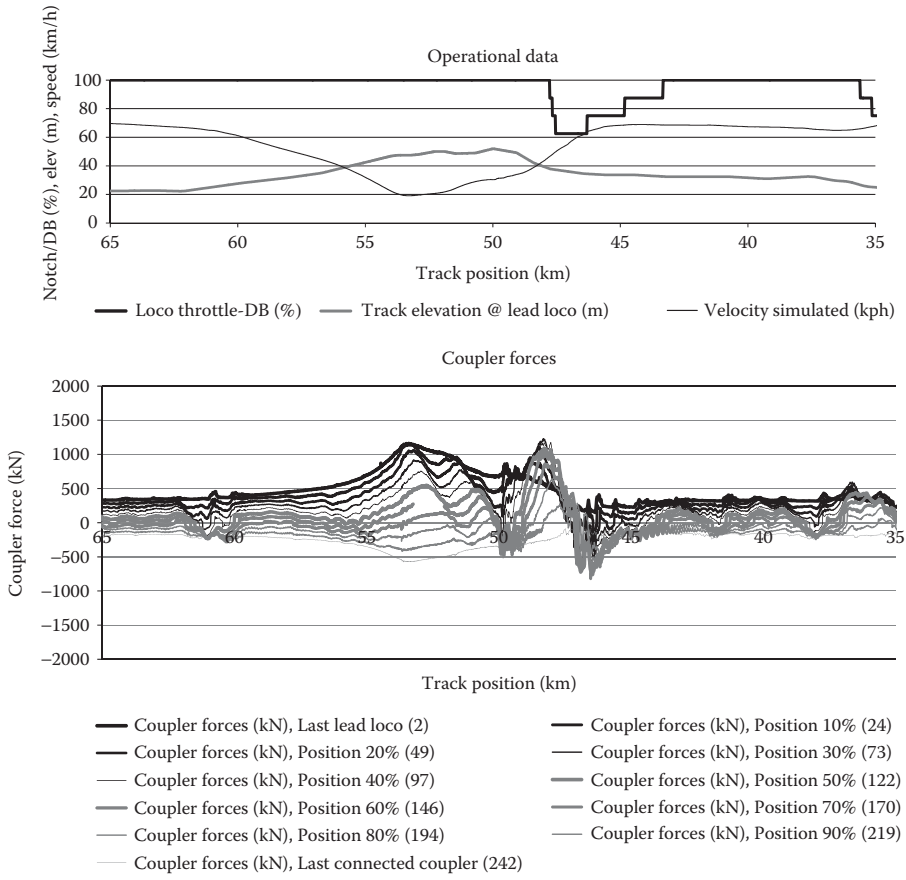

FIGURE 5.71 Operational data and in-train forces—head–tail configuration, 3 locomotives, 240 wagons—plateau profile.

However, the interactions of trains with the local topography and the different effects of different configurations need careful consideration. The configurations given in Table 5.2 show some basic variations.

What will work best for a given heavy haul system is generally a complex decision involving both engineering and operational considerations, so it is important to understand the relative merits of different configurations. In analysing train dynamics across various track topographies, it is usually found that the worst cases of in-train forces are associated with draft forces and traction scenarios. This is in part because locomotive traction force capabilities are generally higher than dynamic brake forces, unless specialised additional dynamic brake capability is added. Secondly, draft forces are usually the primary concern in draw gear components, as higher yield and ultimate strengths are found in compression (buff). This situation is not expected to change, as the coupler knuckle has a secondary function of being a 'mechanical safety fuse', effectively a 'shear pin'. It is the component that engineers

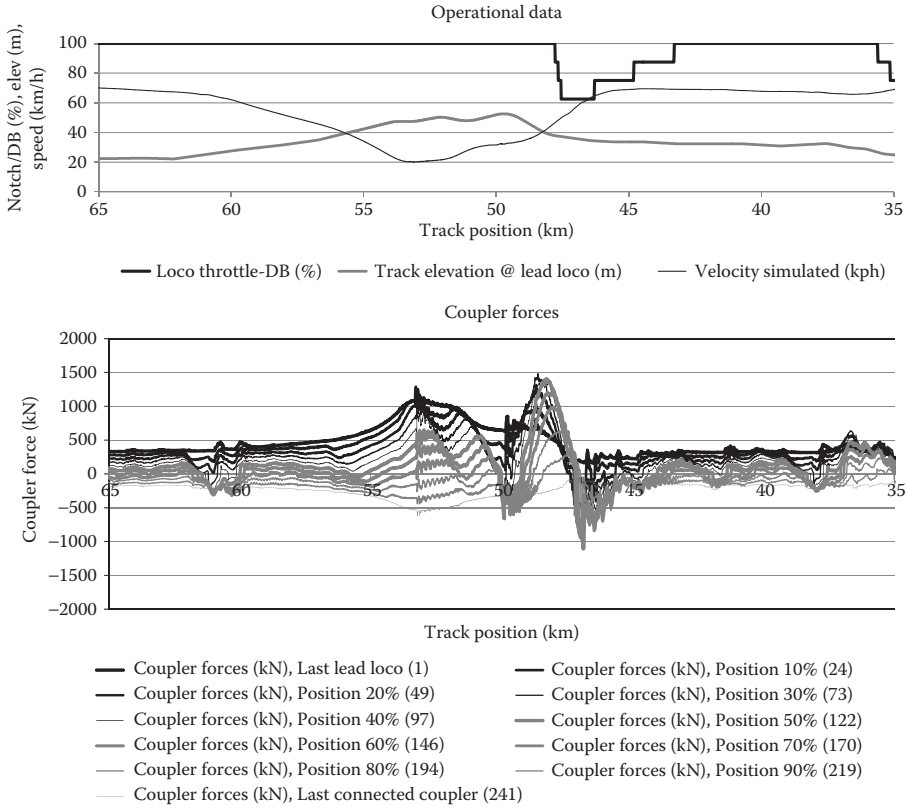

FIGURE 5.72 Operational data and in-train forces—head–tail configuration, 3 locomotives, 240 wagons—parabolic profile.

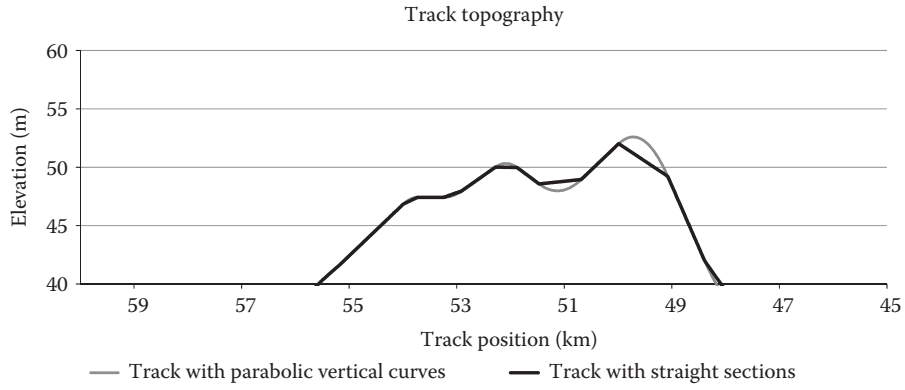

FIGURE 5.73 Track topography.

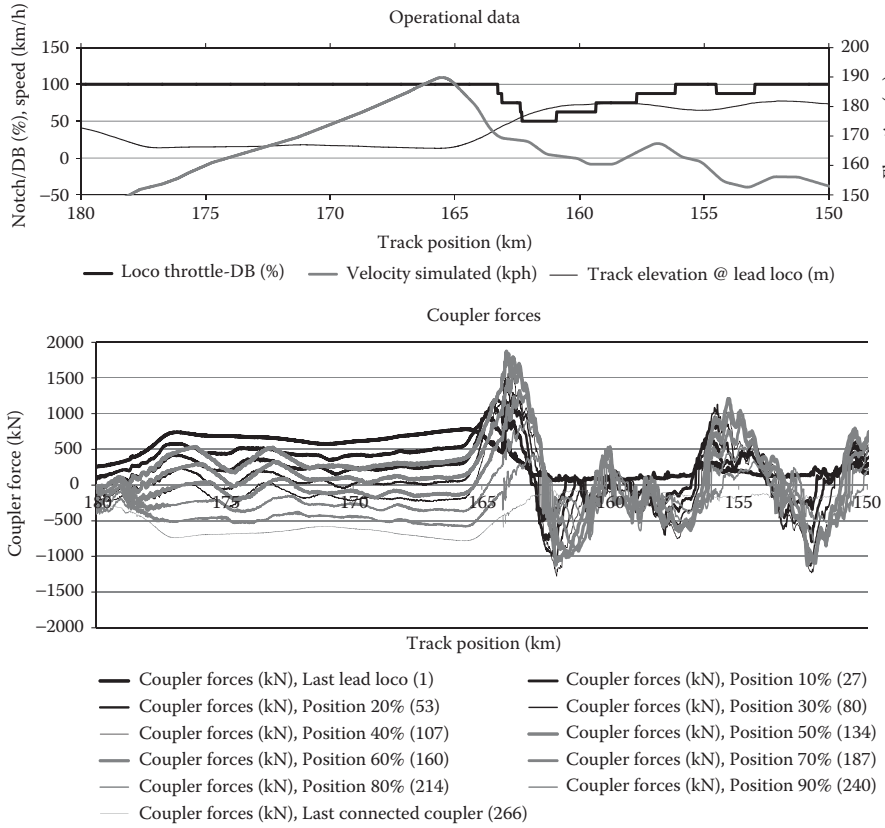

FIGURE 5.74 Operational data and in-train forces—head–mid–tail configuration, 3 locomotives, 264 wagons—synchronised controls.

expect to break first, so as to minimise damage in other areas. It is also relatively easily replaced. Therefore, irrespective of the future designs and innovations, there will always be a need for a 'mechanical safety fuse', and in all likelihood, it will remain the coupler knuckle. This means that limitation of tensile (draft) in-train forces will always be significant in the designing of the train configuration, the allowable grades and the track topography. Brief commentary is now given on each of the distributed power configurations listed in Table 5.2.

5.7.1 Head–Tail Configuration

The head–tail configuration has several obvious advantages and some not so obvious issues that may require careful management. The addition of the locomotives at the tail end of the train reduces tensile (draft) in-train forces, and this can be used to keep draw gear components below yield. It also has the advantage of simple control. In most cases, benefits can be achieved with simple paralleled controls on all locomotives. The rear position of the pusher or banker locomotive/s reduces the tensile forces

in the mid train as the train traverses crests. The design can be adjusted with either more locomotives at the front or equal groups. The configuration also has advantages for traditional brake pipe systems if the brake pipe is also initiated from both lead and tail groups, halving the propagation time. However, there are potential disadvantages. The rear locomotives exert compressive forces on the train during traction. This can be a problem on curves when travelling at speed because compressive forces will increase rollover risks. That said, if the train has a high mass-to-power ratio (which is common in heavy haul trains), the high compressive forces under traction situations will be at slow speeds and, if on curves, the wagons will usually be tracking near the low rail (excess track cant condition), so the compressive force will improve stability. Likewise, if dynamic brakes are being applied at high speed on curves, these tend to also improve the stability by pulling the wagon away from the high rail. Although all of this sounds favourable, the tight curvatures through switches and turnouts could pose some increase in wagon instability risks, particularly with empty wagons. Similarly, the braking situation reveals some unexpected dynamics. It is common practice to only brake the wagons in minimum and service brake applications (so-called locomotives 'bailed off' condition). This, in head-end trains, improves wagon stability. The inertia of the locomotives tends to reduce the severity of deceleration of the lead wagons by applying a tension, while the wagons at the tail of the train are still starting their brake applications (due to pipe delays). This practice is not necessarily good in the head–tail configuration, noting that the tail locomotive group, due to its inertia, will slam into the rear wagon during air braking. A beneficial situation can be achieved by applying the tail locomotive group's air or dynamic brakes while leaving the lead locomotive group unbraked ('bailed off').

5.7.2 Head–Mid Configuration

Comments similar to the head–tail configuration apply here, as mid-train locomotives have a pusher function in some situations. Generally, in-train locations of remotely controlled locomotives do not afford the same reductions in tensile force (draft), and so this configuration is likely to need more instances of independent control. The typical head–mid or head–two-thirds positioning of locomotives can be seen as either two head-end trains together or a head–tail train and a head-end train. With traditional air brake systems, braking is of course improved in the head–tail rake, so the head–two-thirds positioning is the most logical choice for keeping braking behaviours in the wagon rakes similar. The use of equal rakes can result in severe impacts mid train during air braking, as the front rake is braked earlier than the rear. This can be a risk to wagon stability, particularly when wagons are empty.

5.7.3 Head–Mid–Tail Configuration

The head–mid–tail configuration allows the use of equal rakes of wagons and solves the brake impact problem noted in Section 5.7.2. The configuration is effectively two head–tail configurations coupled together. In-train tension problems can be reduced by making the middle locomotive group larger, that is, 1L-120W-2L-120W-1L rather than 2L-120W-1L-120W-1L.

5.8 CONCLUDING REMARKS

As shown in this chapter, the study of longitudinal dynamics has significant implications for design strength of coupling and draft gear components. Heavy haul trains continue to push the limits of train design in both yield strength and fatigue life. In addition, the study of the interaction of longitudinal train dynamics and vehicle dynamics reveals a much more complex area that needs design consideration. The tendency towards shorter couplers increases the risk of lift-off and jack knifing of empty wagons in otherwise-loaded trains. Longitudinal wagon accelerations increase the risk of body pitch and bogie pitch. The use of permanently coupled wagon pairs, quads or eights with reduced interwagon slack is a suitable method of reducing slack action and body/bogie instability. The degree to which these considerations affect design choices in heavy haul systems depends on the minimum curve radius adopted and the maximum expected in-train forces.

The study of longitudinal train dynamics is essential for designing an optimised heavy haul system. It is normal to have several iterations of train configuration, track route, axle load and speeds during the design process. Heavy haul trains continue to explore new limits, with considerations now of 45-tonne axle loads and more than 240 wagons. Recent innovations in automated train control (driverless trains) are expected to provide further precision and efficiencies in the difficult areas where topography results in large mid-train forces or traction pinch points. Electronically controlled braking reduces the need for the adoption of distributed power, as braking performance does not diminish with train length. Despite this, distributed power will often still be needed for lifting the train with limited tensile (draft) forces.

REFERENCES

1. C. Cole, Longitudinal train dynamics. In *Handbook of Railway Vehicle Dynamics*, S. Iwnicki (Ed.), Chapter 9, Taylor & Francis Group, Boca Raton, FL, pp. 239–278, 2006.
2. I.B. Duncan, P.A. Webb, The longitudinal behaviour of heavy haul trains using remote locomotives. In *Proceedings of the 4th International Heavy Haul Conference*, IHHA, Brisbane, Australia, 11–15 September, 1989, pp. 587–590.
3. B.J. Jolly, B.G. Sismey, Doubling the length of coals trains in the Hunter Valley. In *Proceedings of the 4th International Heavy Haul Conference*, IHHA, Brisbane, Australia, 11–15 September, 1989, pp. 579–583.
4. R.D. Van Der Meulen, Development of train handling techniques for 200 car trains on the Ermelo-Richards Bay line. In *Proceedings of the 4th International Heavy Haul Conference*, IHHA, Brisbane, Australia, 11–15 September, 1989, pp. 574–578.
5. M. El-Sibaie, Recent advancements in buff and draft testing techniques. In *Proceedings of the 5th International Heavy Haul Conference*, IHHA, Bejing, China, 6–11 June, 1993, pp. 146–150.
6. M. McClanachan, C. Cole, D. Roach, B. Scown, An investigation of the effect of bogie and wagon pitch associated with longitudinal train dynamics, *Vehicle System Dynamics*, 33(Supp), 1999, 374–385, Swets & Zeitlinger, Lisse, the Netherlands.

7. B. Scown, D. Roach, P. Wilson, Freight train driving strategies developed for undulating track through train dynamics research. In *Proceedings of the Conference on Railway Engineering*, Railway Technical Society of Australasia, Adelaide, Australia, 21–23 May, 2000, pp. 27.1–27.12.
8. S. Simson, C. Cole, P. Wilson, Evaluation and training of train drivers during normal train operations. In *Proceedings of the Conference on Railway Engineering*, Railway Technical Society of Australasia, Wollongong, Australia, 10–13 November, 2002, pp. 329–336.
9. V.K. Garg, R.V. Dukkipati, *Dynamics of Railway Vehicle Systems*, Academic Press, New York, NY, 1984.
10. H.I. Andrews, *Railway Traction: The Principles of Mechanical and Electrical Railway Traction*, Elsevier Science Publishers, New York, 1986.
11. W.W. Hay, *Railroad Engineering* (2nd ed.), John Wiley & Sons, New York, NY, 1982, pp. 69–82.
12. V.A. Profillidis, *Railway Engineering* (2nd ed.), Ashgate Publishing, Aldershot, UK, 2000.
13. C. Cole, Improvements to wagon connection modelling for longitudinal train simulation. In *Proceedings of the Conference on Railway Engineering*, Railway Technical Society of Australasia, Rockhampton, Australia, 7–9 September, 1998, pp. 187–194.
14. L. Muller, D. Hauptmann, T. Witt, TRAIN – A computer model for the simulation of longitudinal dynamics in trains. In *Proceedings of the Conference on Railway Engineering*, Railway Technical Society of Australasia, Rockhampton, Australia, 7–9 September, 1998, pp. 181–186.
15. G.P. Wolf, K.C. Kieres, Innovative engineering concepts for unit train service: The slackless drawbar train and continuous center sill trough train. In *Proceedings of the 4th International Heavy Haul Railway Conference*, IHHA, Brisbane, Australia, 1989, pp. 124–128.
16. G.W. Bartley, S.D. Cavanaugh, The second generation unit train. In *Proceedings of the 4th International Heavy Haul Railway Conference*, IHHA, Brisbane, Australia, 11–15 September, 1989, pp. 129–133.
17. C. Cole, M. McClanachan, M. Spiryagin, Y.Q. Sun, Wagon instability in long trains, *Vehicle System Dynamics*, 50(Supp1), 2012, 303–317.
18. Association of American Railroads, *AAR Manual of Standards and Recommended Practices, Section C – Part II, Design, Fabrication, and Construction of Freight Cars, Section 2.1 Design Data*, pp. C-II-9 – C-II-34, AAR, Washington, DC, 2011.
19. S. Simson, Three axle locomotive bogie steering, simulation of powered curving performance: Passive and active steering bogies, PhD Thesis, Central Queensland University, Rockhampton, Queensland, Australia, 2009. See: http://hdl.cqu.edu.au/10018 / 58747.
20. S. Simson, C. Cole, Idealised steering for hauling locomotives, *Rail and Rapid Transit*, 221(2), 2007, 227–236.
21. S. Simson, C. Cole, Simulation of traction and curving for passive steering hauling locomotive, *Rail and Rapid Transit*, 222(2), 2008, 117–127.
22. Association of American Railroads, *AAR Manual of Standards and Recommended Practices, Section S – Casting Details: Specification M-211 – Foundry and Product Approval Requirements for the Manufacture of Couplers, Coupler Yokes, Knuckles, Follower Blocks and Coupler Parts*, AAR, Washington, DC, 2013.

6 Traction/Adhesion Control Systems and Their Modelling

Nowadays, it is impossible to imagine modern motive power rolling stock without complex microprocessor control and management systems. There are many and varied tasks for such systems. All microprocessor-based systems are very similar in structure. The first level includes the system that is based on a central host computer connected to one or more auxiliary computers, depending on the number of tasks assigned to the system. Programs and data are stored in the memory modules. All these programs are executed in a predetermined sequence. At the second level, there are commonly analogue and digital interfaces which provide connection to analogue and digital peripherals, and modulator subsystems which control the power semiconductor converters. The third level includes low-level signals that are needed to connect the system with the higher layers, that is, external monitoring and diagnostic systems that are outside of the locomotive.

An example of a fully computerised system of a heavy haul diesel-electric locomotive is shown in Figure 6.1. The central computer is responsible for controlling traction power, limiting excitation levels and monitoring feedback of the main generator. The central computer is also responsible for the control and monitoring of diesel engine subsystems, as described in Chapter 2. Furthermore, this computer controls the dynamic braking system and is also responsible for all communication interactions between other computerised systems. The air brake computerised system is responsible for the control of the electric brake valve equipment and monitoring of air brake system parameters gathered from sensors and other active brake components. The traction control system is responsible for the control of power traction equipment such as inverters and converters.

In the case of traction control for heavy haul locomotives, the most important function is to control the traction drive. However, it is worth noting that the mechanical brake control system and auxiliary equipment should also be monitored in detail in order to provide satisfactory operational outcomes. Only a programmable microprocessor traction control system can achieve an economically viable and reliable level of control over a wide range of operational scenarios. However, during simulation and numerical studies of locomotive traction behaviour, such architecture is simplified, as shown in Figure 6.2, and only major input and output signals are used. This approach is commonly used for the investigation of traction/adhesion control strategies and algorithms that generally require the knowledge of the ground speed of a locomotive. This is the reason why a great number of heavy haul locomotive are equipped with radar (also called a radar gun) for the direct measurement of the ground speed.

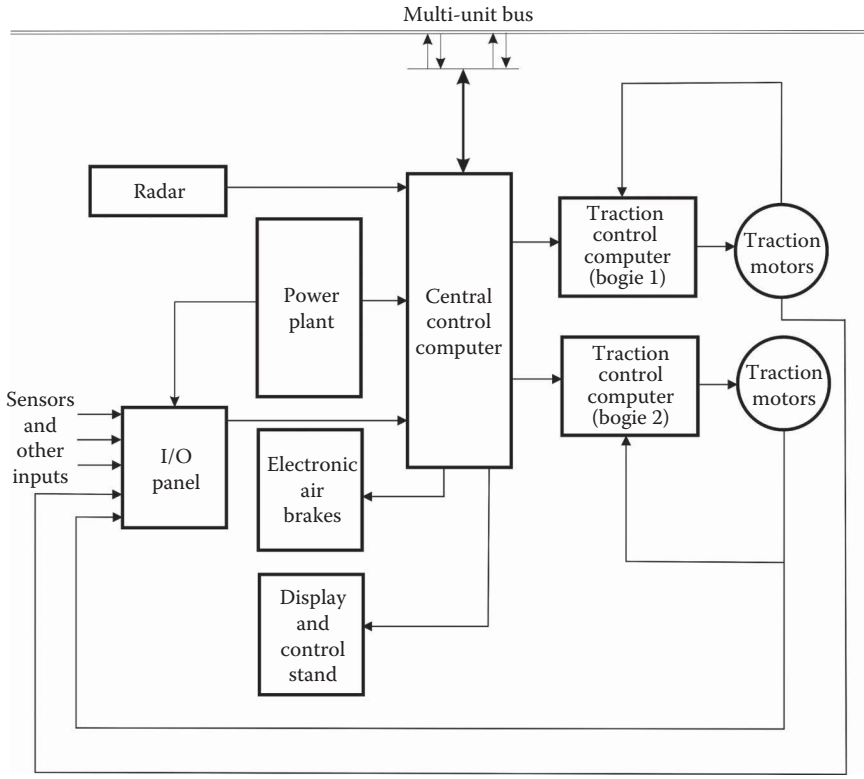

FIGURE 6.1 Example of a computerised system of a heavy haul locomotive.

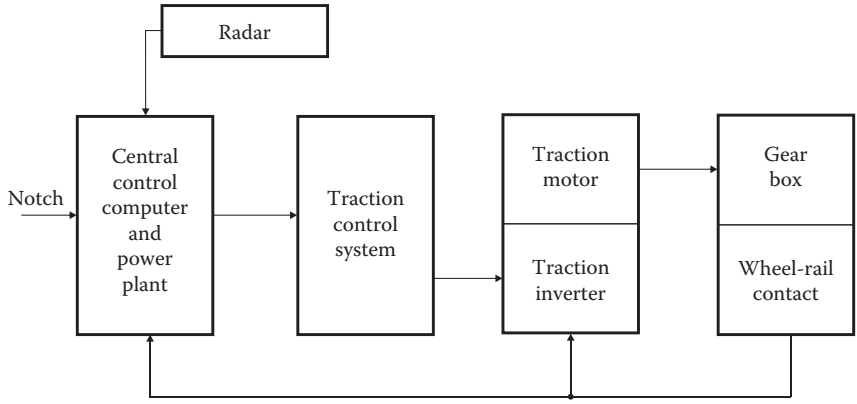

FIGURE 6.2 Example of a simplified locomotive adhesion control system used for simulation studies.

This chapter starts with basic aspects such as classification and design of traction control systems and then describes how to model a simplified adhesion control system for a single wheelset under traction.

6.1 CLASSIFICATION OF TRACTION/ADHESION CONTROL SYSTEMS

The traction/adhesion control systems used on heavy haul locomotives should achieve an optimal adhesion between wheels and rails and avoid any potential damage caused by exceeding the maximum allowable traction torque applied to the wheelset. These systems can be classified according to the method used to achieve this objective:

- Adhesion control strategies;
- Adhesion/creep control algorithms; and
- Design configurations.

6.1.1 Adhesion Control Strategies

A typical heavy haul locomotive is equipped with three types of adhesion control strategies [1]:

- Starting strategy, when the locomotive commences movement;
- Adhesion/creep strategy, when the locomotive operates at a speed higher than 5 km/h;
- Safety mode strategy, used when other strategies have failed.

The starting strategy is designed for starting a hauling movement of the train. It usually does not require the detection of the ground speed because the accuracy of the data obtained from radar at slow speeds is very low. The algorithm for this strategy usually relies on the traction motor speeds and their computed accelerations. This strategy applies for a low speed range only, that is, when the speed is less than 5 km/h.

The adhesion/creep strategies used in heavy haul locomotives act at a speed higher than 5 km/h, and most of them require information about the locomotive ground speed and the traction motor/wheelset rotational speeds. The determination of ground speed requires use of radar operating on the Doppler effect to measure the change in the frequency of a wave sent from an antenna and then detected once reflected back from the ground. The Doppler frequency shift can be defined as

$$f_d = \frac{2V \cdot \cos\alpha}{\lambda} \tag{6.1}$$

Rearranging this equation, the ground (linear) speed of a locomotive is defined as

$$V = \frac{f_d \cdot \lambda}{2\cos\alpha} \tag{6.2}$$

where:

λ is the length of the wave sent from an antenna

α is the angle between the speed vector and the signal vector formed by the antenna orientation

In reality, more than one measurement of the Doppler frequency is involved in this process. This means that a relatively wide range of frequencies, obeying the Gaussian distribution, is in use. This device can also be designed for the calculation of trip distance. Radar systems are very complicated devices, and the error for a signal generated during a speed detection process in practice might be significant. For example, it might achieve an accuracy of 0.5–0.7 km/h for locomotive applications with an acceleration of 1 m/s^2 due to the delay in signal processing.

When an adhesion/creep strategy does not work properly or has failed, then a similar approach to a starting strategy is used that estimates wheel slip within inverter controllers; other alternative approaches to control wheel slip can also be used (subject to the locomotive design).

6.1.2 Adhesion/Creep Control Algorithms

The traction control strategies currently considered for application on heavy haul locomotives can be classified into three groups as follows [2,3]:

- *Monitoring of traction drive behaviour*: Such methods are based on identifying the characteristics of dynamic processes for traction drives. When the adhesion limit is reached at the wheel-rail interface, the system experiences angular fluctuations that can cause severe vibrations with relatively high frequencies (45–65 Hz), particularly if only one wheel loses contact with the rail [4,5].

  For example, in order to monitor adhesion conditions, acceleration and displacement sensors, as well as the values of traction motor currents, can be used. Depending on the design of the traction drives, 2–4 band pass filters are used. These filters are tuned to determine the frequency of angular oscillations of a drive system [4]. In addition, dynamic analysis of the drive gear behaviour based on the vibration of traction motors can be used to detect a situation where the friction condition is low, but it cannot be used for true wheel slip detection algorithms [6].

  However, these approaches are highly dependent on the physical characteristics of suspension elements (e.g., rubber), which can change their characteristics over a short period of time. Therefore, sensors might provide false information to the system, and thus the effectiveness of the control strategy algorithm might decrease.
- *Comparison of traction motor currents*: This method is based on the measurement of traction motor currents and their comparison [7]. This is possible when the angular speeds of the rotors are different, because in this case the currents also deviate from the normal value. However, in real practice, differences in wheel diameters may occur, causing

unbalance in the system, but some advanced algorithms might be able to compensate for this.

- *Slip-based approaches*: In order to estimate wheel slip (creep), the data obtained from angular velocity sensors are processed in order to find a minimal angular velocity for each bogie or for the whole locomotive, and then to compare this velocity with the locomotive ground speed. A value of the longitudinal slip (creep) is estimated based on the following relation:

$$s_{\text{est}} = \frac{w \cdot r - V}{V} \tag{6.3}$$

where:
w is the real angular velocity of a wheelset
V is the locomotive speed
r is the rolling radius of the wheelset

The values of rolling radii for all wheelsets are updated on the locomotive traction control system at each service interval, and rotational speeds of traction motors on some locomotives are recalibrated daily under non-slip conditions to ensure avoiding accumulative errors during locomotive operations. Although the terms 'slip' and 'creep' are often used interchangeably, slip is the additional speed that a wheel might have because of its relative motion at its contact point with the rail, whereas creep is characterised as the slip speed divided by the locomotive speed.

Figure 6.3 shows that the adhesion coefficient depends on the slip in the longitudinal direction. In practice, the slip value should be situated in the practical optimal wheel slip zone for heavy haul locomotives. The need to compromise and reduce the target of control to the level of practical optimal wheel slip (creep) is connected with

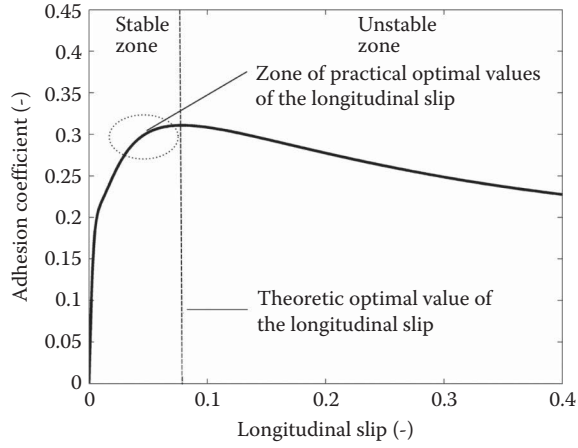

FIGURE 6.3 Example of difference between theoretical and practical optimal slips in the longitudinal direction for a dry friction condition.

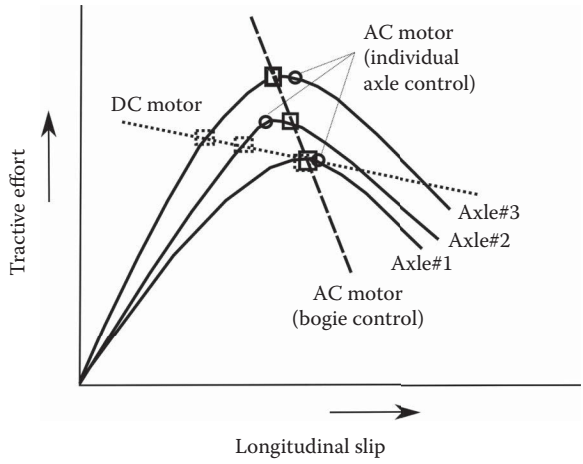

FIGURE 6.4 Axle tractive effort versus wheel creep.

two problems concerning: (a) how to estimate adhesion accurately and (b) how to achieve the needed traction control strategy.

However, in real practice, the situation is more complicated [8], for example, as shown in Figure 6.4 for one three-axle bogie of a heavy haul locomotive. Achievable tractive effort is strongly dependant on the power system design and control algorithms. Furthermore, such algorithms unavoidably work with some uncertainties between the input and output data, which present difficulties when trying to obtain precise results. One such uncertainty is to understand the difference between friction coefficient and adhesion coefficient [9–11]. For the rolling traction/braking mode without slip, the maximum value of the slip-friction coefficient must be higher than the adhesion coefficient for the same contact conditions. In theory, the adhesion coefficient can be defined as the traction force divided by wheel load. Therefore, both of these coefficients describe almost the same physical behaviour, which determines the ratio of the tangential forces to the normal forces. However, the slip-friction coefficient depends only on the physical state of the contacting surfaces, whereas the adhesion coefficient depends on the construction characteristics of rail tracks and the dynamic characteristics of railway vehicles. These characteristics can be modified by the 'unaccounted for' slipping motions, the difference between wheel diameters of wheel pairs, conicity and eccentricity of wheels, track curvature, reallocation of loads between wheels, irregular loads of wheels for the wheel pair, the constraints imposed by the bogie setup, the type of rolling stock, the train configuration, vibrations, and so on. The correct definition of the adhesion condition is also very important for the simulation approaches used to estimate behaviours of rail vehicles.

Different methods for the implementation of traction control systems have been presented in patents and publications [2,3,12–18]. However, the situation of slip detection with a locomotive is not completely solved and still continues to be more complicated for powered railway vehicles because of the differing friction conditions under each of the driven wheelsets. This is also connected with the presence

of a clearing factor when the first running wheelset cleans the rail surface for the following wheelsets. This is an important topic for further more detailed theoretical and experimental studies. In addition, the load distribution between conventional wheelsets (due to vehicle dynamics) leads to different maximum adhesion forces on the wheelsets. However, a slip-based approach is the most commonly used one for modern heavy haul locomotives.

6.1.3 Design Configurations

The traction control systems are commonly divided into three types based on the locomotive power system design:

- Locomotive traction control;
- Bogie traction control; and
- Individual wheelset traction control.

The locomotive traction control system, shown in Figure 6.5a, is where the same torque value is given to all traction motors of a locomotive. This type of traction control system is currently in use in old heavy haul locomotives equipped with a DC traction system.

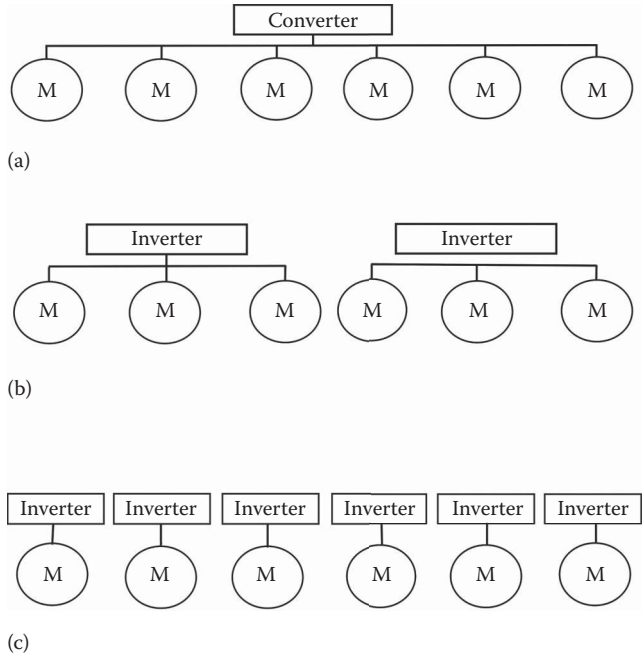

FIGURE 6.5 Examples of traction system designs for a heavy haul locomotive equipped with two three-axle bogies: (a) locomotive traction control, (b) bogie traction control, and (c) individual traction control.

The bogie traction control system, shown in Figure 6.5b and also referred to as group control, is a system in which all wheelsets of the bogie are controlled by one inverter. This system is commonly used on heavy haul locomotives with an AC traction system.

The individual wheelset traction control system, shown in Figure 6.5c and also referred to as axle control, is a system in which each wheelset is controlled by its own traction inverter. This type of traction control system is currently in use in heavy haul locomotives with an AC traction system. Recently, it has also started to be used in some modern heavy haul locomotives equipped with a DC traction system.

Figures 6.6 through 6.8 show modelling principles for all three types of traction control systems based on a slip-based control strategy. Figure 6.6 presents the

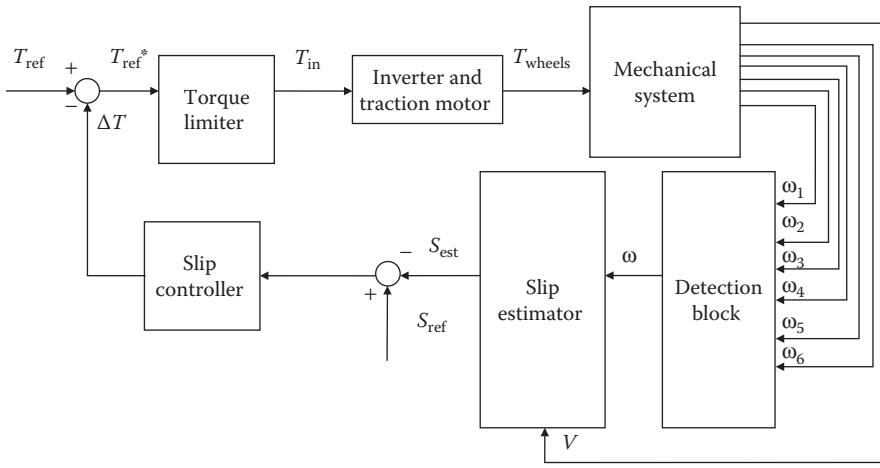

FIGURE 6.6 Locomotive traction control.

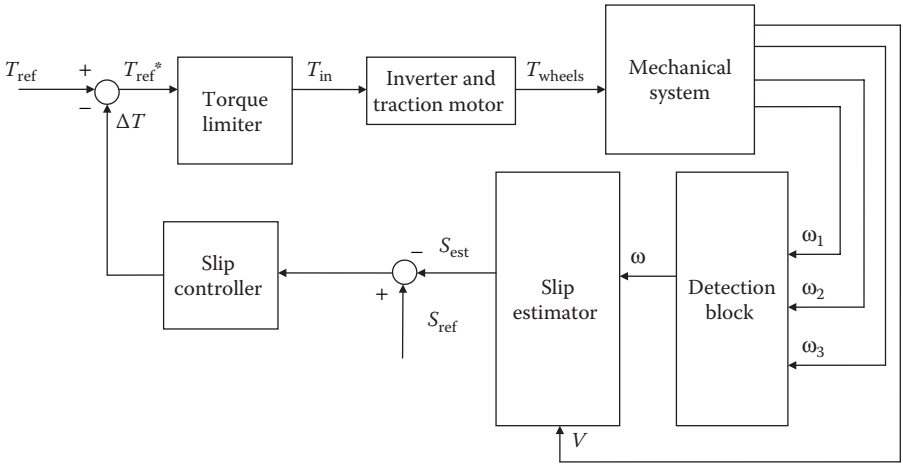

FIGURE 6.7 Bogie traction control (for a single bogie).

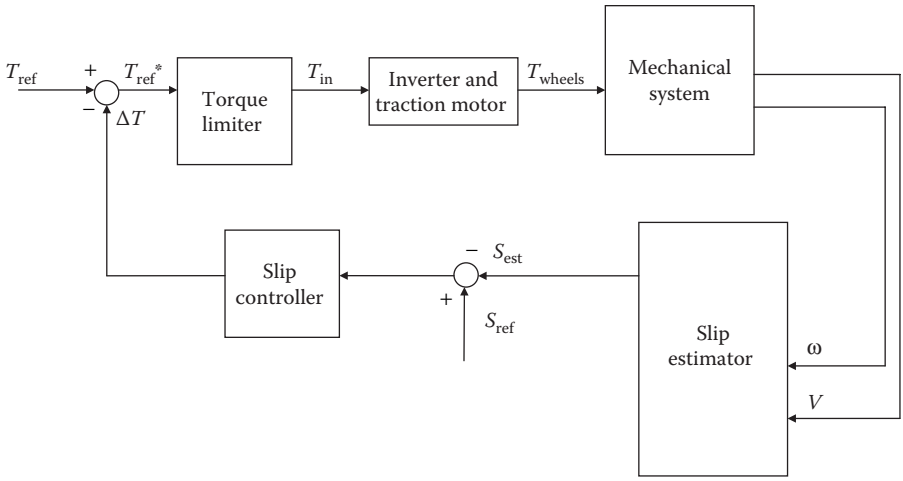

FIGURE 6.8 Individual wheelset traction control (for a single wheelset).

locomotive traction control for a six-axle locomotive. Figure 6.7 presents the bogie traction control for a three-axle bogie. Figure 6.8 presents the individual wheelset traction control, that is, for one motorised wheelset. The difference between the algorithms is the presence of the detection block for a reference axle in the case of the locomotive and bogie traction control systems. The variables shown in these figures are T_{ref} = reference torque (based on the notch position); T_{ref}* = reference torque generated by the control system; T_{in} = input motor torque; T_{wheels} = traction torque applied to the axles; ΔT = torque reduction; ω = angular velocity of a reference axle; $\omega_{1\text{ to }6}$ = angular velocities of individual; s_{est} = estimated longitudinal slip, s_{opt} = optimal longitudinal slip and V = locomotive velocity.

6.2 SIMPLIFIED MODELLING APPROACH

In order to perform modelling, it is necessary to divide the system shown in Figure 6.2 into four subsystems, as shown in Figure 6.9. All four subsystems in a general sense represent a combination of mechanical, electric and control engineering design aspects of a locomotive. In the case of the feedback sensors, these devices are commonly modelled as ideal sensors for the simplified approach. As a result, only three subsystems need to be modelled for traction control studies with such an approach.

6.2.1 Power Plant

For the development of the power plant system, the following approach, as shown schematically in Figure 6.10, has been applied. In this chapter, the diesel-electric locomotive traction system is taken as an example for a simplified modelling

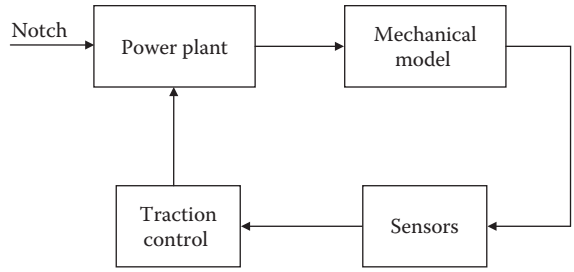

FIGURE 6.9 General modelling approach for locomotive adhesion studies.

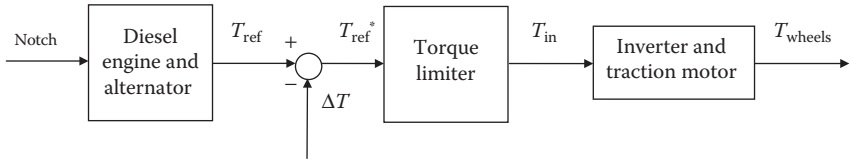

FIGURE 6.10 Modelling approach for a power plant subsystem.

approach based on the oversimplified approach provided in Chapter 5. In this case, the required model for the power plant, assuming that notch level is linearly proportional to motor current, can be derived from the following:

$$\text{for} \quad F_t * v < (N^2/64) * P_{\max}, \qquad F_t = (N/8) * Te_{\max} - k_f * v \tag{6.4}$$

$$\text{else} \quad F_t = (N^2/64) * P_{\max}/v \tag{6.5}$$

where:

F_t is the tractive effort realised by a locomotive, N
v is the locomotive speed, m/s
N is the throttle setting in notches, 0–8
$P_{\max}$ is the maximum locomotive traction horsepower, W
$Te_{\max}$ is the maximum locomotive traction force, N
k_f is the torque reduction, N/(m/s)

In this case, the dynamics of the diesel-alternator system can be described by means of a low-pass filter and use of a Laplace transformation, and can be written for a single wheelset as

$$T_{\text{ref}} = \frac{1}{\tau_1 s + 1} \cdot \frac{F_t r}{n_m} \tag{6.6}$$

where:

τ_1 is a time constant
s is the Laplace variable

r is wheel rolling radius, m
n_m is the number of motorised axles within the locomotive

If the value of the reference torque generated by the control system, T_{ref}^{*}, is higher than the value of the maximum possible torque of the traction motor, it is necessary to use the torque limiter to constrain the driving torque to the motor characteristics.

The inverter and traction motor dynamics can be also presented by means of a low-pass filter and use of a Laplace transformation as

$$T_{\text{wheels}} = \frac{1}{\tau_2 s + 1} T_{in} \tag{6.7}$$

where τ_2 is a time constant. The value of this time constant can be chosen based on the analysis of locomotive log files or can be assumed from results of advanced modelling.

6.2.2 Mechanical Subsystem

For the development of the mechanical system, the approach shown schematically in Figure 6.11 has been applied. All components involved in this modelling approach are described in the following sections.

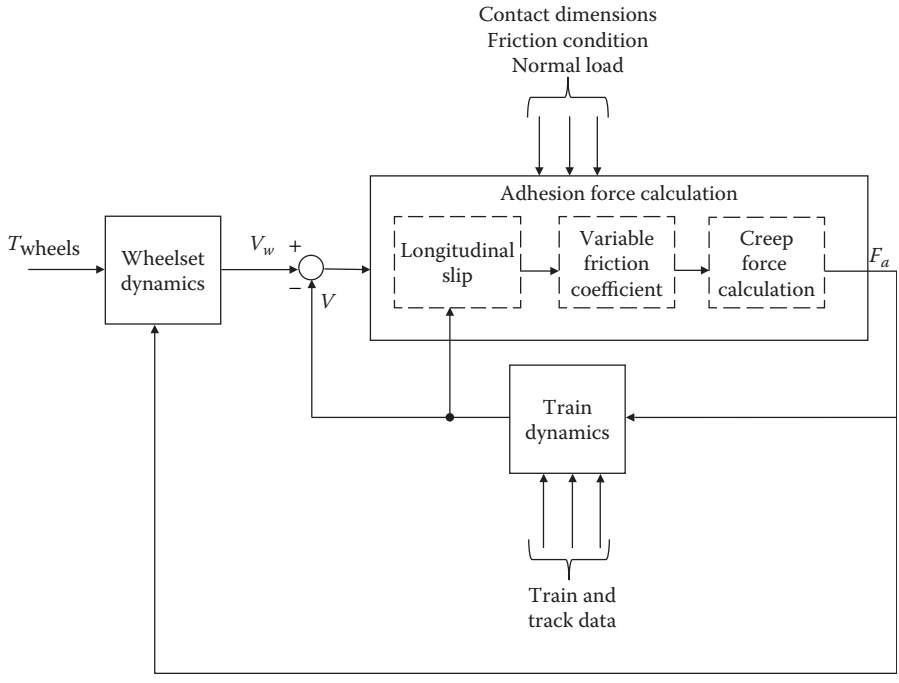

FIGURE 6.11 Modelling approach for a mechanical subsystem.

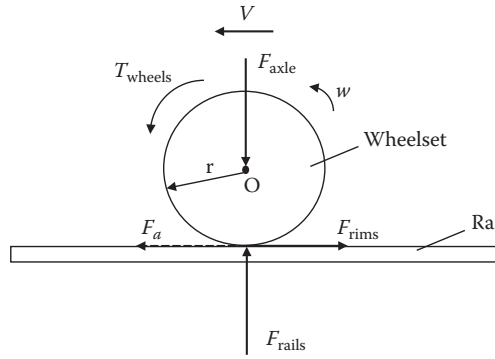

FIGURE 6.12 Forces and torques acting on the wheelset and rails.

6.2.2.1 Wheelset Dynamics

Modelling of the wheelset dynamics requires considering a system separately from train dynamics. In this case, taking into account all forces and torques acting on such a simplified system, the system can be represented as a mass rotating around its centre O, as shown in Figure 6.12.

Traction torque applied to the axles, T_{wheels}, can also be represented by the force acting on the rims of the wheelset:

$$F_{rims} = \frac{T_{wheels}}{r} \tag{6.8}$$

This force is opposed by the wheelset's adhesion force, F_a, which also acts along the track and is discussed in more detail in Section 6.2.2.2. In the static condition (Newton's third law of motion), the rail reaction force, F_{rails}, should be equal to the axle load, F_{axle}. (see how to calculate this force for a locomotive in Section 2.4.1).

The wheel velocity, V_w, can be calculated as

$$V_w = w \cdot r \tag{6.9}$$

In order to model wheelset dynamics, and taking into account Newton's second law of motion, the following equation can be written for the system shown in Figure 6.12:

$$\sum T = J \cdot \dot{w} \tag{6.10}$$

where:

$\sum T$ is the sum of the acting torques

J is the equivalent inertia of the wheelset, which the model should also depict given that the traction motor mass is shared between bogie and axles

$\dot{w}$ is the angular acceleration of the wheelset

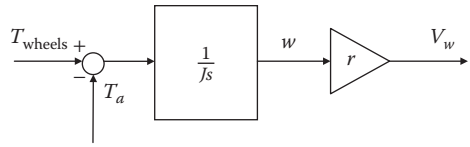

FIGURE 6.13 Modelling approach for wheelset dynamics.

The sum of the acting torques, $\sum T$, can also be defined as

$$\sum T = T_{\text{wheels}} - T_a \tag{6.11}$$

where, T_a is the adhesion torque, also called the load torque, which can be calculated as

$$T_a = F_a \cdot r \tag{6.12}$$

The contributors to resistance to the motion of the wheelset such as bearing friction, torsion stiffness and so on have been neglected in this study because of the simplicity of the modelling approach.

Finally, the modelling approach for wheelset dynamics, based on Equations 6.8–6.12, is shown schematically in Figure 6.13.

6.2.2.2 Adhesion Force Modelling

Further to Equation 6.3, longitudinal slip (creep) can also be defined as

$$s_{\text{est}} = \frac{V_w - V}{V} \tag{6.13}$$

The modelling of a variable friction coefficient is taken from Polach [10], as it has been shown to be reasonable for application in the field of locomotive traction analysis. The variable friction coefficient is defined as

$$\mu = \mu_s((1-A)e^{-B.V_s} + A) \tag{6.14}$$

where:

μ_s is the maximum coefficient of friction
A is the ratio of the limit friction coefficient at infinity slip velocity to the maximum friction coefficient μ_s
V_s is the magnitude of the slip (creep) velocity vector
B is the coefficient of exponential friction decrease, s/m

The slip velocity used for the calculation of the slip-velocity-dependent friction coefficient can be expressed as

$$V_s = V - V_w \tag{6.15}$$

The Polach creep force model [10] is also needed to find the adhesion force between a wheel and the rail. This model has low computational needs and is perfectly suited for a simplified approach. For longitudinal adhesion forces on right and left wheels, we have:

$$F_{r,l} = \frac{2Q\mu}{\pi}\left(\frac{k_A e}{1+(k_A e)^2} + \arctan(k_S e)\right) \quad k_S \le k_A \le 1 \tag{6.16}$$

$$e = \frac{G\pi abC_1}{4Q\mu} s_{\text{est}} \tag{6.17}$$

where:

a and b are the lengths of the semi-axes of the elliptic contact patch
r and l are the indexes for right and left wheels of the wheelset
Q is the wheel load
C_1 is the Kalker's linear theory coefficient
k_A and k_S are reduction factors in the area of adhesion and the area of slip
G is the shear module

Then, the wheel load for each wheel of the wheelset can be calculated as

$$Q = \frac{F_{\text{axle}}}{2} \tag{6.18}$$

Therefore, the adhesion force for a wheelset can be calculated as

$$F_a = F_r + F_l \tag{6.19}$$

6.2.2.3 Train Dynamics

The train dynamics for this single wheelset study is based on the application of Newton's second law, as shown in Figure 6.14. In this case, the following equation can then be written for a single wheelset of a locomotive:

$$\frac{M}{n_m} \cdot \dot{V} = F_a - F_{\text{res}} \tag{6.20}$$

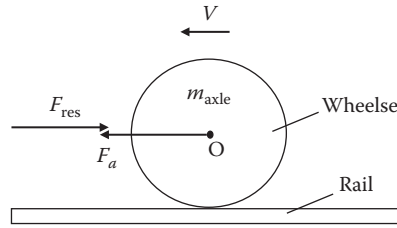

FIGURE 6.14 Train dynamics forces acting on the wheelset.

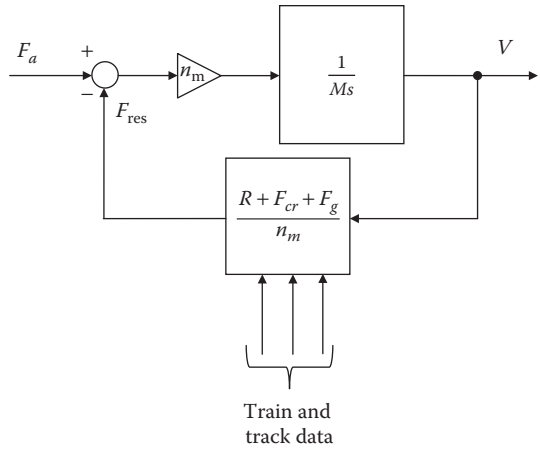

FIGURE 6.15 Modelling approach for train dynamics.

where M is the train mass and F_{res} is the sum of the resistance forces acting on one wheelset of a locomotive, which can be calculated as

$$F_{res} = \frac{R + F_{cr} + F_g}{n_m} \tag{6.21}$$

where:

R is the propulsion resistance
F_{cr} is the curving resistance
F_g is the gravitational component

More detailed information about how to calculate these forces can be found in Chapter 5.

Finally, the modelling approach for train dynamics applicable to a single wheelset, based on Equations 6.20 and 6.21, is shown schematically in Figure 6.15.

6.2.2.4 Modelling of Traction Control Subsystem

Taking into account that only a single wheelset is modelled in this example, it is reasonable for this study to use a simplified individual wheelset traction control, as shown in Figure 6.8. The modelling approach for a traction control subsystem is shown in Figure 6.16. The slip estimator works based on Equation 6.3. A slip error can be defined as

$$e = s_{opt} - s_{est} \tag{6.22}$$

As one can see, the slip control is active when the estimated slip value, s_{est}, is higher than the optimal slip, s_{opt}. In this case, the slip error correction, e_c, can be found as

$$\text{for} \quad e > 0, e_c = 0 \tag{6.23}$$

$$\text{else} \quad e_c = e \tag{6.24}$$

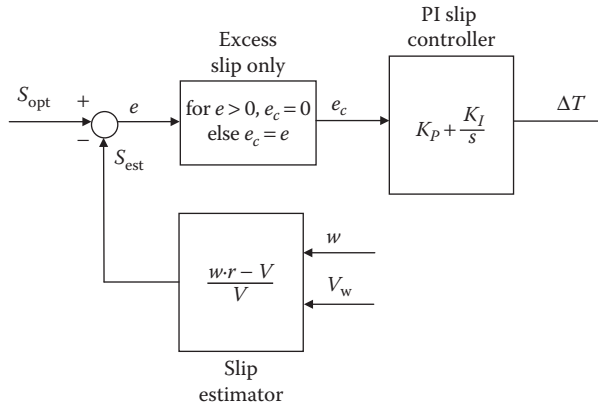

FIGURE 6.16 Modelling approach for traction control subsystem.

The slip controller is a simple controller with proportional and integral action (PI controller), which uses the slip error correction, e_c, as the input to the controller. The control law can be represented by the following equation:

$$\Delta T = K_P \cdot e_c + K_I \cdot \int_{t_1}^{t_2} e_c \, \mathrm{dt} \tag{6.25}$$

where:

K_P and K_I are the proportional and integral gains, respectively, which should be tuned to the applied load

t_1 and t_2 are the previous and current time steps required for the integration process

6.3 SIMPLIFIED TRACTION CONTROL STUDY

This section shows how a traction control study can be performed, taking into account initial train, locomotive, wagon and track parameters, and how a model can be created and implemented in Simulink® to obtain results.

6.3.1 Train, Locomotive and Wagon Parameters

For this simulation process, assume that the train consists of 30 coal wagons hauled by one diesel-electric locomotive. This locomotive has characteristics similar to the locomotive described in the article published by Ramsey et al. [19], and its main design characteristics and parameters required for this simulation study are shown in Table 6.1. The coal wagons are four-axle wagons, and they have a nominal gross mass of 120 tonnes.

TABLE 6.1
Technical Specifications for a Heavy Haul Locomotive

Type	AC Traction Diesel-Electric Locomotive
UIC classification	Co-Co
Tractive effort – starting	600 kN
Tractive effort – continuous at 20 km/h	520 kN
Maximum traction power	2900 kW
Wheel diameter	1067 m
Wheelset mass-inertia (pitch)	1351 kgm^2
Axle load	219.09 kN
Weight	134 tonnes

TABLE 6.2
Polach Contact Model Parameters for AC- and DC-Drive Locomotive Models

Friction Condition	μ_S	A	B	k_A	k_S
Dry	0.47	0.44	0.70	0.60	0.15
Wet	0.30	0.38	0.10	0.29	0.09

6.3.2 Simulation Scenarios

In order to understand the influence of traction control on the dynamic processes, the wheel-rail contact patch friction conditions are switched during the simulation process when the locomotive is running on tangent track. Table 6.2 shows the Polach contact model parameters used in this study for both dry and wet tracks. The behaviours of the adhesion curves using these parameters are very similar to the data published in Ref. [20].

The following scenarios have been applied for this study:

- *Constant speed mode*: The locomotive runs with a constant linear speed of 20 km/h. The notch position is switched from 'idle' to position 8 during the first 20 s and then stays in position 8 until the end of the simulation. This value corresponds to the locomotive speed during continuous tractive effort mode. In order to implement this scenario, the train speed should be equal to 20 km/h. This mode allows checking the response of the traction controller to sudden changes in friction condition.
- *Acceleration mode*: The notch position is switched from 'idle' to position 8 during the first 20 s and then stays in position 8 until the end of the simulation. The locomotive should be accelerated until a speed of 70 km/h is attained. The maximum speed of such locomotives in real-world train operations with fully loaded wagons (120 tonnes gross) is limited to 70 km/h.

In order to make judgements about the performance of traction control and its responses to the input parameters during the simulation process, the following outputs are commonly observed:

- The variation of slip under different friction conditions in the time domain, which is required in order to show that the proposed algorithm is robust in the way it handles such changes; and
- The estimated value of traction coefficient in the time domain, which can be defined as

$$\mu_{\text{est}} = \frac{F_a}{F_{\text{axle}}} \tag{6.26}$$

- Estimated traction coefficient versus estimated slip relationship, which is needed in order to determine the operational range of a traction controller;
- Comparison of reference and adhesion torques, which allows the analysis of how input torques are limited by a traction controller; and
- Locomotive and wheelset speed, in order to ensure that the locomotive runs with the required speed and the wheel slip is present.

6.3.3 Case 1: Constant Speed Mode

The simulation strategy used in this case study example is intended to simulate dry and wet friction conditions. The total simulation time for this case is 100 s. The switch between the adhesion conditions has been done for the constant speed test in the following order: dry-wet-dry. The wet conditions are implemented from 60 to 80 s for this simulation case. The slip threshold, s_{opt}, was limited to 0.07 for the dry friction condition and 0.15 for the wet friction condition.

6.3.3.1 Implementation of the Model in Simulink

The integration approach is based on the aggregation of all relevant existing subsystems, which have been described in the previous sections. The full model in Simulink used for this study is shown in Figure 6.17. In order to simplify the model structure, three additional blocks from the Simulink library have been used for the traction controller (see the PI controller block in Figure 6.17 and its mask parameters in Figure 6.18), notch versus tractive effort in the power plant (see the TE loco block in Figure 6.17 and its mask parameters in Figure 6.19) and adhesion force modelling (see Polach's creep force model block in Figure 6.17 and its mask parameters in Figure 6.20). These modules are based on a set of equations. This is the reason why two Interpreted MATLAB® Functions have been used in the model. The S_{opt}, Notch and Mu_max blocks shown in Figure 6.17 are repeating table blocks used to input time-dependant parameters required for this study in accordance with the constant speed mode scenario described in Section 6.3.2.

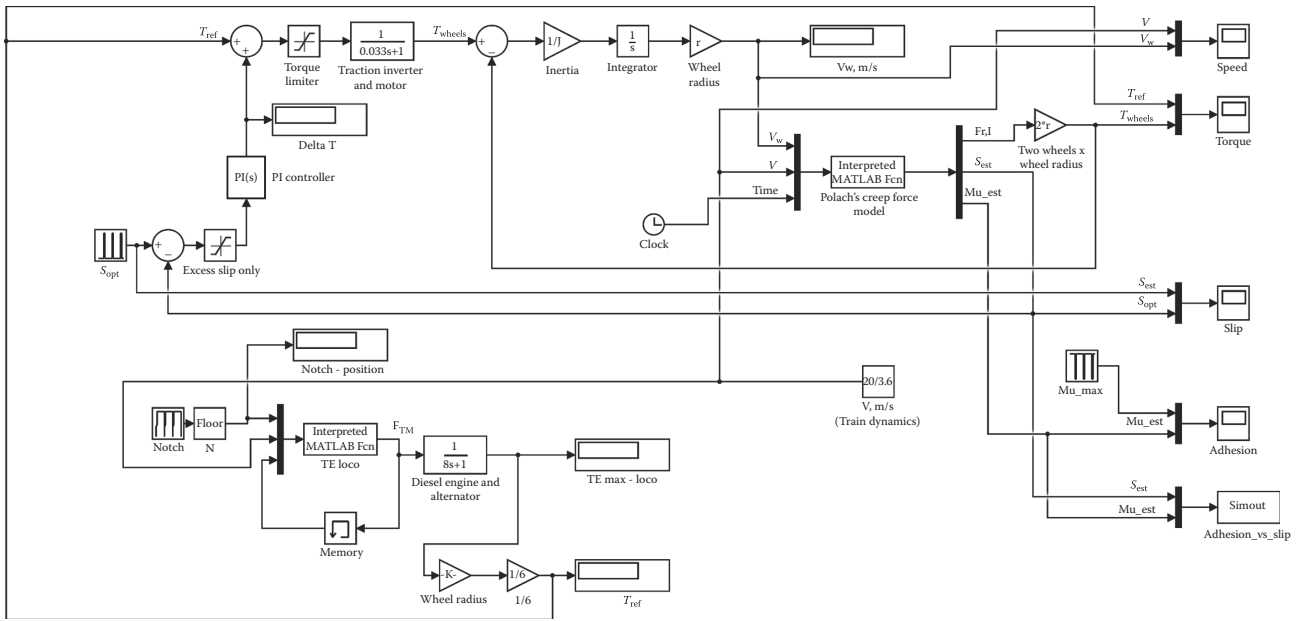

FIGURE 6.17 Full model in Simulink for single wheelset traction control studies with a constant locomotive speed.

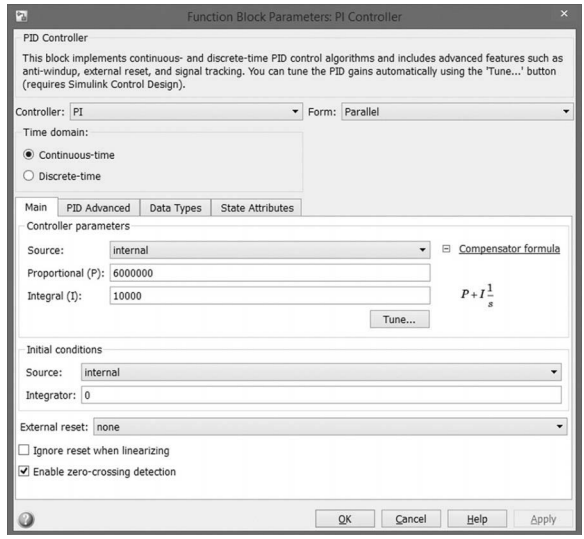

FIGURE 6.18 Parameters of PI controller block for Case 1.

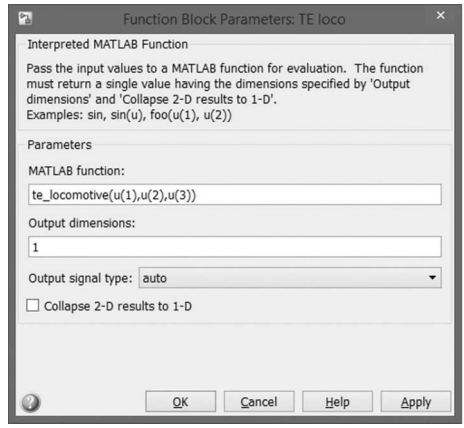

FIGURE 6.19 Parameters of TE loco block for Case 1.

The code for the first Interpreted MATLAB Function, that is, for the TE loco block shown in Figure 6.19, is provided below:

File name: te_locomotive.m

```
function fout = te_locomotive(N,V,Ft)

% N = the throttle setting in notches, 0 to 8
% V = locomotive speed, m/s
% Ft = the tractive effort realised by a locomotive (previous
time step)
```

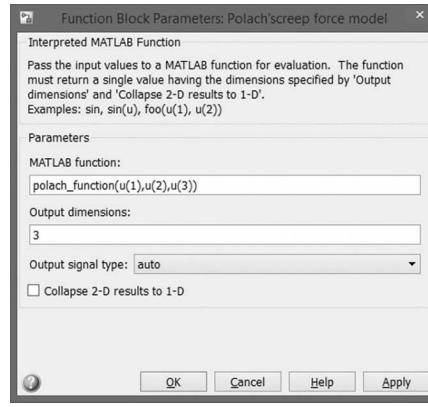

FIGURE 6.20 Parameters of Polach's creep force model block for Case 1.

```
TEmax=600000;
Pmax=2900000;
if ((Ft*V)<((N*N/64)*Pmax))
    Fte=N/8*TEmax-1000*V;
else
     Fte= (N*N/64)*(Pmax/V);
end
fout =[Fte];
```

The code for the second Interpreted MATLAB Function, that is, for Polach's creep force model block shown in Figure 6.20, is provided below:

File name: polach_function.m

```
function fout = polach_function(Vw,V,time)

% Vw = Wheelset linear speed
% V = Locomotive speed
% time = simulation time required for switching between dry
and wet friction
% conditions
% Q = Wheel load
% a = longitudinal half-axis of the contact patch
% b = lateral half axis of the contact patch
% mu_p = friction coefficient
% A = the ratio of the limit friction coefficient at infinity
slip velocity
% to the maximum friction coefficient μs
% B = the coefficient of exponential friction decrease, s/m
% C1 = coefficient of the Kalker's linear theory
% G = the shear module
% F = adhesion force (one wheel)
% s_est = the estimated slip
% mu_est = the estimated traction (adhesion) coefficient
```

```
Q=109545;
a=0.0052;
b=0.0164;

if time<=60
mu_p=0.47;
A=0.44;
B=0.7;
ka=0.6;
ks=0.15;
end

if time>60
mu_p=0.30;
A=0.38;
B=0.10;
ka=0.29;
ks=0.09;
end

if time>80
mu_p=0.47;
A=0.44;
B=0.7;
ka=0.6;
ks=0.15;
end


G=8.4*10^10;
C1=4.100;


wx=Vw-V;

SX=(Vw-V)/V;

muf=mu_p*((1-A)*exp(-B*wx)+A);

FX=0;
EX=G*pi*a*b*C1*SX/(4*Q*muf);
F=2*Q*muf/pi*(ka*EX/(1+ka*ka*EX*EX)+atan(ks*EX));

mu_est=F/Q;
s_est=SX;

fout =[F,s_est,mu_est];
```

In this code, we assume that contact patch dimensions and vertical load are constant during the simulation process.

The model developed was tested using the 'ode2' numerical solver based on Heun's method, with a fixed-time computational time step of 1 ms, which is recommended for such mechatronical systems [21,22].

6.3.3.2 Simulation Results

Figures 6.21 and 6.22 show the calculated values of longitudinal slips (creepages) and traction coefficients for a single wheelset in the time domain. Figure 6.23 presents information regarding the estimated traction coefficient versus estimated slip curve. The comparison of reference and adhesion torques in the time domain is shown in Figure 6.24. In addition, Figure 6.25 presents information on locomotive and wheelset speeds during the constant speed test.

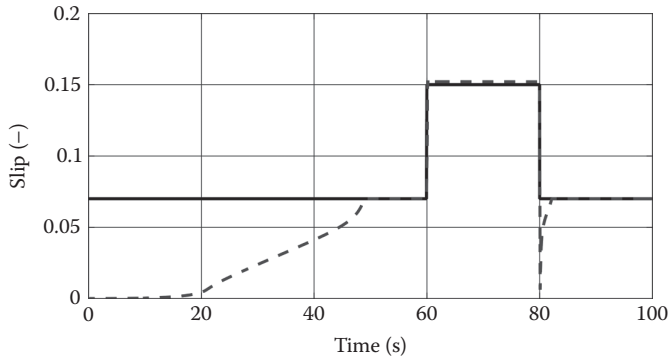

FIGURE 6.21 Comparison of longitudinal slip values in the time domain (solid line – optimal slip, dashed line – estimated slip) for Case 1.

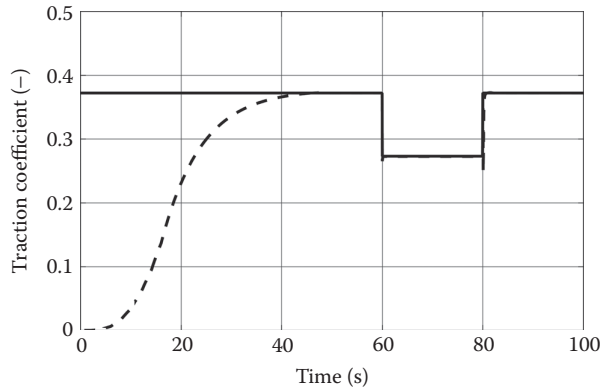

FIGURE 6.22 Comparison of traction coefficient values in the time domain (solid line – maximum possible traction coefficient, dashed line – estimated traction coefficient) for Case 1.

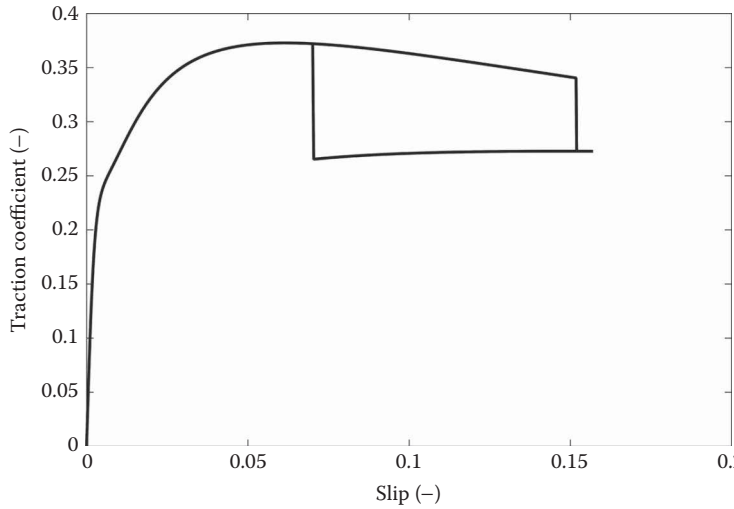

FIGURE 6.23 Slip curve when under traction control for Case 1.

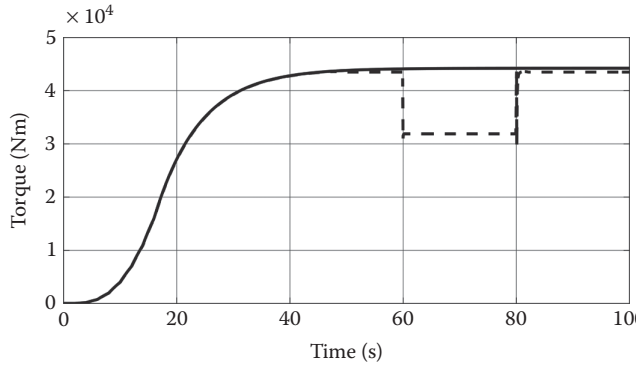

FIGURE 6.24 Comparison of torque values in the time domain (solid line – reference torque, dashed line – realised torque).

This test shows that the behaviour of the system is stable after changes of the friction conditions between wheels and rails. The torque being applied to the wheelset increases and then decreases because of the changes in friction conditions in the wheel-rail contact interface. The main outputs of the proposed system, namely the longitudinal slip and the traction coefficient, are very close to their reference values. This indicates that the PI traction control algorithm achieves almost the optimal adhesion coefficient for both friction conditions. There are still more opportunities for the tuning of P gain and I gain parameters, but it is not required to be perfect in such a simplified modelling as described in this chapter.

Finally, all the results obtained in this simulation confirm that the system recovers very quickly for such a simplified approach.

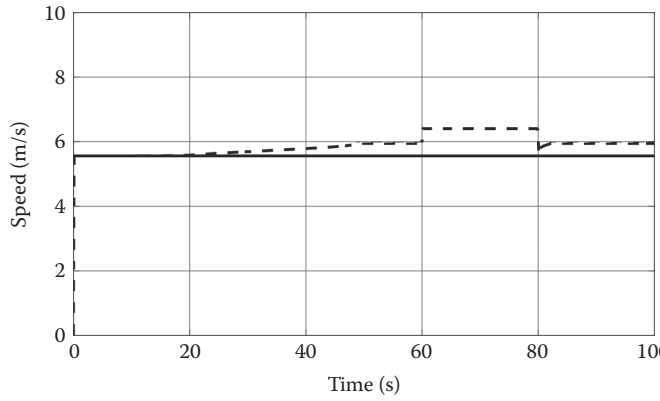

FIGURE 6.25 Comparison of speed values in the time domain (solid line – locomotive speed, dashed line – wheelset linear speed) for Case 1.

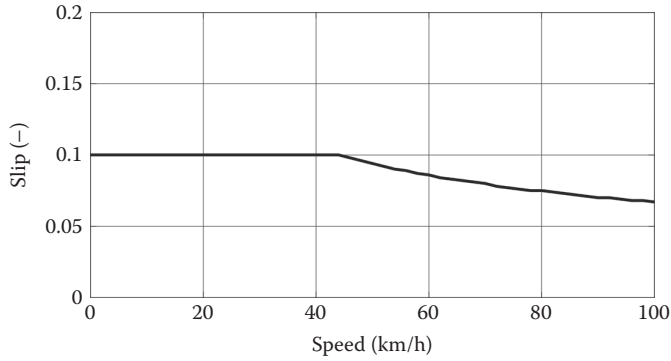

FIGURE 6.26 Slip threshold versus locomotive speed.

6.3.4 Case 2: Acceleration Mode

For the acceleration test, movement along the track under wet adhesion conditions has been simulated. The total simulation time for this case study is 400 s. Assume that the slip threshold, sopt, is given for the wet condition and is dependent on the locomotive speed, as shown in Figure 6.26. In real practice, this relationship depends on certain parameters, which characterise a certain model of a locomotive.

6.3.4.1 Implementation of the Model in Simulink

The integration approach is similar to that described in the previous case for the constant speed mode. The full model in Simulink used for this study is shown in Figure 6.27. Two blocks, namely the PI controller and adhesion force modelling,

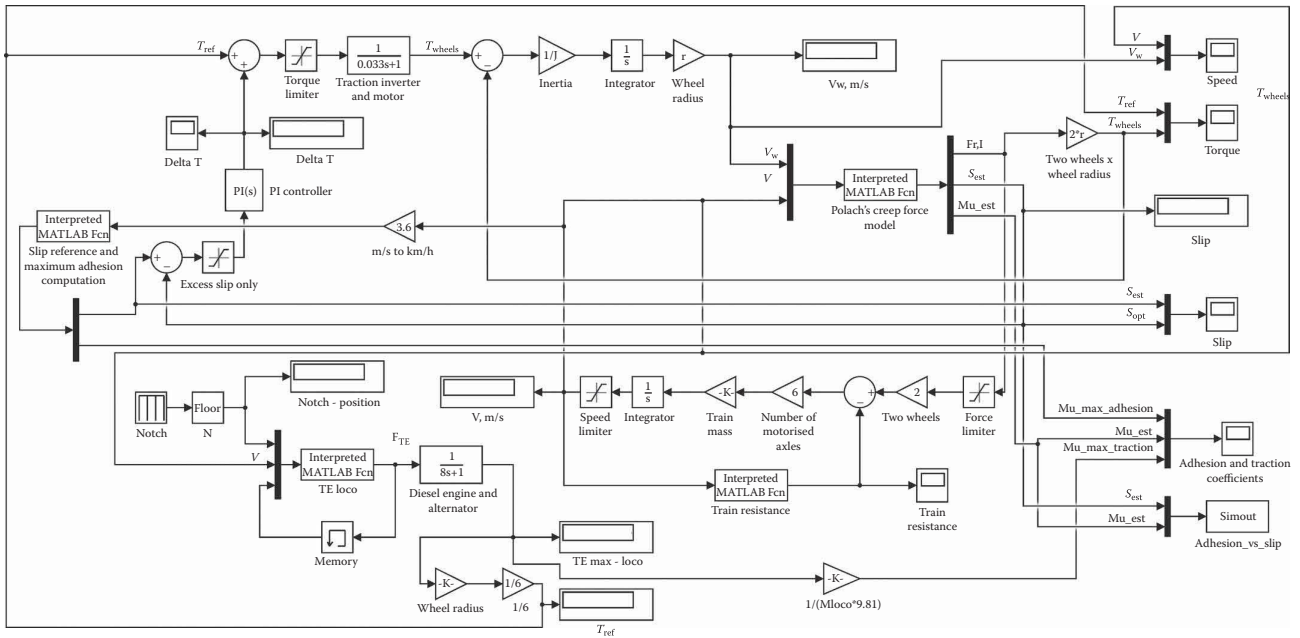

FIGURE 6.27 Full model in Simulink for single wheelset traction control studies for the acceleration mode.

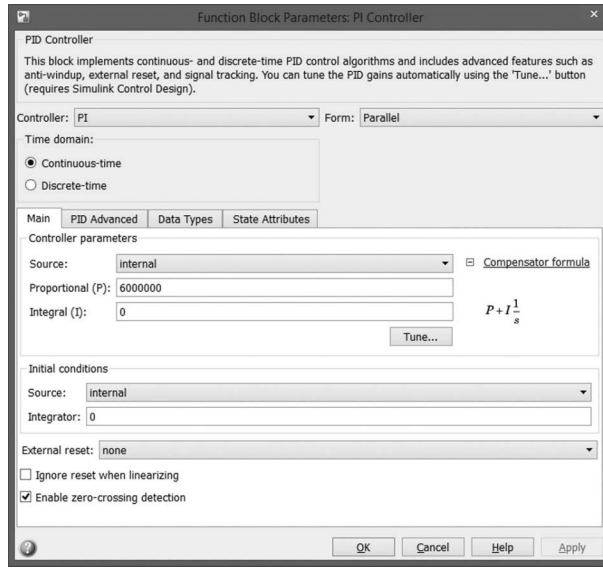

FIGURE 6.28 Parameters of PI controller block for Case 2.

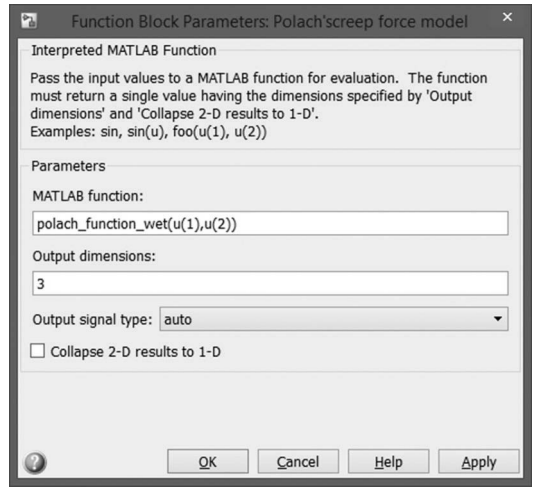

FIGURE 6.29 Parameters of Polach's creep force model block for Case 2.

have been modified in order to reach the objectives of this study, and their mask properties are shown in Figures 6.28 and 6.29, respectively. The slip controller uses only a P gain for this study (I gain equals zero), which provides a compensation of the torque value as required, that is, it is still adjusted to suit the complex non-linear phenomena of the friction process. The code for the modified Interpreted MATLAB

Function, that is, for Polach's creep force model block shown in Figure 6.29, is provided below:

File name: polach_function_wet.m

```
function fout = polach_function_wet(Vw,V)
% Vw = Wheelset linear speed
% V = Locomotive speed
% Q = Wheel load
% a = longitudinal half-axis of the contact patch
% b = lateral half axis of the contact patch
% mu_p = friction coefficient
% A = the ratio of the limit friction coefficient at infinity
slip velocity
% to the maximum friction coefficient μs
% B = the coefficient of exponential friction decrease, s/m
% C1 = coefficient of the Kalker's linear theory
% G = the shear module
% F = adhesion force (one wheel)
% s_est = the estimated slip
% mu_est = the estimated traction (adhesion) coefficient

Q=109545;
a=0.0052;
b=0.0164;

mu_p=0.30;
A=0.38;
B=0.10;
ka=0.29;
ks=0.09;

G=8.4*10^10;
C1=4.100;

wx=Vw-V;

SX=(Vw-V)/V;

muf=mu_p*((1-A)*exp(-B*wx)+A);

FX=0;
EX=G*pi*a*b*C1*SX/(4*Q*muf);
F=2*Q*muf/pi*(ka*EX/(1+ka*ka*EX*EX)+atan(ks*EX));
mu_est=F/Q;
s_est=SX;

fout =[F,s_est,mu_est];
```

Two additional blocks from the Simulink library have been used for the train resistance (see the train resistance block in Figure 6.27 and its mask parameters in Figure 6.30)

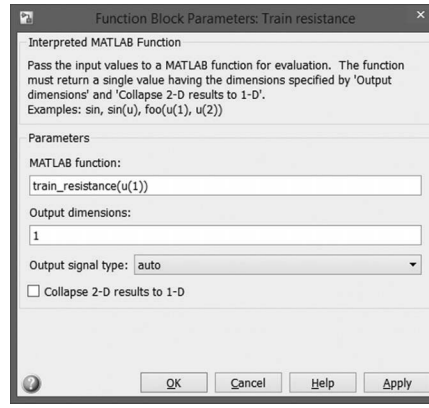

FIGURE 6.30 Parameters of train resistance block for Case 2.

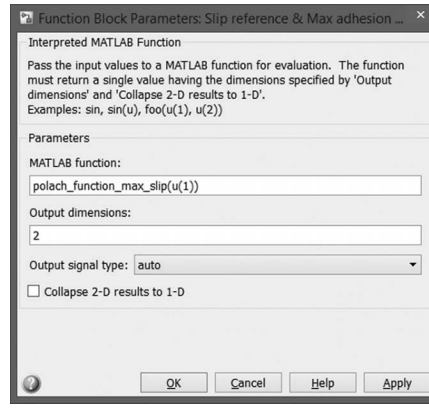

FIGURE 6.31 Parameters of slip reference and maximum adhesion computation block for Case 2.

and the slip reference and maximum adhesion modelling (see the slip reference and maximum adhesion computation block in Figure 6.27 and its mask parameters in Figure 6.31) in order to realise the conditions required for the acceleration study. These modules are based on a set of equations. This is the reason why four Interpreted MATLAB Functions have been used in the model.

The code for the first additional Interpreted MATLAB Function, that is, for the train resistance block shown in Figure 6.30, is provided below:

File name: polach_function_max_slip.m

```
function fout = polach_function_wet(V)

% Vw = Wheelset linear speed
% V = Locomotive speed
% Q = Wheel load
% a = longitudinal half-axis of the contact patch
```

```
% b = lateral half axis of the contact patch
% mu_p = friction coefficient
% A = the ratio of the limit friction coefficient at infinity
slip velocity
% to the maximum friction coefficient μs
% B = the coefficient of exponential friction decrease, s/m
% C1 = coefficient of the Kalker's linear theory
% G = the shear module
% F = adhesion force (one wheel)
% s_est = the estimated slip
% mu_est = the estimated traction (adhesion) coefficient

Q=109545;
a=0.0052;
b=0.0164;

%wet friction condition
mu_p=0.30;
A=0.38;
B=0.10;
ka=0.29;
ks=0.09;

G=8.4*10^10;
C1=4.100;

if V<=45 % in order to replicate the curve shown in Figure 6.26
 SX=0.10;
 N=1;
else
 SX=[0:0.001:1];
 N=1001;
end

for i=1:N

wx(i)=SX(i)*V/3.6;
muf(i)=mu_p*((1-A)*exp(-B*wx(i))+A);
FX(i)=0;
EX(i)=G*pi*a*b*C1*SX(i)/(4*Q*muf(i));
Fx(i)=2*Q*muf(i)/pi*(ka*EX(i)/(1+ka*ka*EX(i)*EX(i))+atan(ks*
EX(i)));
end

[Fmax,number]=max(Fx);

s_max=SX(number);

mu_max=Fmax/Q;

fout =[s_max,mu_max];
```

In this code, we assume that the curve shown in Figure 6.26 is based on Polach's theory. In order to represent this in our model, a special calculation and search algorithm has been realised. Initially, the value of maximum slip is limited to 0.10 for the range of speeds between 0 km/h and 45 km/h. For speeds higher than 45 km/h, the values of adhesion force are calculated for the longitudinal creepage range from 0 to 1, and then the maximum value of calculated force and its corresponding longitudinal creepage are found by the search function. In a similar manner, the maximum possible adhesion coefficient is calculated for the comparison of results.

6.3.4.2 Simulation Results

Figures 6.32 and 6.33 show the calculated values of longitudinal slips (creepages) and traction/adhesion coefficients for a single wheelset in the time domain. Figure 6.34 presents information regarding the estimated traction coefficient versus estimated slip curve. The comparison of reference and adhesion torques in the time domain is shown in Figure 6.35. Figure 6.36 presents information on locomotive

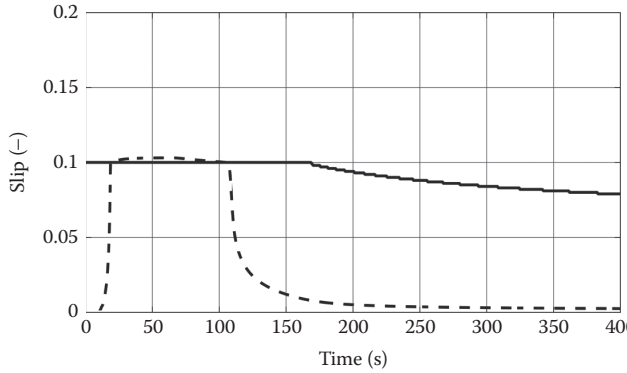

FIGURE 6.32 Comparison of longitudinal slip values in the time domain (solid line – optimal slip, dashed line – estimated slip) for Case 2.

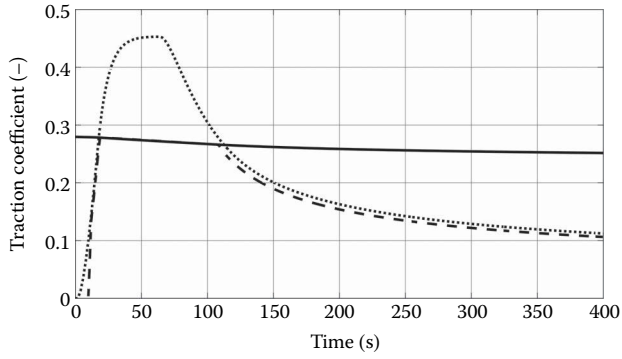

FIGURE 6.33 Comparison of traction coefficient values in the time domain (solid line – maximum possible adhesion coefficient, dotted line – maximum possible traction coefficient, dashed line – estimated traction coefficient) for Case 2.

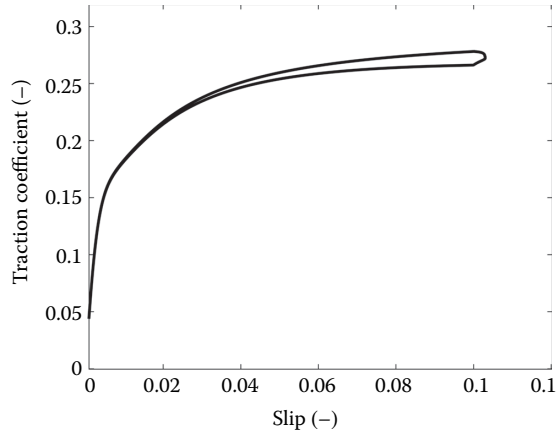

FIGURE 6.34 Slip curve when under traction control for Case 2.

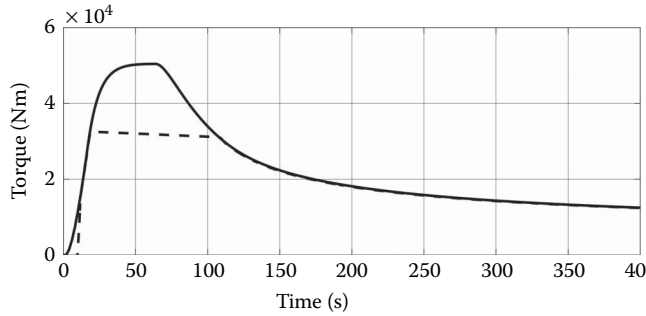

FIGURE 6.35 Comparison of torque values in the time domain (solid line – reference torque, dashed line – realised torque) for Case 2.

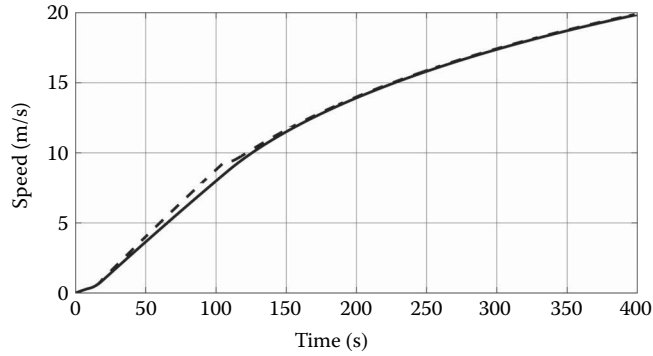

FIGURE 6.36 Comparison of speed values in the time domain (solid line – locomotive speed, dashed line – wheelset linear speed) for Case 2.

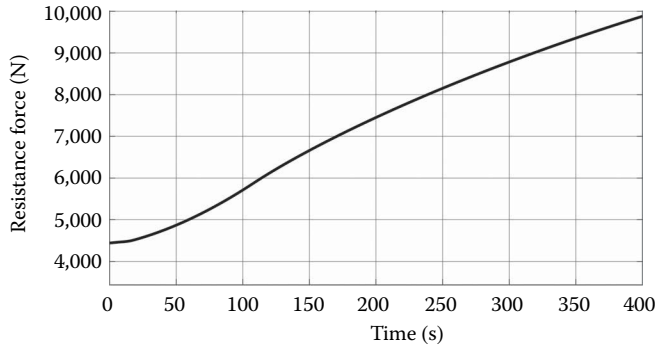

FIGURE 6.37 Resistance force acting on the wheelset in the time domain for Case 2.

and wheelset speed during the acceleration test. In addition, Figure 6.37 shows the train resistance force in the time domain acting on the wheelset during the simulation process.

This test shows that the system behaviour is stable and the traction controller does not allow the maximum slip threshold to be exceeded. When the estimated slip value is lower than the slip threshold value, the traction controller is in the off mode because of the power limit (a torque reference value provided to the system). Some minor differences in slip values that are evident in Figure 6.32 can be solved by means of the introduction of flexible and advanced PI control (e.g., PI-fuzzy logic controller). Finally, all results obtained in the simulation confirm that the system works to properly control the application of traction as required.

6.3.5 Uncertainties in Applying Simplified Modelling for Locomotive Dynamics Studies

The application of such a simplified approach can definitely prove a concept of traction algorithms and can save time in comparison with other simulation techniques. However, this approach does not allow accurate judgements to be made regarding what is going on with the contact forces at the wheel-rail interface, because the contact dimension characteristics are not constant, and track quality is not perfect and has it is own irregularities. If a whole locomotive is taken into consideration, issues of how weight is transferred between axles, how traction influences wheelset steering on curved track and similar factors have to be addressed in the modelling. In addition, there are more questions that need clarification, such as how time constants for use in low-pass filters representing the power plant and inverter-motor dynamics can be delivered at the earliest stages of such studies? How does the electric power system influence the distribution of electrical torques between motors when other than individual wheelset control is in use? How might in-train forces, such as lateral and vertical components of coupler forces, affect the realised traction and how it is applied by traction control algorithms?

Only one answer can be provided to all of these questions—more advanced simulation techniques should be used. Some such simulation approaches and techniques are discussed in Chapters 7, 8 and 9.

REFERENCES

1. M. Spiryagin, P. Wolfs, F. Szanto, C. Cole, Simplified and advanced modelling of traction control systems of heavy-haul locomotives, *Vehicle System Dynamics*, 53(5), 2015, 672–691.
2. D. Frylmark, S. Johnsson, Automatic slip control for railway vehicles, Master's Thesis, Linköpings Universitet, Vehicular Systems, Department of Electrical Engineering, Linköping, Sweden, 2003.
3. M. Spiryagin, V. Spiryagin, Modelling of mechatronic systems of running gears for a rail vehicle, East Ukrainian National University, Lugansk, Ukraine, 2010 (in Ukrainian).
4. A.A. Pavlenko, Dynamics and improvement of traction-adhesion characteristics of locomotive traction drives, PhD Thesis, East Ukrainian State University, Lugansk, Ukraine, 2000 (in Russian).
5. A. Steimel, *Electric Traction – Motive Power and Energy Supply: Basics and Practical Experience*, Oldenbourg Industrieverlag GmbH, Munich, Germany, 2008.
6. T.X. Mei, J.H.Yu, D.A. Wilson, Mechatronic approach for effective wheel slip control in railway traction, *Journal of Rail and Rapid Transit*, 223(3), 2009, 295–304.
7. T. Watanabe, M. Yamashita, Basic study of anti-slip control without speed sensor for multiple motor drive of electric railway vehicles, *IEEE Proceedings of the Power Conversion Conference*, Osaka, Japan, 2–5 April 2002, Vol.3, pp. 1026–1032.
8. R.W. Becker, J.S. Boggess, System considerations for heavy haul diesel-electric locomotives with three phase traction motors, *ASME/IEEE Joint Railroad Conference*, Chicago, IL, 17–19 April 1990, pp. 19–24.
9. M. Spiryagin, K.S. Lee, H.H. Yoo, O. Kashura, O. Kostjukevich, Modeling of adhesion for railway vehicles, *Journal of Adhesion Science and Technology*, 22(10–11), 2008, 1017–1034.
10. O. Polach, Creep forces in simulations of traction vehicles running on adhesion limit, *Wear*, 258, 2005, 992–1000.
11. M. Spiryagin, O. Polach, C. Cole, Creep force modelling for rail traction vehicles based on the Fastsim algorithm, *Vehicle System Dynamics*, 51(11), 2013, 1765–1783.
12. US Patent 6893058 B2, Railway train friction management and control system and method, 17 May 2005.
13. US Patent 5424948, Locomotive traction control system using fuzzy logic, 13 June 1995.
14. US Patent 7027900 B2, Enhanced locomotive adhesion control, 11 April 2006.
15. M. Spiryagin, Y.Q. Sun, C. Cole, S. Simson, I. Persson, Development of traction control for hauling locomotives, *Journal of System Design and Dynamics*, 5(6), 2011, 1214–1225.
16. Y. Tian, S. Liu, W.J.T. Daniel, P.A. Meehan, Comparison of PI and fuzzy logic based sliding mode locomotive creep controls with change of rail-wheel contact conditions, *International Journal of Rail Transportation*, 3(1), 2015, 40–59.
17. Y. Tian, S. Liu, W.J.T. Daniel, P.A. Meehan, Investigation of the impact of locomotive creep control on wear under changing contact conditions, *Vehicle System Dynamics*, 53(5), 2015, 692–709.

18. M. Yamashita, T. Soeda, Development of re-adhesion control method considering axle-weight transfer of electric locomotive, Quarterly Review of Railway Technical Research Institute, 52(1), 2011, 7–12.
19. N. Ramsey, F. Szanto, P. Hewison, Introducing the next generation locomotive to the Australian rail network, *Conference on Railway Engineering CORE2008*, Perth, Australia, 7–10 September 2008.
20. US Patent 7290807, Method and system of limiting the application of sand to a railroad rail, 6 November 2007.
21. J. Belanger, P. Venne, J.N. Paquin, The what, where and why of real-time simulation. *IEEE Power & Energy Society Tutorial*, October 2010, pp. 37–49. http://www.opal-rt.com/technical-document/what-where-and-why-real-time-simulation.
22. M. Spiryagin, Y.Q. Sun, C. Cole, T. McSweeney, S. Simson, I. Persson, Development of a real-time bogie test rig model based on railway specialised multibody software, *Vehicle System Dynamics*, 51(2), 2013, 236–250.

7 Modelling of Locomotives

7.1 INTRODUCTION TO MODELLING APPROACHES

A multibody dynamic system is the one that consists of solid bodies (rigid and flexible bodies) connected to each other by joints and/or couplings such as springs, dampers and actuators that restrict their relative displacements, including rotations. The study of multibody dynamics is the analysis of how the components of mechanisms move under the influence of forces, also known as forward dynamics. A study of the inverse multibody dynamic problems, that is, which forces are necessary to make the mechanical system move in a specific manner, is known as inverse dynamics. Motion analysis is important because product design frequently requires an understanding of how multiple moving parts interact with each other and the surrounding environment. From train locomotives and aircraft to automobiles and assembly lines, moving parts generate loads that are often difficult to predict. Complex mechanical assemblies present design challenges that require a systematic dynamic analysis to be undertaken.

Accurate modelling requires appropriate representations of mechanical systems and compliant parts and connections, as well as complicated physical phenomena such as vibration, friction and noise. Motion analysis software is able to provide a variety of contact modelling functionalities to meet the challenge of quickly evaluating and improving designs for critical characteristics of performance, safety and comfort. Rolling and sliding contacts and impact can readily be represented between various combinations of rigid and/or flexible bodies. More sophisticated methods are used for contact between complex geometries, both rigid and flexible.

Like many physical systems, a train locomotive is a combination of mechanical components actuated by electrical or pneumatic and hydraulic subsystems that are controlled by electronic control units. System models need to fully account for the effects of actuation and control systems to correctly capture the behaviour of the complete assembly.

Modern multibody dynamics software packages can incorporate mechanical models within block diagrams of the control system design software itself, or can directly import the actuators and/or controllers from the controls design software in the mechanical system simulation environment.

In addition, for a mechanical system in which deformation effects are paramount for design analyses, the rigid-body assumption is no longer valid. For such modelling scenarios, some multibody dynamics analysis software packages include fully integrated functionality that allows finite element models to be imported from most major finite element analysis software packages, providing access to convenient modelling and powerful post-processing capabilities.

Comprehensive modelling using multibody dynamics approaches can improve engineering efficiency and reduce product development costs by enabling early system-level design validation. It can be used to evaluate and manage the complex interactions between disciplines, including motion, structures, actuation and controls, to better optimise product designs for performance, safety and comfort. Multibody dynamics solution technology can run non-linear dynamics in a fraction of the time required by finite element analysis solutions. Loads and forces computed by multibody dynamics simulations improve the accuracy of finite element analysis by providing better assessment of how they vary throughout a full range of operating environments.

Multibody dynamics is a branch of classical mechanics concerned with the study of forces and torques and their effect on motion. In the following sections, techniques for developing the dynamic equations of motion for multibody systems (MBSs) consisting of interconnected rigid bodies are briefly introduced [1–4].

7.1.1 Newton–Euler Equations

It is known that the unconstrained three-dimensional motion of a rigid body can be described using six equations—three translational equations of the rigid body and three rotational equations associated with the body. It is important for the origin of the body coordinate system to be fixed to the body mass centre, which can significantly simplify the dynamic equations. In this circumstance, the translational equations are called Newton equations, whereas the rotational equations are called Euler equations. The Newton–Euler equations can be written, for body i in an MBSs, as:

$$\begin{aligned} m_i\mathbf{a}_i &= \mathbf{F}_i \\ J_i\ddot{\theta}_{iz} &= \mathrm{M}_i \end{aligned} \tag{7.1}$$

where:

m_i is the total mass of the rigid body
$\mathbf{a}_i$ is a two-dimensional vector that defines the absolute acceleration of the body mass centre
$\mathbf{F}_i$ is the vector of forces acting on the body mass centre
J_i is the mass moment of inertia defined with respect to the mass centre
M_i is the moment acting on the body
$\ddot{\theta}_{iz}$ is the rotational acceleration about the body mass centre

7.1.2 D'Alembert's Principle and Generalised Forces

Generally, a multibody dynamic system with n coordinates and n_c constraint equations, which are linearly independent, has $(n - n_c)$ independent coordinates, also called the system degrees of freedom (DOFs). Generalised coordinates $\left(\mathbf{q}_j, j = 1, 2,\ldots, m \le (n - n_c)\right)$ are the minimum number of independent coordinates that define the configuration of a system. A constraint is actually represented by the force that prevents a body from moving in a certain path. A more efficient approach to generate the dynamic equations of motion of an MBS, incorporating the constraints on the system, uses D'Alembert's principle, because the kinetic and potential energies of an MBS are much easier to express and calculate than the forces, as energy is a scalar (magnitude

only) whereas force is a vector (magnitude and direction). D'Alembert's principle introduces virtual work into the study of the dynamic equilibrium of an MBS.

The body position vector **r** in an MBS, using a standard coordinate system (Cartesian, spherical, etc.), is related to the generalised coordinates by transformation equations, given by

$$\mathbf{r}_i = \mathbf{r}_i\left(\mathbf{q}_1, \mathbf{q}_2, \ldots, \mathbf{q}_m, t\right), \; i = 1, 2, \ldots, n \tag{7.2}$$

The virtual work of forces acting on an MBS is obtained from the scalar product of each force with the virtual displacement of its point of application, expressed as

$$\delta W = \sum_{i=1}^{n} \mathbf{F}_i \cdot \delta \mathbf{r}_i \tag{7.3}$$

From Equation 7.2, the virtual displacements $\delta \mathrm{r}_i$ are given by

$$\delta \mathbf{r}_i = \sum_{j=1}^{m} \frac{\partial \mathbf{r}_i}{\partial \mathbf{q}_j} \cdot \delta \mathbf{q}_j \tag{7.4}$$

Hence, the virtual work of forces in the system in terms of the generalised coordinates becomes

$$\delta W = \sum_{j=1}^{m} \sum_{i=1}^{n} \mathbf{F}_i \cdot \frac{\partial \mathbf{r}_i}{\partial \mathbf{q}_j} \cdot \delta \mathbf{q}_j$$

The generalised forces can be defined as

$$\boldsymbol{Q}_j = \sum_{i=1}^{n} \mathbf{F}_i \cdot \frac{\partial \mathbf{r}_i}{\partial \mathbf{q}_j}$$

$\boldsymbol{Q}_j$ is known as the generalised force associated with the virtual displacement $\delta \mathbf{q}_j$. On the basis of Newton's equations, Equation 7.3 can be rewritten as

$$\delta W = \sum_{i=1}^{n} \left(\mathbf{F}_i - m_i \mathbf{a}_i\right) \cdot \delta \mathbf{r}_i = 0 \tag{7.5}$$

This equation expresses D'Alembert's principle of dynamic equilibrium of an MBS.

7.1.3 Lagrange's Equation

It is known that the kinetic energy T of the system can be defined by

$$T = \frac{1}{2} \sum_{i=1}^{n} m_i \dot{\mathbf{r}}_i \cdot \dot{\mathbf{r}}_i \tag{7.6}$$

Equation 7.6 is partially differentiated with respect to the generalised coordinates $\mathbf{q}_j$ and the generalised velocities $\dot{\mathbf{q}}_j$, respectively, and the following equations are obtained:

$$\frac{\partial T}{\partial \mathbf{q}_j} = \sum_{i=1}^{n} m_i \dot{\mathbf{r}}_i \cdot \frac{\partial \dot{\mathbf{r}}_i}{\partial \mathbf{q}_j} \quad \text{and} \quad \frac{\partial T}{\partial \dot{\mathbf{q}}_j} = \sum_{i=1}^{n} m_i \dot{\mathbf{r}}_i \cdot \frac{\partial \dot{\mathbf{r}}_i}{\partial \dot{\mathbf{q}}_j} \tag{7.7}$$

Because $\frac{\partial \dot{\mathbf{r}}_i}{\partial \dot{\mathbf{q}}_j} = \frac{\partial \mathbf{r}_i}{\partial \mathbf{q}_j}$, therefore,

$$\frac{\partial T}{\partial \dot{\mathbf{q}}_j} = \sum_{i=1}^{n} m_i \dot{\mathbf{r}}_i \cdot \frac{\partial \mathbf{r}_i}{\partial \mathbf{q}_j} \tag{7.8}$$

Equation 7.8 is differentiated with respect to time and yields:

$$\frac{d}{dt}\frac{\partial T}{\partial \dot{\mathbf{q}}_j} = \sum_{i=1}^{n} m_i \ddot{\mathbf{r}}_i \cdot \frac{\partial \mathbf{r}_i}{\partial \mathbf{q}_j} + \sum_{i=1}^{n} m_i \dot{\mathbf{r}}_i \cdot \frac{\partial \dot{\mathbf{r}}_i}{\partial \mathbf{q}_j} = \boldsymbol{Q}_j + \frac{\partial T}{\partial \mathbf{q}_j}$$

Finally, the above equation results in

$$\boldsymbol{Q}_j = \frac{d}{dt}\left(\frac{\partial T}{\partial \dot{\mathbf{q}}_j}\right) - \frac{\partial T}{\partial \mathbf{q}_j} \tag{7.9}$$

This is an important Lagrange equation based on the dynamic equilibrium of an MBS, incorporating virtual work and generalised coordinates. However, kinematic constraint equations may exist because of connections between bodies or specified motion trajectories in an MBS. The constraints are sometimes considered as the classical constraints, which are usually a set of algebraic equations that define the relative translations or rotations between bodies. In a nonholonomic system, there are possibilities to constrain the relative velocities between bodies. In addition, there are nonclassical constraints that might even introduce a new unknown coordinate. Therefore, Equation 7.9 cannot actually be used in building a dynamics model.

7.1.4 Dynamic Equations

A technique called the augmented formulation [1] can be applied to formulate the dynamic equations of the constrained MBSs.

The constraint equations of an MBS can be written as

$$\mathbf{C}(\mathbf{q},t) = 0 \tag{7.10}$$

where:

$\mathbf{C} = \left[\mathrm{C}_1(\mathbf{q},t)\ \mathrm{C}_2(\mathbf{q},t) \ldots\ \mathrm{C}_{\mathrm{n_c}}(\mathbf{q},t)\right]^{\mathrm{T}}$ is the vector of constraint equations

$\mathrm{n_c}$ is the number of constraint equations

For a virtual displacement $\delta\mathbf{q}$, Equation 7.10 becomes:

$$\mathbf{C}_q \delta\mathbf{q} = 0 \tag{7.11}$$

where $\mathbf{C}_q$ is the constraint Jacobian matrix.

In the augmented formulation, the Lagrange multipliers can be used for both holonomic and nonholonomic systems. Provided that the constraint relationships are velocity-dependent and nonintegrable, the following equation exists:

$$\left(\mathbf{C}_q \delta\mathbf{q}\right)^T \boldsymbol{\lambda} = 0 \tag{7.12}$$

where $\boldsymbol{\lambda} = \left[\lambda_1, \lambda_2, \ldots, \lambda_{n_c}\right]^T$ is the vector of Lagrange multipliers.

Based on the principle of virtual work,

$$\delta W = \left(\mathbf{M}\ddot{\mathbf{q}} - \mathbf{Q}\right)^T \cdot \delta\mathbf{q} = 0 \tag{7.13}$$

where:

$\mathbf{M}$ is the system mass matrix

$\mathbf{Q} = \mathbf{Q}_v + \mathbf{Q}_e$ is the total vector of forces ($\mathbf{Q}_v$ is the vector of centrifugal and inertia forces and $\mathbf{Q}_e$ is the vector of externally applied forces, including gravity, spring, damper and actuator forces)

Equations 7.12 and 7.13 can be combined to yield:

$$\delta\mathbf{q}^T \left(\mathbf{M}\ddot{\mathbf{q}} - \mathbf{Q} + \mathbf{C}_q^T\right) = 0 \tag{7.14}$$

By partitioning the coordinates as dependent and independent, $\mathbf{M}$ and $\mathbf{Q}$ can be written as:

$$\mathbf{M} = \begin{bmatrix} \mathbf{M}_{dd} & \mathbf{M}_{di} \\ \mathbf{M}_{id} & \mathbf{M}_{ii} \end{bmatrix} \text{ and } \mathbf{Q} = \begin{bmatrix} \mathbf{Q}_d \\ \mathbf{Q}_i \end{bmatrix}.$$

where subscripts d and i represent dependent and independent coordinates, respectively. The components of the virtual displacement vector $\delta\mathbf{q}$ in Equation 7.13 are not independent because of the holonomic or nonholonomic constraint equations. It is assumed that λ_k ($k = 1, 2, \ldots, n_c$) is selected, so that:

$$\mathbf{M}_{dd}\ddot{\mathbf{q}}_d + \mathbf{M}_{di}\ddot{\mathbf{q}}_i - \mathbf{Q}_d + \mathbf{C}_{q_d}^T \lambda = 0 \tag{7.15}$$

where $\mathbf{q}_d = \left[q_1, q_2, \ldots, q_{n_c}\right]^T$ are the dependent variables. Substituting Equation 7.15 into Equation 7.14, the following equation is given:

$$\delta\mathbf{q}_i^T \left(\mathbf{M}_{ii}\ddot{\mathbf{q}}_i + \mathbf{M}_{id}\ddot{\mathbf{q}}_d - \mathbf{Q}_i + \mathbf{C}_{q_i}^T \boldsymbol{\lambda}\right) = 0 \tag{7.16}$$

Because $\delta\mathbf{q}_i$ in this equation are independent, therefore,

$$\mathbf{M}_{ii}\ddot{\mathbf{q}}_i + \mathbf{M}_{id}\ddot{\mathbf{q}}_d - \mathbf{Q}_i + \mathbf{C}_{q_i}^{T}\boldsymbol{\lambda} = 0 \tag{7.17}$$

Because $\mathbf{q}_d$ and $\mathbf{q}_i$ are the partitions of $\mathbf{q}$, one equation can be obtained by combining Equations 7.15 and 7.17:

$$\mathbf{M}\ddot{\mathbf{q}} - \mathbf{Q} + \mathbf{C}_q^{T}\boldsymbol{\lambda} = 0 \tag{7.18}$$

The above equation represents a set of differential equations of motion, which, along with the constraint equations, can be solved for the vector of system generalised coordinates $\mathbf{q}$ and the vector of Lagrange multipliers $\boldsymbol{\lambda}$. This equation can be used to develop the dynamic equilibrium equations of motion for the dynamic analysis of an MBS subject to both holonomic and nonholonomic constraints.

7.2 NUMERICAL INTEGRATORS

The differential equations of motion can be solved by various numerical methods that find numerical approximations to the solutions of differential equations. The use of these 'solvers' is also known as 'numerical integration'; however, this term is sometimes taken to mean the computation of integrals. It is known that many differential equations cannot be solved using symbolic computation. For practical purposes in engineering, a numeric approximation to the solution is often sufficient. Therefore, many algorithms can be used to compute such an approximation.

A first-order differential equation is an initial value problem of the form:

$$y'(t) = f(t, y(t)), y(t_0) = y_0 \tag{7.19}$$

where $f(t, y(t))$ is a function of time t and variable $y(t)$. First order means that only the first derivative of $y(t)$ appears in the equation, and higher derivatives are absent because higher-order differential equations of motion can be converted into a larger system of first-order equations by introducing extra variables. For example, the second-order equation $y''(t) = -y(t)$ can be rewritten as two first-order equations: $y'(t) = z(t)$ and $z'(t) = -y(t)$. Numerical methods for first-order solutions often fall into one of two broad categories: linear multistep methods and Runge-Kutta methods. A further division can be realised by dividing the methods into those that are explicit and those that are implicit. The following numerical integrators are widely used in MBS software packages:

- *Euler method*: Selecting an integrator that works according to Euler's explicit method, which is a one-step method with fixed time step, giving an integration error of O(h). The expression is

$$y_{n+1} = y_n + \Delta t \times f\left(t_n, y_n\right) \tag{7.20}$$

where:

y_{n+1} is the value of the integrated variable at time t_{n+1}
y_n is the value of the integrated variable at time t_n
Δt is the time step
$f(t_n, y_n)$ is the value of the integrand at t_n and y_n

- *Midpoint method*: Selecting an integrator that works as a one-step method with fixed time step, giving an integration error of $O(h^2)$. The expression is:

$$y_{n+1} = y_{n-1} + 2 \times \Delta t \times f\left(t_n, y_n\right) \tag{7.21}$$

  where y_{n-1} is the value of the integrated variable at time t_{n-1}.

- *Runge-Kutta method*: Selecting an integrator that works according to the classical fourth-order Runge-Kutta method, which is a four-step method with fixed time step, giving an integration error of $O(h^4)$. The expression is:

$$y_{n+1} = y_{n-1} + \frac{k_1 + 2k_2 + 2k_3 + k_4}{6} \tag{7.22}$$

$$k_1 = \Delta t \times f\left(t_n, y_n\right); \quad k_2 = \Delta t \times f\left(t_n + \frac{\Delta t}{2}, y_n + \frac{k_1}{2}\right); \tag{7.23}$$

$$k_3 = \Delta t \times f\left(t_n + \frac{\Delta t}{2}, y_n + \frac{k_2}{2}\right); \quad k_4 = \Delta t \times f\left(t_n + \Delta t, y_n + k_3\right); \tag{7.24}$$

  where:

  $f\left(t_n + (\Delta t/2), y_n + (k_1/2)\right)$ is the value of the integrand at $t_n + (\Delta t/2)$ and $y_n + (k_1/2)$
  $f\left(t_n + (\Delta t/2), y_n + (k_2/2)\right)$ is the value of the integrand at $t_n + (\Delta t/2)$ and $y_n + (k_2/2)$
  $f(t_n + \Delta t, y_n + k_3)$ is the value of the integrand at $t_n + \Delta t$ and $y_n + k_3$

  As can be seen above, four calculations of the integrand are made for each time step (one at the beginning, one at the end and two in the middle of each time interval).

- *Heun's method*: Selecting an integrator that works as a two-step method with fixed time step, giving an integration error of $O(h^2)$. The expression is:

$$y_{n+1} = y_n + \frac{k_1 + k_2}{2} \tag{7.25}$$

$$k_1 = \Delta t \times f\left(t_n, y_n\right); \quad k_2 = \Delta t \times f\left(t_n + \Delta t, y_n + k_1\right) \tag{7.26}$$

  where $f(t_n + \Delta t, y_n + k_1)$ is the value of the integrand at $t_n + \Delta t$ and $y_n + k_1$.

- *Modified Heun's method*: Involves the use of variable time steps, with their lengths being calculated based on how fast the error increases or decreases between two consecutive time steps.

A simple integration algorithm called the time-stepping integration is used in MBS software packages to calculate the values of displacement and velocity at time step $(n + 1)$ from the displacement, velocity and acceleration at time step (n); thus:

$$\dot{y}_{n+1} = \dot{y}_n + \ddot{y}_n \times \Delta t \tag{7.27}$$

$$y_{n+1} = y_n + \dot{y}_{n+1} \times \Delta t \tag{7.28}$$

where y represents displacement of the DOFs.

This very simple algorithm relies on the fact that changes in force on a DOF over a time step are small. It has been found to be satisfactory in terms of both accuracy and numerical stability with a time step of the order of 1 ms.

7.3 HOW TO MODEL A LOCOMOTIVE

When modelling locomotives using MBS dynamics approaches, the locomotive car body (including all its internal components and main frame, as shown in Figures 2.4 and 3.1) is usually considered as a lumped mass. Similarly, the bogie frame, wheelsets and traction motor assembly, as shown in Figure 3.9, are also considered as lumped masses. Heavy haul locomotives usually have two stages of suspension, primary and secondary, as discussed in Section 3.3, which are commonly modelled with spring and damper elements.

Before detailing the locomotive modelling methodology, it is important to understand how locomotive tractive efforts are applied and transferred. The general concept is shown in Figure 7.1, but it must be recognised that undertaking detailed MBS modelling of a locomotive is much more complicated. Figure 7.1 shows a leading locomotive (i.e., operating at the head of a train); a similar diagram of subsequent locomotives in a train would include coupler forces on the front end of the locomotive.

In Figure 7.1, F_{TWi} $(i = 1, 2\ldots 6)$ indicates the longitudinal creep force for each wheelset under traction conditions. The remainder of this section discusses the

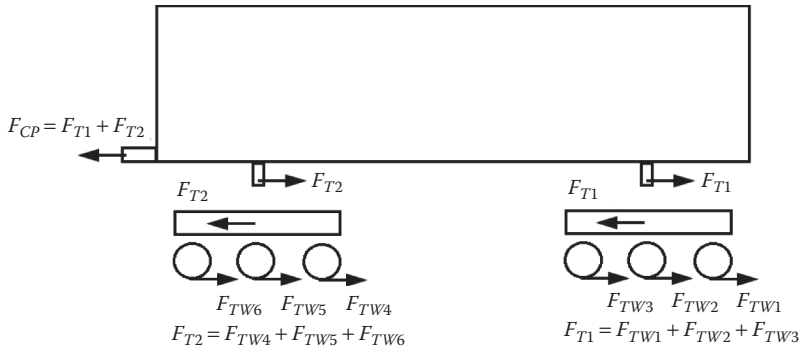

FIGURE 7.1 Simplified force concept of locomotive traction process.

modelling of a locomotive when under traction and provides details of how to model each major component. There is, of course, a very similar concept to be considered with regard to modelling locomotive braking.

7.3.1 Equations of Dynamic Equilibrium: Locomotive Car Body

As stated previously, the locomotive car body, bogie frame, wheelset and traction motor assembly are considered as individual lumped masses. Their local coordination systems are shown in Figure 7.2.

Figure 7.3 shows the free-body diagram of a locomotive car body. For convenience, the origin of the Cartesian coordinate system (X_C, Y_C and Z_C) is positioned at the centre of mass of the car body. Six DOFs describing the motions of the locomotive car body, namely the longitudinal, lateral and vertical displacements (u_C, v_C and w_C) and the roll, pitch and yaw rotations (ϕ_{Cx}, ϕ_{Cy} and ϕ_{Cz}) about the X_C, Y_C and Z_C axes, respectively, are shown in Figure 7.3, as are the various forces acting on the locomotive car body and the relevant dimensions. In contrast to Figure 7.1,

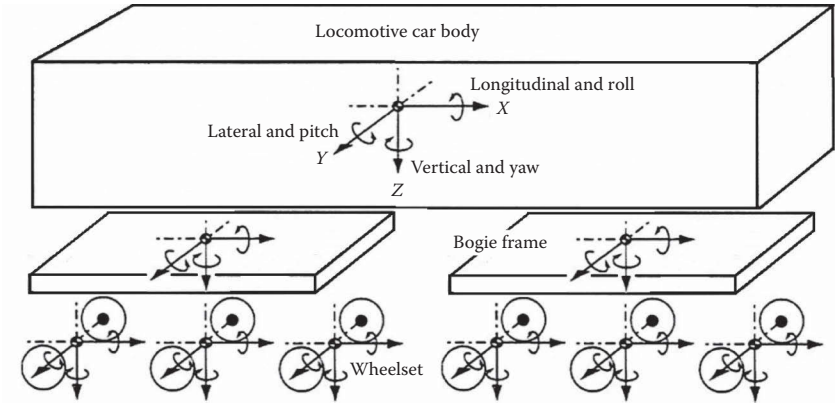

FIGURE 7.2 Local coordinate systems.

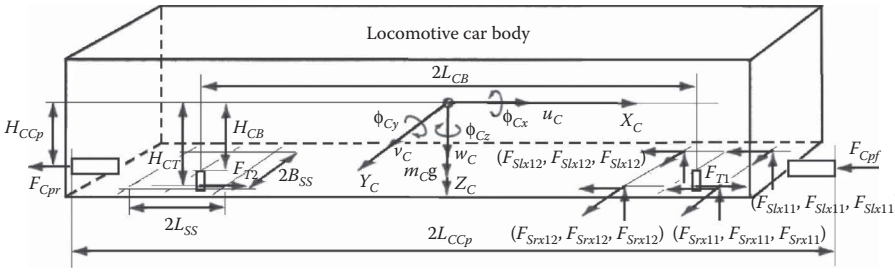

FIGURE 7.3 Free-body diagram of locomotive car body.

which shows the special case of a leading locomotive, Figure 7.3 presents the general case of a locomotive placed in the body of a train, with coupler forces acting on both ends.

When the displacement or the rotation of the locomotive car body varies with time, the motion is governed by Newton's second law. Hence, the total forces acting on a mass (or moments acting about a mass centre) are equal to the mass (or mass moment of inertia) multiplied by their linear (or angular) accelerations. The latter are represented by the second-order differentiation of the various displacements (u, v and w) or rotations (ϕ) with respect to time. In the car body modelling, the directions of longitudinal coupler forces and traction forces are assumed to be in the $X_C Z_C$ vertical plane. In the following dynamic equilibrium equations derived for the locomotive car body, the subscripts used are: l for the left side and r for the right side; x for acting along or rotating about the longitudinal axis, y for the lateral axis and z for the vertical axis; $i = 1$ for the front bogie and $i = 2$ for the rear bogie; $j = 1$ for the front secondary suspension and $j = 2$ for the rear secondary suspension.

7.3.1.1 Longitudinal Dynamic Equilibrium Equation

$$m_C \ddot{u}_C = \sum_{i=1}^{2} F_{Ti} - \sum_{i=1}^{2}\sum_{j=1}^{2} F_{Slxij} - \sum_{i=1}^{2}\sum_{j=1}^{2} F_{Srxij} - F_{Cpf} - F_{Cpr} \tag{7.29}$$

where:

m_C is the locomotive car body mass

F_{Ti} ($i = 1, 2$) is the traction force on the locomotive car body

F_{Slxij} ($i = 1, 2; j = 1, 2$) is the longitudinal secondary suspension force on the left side of the locomotive car body

F_{Srxij} ($i = 1, 2; j = 1, 2$) is the longitudinal secondary suspension force on the right side of the locomotive car body

F_{Cpf} and F_{Cpr} are the longitudinal coupler forces on the front and rear couplers, respectively

7.3.1.2 Lateral Dynamic Equilibrium Equation

$$m_C \ddot{v}_C = \sum_{i=1}^{2}\sum_{j=1}^{2} F_{Slyij} + \sum_{i=1}^{2}\sum_{j=1}^{2} F_{Sryij} \tag{7.30}$$

where:

F_{Slyij} ($i = 1, 2; j = 1, 2$) is the lateral secondary suspension force on the left side of the locomotive car body

F_{Sryij} ($i = 1, 2; j = 1, 2$) is the lateral secondary suspension force on the right side of the locomotive car body

7.3.1.3 Vertical Dynamic Equilibrium Equation

$$m_C \ddot{w}_C = -\sum_{i=1}^{2}\sum_{j=1}^{2} F_{Slzij} - \sum_{i=1}^{2}\sum_{j=1}^{2} F_{Srzij} + m_C g \tag{7.31}$$

where:

F_{Slzij} $(i = 1, 2; j = 1, 2)$ is the vertical secondary suspension force on the left side of the locomotive car body

F_{Srzij} $(i = 1, 2; j = 1, 2)$ is the vertical secondary suspension force on the right side of the locomotive car body

7.3.1.4 Roll Rotational Dynamic Equilibrium Equation

$$J_{Cx}\ddot{\phi}_{Cx} = -H_{CB} \times \sum_{i=1}^{2}\sum_{j=1}^{2}\left(F_{Slyij} + F_{Sryij}\right) + B_{SS} \times \sum_{i=1}^{2}\sum_{j=1}^{2}\left(F_{Slzij} - F_{Srzij}\right) \tag{7.32}$$

where:

J_{Cx} is the car body mass moment of inertia about the X_C axis

H_{CB} is the height between the locomotive car body mass centre and the secondary suspension position

B_{SS} is the semi-lateral width between two secondary suspension positions in a bogie

7.3.1.5 Pitch Rotational Dynamic Equilibrium Equation

$$\begin{aligned} J_{Cy}\ddot{\phi}_{Cy} = &-H_{CB} \times \sum_{i=1}^{2}\sum_{j=1}^{2}\left(F_{Slxij} + F_{Srxij}\right) + \left(L_{CB} + L_{SS}\right) \times \left(F_{Slz11} + F_{Srz11} - F_{Slz22} - F_{Srz22}\right) \\ &+ \left(L_{CB} - L_{SS}\right) \times \left(F_{Slz12} + F_{Srz12} - F_{Slz21} - F_{Srz21}\right) - H_{CCp} \times \left(F_{Cpf} + F_{Cpr}\right) \\ &+ H_{CT} \times \left(F_{T1} + F_{T2}\right) \end{aligned} \tag{7.33}$$

where:

J_{Cy} is the car body mass moment of inertia about the Y_C axis

L_{CB} is the length between the locomotive car body mass centre and the bogie frame mass centre

L_{SS} is the longitudinal length between two secondary suspension positions in a bogie

H_{CCp} is the height between the locomotive car body mass centre and the coupler position

H_{CT} is the height between the locomotive car body mass centre and the pivot assembly or traction rod joint

7.3.1.6 Yaw Rotational Dynamic Equilibrium Equation

$$J_{Cz}\ddot{\phi}_{Cz} = B_{SS} \times \sum_{i=1}^{2}\sum_{j=1}^{2}\left(-F_{Slxij} + F_{Srxij}\right) + \left(L_{CB} + L_{SS}\right) \times \left(F_{Sly11} + F_{Sry11} - F_{Sly22} - F_{Sry22}\right)$$
$$+ \left(L_{CB} - L_{SS}\right) \times \left(F_{Sly12} + F_{Sry12} - F_{Sly21} - F_{Sry21}\right) \tag{7.34}$$

where J_{Cz} is the car body mass moment of inertia about the Z_C axis.

7.3.2 Equations of Dynamic Equilibrium: Bogie Frame

Figure 7.4 shows the free-body diagrams of a bogie frame, indicating the various forces acting on it. These diagrams are specifically for the leading bogie of a locomotive; similar diagrams can be produced for the trailing bogie. The origin of the Cartesian coordinate system (X_B, Y_B, Z_B) is positioned at the centre of mass of the bogie frame. Six DOFs describing the motions of the bogie frame, namely the longitudinal, lateral and vertical displacements (u_B, v_B and w_B) and the roll, pitch and yaw rotations (ϕ_{Bx}, ϕ_{By} and ϕ_{Bz}) about the X_B, Y_B and Z_B axes, respectively, are shown in Figure 7.4. The various forces on the locomotive bogie frame and relevant dimensions are also shown in Figure 7.4. In the bogie modelling, the lateral axis Y_W of the second (or middle) wheelset of the bogie (typical wheelset shown in Figure 7.5) is assumed to be in the vertical Y_BZ_B plane. The directions of longitudinal traction force F_{T1} and the motor system suspended forces acting on the bogie (F_{MS11}, F_{MS12} and F_{MS13}, shown in Figure 7.4c) are assumed to be in the same vertical X_BZ_B plane.

The following dynamic equilibrium equations are derived for the bogie frame of a locomotive's front bogie. Similar conventions regarding the use of subscripts apply here, as noted in Section 7.3.1, except that for the primary suspension forces, $j = 1$ for the front primary suspension, $j = 2$ for the middle primary suspension and $j = 3$ for the rear primary suspension. In addition, as only the leading bogie is discussed here, $i = 1$.

7.3.2.1 Longitudinal Dynamic Equilibrium Equation

$$m_B\ddot{u}_B = -F_{T1} + \sum_{j=1}^{2} F_{Slx1j} + \sum_{j=1}^{2} F_{Srx1j} + \sum_{j=1}^{3} F_{Plx1j} + \sum_{j=1}^{3} F_{Prx1j} \tag{7.35}$$

where:

m_B is the locomotive bogie frame mass

F_{Plx1j} ($j = 1, 3$) is the longitudinal primary suspension force on the left side of the bogie frame

F_{Prx1j} ($j = 1, 3$) is the longitudinal primary suspension force on the right side of the bogie frame

Note that F_{T1} is negative here, because, as shown on Figure 7.1, the direction of F_{T1} on a bogie frame is opposite to the direction of travel of the locomotive.

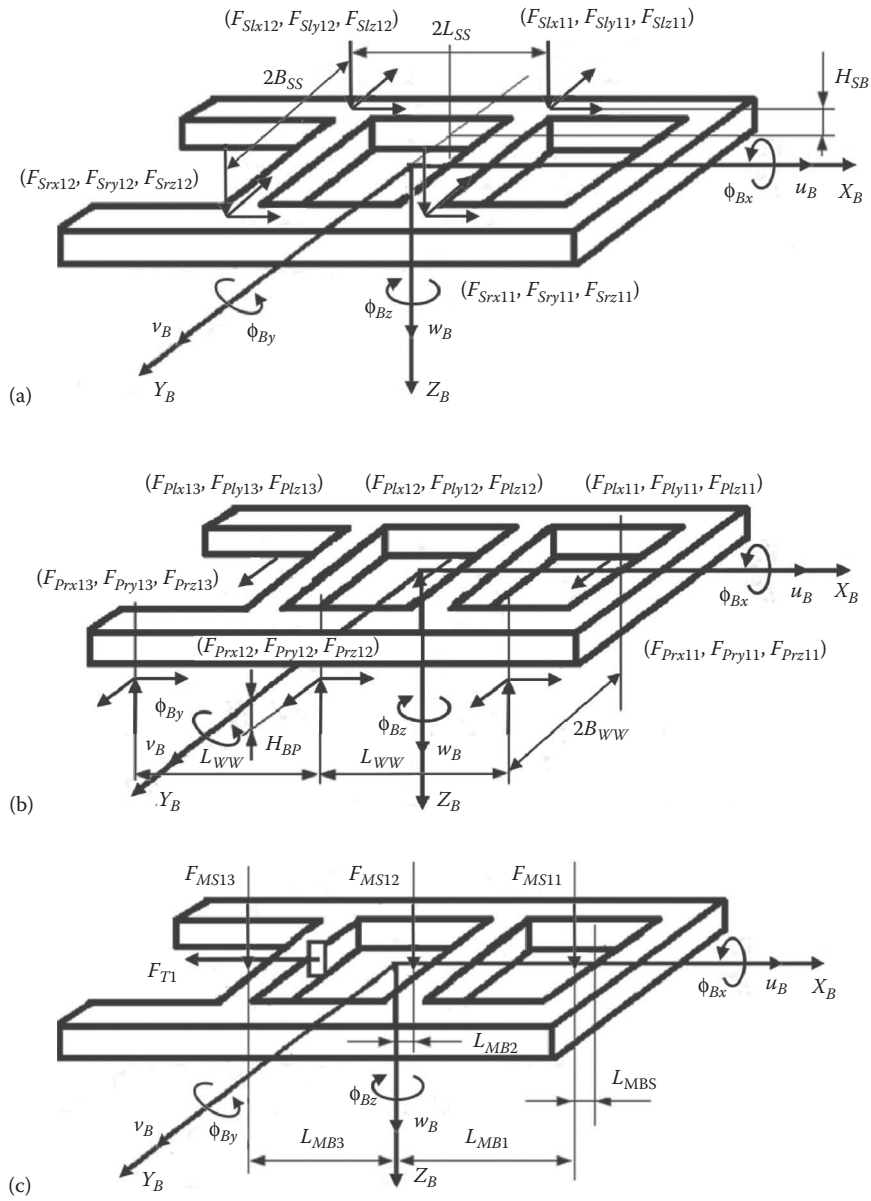

FIGURE 7.4 Free-body diagram of locomotive bogie frame (leading bogie): (a) Secondary suspension forces on bogie frame, (b) primary suspension forces on bogie frame, and (c) other forces on bogie frame.

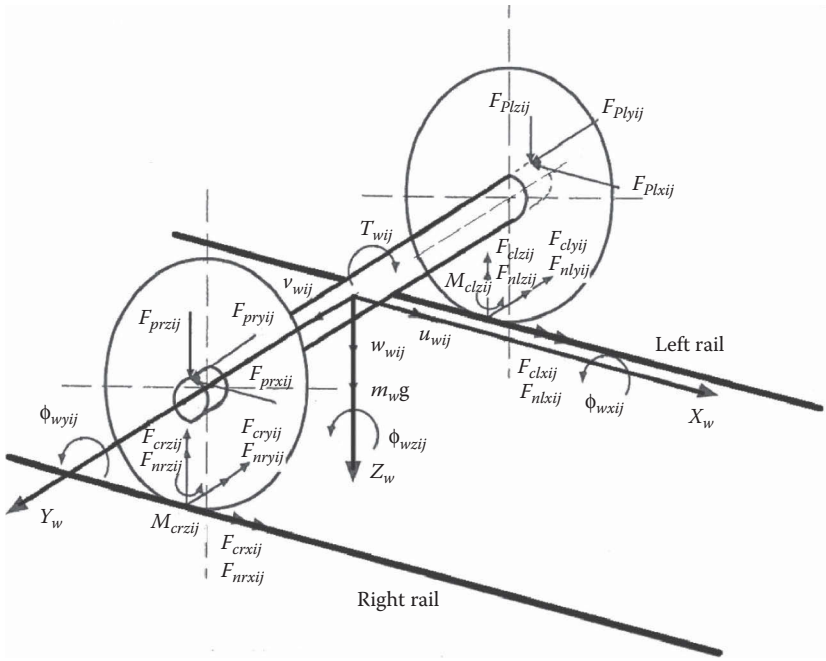

FIGURE 7.5 Free-body diagram of a typical wheelset.

7.3.2.2 Lateral Dynamic Equilibrium Equation

$$m_B\ddot{v}_B = -\sum_{j=1}^{2} F_{Sly1j} - \sum_{j=1}^{2} F_{Sry1j} + \sum_{j=1}^{3} F_{Ply1j} - \sum_{j=1}^{3} F_{Pry1j} \tag{7.36}$$

where:

F_{Ply1j} ($j = 1, 3$) is the lateral primary suspension force on the left side of the bogie frame

F_{Pry1j} ($j = 1, 3$) is the lateral primary suspension force on the right side of the bogie frame

7.3.2.3 Vertical Dynamic Equilibrium Equation

$$m_B\ddot{w}_B = -\sum_{j=1}^{2} F_{Slz1j} - \sum_{j=1}^{2} F_{Srz1j} + \sum_{j=1}^{3} F_{Plz1j} + \sum_{j=1}^{3} F_{Prz1j} + \sum_{j=1}^{3} F_{MS1j} + m_B g \tag{7.37}$$

where:

F_{Plz1j} ($j = 1, 3$) is the vertical primary suspension force on the left side of the bogie frame

F_{Prz1j} ($j = 1, 3$) is the vertical primary suspension force on the right side of the bogie frame

F_{MS1j} ($j = 1, 3$) is the force of the suspended motor on the bogie frame

In bogie modelling, the type of mounting arrangement of the traction motors must be considered, for example, wheelsets driven by traction motors suspended from the bogie frame in this case. The force F_{MS1j} can be approximated as

$$F_{MS1j} = \frac{T_{W1j}}{L_{MBS}} \tag{7.38}$$

where:

T_{W1j} is the drive torque acting on the wheelset

L_{MBS} is the longitudinal distance between the motor centre and the suspension point on the bogie frame

7.3.2.4 Roll Rotational Dynamic Equilibrium Equation

$$\begin{aligned} J_{Bx}\ddot{\phi}_{Bx} = &-H_{SSB} \times \sum_{j=1}^{2}\left(F_{Sly1j} + F_{Sry1j}\right) + B_{SS} \times \sum_{j=1}^{2}\left(-F_{Slz1j} + F_{Srz1j}\right) \\ &- H_{BP} \times \sum_{j=1}^{3}\left(F_{Ply1j} + F_{\mathrm{Pr}y1j}\right) + B_{WW} \times \sum_{j=1}^{2}\left(F_{Plz1j} - F_{Prz1j}\right) \end{aligned} \tag{7.39}$$

where:

J_{Bx} is the mass moment of inertia of the bogie frame about the X_B axis

H_{SSB} is the height between the bogie frame mass centre and the secondary suspension position

H_{BP} is the height between the bogie frame mass centre and the primary suspension position

B_{WW} is the semi-lateral width between two adjacent wheelsets in a bogie

7.3.2.5 Pitch Rotational Dynamic Equilibrium Equation

$$\begin{aligned} J_{Bz}\ddot{\phi}_{Bz} = &-H_{SSB} \times \sum_{j=1}^{2}\left(F_{Slx1j} + F_{Srx1j}\right) + L_{SS} \times \left(-F_{Slz11} - F_{Srz11} + F_{Slz12} + F_{Srz12}\right) \\ &+ H_{BP} \times \sum_{j=1}^{3}\left(F_{Plx1j} + F_{Prx1j}\right) + L_{WW} \times \left(F_{Plz11} + F_{Prz11} - F_{Plz13} - F_{Prz13}\right) \\ &- L_{MB1} \times F_{MS11} - L_{MB2} \times F_{MS12} + L_{MB3} \times F_{MS13} \end{aligned} \tag{7.40}$$

where:

J_{By} is the mass moment of inertia of the bogie frame about the Y_B axis

L_{WW} is the length between two adjacent wheelsets

L_{MM} is the length between the suspension points of two adjacent traction motors

L_{MB} is the length between the bogie frame mass centre and the suspension point of the middle traction motor

7.3.2.6 Yaw Rotational Dynamic Equilibrium Equation

$$J_{Bz}\ddot{\phi}_{Bz} = B_{SS}\times\sum_{j=1}^{2}\left(F_{Slx1j}-F_{Srx1j}\right)+L_{SS}\times\left(F_{Sly12}+F_{Sry12}-F_{Sly11}-F_{Sry11}\right)$$
$$+B_{WW}\times\sum_{j=1}^{3}\left(F_{Plx1j}-F_{Prx1j}\right)+L_{WW}\times\left(F_{Ply11}+F_{Pry11}-F_{Ply13}-F_{Pry13}\right) \quad (7.41)$$

where J_{Bz} is the mass moment of inertia of the bogie frame about Z_B axis.

7.3.3 Secondary Suspension Forces

Figures 7.3 and 7.4 show the free-body diagrams of a locomotive car body and a typical bogie frame, respectively. The secondary suspension forces acting between the car body and the bogie frame along the X, Y and Z directions are expressed in terms of the linear damping and stiffness characteristics, as shown in the following equations.

X direction:

$$F_{Skxij} = C_{Sx}\left[\dot{u}_{Bi}-H_{SB}\dot{\phi}_{Byi}\pm B_{SS}\dot{\phi}_{Bzi}-\left(\dot{u}_{Ci}+H_{CB}\dot{\phi}_{Cyi}\pm B_{SS}\dot{\phi}_{Czi}\right)\right]$$
$$+K_{Sx}\left[u_{Bi}+H_{SB}\phi_{Byi}\pm B_{SS}\phi_{Bzi}-\left(u_{Ci}+H_{CB}\phi_{Cyi}\pm B_{SS}\phi_{Czi}\right)\right] \quad (7.42)$$

Y direction:

$$F_{Skyij} = C_{Sy}\left\{-\dot{v}_{Bi}-H_{SB}\dot{\phi}_{Bxi}+(-1)^{j}L_{SS}\dot{\phi}_{Bzi}+\left[\dot{v}_{Ci}-H_{CB}\dot{\phi}_{Cxi}-(-1)^{i}\left(L_{CB}+\left(-L_{SS}\right)^{i+j}\right)\dot{\phi}_{Czi}\right]\right\}$$
$$+K_{Sy}\left\{-v_{Bi}-H_{SB}\phi_{Bxi}+(-1)^{j}L_{SS}\phi_{Bzi}+\left[v_{Ci}-H_{CB}\phi_{Cxi}-(-1)^{i}\left(L_{CB}+\left(-L_{SS}\right)^{i+j}\right)\phi_{Czi}\right]\right\} \quad (7.43)$$

Z direction:

$$F_{Skzij} = C_{Sz}\left\{\left(\dot{w}_{Bi}\mp B_{SS}\dot{\phi}_{Bxi}+(-1)^{j}L_{SS}\dot{\phi}_{Byi}\right)-\left[\dot{w}_{Ci}\pm B_{SS}\dot{\phi}_{Cxi}+(-1)^{i}\left(L_{CB}+\left(-L_{SS}\right)^{i+j}\right)\dot{\phi}_{Cyi}\right]\right\}$$
$$+K_{Sz}\left\{\left(w_{Bi}\mp B_{SS}\phi_{Bxi}+(-1)^{j}L_{SS}\phi_{Byi}\right)-\left[w_{Ci}\pm B_{SS}\phi_{Cxi}+(-1)^{i}\left(L_{CB}+\left(-L_{SS}\right)^{i+j}\right)\phi_{Cyi}\right]\right\} \quad (7.44)$$

in which C_{Sx}, C_{Sy} and C_{Sz} are the damping coefficients of the secondary suspension along the X, Y and Z axes, respectively, and K_{Sx}, K_{Sy} and K_{Sz} are the stiffness coefficients of the secondary suspension along the X, Y and Z axes, respectively.

In the above equations, when $k = l$, '$\pm$' and '$\mp$' assume '+' and '−', respectively, and when $k = r$, '$\pm$' and '$\mp$' assume '−' and '+', respectively. In addition, $i = 1, 2$ represents the number of bogie frames, and $j = 1, 2$ represents the number of secondary suspensions on the left side or the right side.

7.3.4 Traction Motor Assembly with Wheelset

Motor suspension arrangements are of paramount importance for the reliability of traction motors. The various types of traction motor suspension arrangements used on heavy haul locomotives are described in Section 3.5. For an example of the modelling of a locomotive drive system, the wheelset driven by a bogie-frame-suspended traction motor is selected here. In this case, the mass of the gear wheel is added onto the wheelset.

7.3.4.1 Equations of Dynamic Equilibrium – Wheelset

Figure 7.5 shows the free-body diagram of a typical wheelset. For convenience, the origin of the Cartesian coordinate system (X_w, Y_w, Z_w) is positioned at the centre of mass of the wheelset. The forces acting on the wheelset are also shown in Figure 7.5. The forces include the primary suspension forces (F_{Plxij}, F_{Plyij}, F_{Plzij}, F_{Prxij}, F_{Pryij} and F_{Przij}), the wheel-rail contact normal forces (F_{nlxij}, F_{nlyij}, F_{nlzij}, F_{nrxij}, F_{nryij} and F_{nrzij}), the wheel-rail contact creep forces (F_{clxij}, F_{clyij}, F_{clzij}, F_{crxij}, F_{cryij} and F_{crzij}), moments (M_{clzij} and M_{crzij}), the drive torque (T_{wij}), the friction torque (T_{fij}) and the weight ($m_w g$) of the wheelset. The subscript $i = 1, 2$ represents the number of bogie frames and the subscript $j = 1, 3$ represents the number of wheelsets in each bogie frame, giving a total of six wheelsets.

The motions of each wheelset are described with six DOFs, namely three linear displacements (u_{wij}, v_{wij}, and w_{wij}) along the X_w, Y_w and Z_w axes and three angular rotations (ϕ_{wxij}, ϕ_{wyij}, and ϕ_{wzij}) about the X_w, Y_w and Z_w axes. The differential equations of dynamic equilibrium of a typical wheelset are written as follows.

7.3.4.1.1 *Longitudinal Dynamic Equilibrium of the Wheelset*

$$m_{wij}\ddot{u}_{wij} = F_{clxij} + F_{nlxij} + F_{crxij} + F_{nrxij} - F_{Plxij} - F_{Prxij} \tag{7.45}$$

where m_{wij} is the combined mass of the wheelset and the axle mounted gear wheel.

7.3.4.1.2 *Lateral Dynamic Equilibrium of the Wheelset*

$$m_{wij}\ddot{v}_{wij} = -F_{clyij} - F_{nlyij} - F_{cryij} - F_{nryij} - F_{Plyij} - F_{Pryij} \tag{7.46}$$

7.3.4.1.3 *Vertical Dynamic Equilibrium of the Wheelset*

$$m_{wij}\ddot{w}_{wij} = -F_{clzij} - F_{nlzij} - F_{crzij} - F_{nrzij} + F_{Plzij} + F_{Przij} + m_w g \tag{7.47}$$

7.3.4.1.4 *Roll Dynamic Equilibrium of the Wheelset*

$$\begin{aligned} J_{wxij}\ddot{\phi}_{wxij} = {} & J_{wyij}\frac{V}{r_0}\dot{\phi}_{wzij} + y_{wlij}\left(F_{clzij} + F_{nlzij}\right) - y_{wrij}\left(F_{crzij} + F_{nrzij}\right) \\ & + z_{wlij}\left(F_{clyij} + F_{nlyij}\right) + z_{wrij}\left(F_{cryij} + F_{nryij}\right) + B_{SS}\left(-F_{Plzij} + F_{Przij}\right) \\ & - H_{PW}\left(F_{Plyij} + F_{Pryij}\right) \end{aligned} \tag{7.48}$$

where:

J_{wxij} and J_{wyij} are the combined mass moments of inertia of the wheelset and its larger gear system about the X_w and Y_w axes, respectively

V is the operating speed of the locomotive

r_0 is the nominal wheel radius

(y_{wlij}, z_{wlij}) and (y_{wrij}, z_{wrij}) are the lateral and vertical coordinates of the contact points on the wheelset's left and right wheels, respectively

H_{PW} is the height between the primary suspension position and the wheelset mass centre

7.3.4.1.5 Pitch Dynamic Equilibrium of the Wheelset

$$J_{wyij}\ddot{\phi}_{wyij} = z_{wlij}\left(F_{clxij} + F_{nlxij}\right) + z_{wrij}\left(F_{crxij} + F_{nrxij}\right) + H_{PW}\left(F_{Plxij} + F_{Prxij}\right) - T_{wij} + T_{fij} \quad (7.49)$$

where:

T_{wij} is the drive torque on the wheelset

T_{fij} is the friction torque

7.3.4.1.6 Yaw Dynamic Equilibrium of the Wheelset

$$\begin{aligned} J_{wzij}\ddot{\phi}_{wzij} = &-J_{wy}\frac{V}{r_0}\dot{\phi}_{wxh} + y_{wlij}\left(F_{clxij} + F_{nlxij}\right) - y_{wrij}\left(F_{crxij} + F_{nrxij}\right) \\ &- y_{wlij}\phi_{wzij}\left(F_{clyij} + F_{nlyij}\right) + y_{wrij}\phi_{wzij}\left(F_{cryij} + F_{nryij}\right) \\ &+ B_{WW}\left(-F_{Plxij} + F_{Prxij}\right) - M_{clzh} - M_{crzh} \end{aligned} \quad (7.50)$$

where J_{wzij} is the mass moment of inertia of the wheelset along the Z_w axis.

7.3.4.2 Equations of Dynamic Equilibrium – Traction Motor System

The traction motor housing is bolted onto the bogie frame. The torque from the traction motor transfers to the pinion through a flexible coupling and is then transmitted to the gear wheel through gear meshing. It is noted that the gear wheel is press-fitted onto the axle; one side is installed on the axle through the bearing, and the other side is suspended from the frame beam through a hanger rod. The movement of the gear wheel and the gear box are therefore affected by the wheelset. For this reason, the quality and inertia of the gear and gearbox need to be considered in the modelling of the wheelset. In general calculations of train dynamics and train traction, the mathematical model from the traction motor to the wheel just considers the transmission ratio of the gear box. In fact, the gear meshing in a flexible gear coupling is often considered as a quasistatic state. There is no relative movement and no torque disturbance of motor output.

To understand the dynamic behaviour of the gear system, the gear mesh dynamics equation should be established to acquire the vibration behaviour of the gearing. The transmission gear system can be simplified as a gear torsional vibration model, as shown in Figure 7.6, where θ_p and θ_g are the angular displacements of the driving pinion and driven gear, I_p and I_g are the moments of inertia of the driving pinion and

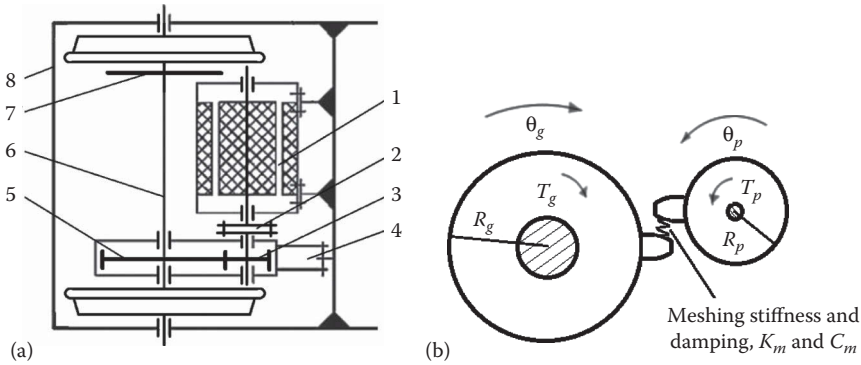

FIGURE 7.6 Traction motor drive system and modelling approach: 1 – traction motor; 2 – flexible coupling; 3 – pinion; 4 – suspension; 5 – gear wheel; 6 – wheelset; 7 – braking plate; and 8 – bogie frame.

driven gear, R_p and R_g are the base radius of the driving pinion and driven gear, i is the transmission ratio, K_m and C_m are the meshing stiffness and meshing damping coefficients, respectively, and T_p and T_g are the torques of the driving pinion and driven gear. The dynamic equations can be described as:

$$\begin{cases} I_p\ddot{\theta}_p + C_m R_p\left(R_p\dot{\theta}_p - R_g\dot{\theta}_g\right) + K_m R_p\left(R_p\theta_p - R_g\theta_g\right) = T_p \\ I_g\ddot{\theta}_g - C_m R_g\left(R_p\dot{\theta}_p - R_g\dot{\theta}_g\right) - K_m R_g\left(R_p\theta_p - R_g\theta_g\right) = T_g \end{cases} \tag{7.51}$$

The relative displacement Δw is defined as:

$$\Delta w = R_p\theta_p - R_g\theta_g \tag{7.52}$$

The above two equations can be combined as:

$$I_p I_g\Delta\ddot{w} + \left(I_g C_m R_p^2 + I_p C_m R_g^2\right)\Delta\dot{w} + \left(I_g C_m R_p^2 + I_p C_m R_g^2\right)\Delta w = I_g R_p T_p + I_p R_g T_g \tag{7.53}$$

From the above expressions, it can be seen that the whole system is a non-linear time-varying stiffness system, the meshing stiffness of the gear is constantly changing in the process of meshing and the contact force between the teeth is also a variable. Even without the external excitation, the inner gear dynamic excitation still has an influence on the gear vibration.

7.3.5 Primary Suspension Forces

Figures 7.3 and 7.4 show the free-body diagrams of a typical bogie frame and a typical wheelset, respectively. The primary suspension forces acting between the bogie frame and the wheelset can be written in the following equations.

The primary suspension force in the longitudinal (X) direction is determined as follows:

$$F_{Pkxij} = C_{Px}\left[\dot{u}_{Bi} + \dot{\phi}_{Biy}H_{BP} \pm \dot{\phi}_{Biz}B_{WW} - \left(\dot{u}_{wij} \pm \dot{\phi}_{wzij}B_{WW}\right)\right] + K_{Px}\left[u_{Bi} + \phi_{Biy}H_{BP} \pm \phi_{Biz}B_{WW} - \left(u_{wij} \pm \phi_{wzij}B_{WW}\right)\right] \tag{7.54}$$

The primary suspension force in the lateral (Y) direction is determined as follows:

$$F_{Pkyij} = \begin{cases} C_{Py}\left[\left(\dot{v}_{Bi} - \dot{\phi}_{Bix}H_{BP} + \dot{\phi}_{Biz}L_{WW}\right) - \dot{v}_{wij}\right] + K_{Py}\left[\left(v_{Bi} - \phi_{Bix}H_{BP} + \phi_{Biz}L_{WW}\right) - v_{wij}\right] & (j=1) \\ C_{Py}\left[\left(\dot{v}_{Bi} - \dot{\phi}_{Bix}H_{BP}\right) - \dot{v}_{wij}\right] + K_{Py}\left[\left(v_{Bi} - \phi_{Bix}H_{BP}\right) - v_{wij}\right] & (j=2) \\ C_{Py}\left[\left(\dot{v}_{Bi} - \dot{\phi}_{Bix}H_{BP} - \dot{\phi}_{Biz}L_{WW}\right) - \dot{v}_{wij}\right] + K_{Py}\left[\left(v_{Bi} - \phi_{Bix}H_{BP} - \phi_{Biz}L_{WW}\right) - v_{wij}\right] & (j=3) \end{cases} \tag{7.55}$$

The primary suspension force in the vertical (Z) direction is determined as follows:

$$F_{Pkzij} = \begin{cases} C_{Pz}\left[-\left(\dot{w}_{Bi} \mp \dot{\phi}_{Bix}B_{WW} - \dot{\phi}_{Biy}L_{WW}\right) + \left(\dot{w}_{wij} \pm \dot{\phi}_{wxij}B_{WW}\right)\right] \\ \quad + K_{Pz}\left[-\left(w_{Bi} \mp \phi_{Bix}B_{WW} - \phi_{Biy}L_{WW}\right) + \left(w_{wij} \pm \phi_{wxij}B_{WW}\right)\right] & (j=1) \\ C_{Pz}\left[-\left(\dot{w}_{Bi} \mp \dot{\phi}_{Bix}B_{WW}\right) + \left(\dot{w}_{wij} \pm \dot{\phi}_{wxij}B_{WW}\right)\right] \\ \quad + K_{Pz}\left[-\left(w_{Bi} \mp \phi_{Bix}B_{WW}\right) + \left(w_{wij} \pm \phi_{wxij}B_{WW}\right)\right] & (j=2) \\ C_{Pz}\left[-\left(\dot{w}_{Bi} \mp \dot{\phi}_{Bix}B_{WW} - \dot{\phi}_{Biy}L_{WW}\right) + \left(\dot{w}_{wij} \pm \dot{\phi}_{wxij}B_{WW}\right)\right] \\ \quad + K_{Pz}\left[-\left(w_{Bi} \mp \phi_{Bix}B_{WW} - \phi_{Biy}L_{WW}\right) + \left(w_{wij} \pm \phi_{wxij}B_{WW}\right)\right] & (j=3) \end{cases} \tag{7.56}$$

in which C_{Px}, C_{Py}, C_{Pz} and K_{Px}, K_{Py}, K_{Pz} are the damping and stiffness coefficients, respectively, of the primary suspension along the X, Y and Z axes.

In the above equations, when $k = l$, '$\pm$' and '$\mp$' assume '+' and '–', respectively, and when $k = r$, '$\pm$' and '$\mp$' assume '–' and '+', respectively. In addition, $i = 1, 2$ represents the number of bogie frames and $j = 1, 2$ and 3 represents the number of primary suspensions on the left side or the right side.

7.3.6 Couplers: Draft Gear Modelling

Rail vehicle connection models are described in detail in Section 5.2.3. Their modelling and simulation can be most challenging because of the high non-linearities of coupler slack, draft gear spring characteristic and stick-slip friction provided by a wedge system. As an example, the rail vehicle connection modelling for autocouplers with friction wedge type draft gear packages is examined in this section [5,6].

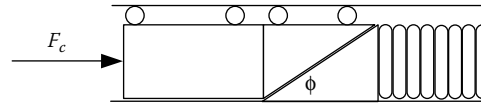

FIGURE 7.7 Free-body diagram of draft gear.

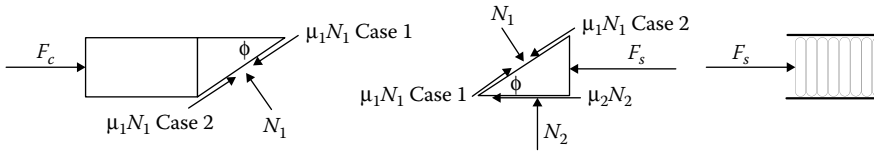

FIGURE 7.8 Force equilibrium states.

The draft gear package can be considered as a single-wedge spring system. The free-body diagram for increasing load (i.e., in compression) is shown in Figure 7.7.

The rollers on the top side of the compression rod represent that the multiple wedges are arranged symmetrically around the outside of the rod in the actual unit. Depending on the direction of motion, the wedge angles and surface conditions, different equilibrium states are possible, as shown in Figure 7.8.

From Figure 7.8, there are two possible cases. Case 1 represents the sliding action in the direction of compression. Case 2 applies if a prejammed state exists. In this case, the rod is held in by the jamming action of the wedge.

The *i*th coupler force for the loading situation in Case 1 is

$$F_{ci} = N_1(\sin\phi + \mu_1 \cos\phi) \tag{7.57}$$

Furthermore, the equations relating the wedge forces to the coupler force and the coil spring force can be developed, again assuming saturated friction states and the direction shown in Case 1, as follows

$$F_{ci} = F_{si}\left(\sin\phi + \mu_1 \cos\phi\right) / \left[\left(\mu_1 - \mu_2\right)\cos\phi + \left(1 + \mu_1\mu_2\right)\sin\phi\right] \tag{7.58}$$

In Equation 7.58, F_{si} is the coil spring force in the *i*th coupler.

Assuming that friction coefficients $\mu_1 = \mu_2 = \mu$ and that both surfaces are saturated, the equation can be reduced to

$$F_{ci} = F_{si}(\mu \cot\phi + 1) / \left[1 + \mu^2\right] \tag{7.59}$$

The other assumption made is that there is no impending motion on the sloping surface due to the seating of the rod and wedge; hence, the value assumed for μ_1 is zero, thereby reducing Equation 7.59 (including the unloading situation) to

$$F_{ci} = F_{si} \tan\phi / (\tan\phi \mp \mu_2) \tag{7.60}$$

$$F_{si} = k(x) \cdot \left(x_i - x_{i-1}\right) + c(x) \cdot \left(\dot{x}_i - \dot{x}_{i-1}\right) \left(i = 1,2,3...\right) \tag{7.61}$$

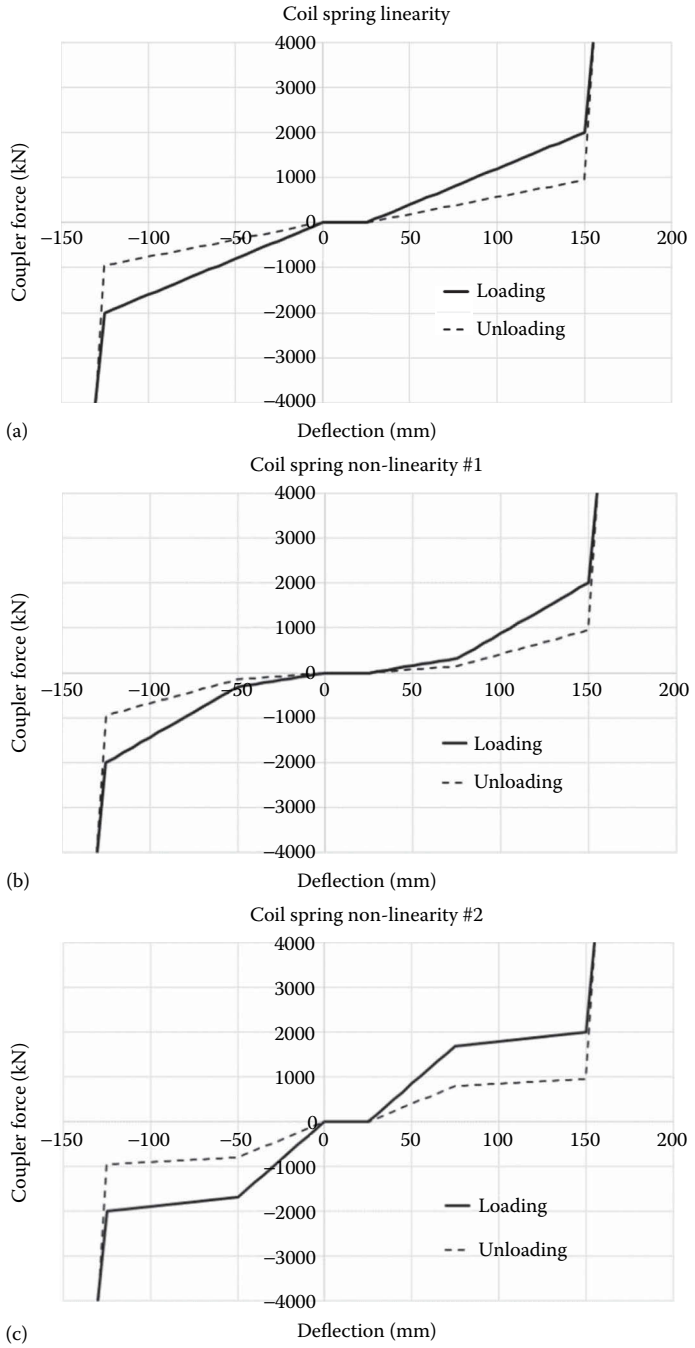

FIGURE 7.9 Examples of three types of coupler forces: (a) Coupler force with linear coil spring, (b) coupler force with hardening non-linear coil spring and (c) coupler force with softening non-linear coil spring.

In Equation 7.60, ∓ represents that '–' is the loading process, whereas '+' is the unloading process.

By way of example, the three stiffness characteristics of coil spring $k(x)$, namely linearity, hardening non-linearity and softening non-linearity, are considered. The corresponding coupler forces calculated through Equation 7.60 are shown in Figure 7.9.

In Figure 7.9, the working region of all couplers is set from –125 to 150 mm, and, at the limit of that working region, the coupler forces are set as –2000 kN and 2000 kN, respectively. Outside the limit of the working region, a locked stiffness value in the order of 80 MN/m is selected. In Figure 7.9, the solid line is the loading process, whereas the dashed line is the unloading process.

7.4 TRACK MODELLING

The cross-sectional and longitudinal views of the mathematical model used in the description of the track subsystem are schematically shown in Figure 7.10a and b, respectively. The model consists of five layers, as shown in that figure, namely (1) the rails and their pads and fastener assemblies, (2) the sleepers, (3) the ballast and the sub-ballast resting on (5) the subgrade. The rails are represented as continuous Timoshenko beams that are discretely supported on the sleepers through fasteners and pads, represented as linear spring and damping elements enclosed within a dashed-line box to signify that the mass of the enclosed components is disregarded. The sleepers are represented with mass and viscoelastic properties by springs and dampers enclosed within a solid-line box to signify that the mass is included. The ballast and sub-ballast blocks are considered as truncated pyramids for calculating their effective mass, stiffness and damping coefficients. The viscoelastic springs and dampers connecting one truncated pyramid to the other represent the continuity of the ballast and the sub-ballast in the lateral and longitudinal directions. The subgrade is modelled as viscoelastic elements without mass, which connect the sub-ballast blocks to the subgrade. The coordinate system and DOFs of each track component are also shown in Figure 7.10. Such track modelling and its variously simplified track models have been previously applied for investigations of track dynamic behaviour and performance [7–21].

7.4.1 Rail

Rail is modelled as a continuous Timoshenko beam, with its vertical deformation and rotation vanishing at both ends so as to be considered as infinitely continuous, as shown in Figure 7.11.

Timoshenko beam theory [22] expresses the equations for the vertical deflection and rotation of the rail at any point under the action of forces as:

$$\begin{cases} \rho A \dfrac{\partial^2 w_R}{\partial t^2} - GAk\left(\dfrac{\partial^2 w_R}{\partial x^2} - \dfrac{\partial \phi_R}{\partial x} \right) = -\displaystyle\sum_{i=1}^{N_s} F_{RSi}\delta(x - x_i) + \sum_{j=1}^{4} P_{WRj}\delta\left(x - x_j\right) \\ \rho I \dfrac{\partial^2 \phi_R}{\partial t^2} - GAk\left(\dfrac{\partial w_R}{\partial x} - \phi_R \right) - EI \dfrac{\partial^2 \phi_R}{\partial x^2} = 0 \end{cases} \tag{7.62}$$

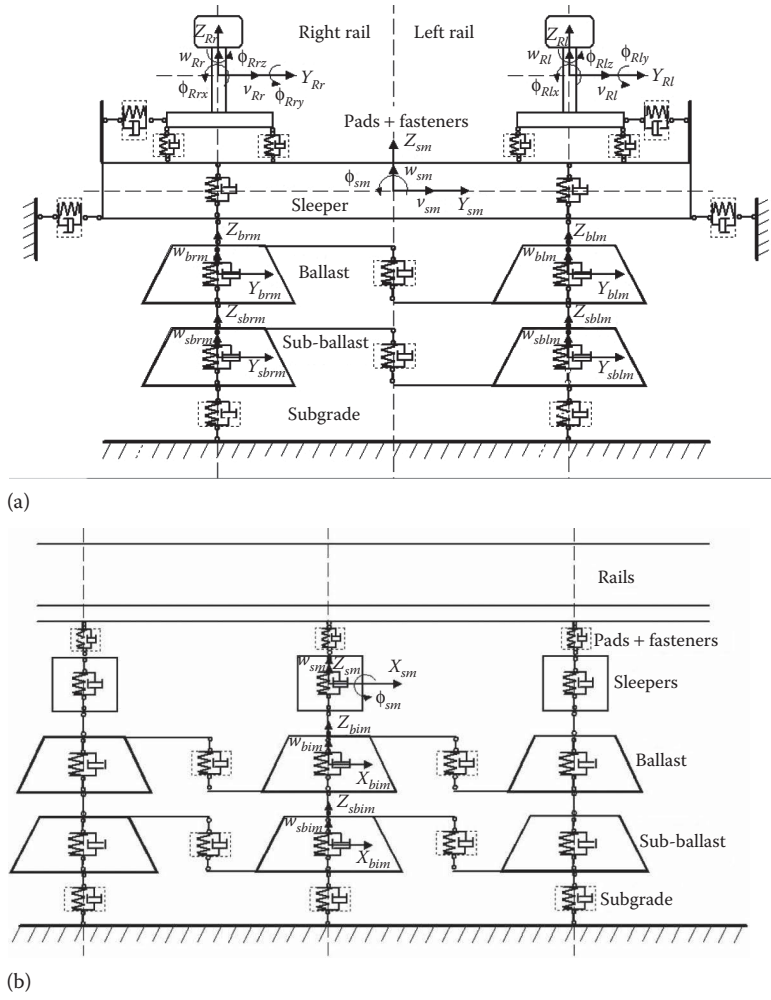

FIGURE 7.10 Schematic diagram of the track model: (a) Cross-sectional view and (b) longitudinal view.

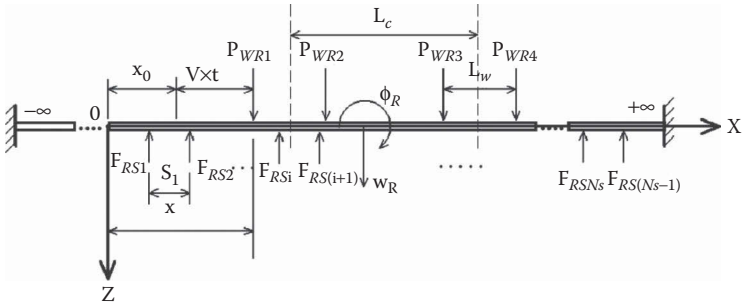

FIGURE 7.11 Timoshenko beam model of rail.

where:

w_R is the vertical deflection of the rail
ϕ_R is the rotation of the rail
ρ is the rail density
A is the rail cross-sectional area
G is the shear modulus of the rail
E is the Young's modulus of the rail material
I is the second moment of area of the rail section
k is the Timoshenko shear coefficient
F_{RSi} is the reaction force between the rail and the ith sleeper
P_{WRj} is the contact force between the jth wheel and the rail
$\delta(x)$ is the Dirac delta function
x_i is the position of the ith sleeper
x_j is the position of the jth wheel
N_s is the number of sleepers considered

The subscripts i and j are used for the sleeper count and the wheel count, respectively.

The vertical deflection w_R and rotation ϕ_R of the rail are obtained using modal superposition, as given by:

$$\begin{cases} w_R = \sum_{h=1}^{N_c} N_w(h,x)\cdot W_h(t) \\ \phi_R = \sum_{h=1}^{N_c} N_\phi(h,x)\cdot \Phi_h(t) \end{cases} \tag{7.63}$$

where:

$N_w(h, x)$ and $N_\phi(h, x)$ are the hth mode shape functions of the vertical deflection and rotation, respectively, of the rail
$W_h(t)$ and $\Phi_h(t)$ are the hth mode time coefficients of the vertical deflection and rotation, respectively, of the rail
N_c is the number of modes considered
x is the linear coordinate along the length of the rail beam

By substituting Equation 7.63 into Equation 7.62, we modify Equation 7.62 (a partial differential equation) to produce Equation 7.64 (an ordinary differential equation). This transformation facilitates the application of the numerical integration method to solve the equations.

$$\begin{cases} \frac{d^2W_h}{dt^2} + \frac{Gk}{\rho}\left(\frac{\Pi h}{L}\right)^2 W_h - \sqrt{\frac{A}{I}}\frac{Gk}{\rho}\left(\frac{\Pi h}{L}\right)\Phi_h = -\sum_{i=1}^{N_s} F_{RSi}N_w(h,x_i) + \sum_{j=1}^{4} P_{WRj}N_w\left(h,x_j\right) \\ \frac{d^2\Phi_h}{dt^2} + \left(\frac{GAk}{\rho I} + \frac{E}{\rho}\left(\frac{\Pi h}{L}\right)^2\right)\Phi_h - \sqrt{\frac{A}{I}}\frac{Gk}{\rho}\left(\frac{\Pi h}{L}\right)W_h = 0 \quad \left(h = 1, 2, \ldots, N_c\right) \end{cases} \tag{7.64}$$

in which L is the length of the rail considered, and the reaction force between the rail and the ith sleeper F_{RSi} is expressed as:

$$F_{RSi} = (C_{pi} + C_{fi}) \sum_{m=1}^{N_c} N_w(m, x_i) \cdot \dot{W}_m + (K_{pi} + K_{fi}) \sum_{m=1}^{N_c} N_w(m, x_i) \cdot W_m - (C_{pi} + C_{fi}) \dot{w}_{si} - (K_{pi} + K_{fi}) w_{si} \quad (7.65)$$

where w_{si} is the vertical displacement of the ith sleeper. C_{pi}, K_{pi} and C_{fi}, K_{fi} are the damping and stiffness coefficients of the ith pad and the ith fastener assembly, respectively.

In Equation 7.64, the contact force P_{WRj} between the jth wheel and the rail is determined by non-linear Hertz contact theory and is given as:

$$P_{WRj}(t) = \begin{cases} C_H \left\{ w_{wj}(t) - w_r(x_{pj}, t) - w_d(t) \right\}^{3/2} & \text{if } w_{wj}(t) - w_r(x_{pj}, t) - w_d(t) > 0 \\ 0 & \text{if } w_{wj}(t) - w_r(x_{pj}, t) - w_d(t) < 0 \end{cases} \quad (7.66)$$

where:

$w_{wj}(t)$ and $w_r(x_{pj}, t)$ are the displacements of the wheel and the rail, respectively, at the jth contact point

$w_d(t)$ is the wheel and/or the rail irregularity function (e.g., an out-of-round wheel, rail corrugation or rail surface geometric irregularity)

C_H is the Hertz contact coefficient that can be deduced from [23] as follows:

$$C_H = \frac{4 G_{wr} \sqrt{R_e}}{3(1 - v_{wr})} \quad (7.67)$$

in which G_{wr} is the shear modulus, v_{wr} is the Poisson's ratio and $R_e = \sqrt{rR}$, where r is the rolling radius of the wheel and $R = \dfrac{\rho_w R_t}{\rho_w - r}$ (ρ_w and R_t are the wheel profile radius and the rail profile radius, respectively).

In Equation 7.66, the contact force P_{WRj} is calculated based on the relative displacement between the wheel and the rail at the point of contact x_{pj}. This point is easily determined by keeping the angle between the vertical diameter of the wheel and the axis of the rail as 90° for the nondefect wheels and rails. However, where defects (in the wheel or the rail) are encountered, the angle between the diameter of the wheel drawn through the point of contact and the axis of the rail varies from 90°. The exact point of contact is determined in such cases by dividing the contact length obtained from static Hertz analysis into smaller segments and checking each segment for potential contact. A similar approach has been reported by Dong et al. [24].

7.4.2 Pads, Fasteners, and Sleepers

Rubber or high-density polyethylene mats that are used as a bearing layer between the rails and the concrete sleepers are commonly known as pads. Rail fasteners

connect the rails and the sleepers together. The elasticity of the fasteners is measured by the spring rate, which is the amount of deflection proportional to the clamping force. In the model, both the pads and the fasteners are modelled as linear springs and dampers without mass.

Sleepers are the track components that tie the two rails together at the required track gauge, thereby providing monolithic action to the track. Sleepers are positioned between the rails and the ballast and are represented in the model by their mass, stiffness and damping properties. The stiffness of sleepers is calculated using the influence coefficient approach by considering the sleepers as beams on an elastic foundation, as proposed by Profillidis [25]. The track structure has been considered as medium quality for the evaluation of the sleeper stiffness. The damping coefficient is then determined based on the values of stiffness and mass.

7.4.3 Ballast and Sub-Ballast

The ballast ensures damping of the traffic-imposed vibrations and distributes the rail vehicle loads evenly to the subgrade. The sub-ballast protects the top surface of the subgrade from penetration of the ballast stone particles, in addition to further distributing the load. Ahlbeck et al. [26] developed the ballast pyramid model based on the theory of elasticity. The ballast—sub-ballast pyramid model assumes that the loading and pressure distribution are uniform throughout the depth. The model is divided into the upper and lower sections, which reflects the actual transmission of the loading. Zhai and Sun [27] defined the vibration of the ballast as a single block, based on the observation that the accelerations of the individual particles in both upper and lower surfaces of the ballast block do not vary significantly, even though such a conclusion is not universal. The oscillating mass of each ballast block is calculated by multiplying the volume of the ballast block by the ballast density. According to Ref. [26], the stiffness of the ith ballast block K_{bl} is

$$K_{bl} = \frac{2\tan\theta_b(L_s - B_s)E_b}{\ln\left[[L_s(2\tan\theta_b H_b + B_s)]/[B_s(2\tan\theta_b H_b + L_s)]\right]} \tag{7.68}$$

in which L_s and B_s are the effective length and width, respectively, of the support area of the rail seat, E_b is the modulus of elasticity of the ballast in N/m^2, θ_b is the internal friction angle of ballast (20° is chosen for ballast, as suggested in Ref. [26]) and H_b is the height of the ballast layer.

Similarly, the stiffness of the ith sub-ballast block K_{sb} is given by

$$K_{sb} = \frac{2\tan\theta_{sb}(L_s - B_s)E_{sb}}{\ln\left[\dfrac{(2\tan\theta_b H_b + L_s)(2\tan\theta_{sb}H_{sb} + 2\tan\theta_b H_b + B_s)}{(2\tan\theta_b H_b + B_s)(2\tan\theta_{sb}H_{sb} + 2\tan\theta_b H_b + L_s)}\right]} \tag{7.69}$$

in which E_{sb} is the modulus of elasticity of the sub-ballast in N/m^2, θ_{sb} is the internal friction angle of the sub-ballast (35° is chosen for sub-ballast) and H_{sb} is the height of the sub-ballast.

The damping coefficients of the ballast and sub-ballast are determined as 40% of their critical damping coefficients. This damping ratio (40%) is considered realistic for earth structures, and these values agree with the range given by Grassie et al. [28] (e.g., the values for post-tamping and pre-tamping of tracks were 30 and 82 kNs/m, respectively).

The oscillating masses of each ballast block M_{bl} and sub-ballast block M_{sb} are given by

$$M_{bl} = \rho_b \left[L_s B_s + H_b \tan\theta_b (L_s + B_s) + \frac{4}{3} H_b^2 \tan^2 \theta_b \right] \tag{7.70}$$

$$M_{sb} = \rho_{sb} \left[(L_s + 2\tan\theta_b)(B_s + 2\tan\theta_b) + H_{sb} \tan\theta_{sb} (L_s + B_s + 4\tan\theta_b) + \frac{4}{3} H_{sb}^2 \tan^2 \theta_{sb} \right] \tag{7.71}$$

The subgrade stiffness K_{sg} is expressed as

$$K_{sg} = E_{sg} (2\tan\theta_{sb} H_{sb} + 2\tan\theta_b H_b + L_s)(2\tan\theta_{sb} H_{sb} + 2\tan\theta_b H_b + B_s) \tag{7.72}$$

in which E_{sg} is the modulus of elasticity of the subgrade in N/m^3.

In the longitudinal direction, the continuity of the ballast and sub-ballast is ensured by including viscoelastic elements (without mass), which connect the blocks of ballast and sub-ballast in their respective layers. The coefficients of these longitudinal springs and dampers are calculated by multiplying their respective vertical stiffness and damping coefficients by a factor of 0.3. This factor is not sensitive to the dynamic responses at the interface between the rail vehicle and the track.

The equations of motion for the *i*th sleeper, ballast block and sub-ballast block are established from the basic dynamic equilibrium concept.

For the *i*th sleeper

$$\begin{aligned} M_s \ddot{w}_{si} &+ \left(C_{pi} + C_{fi} + \frac{C_{sli} C_{bli}}{C_{sli} + C_{bli}} \right) \dot{w}_{si} + \left(K_{pi} + K_{fi} + \frac{K_{sli} K_{bli}}{K_{sli} + K_{bli}} \right) w_{si} \\ &- (C_{pi} + C_{fi}) \sum_{m=1}^{N_c} N_w(m, x_i) \cdot \dot{W}_m - (K_{pi} + K_{fi}) \sum_{m=1}^{N_c} N_w(m, x_i) \cdot W_m \\ &- \frac{C_{sli} C_{bli}}{C_{sli} + C_{bli}} \dot{w}_{bli} - \frac{K_{sli} K_{bli}}{K_{sli} + K_{bli}} w_{bli} = 0 \end{aligned} \tag{7.73}$$

For the *i*th ballast block:

$$\begin{aligned} M_{bl} \ddot{w}_{bli} &+ \left(\frac{C_{sli} C_{bli}}{C_{sli} + C_{bli}} + C_{sbi} + 2C_{jbi} \right) \dot{w}_{bli} + \left(\frac{K_{sli} K_{bli}}{K_{sli} + K_{bli}} K_{sbi} + 2K_{jbi} + \right) w_{bli} \\ &- \frac{C_{sli} C_{bli}}{C_{sli} + C_{bli}} \dot{w}_{si} - \frac{K_{sli} K_{bli}}{K_{sli} + K_{bli}} w_{si} - C_{sbi} \dot{w}_{sbi} - K_{sbi} w_{sbi} - C_{jbi} \dot{w}_{bl(i-1)} \\ &- K_{jbi} w_{bl(i-1)} - C_{jbi} \dot{w}_{bl(i+1)} - K_{jbi} w_{bl(i+1)} = 0 \end{aligned} \tag{7.74}$$

For the *i*th sub-ballast block:

$$M_{sb}\ddot{w}_{sbi}+\left(C_{sbi}+C_{sgi}+2C_{jsbi}\right)\dot{w}_{sbi}+\left(K_{sbi}+K_{sgi}+2K_{jsbi}\right)w_{sbi}$$
$$-C_{sbi}\dot{w}_{bli}-K_{sbi}w_{bli}-C_{jsbi}\dot{w}_{sb(i-1)}-K_{jsbi}w_{sb(i-1)}-C_{jsbi}\dot{w}_{bl(i+1)}$$
$$-K_{jbi}w_{bl(i+1)}=0 \tag{7.75}$$

In Equations 7.73, 7.74 and 7.75, M_s, M_{bl} and M_{sb} are the masses of the sleeper, the ballast block and the sub-ballast block, respectively; C_{sli}, K_{sli}; C_{bli}, K_{bli} and C_{sbi}, K_{sbi} are the damping and stiffness coefficients of the *i*th sleeper, the *i*th ballast block and the *i*th sub-ballast block, respectively; C_{jbi}, K_{jbi} and C_{jsbi}, K_{jsbi} are the damping and stiffness coefficients between the *i*th ballast block and its adjacent ballast blocks and between the *i*th sub-ballast block and its adjacent sub-ballast blocks, respectively; C_{sgi}, K_{sgi} are the damping and stiffness coefficients of the subgrade; w_{bli}, w_{sbi} are the vertical displacements of the *i*th ballast and sub-ballast blocks; $w_{bl(i-1)}, w_{bl(i+1)}$ and $w_{sb(i-1)}, w_{sb(i+1)}$ are the vertical displacements of the ballast and sub-ballast blocks, respectively, adjacent to the *i*th ballast and sub-ballast blocks.

7.4.4 Dynamics of Complete Locomotive-Track System

The equations of the complete locomotive-track system are obtained by assembling the equations from Section 7.3 and Sections 7.4.1 through 7.4.3 in a matrix form, as shown in Equations 7.76 and 7.77 for the locomotive and rail track, respectively.

$$\left[M_L\right]\left\{\ddot{q}_L\right\}+\left[C_L\right]\left\{\dot{q}_L\right\}+\left[K_L\right]\left\{q_L\right\}=\left\{F_{LT}\right\} \tag{7.76}$$

where:

M_L, C_L and K_L are the mass, damping and stiffness matrices of the locomotive subsystem

q_L is the displacement vector of the locomotive subsystem

F_{LT} is the interface force vector between the locomotive and the track subsystems consisting of the wheel-rail contact normal forces, tangent creep forces and creep moments about the normal direction to the wheel-rail contact plane, which are discussed and determined in Section 7.5.

$$\left[M_T\right]\left\{\ddot{q}_T\right\}+\left[C_T\right]\left\{\dot{q}_T\right\}+\left[K_T\right]\left\{q_T\right\}=\left\{\widetilde{F}_{LT}\right\} \tag{7.77}$$

where:

M_T, C_T and K_T are the mass, damping and stiffness matrices of the track subsystem

q_T is the displacement vector of the track subsystem, which includes the modal and physical displacements

$\widetilde{F}_{LT}$ is the combined interface force vector between the locomotive and the track subsystems

7.5 CONTACT MODELLING AT THE WHEEL-RAIL INTERFACE

Research on wheel-rail contact mechanics has a history that goes back to 1926, when Carter [29] provided a two-dimensional solution for rolling contact by applying the Hertz normal contact theory. In 1958, Johnson [30] provided a two-dimensional solution, including spin and in 1964, Johnson and Vermeulen together [31] obtained a closed-formula solution for rolling contact problems including both longitudinal and lateral creepages. Kalker [32] generated a successful linear theory in 1967 which provided the basis of other approaches, notably the 1982 simplified theory of Kalker [33], the 1983 model of Shen, Hedrick and Elkins [34] and the 1999 model and associated FASTSIM computer code of Polach [35]. Kalker [36] also extended his previous work to three-dimensional elastic bodies in rolling contact in 1990.

In this section, basic wheel-rail normal contact theory is initially introduced, along with wheel-rail normal contact forces, and then the various wheel-rail tangential contact theories and methods for the determination of tangential forces are described.

7.5.1 Wheel-Rail Contact – The Normal Problem

Despite their small size, wheel-rail contact patches are difficult to analyse, partly because of the complex wheel and rail geometry involved, particularly as wheelsets move laterally and yaw as they travel along the track [37–39]. One of the first steps in the analysis is to determine the shape, size, normal force on and pressure distribution within wheel-rail contact patches, as determined from vehicle weight and wheel-rail geometry [40]. Point or nonconformal contact usually occurs between wheels and rails, but some combinations of new and/or worn wheel and rail profiles can result in conformal contact that occurs along a rail [38]. During flanging, or when a rail vehicle passes over a turnout, it is also possible for two or more contact patches to form at each wheel-rail interface [41]. Further complications arise because of the highly concentrated stresses in contact areas, as well as the open nature of the system where contaminants such as water, dust and even small stones or leaves can affect the contact conditions [39]. Once the normal contact force and contact patch shapes have been found, the tangential force distribution within the contact patches can be calculated.

In light of this, wheel-rail contact modelling is an important part of locomotive traction analysis and rail vehicle dynamics in general, and several methods have been devised to model contact patch phenomena. The following section describes Hertz theory, which is widely used to calculate normal pressure distributions in the contact patch for MBS studies.

7.5.1.1 Normal Contact (Hertz) Theory

Nonconformal contact between two surfaces was first studied by Hertz [38,42]. Two bodies in nonconformal contact, which are the wheel and the rail in the railway case, are assumed to be elastic, frictionless half-spaces with continuous contact surfaces. These are loaded over an elliptical contact patch that is small in comparison with the dimensions and surface radii of the contacting bodies. Body surface curvatures are assumed to be constant in the contact patch, allowing the contact surface to be flat. The assumption of two half-spaces in nonconformal contact allows the resulting

semi-ellipsoidal pressure distribution in the contact patch to be separately considered from the bodies' general stress state; in other words, stresses in the contact area vanish some distance away from it [38,39].

The semi-axes a and b of the contact ellipse can be found with the following formulas in [38,43].

$$
\begin{aligned}
&a = m \cdot \sqrt[3]{\frac{3\pi \cdot N \cdot (k_1 + k_2)}{4 \cdot k_3}}, \quad b = n \cdot \sqrt[3]{\frac{3\pi \cdot N \cdot (k_1 + k_2)}{4 \cdot k_3}} \\
&k_1 = \frac{1 - \upsilon_R{}^2}{E_W}, \quad k_2 = \frac{1 - \upsilon_W{}^2}{E_R}, \quad k_3 = \frac{1}{2}\left[\frac{1}{r_1} + \frac{1}{r_1'} + \frac{1}{r_2} + \frac{1}{r_2'}\right], \\
&k_4 = \frac{1}{2} \cdot \sqrt[2]{\left(\frac{1}{r_1} - \frac{1}{r_1'}\right)^2 + \left(\frac{1}{r_2} - \frac{1}{r_2'}\right)^2 + 2\left(\frac{1}{r_1} - \frac{1}{r_1'}\right)\left(\frac{1}{r_2} - \frac{1}{r_2'}\right)\cos 2\psi}, \\
&\theta = \arccos\left(\frac{k_4}{k_3}\right)
\end{aligned}
\tag{7.78}
$$

where:

a, b are the contact ellipse semi-axes

k_1, k_2, k_3, k_4 are coefficients based on wheel and rail material and geometric properties

m, n are the Hertz coefficients, described in the following paragraph

N is the normal contact force

v_R is Poisson's ratio for rail material

v_W is Poisson's ratio for wheel material

E_R is elastic modulus for rail material

E_W is elastic modulus for wheel material

r_1 is the principal rolling radius of the wheel at the contact point

r_1' is the principal transverse radius of the wheel profile curvature at the contact point

r_2 is the principal rolling radius of the rail at the contact point, assumed to be infinite

r_2' is the principal transverse radius of the rail profile curvature at the contact point

θ is the angle between contacting planes

ψ is the yaw angle between the longitudinal direction of a wheelset and track centreline

m and n are coefficients that can be calculated using the following formulas [39], allowing for the interval $0 < n/m < \infty$.

$$
A = \frac{1}{2}\left(\frac{1}{r_1} + \frac{1}{r_2}\right), \quad B = \frac{1}{2}\left(\frac{1}{r_1'} + \frac{1}{r_2'}\right), \quad n\left(\frac{A}{B}\right) = m\left(\frac{1}{A/B}\right) \tag{7.79}
$$

where:

A is the rolling (longitudinal) curvature at contact point

B is the transverse (lateral) curvature at contact point

TABLE 7.1
Hertz Coefficients for $0° \leq \theta \leq 180°$

θ°	0	5	10	30	60	90	120	150	170	175	180
A/B	0	0.002	0.008	0.072	0.333	1.000	3.000	13.93	130.6	524.6	∞
n/m = b/a	0	0.021	0.047	0.181	0.483	1.000	2.072	5.538	21.26	47.20	∞
M	∞	11.238	6.612	2.731	1.486	1.000	0.717	0.493	0.311	0.238	0

Source: Ayasse, J.-B. and Chollet, H., Wheel-rail contact, *Handbook of Railway Vehicle Dynamics*, S. Iwnicki (ed.), Taylor & Francis Group, Boca Raton, FL, pp. 85–120, 2006.

Alternatively, the coefficients m and n can be interpolated from Table 7.1.

As the pressure distribution in the contact patch is semi-ellipsoidal, the contact pressure along the contact patch's longitudinal x and lateral y axes is given by [44]:

$$p_z(x,y) = \frac{3N}{2\pi ab}\sqrt{1-\left(\frac{x}{a}\right)^2-\left(\frac{y}{b}\right)^2} \tag{7.80}$$

where:
p is the contact pressure
x is the longitudinal contact patch axis
y is the lateral contact patch axis

The total normal force is derived by integration of Equation 7.80 [45]:

$$N = \int_{-b}^{b}\int_{-a}^{a} p_z(x,y)\,dxdy$$

Hertz theory is widely used today to estimate the size of and stress distribution within contact patches for use in vehicle dynamic analysis and many tangential contact algorithms, but there are a few drawbacks to consider when conducting more advanced simulations such as traction modelling, flanging and vehicle response to turnouts. Although modifications can be made to detect multiple contact points, there are problems with modelling slender contact ellipses such as occur, for example, when contact is made with the inside corner of the high rail during flanging. As Hertz theory is concerned with only nonconformal contact and assumes an elliptical contact patch shape, it understandably cannot model conformal contact and has trouble modelling nonelliptical contact patches [39,46–48].

7.5.2 Wheel-Rail Tangential Contact Modelling

After the normal problem is solved, the common modelling approach is to find contact stresses and creep forces at the wheel-rail interface. Although different theories

can be used for tangential contact modelling, not all of them are appropriate for locomotive traction and braking studies. However, the theories described in this section provide a general understanding of the modelling principles of the physical processes at the contact interface, which are used as a basis for creep force modelling at the wheel-rail interface for locomotives under traction and braking.

7.5.2.1 Kalker Linear Theory

In order to solve the stationary tangential contact problem, Kalker used an analytical approach. With the assumption that the normal contact is Hertzian and that the stick zone covers the entire contact patch, Kalker solved the constitutive equations in 1967 by assuming the tangential stress distribution to be of a polynomial form. In principle, it is possible to apply higher-order polynomials as an approximation, but the complexity of the calculations increases with the number of polynomial coefficients. Using a special-order approximation method, Kalker found a linear relation between the tangential force and the creepage. Assuming steady-state rolling contact, the creep forces and the spin moment can be described in matrix form, as follows, using creep coefficients c_{ik}, which have been calculated by Kalker:

$$\begin{bmatrix} F_x \\ F_y \\ M \end{bmatrix} = -Gab \begin{bmatrix} c_{11} & 0 & 0 \\ 0 & c_{22} & \sqrt{ab}c_{23} \\ 0 & -\sqrt{ab}c_{23} & abc_{33} \end{bmatrix} \begin{bmatrix} \zeta_x \\ \zeta_y \\ \varphi \end{bmatrix}, \quad \frac{\nu}{G} = \frac{1}{2}\left[\frac{\nu_W}{G_W} + \frac{\nu_R}{G_R}\right] \tag{7.81}$$

where:

a and b are the semi-axes of the contact ellipse
G is the combined shear modulus of rigidity of rail and wheel materials
G_R is the shear modulus of rigidity for rail material
G_W is the shear modulus of rigidity for wheel material
v is combined Poisson's ratio of rail and wheel materials
v_R is Poisson's ratio for rail material
v_W is Poisson's ratio for wheel material
c_{11}, c_{22}, c_{23}, c_{33} are Kalker's creepage and spin coefficients
ζ_x, ζ_y, φ are the longitudinal, lateral and spin creepages, respectively

The methods used to calculate creepages are briefly described by first referring to Figure 7.12, which depicts a wheel rolling over a rail at the contact point *P*.

The symbols used in Figure 7.12 are:

$\dot{u}_w$ is the wheel velocity
$\dot{\phi}_{wy}$ is the wheel angular velocity
n_R is unit normal to wheel-rail surfaces at contact point
t_{R1} is unit longitudinal tangent to wheel-rail surfaces at contact point
t_{R2} is unit lateral tangent to wheel-rail surfaces at contact point
P is the contact point

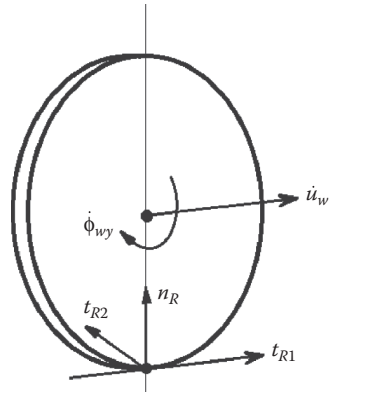

FIGURE 7.12 Wheel-rail contact frame.

The longitudinal, lateral and spin creepages can now be defined as follows:

$$\begin{cases} \zeta_x = \dfrac{(\dot{u}_{WP} - \dot{u}_{RP}) \cdot t_{R1}}{V} \\ \zeta_y = \dfrac{(\dot{v}_{WP} - \dot{v}_{RP}) \cdot t_{R2}}{V} \\ \varphi = \dfrac{(\dot{\phi}_{WP} - \dot{\phi}_{RP}) \cdot n_R}{V} \end{cases} \tag{7.82}$$

where:

V is the locomotive velocity

$\dot{u}_P$, $\dot{v}_P$ and $\dot{\phi}_P$ are longitudinal and lateral velocities and yaw rotation velocity, respectively, at contact point P

ζ_x is longitudinal creepage

ζ_y is lateral creepage

φ is spin creepage

subscripts used are W for wheel and R for rail

7.5.2.2 Kalker Simplified Theory

In the simplified theory of wheel-rail rolling contact, an approximate relation between the tangential surface displacement (u_W, v_W) of the wheel and the tangential surface traction (p_{Wx}, p_{Wy}) acting on the wheel is assumed as:

$$(u_W, v_W) = L_W (p_{Wx}, p_{Wy}) \tag{7.83}$$

where L_W is a flexibility parameter, effectively $1/E_W$, where E_W is the modulus of elasticity of the wheel material.

It should be noted that the normal displacement cannot be approximated by a relationship similar to Equation 7.83 because of the lack of accuracy in the normal

simplified relationship. Hertz theory, whereby the contact becomes elliptical and the normal traction distribution is semi-ellipsoidal, is used instead.

Considering the rail surface that is in contact with the wheel, Newton's third law requires that the following relationship exists between the surface tractions acting on the wheel and rail:

$$(p_{Wx}, p_{Wy}) = -(p_{Rx}, p_{Ry}) \tag{7.84}$$

The displacement difference can be written as

$$(u,v) = (u_W - u_R, v_W - v_R) = (L_W + L_R)(p_x, p_y) = L_{WR}(p_x, p_y) \tag{7.85}$$

Under linear theory, the stick area covers the entire elliptical contact area U, where $\left(U = \left\{(x,y,z) | z = 0, (x/a)^2 + (y/a)^2 \le 1\right\}\right)$, and this assumption corresponds to only small tractions. With the simplified approximation of $(u, v) = L_{WR}(p_x, p_y)$, and for steady state rolling, the following equation can be derived:

$$(p_x, p_y) = \begin{cases} \dfrac{\left(\zeta_x x - \varphi xy + k(y),\ \zeta_y x + \dfrac{\varphi x^2}{2} + l(y)\right)}{L_{WR}} & x \in U \\ (0,\ 0) & x \notin U \end{cases} \tag{7.86}$$

where k and l are arbitrary functions of y for which their derivatives with respect to x vanish.

In the contact patch, the leading edge is denoted by: $x_L = a(y) > 0$, $\left(a(y) = a\sqrt{1-(y/b)^2}\right)$, and the trailing edge is then $x_T = -a(y) < 0$. Therefore, $k(y)$ and $l(y)$ can be written as:

$$\begin{cases} k(y) = -\zeta_x a(y) + \varphi a(y) y \\ l(y) = -\zeta_y a(y) - \varphi a(y)^2 y \end{cases} \tag{7.87}$$

For the stick case, the relationships between tangential forces and creepages are expressed as:

$$\begin{cases} F_x = \displaystyle\int_{-b}^{b} \int_{-a(y)}^{a(y)} p_x(x,y)\, dxdy = -\frac{8a^2 b \zeta_x}{3L} \\ F_y = \displaystyle\int_{-b}^{b} \int_{-a(y)}^{a(y)} p_y(x,y)\, dxdy = -\frac{8a^2 b \zeta_y}{3L} - \frac{\pi a^3 b \varphi}{4L} \end{cases} \tag{7.88}$$

These are the forces calculated by the simplified theory. On the other hand, F_x and F_y can be calculated by the exact theory of elasticity, as shown in Equation 7.81.

The flexibility parameter L_{WR} shown in Equation 7.85 can be calculated by equating the coefficients of ζ_x, ζ_y and φ from both the simplified theory and the exact theory, giving three expressions for flexibilities as

$$\begin{cases} \text{for } \zeta_x,\ L_1 = \dfrac{8a}{3Gc_{11}} \\ \text{for } \zeta_y,\ L_2 = \dfrac{8a}{3Gc_{22}} \\ \text{for } \varphi,\ L_3 = \dfrac{\pi a^2}{4G\sqrt{ab}c_{23}} \end{cases} \tag{7.89}$$

The value of L_{WR} as a weighted mean of the range of L_i ($i = 1, 2, 3$) can be formed as

$$L_{WR} = \frac{L_1|\zeta_x| + L_2|\zeta_y| + L_3|\varphi|\sqrt{ab}}{\sqrt{\zeta_x^2 + \zeta_y^2 + ab\varphi^2}} \tag{7.90}$$

The longitudinal and lateral components of total creepage (relative slip) are given as

$$\begin{cases} s_x = \zeta_x - \varphi y - L_{WR}\dfrac{\partial p_x}{\partial x} = \zeta_x - \varphi y - L_{WR}\dfrac{p_x(x,y) - p_x(x-\Delta x, y)}{\Delta x} \\ s_y = \zeta_y + \varphi x - L_{WR}\dfrac{\partial p_y}{\partial x} = \zeta_y + \varphi x - L_{WR}\dfrac{p_y(x,y) - p_y(x-\Delta x, y)}{\Delta x} \end{cases} \tag{7.91}$$

In the stick area, $s_x = s_y = 0$, and this yields:

$$\begin{cases} p_x(x-\Delta x, y) = \dfrac{(\zeta_x - \varphi y)\Delta x}{L} + p_x(x,y) \\ p_y(x-\Delta x, y) = \dfrac{(\zeta_y + \varphi x)\Delta x}{L} + p_y(x,y) \end{cases} \tag{7.92}$$

For the slip area, the following algorithm is used.

Step 1

Determine the tangential force with rigid slip:

$$\begin{cases} p'_x(x-\Delta x, y) = p_z\mu(\zeta_x - \varphi y)/|\zeta_x - \varphi y| \\ p'_y(x-\Delta x, y) = p_z\mu(\zeta_y + \varphi x)/|\zeta_y + \varphi x| \end{cases} \tag{7.93}$$

where:

μ is the coefficient of friction

$p_z(x, y)$ is the normal pressure

In the simplified theory, $p_z(x, y)$ can be determined as

$$p_z(x,y) = \frac{2F_z}{\pi ab}\left\{1-(x/a)^2-(y/b)^2\right\} \tag{7.94}$$

where F_z is the compressive force.

Step 2

Calculate the longitudinal and lateral components of total creepage (relative slip) as

$$\begin{cases} s_x \approx \zeta_x - \varphi y - L_{WR}\dfrac{p_x(x,y)-p'_x(x-\Delta x,y)}{\Delta x} \\ s_y \approx \zeta_y + \varphi x - L_{WR}\dfrac{p_y(x,y)-p'_y(x-\Delta x,y)}{\Delta x} \end{cases} \tag{7.95}$$

Again, determine the tangential forces with slip as

$$\begin{cases} p''_x(x-\Delta x,y) = p_z\mu(s_x)/|s_x| \\ p''_y(x-\Delta x,y) = p_z\mu(s_x)/|s_x| \end{cases} \tag{7.96}$$

Step 3

Compare:

$$\begin{cases} |p''_x - p'_x| < \varepsilon \\ |p''_y - p'_y| < \varepsilon \end{cases} \tag{7.97}$$

If true, we get the tangential value; if false, go back to repeat Steps 1–3.

If the previous slip value is known, it can be used as the initial value to replace the rigid slip values in Step 1.

One advantage of Kalker's simplified theory over other theories such as those of Shen–Hedrick–Elkins and Polach is that detailed information about the contact area can be provided, for example, the adhesion (stick) and slip areas of the contact zone which are useful for analysis of wear.

Figure 7.13 shows the adhesion and slip areas obtained by using Kalker's simplified theory with various combinations of creepages [36].

7.5.2.3 Creep Force Law of Shen–Hedrick–Elkins

A heuristic method to describe creep-force curves based on Kalker's linear theory and the Johnson and Vermeulen model [31] was provided by Shen, Hedrick and Elkins [34]. Firstly, the linear creep forces can be calculated and then the resultant creep force is written as:

$$F_r = \sqrt{F_x^2 + F_y^2} \tag{7.98}$$

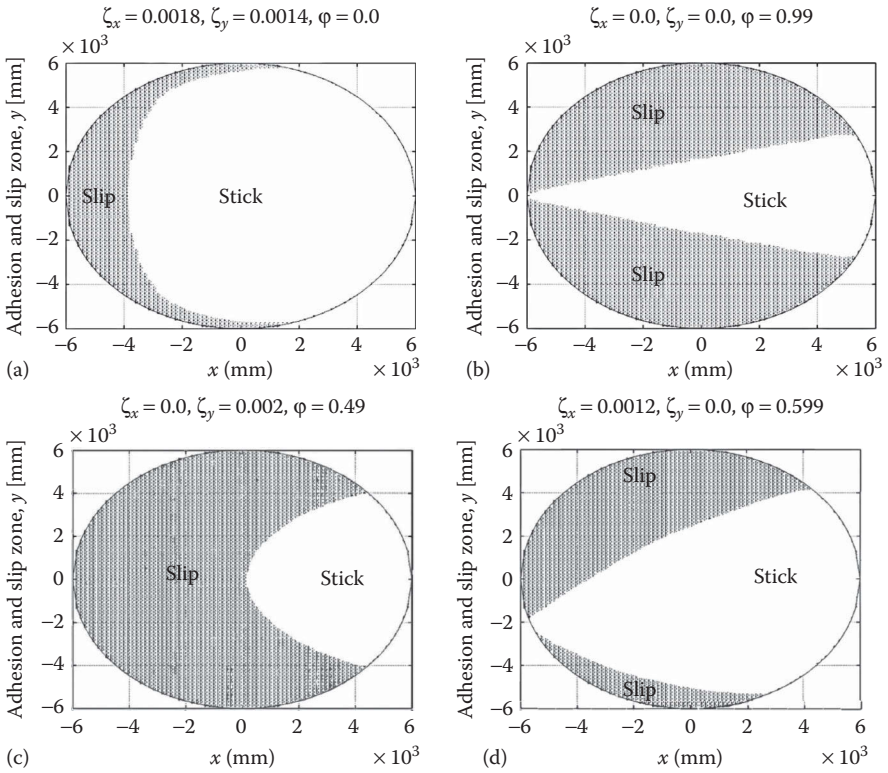

FIGURE 7.13 Regions of adhesion and slip: (a) Longitudinal/lateral creepag without spin, (b) pure spin, no longitudinal/lateral creepag, (c) lateral creepag with spin, and (d) longitudinal creepag with spin.

By means of the theory of Johnson and Vermeulen [31], let

$$F_r' = \begin{cases} \mu N \left[\dfrac{F_r}{\mu N} - \dfrac{1}{3}\left(\dfrac{F_r}{\mu N} \right)^2 + \dfrac{1}{27}\left(\dfrac{F_r}{\mu N} \right)^3 \right], & F_r \le 3\mu N \\ \mu N, \quad F_r > 3\mu N \end{cases} \tag{7.99}$$

then, introducing a modified coefficient,

$$\varepsilon = \frac{F_r'}{F_r} \tag{7.100}$$

yields the creep forces as:

$$\begin{cases} F_x' = \varepsilon F_x \\ F_y' = \varepsilon F_y \\ M_z' = \varepsilon M_z \end{cases} \tag{7.101}$$

The Shen–Hedrick–Elkins method is a heuristic description model that can only be applied to establish a creep-force curve. It is does not give an evaluation of what happens inside the contact patch, such as evaluating the levels of slip and stress or determining the location of the stick and slip zones.

7.5.2.4 Polach Approach

Another way to determine the creep forces was provided by Polach [35]. He modified Kalker's simplified method to include a variable friction coefficient. The contact area is assumed elliptical with semi-axes a and b and normal stress distribution in accordance with Hertz theory. The distribution of the normal stress σ and the tangential stress τ can be seen in Figure 7.14.

The maximum value of tangential stress at any arbitrary point is

$$\tau_{\max} = \mu\sigma \tag{7.102}$$

where μ is the coefficient of friction.

The resultant tangential creep force (without spin) is given by

$$F = \frac{2N\mu}{\pi}\left(\frac{k_A\varepsilon}{1+(k_A\varepsilon)^2} + \arctan(k_S\varepsilon)\right),\ k_S \le k_A \le 1 \tag{7.103}$$

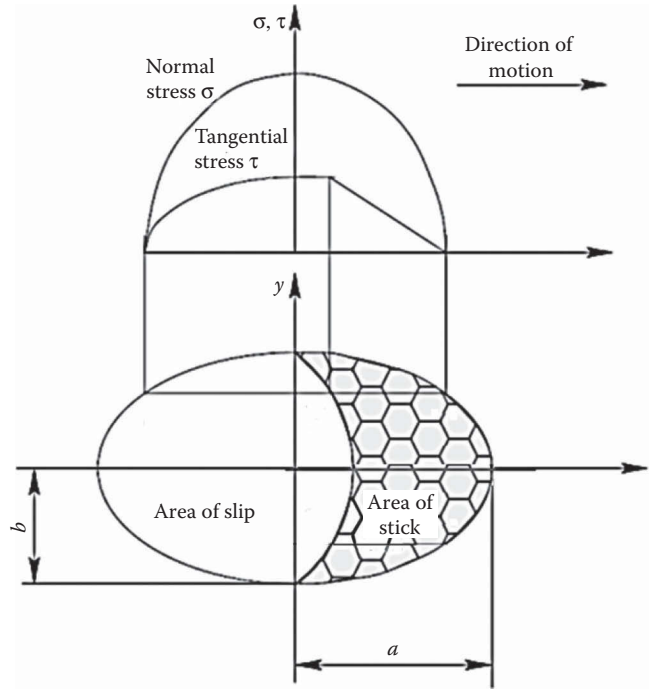

FIGURE 7.14 Distribution of normal and tangential stresses in the wheel-rail contact area. (From Polach, O., *Vehicle Syst. Dyn.*, 33(S), 728–739, 1999.)

with

$$\varepsilon = \frac{2}{3}\frac{C\pi a^2 b}{N\mu}s \tag{7.104}$$

where:

C is the proportionality coefficient (derived from Kalker's linear theory) characterising the contact shear stiffness in N/m^3

k_A and k_S are the reduction factors in the areas of adhesion and slip, respectively

For the longitudinal direction, we get

$$\varepsilon = \frac{1}{4}\frac{G\pi abkc_{11}}{N\mu}s_x \tag{7.105}$$

where s_x is the longitudinal component of the total creepage (relative slip).

$$k = \frac{k_A + k_S}{2}; s = \sqrt{s_x^2 + s_y^2} \tag{7.106}$$

The creep forces F_x and F_y are given by

$$F_i = F\frac{s_i}{s}, \quad i = x, y \tag{7.107}$$

7.5.2.5 Comparison of Kalker Simplified, Shen–Hedrick–Elkins and Polach Approaches

The creep-force laws of the Kalker simplified, Shen–Hedrick–Elkins and Polach theories are widely used in railway vehicle dynamic simulations. However, a comparison is important to provide an understanding of the appropriate modelling applications for each. Generally speaking, Kalker's simplified theory (FASTSIM) can provide better accuracy than the Shen–Hedrick–Elkins and Polach models, but it requires more computing time. However, FASTSIM can also provide information regarding the distribution of the stick (adhesion) and slip zones on the contact area. This information is useful for variable friction analysis and wear prediction. In order to compare the results, reduced creepages and tangential forces are used. The reduced creepages are defined as:

$$\begin{cases} \zeta'_x = \dfrac{abG}{\mu F_z} c_{11}\zeta_x \\ \zeta'_y = \dfrac{abG}{\mu F_z} c_{22}\zeta_y \\ \varphi' = \dfrac{(ab)^{3/2} G c_{23}}{\mu F_z}\varphi \end{cases} \tag{7.108}$$

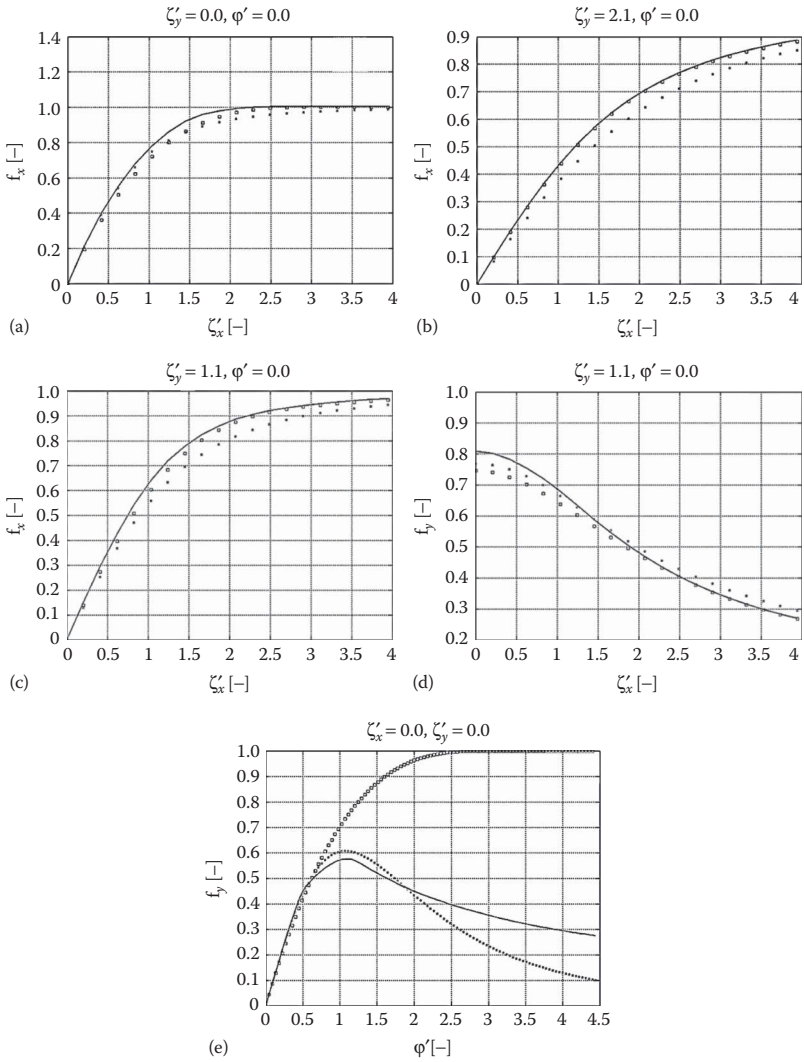

FIGURE 7.15 Comparison of results from FASTSIM (solid line), Shen-Hedrick-Elkins (square dot line) and Polach (circular dot line) models: (a) Longitudinal force, no lateral or spin creepage, $a/b = 1$, (b) longitudinal force, no spin, lateral creepage = 2.1, $a/b = 1$, (c) longitudinal force, no spin, lateral creepage = 1.1, $a/b = 1$, (d) lateral force, no spin, lateral creepage = 1.1, $a/b = 1$, and (e) lateral force, no longitudinal/lateral creepage, $a/b = 1$.

and the reduced forces are:

$$\left(F_x', F_y'\right) = -\frac{(F_x, F_y)}{(\mu F_z)} \tag{7.109}$$

Figure 7.15 illustrates the differences among the theories, with various combinations of creepages; note that (a–c) show longitudinal force versus longitudinal

creepage, (d) shows lateral force versus longitudinal creepage and (e) shows lateral force versus spin.

According to Kalker's results, the maximum error between FASTSIM and Kalker's exact contact theory (using the CONTACT program developed by Kalker based on his exact contact theory) is about 10% for the case of pure spin. The error between Polach and FASTSIM is smaller than that between Shen-Hedrick-Elkins and FASTSIM. However, both the Shen–Hedrick–Elkins and Polach models are not suitable for situations of high spin. For both longitudinal and lateral creepages, results show that the Shen–Hedrick–Elkins model is better than the Polach model in comparison with FASTSIM. Provided that the calculation speed is not the primary consideration, FASTSIM should be selected for vehicle dynamic simulations and should be used as the basis for traction adhesion analysis.

7.5.3 Friction and Adhesion Coefficients

In this discussion, it is necessary to understand the difference between a friction coefficient and an adhesion coefficient [49]. For the rolling traction/braking mode without slip, the maximum value of friction coefficient must be higher than the adhesion coefficient for the same contact conditions. In theory, the adhesion coefficient can be defined as traction force divided by wheel load [50]. Therefore, both these coefficients describe almost the same physical behaviour, which determines the ratio of the tangential force to the normal force. However, the friction coefficient depends only on the physical state of the contacting surfaces, whereas the adhesion coefficient depends on the construction characteristics of rail tracks and the dynamic characteristics of rail vehicles. Hence, the adhesion coefficient can be modified by 'unaccounted for' slipping motions, the difference between wheel diameters of wheel pairs, conicity and eccentricity of wheels, track curvature, reallocation of loads between wheels, irregular loads of wheels for the wheelset, the constraints imposed by the bogie setup, the type of rolling stock, the train configuration, vibrations, and so on. Some examples of typical values of friction coefficients for a variety of rail surface conditions measured using a hand-pushed rail tribometer are given in Table 7.2.

Most tangential wheel-rail contact models are designed for use in vehicle dynamics simulations, which focus on evaluating vehicle behaviour such as responses to track disturbances and determining the critical speed. Because large creepages are rarely encountered in vehicle dynamics simulations, creep-force versus creep models with creep saturation characteristics are not really applicable for such studies. For the constant friction coefficient used in such vehicle dynamics simulations, the friction force increases to the saturated value when slip occurs over the whole contact area. However, such an approach cannot be used for modelling the real behaviour of a heavy haul locomotive, because, as mentioned earlier, the static friction coefficient is greatly affected by material properties and surface conditions [37,49,51,52]. Despite a large number of investigations on this topic [53], the classical models described in Sections 7.5.1 and 7.5.2 cannot represent the creep-force characteristics at large creepages, in agreement with the typical measurements on locomotives and

TABLE 7.2
Friction Coefficients

Condition	Coefficient of Friction
Sunshine, dry rail, 19°C	0.6–0.7
Recent rain, 5°C	0.2–0.3
Grass on rail, 8°C	0.05–0.1
Damp-leaf film on rail, 8°C	0.05–0.1

Source: Olofsson, U., Adhesion and friction modification, *Wheel-Rail Interface Handbook*, R. Lewis, U. Olofsson (eds.), Woodhead Publishing, Cambridge, UK, 2009.

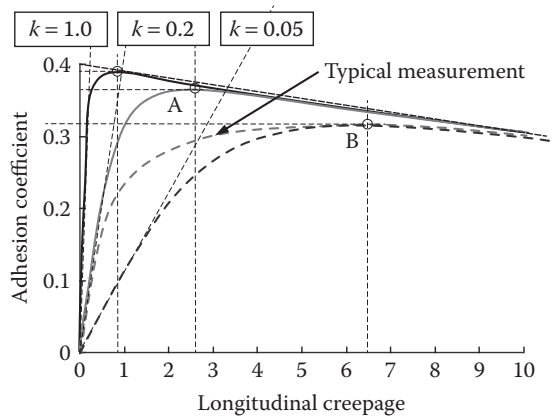

FIGURE 7.16 Modelling of creep force characteristic using falling friction coefficient and different reduction factors *k*. There is disagreement between the modelled creep force characteristic shape and its typical shape from measurements on wet rail. (From Spiryagin, M. et al., *Vehicle Syst. Dyn.*, 51, 1765–1783, 2013.)

other traction vehicles; see the longitudinal creepage versus adhesion coefficient curves in Figure 7.16 [54]. A justification of model parameters with regard to their slope at very small creepages requires rather moderate values of the factor (*k*) used to reduce the coefficients of Kalker's linear theory, resulting in the maximum adhesion occurring at creepage values smaller than those found in field measurements (point A in Figure 7.16). A justification of model parameters with regard to the maximum adhesion (point B) requires a very small value of the reduction factor, which is too low as compared with the values reported from measurements. In addition, it is possible to see that the results obtained from experiments are not covered by the adaptation of the friction coefficient. Furthermore, as shown in Figure 7.16, the reduced initial slope and the reduced friction coefficient at high creepages are not sufficient to achieve good agreement with typical field measurements [53–55].

The modelling of creep forces at large creepages, and especially at very low adhesion conditions, was solved in the Polach algorithm [53,55], which not only applies the variable friction coefficient but also represents the change of creep-force curves with increasing creep due to non-linearity of the tangential contact flexibility, in agreement with measurements on real locomotives, especially in low-adhesion conditions. However, the Polach algorithm is based on a simplified model [35] developed for fast calculation purposes. The model provides reliable results, but the differences can be observed compared with the exact theory and the FASTSIM code, as discussed by Vollebregt et al. in Ref. [56]. In order to improve the accuracy of such creep-force studies, some other models have been developed [54,57–62]. Two of these models used by the authors in their locomotive traction and braking studies are described in Section 7.8.

7.5.4 Tangential Forces, Including Variable Friction Coefficient

In the force-slip traction curves, there should be a reduction in the maximum possible tangential force at the contact, as the slip increases beyond the saturation point [35,53]. The creep-force law with constant friction coefficient could be adapted for solving some problems in which the wheel on rail slippages are under the saturation case. However, the slips are often large enough to affect the friction coefficient during the following situations:

- Control of the traction torque on start-up;
- During curve negotiation;
- Under conditions of dynamic instability, for example, wheel unloading due to track irregularity or vehicle body pitch and roll; and
- Presence of contaminants at the wheel-rail contact interface.

In the Polach model [53,55], the variable friction coefficient can be expressed as

$$\mu = \mu_s \left[(1 - A) e^{-Bw} + A \right] \tag{7.110}$$

where:

w is the magnitude of the slip (creep) velocity vector
B represents the coefficient of exponential friction decrease in m/s
A is the ratio of limit friction coefficient μ_∞ at infinite slip velocity to the maximum friction coefficient μ_S, given as:

$$A = \frac{\mu_\infty}{\mu_s} \tag{7.111}$$

Then Equations 7.103–7.107 are used for the calculation of creep forces.

In the modified FASTSIM model [54], the modelling of a variable friction coefficient is taken from Polach [53,55] (see Equation 7.110). It is assumed that the reduction factor k abates with the increasing ratio of the area of slip to the area of adhesion. Therefore, it requires a mathematical description of the change of the ratio between the area of slip and the area of adhesion as a function of creepage. The gradient of

the tangential stress, as used in the Polach model, can be used for this mathematical description. Because the tangential stress distribution in the Polach model is transformed to a hemisphere [35,53,55], the gradient of the tangential stress in this transformed model directly represents the ratio between the area of slip and the area of adhesion as a function of creepage. The gradient of the tangential stress from the Polach model is therefore used in FASTSIM to express the reduction factor k as a function of creepage. The parameters of the modified FASTSIM creep-force model are adjusted for the longitudinal creep direction by comparisons with field measurements. They are then used for modelling of creep forces for general creep and spin conditions. This is considered to be an acceptable assumption, because the creep can reach very large values in only the longitudinal direction (due to either traction or braking); however, the lateral and spin creepages remain limited.

The proposed variable stiffness reduction factor k is given by

$$k = k_0 \left(\alpha_{\text{inf}} + \frac{1 - \alpha_{\text{inf}}}{1 + \beta\varepsilon} \right) \tag{7.112}$$

where:

- k_0 is the initial value of Kalker's reduction factor at creep values close to zero, $0 < k_0 \leq 1$
- α_{inf} is the fraction of the initial value of the Kalker's reduction factor at creep values approaching infinity, $0 \leq \alpha_{\text{inf}} \leq 1$
- β is a nondimensional parameter related to the decrease of the contact stiffness with the increase of the slip area size, $0 \leq \beta$
- ε is a parameter that describes the gradient of the tangential stress in the stress distribution transformed to a hemisphere, according to Polach [35,53,55]

The latter parameter also represents the ratio of the slip area to the area of adhesion:

$$\varepsilon = \frac{1}{4} \frac{G \pi a b k_0 c_{11}}{N \mu} s \tag{7.113}$$

where:

- G is the shear modulus
- a and b are the semi-axes of the contact ellipse in the longitudinal and lateral directions, respectively
- c_{11} is Kalker's coefficient for the longitudinal direction
- N is wheel load
- μ is the coefficient of friction (see Equation 7.110)
- s is the total creep/relative slip

The total creep is computed as the vectorial sum of longitudinal and lateral creepages, whereby the lateral creepage considers the contribution of spin as used by Polach in Ref. [35]:

$$\zeta_{y\varphi} = \zeta_y + \varphi a \tag{7.114}$$

where φ is the relative spin, rad/m, and a is the contact ellipse semi-axis. If the values of lateral creep and spin have opposite signs and the total lateral creepage is lower than the pure lateral creep, the higher absolute value of $\zeta_{y\varphi}$ and ζ_y is selected.

Then, the total creepage can be defined as

$$s = \sqrt{\zeta_x^2 + \zeta_{y\varphi}^2} \tag{7.115}$$

Finally, the contact flexibility coefficient L_{WR} defined by Kalker [33,63] is increased, and the new value L_{WR}^* is calculated as

$$L_{WR}^* = \frac{L_{WR}}{k} \tag{7.116}$$

or alternatively, the Kalker's coefficients c_{11}, c_{22}, c_{23} are each reduced by multiplying them by the stiffness reduction factor k.

Figures 7.17a–g present comparisons of the calculation results by using the Polach model [53] and the modified FASTSIM [53], with measurements performed on real locomotives [64–68].

The modification of Kalker's FASTSIM [54] provides results at large creepages, which are similar to the Polach model [53], without affecting the proven FASTSIM modelling at small creepages. The modified FASTSIM model can be used instead of the Polach model in multibody simulations, with application of large tractive or braking efforts under various contact conditions such as dry, wet and polluted, if information required in Polach's algorithm is not available, for example, the stress distribution in the contact area.

7.6 MULTIBODY DYNAMICS SOFTWARE PACKAGES FOR RAIL VEHICLE-TRACK INTERACTION SIMULATION

The dynamic behaviour of locomotives due to wheel-rail interactions can be simulated using commercial software packages. As presented previously in this chapter, the dynamic modelling of rail vehicle-track interaction is typically described by a series of ordinary differential equations or partial differential equations. As such, a mathematical model incorporates complex wheel-rail contacts and real-world suspension elements such as friction, bumpstops, shear springs and the like, and the equations become non-linear. This requires numerical methods to solve the equations. A numerical simulation is undertaken by stepping through multiple time intervals and calculating the integral of the derivatives by approximating the area under the derivative curves. Some methods use a fixed step through the interval, and others use an adaptive step that can shrink or grow automatically to maintain an acceptable error tolerance. This is the way that every multibody dynamics software package works.

Several commercial software packages are currently available for the comprehensive simulation of rail vehicle-track interaction dynamic behaviour. Simulations using these software packages have provided many benefits to the rail industry and its regulators. Firstly, modelling of rail vehicle dynamics can be performed to give a virtual dynamic response close to that of the actual system. This is very useful and

important in vehicle derailment investigation and prevention, as well as in vehicle lateral hunting stability analysis. Secondly, some rail vehicle standards and acceptance procedures now allow dynamic simulations to be substituted for physical field tests, saving significant costs. Finally, the simulation of rail vehicle dynamic behaviour is an essential part of rail vehicle design, especially for suspension element designs.

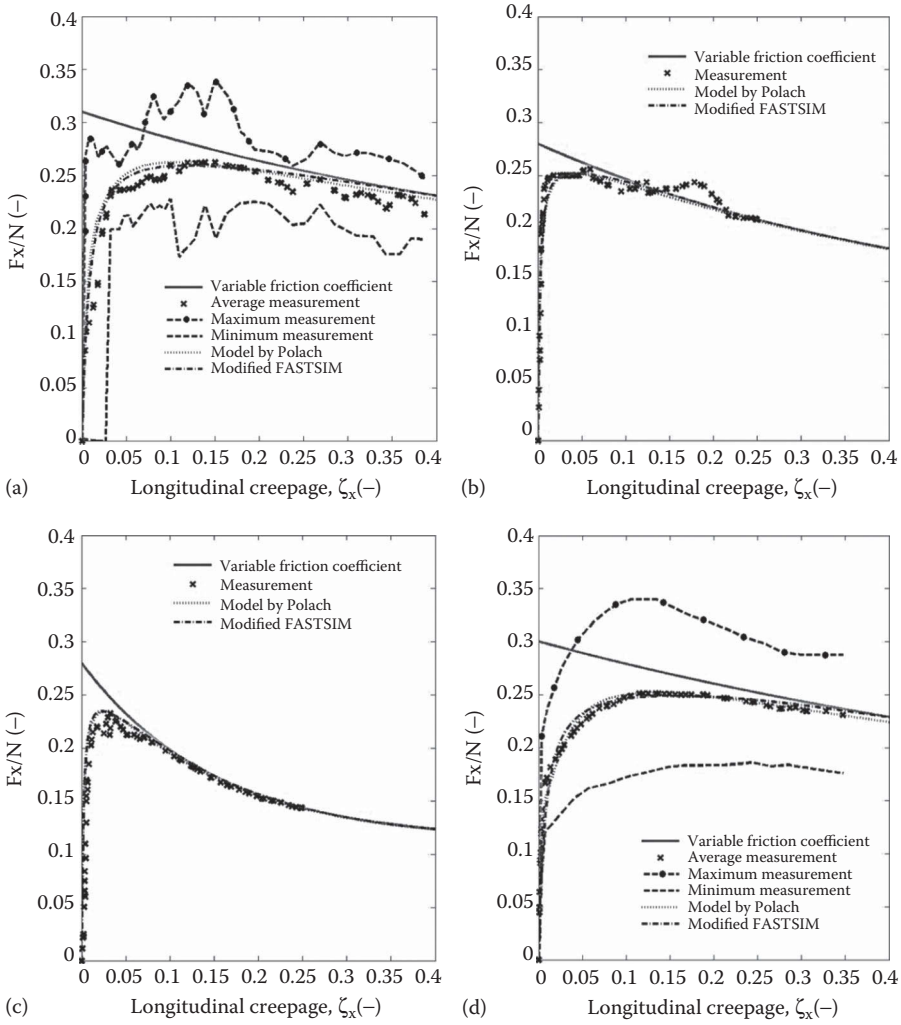

FIGURE 7.17 Comparison of results using Polach model and modified FASTSIM with measurements for some locomotives: (a) Locomotive SBB 460 (From Polach, O., SBB 460 Adhäsionsversuche, Technical Report No. 414, SLM Winterthur, 1992.) (wet wheel-rail contact, 40 km/hr), (b) locomotive 12X (From Polach, O., *Eisenbahningenieur*, 53, 50–57, 2002.) (wet wheel-rail contact, 20 km/h), (c) locomotive 12X (From Polach, O., *Eisenbahningenieur*, 53, 50–57, 2002.) (wet wheel-rail contact, 60 km/h), (d) locomotive SD45X (From Logston Jr., C.F. and Itami, G.S., *ASME J. Eng. Ind.*, 102, 275–281, 1980.) (wet wheel-rail contact).

(*Continued*)

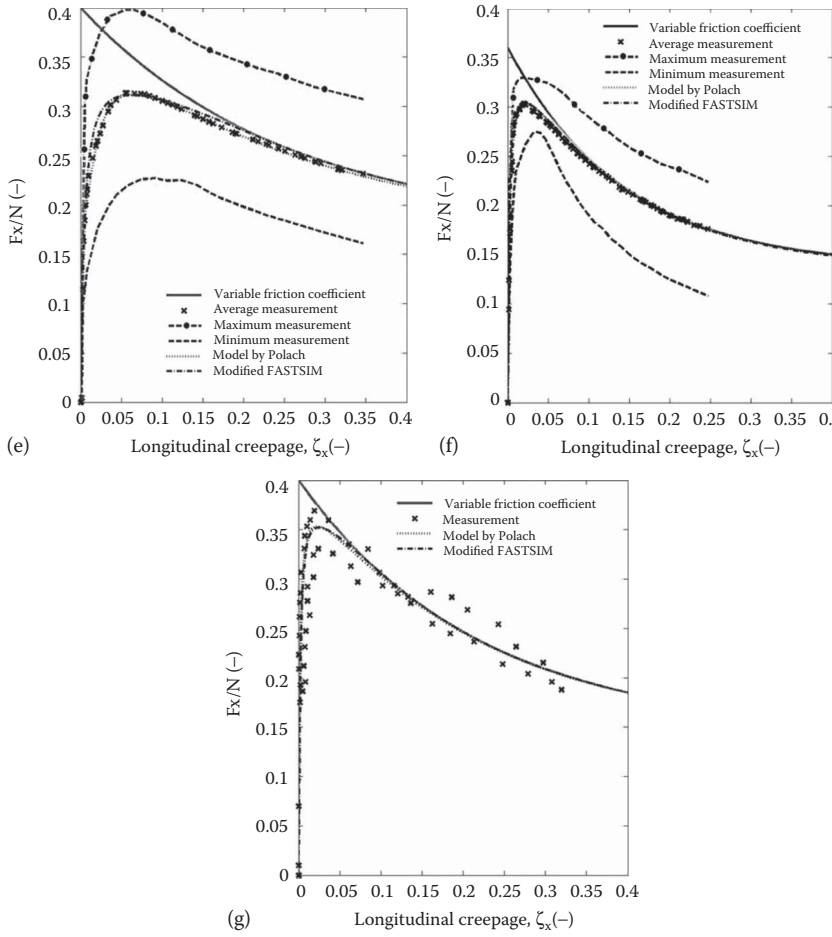

FIGURE 7.17 (CONTINUED) Comparison of results using Polach model and modified FASTSIM with measurements for some locomotives: (e) locomotive SD45X (From Logston Jr., C.F. and Itami, G.S., *ASME J. Eng. Ind.*, 102(3), 275–281, 1980.) (dry wheel-rail contact), (f) locomotive DB127 (From Engel, B. et al., *Elektrische Bahnen*, 96(6), 201–209, 1998.) (dry wheel-rail contact, 36 km/hr), and (g) locomotive S252 (From Lang, W. and Roth, G., *Eisenbahntechnische Rundschau*, 42(1–2), 61–66, 1993.) (dry wheel-rail contact, 30 km/hr).

Parametric sensitivity studies through the use of such simulations can ensure that a rail vehicle design reaches an optimum outcome.

The following subsections briefly introduce some widely used commercial software packages for the detailed simulation of rail vehicle dynamic behaviour.

7.6.1 NUCARS®

NUCARS®, developed by the Transportation Technology Centre Inc, a wholly owned subsidiary of the Association of American Railroads, has been accepted as an

industry standard in North America and widely adopted elsewhere [69]. NUCARS, as a computer simulation model of a general multibody rail vehicle dynamics system, can perform a variety of roles, which include:

- Simulation and prediction of the dynamic response of any rail vehicle to specified track conditions or on any type of track geometry, including special track work such as turnouts and guardrails;
- Evaluation of new or existing vehicle designs, as well as performance of failure analyses such as derailment studies and dynamic stability analysis; and
- Investigation of potential modifications of vehicle designs to improve ride quality.

NUCARS is designed with the following capabilities and features:

- Track geometry inputs may be either theoretical or actual track measurements, including track alignment, gauge, cross-level, curvature and superelevation and turnout geometry;
- Wheel-rail force calculations are undertaken using Kalker's exact non-linear creep theory and allow for two-point wheel-rail contact, measured or theoretical wheel and rail profile shapes, rail profiles (may vary along the track), wheel profiles (may be specified individually for each wheel), coefficient of friction (may vary along the track and across the wheel-rail surface), wheel flange back contact for guard rails, turnouts and special trackwork;
- Optional wheel-rail force calculations include traction and braking forces, torsionally flexible axles, independent rotating wheels, torsional links between axles and drive gears on axles;
- Vehicle bodies may be flexible, with up to 89 modes in each principal direction;
- Suspensions described as combinations of connection elements, including parallel and series springs and dampers; hysteresis elements; stops and gap elements; friction line and surface elements, including stick/slip; friction wedges with optional toe in/out for three-piece bogies; air springs simulated as combinations of standard connection elements and active suspensions;
- NUCARS outputs include all body motions, velocities and accelerations; eigenvalues and eigenvectors; wheel-rail contact point geometry, creepages, creep forces and contact stresses; suspension forces and motions; and wheel and rail wear indices on flange/gauge face and tread/railhead.

7.6.2 GENSYS®

GENSYS is designed as a general multipurpose software package for modelling mechanical, electrical and/or multibody systems. Modelling of rail vehicles using computers was begun by ASEA (Allmänna Svenska Elektriska Aktiebolaget or General Swedish Electrical Company) in Sweden in 1971 in the lead up to the development by that company of the X2000 high-speed tilt train. After initially producing a linear program in the frequency domain to model a bogie frame with two wheelsets called LSTAB, a non-linear time-domain simulation program called SIMFO

TABLE 7.3
Main Elements of GENSYS Software

	Main Calculation Programs in GENSYS
QUASI	Quasistatic analysis
MODAL	Modal analysis
FRESP	Frequency-response analysis
TSIM	Time-domain integration
	Pre-processors in GENSYS
TRACK	Generation of track irregularity files
KPF	Generation of wheel-rail geometrical properties
MISC	Miscellaneous programs for vehicle and track property input, etc.
NPICK	Adding flexible modes to rigid bodies
OPTI	Runs sequences of calculations
	Post-processors in GENSYS
GPLOT	Three-dimensional visualisation and animation program
GLPLOT	Similar to GPLOT, but an improved appearance
MPLOT	Two-dimensional or three-dimensional plotting of the results

quickly evolved to model a whole railway vehicle. In 1992, a three-dimensional general multibody dynamics analysis program called GENSYS was developed. At that time, the responsibility for the software package moved to a new company, AB DEsolver, which now has the sole task of developing and supporting the package. GENSYS is a software tool for modelling rail vehicles running on tracks [70], and the main functions in GENSYS are listed in Table 7.3.

All the four major calculation programs are very general in their basic design, and the GENSYS input data syntax makes it easy to create models of systems. If a subsystem is written in an m-file for MATLAB® or Octave, it is possible to initiate a co-simulation with the cosim_server command. The coupling between wheel and rail can be modelled in many ways. The GENSYS package can also simulate a system combining multiple flexible and rigid bodies. Examples of typical GENSYS locomotive [70] and bogie models [71] are shown in Figures 7.18–7.20.

The following are the main applications of GENSYS for rail vehicle dynamic analysis:

- Critical speed;
- Vehicle behaviour in traction and braking;
- Wheel unloading on track twists;
- Car body roll coefficient;
- Maximum track shift forces;
- Maximum flange-climb ratio;
- Vehicle overturning;
- Ride comfort and motion sickness;
- Wheel and rail wear rates;
- Co-simulation for traction, braking and other studies;

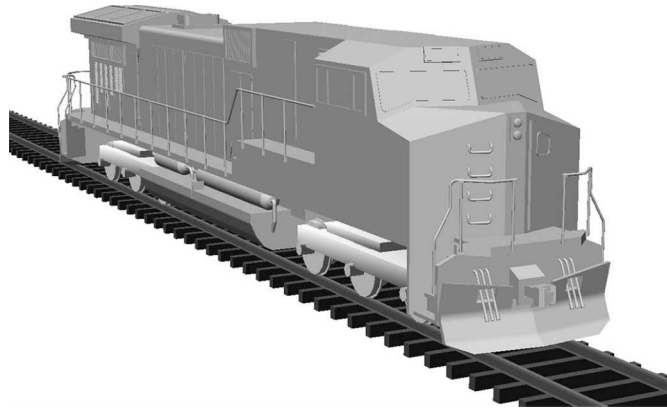

FIGURE 7.18 Typical heavy haul Co-Co diesel-electric locomotive model generated in GENSYS. (©AB DESolver, Östersund, Sweden. With permission.)

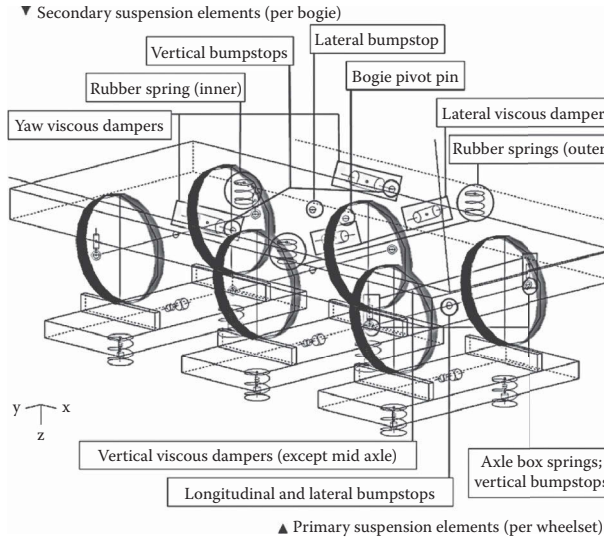

FIGURE 7.19 GENSYS model of rigid locomotive bogie. (From George, A.L., Theoretical and numerical investigation on traction forces for high adhesion locomotives, MEng Thesis, Central Queensland University, Rockhampton, Australia, 2015.)

- Prediction of risk of rolling contact fatigue;
- Prediction whether wheel profiles will be stable or not; and
- Prediction of the risk of wheel squeal and rail corrugation.

Examples of locomotive dynamics analysis using GENSYS are given in Section 7.8. Examples of the development of a co-simulation interface between GENSYS and MATLAB–Simulink® and of the full mechatronic system of a heavy haul locomotive are given in Chapter 9.

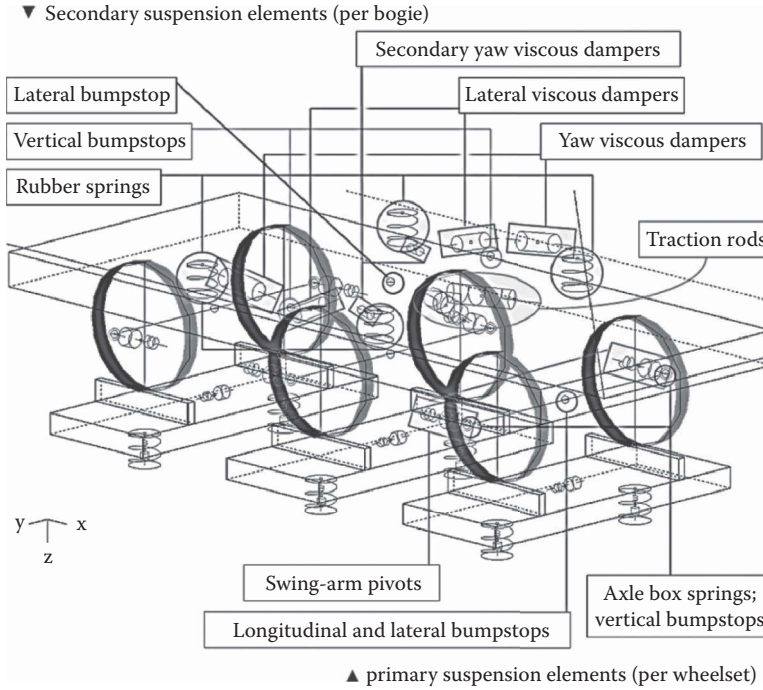

FIGURE 7.20 GENSYS model of semi-steering locomotive bogie. (From George, A.L., Theoretical and numerical investigation on traction forces for high adhesion locomotives, MEng Thesis, Central Queensland University, Rockhampton, Australia, 2015.)

7.6.3 VAMPIRE®

The owner of VAMPIRE is the DeltaRail Group Ltd, whose predecessors were AEA Technology Rail and British Rail Research, which had been world-leading authorities in the field of rail vehicle dynamics and wheel-rail interaction for many years [72,73]. Unlike many other multibody dynamics packages, VAMPIRE is particularly designed to analyse the behaviour of rail vehicles. Therefore, VAMPIRE allows assembling a mathematical model of almost any rail vehicle configuration and offers detailed models of suspension components and elements important to rail vehicle behaviour, such as air springs. It is claimed that running VAMPIRE is significantly faster than other general multibody packages. The latest version, VAMPIRE Pro, includes all the pre- and post-processing options required to investigate railway-related issues from vehicle design and acceptance to in-service issues, track damage and accident investigation; see Table 7.4 for details.

Based on Table 7.4, and similar to GENSYS, the analysis capabilities of VAMPIRE can be extended through the use of VAMPIRE Control (MATLAB-Simulink interface) to co-simulate control algorithms for active or specialist suspensions. More importantly, in order to provide a means for users of VAMPIRE to model and simulate more complex problems, a User Subroutine Facility is available. This facility allows

TABLE 7.4
Main Elements of VAMPIRE Software

Pre-processors	Generating and visualising wheel-rail contact data, model building and track plotting
Analysis Programs	Linear eigenvalue and response analysis, non-linear transient response analysis, quasistatic curving analysis and static analysis
	Can be extended by the use of VAMPIRE user subroutines or VAMPIRE control (MATLAB–Simulink interface) and the in-line processing of simulation data
Post-processors	Extensive plotting facilities for simulation data, statistical analysis, data filtering, channel arithmetic, data extractor and peak counting
	Vehicle acceptance and wheel and rail wear analysis
Animation	Transient response animations and eigenvalue modes animations

users to write their own algorithms or subroutines to, for example, model and investigate the behaviour of active and other novel suspensions, simulate control systems and extend the functionality of the standard transient analysis program, and so on.

Many studies have been published in which VAMPIRE has been used to undertake simulations of heavy haul locomotives. Several of these studies that address the issues of curving of three-axle bogies under traction are included in Refs. [74–78]. A locomotive model generated in VAMPIRE and typical analysis are shown in Figure 7.21 [79].

7.6.4 VI-RAIL®

VI-RAIL is built upon the MSC Software product MSC Adams, one of the world's leading mechanical system simulation tools. VI-RAIL is a specialised simulation software package for railway engineering [80], allowing rail vehicle engineers to build and test functional virtual prototypes of complex rail vehicle designs, to realistically simulate full-motion dynamic behaviours, to evaluate and manage the complex interactions between rail vehicle and tracks and to better optimise rail vehicle designs for performance, safety and comfort.

VI-RAIL software allows users to select from two operational modes:

- A standard interface, which allows the users to input data into existing design templates to run both standard and custom design tests; and
- Template-builder mode, which enables experienced users to create their own design templates from libraries of core and user-defined modelling elements.

VI-RAIL software can be used for dynamic simulations of wheel-rail contact and track loads; cargo tie-down effectiveness; auxiliary equipment; suspension and coupler designs; predictions of wear; analyses of curving, stability and creep; and event reconstruction.

The software allows users to instantly see the effects of design changes on rail vehicle performance in high-speed animation and to easily detect component interferences, excessive wear, instability and performance limitations. Users are also able to plot key parameters in graphs to compare results from different designs.

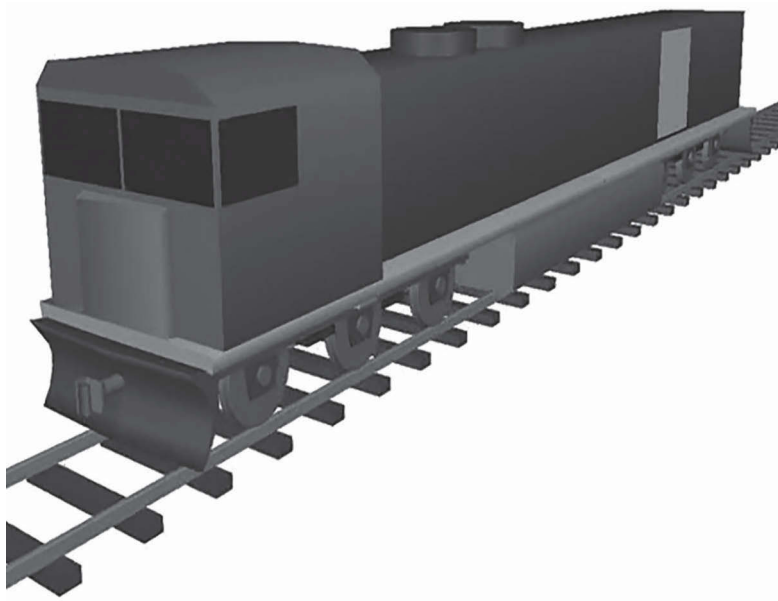

(a)

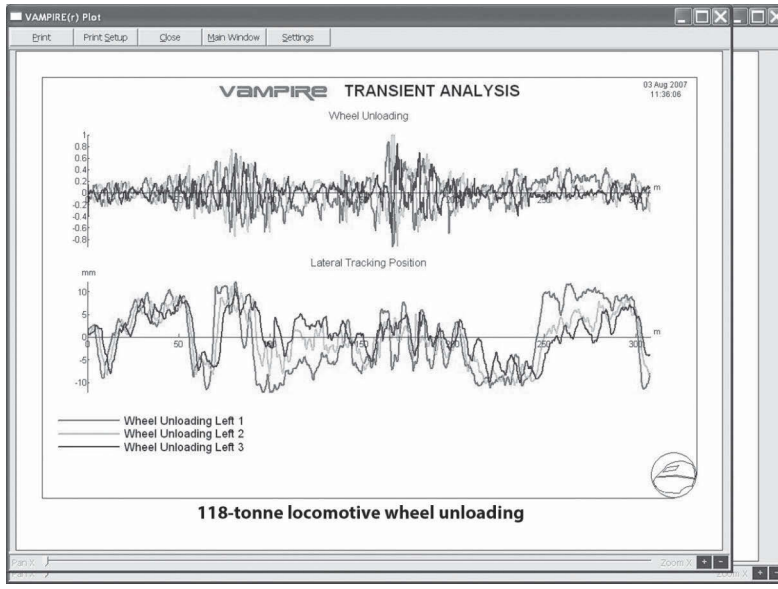

(b)

FIGURE 7.21 Locomotive modelling in VAMPIRE: (a) Locomotive model and (b) typical analysis output. (From Simson, S., Three axle locomotive bogie steering, simulation of powered curving performance, Passive and active steering bogies, PhD Thesis, Central Queensland University, Rockhampton, Queensland, Australia, 2009.)

7.6.5 SIMPACK®

As a general-purpose MBS software package, SIMPACK can be used for the dynamic analysis of any mechanical or mechatronic system. The module SIMPACK Rail enables engineers to generate and solve virtual three-dimensional rail vehicle and track models in order to predict and visualise motion, coupling forces and stresses [81]. SIMPACK originated from a collaboration project between the German aerospace research centre DLR and the central technology department of the MAN group in 1987. The SIMPACK Rail add-on module was developed in a joint project with Siemens Transportation Systems and was made available in 1996. SIMPACK Rail is widely used by railway operators and engineering service providers. In 2014, SIMPACK and SIMPACK Rail became part of the Dassault Systèmes SIMULIA brand.

SIMPACK Rail's main advantages are as follows:

- One common, clear and modern user interface covering all modelling and post-processing;
- Unlimited flexibility in modelling, from a single wheel on a rail to a complete train;
- Fast, robust and reliable solver, designed for high-frequency transient analyses up into the acoustic range;
- Redundancy-saving modelling through referencing an arbitrary number of other SIMPACK models in any level (substructuring), with automatic connection and powerful inheritance and overwriting mechanisms;
- Interfaces to all major finite element analysis packages for importing flexible bodies or undertaking co-simulation;
- Easy model scalability and switching between different levels of detail;
- Separation of models and scenarios;
- Element and model 'diff tool' for easy comparison of models or parts thereof;
- Versatile post-processing, with extensive filter library;
- Built-in object-oriented scripting language, based on both JavaScript and Windows COM scripting; and
- Powerful programming interface for adding user functionality.

SIMPACK Rail can be used for the analysis and design of any type of rail-based vehicle. Its main fields of application are as follows:

- Homologation, certification and assessment of new and modified rail vehicles;
- Rail-wheel forces in tangent track and curves;
- Derailment safety;
- Critical speed and hunting stability;
- Ride comfort;
- Crosswind safety;
- Rail and wheel profile wear and rolling contact fatigue analysis;
- Gauging;
- Drivetrain dynamics, traction and braking (see Figures 7.22 through 7.24 [82,83] for locomotive bogie and nose-suspension drive modelling arrangements in SIMPACK);

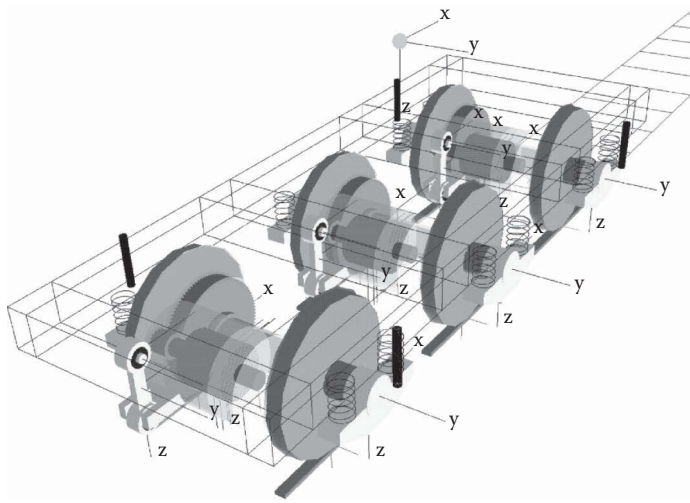

FIGURE 7.22 Locomotive bogie model in SIMPACK. (©Siemens AG, Munich, Germany. With permission; Pfleger, E., Simulation of the dynamic behaviour of nose-suspension drives for rail vehicles: Using SIMPACK-Gear Wheel, SIMPACK User-Meeting 2006, Baden-Baden, Germany, March 21–23, 2006.)

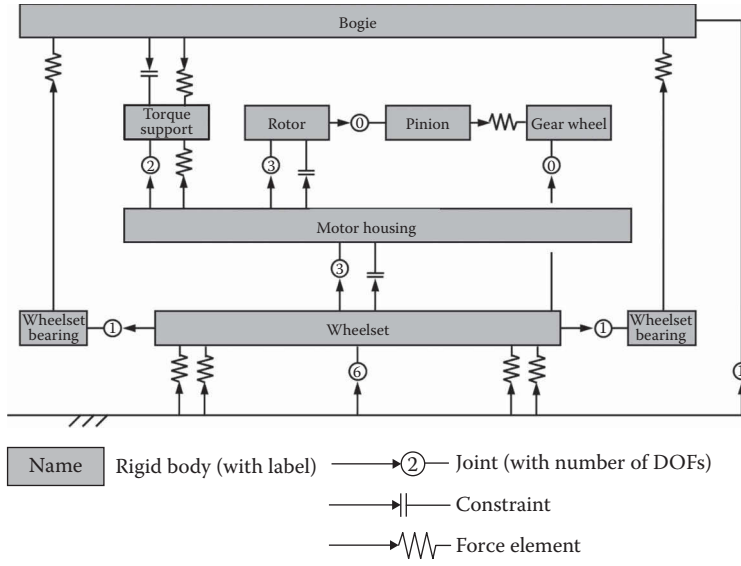

FIGURE 7.23 Traditional modelling of nose-suspension drive in SIMPACK, giving correct bearing forces only without motor torque. (©Siemens AG, Munich, Germany. With permission; Pfleger, E., Simulation of the dynamic behaviour of nose-suspension drives for rail vehicles: Using SIMPACK-Gear Wheel, SIMPACK User-Meeting 2006, Baden-Baden, Germany, March 21–23, 2006.)

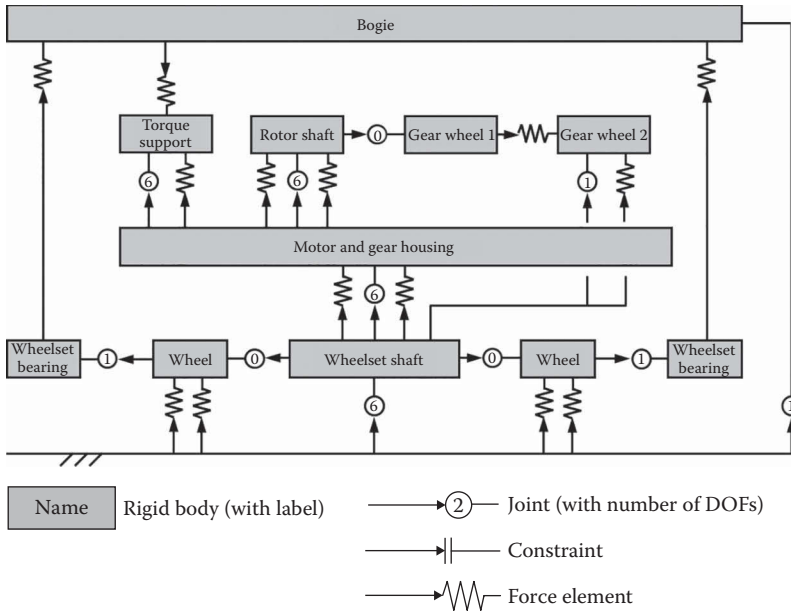

FIGURE 7.24 More sophisticated modelling of nose-suspension drive in SIMPACK, incorporating motor torque effects. (©Siemens AG, Munich, Germany. With permission; Pfleger, E., Parameter-Excited Vibrations in Rail Vehicle Drives, SIMPACK User-Meeting 2007, Bad Godesberg, Germany, November 20–22, 2007.)

- Train/track dynamics, bridge, slab track and turnout design;
- Pantograph/overhead line dynamics;
- Derailment analysis;
- Component design and optimisation (suspension, couplers, buffers, drivetrains, gearboxes and engines); and
- Real-time (hardware-in-the-loop) simulation.

SIMPACK provides the following main solvers:

- Preload and equilibrium;
- Time-domain integration with the main integrator SODASRT 2, plus various variable and fixed stepsize integration methods;
- Kinematics;
- Measurements for re-evaluating a time domain or kinematics solver run with reduced or additional outputs or reduced stepsize;
- Eigenmodes;
- Linear response and transfer functions; and
- Operating deflection shapes.

SIMPACK offers a large number of advanced modelling elements, including:

- Coil spring elements with shear-bending cross-coupling;
- Non-linear elastomer elements with static and dynamic hystereis;
- One-dimensional and two-dimensional friction elements with various characteristics;
- Generic two-dimensional and three-dimensional contact between rigid and flexible bodies; and
- Air spring system with level control, tanks, differential pressure and other valves.

Modelling elements for heavy-haul locomotive simulation are as follows:

- Flexible bodies for truck frames, wheelset shafts, wheels, gearboxes, shafts and car body;
- Drivetrain elements covering all types of gearwheels, journal and rolling bearings, cardan shafts, spline couplings and clutches;
- Controllers, filters and other control loop elements;
- Asynchronous motor with three-phase voltage input and skin effect; and
- Elements for combustion engine modelling, such as chains with flexible guides, belts, valve springs with internal dynamics and contact between the coils, hydraulic lash adjuster, gas force excitations and so on.

Modelling the wheel and rail contact interface offers advanced and accurate contact algorithms for both equivalent elliptic and nonelliptic contacts, including an interface to Kalker CONTACT software. The user can visualise contact patches, their forces and surface stresses in SIMPACK's post-processor. SIMPACK supports variable rail profiles for turnouts and crossings, roller rigs and out-of-round wheels. Various friction weighting functions are available for modelling flange lubrication, macroslip friction reduction for traction, braking analyses and much more. For linear stability analyses, there are different methods to automatically quasilinearise the rail-wheel contact geometry. The rail-wheel contact situation can be used as an input to wear simulations of rail and wheel profiles.

Track layout and irregularities can be defined separately from each other, either from synthetic input or from measured track data. The track foundation can be rigid or flexible, with arbitrary suspension modelled by standard SIMPACK elements. Flexible track structures such as turnouts or bridges can be imported from finite element analysis software.

SIMPACK's post-processor allows creating large reports with multiple page sets and pages. A page may contain any combination of three-dimensional animations (in time and frequency domains), two-dimensional and three-dimensional diagrams and text. Live texts and annotations, written in JavaScript code, can be used to display model status and results in text format at any place in a diagram or a text box. The user can animate the results in three dimensions while simultaneously watching how cursors run along the curves in the diagrams. Even results of different solver

runs or different models can be displayed simultaneously. A vast number of signal filters allow complete data processing within the SIMPACK framework.

There are also multiple interfaces for co-simulation and model import/export:

- SIMAT co-simulation interface between SIMPACK and Simulink;
- Standalone S-Function export for co-simulation;
- MatSIM to compile a Simulink model and import it into SIMPACK;
- Import of Functional Mockup Unit (FMU) for co-simulation and model exchange;
- Export of FMU for co-simulation
- Export of the state-space matrices A, B, C and D to MATLAB; and
- Direct export of simulation results to MATLAB format.

SIMPACK's SIMAT module enables a direct co-simulation interface between SIMPACK and Simulink. In this way, a SIMPACK multibody model can be combined with any control, hydraulic, pneumatic or electronic system designed in Simulink to have a full Software-in-the-Loop simulation. SIMAT provides an S-Function, which can be imported into any Simulink model. Both SIMPACK and Simulink use their own integrators, and therefore, all model elements are supported.

The SIMAT module also comes with an S-Function export feature for co-simulation to generate a standalone S-Function of a complete SIMPACK model. This S-Function for co-simulation can be imported into any Simulink model and requires no SIMPACK installation; however, it needs the required solver licenses.

SIMPACK MatSIM provides the ability to generate a standalone library of a Simulink model to directly import this into the SIMPACK environment. Most, but not all, Simulink elements are supported. With this feature, a control system designed in Simulink can be imported directly into SIMPACK to connect with the multibody model.

SIMPACK also supports the Functional Mockup Interface, which is standardised by an independent association [84]. The FMUs for co-simulation and model exchange can be imported directly into SIMPACK to combine SIMPACK models with any electronic, control and hydraulic systems. SIMPACK also supports the export of standalone FMUs for co-simulation. This feature exports a complete SIMPACK model (with no restrictions in modelling) into the FMU format for co-simulation. No SIMPACK installation is required to run this standalone SIMPACK FMU in another tool; however, it does need the required solver licenses.

Besides enabling technical connectivity between different software packages, the model export and import functionalities also give users the possibility to share their models with providers, customers or partners, without disclosing the actual model structure or other modelling details. The exported S-Functions or FMUs contain a user-defined interface that defines inputs and outputs and a selected set of parameters, but no deeper insight into the models is possible.

Finally, the SIMPACK state-space matrices export enables the feature to export A, B, C and D matrices of a linearised SIMPACK model around a specific operating point. The matrices are written in M-File format, which can be directly read into

MATLAB for further model analysis or control design. The SIMPACK–MATLAB result export enables the export of SIMPACK results directly in the MAT-File format for loading into the MATLAB environment for further post-processing.

7.6.6 Universal Mechanism

Universal Mechanism (UM) is a multibody dynamics program for the simulation of kinematics and dynamics of mechanical systems, developed at the Laboratory of Computational Mechanics of Bryansk State Technical University, Russia [85]. This program includes a number of modules specifically oriented to the simulation of railway vehicle dynamics, namely:

- UM Loco, which allows the user to efficiently create fully parameterised models of rail vehicles for the analysis and optimisation of vehicle dynamic behaviour, for wheel-rail interface and rollingstock performance management and for rail vehicle simulation;
- UM Train and UM Train3D, which are capable of calculating longitudinal train dynamics with user-specified train make-up (numbers of locomotives and wagons, axle loads and the like), simplified and three-dimensional vehicle models, different braking and traction modes, draft gear characteristics and railway track macrogeometry of any configuration;
- UM Wheel-Rail Wear for railway wheel and rail profile wear prediction; and
- UM RCF for simulation of the accumulation of rolling contact fatigue damage to rail vehicle wheels.

In some cases, to obtain more accurate solutions and to perform durability analysis, it is necessary to introduce flexible vehicle bodies imported from ANSYS or NASTRAN, in contrast to rigid flexible bodies, into the modelling. This can be done with the help of the UM FEM and UM Durability modules.

Simulations are performed in the time domain by means of numeric integration of differential or differential-algebraic equations of motion. UM supports two methods for automatic generation of equations of motion: symbolic and numeric-iterative. For complex models with many DOFs, symbolic generation helps accelerate numerical simulation by up to 30%–50% in comparison with numerical generation.

Online animation of motion and plots of dynamic performance are available during simulation, including linear and angular coordinates, velocities and accelerations, active forces and moments and, reaction forces and the like. UM allows the user to create fully parameterised models of rail vehicles. Geometrical, inertia and force parameters may be specified via variable parameters. The parameterisation of a model is the basis for effective analysis and optimisation of its dynamic behaviour. UM is able to directly interface with most popular CAD programs to accelerate the creation of models.

The locomotive and bogie models shown in Figure 7.25 allow the analysis of dynamic performances of the locomotive in tangent sections and curves, with constant or variables speed and so on. The dynamic performances are usually

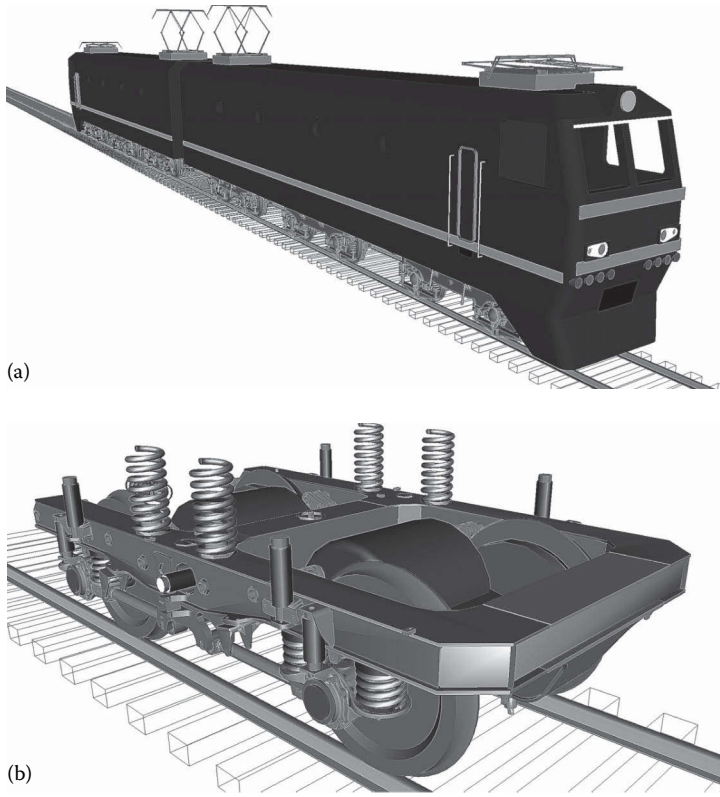

FIGURE 7.25 Typical locomotive modelling using Universal Mechanism (UM): (a) Locomotive model and (b) bogie model. (©Computational Mechanics Ltd., Bryansk, Russia. With permission.)

evaluated, which are the same as in the field tests, including guiding and frame forces, derailment criteria, lateral and vertical accelerations, dynamic factors and wear factors in wheel-rail contacts. UM Loco includes a contact animation window that allows a designer to observe features of the wheel-rail geometry and forces at the contact interface, to determine whether the contact is single point or two point, to observe the dynamic behaviour of wheelsets in curves and so on. This is very useful for determining of the critical speed of a railway vehicle, studying the features of the interaction between wheels and rails and observing wheel climb and derailment situations. A special tool for the creation of track irregularities is also included, supporting point-wise input of irregularities and import of measured irregularities. Both standard wheelsets and wheelsets with independently rotating wheels are included.

UM software allows the simulation of locomotive bogies with various degrees of detail and complexity. As an example, a powered wheelset assembly is shown in Figure 7.26, and the schematic of its model, as developed in UM, is presented in Figure 7.27.

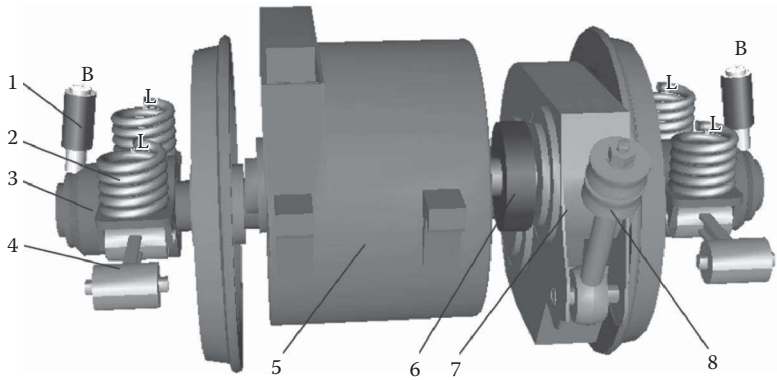

FIGURE 7.26 Model of powered wheelset assembly: 1 – damper; 2 – primary suspension; 3 – axle-box; 4 – traction rod; 5 – traction motor; 6 – elastic coupling; 7 – reduction gearbox; and 8 – reducer suspension rod. (©Computational Mechanics Ltd., Bryansk, Russia. With permission.)

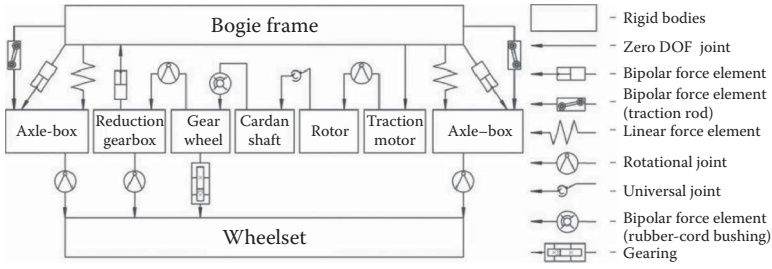

FIGURE 7.27 Schematic of wheelset traction motor assembly. (©Computational Mechanics Ltd., Bryansk, Russia. With permission.)

The traction motor casing is rigidly fixed to the bogie frame. The rotor is connected to the motor casing by the rotational joint. The cardan shaft has two DOFs relative to the rotor. The rubber annulus coupling is modelled by a bushing force element. The shaft transmits the traction torque via the coupling to the gear wheel of the reducer. The reduction gearbox is connected to the wheelset by the rotational joint and suspended from the bogie frame by a linear bipolar force element. A joint of the generalised type introduces the rotational DOF of the rotor relative to the motor casing. A rotational joint could also be used, in which case the traction torque is described as a numerical value of the joint torque.

Furthermore, the electromechanical motor can be described by using the special UM Block Editor tool, intended for the description of block diagrams showing the interfacing of schemas, or by using third-party software, for example, MATLAB–Simulink.

The UM includes the following algorithms for computing creep forces:

- *Mueller's method*: A very fast and simple model for computation of creep forces according to analytic expressions containing a creep factor;

- *FASTSIM*: The well-known and the most frequently used algorithm for creep forces by Kalker;
- *FASTSIM A*: A semi-analytic modification of the classical FASTSIM algorithm;
- *Minov's model*: Used as a rule for simulation of traction and braking modes and based on experimental dependence of adhesion force on sliding velocity;
- *Nonelliptical model*: Used for simulation of conformal contact, which is important for the simulation of dynamics of vehicles with worn profiles or the evolution of wheel and rail profiles due to wear;
- *Multipoint nonelliptical model*: The most universal contact model without any restrictions on the number of contact patches that are useful, for example, for simulation of passage through a switch; and

To calculate creep forces for locomotive traction or braking modes, the dependence of the coefficient of friction on sliding velocity, according to the Polach model, is available.

UM supports four co-simulation techniques:

- Exporting code from UM to Simulink (UM Control/CoSimulation);
- Exporting code from Simulink to UM (UM Control/MATLAB Import);
- Importing user's code written in C/Fortran/Pascal and compiled as DLL to UM (UM Control/User-defined routines);
- Importing models described as structural diagrams (in Simulink style) to UM without requiring MATLAB–Simulink (UM Control/Block Editor).

UM Control/User-defined routines are usually used for incorporating into UM various mathematical models of forces or control systems that are impossible to describe with the help of the built-in force elements. External libraries have a list of input and output signals, as well as a list of related parameters. During the integration of the external library and UM model, external library input signals are connected with UM variables to describe kinematical performances. Output signals are connected with UM parameters that represent/replicate forces and torques acting on a mechanical system.

UM Control/Block Editor is a separate additional tool used to describe structure diagrams with the help of basic functional elements. The Block Editor is somewhat similar to the Simulink tool from the MATLAB–Simulink software package. Schemas created in the Block Editor are connected to the UM environment in the same way as the MATLAB–Simulink models or User-defined routines. Both the Block Editor and MATLAB Import tools have very similar approaches in the description of structure diagrams and their connection to dynamic models in the UM environment. Block Editor supports all the major and most commonly used block diagrams and allows simulation of the majority of practical applications. However, in contrast to MATLAB–Simulink, Block Editor does not have specific libraries for processing of neural networks or support libraries of fuzzy logic.

Block Editor can be recommended for the modelling of block diagrams of low and medium complexity. If the capabilities of Block Editor are not sufficient for

some specific problems, then it is recommended to use MATLAB–Simulink along with MATLAB Import.

Some examples of the application of a co-simulation approach in UM can be found in Refs. [86–88].

7.7 LOCOMOTIVE MODEL ACCEPTANCE PROCEDURE

Before a new class of railway locomotive is put into operational service, the prototype/s must successfully undergo a comprehensive set of experimental tests, theoretical calculations and simulations to prove compliance with the dynamic performance specified by the locomotive manufacturer and/or operator. In addition, locomotives that are either substantially modified or relocated to a new location with significantly different track parameters need to undergo physical tests, so that their dynamic performance can be assessed, which can be both time consuming and expensive for rail operators. In the case of modified or relocated locomotives, it is possible to reduce the time and resources required for dynamic behaviour tests by the use of virtual multibody locomotive models in place of the actual locomotive tests. Several verified MBS packages such as GENSYS, NUCARS, SIMPACK and VAMPIRE are available for this purpose, with their underlying mathematical modelling theories now considered to be well tested and reliable. It may also be advantageous to use multibody models in association with additional scripts to model systems such as traction and pneumatic/dynamic braking in the initial design phase of new locomotives.

Before mathematical locomotive models can be used for detailed simulations, basic tests need to be performed to validate their static and dynamic behaviours. The criteria for acceptable model performance in these tests should be clearly defined, so that any significant errors present can be identified and corrected. Although several standards exist worldwide to govern locomotive dynamic behaviour, there is a lack of documentation regarding the validation process for multibody locomotive models. These standards normally specify a range of static and dynamic tests to determine the locomotive performance in critical areas such as the ability to negotiate sharp curves and any susceptibility to hunting. These tests may be variously conducted on laboratory equipment, test tracks or operating railways.

A Locomotive Model Acceptance Procedure (LMAP), as proposed by Spiryagin et al. in Ref. [89], is discussed in this section. Although its specific purpose is to evaluate the models of Australian freight and heavy haul locomotives, which required such a process to satisfy relevant Australian Standards, the procedure could readily be modified to suit the needs of other countries and various types of locomotives. Table 7.5 shows what this procedure covers.

7.7.1 Locomotive Modelling

In order to demonstrate the process of detailed simulations for the LMAP, a typical locomotive widely used in heavy haul transportation in Australia is selected, for which to create a model using the GENSYS software. The selected locomotive has a

TABLE 7.5
Locomotive Model Acceptance Procedure

Stage 1	Basic locomotive model checking/debugging
Stage 2	Tests currently included in Australian Standards
	A: Rolling stock outlines
	B: Track forces and stresses
	C: Dynamic behaviour (time-stepping analyses required)
Stage 3	Tests not included in Australian Standards
	A: Traction tests
	B: Braking tests

Co-Co wheel arrangement, meaning that the car body is connected to two three-axle bogies, with each axle being independently driven by its own traction motor.

The locomotive multibody model is constructed from nine rigid bodies, namely one car body, two bogie frames and six wheelsets, which are connected together through secondary and primary suspensions. The masses and moments of inertia of the traction motor assemblies are therefore incorporated into neighbouring wheelset and bogie frame bodies. The assumption is made that one-third of each traction motor assembly's mass (and moment of inertia) is added to its corresponding wheelset (one traction motor per wheelset) and the remaining two-thirds are added to the bogie frames (three traction motors per bogie). All bodies in the locomotive model are given six DOFs, except that each wheelset pitch angle is constrained to zero.

Rails are modelled as separate massless elements under each wheel, which can be connected with up to three wheel-rail contact points. Each contact point is assumed to have linear stiffness and damping acting normal to the contacting wheel-rail surfaces. The two rails under each wheelset are connected to a body that represents the track (sleepers) with lateral and vertical stiffness and damping units. The track bodies have mass and are allowed to move in the lateral and vertical directions and rotate in yaw with three DOFs. These are, in turn, connected to the ground with a series stiffness-damping unit in the lateral direction and two pairs of stiffness and series stiffness-damping units, for both the right and left sides of the track, respectively, in the vertical direction. Overall views of the locomotive multibody model, the bogie model and the rail and track structure model are shown in Figure 7.28 [71].

Brief descriptions of elements of the secondary and primary suspension connections in the locomotive model are given below:

Secondary suspension elements:

- *Rubber springs*: On each bogie frame, there are three rubber springs on which the locomotive car body rests. Compressive stiffness is high to support car body weight, whereas low shear stiffness allows car body yaw rotation relative to the bogie in curves.

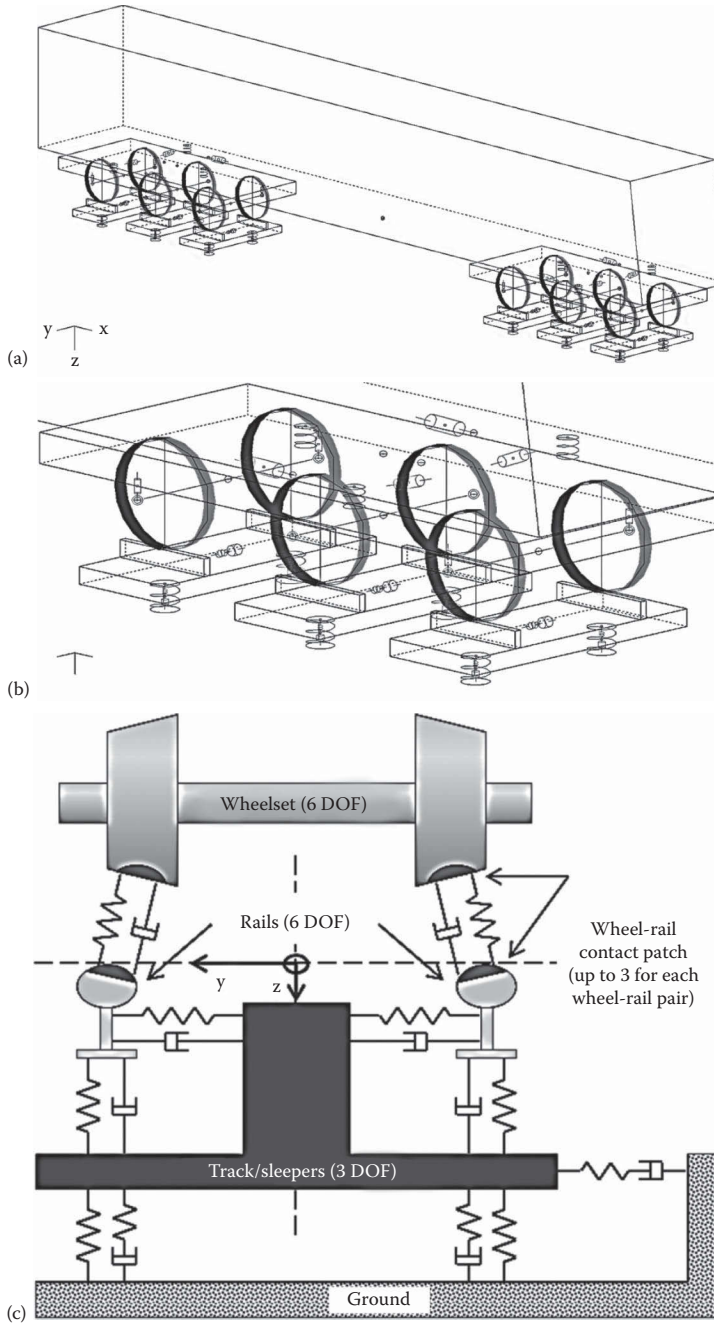

FIGURE 7.28 Locomotive modelling elements: (a) Locomotive multibody model, (b) rigid bogie connections model, and (c) track structure model. (From George, A.L., Theoretical and numerical investigation on traction forces for high adhesion locomotives, MEng Thesis, Central Queensland University, Rockhampton, Australia, 2015.)

- *Yaw viscous dampers*: Non-linear dampers mitigate relative yaw vibrations between the bogie frames and the car body. In conjunction with the lateral viscous dampers, they help to control bogie hunting.
- *Lateral viscous dampers*: Assist with controlling bogie hunting but have little effect on limiting relative yaw between the bogie frames and the car body.
- *Lateral bumpstops*: Limit relative displacements of the bogie frame in the lateral direction at the bogie frame centre. Side play of 60 mm is allowed (30 mm left/right from centre).
- *Vertical bumpstops*: Limit relative displacements of the bogie frame in the vertical direction on the left/right sides of the bogie frame. Vertical travel of 50 mm is allowed (25 mm up/down from rest position).
- *Bogie pivot pin*: Transfers tractive effort (longitudinal) and cornering (lateral) forces from the bogie to the car body. These are modelled with two non-linear springs constrained to move in the longitudinal and lateral directions, respectively. Free play of 4 mm (±2 mm from centre) is provided for in both directions.

Primary suspension elements: Elements in the primary suspension, except for bumpstops, were assumed to be linear.

- *Axle-box springs*: These are modelled as single springs with parallel dampers, and are positioned at the ends of wheelsets. Like the rubber springs in the secondary suspension, they have high compressive stiffness to support the car body and bogie frame, but are soft in shear to allow lateral and longitudinal wheelset movements.
- *Vertical viscous dampers*: Provide additional damping to reduce vertical wheelset vibrations in response to track irregularities. They are fitted only to the leading and trailing axles in each bogie.
- *Longitudinal bumpstops*: Allow limited relative displacements of the wheelsets in the longitudinal direction at the wheelset centres. Longitudinal travel of 10 mm is allowed (5 mm forwards/backwards from centre).
- *Lateral bumpstops*: Located in the same positions as longitudinal bumpstops (one per wheelset). Side play of 22 mm (11 mm left/right from centre) is allowed for the leading and trailing axles, whereas mid axles have 60 mm (30 mm left/right). Stiffness characteristics also differ between leading/trailing and mid-axle bumpstops.
- *Vertical bumpstops*: Allow limited relative displacements of wheelsets in the vertical direction on the left/right sides of wheelsets. Vertical travel of 50 mm is allowed (25 mm up/down from rest position).

The locomotive model parameter values are given in Table 7.6.

7.7.2 Methodology in LMAP

As the proposed LMAP is intended for use in Australia, the terminology is based on the LMAP used in the Rail Industry Safety and Standards Board (RISSB)/Australian

TABLE 7.6
Locomotive Model Parameters

Parameter	Value	Units
Dimensions		
Coupler longitudinal distance from car body Centre of Gravity (CoG)	22	m
Nominal coupler height above rail level	0.885	m
Bogie pivot longitudinal distance from car body CoG	7.095	m
Bogie pivot longitudinal distance (outwards) from bogie frame CoG	0.45	m
Bogie semi-wheelbase	1.85	m
New wheel diameter	1.067	m
Total mass	134000	kg
Car Body		
CoG height above rail level	1.93	m
Mass	91600	kg
Moment of inertia, roll	177095	kgm^2
Moment of inertia, pitch	3793457	kgm^2
Moment of inertia, yaw	3772695	kgm^2
Bogie Frame		
CoG height above rail level	0.733	m
Mass	11000	kg
Moment of inertia, roll	4826	kgm^2
Moment of inertia, pitch	33585	kgm^2
Moment of inertia, yaw	37234	kgm^2
Wheelsets		
CoG height above rail level for new (unworn) wheels	0.5335	m
Mass	3400	kg
Moment of inertia, roll and yaw	2134	kgm^2
Moment of inertia, pitch	1432	kgm^2
Secondary Suspension		
Rubber springs – longitudinal distance from bogie frame CoG	0.925	m
Outer springs		
Lateral distance from bogie CoG	1.272	m
Longitudinal and lateral shear stiffness	188.4	kN/m
Vertical stiffness	10	MN/m
Inner/central springs		
Longitudinal and lateral shear stiffness	376.8	kN/m
Vertical stiffness	20	MN/m
Traction rods		
Stiffness	25	MN/m
Damping coefficient	100	kNs/m

(*Continued*)

TABLE 7.6 (*Continued*)
Locomotive Model Parameters

Parameter	Value	Units
Bogie centre pins		
Stiffness at 2 mm displacement (expansion/compression)	0	kN/m
Stiffness at 40 mm displacement	60	kN/m
Stiffness from 41 mm displacement	1	GN/m
Lateral viscous dampers		
Longitudinal distance from bogie CoG	0.925	m
Damping coefficient	40	kNs/m
Yaw viscous dampers		
Lateral distance from bogie CoG	1.078	m
Series stiffness	45	MN/m
Damping coefficient (at 32 mm expansion/compression)	4.6	kNs/m
Blow-off point (at 1.032 m expansion/compression)	6.8	kNs/m
Secondary yaw viscous dampers – damping coefficient	200	kNs/m
Primary Suspension		
Axle box lateral position from wheelset CoG	1.078	m
Coil springs		
Longitudinal shear stiffness	45	MN/m
Lateral shear stiffness	2.25	MN/m
Vertical stiffness	782	kN/m
Damping coefficient	10	kNs/m
Vertical viscous dampers (except mid axle)	60	kNs/m

Source: George, A.L., Theoretical and numerical investigation on traction forces for high adhesion locomotives, MEng Thesis, Central Queensland University, Rockhampton, Australia, 2015.

Standards [90–92]. The proposed LMAP process has been split into three main 'stages' as follows.

7.7.2.1 Stage 1: Basic Locomotive Model Checking/Debugging

Stage 1 consists of tests to ensure that the model code used is free of errors and that the multibody model behaves as expected when basic (static and dynamic) analyses are performed. As the RISSB/Australian Standards do not contain provisions for the debugging of multibody locomotive models, the tests adopted in Stage 1 are based mainly on the GENSYS online documentation [93]. The procedures and acceptance criteria for Stage 1 tests can be summarised as follows:

1. Automatic syntax error checking: *Procedure:* Run the model code as input to an automatic code-checking program or other available tools. *Acceptance criteria:* No syntax/coding errors or extremely soft/stiff connections in the model code.

2. Visual model check: *Procedure:* View the model in a three-dimensional plotting program. *Acceptance criteria:* All bodies and connections should be correctly placed and dimensioned.
3. Quasistatic analyses:
   a. Vertical car body displacement: *Procedure:* Allow only vertical car body movement and displace it 5 cm in the downwards direction. *Acceptance criteria:* Both bogies deflect symmetrically, whereas wheel loads increase linearly in proportion to total primary and secondary suspension stiffness.
   b. Lateral car body displacement: *Procedure:* Allow only lateral car body movement and displace it 5 cm in the positive direction (right). *Acceptance criteria:* Both bogies deflect symmetrically, having negative roll displacements relative to the track.
4. Modal (eigenvalue) analysis: *Procedure*: Perform a modal analysis on the locomotive model at zero speed. Look for basic modes/eigenvalues. *Acceptance criteria:* Errors such as negatively damped and excessively high eigenvalues (upwards of ~5000 rad/s) should not be present.
5. Time-stepping analysis: Numerical instabilities: *Procedure:* Perform two time-stepping analyses on the locomotive model, with both fine and coarse time steps, at maximum design speed. *Acceptance criteria:* There should be no unexpected motions in the model. Initial disturbances should stabilise at the same time, regardless of the time step value.
6. Critical speed estimation: *Procedure:* Perform a time-stepping analysis with the locomotive at a very high speed (~300 km/h). Lateral instabilities are provoked with an initial excitation. Wheelset hunting stops near ±10 km/h of the locomotive's critical speed. *Acceptance criteria:* The approximate critical speed should be >110% of the maximum design speed of the locomotive.

7.7.2.2 Stage 2: Tests Currently Included in Standards

Stage 2 consists of static and dynamic tests that are presently included in the RISSB/Australian Standards for freight rolling stock, namely AS 7507.1 [90] for rolling stock outlines, AS 7508.1 [91] for track forces/stresses and AS 7509.1 [92] for dynamic behaviours. Procedures and acceptance criteria for Stage 2 tests can be summarised as follows:

Stage 2A: Rollingstock outlines

1. Static suspension heights: *Procedure:* Perform quasistatic analyses on the locomotive for both maximum and minimum operational weights to find the maximum and minimum static heights. *Acceptance criteria*: No part of the locomotive should infringe its applicable static (cross-sectional) outline.
2. Basic kinematics – sway: *Procedure:* Determine body roll and lateral translation relative to the wheelset centreline when the locomotive is tilted (e.g., when cornering). *Acceptance criteria:* No part of the locomotive should infringe its applicable basic kinematic (cross-sectional) outline.

a. Cant test rig: *Procedure:* Raise the locomotive in multiple increments up to its maximum applicable track cant (superelevation) on one side and then lower it back to zero cant. Do the same with the other side to get a hysteresis curve of lateral and roll movements versus applied cant.
b. On-track test (dynamic): *Procedure:* Perform a time-stepping (quasi-static) analysis, with the locomotive curving at maximum cant deficiency, as close to maximum speed as possible.
c. On-track test (static): *Procedure:* Perform a quasistatic analysis of the locomotive at maximum cant when stationary.

Stage 2B: Track forces and stresses

1. Axle loads and P/D ratios: *Procedure:* Wheelset loads can be obtained from either a quasistatic analysis at 0 km/h or a quasistatic/time-stepping analysis at 10 km/h. The P/D ratio is simply wheel load divided by wheel diameter. *Acceptance criteria:* Wheelset/axle loadings and P/D ratios cannot exceed prescribed limits.
2. P2 forces: *Procedure:* This is simply obtained using the equation described in AS 7508.1 [91]. *Acceptance criteria:* P2 forces cannot exceed prescribed limits.
3. Lateral track-shifting forces: *Procedure:* Perform time-stepping analyses for situations (if any) where the locomotive will experience unbalanced lateral acceleration $\geq 0.72\,m/s^2$ (for 1435 mm standard gauge track) in curves. *Acceptance criteria:* The sum of lateral wheelset forces on each axle cannot exceed the limits defined in Ref. [91].
4. Lateral wheel-to-rail forces: *Procedure:* Run the locomotive through various curves whose speed, cant and radius result in an unbalanced lateral acceleration of $0.73\,m/s^2$ by using time-stepping analyses. *Acceptance criteria:* Lateral wheel-rail forces cannot exceed the limits defined in Ref. [91].

Stage 2C: Dynamic behaviour (time-stepping analyses are required, unless otherwise noted)

1. Hunting: *Procedure:* Run the locomotive model over a ≥2 km section of smooth, straight track at 110% of the maximum design speed. *Acceptance criteria:* Lateral and vertical acceleration limits at the bogie centres cannot be exceeded. Significant hunting motions of the wheelsets cannot occur during the test.
2. Base ride accelerations: *Procedure:* Run the locomotive over the track that represents the roughest track encountered in service. Straight track will suffice. *Acceptance criteria:* Lateral and vertical acceleration limits at the bogie centres cannot be exceeded.
3. Horizontal and vertical curve negotiation: *Procedure:* Measure displacements of locomotive bodies when traversing the minimum radius horizontal and vertical curves encountered in service (at low speeds). *Acceptance criteria:* Clearances between the car body, bogie frames and wheelsets should

allow the locomotive to traverse the track geometry without derailing or being damaged. Suspension elements/parameters and wheel-rail profiles may also have an effect.

4. Transition curve negotiation:
   a. Twist test: *Procedure:* The static locomotive model is placed on a cant ramp designed to impart (underframe) twisting forces. Wheelsets of interest—in this case, the leading wheelset of the first bogie—are then incrementally raised and lowered on both sides in a similar manner to Stage 2A, Test 2a, to obtain a hysteresis curve showing wheel unloading versus applied wheelset cant. *Acceptance criteria:* The average wheel unloading for the analysed wheelset cannot exceed 60%.
   b. Bogie rotational resistance: *Procedure:* Determine the torque required to rotate the bogies relative to the car body by either running the model through a minimum-radius curve at a speed typical of operational conditions or rotating one bogie while the locomotive is static. *Acceptance criteria:* The *X*-factor calculated for the bogie should be less than 0.1.
   c. Alternate on-track assessment: *Procedure:* Run the locomotive model at 10 km/h through a minimum radius curve with a prescribed cant irregularity in the exit transition. *Acceptance criteria:* Limits on maximum axle (sum) L/V (Y/Q) ratios and wheel L/V ratios sustained for 50 ms cannot be exceeded.
5. Rollover: *Procedure:* Perform time-stepping analyses for situations (if any) where the locomotive will experience unbalanced lateral acceleration $\geq 0.72\ m/s^2$ (for 1435 mm standard gauge track) in curves. *Acceptance criteria:* The vertical unloading for wheels on the low rail cannot be greater than 60%.
6. Isolated track irregularities: *Procedure:* Run the locomotive at a range of speeds up to 110% of the design speed over irregularities constituting a flat hump (vertical), a curved dip (vertical) and curve entry irregularities (lateral). *Acceptance criteria:* Prescribed limits for maximum lateral/vertical accelerations, vertical wheel-rail forces and sum axle L/V ratios cannot be exceeded.
7. Cyclic track irregularities: *Procedure:* Run the locomotive at a range of speeds up to 110% of the design speed for the following cases: (a) pitch and bounce (vertical parallel rail disturbances), (b) harmonic roll (vertical staggered rail disturbances) and (c) curve entry irregularities (variations in cant imbalance). *Acceptance criteria:* Prescribed limits for maximum lateral/vertical accelerations, vertical wheel-rail forces and sum axle L/V ratios cannot be exceeded.
8. Longitudinal forces in curves: *Procedure:* Calculations are first carried out to determine wheel unloading limits and to determine whether they will be breached for a locomotive experiencing longitudinal buff/draft forces in a small-radius curve. If the calculated limit is not exceeded but the calculated wheel unloading is greater than 90%, a time-stepping analysis is required.

The locomotive is simulated to run in a small-radius curve, with either separate rolling stock models coupled to it to provide buff/draft forces or by applying coupler forces to the locomotive model that are determined using longitudinal train simulation. *Acceptance criteria:* The calculated wheel unloading limit should not be exceeded. Any wheel lift during simulations results in failure.

7.7.2.3 Stage 3: Tests Not Included in Standards (Traction and Braking)

Locomotive traction and braking tests are contained in Stage 3 because they are not covered in the Australian Standards. In addition to a mechanical multibody model, these require modelling of traction and/or braking systems. A brief summary of the tests in Stage 3 is given as follows:

Stage 3A: Traction tests

1. Gradient starting: *Procedure:* Determine the longitudinal coupler force exerted on the locomotive when hauling the heaviest permissible train up a given gradient. Apply this coupler force to the locomotive model and have it start from rest on straight, level track. *Acceptance criteria:* The locomotive (and the train) should be able to accelerate to balance speed without exceeding the traction equipment's short-time thermal rating.
2. All-weather adhesion limit: *Procedure:* Start the locomotive and the train (the latter simulated with applied longitudinal coupler forces) at line speed on dry, level straight track before climbing a 1 km incline. At 500 m up the incline track, change friction from dry to wet to simulate the application of water sprays on the locomotive. *Acceptance criteria:* The test fails if speed drops below 10 km/h, excessive uncontrolled wheelslip occurs and/or the traction equipment's short-time thermal rating is exceeded.
3. Tractive effort-speed for dry/wet rail: *Procedure:* Run the locomotive and train from rest on straight track up to balance speed. The track can be on a gradient, but level track will suffice. Record tractive effort, speed, throttle reading, wheelslip, sanding applications and the time taken to accelerate to balance speed during the test. *Acceptance criteria:* Excessive wheelslip is not allowed.
4. Continuous tractive effort for dry/wet rail: *Procedure:* Starting at balance speed, run the locomotive on a straight track. The track can be on a gradient, but level track will suffice. *Acceptance criteria:* The locomotive must be able to maintain its balance speed without excessive wheelslip.
5. Balance speed acceleration test: *Procedure:* This is similar to Stage 3A, Test 1; however, the objective is to record the time taken for the locomotive to accelerate to balance speed with its given gradient and load. *Acceptance criteria:* Criteria are similar to that for Stage 3A, Test 1, with the additional requirement that the time taken to accelerate to balance speed should be similar to the data provided by the locomotive manufacturer (however, this is not strictly a criterion for failure).

Stage 3B: Braking tests

1. Stopping distances: *Procedure:* A locomotive and train are to be tested on dry, straight track. It is preferred to have level track, but constant gradients can also be used. Shortly after the train has started at speed, apply the (emergency/dynamic/pneumatic) brakes and record the distance and time elapsed while the train slows to a stop. Multiple speeds should be tested. *Acceptance criteria:* Excessive wheelslip cannot occur, and the train must be able to slow to a complete stop. Braking time and distance (with the train) should be similar to the data provided by the locomotive manufacturer (however, this is not strictly a criterion for failure) and within the limits imposed by the locomotive operator.
2. Gradient parking: This test should be considered only if parking brake mechanisms are being tested. *Procedure:* Start the locomotive at rest on a 1:30 gradient, with the parking brake on. *Acceptance criteria:* The parking brake should be strong enough to secure the locomotive indefinitely. No movement is allowed.
3. Static test: Consider this test only if pneumatic braking is modelled. *Procedure:* Apply the locomotive air brakes when it is at rest. Simulation of the air brakes alone (rather than the multibody model) should suffice. *Acceptance criteria:* The air brakes should function properly, with appropriate air pressures, apply/release times and brake block forces.
4. Deceleration rates: *Procedure:* Linked to the results out of Stage 3B, Test 1. Deceleration rates can either be recorded directly or calculated from the deceleration times and distances recorded earlier. *Acceptance criteria:* Braking deceleration rates should be similar to the data provided by the locomotive manufacturer (however, this is not strictly a criterion for failure) and within the limits imposed by the locomotive operator.

7.7.3 Simulated Case Studies for Locomotive Model Validation

Owing to the lack of available data from physical testing under actual operational conditions and the consequent lack of quantitative measurements for verifying the locomotive model, it is assumed that compliance with standards referenced in the LMAP constitutes successful test outcomes. Obviously, a locomotive model should accurately replicate the capabilities of its real counterpart. Discussion follows of the various scenarios examined as part of ensuring that the locomotive model used to demonstrate the LMAP process can be considered sound.

With vertical car body displacement applied to the locomotive model, the car body and bogie frames are displaced downwards as expected, as shown in Figure 7.29a. Simulation results should show that vertical wheel-rail contact forces have increased in response to the car body displacement and are equal across all wheels. From Figure 7.29b, it can be seen that the lateral car body displacement causes additional roll displacement in the car body and the bogie frame. It is apparent that the secondary suspensions for the locomotive model are much stiffer than their primary suspensions.

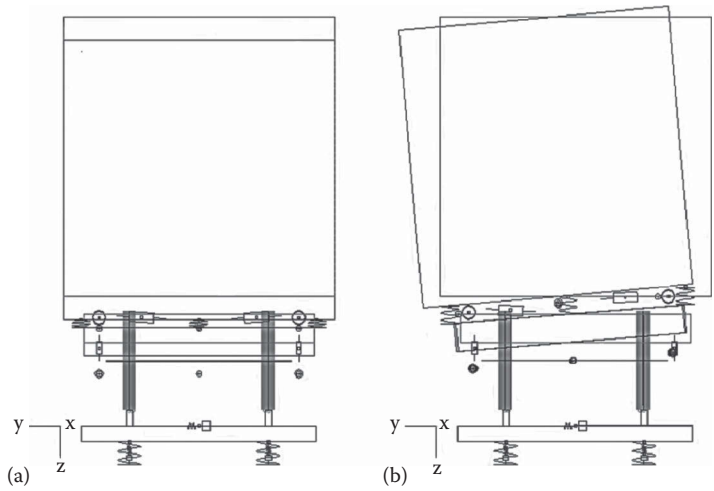

FIGURE 7.29 Front views of model undergoing Stage 1 car body displacements: (a) Model undergoing vertical car body displacement and (b) model undergoing lateral car body displacement. (From George, A.L., Theoretical and numerical investigation on traction forces for high adhesion locomotives, MEng Thesis, Central Queensland University, Rockhampton, Australia, 2015.)

TABLE 7.7
Approximate Locomotive Model Stabilisation Times

Locomotive Speed	20 km/h	70 km/h	115 km/h
	Model Stabilisation Times (s)		
Fine time step (0.1 ms)	2.3	2.3	2.3
Coarse time step (1 ms)	1.8	1.8	1.8

Source: George, A.L., Theoretical and numerical investigation on traction forces for high adhesion locomotives, MEng Thesis, Central Queensland University, Rockhampton, Australia, 2015.

The potential for numerical instability is checked by running the model over a straight and level section of an ideal track at different speeds. It is required that the locomotive model becomes stable once all vertical wheel-rail forces have stabilised using both fine and coarse time steps.

Approximate stabilisation times for the locomotive model, speeds and solver time steps are summarised in Table 7.7. Stabilisation times do not vary with speed, but they do increase with decrease in time step.

A quick method of estimating the critical hunting speed of a locomotive model is to start it off at a high speed, with an initial lateral disturbance being applied to the car body, and then decelerate it at a fixed rate until hunting motions in the

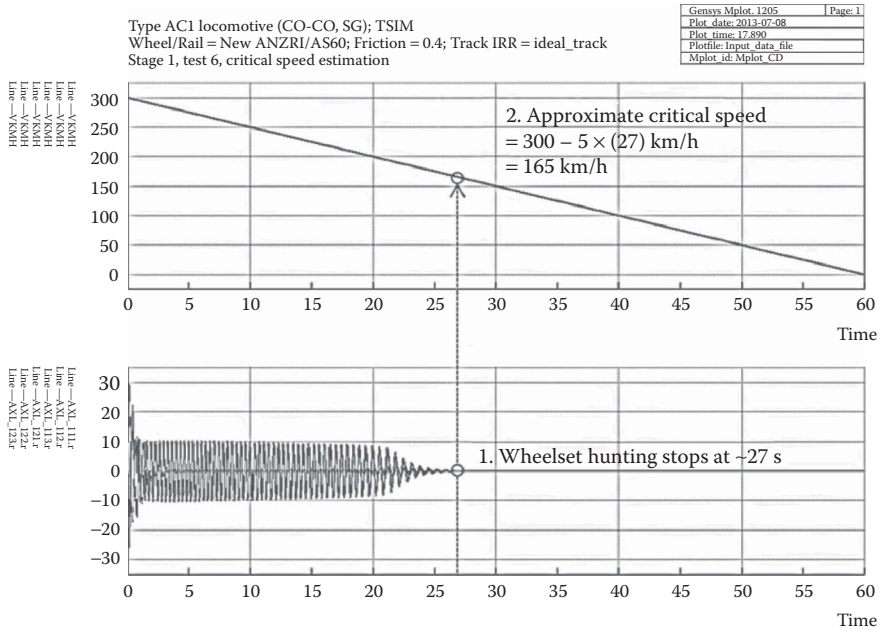

FIGURE 7.30 Determining approximate critical hunting speed. (From George, A.L., Theoretical and numerical investigation on traction forces for high adhesion locomotives, MEng Thesis, Central Queensland University, Rockhampton, Australia, 2015.)

wheelsets stop. From Figure 7.30, it can be seen that the hunting speed is approximately 165 km/h for this locomotive. A heavy haul locomotive's normal maximum operational design speed is approximately 90 km/h; therefore, the modelling satisfies the acceptance criterion with regard to hunting.

Other tests specified in Stage 2 are also performed. For example, the maximum lateral and vertical accelerations of the car body at the bogie centres during hunting motions at high speed are simulated and evaluated; all are found to satisfy the limits required in the standards. Another example concerns cyclic track irregularities, which create locomotive pitch and bounce. In this test, the locomotive model is run over a test track with cyclic vertical track centreline disturbances specified in the standard. The maximum lateral and vertical accelerations at the bogie centre, the maximum wheel unloading and the maximum sum axle L/V ratio that occur for a period of more than 50 ms are evaluated, and all values are much less than the allowable limits.

As mentioned previously, Stage 3 tests deal with traction and braking and are not included in Australian Standards. It is somewhat of a 'debugging' exercise to ensure that both the variable friction modelling and the traction control system in the locomotive model work properly. Results are used to select the optimum longitudinal creep values for the locomotive model at maximum continuous tractive effort for dry and wet track surfaces. For this analysis, the creep/slip range to be simulated is 0%–30%,

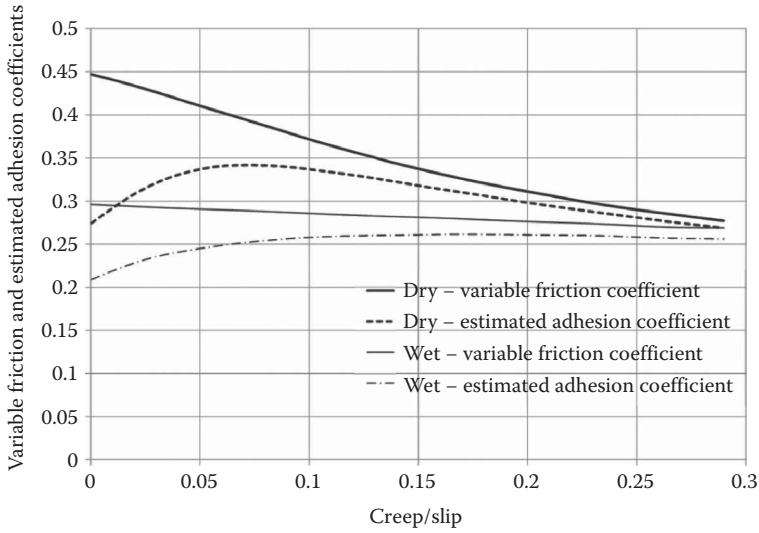

FIGURE 7.31 Variable friction and estimated adhesion curves. (From George, A.L., Theoretical and numerical investigation on traction forces for high adhesion locomotives, MEng Thesis, Central Queensland University, Rockhampton, Australia, 2015.)

with the rate of creep increase being 0.1% per second (total modelling time is 300 s). For both dry and wet track conditions, the locomotive model is run at its maximum continuous tractive effort rating and then a variable friction coefficient and an approximate adhesion coefficient are plotted against creep/slip, as shown in Figure 7.31.

The acceptance criteria are that no uncontrolled wheelslip or other traction control system malfunctions should occur over the tested creep/slip range and that no significant interference/vibrations should be present in the plotted data.

An LMAP for use in MBS software has been described, and sample tests have been conducted using a locomotive model in GENSYS. These simulated case studies show that simulation of locomotive dynamic behaviour in MBS software is not only possible, but can also identify issues with a locomotive model that might otherwise be overlooked.

7.8 EXAMPLES OF HEAVY HAUL LOCOMOTIVE DYNAMIC BEHAVIOUR STUDIES IN GENSYS

Three examples have been selected to illustrate the applications of heavy haul locomotive modelling in GENSYS. The first is the assessment of an air suspension design suitable for application in a heavy haul locomotive; the second examines the optimisation of primary suspension characteristics for heavy haul locomotives; and the third demonstrates the application of inverse modelling of a heavy haul locomotive to determine the wheel-rail contact forces based on the accelerations measured on the locomotive's car body and bogie.

7.8.1 Application of Adjustable Air Suspension under Traction Control

During the operation of a locomotive in traction or braking mode, the body weight is distributed between bogies in different proportions depending on many factors. Each bogie and wheelset thus experience different traction coefficients. The adhesion coefficient is dependent not only on the tractive or braking effort but also on vertical wheel loading. Here, we will examine several design variations of a Co-Co locomotive equipped with adjustable secondary air suspension by using rail vehicle multibody modelling software with a view to optimising adhesion.

The various types of traction control currently in use do not provide a perfect solution for the realisation of maximum possible tractive efforts for heavy haul locomotives equipped with three-axle bogies [94,95]. It should be emphasised that locomotive traction behaviour is dependent on the parameters of the primary and secondary suspension systems [79,96–98]. Mechanical optimisation of the suspension is not a very attractive option because it can be optimised only for some specific tasks on specific tracks. To achieve more generic outcomes applicable for a broader range of operational conditions, it is necessary to work on the characteristics of the secondary suspension and to use an active spring suspension instead of a conventional design. This can be achieved for vertical suspension using an 'air pump' controlled air spring. However, traction studies in this field have not yet been performed to progress further development of this air suspension design.

In order to show the impact of an active secondary suspension system equipped with air springs, we will analyse three design variations of the secondary suspension, namely conventional springs, uncontrolled air springs and fully controlled air springs. Taking into account that typical heavy haul locomotives are equipped with a bogie traction control system, the proposed approach is to systematise the combination of aspects for both the secondary suspension system and the traction control system and to assess the implications of the various designs by means of analysing the results obtained from the numerical studies performed in GENSYS multibody software [99].

7.8.1.1 Secondary Suspension Design and Its Modelling Approach

Figure 7.32 shows the basic design of the proposed heavy haul locomotive. Four air springs are mounted on each bogie as the main elements of the secondary suspension, with each spring having its own individual air supply and control system. These substitute for the rubber elements used in conventional designs.

Considerable work has been undertaken on the modelling of air springs for vehicle dynamics and efforts have been put towards developing very accurate relationships with data obtained from laboratory experiments. Taking into account that the traction coefficient is highly dependent on weight distribution, it is reasonable to focus on modelling the air spring in only the vertical direction. The simplified model shown in Figure 7.32 has been verified in experiments [100]; model parameters are the air spring stiffness (k), the damping coefficient (c) and the controllable force (F). The stiffness, k, can be obtained in N/m, as

$$k = \frac{nA_{eff}^2 p_0}{V_0} \tag{7.117}$$

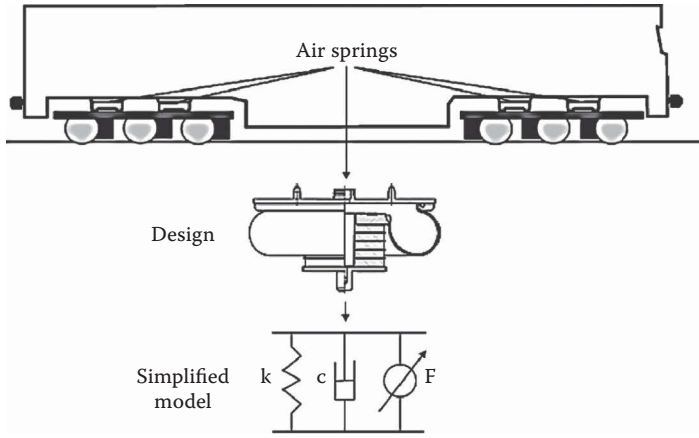

FIGURE 7.32 Heavy haul locomotive equipped with secondary air spring suspension and its simplified air spring model. (From Spiryagin, M. et al., Investigation of the application of adjustable air suspension under traction control for heavy haul locomotives, *Proceedings of the Stephenson Conference: Research for Railways*, IMechE, London, UK, April 21–23, pp. 549–558, 2015.)

where:

p_0 is the pressure in the air spring (N/m^2)
A_{eff} is the effective area of the air spring (m^2)
V_0 is the nominal volume of the air spring (m^3)
n is the polytrophic index, which equals 1 for slow, static deformation of the air spring and 1.3–1.4 for dynamic deformation [101]

A polytrophic index of 1.4 has been assumed in the simulation of dynamic processes in the air springs.

Lobachev [102] indicates that the area of the air spring changes by approximately 5% when the height is changed under testing. Therefore, a simplification of constant effective area has been made in this analysis. The main characteristics of the air spring, presented in Table 7.8, have been chosen based on the air spring design for the 138-tonne locomotive with three-axle bogies, described in Ref. [102].

Ref. [102] shows that the dynamic pressure change under lateral dynamics studies for curves can add approximately 20% to the working pressure in air springs. Therefore, it looks reasonable to assume that the maximum allowable pressure of the air spring can be limited to 106 N/m^2, as done by Docquier [103].

7.8.1.2 Locomotive Modelling in GENSYS

Three simulation cases are investigated to show traction behaviour of locomotives equipped with conventional, noncontrolled and controlled secondary suspension systems. The two mechanical models of a heavy haul locomotive with a semi-steering (yaw-relaxed, self-steering) bogie design required for this study have been implemented in GENSYS. These models have different elements in their secondary

TABLE 7.8
Main Characteristics of the Air Spring

Parameter	Value
Height	0.21 m
Effective area	0.212 m^2
Nominal volume	0.027 m^3
Working pressure	550000 N/m^2

Source: Lobachev, N.A., Pneumatic support and connection system between the locomotive body and bogies, PhD Thesis, All-Union Scientific Research Diesel Locomotive Institute, Kolomna, USSR, 1983 (in Russian).

suspension system, as shown in Figure 7.33. The model in Figure 7.33a has characteristics as installed on a standard locomotive bogie with conventional suspension, and the bogie model in Figure 7.33b is for the proposed heavy haul locomotive with air springs, as shown in Figure 7.32. The overall locomotive parameters for both models are set out in Table 7.9.

The full locomotive model consists of the car body, two bogie frames, twelve axle boxes and six wheelsets, all of which are modelled as rigid masses with six DOFs. Constraints between each wheelset and its axle boxes are implemented in the model. In the lateral direction, a linear spring element is used between each axle box and the wheelset in order to model a potential clearance between these two bodies. In wheel-rail contact modelling, the rails are modelled as massless bodies. Three springs are provided normal to each wheel-rail contact interface, allowing three separate contact patches to be in contact simultaneously (Figure 7.28). The rails are connected to the track via springs and dampers in the lateral and vertical directions. Creep forces are calculated based on the method developed by Polach [53].

7.8.1.3 Control Systems

A typical traction control system that acts individually for each bogie, and that is used both for a standard locomotive and for a locomotive with an uncontrolled secondary air suspension system, is shown in Figure 7.34a. The advanced traction control system, which includes an additional control system for the air spring secondary suspension, is shown in Figure 7.34b. Both have been created as subroutines in GENSYS.

The variables shown in Figure 7.34 are T_{ref} = reference torque; T_{ref}* = reference torque generated by the control system; T_{in} = input motor torque; T_{wheels} = traction torque applied to the axles; ΔT = torque reduction; ω = angular velocity of a reference axle; ω_1, ω_2 and ω_3 = angular velocity of front, middle and rear axles, respectively; s_{est} = estimated longitudinal slip; s_{opt} = optimal longitudinal slip; h_1,..,h_8 = heights for each air spring; F_{a1},..,F_{a8} = actuator forces acting in the vertical direction and dependent on the supply pressure to each air spring. The dynamics of the inverters and traction motors are modelled by means of a low-pass filter. It is assumed that sensors similar to those described in Ref. [103] can be used for a proposed

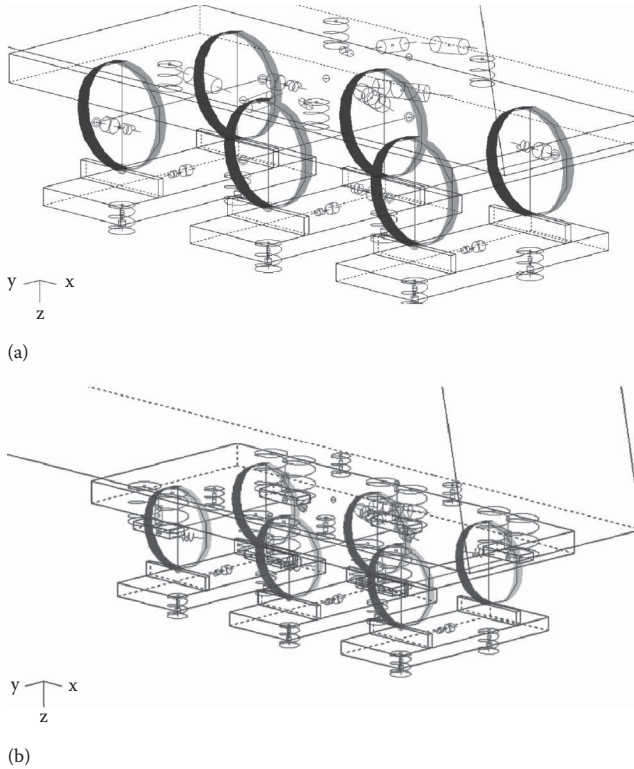

FIGURE 7.33 Conventional and proposed locomotive bogie models: (a) Conventional secondary suspension and (b) air spring secondary suspension. (From Spiryagin, M. et al., Investigation of the application of adjustable air suspension under traction control for heavy haul locomotives, *Proceedings of the Stephenson Conference: Research for Railways*, IMechE, London, UK, April 21–23, pp. 549–558, 2015.)

suspension control subsystem with an individual algorithm for each air spring based on simple fuzzy logic rules that tries to equalise heights of the air springs for each bogie, that is, the suspension control of the locomotive's front bogie is independent of the suspension control of its rear bogie.

7.8.1.4 Simulation and Results

The locomotive simulation is run on a straight track with ideal track conditions. An all-weather adhesion limit of 35% is used because it can be assumed that this level can be realised with a 97% probability on dry rail. An adjustable longitudinal coupler force has been attached to the locomotive model in order to maintain a constant speed of 22 km/h, which is chosen because it is the continuous mode speed, that is, the speed at which the locomotive experiences maximum creep forces. As mentioned previously, three simulation cases are performed in order to compare three secondary suspension design variants. The comparisons of results for axle load distribution, traction coefficient and tractive effort for each design variant are shown

TABLE 7.9
Parameters for the Multibody Locomotive Model

Parameter	Value
Locomotive Car Body	
Centre of gravity, vertical distance above top of rail	1.93 m
Mass	90000 kg
Moment of inertia, roll/pitch/yaw	174002/3727195/3706796 kgm^2
Bogie Frame	
Centre of gravity, vertical distance above top of rail	0.733 m
Mass	12121 kg
Moment of inertia, roll/pitch/yaw	5318/37007/41029 kgm^2
Axle Box	
Centre of gravity, vertical distance above top of rail	0.5335 m
Mass	200 kg
Moment of inertia, roll/ pitch/ yaw	50/50/50 kgm^2
Wheelsets (with the traction motor mass shared between bogie and axles)	
Centre of gravity, vertical distance above top of rail	0.5335 m
Mass	2893 kg
Moment of inertia, roll/pitch/yaw	2067/1387/2067 kgm^2
Secondary Suspension	
Vertical stiffness per spring (conventional design)	7870 kN/m
Vertical stiffness per spring (design with air springs)	1281 kN/m
Vertical damper per spring (design with air springs)	1 kNs/m
Other Dimensions	
Wheel diameter	1.067 m
Axle spacing	1.9 m
Bogie spacing	13.7 m

in Figures 7.35–7.37. Maximum tractive efforts have been applied to the wheelsets in order to perform this study. In theory, the maximum tractive effort of 420 kN assumed for this speed can be achieved with the optimal slip value set to 0.08.

The axle load results presented in Figure 7.35 show that axle loads are not perfectly distributed for the conventional and uncontrolled air spring secondary suspension designs and that there is only a slight difference between these two designs. However, the controlled secondary air spring suspension design comes closest to achieving the equalising of weight loads between axles, giving a positive indication that it would lead to the reduction of the maximum vertical wheel load experienced under traction.

Figure 7.36 confirms that there are additional benefits of using the controlled air spring secondary suspension design, indicating that the middle and trailing axles are very close to reaching the required traction coefficient of 0.35. By contrast, the

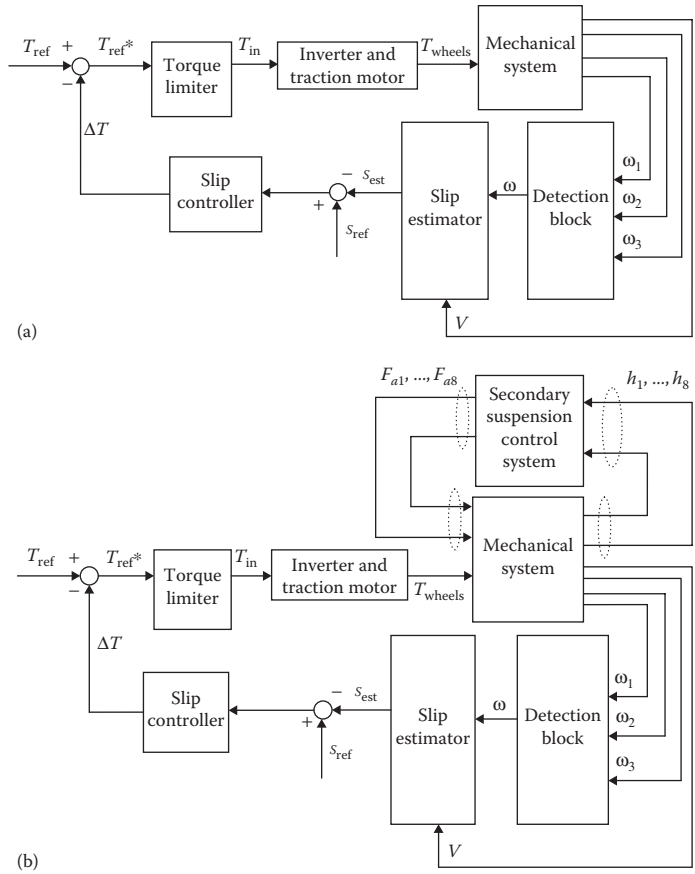

FIGURE 7.34 Traction control algorithms: (a) Standard approach and (b) advanced approach. (From Spiryagin, M. et al., Investigation of the application of adjustable air suspension under traction control for heavy haul locomotives, *Proceedings of the Stephenson Conference: Research for Railways*, IMechE, London, UK, April 21–23, pp. 549–558, 2015.)

uncontrolled air spring secondary suspension design leads to a significant reduction of traction coefficient, performing worse than even the conventional design. The uncontrolled air spring design also achieves the poorest tractive effort result, as shown in Figure 7.37. However, the controlled air spring secondary suspension design seems a good solution because it achieves a 10% increase in drawbar pull compared with the conventional design.

In summary, the uncontrolled air spring suspension gives the poorest results for all performance parameters because of its soft stiffness characteristics, which would be totally inappropriate for use on heavy haul locomotives in which high traction is required. The conventional secondary suspension shows better results than the uncontrolled air spring suspension design, but it still cannot match the performance of a locomotive equipped with a controlled air spring suspension system.

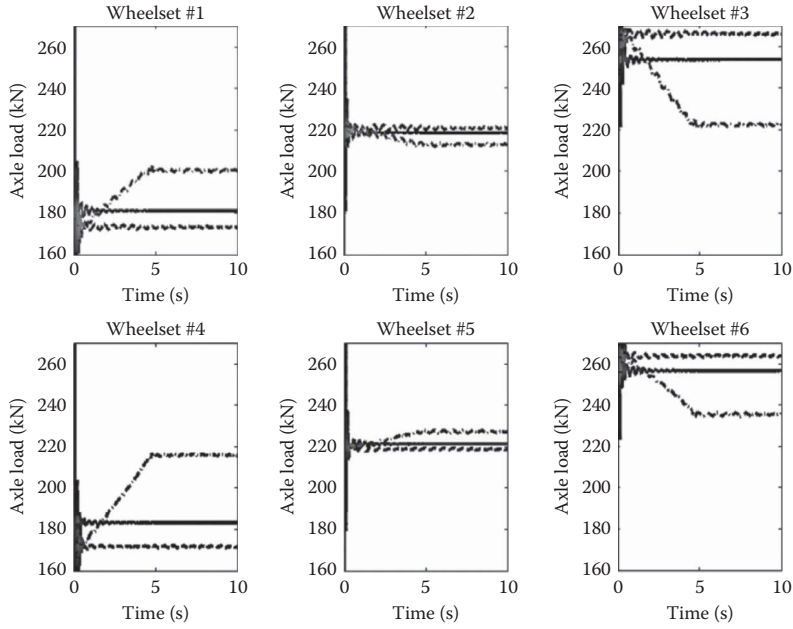

FIGURE 7.35 Axle load results in the time domain for conventional secondary suspension (solid line), uncontrolled air spring secondary suspension (dash-dot line) and controlled air spring secondary suspension (dashed line). (From Spiryagin, M. et al., Investigation of the application of adjustable air suspension under traction control for heavy haul locomotives, *Proceedings of the Stephenson Conference: Research for Railways*, IMechE, London, UK, April 21–23, pp. 549–558, 2015.)

7.8.2 Optimisation of Primary Suspension Characteristics for Heavy Haul Locomotives

Heavy haul locomotives can achieve an improvement in their tractive effort by means of equalisation of weight loadings between wheelsets to suit adhesion conditions. However, this is not a perfect solution, because adhesion limit variability can lead to the overloading of wheelsets with poor adhesion conditions along with insufficient loading on wheelsets with better adhesion conditions. The mechanical design of the primary suspension has a big influence on locomotive performance under both traction and braking operating modes. For example, increase in primary suspension stiffness can result in decrease in the weight utilisation of the leading wheelset of each bogie. In addition, the yaw stiffness of the primary suspension is an important parameter for optimising the radial steering process of wheelsets. It is necessary to find a balanced outcome between weight loading, stiffness and steering ability in order to provide optimal performance. During locomotive movement in traction or braking modes, the weight of a locomotive body is distributed between bogies in different proportions, depending on many factors. The design of a Co-Co locomotive with variations of the primary suspension design characteristics is examined here by means of numerical experiments using the GENSYS multibody software package [104].

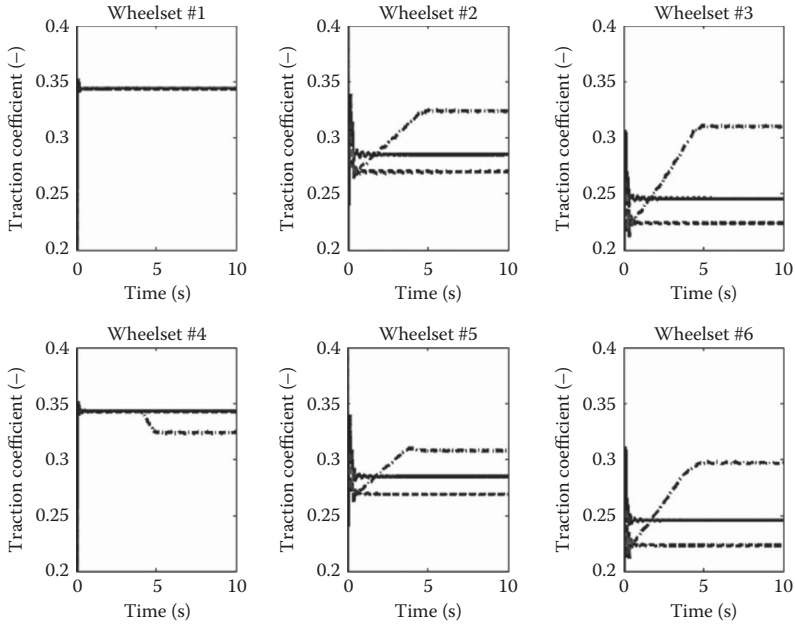

FIGURE 7.36 Axle traction coefficient results in the time domain for conventional secondary suspension (solid line), uncontrolled air spring secondary suspension (dash-dot line) and controlled air spring secondary suspension (dashed line). (From Spiryagin, M. et al., Investigation of the application of adjustable air suspension under traction control for heavy haul locomotives, *Proceedings of the Stephenson Conference: Research for Railways*, IMechE, London, UK, April 21–23, pp. 549–558, 2015.)

Evaluation of a locomotive design is a multicriteria, statistical and nondeterministic task. Among the many variants of design configuration, it is necessary to choose the most appropriate. The primary criteria for the effectiveness of the dynamic interaction between a locomotive and the track are as follows:

- Values of vertical forces and accelerations;
- Values of horizontal forces and accelerations;
- Utilisation of adhesion weight;
- Total tractive effort on the specified track; and
- The so-called comprehensive estimation criterion for tractive-dynamic qualities of locomotives, which can be obtained as a vector sum of the relative estimations of the other factors.

To make the correct decisions in this area, it is necessary to evaluate the many factors that affect the process outputs. The factors that most significantly affect the nature of these outputs should be analysed and others can be ignored. This reduces the amount of research, timeframes and material costs and simplifies the mathematical models that describe the objects or processes under investigation, all of which allow appropriate intensification of the research.

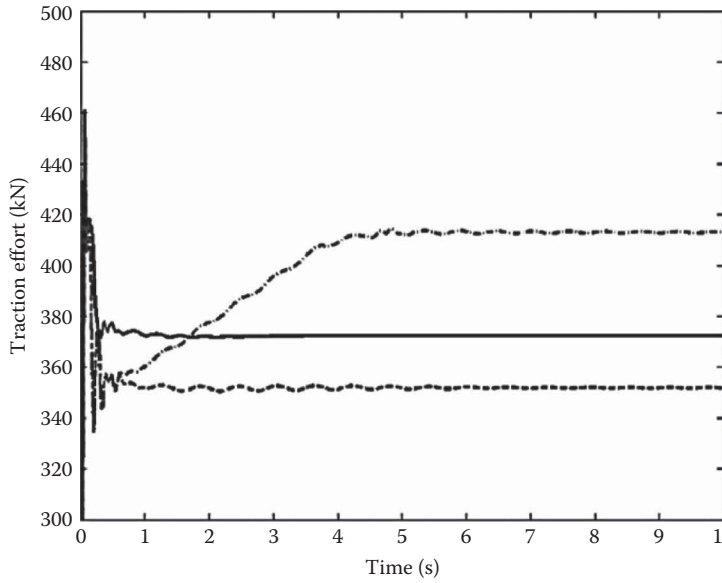

FIGURE 7.37 Locomotive tractive effort results in the time domain for conventional secondary suspension (solid line), uncontrolled air spring secondary suspension (dash-dot line) and controlled air spring secondary suspension (dashed line). (From Spiryagin, M. et al., Investigation of the application of adjustable air suspension under traction control for heavy haul locomotives, *Proceedings of the Stephenson Conference: Research for Railways*, IMechE, London, UK, April 21–23, pp. 549–558, 2015.)

Modelling is defined as an organised scientifically based analysis procedure that reflects the behaviour of the real system in order to explain the processes working in that system and the influence of the individual parameters on those processes.

During the development of a model, it is commonly necessary to solve a number of problems. The first range of problems is related to the methodology for creating the model: the choice of dimensions in the model and its variables, its identification and the choice of the oscillations from moving over the track. The second range is associated with providing a rational technology for the modelling issues.

The characteristics of elastic elements and connections between a bogie frame and wheelsets (primary suspension) and between a bogie frame and the locomotive body (secondary suspension) determine tractive and dynamic parameters of the running gear and the processes occurring in the contact zones between the wheels and the rails.

It is advisable to introduce realistic characteristics in running gear models based on the results obtained from experimental investigations.

Grassie and Elkins [105] studied the behaviour of a conventional two-axle bogie with tractive effort and stated that 'the ability of a bogie to steer deteriorates as tractive effort increases'. However, this statement needs to be verified for a three-axle bogie. Some research in the field of suspension design has been undertaken

in Ukraine in order to understand the behaviour of locomotives equipped with two three-axle bogies under traction on tangent track [96,97]. Similar research for curved track has been performed in Australia, which shows the influence of the bogie design on the steering ability [74–76,79,106].

Here, the focus is on primary suspension, because detailed descriptions and models of such systems are poorly represented for heavy haul locomotives in other publications and even small changes in the parameters and design can lead to significant changes in the final results.

7.8.2.1 Locomotive Mechanical Model

The primary suspension design commonly used in heavy haul locomotive bogies, which has the axle box connected to the bogie frame with coil springs and a traction rod as shown in Figure 3.21, is used for this study. The mechanical model of heavy haul locomotive with a conventional semi-steering bogie design implemented in GENSYS, as shown in Figure 7.33a, and with the characteristics documented in Table 7.9 for the conventional secondary suspension is again used. The model comprises 21 rigid bodies, namely a locomotive body, two bogie frames, twelve axle boxes and six wheelsets; the constraints applied to these bodies are presented in Table 7.10. The traction motor mass has been shared between the bogie frame and its wheelsets.

The primary suspension between the bogie frame and each axle box includes the following:

- Two coil springs: Each is a stiffness connection with coil spring element;
- *One hydraulic shock absorber*: A damping connection with linear damper element acting in the vertical direction;
- *One traction rod*: A spring connection with linear spring element acting in the longitudinal direction;
- *One lateral bumpstop*: A spring connection with linear spring element acting in the lateral direction; and
- *One vertical bumpstop*: A spring connection with linear spring element acting in the vertical direction.

TABLE 7.10
Constraints on Bodies

	***x*-Longitudinal**	***y*-Lateral**	***z*-Vertical**	***f*-Roll**	***k*-Pitch**	***p*-Yaw**
Locomotive body	√	√	√	√	√	√
Bogie frame	√	√	√	√	√	√
Axle box	√	√	√	√	√, $v_k = 0$	√
Wheelset	√	√	√	√	√, $k = 0$	√

Note: √ = Degree considered; $k = 0$ and $v_k = 0$ refer to pitch angle and axle box angle velocity being fixed to be equal to zero.

A linear spring element is used in the lateral direction between the axle box and the wheelset in order to model a possible clearance between two bodies.

7.8.2.2 Simulation and Results

The Polach creep-force calculation method [53] is used in order to model the locomotive behaviour under traction. The simplified traction control system has been introduced in the model, which allows smooth change in the angular velocity of the wheelsets in order to reproduce the required longitudinal creepage and achieve the desired traction. This system has been implemented as a subroutine in GENSYS and is similar to the one published in Ref. [95].

The locomotive runs on tangent and curved tracks with ideal track conditions. Different coefficients of friction have been used in the simulation cases for tangent and curved tracks. For the former, it is assumed that the maximum coefficient of friction for Polach's model is 0.47; for the latter, it is assumed that the maximum coefficient varies from 0.23 to 0.47 for the different contact conditions on the high and low rails, respectively. The locomotive is set in Notch 8 and runs with a constant speed of 22 km/h (continuous traction mode).

In order to accurately reproduce the behaviour of the locomotive on the curved track, the lateral coupler forces are attached to the locomotive model based on approximate results obtained from the methodology described in Ref. [79]. Simulation scenarios have been extended to study the locomotive behaviour with a variety of primary suspension stiffness, as described in Refs. [96,97].

The influence of coil spring stiffness on the change of vertical axle loads is initially investigated. The results realised by the locomotive under high tractive efforts are presented in Figure 7.38 and show that the values of vertical stiffness change the situation of load distribution between the locomotive axles. This indicates that stiffness might have significant effects on the traction characteristics under real operational conditions.

Subsequently, the influence of an installation position of a traction rod on the bogie frame is investigated in both nontraction and traction modes. The results presented in Figure 7.39 confirm the statement published in Ref. [105] that steering ability deteriorates under high tractive effort conditions. However, it can be seen that the modification of the design by means of varying the traction rod installation angle can compensate for such deterioration. This also confirms the results published in Ref. [98], which have been obtained for a design with two traction rods (radius links) based on kinematic analysis and experimental results.

Taking into account that the model does not fully represent the actual operational primary suspension characteristics because of some simplification of the suspension design (no variation in stiffness values in different directions for rubber elements used in traction rods, no connections of traction motors, etc.), it is recommended that the usage of the total stiffness approach during modelling should be restricted to conceptual studies because it does not allow an adequate judgement about suspension behaviour to be made, especially in cases when bogie component design alignment modifications (rather than just changes in component parameters) are planned to be performed.

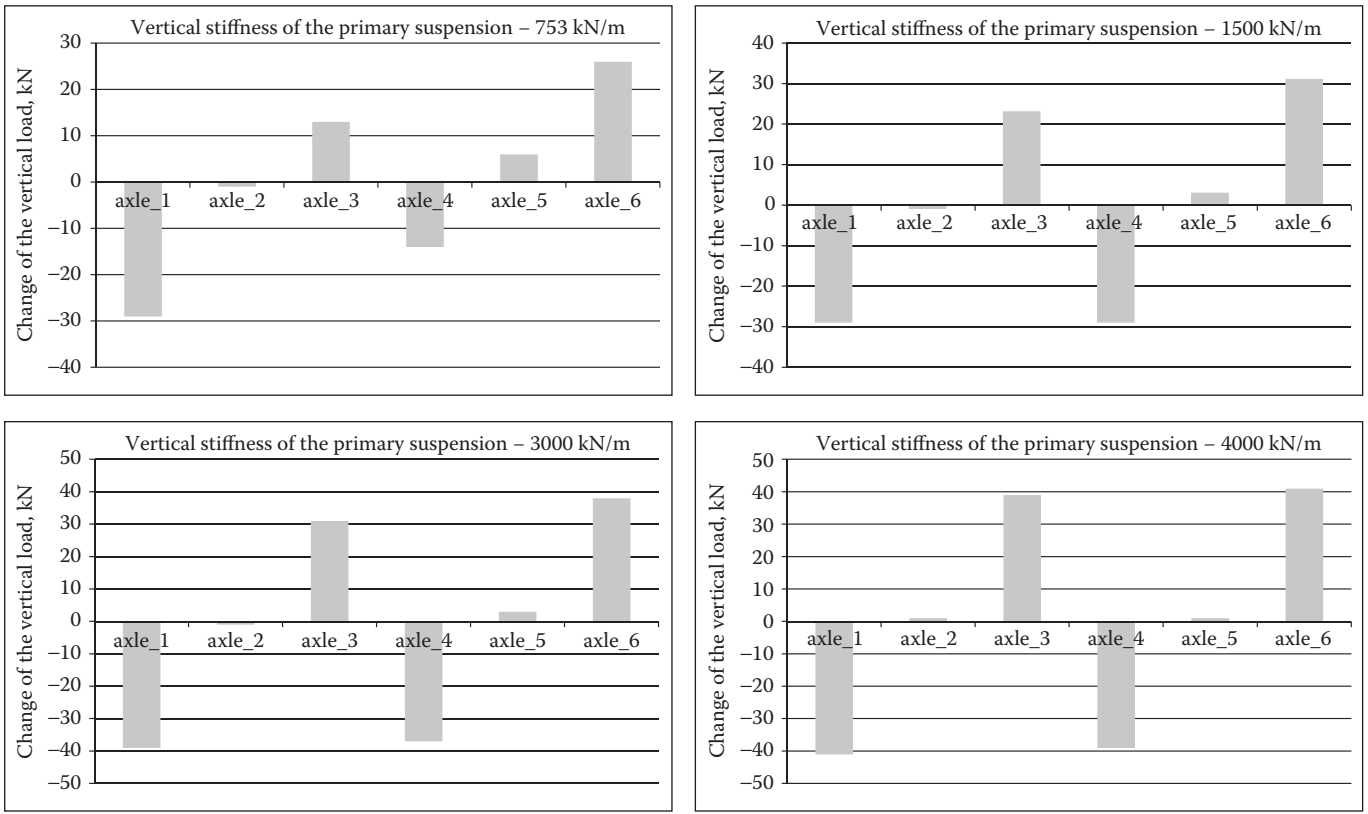

FIGURE 7.38 Change of vertical axle loads for different primary suspension vertical stiffness. (From Spiryagin, M. et al., Optimisation of primary suspension characteristics for heavy haul locomotives, *Proceedings of the 10th World Congress on Railway Research*, CRC for Rail Innovation, Sydney, Australia, November 25–28, 2013.)

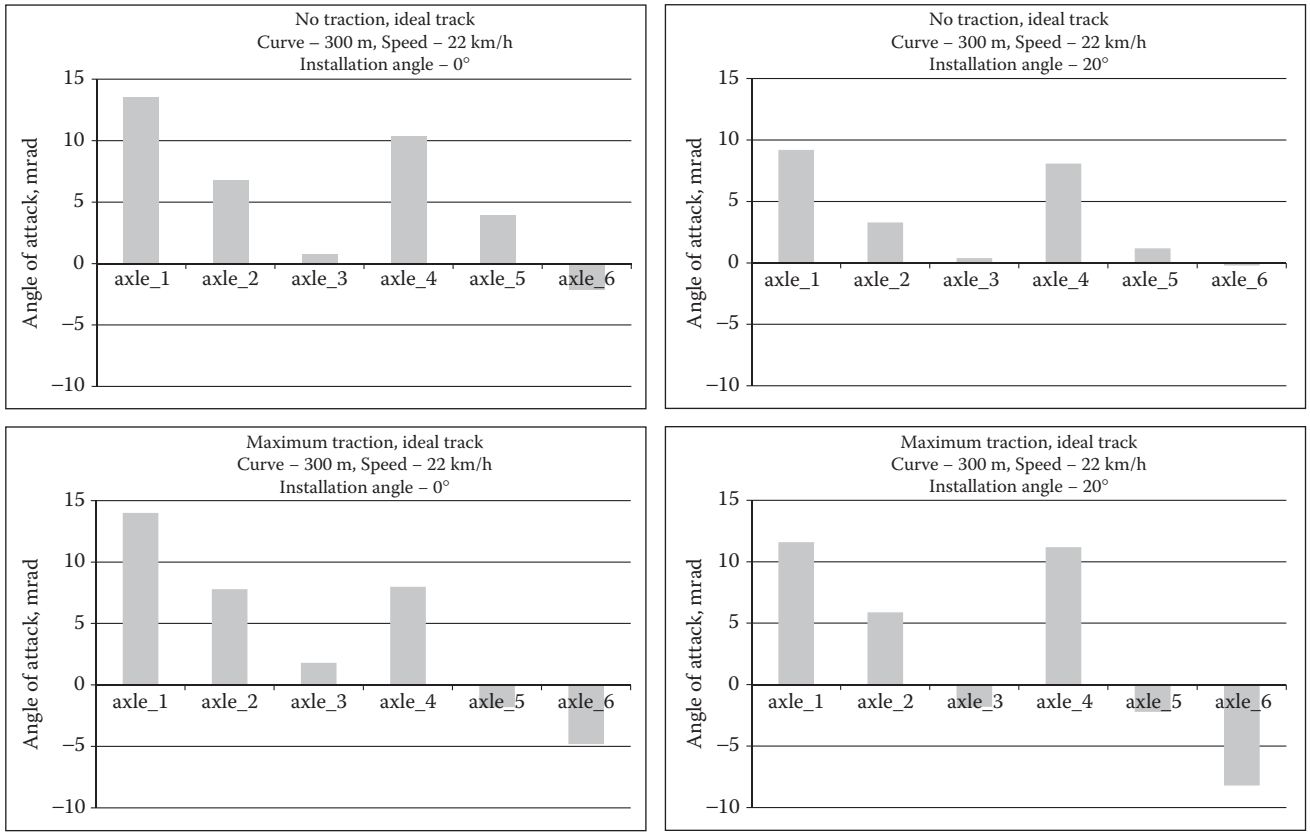

FIGURE 7.39 Angle of attack results for the nontraction and traction modes for varying installation angles of the traction rod. (From Spiryagin, M. et al., Optimisation of primary suspension characteristics for heavy haul locomotives, *Proceedings of the 10th World Congress on Railway Research*, CRC for Rail Innovation, Sydney, Australia, November 25–28, 2013.)

7.8.3 Heavy Haul Locomotive Dynamic Inverse Modelling

Locomotives (and wagons) generate and are subjected to dynamic forces in the vertical and lateral directions when they run on straight or curved tracks with irregularities in track geometry. Depending on the severity of those irregularities, significant dynamic forces can occur in the lateral and vertical directions. Simultaneous occurrence of lateral and vertical dynamic loading has the potential to damage rails and wheels and/or cause derailments. Understanding the dynamic behaviour of a heavy haul locomotive is very important for railway operations. Accelerations on locomotive components can easily be measured because of the excellent range of transducers now available. The problem is how to predict wheel-rail contact dynamic forces based on those measured accelerations. This is an inverse identification problem that can be defined as determining system inputs based on known responses, boundary conditions and system modelling. To solve this problem, an inverse model of the system has to be developed and validated.

Therefore, to evaluate wheel-rail contact dynamic forces based on the known accelerations on locomotive components, an inverse prediction model is developed as described in the following sections. In order to verify this prediction model, a comprehensive locomotive model is generated using GENSYS. The accelerations on the car body and the bogie frames from GENSYS simulations due to a typical short-wavelength irregularity in track geometry are used as the inputs to the prediction model. The prediction calculations are carried out using the modified Newmark – β numerical integration method. The inverse model's predicted outputs of various dynamic forces are compared with those generated from detailed GENSYS model.

7.8.3.1 Locomotive Dynamics Inverse Modelling

Details of the lateral and vertical locomotive dynamic inverse car body and bogie models are shown in Figure 7.40 [107].

The inverse modelling process can be described as follows:

- Knowing the lateral and vertical accelerations of the locomotive car body and of the two bogie frames at the secondary suspension positions, double integrations are carried out to obtain their velocities and displacements. The secondary suspension forces can then be determined by multiplying the stiffness and damping coefficients of the suspension springs and dampers by their relative displacements and velocities, respectively.
- The dynamic equivalent equations are established for the bogie frames and the wheelsets. This dynamic system is then subjected to the secondary suspension forces.
- A numerical method is applied to solve the equations, allowing the primary suspension and wheel-rail contact forces to be determined.

7.8.3.2 Bogie Frame

Five DOFs describing the motions of the bogie frame, namely the lateral and vertical displacements (v_B and w_B) and the roll, pitch and yaw rotations (ϕ_{Bx}, ϕ_{By} and ϕ_{Bz}) about the X_B, Y_B and Z_B axes, respectively, are used. In Figure 7.40b, the dynamic equivalent equations of each bogie frame ($i = 1, 2$) can be written as

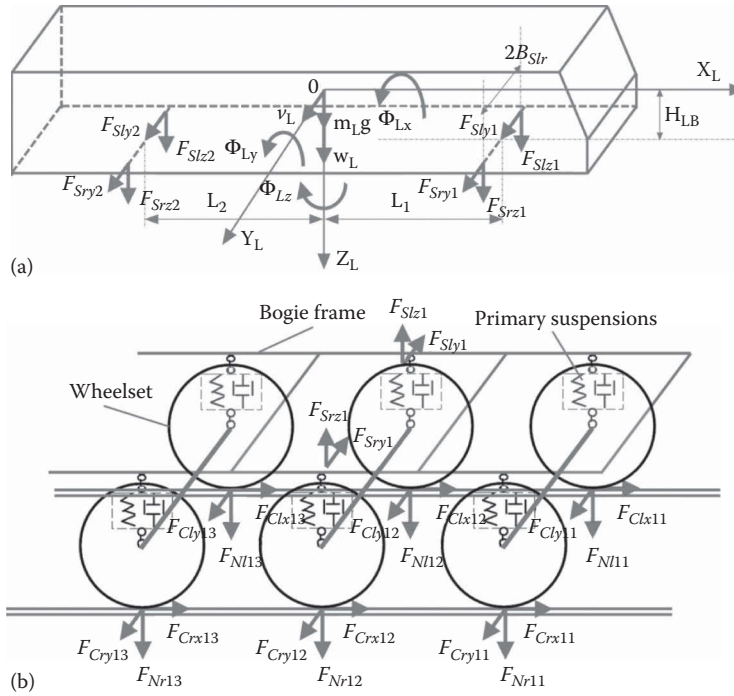

FIGURE 7.40 Inverse locomotive car body and bogie models: (a) Locomotive car body model and (b) bogie model. (From Sun, Y.Q. et al., *Proceedings of the Stephenson Conference: Research for Railways*, IMechE, London, UK, April 21–23, pp. 71–81, 2015.)

$$\begin{bmatrix} m_B & 0 & 0 & 0 & 0 \\ 0 & m_B & 0 & 0 & 0 \\ 0 & 0 & J_{Bx} & 0 & 0 \\ 0 & 0 & 0 & J_{By} & 0 \\ 0 & 0 & 0 & 0 & J_{Bz} \end{bmatrix} \begin{Bmatrix} \ddot{v}_{Bi} \\ \ddot{w}_{Bi} \\ \ddot{\phi}_{Bxi} \\ \ddot{\phi}_{Byi} \\ \ddot{\phi}_{Bzi} \end{Bmatrix}$$

$$= \begin{Bmatrix} -F_{Sryi} - F_{Slyi} + \sum_{j=1}^{3} \left(F_{Pryij} + F_{Plyij} \right) \\ -F_{Srzi} - F_{Slzi} + \sum_{j=1}^{3} \left(F_{Przij} + F_{Plzij} \right) \\ (F_{Slzi} - F_{Srzi}) B_{Slr} + \left[\sum_{j=1}^{3} \left(F_{Przij} + F_{Plzij} \right) \right] B_{Plr} \\ \left[-(F_{Przi1} - F_{Plzi1}) + (F_{Przi3} - F_{Plzi3}) \right] Lw \\ \left[(F_{Pryi1} + F_{Plyi1}) - (F_{Pryi3} + F_{Plyi3}) \right] Lw \end{Bmatrix}$$

$$\left[M_B \right] \left\{ \ddot{q}_B \right\} = \left\{ F_{SPi} \right\} \quad (i = 1, 2) \tag{7.118}$$

In Equation 7.118, m_B and J_B represent the mass and the mass inertia moment of each bogie frame. F_S and F_P represent the secondary and primary suspension forces. B_{Slr} and B_{Plr} are the lateral distances between secondary and primary suspensions of each bogie frame, respectively. L_W is the longitudinal distance between two adjacent wheelsets. It is assumed that the mass centre of each bogie frame is in the same vertical plane as the secondary and primary suspension forces on the second (centre) wheelset of each bogie.

7.8.3.3 Wheelset

Four DOFs describing the motions of a wheelset, namely the lateral and vertical displacements (v_W and w_W) and the roll and the yaw rotations (ϕ_{Bx} and ϕ_{Bz}) about the X_W and Z_W axes, respectively, are used. In Figure 7.40b, the dynamic equivalent equations of each wheelset ($i = 1, 2$ and $j = 1, 2, 3$) can be written as

$$\begin{bmatrix} m_W & 0 & 0 & 0 \\ 0 & m_W & 0 & 0 \\ 0 & 0 & J_{Wx} & 0 \\ 0 & 0 & 0 & J_{Wz} \end{bmatrix} \begin{Bmatrix} \ddot{v}_{Wij} \\ \ddot{w}_{Wij} \\ \ddot{\phi}_{Wxij} \\ \ddot{\phi}_{Wzij} \end{Bmatrix} = \begin{Bmatrix} F_{PWyij} \\ F_{PWzij} \\ M_{PWxij} \\ M_{PWzij} \end{Bmatrix}$$

$$\left[M_W\right]\left\{\ddot{q}_{Wij}\right\} = \left\{F_{PWij}\right\} \quad \left(i = 1,\ 2 \text{ and } j = 1,\ 2 \text{ and } 3\right) \tag{7.119}$$

$$\begin{Bmatrix} F_{PWyij} \\ F_{PWzij} \\ M_{PWxij} \\ M_{PWzij} \end{Bmatrix} = \begin{Bmatrix} -F_{plyij} - F_{plyij} + F_{Clyij} + F_{Cryij} \\ -F_{plzij} - F_{przij} + F_{Nlzij} + F_{Nrzij} \\ Jw_y \dfrac{V}{r_0}\dot{\phi}_{Wzij} - r_0\left(F_{Clyij} + F_{Cryij}\right) + B_{Wlr}\left(F_{Nrzij} - F_{Nlzij}\right) + B_{Plr}\left(F_{Plzij} - F_{Przij}\right) \\ -Jw_y \dfrac{V}{r_0}\dot{\phi}_{Wxij} + B_{Wlr}\left(F_{Clxij} + F_{Crxij}\right) + B_{Wlr}\phi_{Wzij}\left(F_{Clyij} - F_{Cryij}\right) \end{Bmatrix}$$

In Equation 7.119, m_W and J_W represent the mass and the mass moment of inertia of the wheelsets, respectively.

7.8.3.4 Wheel-Rail Contact Forces

The wheel-rail normal force can be determined using the following equation:

$$\begin{cases} F_{Nlzij} = C_H\left[(w_{wij} - B_{Wlr}\phi_{Wxij}) - \mu_l(x)\right]^{\frac{3}{2}}, \ \text{if}\left[(w_{Wij} - B_{Wlr}\phi_{Wxij}) - \mu_l(x)\right] \le 0, \ F_{Nlzij} = 0 \\ F_{Nrzij} = C_H\left[(w_{wij} - B_{Wlr}\phi_{Wxij}) - \mu_r(x)\right]^{\frac{3}{2}}, \ \text{if}\left[(w_{Wij} + B_{Wlr}\phi_{Wxij}) - \mu_r(x)\right] \le 0, \ F_{Nrzij} = 0 \end{cases} \tag{7.120}$$

In Equation 7.120, C_H is the Hertz contact coefficient, $\mu(x)$ describes the track irregularities and B_{Wlr} is the lateral distance between the wheel-rail contact point and the track centreline.

The longitudinal and lateral creep forces are determined based on Polach's theory:

$$F_C = \frac{2F_N\mu}{\pi}\left(\frac{\varepsilon}{1+\varepsilon^2}+\arctan\varepsilon\right) \text{ with } \varepsilon = \frac{1}{4}\frac{G\pi abc_{mm}}{F_N\mu}s \tag{7.121}$$

In Equation 7.121, G is the shear modulus, a and b are the semi-axes of the contact ellipse, μ is the coefficient of friction, s is the total creep and c_{mm} is the coefficient from Kalker's linear theory. The latter two terms are obtained as follows:

$$s = \sqrt{{s_x}^2+{s_y}^2} \text{ and } c_{mm} = \sqrt{\left(c_{11}\frac{s_x}{s}\right)^2+\left(c_{22}\frac{s_y}{s}\right)^2}$$

where c_{11} and c_{22} are the coefficients from Kalker's linear theory and s_x and s_y are the creep in the longitudinal (X) and lateral (Y) directions, respectively, which are obtained as follows:

$$\begin{cases} s_{lxij} = +B_{Wlr}\dfrac{\dot{\phi}_{Wzij}}{V}+\dfrac{\lambda y}{r_0} \\ s_{rxij} = -B_{Wlr}\dfrac{\dot{\phi}_{Wzij}}{V}-\dfrac{\lambda y}{r_0} \end{cases}, \quad \begin{cases} s_{lyij} = \dfrac{\dot{v}_{Wij}}{V}-\phi_{Wzij} \\ s_{ryij} = \dfrac{\dot{v}_{Wij}}{V}-\phi_{Wzij} \end{cases}$$

Based on Equations 7.118 and 7.119, the dynamic equivalent equations of an inverse locomotive model can be written as the matrix form of:

$$[M_w]\{\ddot{q}_w\}+[C_w]\{\dot{q}_w\}+[K_w]\{q_w\}=\{F_w\} \tag{7.122}$$

In Equation 7.122, $[M_W]$, $[C_W]$ and $[K_W]$ are the mass, damping and stiffness matrixes of the inverse locomotive model and $\{q_W\}$ and $\{F_W\}$ are the displacement vector and the force vector, respectively. The total DOFs are 34. The secondary suspension forces in Equation 7.122 are known, and therefore, the wheel-rail contact forces can be predicted through calculations using the numerical integration Newmark-β method.

7.8.3.5 Locomotive Dynamics Modelling Using GENSYS

The locomotive model is developed in GENSYS in a way similar to that described in previous sections.

Secondary suspensions to connect the locomotive car body and one bogie frame comprise:

- Four coil springs;
- Two stiffness elements representing traction rods at the direction specified by the coupling's attachment points;
- One lateral bumpstop element; and
- Two vertical bumpstop elements.

Primary suspensions to connect the bogie frame and two axle boxes of one wheelset comprise:

- Four coil springs;
- Two stiffness elements representing traction rods at the direction specified by the coupling's attachment points;
- Two vertical damping elements representing hydraulic shock absorbers at the direction specified by the coupling's attachment points;
- Two lateral bumpstop elements; and
- Two vertical bumpstop elements.

Primary suspensions to connect the bogie frame and one traction motor comprise:

- One vertical stiffness element and one vertical damping element representing traction motor hydraulic shock absorbers at the direction specified by the coupling's attachment points;
- Two lateral bumpstop elements; and
- Two vertical bumpstop elements.

The various locomotive parameters used for the simulations are listed in Table 7.11.

7.8.3.6 Case Study

A track cross-level geometry irregularity composed of a 20 mm half-sine wave dip with a semi-span of 6 m on the right rail and, directly opposite this, a similar 20 mm rise on the left rail is selected for the case study. The secondary suspension lateral and vertical forces obtained from the direct GENSYS simulation and predicted by the inverse modelling are shown in Figure 7.41.

The lateral and vertical secondary suspension forces shown in Figure 7.41 are then applied as the external forces acting on the two bogies. Figures 7.42 and 7.43 show the vertical primary suspension forces and the vertical wheel-rail contact forces that result on the first wheelset of the front bogie frame.

Simple inverse locomotive modelling can give reasonable and useful predictions of locomotive component connection forces and wheel-rail contact forces based on the measurements of acceleration on locomotive components caused by irregularities in track geometry. It will be noticed that the results from the inverse modelling have some minor differences from those using the detailed GENSYS model. Further improvements of the inverse model and selection of better integration and/or prediction methods are necessary to achieve more accurate outcomes.

TABLE 7.11
Locomotive Parameters

Parameter	Value	Unit
Locomotive car body mass	87180	kg
Mass moment of inertia of locomotive car body about *X* axis (roll)	168550	kgm^2
Mass moment of inertia of locomotive car body about *Y* axis (pitch)	3610410	kgm^2
Mass moment of inertia of locomotive car body about *Z* axis (yaw)	3590650	kgm^2
Mass of bogie frame	14860	kg
Mass moment of inertia of bogie frame about *X* axis	6520	kgm^2
Mass moment of inertia of bogie frame about *Y* axis	45370	kgm^2
Mass moment of inertia of bogie frame about *Z* axis	50300	kgm^2
Wheelset mass	2850	kg
Mass moment of inertia of wheelset about *X* and *Z* axes	1789	kgm^2
Mass moment of inertia of wheelset about *Y* axis	1200	kgm^2
Stiffness coefficient of secondary suspension along *Z* axis	2.138×10^3	kN/m
Stiffness coefficient of secondary suspension along *X* and *Y* axes	1.2×10^3	kN/m
Longitudinal distance from the mass centre of locomotive car body to the mass centre of the front and the rear bolsters	7.095	m
Semi-lateral distance between the left and the right secondary suspensions in a bogie	1.012	m
Height between the mass centres of the locomotive car body and the bogie frame	1.93–0.733	m
Height between the mass centres of bogie frame and wheelset	0.733–1.067/2	m
Height of car body floor	1.5	m
Stiffness coefficient of primary suspension along *Z* axis	0.73×10^3	kN/m
Stiffness coefficient of primary suspension along *X* axis	24×10^3	kN/m
Stiffness coefficient of primary suspension along *Y* axis	3.5×10^3	kN/m
Damping coefficient of primary suspension along *Z* axis	5	kNs/m
Damping coefficient of primary suspension along *X* axis	25	kNs/m
Damping coefficient of primary suspension along *Y* axis	15	kNs/m
Semi-lateral distance between the left and the right primary suspensions	1.012	m
Longitudinal distance between two adjacent wheelsets	1.85	m
Wheel diameter	1.067	m

Source: Sun, Y.Q. et al., Prediction of wheel-rail contact forces based on a heavy haul locomotive dynamic inverse modelling, *Proceedings of the Stephenson Conference: Research for Railways*, IMechE, London, UK, April 21–23, pp. 71–81, 2015.

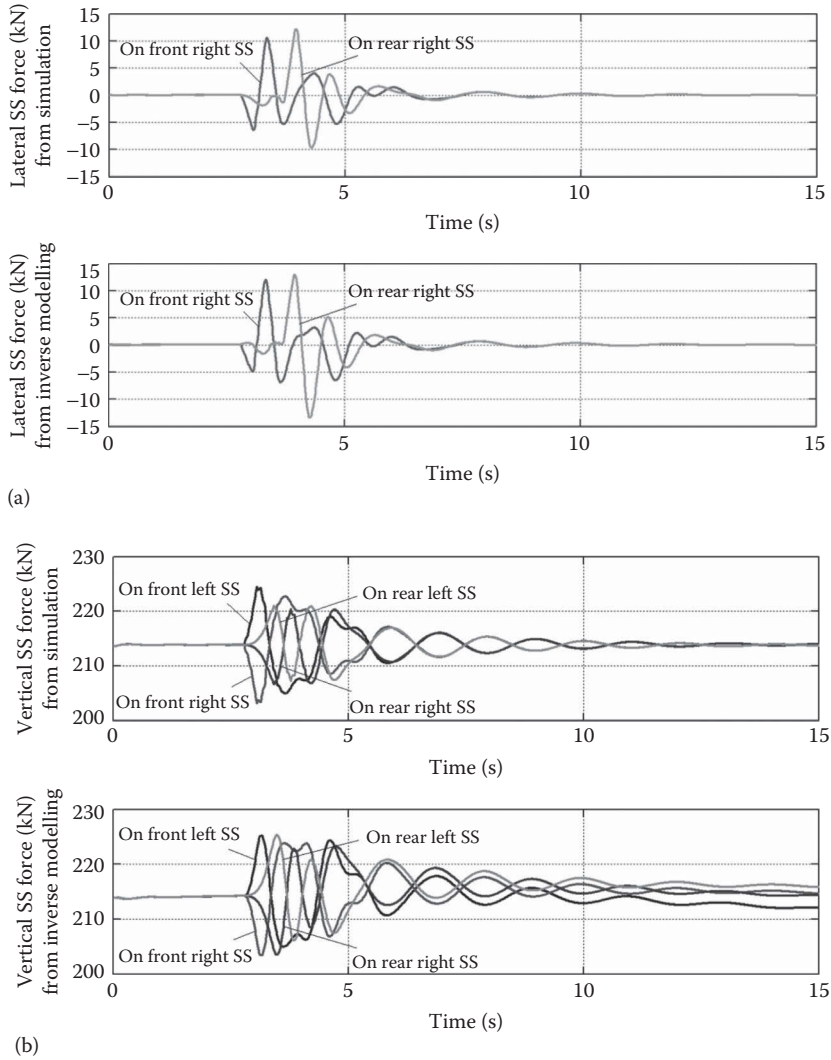

FIGURE 7.41 Secondary suspension (SS) forces: (a) Lateral forces from simulation (top) and from inverse modelling (bottom) and (b) vertical forces from simulation (top) and from inverse modelling (bottom). (From Sun, Y.Q. et al., Prediction of wheel-rail contact forces based on a heavy haul locomotive dynamic inverse modelling, *Proceedings of the Stephenson Conference: Research for Railways*, IMechE, London, UK, April 21–23, pp. 71–81, 2015.)

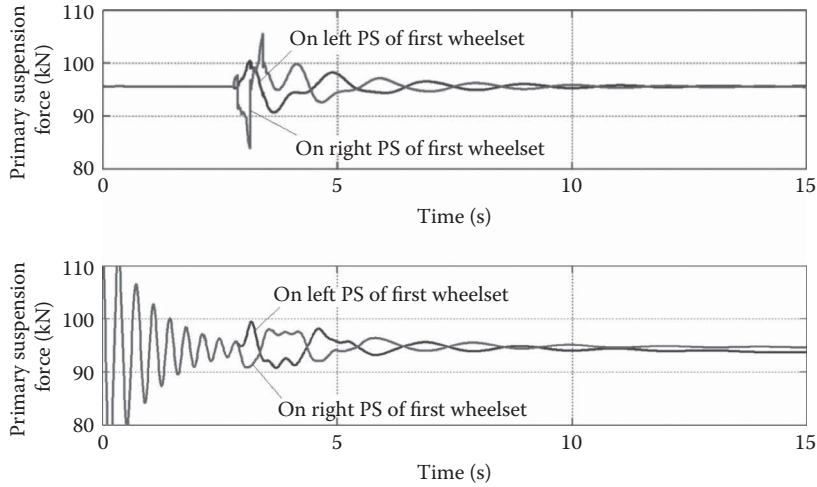

FIGURE 7.42 Vertical primary suspension (PS) forces from simulation (top) and from inverse modelling (bottom). (From Sun, Y.Q. et al., Prediction of wheel-rail contact forces based on a heavy haul locomotive dynamic inverse modelling, *Proceedings of the Stephenson Conference: Research for Railways*, IMechE, London, UK, April 21–23, pp. 71–81, 2015.)

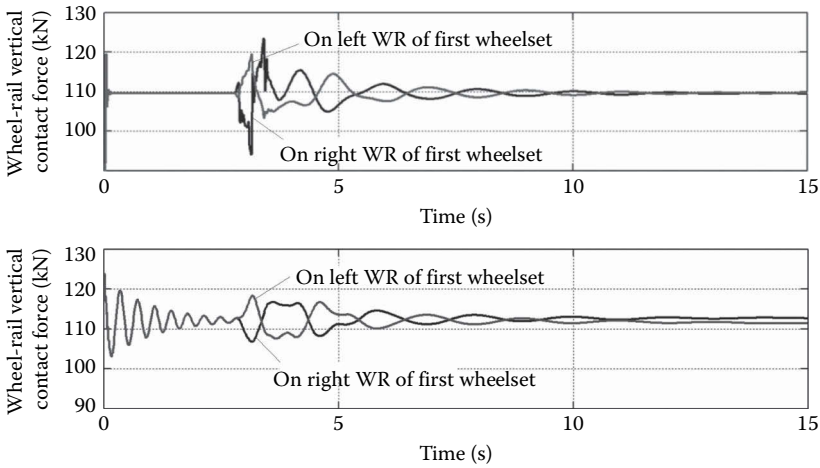

FIGURE 7.43 Vertical wheel-rail (WR) contact forces from simulation (top) and from inverse modelling (bottom). (From Sun, Y.Q. et al., Prediction of wheel-rail contact forces based on a heavy haul locomotive dynamic inverse modelling, *Proceedings of the Stephenson Conference: Research for Railways*, IMechE, London, UK, April 21–23, pp. 71–81, 2015.)

REFERENCES

1. A.A. Shabana, *Dynamics of Multibody Systems* (3rd ed.), Cambridge University Press, New York, NY, 2005.
2. J.G. De Jalon, E. Bayo, *Kinematic and Dynamic Simulation of Multibody Systems: The Real-Time Challenge*, Springer-Verlag, New York, NY, 1994.
3. W. Schiehlen, Multibody system dynamics: Roots and perspectives, *Journal of Multibody System Dynamics*, 1(2), 1997, 149–188.
4. S. Iwnicki (ed.), *Handbook of Railway Vehicle Dynamics*, CRC Press, Boca Raton, FL, 2006.
5. C. Cole, Y.Q. Sun, Simulated comparisons of wagon coupler systems in heavy haul trains, *Rail and Rapid Transit*, 220(3), 2006, 247–256.
6. Y.Q. Sun, Q. Wu, M. Spiryagin, C. Cole, Determination of dynamic characteristics of draft gears of heavy haul train using collision simulations. In *Proceedings of 11th International Heavy Haul Association Conference*, 21–24 June 2015, IHHA, Perth, Australia, pp. 274–280.
7. Y.Q. Sun, C. Cole, M. Spiryagin, Study on track dynamic forces due to rail short-wavelength dip defects using rail vehicle-track dynamics simulations, *Journal of Mechanical Science and Technology*, 27(3), 2013, 629–640.
8. Y.Q. Sun, C. Cole, Vertical dynamic behaviour of three-piece bogie suspensions with two types of friction wedge, *Journal of Multibody System Dynamics*, 19(4), 2008, 365–382.
9. Y.Q. Sun, S. Simson, Wagon-track modelling and parametric study on rail corrugation initiation due to wheel stick-slip process on curved track, *Wear*, 265(9–10), 2008, 1193–1201.
10. Y.Q. Sun, C. Cole, Comprehensive wagon-track modelling for simulation of three-piece bogie suspension dynamics, *Journal of Mechanical Engineering Science*, 221(8), 2007, 905–917.
11. Y.Q. Sun, S. Simson, Nonlinear three-dimensional wagon-track model for the investigation of rail corrugation initiation on curved track, *Vehicle System Dynamics*, 45(2), 2007, 113–132.
12. Y.Q. Sun, M. Dhanasekar, Importance of track modelling to the determination of the critical speed of wagons, *Vehicle System Dynamics*, 41(S1), 2004, 232–241.
13. Y.Q. Sun, M. Dhanasekar, D. Roach, A 3D model for the lateral and vertical dynamics of wagon–track systems, *Rail and Rapid Transit*, 217(1), 2002, 31–45.
14. Y.Q. Sun, M. Dhanasekar, A dynamic model for the vertical interaction of the rail track and wagon system, *International Journal of Solids and Structures*, 39(5), 2002, 1337–1359.
15. Y.Q. Sun, C. Cole, C. Bossomworth, Early detection of wheel flats using wagon body acceleration measurements. In *Proceedings of the Conference on Railway Engineering: Rail – Rejuvenation & Renaissance*, Railway Technical Society of Australasia, Wellington, New Zealand, 12–14 September 2010, pp. 230–239.
16. Y.Q. Sun, C. Cole, M. Kerr, S. Kaewunruen, Use of simulations in determination of wheel impact forces P1 and P2 due to rail dip defects. In *Proceedings of AusRAIL PLUS 2009 Conference*, Informa Australia, Adelaide, Australia, 17–19 November 2009, pp. 1–11.
17. Y.Q. Sun, S. Simson, Wagon-track modelling and parametric study on rail corrugation initiation due to wheel stick-slip process on curved track. In *Proceedings of 7th International Conference on Contact Mechanics and Wear of Rail/Wheel Systems*, Institute of Materials Engineering Australasia, Brisbane, Australia, 2006, pp. 573–581.

18. Y.Q. Sun, C. Cole, The effect of wedge friction conditions on the dynamic wheel-rail contact force on short wavelength defects. In *Proceedings of the ASME/IEEE Joint Rail Conference: Restoring and Upgrading Rail Infrastructure*, *Rolling Stock and Systems*, IEEE, Atlanta, GA, 4–6 April 2006, pp. 37–43.
19. Y.Q. Sun, S. Simson, Vehicle-track modelling for rail corrugation initiation investigation. In *Proceedings of the ASME/IEEE Joint Rail Conference: Research and Testing for Industry Advancement*, IEEE, Pueblo, CO, 16–18 March 2005, pp. 65–71.
20. Y.Q. Sun, M. Dhanasekar, D. Roach, Effect of track geometry irregularities on wheel-rail impact forces. In *Proceedings of the Conference on Railway Engineering: New Horizons for Rail*, Railway Technical Society of Australasia, Darwin, Australia, 20–23 June 2004, pp. 03.1–03.7.
21. Y.Q. Sun, M. Dhanasekar, Influence of the railway track parameters to the vertical and lateral impact. In *Proceedings of the Conference on Railway Engineering: Cost Efficient Railways through Engineering*, Railway Technical Society of Australasia/Rail Track Association of Australia, Wollongong, Australia, 10–13 November 2002, pp. 373–382.
22. C.L. Dym, I.H. Shames, *Solid Mechanics: A Variational Approach*, McGraw-Hill, New York, NY, 1973.
23. K.L. Johnson, *Contact Mechanics*, Cambridge University Press, Cambridge, UK, 1985.
24. R.G. Dong, S. Sankar, R.V. Dukkipati, A finite element model of railway track and its application to the wheel flat problem, *Rail and Rapid Transit*, 208(1), 1994, 61–72.
25. V.A. Profillidis, *Railway Engineering* (2nd ed.), Ashgate Publishing, Aldershot, UK, 2000.
26. D.R. Ahlbeck, H.C. Meacham, R.H. Prause, The development of analytical models for railroad track dynamics. A.D. Kerr (ed.). In *Railroad Track Mechanics & Technology: Proceedings of a Symposium held at Princeton University in April 1975*, Pergamon Press, New York, NY, 1978, pp. 239–263. ISBN: 9780080219233.
27. W. Zhai, X. Sun, A detailed model for investigating interaction between railway vehicle and track, *Vehicle System Dynamics*, 23(S1), 1994, 603–615.
28. S.L. Grassie, R.W. Gregory, D. Harrison, K.L. Johnson, The dynamic response of railway track to high frequency vertical excitation, *Journal of Mechanical Engineering Science*, 24(2), 1982, 77–90.
29. F.W. Carter, On the action of a locomotive driving wheel, *Proceedings of the Royal Society of London – Series A*, 112(760), 1926, 151–157.
30. K.L. Johnson, The effect of spin upon the rolling motion of an elastic sphere upon a plane, *Journal of Applied Mechanics*, 25(3), 1958, 332–338.
31. K.L. Johnson, P.J. Vermeulen, Contact of non-spherical bodies transmitting tangential forces, *Journal of Applied Mechanics*, 31(2), 1964, 338–340.
32. J.J. Kalker, A strip theory for rolling with slip and spin, *Proceedings Koninklijke Nederlandse Akademie van Wetenschappen, Series B*, 70(1), 1967, 10–62.
33. J.J. Kalker, A fast algorithm for the simplified theory of rolling contact, *Vehicle System Dynamics*, 11, 1982, 1–13.
34. Z.Y. Shen, J.K. Hedrick, J.A. Elkins, A comparison of alternative creep-force models for rail vehicle dynamic analysis. In *The Dynamics of Vehicles on Roads and Tracks, Proceedings of the 8th IAVSD Symposium*, J.K. Hedrick (ed.), MIT, Cambridge, MA, 15–19 August 1983, pp. 591–605.
35. O. Polach, A fast wheel-rail forces calculation computer code, *Vehicle System Dynamics*, 33(S), 1999, 728–739.
36. J.J. Kalker, *Three-Dimensional Elastic Bodies in Rolling Contact*, Kluwer Academic Publishers, Dordrecht, The Netherlands, 1990.
37. U. Olofsson, R. Lewis, Tribology of the wheel-rail contact. In *Handbook of Railway Vehicle Dynamics.* S. Iwnicki (ed.), Taylor & Francis Group, Boca Raton, FL, 2006, pp. 121–141.

38. A.A. Shabana, K.E. Zaazaa, H. Sugiyama, *Railroad Vehicle Dynamics: A Computational Approach*, CRC Press, Boca Raton, FL, 2008.
39. J-B. Ayasse, H. Chollet, Wheel-rail contact. In *Handbook of Railway Vehicle Dynamics*. S. Iwnicki (ed.), Taylor & Francis Group, Boca Raton, FL, 2006, pp. 85–120.
40. A.H. Wickens, A history of railway vehicle dynamics. In *Handbook of Railway Vehicle Dynamics*. S. Iwnicki (ed.), Taylor & Francis Group, Boca Raton, FL, 2006, pp. 5–38.
41. O. Polach, M. Berg, S.D. Iwnicki, Simulation. In *Handbook of Railway Vehicle Dynamics*. S. Iwnicki (ed.), Taylor & Francis Group, Boca Raton, FL, 2006, pp. 359–421.
42. H. Hertz, Über die berührung fester elastischer Körper und über die Harte (On the contact of rigid elastic solids and on hardness). In *Verhandlungen des Vereins zur Beförderung des Gewerbefleisses*, Leipzig, Universitätsbibliothek Johann Christian Senckenberg, 1882, pp. 449–463.
43. D.J. Thompson, A.D. Monk-Steel, C.J.C. Jones, P.D. Allen, S.S. Hsu, S.D. Iwnicki, Railway noise: curve squeal, roughness growth, friction and wear, Rail Research UK Report RRUK/A3/1, 2003.
44. K.E. Zaazaa, A.L. Schwab, Review of Joost Kalker's wheel-rail contact theories and their implementation in multibody codes. In *ASME 2009 International Design Engineering Technical Conferences & Computers and Information in Engineering Conference*, ASME, San Diego, CA, 2009, pp. 1–11.
45. J.J. Kalker, Rolling contact phenomena: Linear elasticity. In *Rolling Contact Phenomena*. B. Jacobson, J.J. Kalker (eds), Springer-Verlag, New York, NY, 2000, pp. 1–84.
46. X. Quost, M. Sebes, A. Eddhahak, J.B. Ayasse, H. Chollet, P.-E. Gautier, F. Thouverez, Assessment of a semi-Hertzian method for determination of wheel-rail contact patch, *Vehicle System Dynamics*, 44(10), 2006, 789–814.
47. J. Piotrowski, H. Chollet, Wheel-rail contact models for vehicle system dynamics including multi-point contact, *Vehicle System Dynamics*, 43(6–7), 2005, 455–483.
48. J. Piotrowski, W. Kik, A simplified model of wheel/rail contact mechanics for non-Hertzian problems and its application in rail vehicle dynamic simulations, *Vehicle System Dynamics*, 46(1–2), 2008, 27–48.
49. M. Spiryagin, K.S. Lee, H.H. Yoo, O. Kashura, O. Kostjukevich, Modeling of adhesion for railway vehicles, *Journal of Adhesion Science and Technology (JAST)*, 22(10–11), 2008, 1017–1034.
50. International Heavy Haul Association, *Guidelines to Best Practices for Heavy Haul Operations: Management of the Wheel and Rail Interface*, Virginia Beach, VA, 2015.
51. U. Olofsson, Adhesion and friction modification. In *Wheel-Rail Interface Handbook*. R. Lewis, U. Olofsson (eds), Woodhead Publishing, Cambridge, UK, 2009.
52. C. Tomberger, P. Dietmaier, W. Sextro, K. Six, Friction in wheel-rail contact: A model comprising interfacial fluids, surface roughness and temperature, *Wear*, 271(1–2), 2011, 2–12.
53. O. Polach, Creep forces in simulations of traction vehicles running on adhesion limit, *Wear*, 258(7–8), 2005, 992–1000.
54. M. Spiryagin, O. Polach, C. Cole, Creep force modelling for rail traction vehicles based on the Fastsim algorithm, *Vehicle System Dynamics*, 51(11), 2013, 1765–1783.
55. O. Polach, Influence of locomotive tractive effort on the forces between wheel and rail, *Vehicle System Dynamics*, 35(S), 2001, 7–22.
56. E.A.H. Vollebregt, S.D. Iwnicki, G. Xie, P. Shackleton, Assessing the accuracy of different simplified frictional rolling contact algorithms, *Vehicle System Dynamics*, 50(1), 2011, 1–17.
57. J.G. Gimenez, A. Alonso, E. Gomez, Introduction of a friction coefficient dependent on the slip in the FastSim algorithm, *Vehicle System Dynamics*, 43, 2005, 233–244.

58. J. Piotrowski, Kalker's algorithm Fastsim solves tangential contact problems with slip-dependent friction and friction anisotropy, *Vehicle System Dynamics*, 48, 2010, 869–889.
59. A. Rovira, A. Roda, R. Lewis, M.B. Marshall, Application of Fastsim with variable coefficient of friction using twin disc experimental measurements, *Wear*, 274–275, 2012, 109–126.
60. B. Croft, C. Jones, D. Thompson, Velocity-dependent friction in a model of wheel–rail rolling contact and wear, *Vehicle System Dynamics*, 49(11), 2011, 1791–1802.
61. K. Six, A. Meierhofer, G. Müller, P. Dietmaier, Physical processes in wheel–rail contact and its implications on vehicle–track interaction, *Vehicle System Dynamics*, 53(5), 2015, 635–650.
62. E. Vollebregt, Numerical modeling of measured railway creep versus creep-force curves with CONTACT, *Wear*, 314(1–2), 2014, 87–95.
63. J.J. Kalker, On the rolling contact of two elastic bodies in the presence of dry friction, PhD Thesis, Delft University of Technology, Delft, The Netherlands, 1967.
64. O. Polach, SBB 460 Adhäsionsversuche, Technical Report No. 414, SLM Winterthur, 1992.
65. O. Polach, Optimierung moderner Lok-Drehgestelle durch fahrzeugdynamische Systemanalyse, *Eisenbahningenieur*, 53(7), 2002, 50–57.
66. C.F. Logston Jr., G.S. Itami, Locomotive friction-creep studies, *ASME Journal of Engineering for Industry*, 102(3), 1980, 275–281.
67. B. Engel, H.P. Beck, J. Alders, Verschleißreduzierende Radschlupfregelung mit hoher Kraftschlussausnutzung, *Elektrische Bahnen*, 96(6), 1998, 201–209.
68. W. Lang, G. Roth, Optimale Kraftschlussausnutzung bei Hochleistungs-Schienenfahrzeugen, *Eisenbahntechnische Rundschau*, 42(1–2), 1993, 61–66.
69. Transportation Technology Center, Inc., NUCARS, 2015. See: http://www.aar.com/nucars/about.php.
70. AB DEsolver, GENSYS.1508 Home Page, 2015. See: http://www.gensys.se/index.html#
71. A.L. George, Theoretical and numerical investigation on traction forces for high adhesion locomotives, MEng Thesis, Central Queensland University, Rockhampton, Australia, 2015.
72. L. Rawlings (ed.), *VAMPIRE (Version 4.32) User Manual*, AEA Technology, Derby, UK, 2004.
73. DeltaRail, VAMPIRE Pro V6.00 Help Manual, 2012. See: http://www.vampire-dynamics.com.
74. S.A. Simson, C. Cole, Simulation of traction and curving for passive steering hauling locomotives, *Rail and Rapid Transit*, 222(2), 2008, 117–127.
75. S. Simson, C. Cole, Parametric simulation study of traction curving of three axle steering bogie designs, *Vehicle System Dynamics*, 46(S1), 2008, 717–728.
76. S.A. Simson, C. Cole, Simulation of curving at low speed under high traction for passive steering hauling locomotives, *Vehicle System Dynamics*, 46(12), 2008, 1107–1121.
77. S. Simson, C. Cole, An active steering bogie for heavy haul diesel locomotives. In *Proceedings of the Conference on Railway Engineering: Rail – The Core of Integrated Transport*, Railway Technical Society of Australasia, Perth, Australia, 7–10 September 2008, pp. 481–488.
78. S. Simson, C. Cole, Control alternatives for yaw actuated force steered bogies. In *Proceedings of the 17th International Federation of Automatic Control World Congress*, IFAC, Seoul, Korea, 6–11 July 2008, pp. 8281–8286.
79. S. Simson, Three axle locomotive bogie steering, simulation of powered curving performance. Passive and active steering bogies, PhD Thesis, Central Queensland University, Rockhampton, Queensland, Australia, 2009.
80. VI-RAIL, 2015. See: http://www.vi-grade.com/index.php?pagid=rail.

81. Simpack GmbH, SIMPACK Multi-Body Simulation Software: Rail. See: http://www.simpack.com/industrial_sectors_rail.html
82. E. Pfleger, Simulation of the dynamic behaviour of nose-suspension drives for rail vehicles: Using SIMPACK-Gear Wheel, SIMPACK User-Meeting 2006, Baden-Baden, Germany, 21–23 March 2006. See: http://www.simpack.com/fileadmin/simpack/doc/usermeeting06/um06_siemens-pfleger.pdf
83. E. Pfleger, Parameter-Excited Vibrations in Rail Vehicle Drives, SIMPACK User-Meeting 2007, Bad Godesberg, Germany, 20–22 November 2007. See: http://www.simpack.com/fileadmin/simpack/doc/usermeeting07/um07_siemens-ad_pfleger.pdf
84. T. Blochwitz, M. Otter, M. Arnold, C. Bausch, C. Clauß, H. Elmqvist, A. Junghanns, J. Mauss et al., The functional mockup interface for tool independent exchange of simulation models. In *Proceedings of the 8th International Modelica Conference*, Modelica Association, Dresden, Germany, 20–22 March 2011, pp. 105–114.
85. Universal Mechanism, User's Manual – Simulation of rail vehicle dynamics – Version 7.0, 2013, Laboratory of Computational Mechanics, Bryansk State Technical University, Russia. See: http://www.universalmechanism.com/en/pages/index.php?id=3.
86. R.V. Kovalev, G.A. Fedyaeva, V.N. Fedyaev, Modelling of an electro-mechanical system of locomotives, Sbornik Trudov of DIIT, no. 14, 2007, pp. 123–127 (in Russian). See: http://www.universalmechanism.com/index/download/elmechloco pdf.
87. V.N. Fedyaev, Influence of electrical and mechanical subsystems of a shunting locomotive on the realization limit tractive efforts, PhD Thesis, Bryansk State Technical University, Bryansk, Russia, 2006 (in Russian).
88. G.A. Fedyaeva, Forecasting of dynamic process under transient and emergency mode for traction drives with asynchronous motors, DSc Thesis, Moscow State Railway University, Moscow, Russia, 2008 (in Russian).
89. M. Spiryagin, A. George, Y.Q. Sun, C. Cole, T. McSweeney, S. Simson, Investigation of locomotive multibody modelling issues and results assessment based on the locomotive model acceptance procedure, *Rail and Rapid Transit*, 227(5), 2013, 453–468.
90. Standards Australia and Rail Industry Safety & Standards Board, AS7507.1: Railway Rolling Stock – Rolling Stock Outlines – Part 1: Locomotive Rolling Stock, 2009, Sydney, Australia.
91. Standards Australia and Rail Industry Safety & Standards Board, AS7508.1: Railway Rolling Stock – Track Forces and Stresses – Part 1: Locomotive Rolling Stock, 2009, Sydney, Australia.
92. Standards Australia and Rail Industry Safety & Standards Board, AS7509.1: Railway Rolling Stock – Dynamic Behaviour – Part 1: Locomotive Rolling Stock, 2009, Sydney, Australia.
93. AB DEsolver, GENSYS.1508 Reference Manual – Rail Road Applications, 2015. See: http://www.gensys.se/doc_html/analyse_sum.html.
94. M. Spiryagin, C. Cole, Y.Q. Sun, T. McSweeney, V. Spiryagin, N. Gorbunov, A. Golubenko, Heavy haul locomotive suspension behaviour under bogie and individual wheelset traction control strategies. In *23rd Symposium on Dynamics of Vehicles on Roads and Tracks (IAVSD2013)*, Southwest Jiaotong University, Qingdao, China, 19–23 August, 2013.
95. M. Spiryagin, Y.Q. Sun, C. Cole, S. Simson, I. Persson, Development of traction control for hauling locomotives, *Journal of System Design and Dynamics*, 5(6), 2011, 1214–1225.
96. N. Gorbunov, Theory and practical realization of the system approach in the construction of the carriage of locomotive, DSc Thesis, East Ukrainian National University, Lugansk, Ukraine, 2006 (in Russian).
97. V. Spiryagin, Improvement of dynamic interaction between the locomotive and railway track, PhD Thesis, East Ukrainian National University, Lugansk, Ukraine, 2004 (in Russian).

98. M. Spiryagin, H.H. Yoo, K.S. Lee, V. Spiryagin, M. Gorbunov, Investigation of influence of constraints with radius links on locomotive axle load distribution and wheelset steering ability, *Journal of Mechanical Science and Technology*, 27(7), 2013, 629–640.
99. M. Spiryagin, V. Spiryagin, P. Wolfs, C. Cole, Y.Q. Sun, I. Persson, Investigation of the application of adjustable air suspension under traction control for heavy haul locomotives. In *Proceedings of the Stephenson Conference: Research for Railways*, IMechE, London, UK, 21–23 April 2015, pp. 549–558.
100. J. Wang, Nonlinear modelling and h-infinity model reference control of pneumatic suspension system, PhD Thesis, Iowa State University, Ames, IA, 2012.
101. B.M. Ibraev, Parameters of pneumatic suspension of a rail bus for Kazakh railways, PhD Thesis, Moscow State Railway University (MIIT), Moscow, Russia, 2009 (in Russian).
102. N.A. Lobachev, Pneumatic support and connection system between the locomotive body and bogies, PhD Thesis, All-Union Scientific Research Diesel Locomotive Institute, Kolomna, Russia, 1983 (in Russian).
103. N. Docquier, Multiphysics modelling of multibody systems: Application to railway pneumatic suspensions, PhD Thesis, Université Catholique de Louvain, Belgium, 2010.
104. M. Spiryagin, C. Cole, Y.Q. Sun, T. McSweeney, V. Spiryagin, N. Gorbunov, A. Golubenko, Optimisation of primary suspension characteristics for heavy haul locomotives. In *Proceedings of the 10th World Congress on Railway Research*, CRC for Rail Innovation, Sydney, Australia, 25–28 November 2013.
105. S.L. Grassie, J.A. Elkins, Tractive effort, curving and surface damage of rails: Part 1 — Forces exerted on the rails, *Wear*, 258, 2005, 1235–1244.
106. S. Simson, C. Cole, Idealised steering for hauling locomotives, *Rail and Rapid Transit*, 221(2), 2007, 227–236.
107. Y.Q. Sun, M. Spiryagin, C. Cole, Prediction of wheel-rail contact forces based on a heavy haul locomotive dynamic inverse modelling. In *Proceedings of the Stephenson Conference: Research for Railways*, IMechE, London, UK, 21–23 April 2015, pp. 71–81.

8 Locomotive Power Systems Modelling

8.1 INTRODUCTION

This chapter will present some models for the major power systems components of a heavy haul locomotive and present two case studies: an electric locomotive with AC traction and a diesel-electric locomotive with AC traction. Any practically useful model has the following properties:

- The model should replicate the behaviours of the physical system that are important in the context of the problem under study.
- The model results should have an acceptable level of accuracy.
- The model should avoid unnecessary complexity.

Increasing the complexity of a model does not necessarily lead to improved performance. It certainly extends the time required to establish the model parameters, increases the computational burden and may adversely affect the numerical stability of the simulation. This book focuses on the electromechanical simulation of the locomotives, primarily for studies in train and rail vehicle dynamics. Some important aspects of locomotive performance are beyond the scope of this book. Two examples include the impact of locomotives on electrical power quality in the railway overhead traction power supply system and the thermal modelling of the locomotive's electrical equipment. Although these are important topics, it is more productive to develop several models that are carefully tailored to deal with different problem domains.

8.2 DIESEL ENGINE MODELLING

In heavy haul operations, the tractive effort is controlled by the throttle notch setting [1]. The throttle setting takes discrete values from the idle position, or notch zero, through to notch eight. The available steady state power approximately follows a square-law relationship, as given below:

$$P_n = \frac{n^2}{64} P_{\text{rated}} \tag{8.1}$$

where:

P_n is the notch power
P_{rated} is the rated power in notch 8
n is the discrete notch number, which takes a range from zero to eight

For a locomotive power system model, the major features to be captured for the diesel engine are the time delays in the diesel power output in response to throttle changes. A locomotive diesel engine will require tens of seconds to appreciably change its power output. These rates of change are imposed by a range of mechanical considerations, such as the engine temperature and the emission control requirements. From a simulation perspective, these limitations are best captured by lookup tables and rate-limiting functions. In a simple model, Equation 8.1 can be applied to calculate a notch power and then a rate limitation could be applied. A slightly more sophisticated approach uses lookup tables populated with manufacturer's data for the engine's revolutions per minute (rpm) and power in each notch, as illustrated in the example shown in Figure 8.1 and Table 8.1. The throttle notch setting is converted into a target for the diesel engine rotational speed. The rotational speed is subject to a ramp rate limit that can be inferred from the manufacturer's published data.

Figure 8.1 includes a 'power capability' signal. For the purposes of maintaining stability during simulation, and in a physical locomotive, it is important to impose limitations on the power electronic systems to ensure that the traction motors do not exceed the capability of the diesel generation. Power electronic drives are highly responsive and are able to change their power demands far more quickly than the diesel engine. In a physical locomotive, excessive power demands from the traction system would cause the DC bus voltage to collapse, and this ultimately causes a loss of torque in the traction motors. This is undesirable because the loss of torque is uncontrolled and the recovery of the drive system may be dynamically unstable.

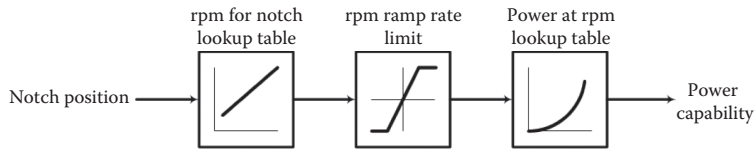

FIGURE 8.1 Diesel locomotive engine rpm rate limits and power capability.

TABLE 8.1
Diesel Engine rpm and Power Capability

Notch Position	Rotational Speed (rpm)	Power (kW)
0–Idle	200	0
1	269	133
2	343	294
3	490	665
4	568	945
5	651	1253
6	729	1820
7	820	2400
8	904	2757

Source: M. Spiryagin et al., *Vehicle System Dynamics*, 53(5), 672–691, 2015.

The engine power capability has to be converted into electrical generation at the DC bus. This is accomplished by the traction alternator. The alternator produces a variable frequency and a variable voltage output that is converted into DC by using diode rectifiers. Most commonly, three-phase alternators and rectifiers are used. The steady-state DC voltage is

$$V_{\mathrm{dc}} = \frac{3\sqrt{2}}{\pi} V_{\mathrm{ll}} - R_c I_{\mathrm{dc}} \tag{8.2}$$

where:

V_{dc} and I_{dc} are the DC output voltage and load current, respectively
V_{ll} is the unloaded alternator voltage
R_c is the commutation resistance

The commutation resistance is a virtual lossless term that captures the alternator voltage drop due to the synchronous alternator inductance and is given by

$$R_c = \frac{3}{\pi} X_s \tag{8.3}$$

where X_s is the alternator synchronous reactance.

The commutation resistance is significant, and may be in the range of 0.5–1.0 in per unit terms using the alternator DC voltage and current ratings as a base. The alternator voltage, V_{ll}, depends on the rotational speed and the field excitation as follows:

$$V_{\mathrm{ll}} = k\left(I_f\right) I_f N_{\mathrm{mech}} \tag{8.4}$$

where:

N_{mech} is the rotational speed of the alternator
I_f is the field current
$k(I_f)$ is a field magnetisation function

The field magnetisation function is a constant for lower field current values but exhibits saturation at the higher field currents. The alternator subsystem includes a closed-loop voltage regulator that adjusts the field voltage to maintain a specified output voltage, as shown in Figure 8.2. The voltage set point in Figure 8.2, as in many heavy haul applications, is a function of both throttle notch position and train speed. At lower speeds, the traction motors operate in the constant torque region and a minimum DC bus voltage is required to maintain the motor flux. The drive efficiency is maximised if the DC bus voltage is regulated to be just above the minimum requirement. In Figure 8.2, a two-dimensional lookup table adjusts the alternator output voltage as a function of notch and train speed. The output of the lookup table is compared to the actual DC bus voltage to form an error signal that drives the DC bus voltage regulator. Normally, this is a proportional–integral–derivative regulator and achieves a voltage regulation response time of a few hundred milliseconds, subject to the constraints imposed by alternator shaft speed and field

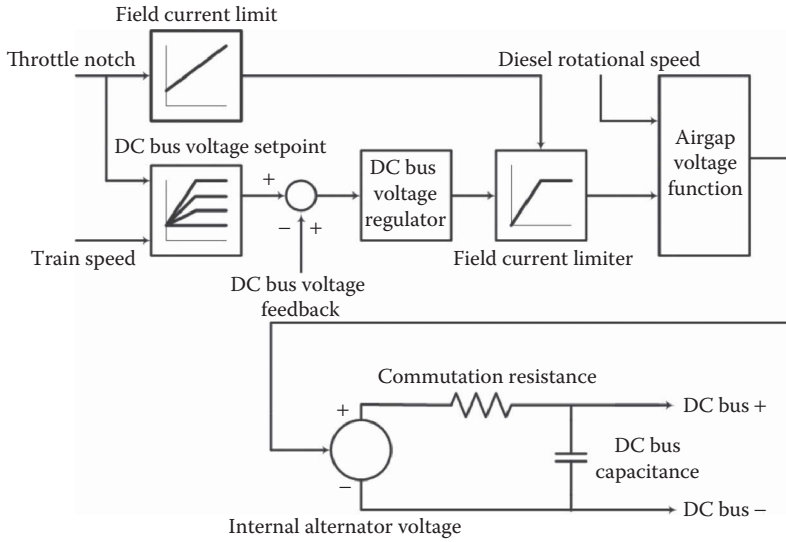

FIGURE 8.2 Alternator voltage regulator.

current limits. An important constraint is that, owing to limits on the field current and saturation effects, higher voltages require higher alternator speeds. High alternator voltages will not be available if the diesel engine shaft speed is low. The rotational speed of the diesel engine imposes both a voltage constrain on the output of the alternator and a power constraint.

The alternator voltage and power constraints are clearly visible at the DC bus. Functionally, an inverter converts DC power to AC power. As inverters have negligible internal energy storage, their operation is constrained by the requirement for instantaneous power balance. A rapid change in the traction motor torque results in an equivalent rapid change in its power output. This is instantaneously visible at the DC bus bar. There will be limited storage, perhaps 1 MJ or 1 MWs, at the DC bus bar in the form of capacitors. The capacitors are readily modelled as an integrator by using the fundamental element equation:

$$v_c(t) = v_c(t_0) + \int_{t_0}^{t} i_c(t)\,\mathrm{d}t \tag{8.5}$$

where:

$v_c(t)$ and $i_c(t)$ are the capacitor voltage and current, respectively
$v_c(t_0)$ is the initial capacitor voltage

A rapid transient event, such as a wheel breakaway and rapid re-adhesion, may be dealt with using the DC bus capacitance storage ability [1]. A rapid reduction in the inverter power will cause the DC bus voltages to rise, and this can be managed by the rapid connection of braking resistors. However, any prolonged event,

such as a step increase in tractive power, must be accommodated by a matching increase in generation.

The traction system load acts as a constant power load. In a power system, it is well known that loads of the constant power type can produce a specific type of instability. If the voltage available to a constant power load reduces, it will compensate by increasing its current. The increase in current will further reduce the voltage available if the source of supply is limited. A runaway voltage collapse may result. For a locomotive, a rapid increase in tractive effort will increase the current drawn from the DC bus bar, reducing its voltage. The voltage reduction will, in turn, cause the DC current to increase further, given that the inverter power is determined by the motor load. The generation at the DC bus will be limited by the diesel engine capability, and it is inevitable that the DC bus voltage will collapse if the alternator cannot keep pace with the load demand. For sudden increases in tractive effort, the dynamics of the diesel engine and the alternator excitation system will be the stability-determining factor.

8.3 TRANSFORMER MODELLING

For the purposes of electromechanical modelling of the locomotive tractive effort, the locomotive transformer may be modelled using the conventional mains frequency equivalent circuit model shown in Figure 8.3. In terms of a per unit comparison to general-purpose industrial transformers, the winding losses due to the primary and secondary winding resistances, r_p and r_s, respectively, are higher by a factor of up to 4 times [2]. The core losses, represented by r_m, and the magnetising currents, represented by L_m, are generally twice as high. This reflects the limitations on space and the intensive forced cooling of the design. The primary and secondary leakage reactances, L_{lp} and L_{ls}, are generally higher than those found in general-purpose distribution transformers and may reach 20% on a per unit basis.

The traction transformer is likely to have multiple secondary windings to provide supply to several converters. In this case, the transformer may be represented by:

- A number of single-phase, two-winding transformers; or
- A single transformer with multiple secondary windings, where the primary winding load current is proportional to the sum of the secondary ampere turns. Each secondary winding may have different primary-secondary leakage reactances.

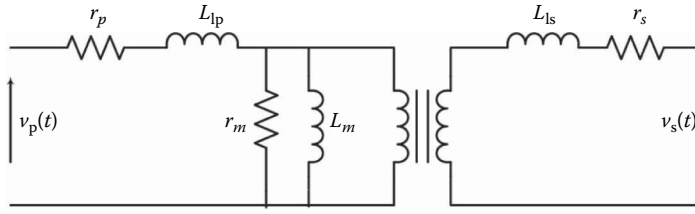

FIGURE 8.3 Traction transformer model.

The major concern in tractive effort modelling is the secondary voltage regulation. For a multiple converter model, the approaches are equivalent if all of the windings are equally loaded. Some differences will emerge if some converters are out of service.

The thermal issues and higher-frequency harmonic performance of the transformer will not be considered in this model. In these cases, a finite element approach may be used to determine the transformer behaviour.

The traction transformer will be paired with a converter to produce a DC supply for the traction system. The most common approaches are:

- Controlled thyristor/diode rectifiers for DC traction systems; and
- Pulse width modulated (PWM) converters, which produce a regulated DC bus for the supply of power to AC traction systems.

For the thyristor-based rectifiers, the traction transformer is subject to significant harmonic currents flows, and this gives rise to additional winding losses. The transformer leakage reactances have a profound effect on the rectifier commutation process, and the design of these two items must be carefully coordinated.

The PWM AC-DC converters are based on single-phase, four-switch bridge (B4) inverters, as shown in Figure 8.4. These converters are topologically identical to single-phase DC–AC inverters. Although the terminology 'inverter' indicates a DC to AC power conversion device, the B4 converter allows bidirectional power flow. Power may be transferred in either direction between the AC system and the DC system. The converter is equally capable as an inverter, with DC to AC power flow, or as a rectifier, with power flow from the AC to the DC terminals. The PWM rectifier is more complex than the thyristor rectifier but has two important operational advantages:

- The traction transformer current and the locomotive current are sinusoidal. The low-frequency harmonics found in thyristor rectifiers are removed.
- The converter allows energy recovered during dynamic braking to be returned to the overhead traction power supply system.

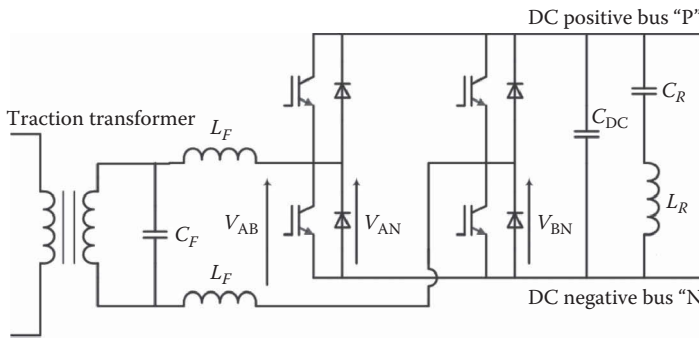

FIGURE 8.4 AC-DC bidirectional traction power supply.

The converter system shown in Figure 8.4 includes the following components:

- A switching frequency filter composed of two inductors labelled L_F, and the capacitor labelled C_F. This results in sinusoidal transformer voltages and currents, and ensures that no harmonic losses occur in the transformer. These filters are physically small, and the effective switching frequency is a few kilohertz;
- A DC bus capacitor, C_{DC}, which is necessary to balance the high-frequency power flows of the rectifier and the traction inverters;
- A '2ω' resonant filter, consisting of the inductor, L_R, and the capacitor, C_R, to accommodate power flows that occur at twice the mains power supply frequency. The technical need for this filter will be revisited in the following section on inverter modelling.

8.4 INVERTER MODELLING

All AC traction motors are controlled with the help of inverters that produce variable frequency electric power by using power electronic switching devices. Switching power conversion is a theoretically lossless power conversion method, and the practical power conversion efficiencies are typically more than 97%. Figure 8.5 shows the six-switch bridge (B6) inverter, which is able to convert DC power to three-phase variable frequency AC power. In this case, the power switching devices are insulated gate bipolar transistors (IGBTs). These are extremely popular low-cost devices that

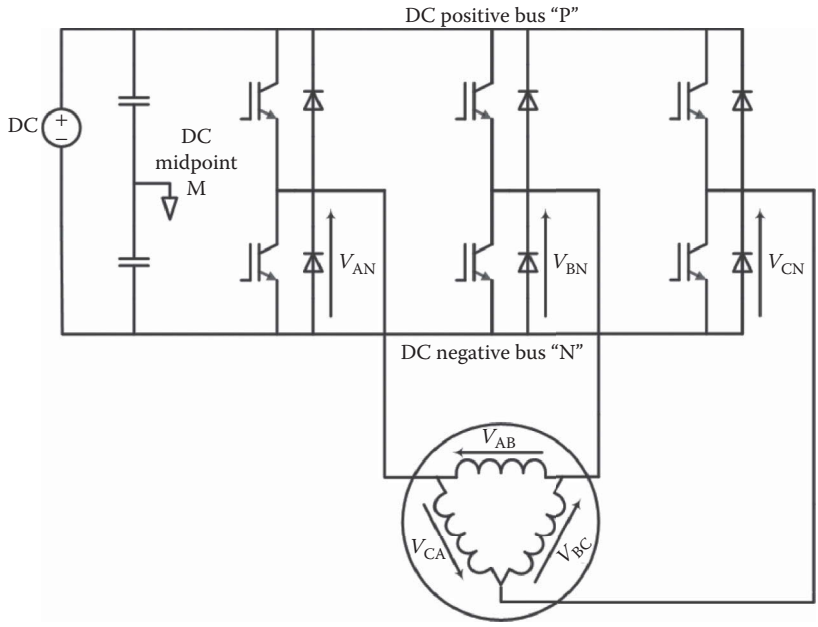

FIGURE 8.5 B6 inverter with a traction motor.

account for most of the industrial variable speed drive market. For railway applications, the voltage ratings for IGBTs are somewhat restrictive. Common low-cost IGBTs have 1200 and 1700 V ratings, and these are optimised for the industrial drive applications at 480 and 690 V, respectively. In a B6 inverter using the best space vector modulation schemes, the DC bus voltage must be equal to the peak of the AC line-to-line voltage. The switching device voltage stress is equal to the DC bus voltage. For a 690 V drive, the 1700 V IGBT is stressed to 60% of its voltage rating, which is practically acceptable from a reliability perspective.

Higher voltages are desirable in heavy haul systems. For motors of several hundred kilowatts, higher voltage ratings reduce the stator currents; this provides manufacturing advantages in constructing the windings which must carry a few hundred amperes. The upper limit on the range of desirable currents is somewhat arbitrary, but if 400 A is selected as a limit, then the power rating of a 690 V motor is approximately 400 kW. This is clearly at the low end of the heavy haul range.

The voltage supplied to the AC motor can be increased by using high-voltage rating switching devices or multilevel inverter designs [3]. The multilevel converters use inexpensive lower-voltage devices in more complex inverter topologies to synthesise higher motor voltages. IGBT devices can be easily applied in the neutral-point-clamped inverter, shown in Figure 8.6. This is the most popular of the multilevel converter designs and has found wide applications in rail traction systems. The switch voltage stress is only half the DC bus voltage, and this topology doubles the voltage applied to the traction motor, and with 1700 V IGBTs, 1400 V is readily achievable. This extends the traction motor power range to approximately 800 kW.

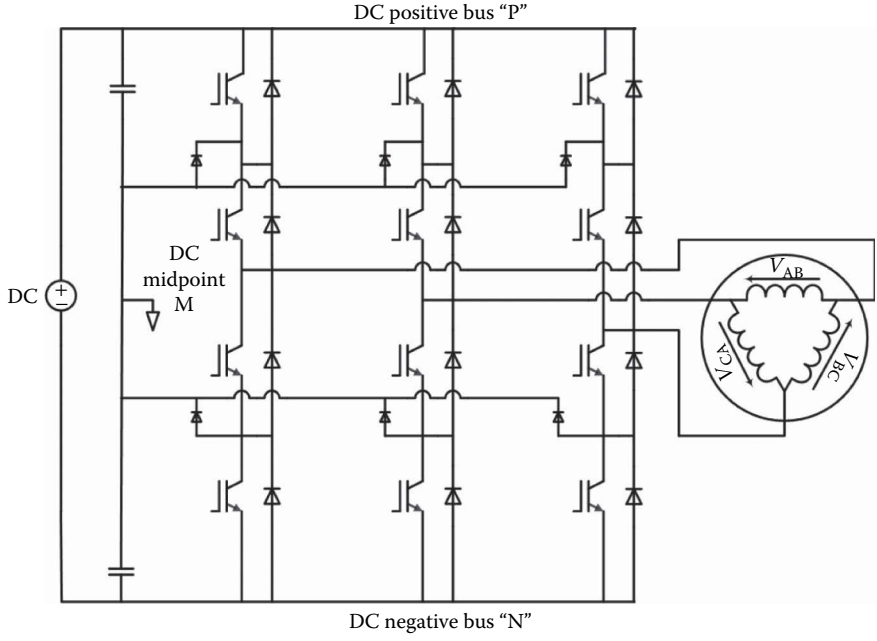

FIGURE 8.6 Neutral-point-clamped inverter with a traction motor.

For direct torque control or field-oriented control (FOC), the neutral-point-clamped inverter offers a higher number of voltage states than the B6 inverter. This allows smoother control for the same device switching frequency.

Although IGBTs are pervasive in the industrial drive market, the achievable line-to-line voltages are still somewhat low for motors that approach 1 MW. Other power devices are available. At the power and voltage levels prevalent in heavy haul applications, that is, a few hundred kilowatts to 1 or 2 MW per inverter, with DC bus voltages ranging up to approximately 3 kV, gate turn-off thyristors and integrated gate-commutated thyristors have been widely applied. These devices have voltage ratings of up to and beyond 5 kV and, in a B6 topology traction motor, voltages in the 2 kV range are routinely achieved. The IGBT has a significant switching speed advantage, which allows higher switching frequencies and better current control. In light of recent technology developments, silicon carbide IGBTs are becoming available. This technology can offer a two- to three-fold improvement in voltage ratings, which puts the heavy haul inverter applications well within reach.

The pairing of AC machines with PWM inverters in a variable drive was first proposed by Schoung and Stemmler in 1964 [4]. The key realisation within that paper was that the currents in an induction machine would be driven by the average value of a PWM stator voltage. In an AC drive, the switching rate is purposefully selected so that the motor currents are relatively sinusoidal. The leakage reactances of the machine block the flow of switching frequency currents. The magnetising flux is largely sinusoidal and the rotor currents are even further filtered by the rotor leakage reactance. The fundamental currents produce the majority of the machine torque. Any torques due to the switching frequency currents are treated as a parasitic element. In most drive applications, it is unnecessary to model the switching behaviour of the inverter as the switching frequency currents are minimised by design. The inverter elements are often modelled using the 'state-space averaged' approach [5]. In this approach, a single-phase inverter is replaced by two elements:

- A controlled voltage source that provides a continuous and controllable output at the inverter terminals; and
- A controlled current source at the DC terminals that draws a current that reflects the instantaneous power demand resulting from the flow of load current.

The state-space averaged model for a single-phase inverter is shown in Figure 8.7. The averaged output voltage is a product of the duty cycle, which is a continuous variable that ranges between –1 and +1, and the DC bus voltage at the converter input terminals. That is

$$v_o(t) = d(t) \times v_i(t) \tag{8.6}$$

where:

$d(t)$ is the duty cycle

$v_o(t)$ and $v_i(t)$ are the output and input voltages, respectively

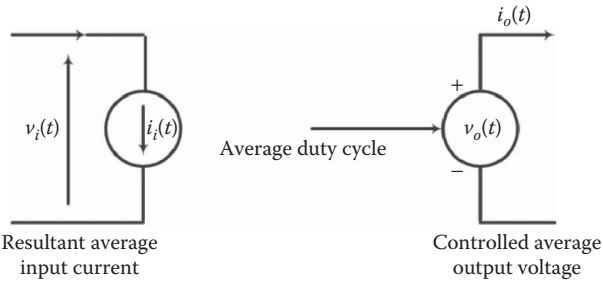

FIGURE 8.7 State-space averaged single-phase inverter.

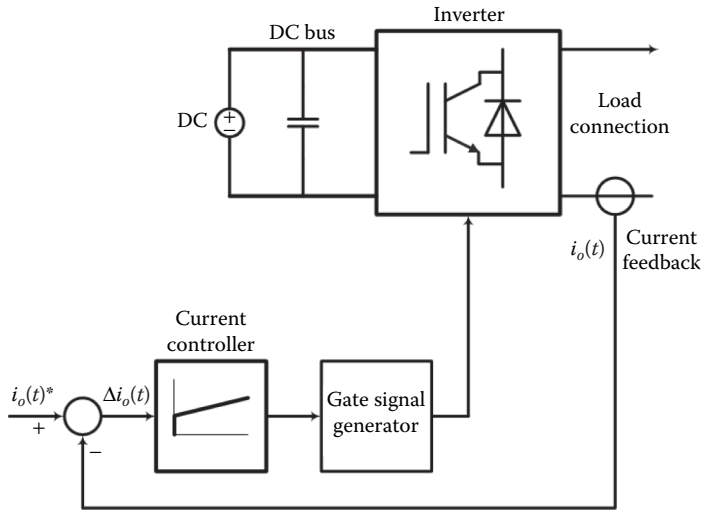

FIGURE 8.8 Inverter current control.

Instantaneous power balance requires the power at the input and output ports to balance, giving the constraint equation:

$$i_o(t) \times v_o(t) = i_i(t) \times v_i(t) \tag{8.7}$$

In many instances, an inverter will be current controlled [6], as shown in Figure 8.8. In this case, the load is assumed to be inductive so that the average current responds, over several switching periods, to the average inverter voltage. A responsive current control has several advantages. In controlled torque drives, the motor currents control the fluxes and torque more directly than the stator voltages. From a practical standpoint, current controlled inverters have an inherent overload protection if the allowable current demand signal is limited. In this case, the instantaneous power balance equation, Equation 8.7, naturally still applies. The resulting space averaged model is shown in Figure 8.9.

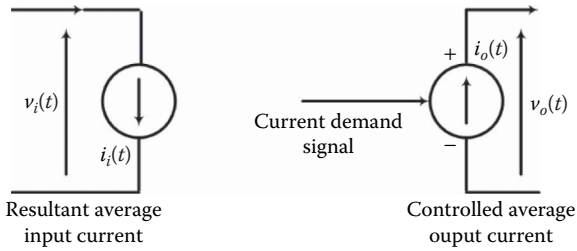

FIGURE 8.9 State-averaged inverter with output current control.

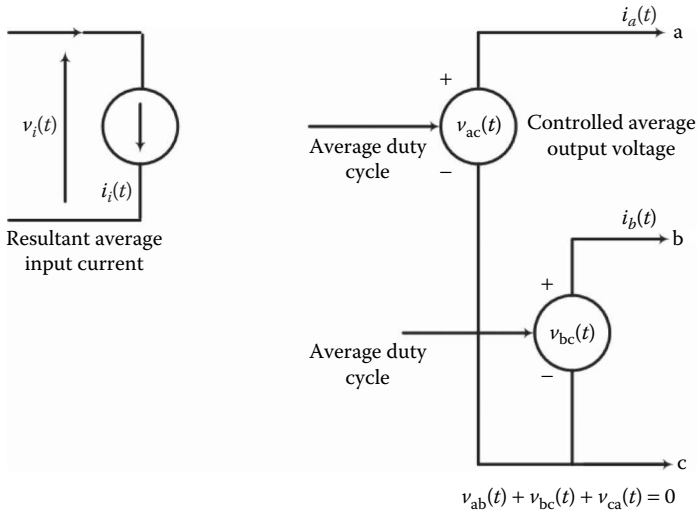

FIGURE 8.10 Three-phase state-averaged voltage output model.

For most drives, three-phase models are required. The voltage- and current-controlled forms are shown in Figures 8.10 and 8.11. An important point is that the three-phase inverter has three output terminals but only two degrees of freedom. A constraint is imposed by Kirchoff's current law for the current-controlled outputs. The three terminal currents must sum to zero. Kirchoff's voltage law imposes a constraint for the voltage-controlled outputs, where the line-to-line voltages sum to zero. The power can be calculated using the two-wattmeter formula, and this equation becomes:

$$i_i(t) \times v_i(t) = i_a(t) \times v_{ac}(t) + i_b(t) \times v_{bc}(t) \tag{8.8}$$

where:

$i_a(t)$ and $i_b(t)$ are the a and b phase currents, respectively

$v_{ac}(t)$ and $v_{bc}(t)$ are the ab and bc line-to-line voltages, respectively

These models allow bidirectional power flow and naturally support dynamic braking in heavy haul applications. An induction motor automatically regenerates if the stator

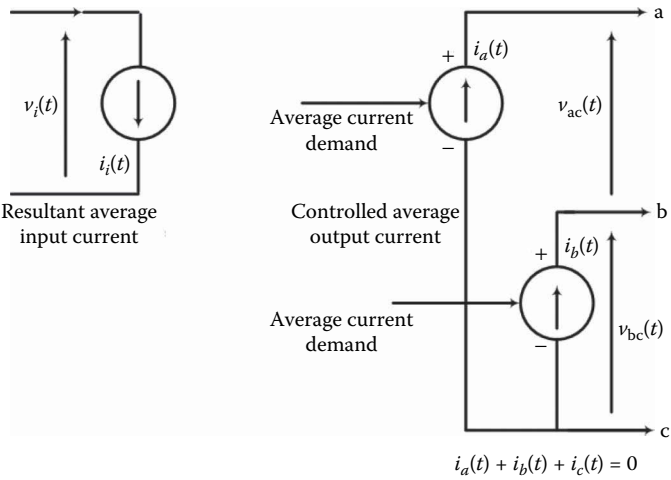

FIGURE 8.11 Three-phase state-averaged current output model.

frequency drops below the electrical frequency, and this occurs naturally in both direct torque control and FOC drives when the torque set point becomes negative.

The correct modelling for a drive system requires that the constant torque and constant power regions are properly captured. The state-space models assume that there is sufficient voltage available at the DC link to achieve the phase terminal voltages that would be required to produce the average currents or voltages. If the drive operates in a region where the DC bus voltage is less than that required for current control, then the inverter modelling must change. There are two possibilities:

- To change to a switched mode of operation; or
- To ensure that field weakening is imposed so that the motor voltages always remain just within the capability of the inverter.

The transition to a switching mode automatically introduces field weakening and a constant power mode of operation. A disadvantage is that the transition does introduce a discontinuity into the simulation and disturbances in the motor torque. For either method, knowledge of the inverter voltage capability is required. Figure 8.12 shows the reachable voltage space for the B6 inverter with a DC bus voltage of E. The inverter can produce six non-zero output voltage vectors. Any stator voltage phasor within the shaded hexagon can be produced by pulse width modulation, where a sequence of the six vectors is sequentially applied.

Sinusoidal voltages are produced if the phasor follows a circular trajectory. The largest circle that can be placed wholly in the reachable hexagon has a radius of $E/\sqrt{3}$. This is the maximum undistorted value of the peak phase voltage. The maximum undistorted line-to-line voltage has a peak value of E. It is possible to produce a slightly higher fundamental line-to-line voltage by forcing the inverter to run in the square wave mode. The voltage phasor then follows the edge of the reachable hexagon. The resulting line-to-line voltage is shown in Figure 8.13.

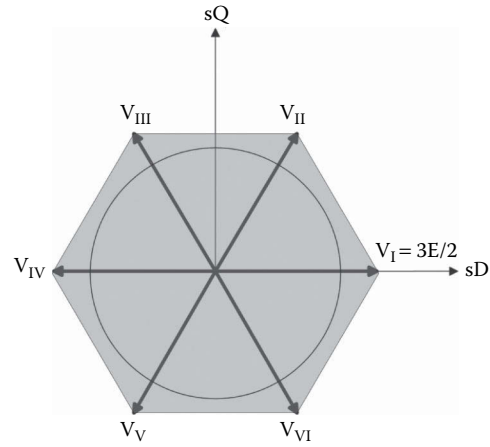

FIGURE 8.12 B6 reachable voltage space.

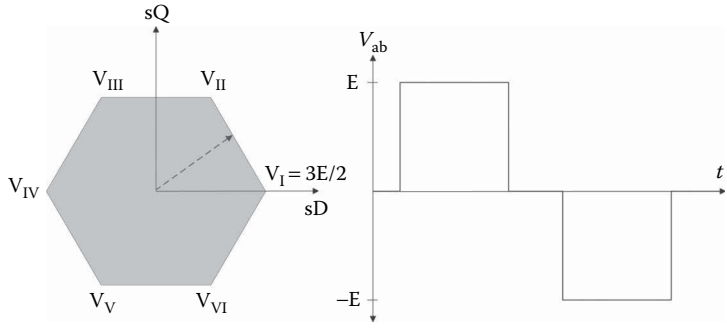

FIGURE 8.13 B6 inverter square wave mode.

In this case, the peak value of the fundamental voltage of the line-to-line waveform is

$$V_{\text{llpeak1}} = \frac{2\sqrt{3}}{\pi} E = 1.103E \tag{8.9}$$

The space-averaged models are also directly applicable for PWM rectifiers in electric locomotives where AC energy from the traction transformer is to be converted into DC energy at the DC bus bars. These are current-controlled single-phase converters. The power balance equation, Equation 8.7, applies. Consider the case in which the rectifier is controlled to draw a sinusoidal current from the traction transformer, where the transformer voltages and currents are

$$v_i(t) = \sqrt{2}\ V_{\text{rms}} \sin(\omega t) \tag{8.10}$$

$$i_i(t) = \sqrt{2}\ I_{\text{rms}} \sin(\omega t + \phi) \tag{8.11}$$

The converter input and output powers are equal to:

$$i_o(t) \times v_o(t) = i_i(t) \times v_i(t) = V_{\text{rms}} I_{\text{rms}} \left[\cos(\phi) - \cos(2\omega t + \phi) \right] \tag{8.12}$$

The rectifier power has an average value, $V_{\text{rms}}I_{\text{rms}}$ [cos(ϕ)], which is responsible for the average power flow. Most often, the converter will operate at cos(ϕ) = 0, that is, normal rectification, or at cos(ϕ) = π, which is the regenerative mode where braking energy can be returned to the overhead system. The output power also contains an oscillatory term, $-V_{\text{rms}}I_{\text{rms}}$ [cos(2ω*t* + ϕ)], at twice the mains frequency. This is very significant in terms of power. For example, in a 5 MW AC locomotive, the average power term is naturally 5 MW, but the instantaneous term varies between +5 MW and –5 MW. The total rectifier power varies between 0 MW and 10 MW. The power flows can be averaged with energy storage at the DC bus. The typical exchanges vary with the supply frequency, but are less than 10 kJ. If the rectifier output voltage is a fixed DC voltage, *E*, then the output current becomes:

$$i_o(t) = \frac{V_{\text{rms}} I_{\text{rms}}}{E} \left[\cos(\phi) - \cos(2\omega t + \phi) \right] \tag{8.13}$$

The current produced by the *2*ω term has to be carried by the DC bus filters shown in Figure 8.4. The filter size can be reduced by adding the resonant link consisting of the inductor L_R and the capacitor C_R. This link provides a low impedance path at the *2*ω frequency. Energy storage, which averages the power flows, is provided by both the capacitor and the inductor.

8.5 TRACTION MOTOR MODELLING

The traction motor models should be based upon manufacturer's data or the experimental measurement of the key parameters. The motor name plate will provide some key data such as the rated currents and voltages. The key experimental measurements are as follows:

- For induction motors — the no-load test and the locked rotor test, which will determine the machine resistances and inductances;
- For DC motors — unloaded motor speed at full-field and partial-field conditions, as this determines the back electromotive force and torque constant (these have the same numeric value); and
- For all motors — the DC resistances of all accessible windings.

For an AC traction motor, the following parameters are generally required:

- The rated line-to-line voltage and the rated frequency;
- The stator and rotor leakage inductance;
- The mutual inductance (the magnetising inductance less the stator leakage reactance); and
- The stator and rotor resistances.

For some commercial drive models that integrate a motor and a controller, for example, MATLAB®-Simulink®, the rated flux is required. This is calculated from:

$$\lambda_{\text{rated}} = \frac{V_{\text{ll}}}{\sqrt{3}2\pi f_{\text{rated}}} \tag{8.14}$$

where:

λ_{rated} is the root mean square (rms) value of the rated flux
V_{ll} is a rated motor line-to-line voltage
f_{rated} is a base frequency corresponding to the rated frequency and flux

For a separately excited DC motor, the following parameters will be required:

- The rated armature voltage and current;
- The armature resistance and inductance (inclusive of compensation windings and interpoles);
- The rated field winding voltage and current;
- The field winding resistance and inductance (if the field dynamics are to be incorporated); and
- The back electromotive force/torque constant as a function of the field current.

Inappropriate motor parameters may adversely affect the modelling in ways that are not immediately apparent. For a modeller, this is a dangerous situation in that a simulation may appear to run correctly but may ultimately produce unrealistic results. As an example, the inductances within an induction motor model have a profound effect on the slip characteristics. A simulation study of a slip control system would be adversely affected by a modelling error of this type. These types of modelling error are detectable. As a model confirmation exercise, it is advisable to take simplified models of the traction motor, AC or DC, operated from fixed voltage sources, and to evaluate the motor performance with static loads. Major parameters such as currents, efficiency and, in the case of an AC motor, slip and power factor should be assessed against expectations.

A valuable tool in the evaluation and verification of machine parameters is the per unit system. The per unit system expresses the machine parameters as ratios relative to a base impedance. For a traction motor, the base impedance is a load that would draw an equivalent current at the rated motor voltage. The motor parameters expressed in per unit terms will fall within a limited range. Motors of similar power ratings will have similar per unit parameters, even if the terminal voltages and currents are markedly different.

Consider the traction motor studied in Chapter 4. This machine has a rated phase voltage of 1170 Vrms and a phase current of 167 A. The base impedance is 7.02 Ω. For a 29 Hz machine, this equates to a base inductance of 38.5 mH. The magnetising inductance is 3 times the base inductance, which indicates that the magnetising current is one-third of the motor's rated current. This is a reasonable outcome for

an induction motor. The stator and rotor resistances are 1.8% of base resistance, which indicates that the copper losses at full load will be 3.6% of the motor's kilovolt amperes rating. Again, for an efficient machine, this is a reasonable ratio. The stator and rotor leakage inductances are 8.1% as a portion of the base inductance. These are reasonable values and result in satisfactory slip and breakdown torque performances as detailed in Chapter 4.

8.6 POWER SYSTEM MODELLING FOR HEAVY HAUL LOCOMOTIVES IN SIMULINK

Two case studies are now presented. Both are AC traction systems using induction motors and an FOC drive system. The first case represents an electric locomotive and the second represents a diesel-electric system. In both cases, state-space average models are used and a fixed time step of 20 µs is applied. The state-space approach avoids the production of switching events, as would otherwise occur in the power electronic systems. Switched models are normally solved with variable time step solvers that allow very small time steps, even less than 1 ns, in the vicinity of the power device switching events so that the switching transition is correctly solved. The use of a fixed time step greatly simplifies the integration with the mechanical system models. The avoidance of very short time steps allows the electrical systems to be integrated with the mechanical systems while still achieving a reasonable simulation runtime.

8.6.1 Case Study 1: AC Electric Locomotive

An overview of the power system is presented in Figure 8.14. The locomotive is a Co-Co configuration and has one traction inverter for each bogie. Each inverter supplies three traction motors which are connected directly in parallel. The traction motors are described in Table 8.2. The traction inverter utilises field-oriented torque control. The DC bus voltage is 2650 V. This is just sufficient for a 2027 V motor if the inverter is driven into the square wave mode at high speed. The required peak voltage for the motor is 2866 V. In the square wave mode, the maximum value of the line-to-line voltage available from the inverter is, from Equation 8.19, 2061 Vrms or 2915 Vpeak. The maximum undistorted line-to-line voltage is 1874 Vrms.

In this simulation, parts of the MATLAB Simulink AC3 drive module were used to build the drive system model [7]. The AC3 model is included in the SimPowerSystems libraries and is an indirect rotor-based FOC drive that uses a state-space averaged approach. The model is a Simulink masked subsystem. It is possible to unmask the subsystem and edit the model. The major changes included the removal of the existing DC power supply and braking chopper, and the introduction of two additional traction motors.

The inverter is modelled using a three-phase current controlled state-space averaging approach. Field weakening is introduced above 29 Hz to maintain the stator voltage within the 2915 Vpeak fundamental voltage, which can be achieved with a

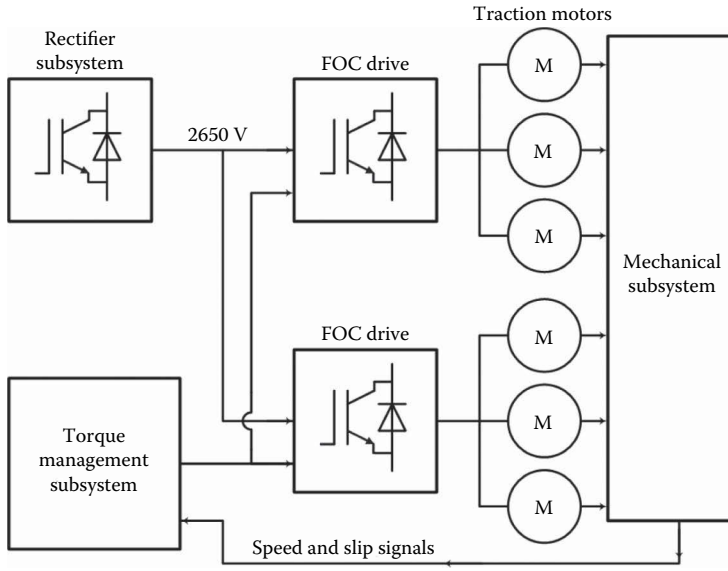

FIGURE 8.14 Electric locomotive power system overview.

TABLE 8.2
Traction Motor Parameters

Parameter	Value	Per Unit Value
Real power rating	500 kW	0.85
Apparent power rating	585 kVA	1.0
Line-to-line voltage	2027 Vrms	1.0
Number of phases	3	
Base frequency	29 Hz	1.0
Number of poles	4	
Stator resistance	132 mΩ	1.9%
Stator reactance	3.14 mH	8.1%
Rotor resistance	132 mΩ	1.9%
Rotor reactance	3.14 mH	8.1%
Magnetising resistance	1240 Ω	176
Magnetising reactance	117 mH	3.0

Source: M. Spiryagin et al., *Vehicle System Dynamics*, 53(5), 672–691, 2015.

2650 V bus. For these motors, the rated flux may be calculated using Equation 8.14. This provides a value of 9.08 Wb peak. In practice, the motor flux in the loaded condition will be slightly less because of the voltage drops on the winding resistances and leakage reactances. In this simulation, a flux of 8.5 Wb peak was set to maintain the motor voltages within the inverter limits.

TABLE 8.3
Locomotive Torque Limits by Notch

Notch Position	Torque Limit (kNm)
0–Idle	0
1	5.041
2	10.082
3	17.643
4	25.205
5	32.788
6	40.327
7	47.889
8	54.442

Source: M. Spiryagin et al., *Vehicle System Dynamics*, 53(5), 672–691, 2015.

The mechanical subsystem includes the gearboxes, a Polach wheel-rail contact patch model [8], and an inertia model for the vehicle mass. The key mechanical parameters are:

- Gearbox ratio 90/17;
- Wheel diameter 1.052 m; and
- Vehicle mass 120 tonnes, which corresponds to the complete locomotive.

The torque control system provides torque set points to the inverters in response to the throttle notch settings. Additional limits on torque, based on the train speed, are imposed to maintain the DC power demand below 3 MW. In addition, a slip-limiting system is included to restrict the maximum wheel slip to 0.05 per unit [9–10]. For this locomotive, the notch torque settings for all six traction motors combined are shown in Table 8.3 [1]. The torque ramp rate limit is 18.147 kNm/s. This is selected to allow full torque to be achieved in 3 s.

The schematic diagram of the rectifier subsystem is shown in Figure 8.4. This subsystem includes the following equipment:

- A traction transformer with the following ratings: 3 MVA; 25 kV: 1500 V; primary and secondary leakage reactance 8%; primary and secondary resistance 0.2%; magnetising reactance 500 per unit; and core loss resistance 500 per unit;
- A current B4 converter modelled using the state-space approach, as outlined in Figures 8.8 and 8.9;
- A DC bus capacitor of 3600 μF;
- A 2ω resonant filter, tuned to 100 Hz with a quality factor (Q) of 15, with a 3600 μF capacitor and a 0.7036 mH inductor;

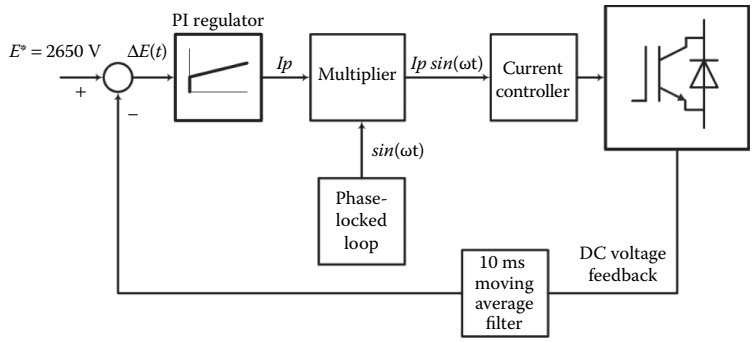

FIGURE 8.15 DC bus voltage regulator.

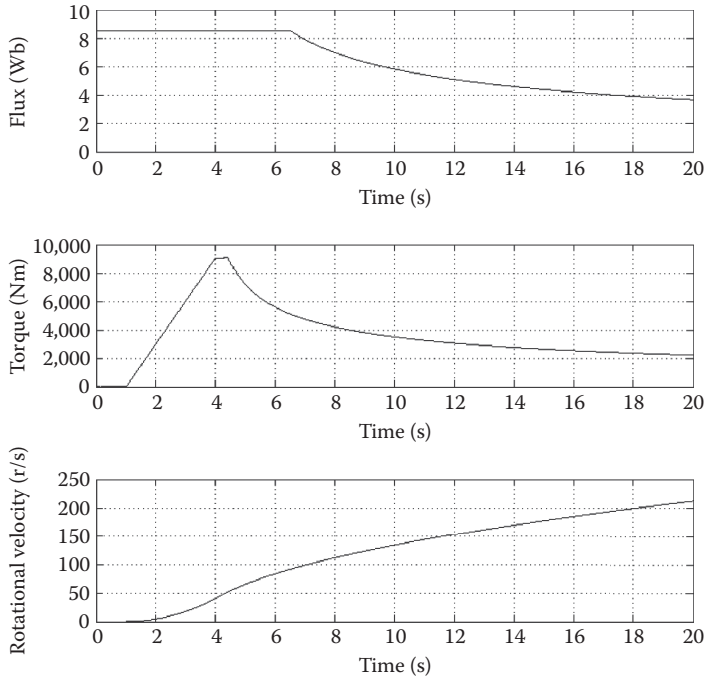

FIGURE 8.16 Traction motor flux, torque and rotational speed of AC electric locomotive.

- A phase-locked loop to provide a sine wave reference signal synchronised to the traction transformer secondary voltage; and
- A proportional-integral (PI) controller, which controls the DC bus voltage to 2650 V, as outlined in Figure 8.15.

Figures 8.16–8.19 show the results for the acceleration of the locomotive from standstill, with the maximum notch selected at $t = 1$ s. In this locomotive, the

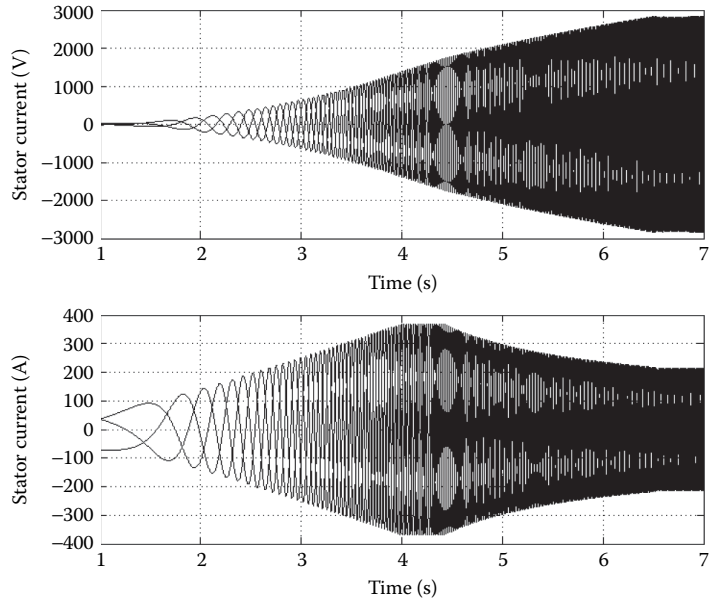

FIGURE 8.17 Stator voltage and current for one traction motor of AC electric locomotive.

notch torque limit is 54.4 (9.1 kNm per traction motor). This is a short-time rating, which is significantly higher than the steady-state rating of the motors, which is 5.45 kNm. The torque is ramp rate limited, and full torque can be obtained within 3 s. Figure 8.16 shows the torque production of a single motor, along with the rotational speed and the machine flux. The torque is zero up to $t = 1$ s and then ramps linearly to the notch 8 setting of 9.1 kNm at 4 s. The full torque is held until 4.5 s where a torque limit is imposed to restrict the DC traction power to 3 MW, as the locomotive accelerates. The flux is constant at 8.5 Wb until approximately 6.5 s where the motor reaches its rated frequency of 29 Hz. After that point, field weakening occurs.

Figure 8.17 shows the stator currents and voltages, displayed over the period from 1 to 7 s. This captures the full ramp up of the machine voltage and the start of field weakening. The monotonic increase of the motor current and voltage frequency can be seen in the first seconds of the acceleration. The current magnitudes can be seen to respond to the torque demand. In this simulation, field weakening is used to limit the motor voltage to the inverter capability. The Simulink FOC model was modified to disable the transition to the switching mode. The motor flux value, 8.5 Wb (peak), results in a peak line-to-line voltage of less than 2850 V, which is within the inverter capability.

Figure 8.18 shows the rectifier power and the current drawn from the 25 kV overhead traction power supply system. The DC power rises rapidly from 1 to 4 s as the torque increases linearly with the acceleration of the locomotive. After 4 s, the power increases linearly as the torque is fixed and the locomotive acceleration is nearly constant. At 4.5 s, the torque control system reduces the drive torque

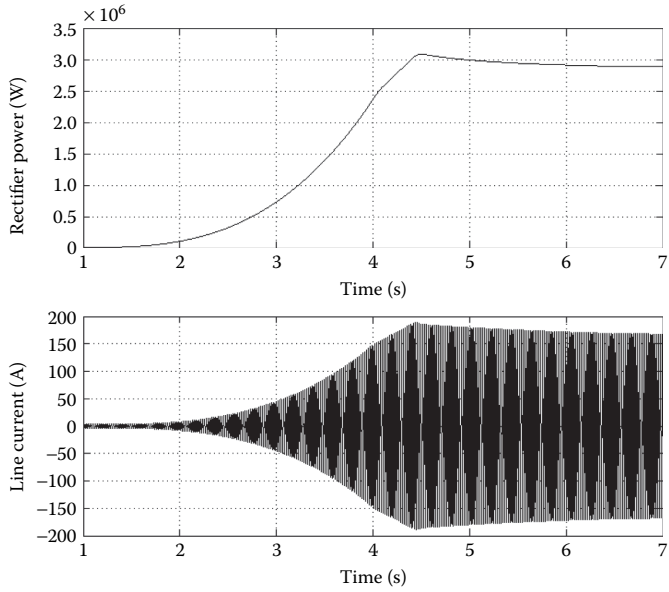

FIGURE 8.18 Rectifier power and 25 kV system current.

to limit the rectifier subsystem power to 3 MW. The rectifier power is directly reflected in the envelope of the 25 kV overhead system current. Three megawatts equates to 120 Arms or 170 Apeak.

Figure 8.19 shows the operation of the rectifier from 6.8 to 7.0 s. In this period, the rectifier is operating at nearly steady state. The input voltage and current waveforms are sinusoidal and unity power factor. The DC bus output voltage has approximately 50 Vpp ripple at the 2ω frequency—100 Hz in this case. The DC bus filter consists of the DC bus capacitor and a series resonant link, and these carry 700 Arms of 100 Hz current.

8.6.2 Case Study 2: AC Diesel-Electric Locomotive

An equipment overview for the diesel-electric case study is seen in Figure 8.20. This example is based on Ref. [1]. The AC drive systems are identical to the electric locomotive case, but the DC bus is now powered by a generator subsystem. The torque control subsystem still has the same notch torque limits as the electric locomotive, but the torque ramp rate is reduced to 3.402 kNm/s. It now requires at least 16 s to achieve full torque from a zero initial condition. This is equivalent to 2 s per notch position. The torque control subsystem is further constrained by a power capability signal provided by the generator. The torque may be limited if, given the train speed, the real power capability of the diesel engine would be exceeded. The torque control system provides notch and train speed signals to the generator. This subsystem incorporates a diesel engine model, as described in Figure 8.1. The diesel rotational speed and power capability with each notch setting are shown in Table 8.1. In this

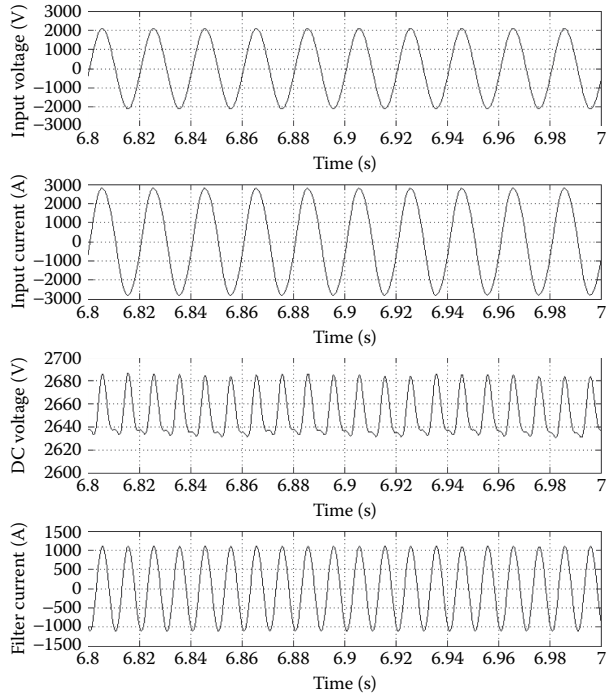

FIGURE 8.19 Rectifier input voltage and current, DC output voltage and filter current.

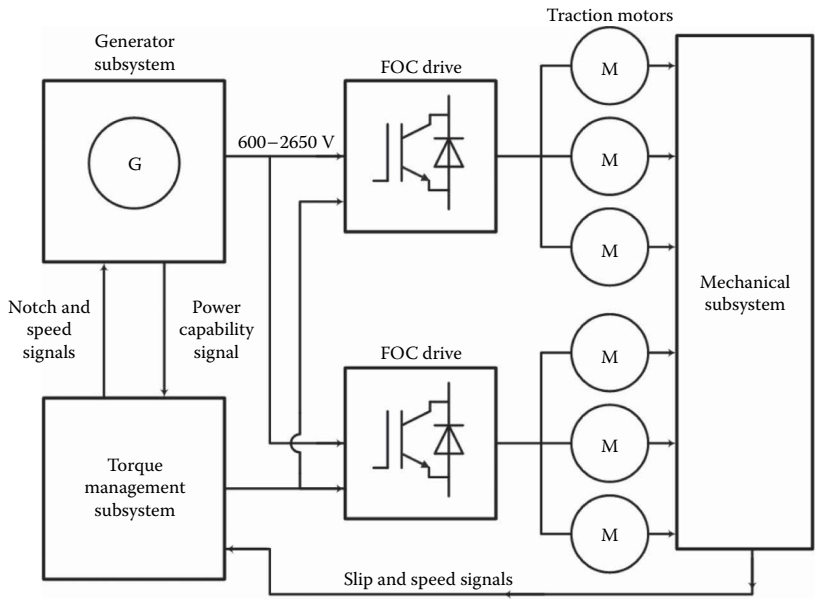

FIGURE 8.20 Diesel-electric power system overview.

TABLE 8.4
Generator Subsystem Lookup Table Data

Notch	Field Current Limit (A)	$K(I_f)$ ($VA^{-1}\,rpm^{-1}$)
0–Idle	0	0.0544
1	79	0.0544
2	79	0.0544
3	95	0.0480
4	99	0.0480
5	102	0.0480
6	105	0.0480
7	107	0.0480
8	109	0.0480

case, the diesel engine requires 16 s to transition from idle to full speed, and this establishes a ramp rate limit of 44 rpm/s.

The alternator model is described in Figure 8.2. The commutation resistance is 0.92 Ω and the DC bus capacitance is 1440 μF. The generator field current limits and the air gap factor are determined from lookup tables. These data are shown in Table 8.4. The generator voltage is a function of notch and vehicle speed. Table 8.5 shows the generator voltage lookup table. The notch setting is a discrete variable, but speed is a continuous variable. Linear interpolation is used to determine the voltage variation with speed.

Figure 8.21 shows the torque production of a single motor, along with the rotational speed and the machine flux. Figures 8.22–8.25 show the results for the acceleration of the diesel-electric locomotive from standstill with the maximum notch, notch 8, selected at $t = 1$ s. In this locomotive, the notch torque limit is 54.4 kNm, or 9.1 kNm per traction motor. As in the electric locomotive case, this is a short-time rating, which is significantly higher than the steady-state rating of the motors which is 5.45 kNm. The torque is ramp rate limited, and full torque can be obtained within 16 s.

The torque is zero to $t = 1$ s and then ramps linearly towards the notch 8 setting at the ramp rate limit, which is 0.57 kNm/s at the machine level. The machine torque does not reach the notch torque setting, as, shortly after 6 s, the locomotive reaches the power capability of the generator. The diesel engine has a rotation speed that is less than 500 rpm and a power capability of less than 600 kW at this time. The machine torque remains power limited for the rest of the simulation period. The torque remains between 3 kNm and 3.7 kNm and varies with the generator power and vehicle speed. At $t = 17$ s, the generator is at full power and torque declines as the locomotive continues to accelerate. In this simulation, only the locomotive is considered. In the absence of a trailing load, it can accelerate quickly. In heavier trains, the traction motor torques may reach the notch 8 limit as the vehicle speeds attained during the generator ramp time is much lower.

The flux is constant at 8.5 Wb until approximately 14 s, where the machine reaches its rated frequency of 29 Hz. After that point, field weakening occurs.

TABLE 8.5
Generator Voltage Lookup Table Data

	Locomotive Velocity (m/s); Traction Machine (rpm)							
Notch	**0 m/s; 0 rpm**	**0.97 m/s; 93 rpm**	**7.66 m/s; 735 rpm**	**13.2 m/s; 1265 rpm**	**14.7 m/s; 1415 rpm**	**26.1 m/s; 2500 rpm**	**27.6 m/s; 2655 rpm**	**36.5 m/s; 3500 rpm**
Idle	620 V	620 V	620 V	620 V	620 V	620 V	620 V	620 V
1	620 V	620 V	620 V	620 V	620 V	620 V	620 V	620 V
2	880 V	880 V	880 V	880 V	880 V	880 V	880 V	880 V
3	1200 V	1200 V	1295 V	1295 V	1295 V	1295 V	1295 V	1295 V
4	1410 V	1410 V	1540 V	1540 V	1540 V	1540 V	1540 V	1540 V
5	1500 V	1500 V	1760 V	1760 V	1760 V	1760 V	1760 V	1760 V
6	1500 V	1500 V	2130 V	2130 V	2130 V	2130 V	2130 V	2130 V
7	1500 V	1500 V	2400 V	2430 V	2430 V	2430 V	2430 V	2430 V
8	1500 V	1500 V	2650 V	2650 V	2650 V	2650 V	2650 V	2650 V

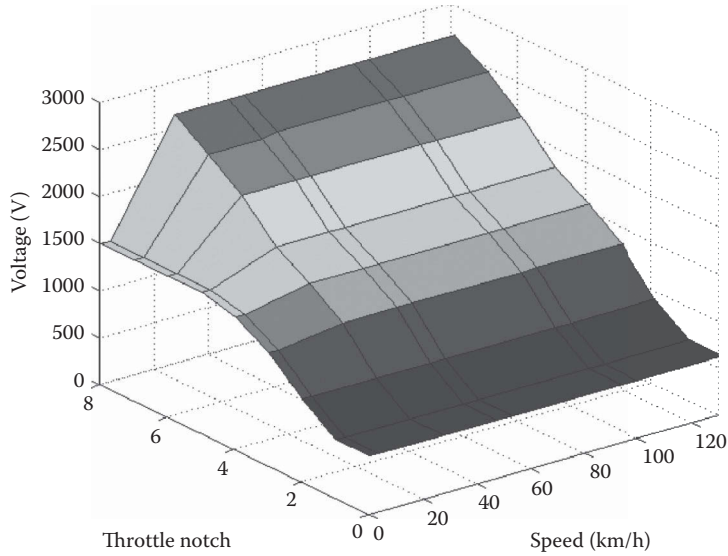

FIGURE 8.21 Generator notch/speed voltage dependency.

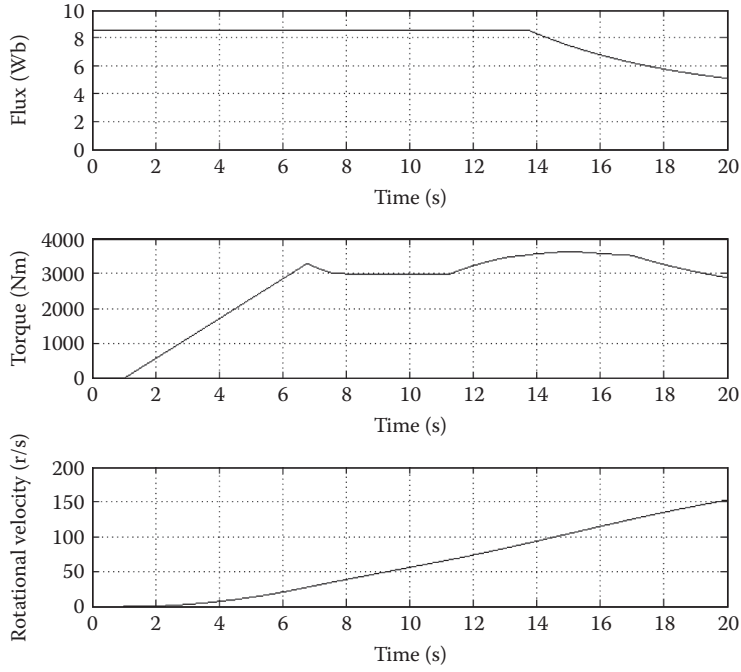

FIGURE 8.22 Traction motor flux, torque and rotational speed of AC diesel-electric locomotive.

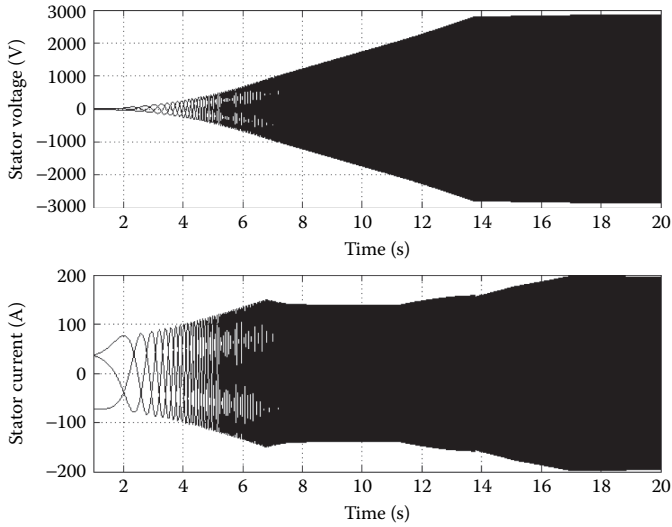

FIGURE 8.23 Stator voltage and current for one traction motor of AC diesel-electric locomotive.

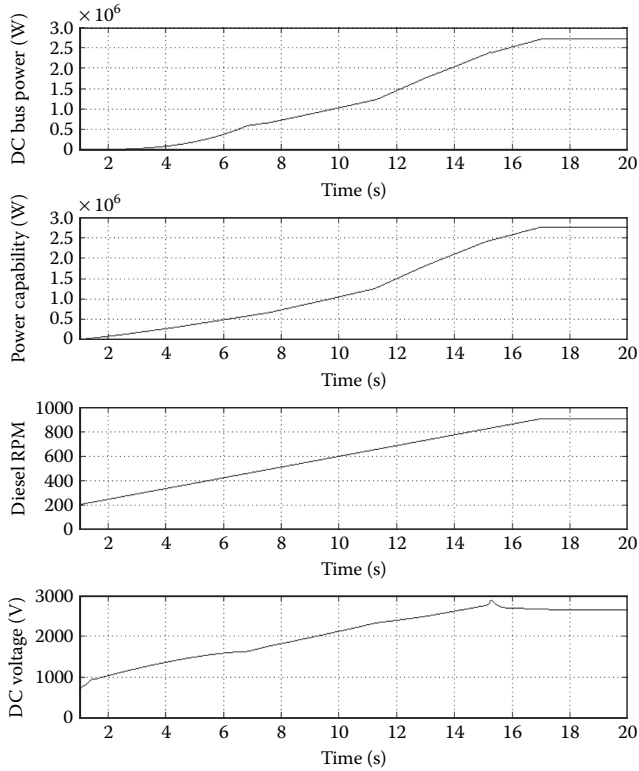

FIGURE 8.24 Generator power, power capability, rpm and voltage.

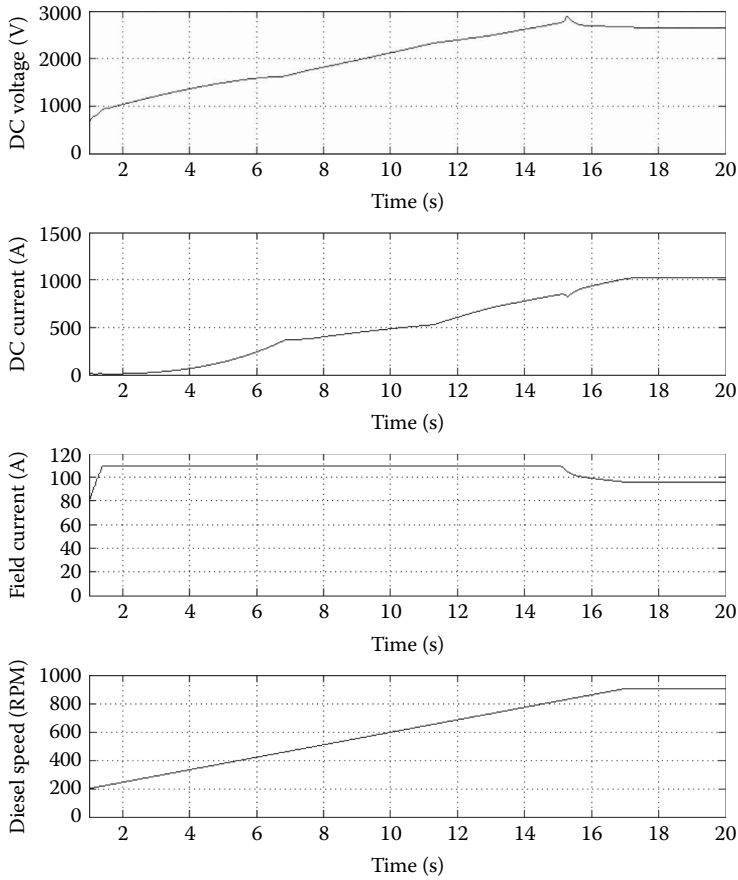

FIGURE 8.25 Generator voltage, current, excitation and rpm.

This does not have a torque impact, as the torques are already strongly limited by the available power.

Figure 8.23 shows the stator currents and voltages, displayed over the period from 1 to 20 s. This captures the full ramp up of the motor voltage and the start of field weakening at $t = 14$ s. The monotonic increase of the motor current and voltage frequency can be seen in the first seconds of the acceleration. The current magnitudes can be seen to respond to the torque demand. As in the electric locomotive case, field weakening is used to limit the motor voltage to the inverter capability.

Figure 8.24 shows the performance of the generator subsystem. This simulation case is the most dynamically demanding for the generator subsystem, as the locomotive can accelerate rapidly and higher speeds allow quick changes in traction power.

The first trace is the power demand imposed by the traction inverters upon the DC bus during the simulation. The DC power demand is actively limited by the torque control system to ensure that the power capability of the generator is not exceeded. The second trace is the generator power capability, which exceeds the

traction system demand until shortly after $t = 6$ s. After that time, the DC bus power tracks the generator capability.

The power capability is determined from the diesel engine rpm from a lookup table. The third trace is the diesel engine rotational speed. The machine starts at idle, 200 rpm, and accelerates at 44 rpm/s from $t = 1$ s. Full speed of 904 rpm is achieved at 17 s.

Figure 8.25 shows further details on the generator operation. The first trace is the generator voltage. The full voltage is reached just after 14 s. To achieve the necessary voltages during the ramp-up period, the alternator field current, shown as the third trace, is at the notch limit of 109 A. As the engine rotational speed is low, the internal alternator voltage is also low. There will always be a delay in establishing the generator voltage because of the rate limits on the diesel engine speed. A slight overshoot in voltage is seen near $t = 15$ s. This corresponds to an overshoot of the PI voltage regulator, as seen in Figure 8.2. Before that point, the field currents had been at the notch 8 current limit of $109A$. The PI regulator has to rapidly reduce its output current demand to limit the voltage as the diesel engine is still increasing its rotational speed when the 2650 V set point is reached.

8.7 CONCLUSIONS

This chapter has introduced a range of appropriate modelling concepts and models that can be used to develop practical and useful simulation models. Models have been introduced for the traction transformer- and generator-based power supplies. The time delays that occur in the diesel subsystems have been examined and approaches based on lookup tables and rate-limiting systems have been described. These are intended to be suitable and tractable for power systems simulations and do not attempt to model the full range of diesel engine behaviours.

An explanation has been given of the state-space averaging methods that are widely applied for traction inverter modelling. Traction system inverters are specifically designed so that the motor currents are largely sinusoidal; this allows the approach to be readily applied. This permits simulations to be conducted with a fixed time step that is orders of magnitude larger than may be required in a switching model.

Finally, two Simulink demonstration case studies are presented for a complete electric locomotive and a complete diesel-electric locomotive power system. In each case, an unloaded locomotive accelerates at its maximum notch setting for 20 s. This allows the DC supplies, the traction inverters and the traction motors to operate from standstill, through the constant torque mode and well into the field weakening regime.

REFERENCES

1. M. Spiryagin, P. Wolfs, F. Szanto, C. Cole, Simplified and advanced modelling of traction control system of heavy haul locomotives, *Vehicle System Dynamics*, 53(5), 2015, 672–691.
2. H. Kamijo, H. Hata, H. Fujimoto, A. Inoue, K. Nagashima, K. Ikeda, M. Iwakuma, F. Funaki, Y. Sanuki, A. Tomioka, H. Yamada, K. Uwamori, S. Yoshida, Test of superconducting traction transformer for railway rolling stock, *IEEE Transactions on Superconductivity*, 17(2), 2007, 1927–1930.

3. L.G. Franquelo, J. Rodriguez, J.L. Leon, S. Kouro, The age of multilevel converters arrives, *IEEE Industrial Electronics Magazine*, 2(2), 2008, 28–39.
4. A. Schoung, H. Stemmler, Static frequency changers with subharmonic control in conjunction with reversible variable speed ac drives, *Brown Boveri Review*, 51(8–9), 1964, 555–577.
5. B.K. Bose, *Power Electronics and Variable Frequency Drives: Technology and Applications*, IEEE Press, Piscataway, NJ, 1996.
6. M.O. Kazmierkowski, L. Malesani, Current control techniques of three-phase voltage-source PWM converters: A survey, *IEEE Transactions on Industrial Electronics*, 45(5), 1998, 691–703.
7. R. Mathew, F. Flinders, W. Oghanna, Locomotive "total systems" simulation using SIMULINK, *Proceedings of International Conference on Electric Railways in a United Europe*, 27–30 March 1995, Amsterdam, the Netherlands, pp. 202–206.
8. O. Polach, Creep forces in simulations of traction vehicles running on adhesion limit, *Wear*, 258(7–8), 2005, 992–1000.
9. M. Spiryagin, O. Polach, C. Cole, Creep force modelling for rail traction vehicles based on the Fastsim algorithm, *Vehicle System Dynamics*, 51(11), 2013, 1765–1783.
10. M. Spiryagin, Y.Q. Sun, C. Cole, S. Simson, I. Persson, Development of traction control for hauling locomotives, *Journal of System Design and Dynamics*, 5(6), 2011, 1214–1225.

9 Advanced Simulation Methodology

The design concept of locomotives that was introduced more than 200 years ago continues to be further developed and improved. The progress of science and technology, especially in the field of computer modelling, allows rapid adoption of new and advanced forms of traction to powered railway vehicles. Recent publications [1,2] show that the design process requires the application of modern and advanced simulation techniques and tools.

At the simulation stage of locomotives, it is highly desirable to evaluate the whole mechatronic vehicle system [3,4] and test it under a variety of specific loads and operational scenarios. This requires the application of specialised software tools, the development of a mechatronic system (control system and vehicle dynamics model) and verification.

The simulation methodology commonly used for rail traction vehicles can be divided into the following simulation stages [5]:

- Simulation of longitudinal train dynamics [1,2];
- Modelling of creep forces at the wheel-rail interface [6–11];
- Simulation of purely mechanical systems in multibody software packages [1,2,12];
- Modelling and simulation of electric and traction control systems [13,14];
- Simulation of a controlled mechanical system (simplified mechatronic system) in dynamic and multibody software packages [15–17];
- Simulation of the full locomotive mechatronic system by means of co-simulation between multibody software and power engineering/control software [2,18,19]; and
- Validation and verification [1,17,20].

The concept of the implementation of the advanced simulation methodology, which is used in research studies and engineering tasks, can be presented as shown in Figure 9.1.

The verification of full locomotive models can be performed in a way similar to the locomotive model acceptance procedure described in Chapter 7. More advanced validation approaches require comparison of simulation results with experimental data gathered with special measurement devices or with operational data stored in logs of locomotive diagnostics systems.

The results obtained during simulations can then be transferred to other applications such as finite element analysis, computational aerodynamics, noise evaluation, specialised in-house and other software packages. These results can also be used for experimental programs, which are based on software-in-the-loop or hardware-in-the-loop techniques, for component testing and validation.

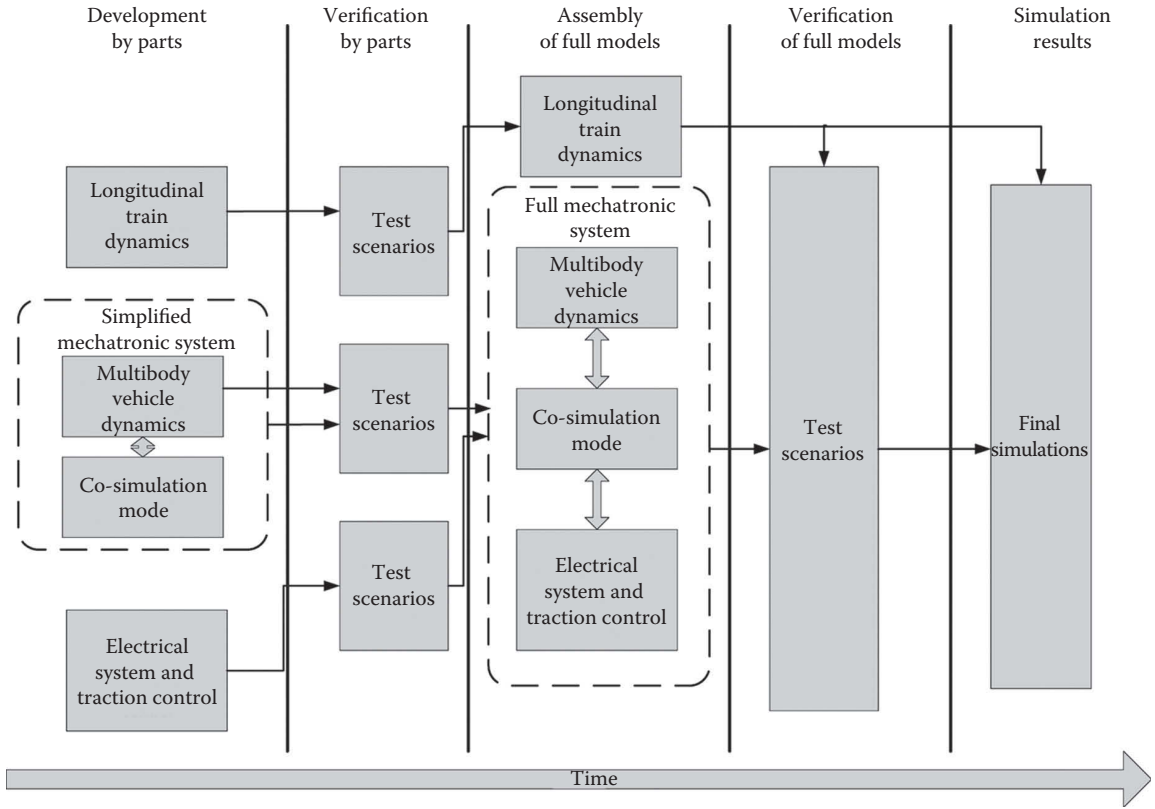

FIGURE 9.1 Concept of implementation of the advanced simulation methodology.

This chapter presents some examples of how to use a co-simulation technique in the studies of dynamic behaviour of locomotives, which can be achieved through data exchange processes between two software packages, with a predefined time step for that data exchange. The data exchange processes are usually based on three types of communication techniques:

- Integrated memory-shared communication between software products;
- Network data exchange; and
- Exporting code from one package to another.

All of these techniques have their own advantages and disadvantages; the decision about which technique is best to use is usually based on the initial requirements and existing hardware or software limitations.

In addition, this chapter presents an example of how to use the results delivered from a longitudinal train dynamics simulator in studies of heavy haul locomotive dynamics performed in a multibody software package.

9.1 CO-SIMULATION AND ITS APPLICATION

It has begun to be a common practice to use Simulink® software included in the MATLAB® package in locomotive dynamics studies. This is because this software is a very powerful tool and allows the development of any components of the locomotive model as well as its full mechatronic system. Simulink is also very friendly for the development of data exchange connections with multibody packages [2,19,21–23]. It makes the process of simulating locomotive dynamic behaviour under different operational conditions relatively easy [2,7,8,24–31].

9.1.1 Development of the Co-Simulation Client Interface

This chapter uses the GENSYS multibody software package to model a mechanical system of a heavy haul locomotive. Since the development of version 10.10 of GENSYS software, this package includes a server co-simulation interface, which allows the creation of the client interface in the Simulink environment. The co-simulation approach between GENSYS and Simulink has been developed based on the data exchange between these software tools by means of the Transmission Control Protocol/Internet Protocol (TCP/IP) protocol [32]. The development of client interface has been described in Refs. [2,19]. This chapter presents the development of the client interface in MATLAB/Simulink, taking into consideration that GENSYS runs on a 64-bit Linux platform and MATLAB/Simulink runs in a 64-bit Windows environment in this example. The architecture for such a co-simulation process is shown in Figure 9.2.

FIGURE 9.2 Architecture of the co-simulation process.

With regard to the existing requirements provided by GENSYS and described in Ref. [33], the co-simulation is executed by the tsim script of the CALC program. In this case, this program is a server, which can be called 'server_tsim'. The existing interface works under TCP/IP protocol version 4. On the basis of the information presented in Figure 9.2 and analyses of the existing solutions in this field, it is clear that the client interface needs to be realised under the Win64 architecture. Therefore, the approach described in Refs. [2,19,32] has been totally modernised in terms of our current co-simulation requirements and needs.

Simulink includes a very powerful tool for writing program code based on the S-function mechanism. An S-function called 'client_tsim' was written in C language and represents a client interface between GENSYS and Simulink. After creation, the client_tsim function was compiled with Mex-compiler in order to use it inside Simulink. For writing the client_tsim function, the following callback functions have been implemented inside the S-function:

- mdlStart;
- mdlCheckParameters;
- mdlInitializeSizes;
- mdlInitializeSampleTimes;
- mdlInitializeConditions;
- mdlOutputs; and
- mdlTerminate.

The function mdlStart is needed to define names and/or values of input and output parameters, presented in Figure 9.3, and store them in arrays for further use by other functions. The client user interface shown in this figure is created with Create Mask for the S-function block. Figure 9.3 also shows that the IP address of server_tsim and its port number are required for establishing connection between server and client. An example of the open-loop co-simulation in Simulink for the six-axle locomotive traction control problem is presented in Figure 9.4.

The function mdlCheckParameters is used for the validation and verification of the function block parameters, presented in Figure 9.3.

The 'sizes' information is used by Simulink to determine the characteristics of the S-function block (number of inputs, outputs, states, etc.). These characteristics are included in mdlInitializeSizes.

The function mdlInitializeSampleTimes is used in order to specify a value of sample time for our S-function in Simulink.

For the initialisation that must be carried out at each time step, the function mdlInitializeConditions is used. It initialises the connection between programs by means of using the Windows socket described in the Windows socket API library Ws2_32.lib for the Win64 platform. The parameters IP address and port number are used here for the TCP communication process.

The function mdlOutputs is used to start and stop the co-simulation process and for data exchange between client_tsim and server_tsim at each time step. The flowchart for the data exchange process is shown in Figure 9.5. The command 'run_tout' is sent to server_tsim in order to start the calculation process for one-time iteration.

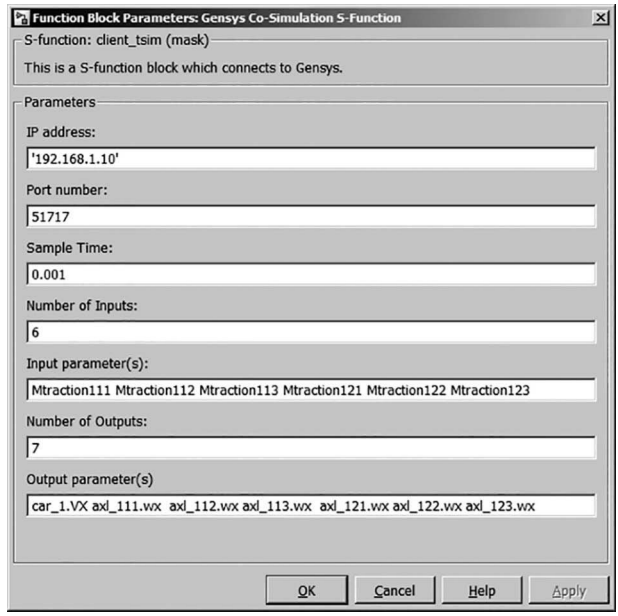

FIGURE 9.3 The client_tsim input and output data dialog box.

For receiving output parameters in the output data dialog box (see Figure 9.3), the following sequence of commands is used:

- Send the command 'ask_iadr <output parameter>' in order to find the addresses of the variables that need to be overwritten, and server_tsim replies with the address of the variable (var_address);
- Send the command 'put_iadr <var_address> <value>' in order to change/overwrite a variable. After sending the first argument, server_tsim sends a request to input the second argument. After sending the second argument (the new value of the variable), server_tsim replies with a zero, indicating that the new value was successfully inserted in the main memory.

A similar sequence of commands is used for sending input parameters (Figure 9.3) to server_tsim:

- Send the command 'ask_iadr <input parameter>' in order to find the addresses of the variables that need to be read, and server_tsim replies with the address of the variable (var_address).
- Send the command 'get_iadr <var_address>' in order to retrieve a value from server_tsim, and server_tsim replies with the value of the variable.

The function mdlTerminate is a mandatory function. In order to stop the simulation on the server_tsim side, the command 'run_stop' is used to send a stop command

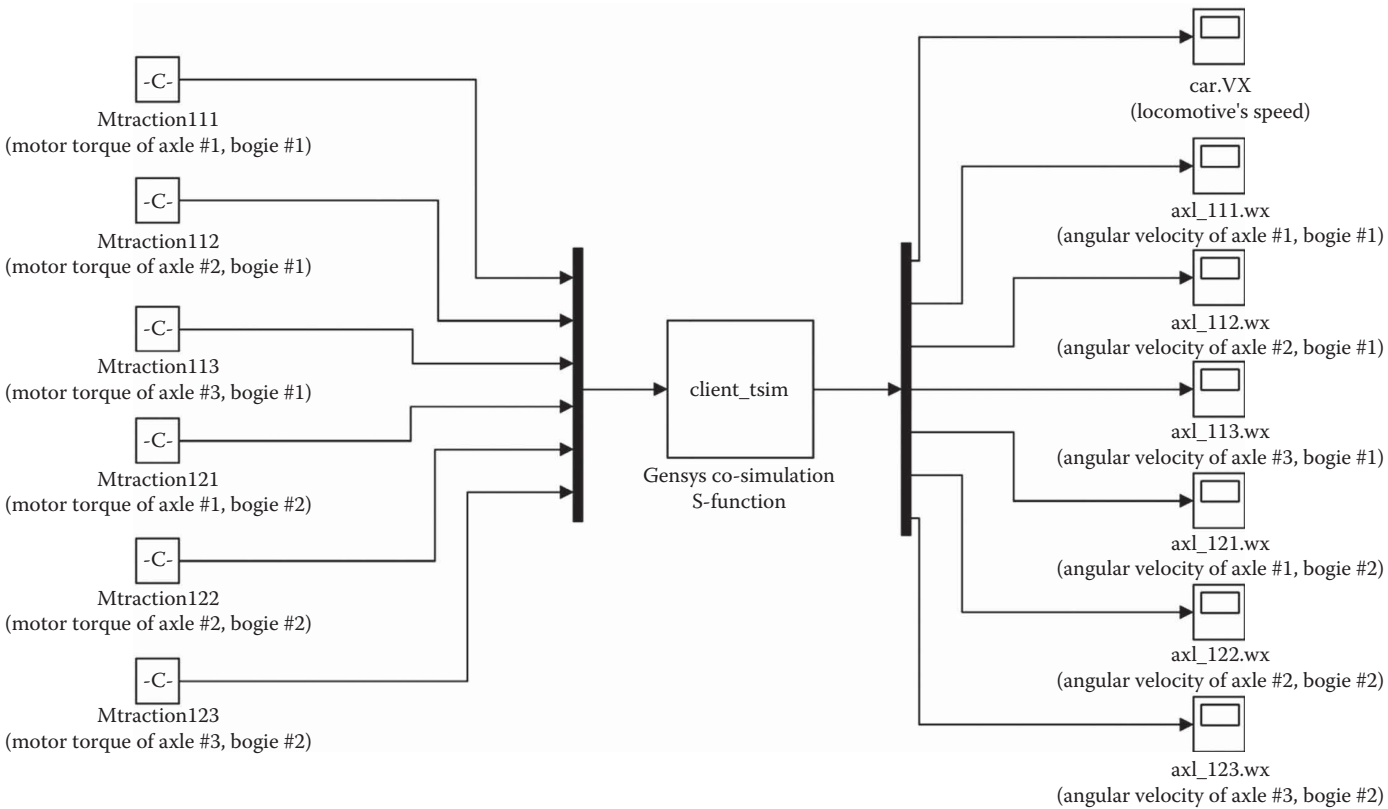

FIGURE 9.4 Example of open-loop co-simulation for six-axle locomotive in Simulink.

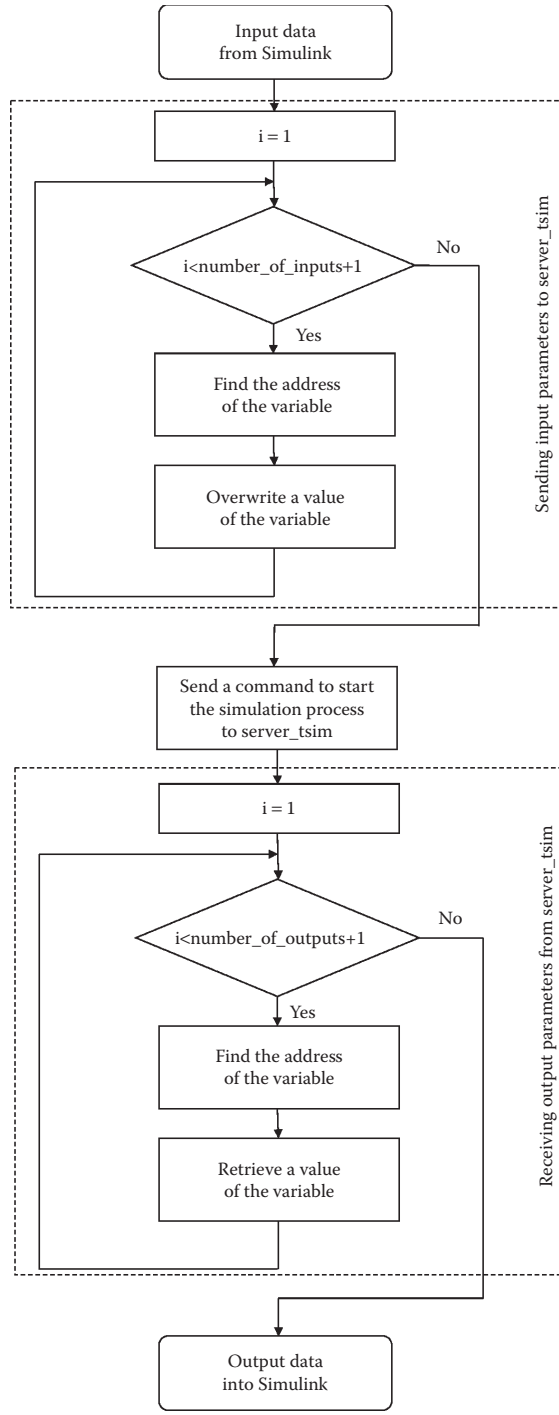

FIGURE 9.5 Algorithm flowchart written inside the mdlOutputs routine.

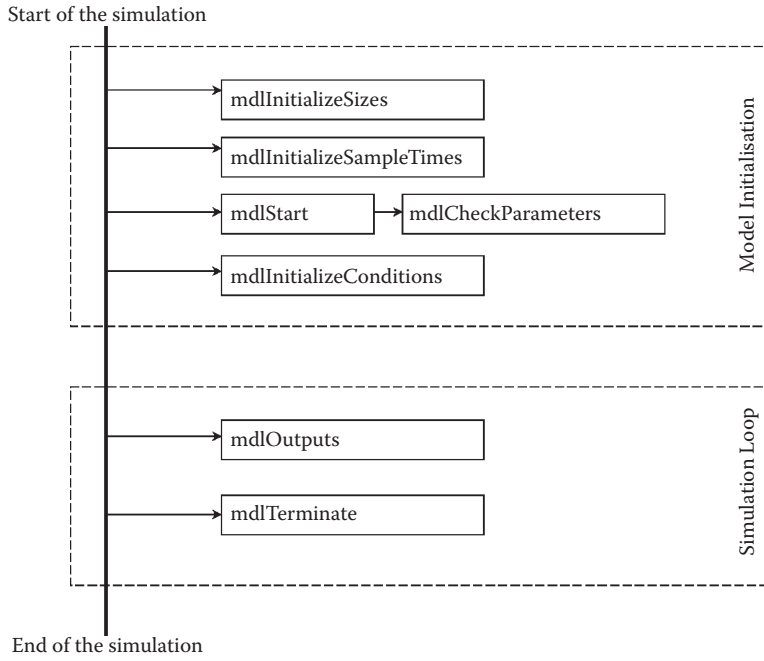

FIGURE 9.6 Structure of model initialisation and simulation loop in Simulink.

inside of this function. As a result, both server_tsim and client_tsim close the TCP/IP connection between the GENSYS and Simulink software products.

The overall sequence of implemented functions is presented in Figure 9.6. The figure shows the order in which the Simulink engine invokes the functions. The mdlInitializeSizes and mdlInitializeSampleTimes functions are executed during initialisation and all time steps during the simulation loop. The other functions inside the Model Initialisation rectangle are executed only once during the initialisation process. The functions from the Simulation Loop rectangle are executed at each time step during the simulation process.

The S-function was written to run in the discrete time mode, which allows the possibility of using the model created in Simulink for further research with real-time simulations. The code of the S-function is provided below:

```
/* File : client_tsim.c
* Abstract:
* Gensys model (tsim co-simulation) Function block for Win64
OS platform
*/
#define S_FUNCTION_NAME client_tsim
#define S_FUNCTION_LEVEL 2
#include "simstruc.h"
#include "winsock2.h"
#include "windows.h"
```

```
#include "string.h"
#include "mex.h"
#include <stddef.h>
#include <stdio.h>
#include <stdlib.h>
/* Link with Ws2_32.lib */
#pragma comment (lib, "Ws2_32.lib")
/* The macro substitutions are defined below */
#define U(element) (*uPtrs[element]) /* Pointer to Input
Port0 */
#define ADDRESS_IDX 0
#define ADDRESS_PARAM(S) ssGetSFcnParam(S,ADDRESS_IDX)

#define PORTNUMBER_IDX 1
#define PORTNUMBER_PARAM(S) ssGetSFcnParam(S,PORTNUMBER_IDX)

#define SAMPLE_TIME_IDX 2
#define SAMPLE_TIME_PARAM(S) ssGetSFcnParam(S,SAMPLE_TIME_IDX)
#define NUMBER_INPUTS_IDX 3
#define NUMBER_INPUTS_PARAM(S)
ssGetSFcnParam(S,NUMBER_INPUTS_IDX)
#define INPUTS_IDX 4
#define INPUTS_PARAM(S) ssGetSFcnParam(S,INPUTS_IDX)

#define NUMBER_OUTPUTS_IDX 5
#define NUMBER_OUTPUTS_PARAM(S)
ssGetSFcnParam(S,NUMBER_OUTPUTS_IDX)
#define OUTPUTS_IDX 6
#define OUTPUTS_PARAM(S) ssGetSFcnParam(S,OUTPUTS_IDX)

#define NPARAMS 7
#define MAX_NUMBER_OF_INPUTS 100
/* The declaration list of variables */
SOCKET mySocket;
long double f;
unsigned char p[128];
int port;
int number_inputs, number_outputs;
char *input_5, *input_7, *hostname;
static char *msg[35];
unsigned char *input_names[100], *output_names[100];
unsigned char server_command[128];
unsigned char c;
unsigned char dataparameters[100];
int numberofinputparameters, numberofoutputparameters;
/*====================*
* S-function methods *
*====================*/

#define MDL_START
static void mdlStart(SimStruct *S)
```

```
{
       int i;
     int   m,l,h,g;
       int numberofchars;

/* INPUT_NAMES: this section allows getting the name of input
parameters and store them in the array*/
            number_inputs=(int)
mxGetScalar(NUMBER_INPUTS_PARAM(S));
           numberofchars=mxGetNumberOfElements
(INPUTS_PARAM(S))+1;
            input_5=calloc(1000, sizeof(char));
            mxGetString(INPUTS_PARAM(S), input_5,
numberofchars);

             for (i=0;i<MAX_NUMBER_OF_INPUTS;i++) {
                  input_names[i]=calloc(100, sizeof(char));
             }

             m=0; l=0;
             for (i=0;i<numberofchars;i++)
                 {
                      c=input_5[i];
                        if ((c==' ')||(c=='\0')) {
                             dataparameters[l]='\0';
                             strcat(input_names[m],
                             dataparameters);
                               l=0;
                               m++;
                        }
                        else {
                            dataparameters[l]=c;
                             l++;
                        }
             }
             numberofinputparameters=m;

/* INPUT_NAMES: the end of this section*/

/* OUTPUT_NAMES: this section allows getting the name of input
parameters and store them in the array*/

            number_outputs=(int)
mxGetScalar(NUMBER_OUTPUTS_PARAM(S));
           numberofchars=mxGetNumberOfElements
(OUTPUTS_PARAM(S))+1;
            input_7=calloc(1000, sizeof(char));
            mxGetString(OUTPUTS_PARAM(S), input_7,
numberofchars);

             for (i=0;i<MAX_NUMBER_OF_INPUTS;i++) {
```

```
                output_names[i]=calloc(100, sizeof(char));
            }


            m=0; l=0;
            for (i=0;i<numberofchars;i++)
                {
                    c=input_7[i];
                      if ((c==' ')||(c=='\0')) {
                          dataparameters[l]='\0';
                            strcat(output_names[m],
dataparameters);
                            l=0;
                            m++;
                      }
                      else {
                          dataparameters[l]=c;
                          l++;
                      }
            }
            numberofoutputparameters=m;

/* OUTPUT_NAMES: the end of this section*/

/*Get host name from the input data*/
     numberofchars=mxGetNumberOfElements(ADDRESS_PARAM(S))+1;
     hostname=calloc(1000, sizeof(char));
     mxGetString(ADDRESS_PARAM(S), hostname, numberofchars);

   /* Get host name from the input data: the end of this
section*/

/*Get port from the input data*/
        port=(int) mxGetScalar(PORTNUMBER_PARAM(S));
/* Get port from the input data: the end of this section*/

     }
#define MDL_CHECK_PARAMETERS
#if defined(MDL_CHECK_PARAMETERS) && defined(MATLAB_MEX_FILE)
 /* Function: mdlCheckParameters
================================================
  * Abstract:
  *    Validate our parameters to verify they are okay.
  */
 static void mdlCheckParameters(SimStruct *S)
 {
     mwSize buflen;

/* Check 1st & 2nd parameters: ADDRESS/PORTNUMBER parameters */
     {
        if (mxGetNumberOfElements(PORTNUMBER_PARAM(S)) <= 0) {
```

```
            ssSetErrorStatus(S,"The port number (parameter)
is wrong");
            return;
        }
        if ((mxGetScalar(PORTNUMBER_PARAM(S)) <= 0)
||(mxGetScalar(PORTNUMBER_PARAM(S)) >= 65535)){
            ssSetErrorStatus(S,"The port number (parameter)
is wrong");
            return;
         }
    }
/* Check 3rd parameter: Sample Time of Block */
    /* The block sample time must be greater than
zero (0.0) */
    {
        if (*mxGetPr(SAMPLE_TIME_PARAM(S)) <= 0.0) {
            ssSetErrorStatus(S,"The block sample rate
(3rd parameter) "
                               "must be greater than zero");
            return;
        }
    }

/* Check 4th parameter: Number of Inputs*/

      number_inputs=(int) mxGetScalar
(NUMBER_INPUTS_PARAM(S));

/* Check 5th parameter: Input parameters */

           buflen = mxGetNumberOfElements(INPUTS_PARAM(S)) + 1;

       /* Copy the string data from string_array_ptr and
place it into input_5 */
         if (mxGetString(INPUTS_PARAM(S), input_5, buflen)
!= 0) {
           ssSetErrorStatus(S,"Could not convert string data");
             return;
        }

/* Check 6th parameter: Number of outputs */
         number_outputs=(int)
mxGetScalar(NUMBER_OUTPUTS_PARAM(S));
      /* Check 7th parameter: Output parameters */

         /* Copy the string data from string_array_ptr and
place it into input_7


         if (mxGetString(OUTPUTS_PARAM(S), input_7, buflen)
!= 0) {
```

```
            ssSetErrorStatus(S,"Could not convert string
data");
              return;
         } */

 }
#endif /* MDL_CHECK_PARAMETERS */
/* Function: mdlInitializeSizes
=============================================
* Abstract:
*    The sizes information is used by Simulink to determine
the S-function
*    block's characteristics (number of inputs, outputs,
states, etc.).
*/
static void mdlInitializeSizes(SimStruct *S)
{
   /* See sfuntmpl_doc.c for more details on the macros below */
   ssSetNumSFcnParams(S, NPARAMS); /* Number of expected
parameters */

#if defined(MATLAB_MEX_FILE)
    if (ssGetNumSFcnParams(S) == ssGetSFcnParamsCount(S)) {
        mdlCheckParameters(S);
        if (ssGetErrorStatus(S) != NULL) {
            return;
        }
    } else {
        return; /* Parameter mismatch will be reported by
Simulink */
    }
#endif
    {
        int iParam = 0;
        int nParam = ssGetNumSFcnParams(S);
        for ( iParam = 0; iParam < nParam; iParam++ )
        {
            switch ( iParam )
            {
              default:
                ssSetSFcnParamTunable( S, iParam,
SS_PRM_SIM_ONLY_TUNABLE );
                break;
            }
        }
  }
  if (!ssSetNumInputPorts(S, 1)) return;
          ssSetInputPortWidth(S, 0, number_inputs);
            ssSetInputPortDirectFeedThrough(S, 0, 1);
          ssSetInputPortOverWritable(S, 0, 1);
          ssSetInputPortOptimOpts(S, 0, SS_REUSABLE_AND_LOCAL);
```

```
  if (!ssSetNumOutputPorts(S, 1)) return;
          ssSetOutputPortWidth(S, 0, number_outputs);
         ssSetOutputPortOptimOpts(S, 0,
SS_REUSABLE_AND_LOCAL);
  ssSetNumSampleTimes(S, 1);
  ssSetNumRWork(S, 0);
  ssSetNumIWork(S, 0);
  ssSetNumPWork(S, 0);
  ssSetNumModes(S, 0);
  ssSetNumNonsampledZCs(S, 0);
  ssSetOptions(S, SS_OPTION_WORKS_WITH_CODE_REUSE |
SS_OPTION_EXCEPTION_FREE_CODE );
}
/* Function: mdlInitializeSampleTimes
=========================================
* Abstract:
*    Specify that we have a value of sample time.
*/
static void mdlInitializeSampleTimes(SimStruct *S)
{
ssSetSampleTime(S,0,mxGetScalar(ssGetSFcnParam(S,2)));
}
#define MDL_INITIALIZE_CONDITIONS
/* Function: mdlInitializeConditions
========================================
* Abstract:
*   This method is used for the initialization that must be
carried out
*   each time the subsystem becomes enabled.
*/
static void mdlInitializeConditions(SimStruct *S)
{
WORD wVersionRequested;
WSADATA data;
int n;
struct in_addr addr = { 0 };

/*The sockaddr_in structure specifies the address family,
  IP address, and port of the server to be connected to.
*/
 struct sockaddr_in{
  short sin_family;
  unsigned short sin_port;
  struct in_addr sin_addr;
  char sin_zero[8];
 };
 struct sockaddr_in clientService;
/* Initialize Winsock */
WSAStartup(wVersionRequested, &data);
mySocket=socket(PF_INET, SOCK_STREAM, 0);
if (mySocket == INVALID_SOCKET) {
```

```
         ssSetErrorStatus(S,"ERROR in creating mySocket");
             WSACleanup();
    return 1;
 }
clientService.sin_family = PF_INET;
clientService.sin_addr.s_addr = inet_addr( hostname );
clientService.sin_port = htons(port);
n=connect(mySocket, (SOCKADDR*) &clientService,
sizeof(clientService) );
                 if (n<0) {
              ssSetErrorStatus(S,"ERROR connecting");
                   WSACleanup();
                   }
}
/* Function: mdlOutputs
=================================================
*
*/
static void mdlOutputs(SimStruct *S, int_T tid)
{
     real_T x0,x1, data;
       int_T portWidth = ssGetInputPortWidth(S,0);
       InputRealPtrsType uPtrs = ssGetInputPortRealSignalPtr
s(S,0);
     real_T *y = ssGetOutputPortSignal(S,0);
     int_T i, n, ins;
       char_T command1[128];
       char_T command2[128];
     UNUSED_ARG(tid); /* not used in single tasking mode */

/* Start sending input parameters to the server*/
       for (i=0;i<numberofinputparameters;i++)
           {
            sprintf(&server_command,"ask_iadr");
            n=send( mySocket, &server_command,
(strlen(&server_command)+1), 0 );
                 if (n<0) {
             ssSetErrorStatus(S,"ERROR writing to socket");
                  }
            Sleep(0.1);
            memset(&server_command[0], 0,
sizeof(server_command));
            n=recv( mySocket, &server_command, 128, 0 );
      if (n<0) {
             ssSetErrorStatus(S,"ERROR reading from socket");
                  }
            Sleep(0.1);
             /************************ ask_iadr
************************************/
            n=send( mySocket, input_names[i],
(strlen(input_names[i])+1), 0 );
```

```
      if (n<0) {
              ssSetErrorStatus(S,"ERROR writing to socket");
      }
             Sleep(0.1);
              memset(&server_command[0], 0,
sizeof(server_command));
             n=recv( mySocket, &server_command, 128, 0 );
      if (n<0) {
              ssSetErrorStatus(S,"ERROR reading from socket");
      }
             Sleep(0.1);
              /************************** put_iadr
****************************************/
             sprintf(&command1,"put_iadr");
             n=send( mySocket, &command1,
(strlen(&command1)+1), 0 );
      if (n<0) {
              ssSetErrorStatus(S,"ERROR writing to socket");
      }
             Sleep(0.1);
             memset(&command1[0], 0, sizeof(command1));
             n=recv( mySocket, &command1, 128, 0 );
      if (n<0) {
              ssSetErrorStatus(S,"ERROR reading from socket");
      }
             Sleep(0.1);
             /*xxxxxxx put_iadr:first argument xxxxxx*/
             ins=atoi(&server_command);
             sprintf(&command1,"%d",ins);
             n=send( mySocket, &command1,
(strlen(&command1))+1, 0 );
      if (n<0) {
              ssSetErrorStatus(S,"ERROR writing to socket");
      }
             Sleep(0.1);
             memset(&server_command[0], 0,
sizeof(server_command));
             n=recv( mySocket, &server_command, 128, 0 );
      if (n<0) {
              ssSetErrorStatus(S,"ERROR reading from socket");
      }
             Sleep(0.1);
             /*xxxxxxx put_iadr:second argument xxxxxx*/
             data=((real_T)(*uPtrs[i]));
             sprintf(&command2,"%e",data);
             n=send( mySocket, &command2,
(strlen(&command2)+1), 0 );
      if (n<0) {
              ssSetErrorStatus(S,"ERROR writing to socket");
      }
             Sleep(0.1);
```

```
            memset(&server_command[0], 0,
sizeof(server_command));
            n=recv( mySocket, &server_command, 128, 0 );
      if (n<0) {
             ssSetErrorStatus(S,"ERROR reading from socket");
      }
            Sleep(0.1);
}
/* End sending input parameters to the server*/
/* To send a command to start simulation the server */
            sprintf(&server_command,"run_tout");
            n=send( mySocket, &server_command, 9, 0 );
      if (n<0) {
             ssSetErrorStatus(S,"ERROR writing to socket");
      }
            Sleep(0.1);
            n=recv( mySocket, &server_command, 128, 0 );
      if (n<0) {
             ssSetErrorStatus(S,"ERROR reading from socket");
      }
            Sleep(0.1);
/* Start receiving output parameters to the server*/
       for (i=0;i<numberofoutputparameters;i++)
      {
            sprintf(&server_command,"ask_iadr");
            n=send( mySocket, &server_command,
(strlen(&server_command)+1), 0 );
      if (n<0) {
             ssSetErrorStatus(S,"ERROR writing to socket");
      }
            Sleep(0.1);
             memset(&server_command[0], 0,
sizeof(server_command));
            n=recv( mySocket, &server_command, 128, 0 );
      if (n<0) {
             ssSetErrorStatus(S,"ERROR reading from socket");
      }
            Sleep(0.1);
            /************************ ask_iadr
*******************************/
            n=send( mySocket, output_names[i],
(strlen(output_names[i])+1), 0 );
      if (n<0) {
             ssSetErrorStatus(S,"ERROR writing to socket");
      }
            Sleep(0.1);
            memset(&server_command[0], 0,
sizeof(server_command));
            n=recv( mySocket, &server_command, 128, 0 );
      if (n<0) {
             ssSetErrorStatus(S,"ERROR reading from socket");
```

```
      }
             Sleep(0.1);
             /************************** get_iadr
*************************************/
             sprintf(&command1,"get_iadr");
             n=send( mySocket, &command1,
(strlen(&command1)+1), 0 );
      if (n<0) {
              ssSetErrorStatus(S,"ERROR writing to socket");
      }
             Sleep(0.1);
             memset(&command1[0], 0, sizeof(command1));
             n=recv( mySocket, &command1, 128, 0 );
      if (n<0) {
              ssSetErrorStatus(S,"ERROR reading from socket");
      }
             Sleep(0.1);
             /*xxxxxxx get_iadr:first argument xxxxxx*/
             ins=atoi(&server_command);
             sprintf(&command1,"%d",ins);
             n=send( mySocket, &command1,
(strlen(&command1))+1, 0 );
      if (n<0) {
              ssSetErrorStatus(S,"ERROR writing to socket");
      }
             Sleep(0.1);
             memset(&server_command[0], 0,
sizeof(server_command));
             n=recv( mySocket, &server_command, 128, 0 );
      if (n<0) {
              ssSetErrorStatus(S,"ERROR reading from socket");
      }
             Sleep(0.1);
            y[i]=atof(&server_command);
}
/* End receiving output parameters to the server*/
}
/* Function: mdlTerminate
=============================================================
* Abstract:
*    No termination needed, but we are required to have this
routine.
*/
static void mdlTerminate(SimStruct *S)
{
   int_T i, n;
             free(input_5);
             for (i=0;i<MAX_NUMBER_OF_INPUTS;i++) {
           free(input_names[i]);
      }
             sprintf(&server_command,"run_stop");
```

```
            n=send( mySocket, &server_command, 9, 0 );
      if (n<0) {
            ssSetErrorStatus(S,"ERROR writing to socket");
      }
            Sleep(0.1);
            closesocket(mySocket);
            UNUSED_ARG(S); /* unused input argument */
            WSACleanup();
}
#ifdef MATLAB_MEX_FILE      /* Is this file being compiled as
a MEX-file? */
#include "simulink.c"       /* MEX-file interface mechanism */
#else
#include "cg_sfun.h"        /* Code generation registration
function */
#endif
```

After the file client_tsim.c has been saved, it is necessary to compile it in MATLAB as follows:

```
>>mex client_tsim.c
```

Finally, the file client_tsim.mexw64 should be created, and the client interface is now ready for co-simulation.

9.1.2 Case Studies

Two case studies for the modelling of a locomotive with a bogie traction control strategy, based on both simplified and complex modelling approaches, are now presented. Both cases are focused on understanding the dynamic behaviour for a typical locomotive (Co-Co) with bogie traction control operated in the traction mode [30]. This discussion will seek to answer a fundamental question. What level of modelling complexity is necessary for the investigation of the operational dynamic behaviours of a heavy haul locomotive?

9.1.2.1 Multibody Model of a Heavy Haul Locomotive in GENSYS

A typical Australian heavy haul locomotive has been chosen for this study. The locomotive has a Co-Co axle arrangement, as shown in Figure 9.7a, and consists of 33 bodies (1 car body, 2 bogie frames, 12 axle boxes, 6 motor housings, 6 rotors and 6 wheelsets). All bodies have been modelled as rigid masses with 6 degrees of freedom. Some constraints are set on these bodies, as listed in Table 9.1.

The connection between the car body and one bogie frame includes:

- Four rubber springs, which are modelled as four coil spring elements acting in longitudinal, lateral and vertical directions;
- Two traction rods, where each rod is modelled as a linear spring element acting in parallel with a linear damper; and

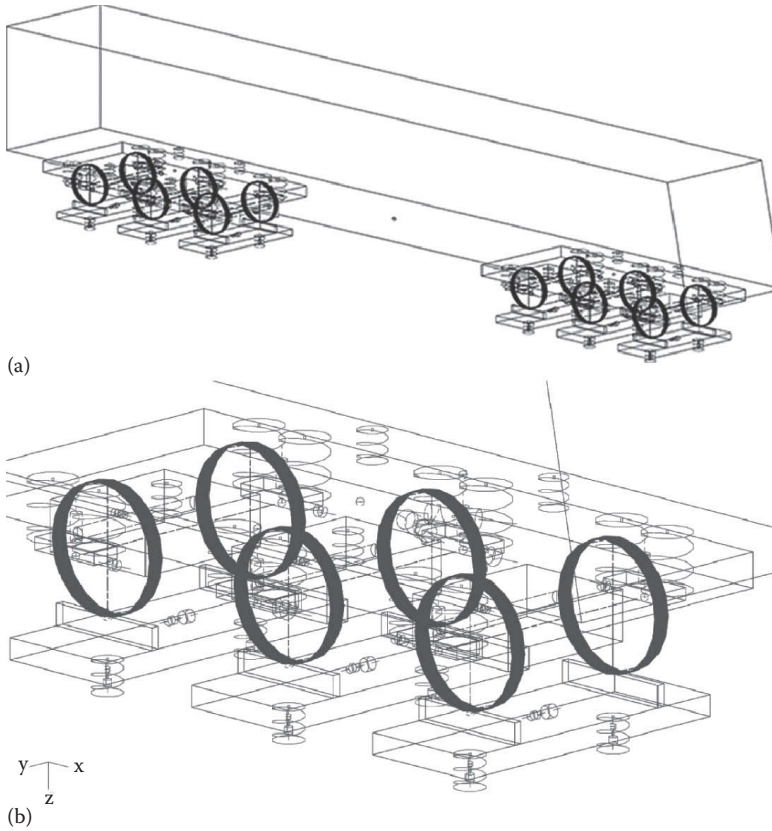

FIGURE 9.7 Locomotive model in GENSYS [30]: (a) whole locomotive and (b) front bogie.

TABLE 9.1
Constraints on Bodies

	x-Longitudinal	y-Lateral	z-Vertical	f-Roll	k-Pitch	p-Yaw
Locomotive car body	√	√	√	√	√	√
Bolster	√	√	√	√	√	√
Sideframe	√	√	√	√	√	√
Axle box	√	√	√	√	√, $v_k = 0$	√
Wheelset	√	√	√	√	√, $k = 0$	√
Motor housing	√	√	√	√	√	√
Rotor	√	√	√	√	√, $k = 0$	√

Note: √ = Degree considered; $k = 0$ and $v_k = 0$ represent that body pitch angle and axle box angle velocity are fixed to be equal to zero.

- One lateral and two vertical bumpstops, which are modelled as nonlinear spring elements acting in the corresponding directions.

The primary suspension between a bogie frame and an axle box is modelled as:

- Two coil spring elements acting in longitudinal, lateral and vertical directions;
- One longitudinal traction rod modelled as a linear spring element;
- One linear vertical damping element on each axle box;
- One vertical bumpstop; and
- One lateral bumpstop with a nonlinear characteristic, with the middle wheelset having a different characteristic in comparison with the leading and trailing wheelsets, in order to model a different clearance between its wheelset and the axle box.

Constraints between the wheelsets and their axle boxes are used in the model.

The traction motor is a nose-suspended motor. The motor has been modelled as two bodies, comprising a motor housing and a rotor as shown in Figure 9.7b, and is based on the approaches described in Ref. [32]. Therefore, those two bodies have been constrained. The motor housing is connected to the wheelset on one end through constraints, and a spring element is used on the other end to connect the housing to the bogie frame.

For the modelling of the gearbox, a special subroutine has been developed based on kinematic relations between torques and angular velocities, taking into account energy conversion efficiency. The assumption that has been made for the model is that the connection between the rotor and the wheelset is perfectly stiff. The processes of interaction between a gear and a pinion have not been considered for this study.

The main parameters of the locomotive represented in the simulation model are presented in Table 9.2.

The wheel and rail profiles used are for standard new S1002 wheels and new UIC60 rail. In wheel-rail contact modelling, the rails are modelled as massless bodies. Three springs normal to the wheel-rail contact surface are used in the contact subroutine. This allows simultaneous modelling of three different contact surfaces in the wheel-rail contact. The normal contact forces are also solved by these three springs. The rails are connected to the track via springs and dampers in the lateral and vertical directions. The calculations of creep forces are made using the modified FASTSIM algorithm, as described in Chapter 7. The model parameters have been assumed for the speed of 22.5 km/h for the three friction conditions as presented in Table 9.3. The effects of speed and creepage on the longitudinal adhesion characteristics for these friction conditions are shown in Figures 9.8 through 9.10.

9.1.2.2 Simulation Scenario

The simulations have been performed for two models that differ only in their power system modelling approaches. For the case of checking of a fast event, the locomotive model was run on a straight track with no track geometry errors at a constant speed of 22.5 km/h (assumed continuous speed).

TABLE 9.2
Parameters for Multibody Model of Heavy Haul Locomotive

Car Body	
Centre of gravity, vertical	1.930 m
Mass	90510 kg
Moment of inertia, roll	132193 kgm^2
Moment of inertia, pitch	3394125 kgm^2
Moment of inertia, yaw	3390553 kgm^2
Bogie Frame	
Centre of gravity, vertical	0.733 m
Mass	4903 kg
Moment of inertia, roll	3629 kgm^2
Moment of inertia, pitch	14453 kgm^2
Moment of inertia, yaw	17659 kgm^2
Wheelset	
Centre of gravity, vertical	0.5016 m
Mass	2036 kg
Moment of inertia, roll	1231 kgm^2
Moment of inertia, pitch	255 kgm^2
Moment of inertia, yaw	1231 kgm^2
Axle Box	
Centre of gravity, vertical	0.5016 m
Mass	239 kg
Moment of inertia, roll	50 kgm^2
Moment of inertia, pitch	50 kgm^2
Moment of inertia, yaw	50 kgm^2
Other Dimensions	
Wheel spacing	1.9 m
Bogie spacing	13.7 m
Gauge	1.435 m
Motor Housing	
Centre of gravity, vertical	0.5086 m
Mass	2390 kg
Moment of inertia, roll	508 kgm^2
Moment of inertia, pitch	480 kgm^2
Moment of inertia, yaw	453 kgm^2
Rotor	
Centre of gravity, vertical	0.5016 m
Mass	710 kg
Moment of inertia, roll	100 kgm^2
Moment of inertia, pitch	16 kgm^2
Moment of inertia, yaw	100 kgm^2
Secondary Suspension	
Vertical stiffness	7870 kNs/m
Longitudinal and lateral stiffness (side springs)	157 kN/m
Traction rod (between car body and bogie frame):	25000 kN/m
Stiffness	100 kNs/m
Damper	
Primary Suspension	
Vertical stiffness (one spring)	379 kN/m
Vertical damper	45 kNs/m
Longitudinal stiffness	200 kN/m
Lateral stiffness	200 kN/m
Traction rod (between axle box and bogie frame)	31000 kN/m

TABLE 9.3
Parameters for Modified FASTSIM Algorithm

	Friction Conditions at Wheel-Rail Interface		
Model Parameters	**Dry**	**Wet**	**Greasy**
V (km/h)	22.5	22.5	22.5
k_0	0.14	0.1	0.08
α_{inf}	0.025	0.02	0.015
β	0.85	0.8	0.65
μ_s	0.44	0.3	0.23
A	0.43	0.39	0.70
B (s/m)	0.72	0.17	0.07

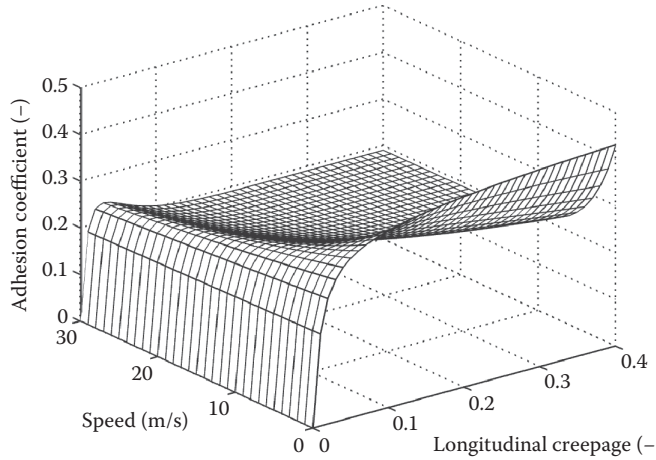

FIGURE 9.8 Calculated dependence of maximum adhesion coefficient on longitudinal creepage and vehicle velocity for the dry friction condition.

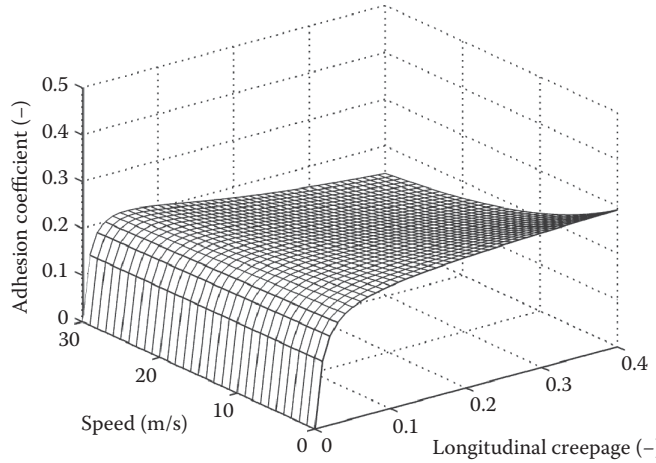

FIGURE 9.9 Calculated dependence of maximum adhesion coefficient on longitudinal creepage and vehicle velocity for the wet friction condition.

The operational scenario for these simulations is based on the following rules and conditions:

- Notch position goes from 'idle' to 8 during the first 2 s, after which it remains at Notch 8.
- Dry friction condition is used for locomotive running, except for switching to 'wet friction condition' from 25 to 30 s, and to 'greasy friction condition' from 40 to 45 s.
- Slip threshold for the traction control system is set to 0.05.

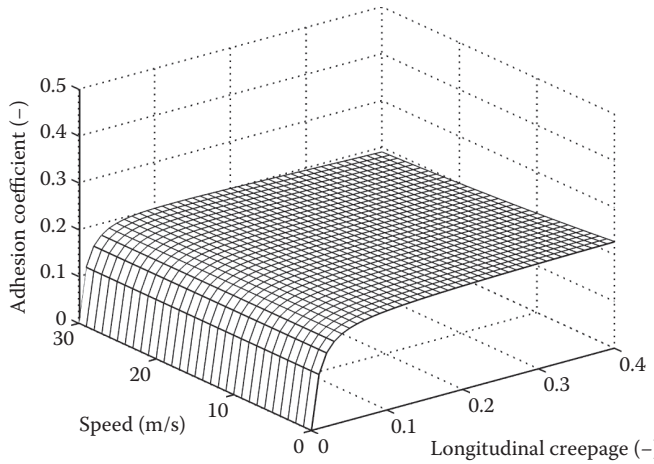

FIGURE 9.10 Calculated dependence of maximum adhesion coefficient on longitudinal creepage and vehicle velocity for the greasy friction condition.

During the simulation, a modified Heun's method with a time step of 1 ms should be used as the GENSYS solver. In Simulink, the discrete (no continuous states) solver with a fixed-step size of 1 ms should be chosen for a simplified modelling and 2 μs for an advanced modelling of traction control systems.

9.1.2.3 Case Study 1: Simplified Approach: Multibody Model and Traction Control System

The integration approach is based on the aggregation of all relevant existing subsystems, which have been described in Chapter 7, for a simplified approach. The full model in Simulink used for this study is shown in Figure 9.11. The inputs and outputs of the co-simulation client interface are exactly the same as shown in Figures 9.3 and 9.4.

9.1.2.4 Case Study 2: Full Locomotive Model

An implemented model for the traction system includes the following elements, as described in Chapter 8:

- A physics-based model for the traction machine (and this is implemented using a coupled inductor model in the case of the induction machine);
- A model for the power electronics-based inverter and its controls;
- A model for the inverter DC bus that includes the DC storage capacitors and dynamic brake resistors; and
- A model for the alternator, its excitation and rectifier subsystems, and the diesel prime mover.

MATLAB SimPowerSystems library was chosen as a basis for the modelling tool. An indirect torque-regulated field-oriented control system was implemented, with a single inverter per bogie supplying its three traction motors, as shown in Figure 9.12.

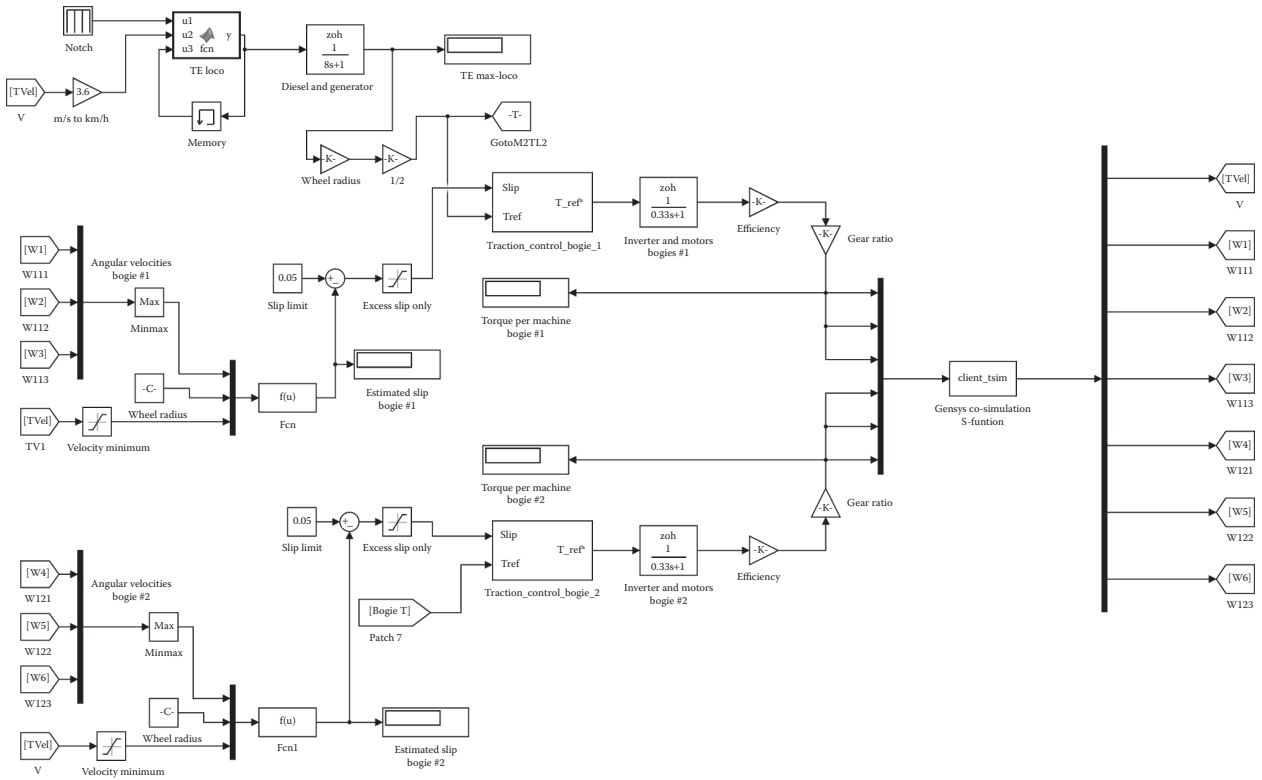

FIGURE 9.11 Simplified locomotive traction system model in Simulink.

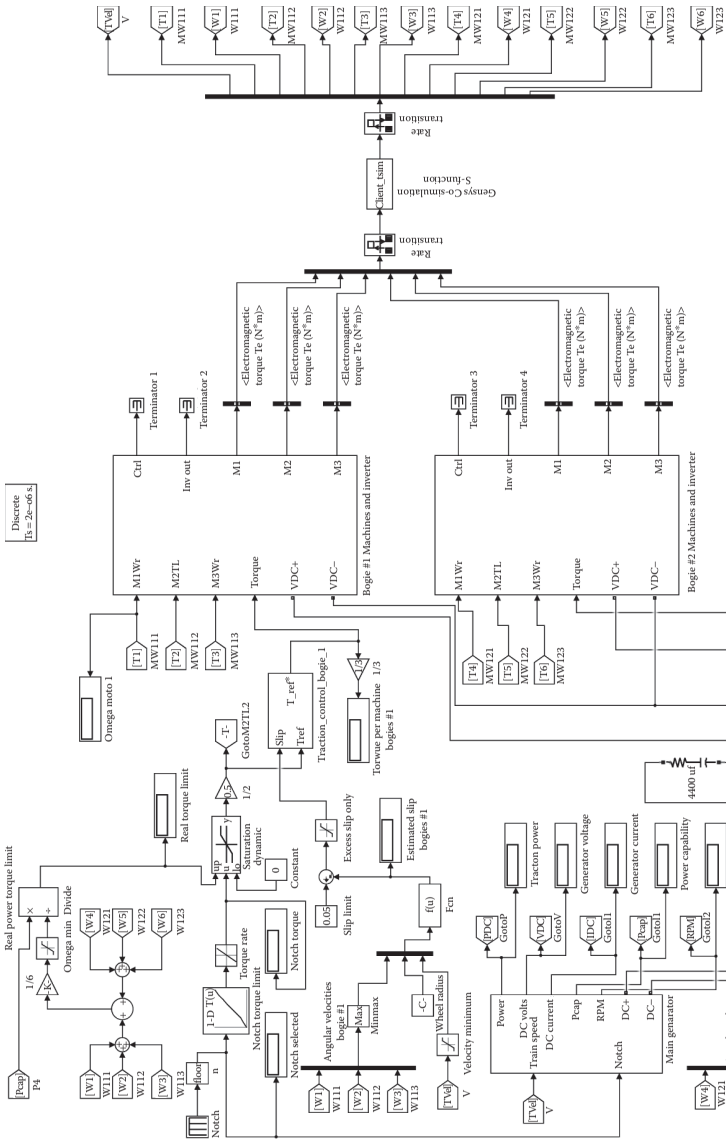

FIGURE 9.12 Full locomotive traction system model in Simulink.

The simulation is performed with a time step of 2 μs for the traction power system. The time for the data transfer rate through the co-simulation interface is set to 1 ms. The inputs of the co-simulation client interface are exactly the same as for the simplified approach, but outputs are extended with additional parameters such as angular speeds of traction motors.

9.1.2.5 Simulation Results

During the simulations, both cases showed locomotive speeds very close to the target speed of 22.5 km/h (6.25 m/s), as shown in Figure 9.13.

Taking into account that the diesel-generator subsystem has also been simplified for the case of the simplified model, it is possible to say that the two locomotive models produce some significant differences in traction effort (TE) characteristics between 0 s and 15 s, as shown in Figure 9.14. Subsequently however, the output TE values are very close to each other, allowing the following statements to be made regarding the comparison results presented in Figures 9.15–9.18. The initial differences are caused by the power limitations imposed by the diesel generator in the advanced model. In the idle position, the diesel engine is operating at 200 rpm. To achieve the full tractive effort, the diesel engine needs to accelerate to its rated speed of 904 rpm. This requires 16 s and is reflective of actual locomotive performance.

The advanced model captures a slip equalisation effect caused by operating the three traction motors from a common inverter for each bogie. This forces the slip on each wheelset of that bogie to be similar. If one wheelset within a bogie develops a higher slip than its peers, the dynamics of the driving induction machine cause the motor torque to rapidly decrease. A positive feature of operation with approximately

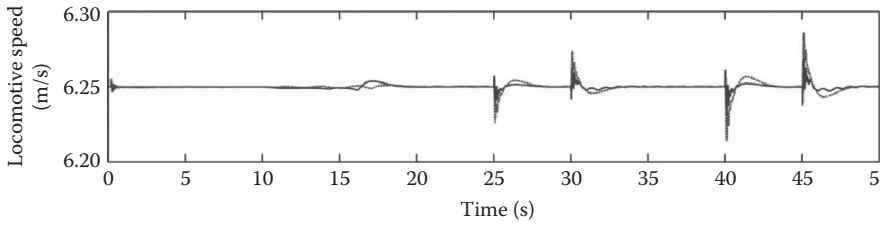

FIGURE 9.13 Locomotive speed in the time domain (solid line—advanced model, dashed line—simplified model).

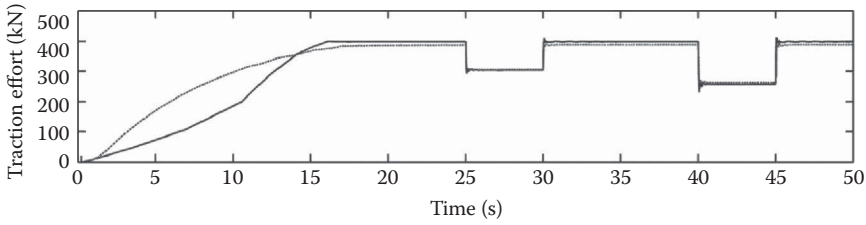

FIGURE 9.14 Locomotive traction effort in the time domain (solid line—advanced model, dashed line—simplified model).

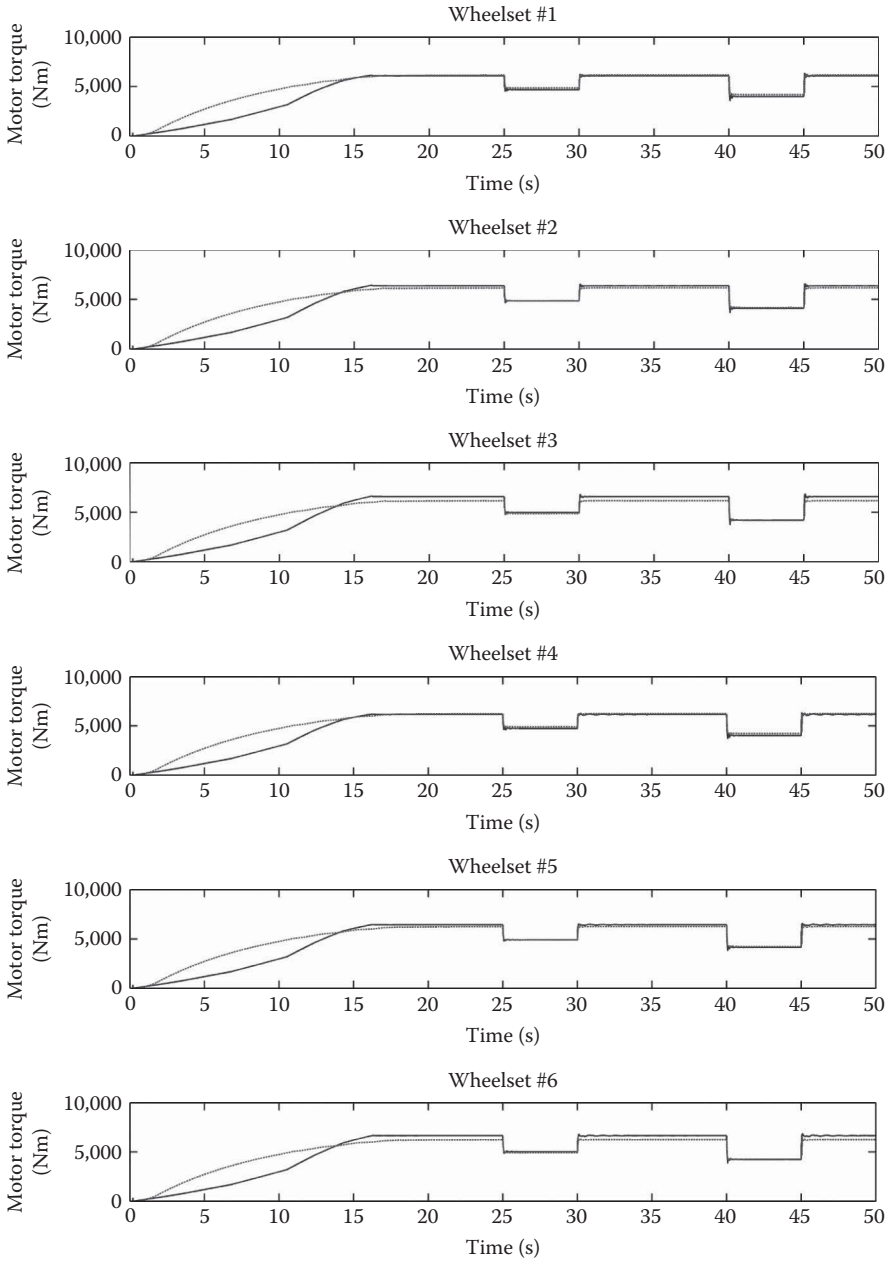

FIGURE 9.15 Comparison of motor torque value in the time domain (solid line—advanced model, dashed line—simplified model).

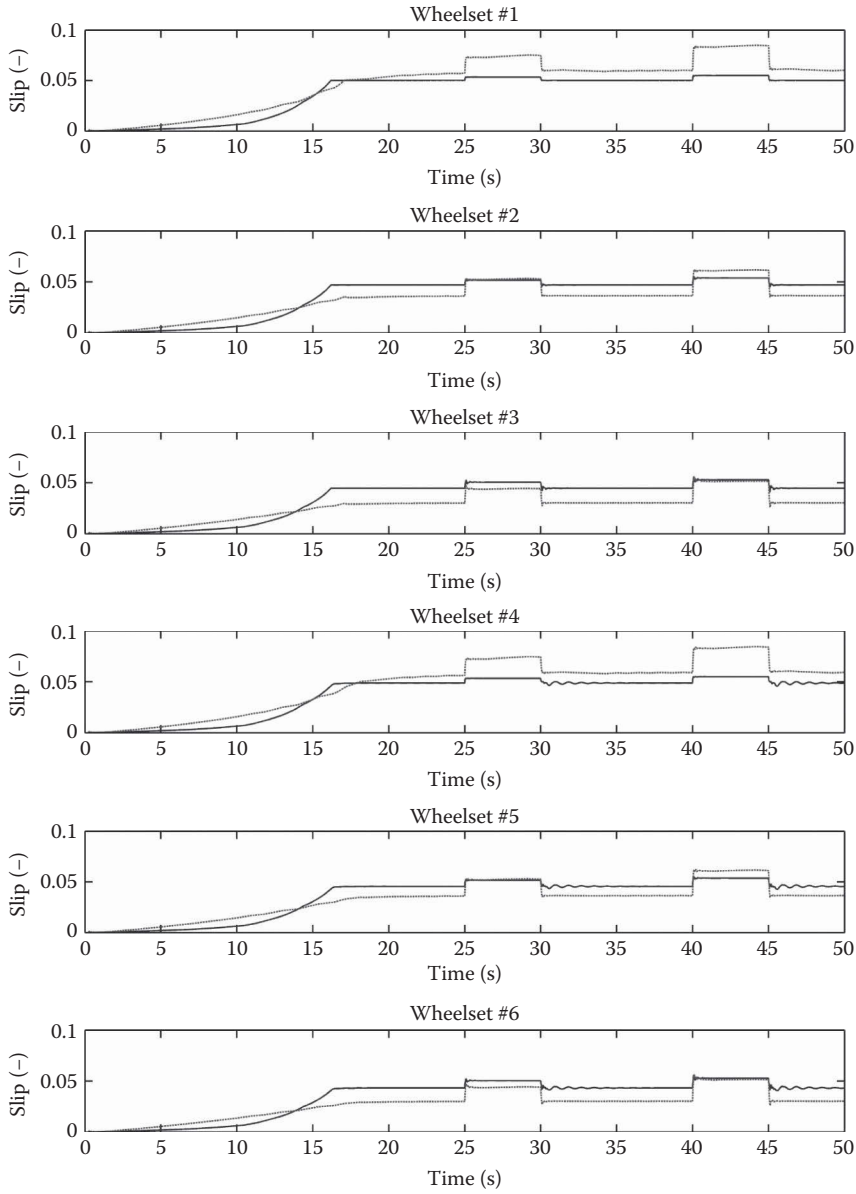

FIGURE 9.16 Comparison of longitudinal slip value in the time-domain (solid line—advanced model, dashed line—simplified model).

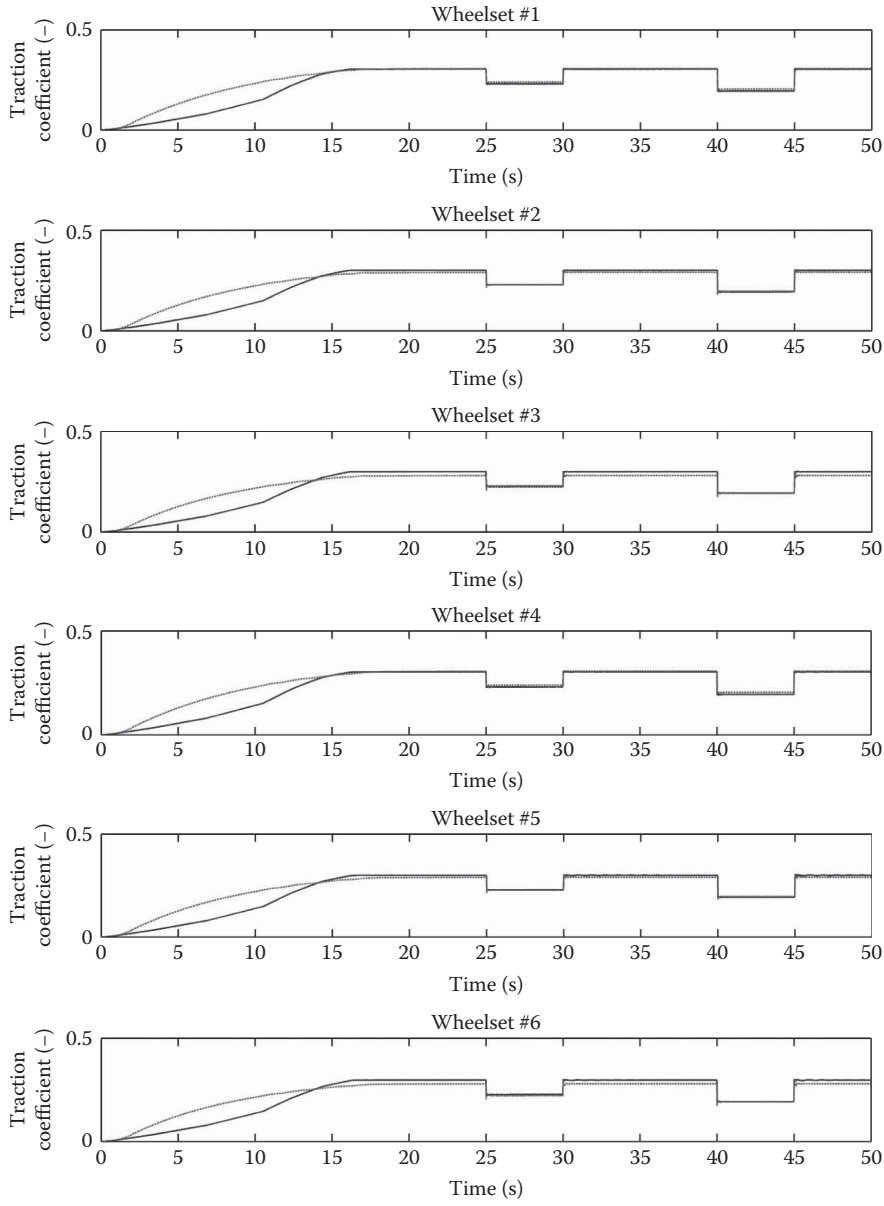

FIGURE 9.17 Comparison of traction coefficient value in the time domain (solid line—advanced model, dashed line—simplified model).

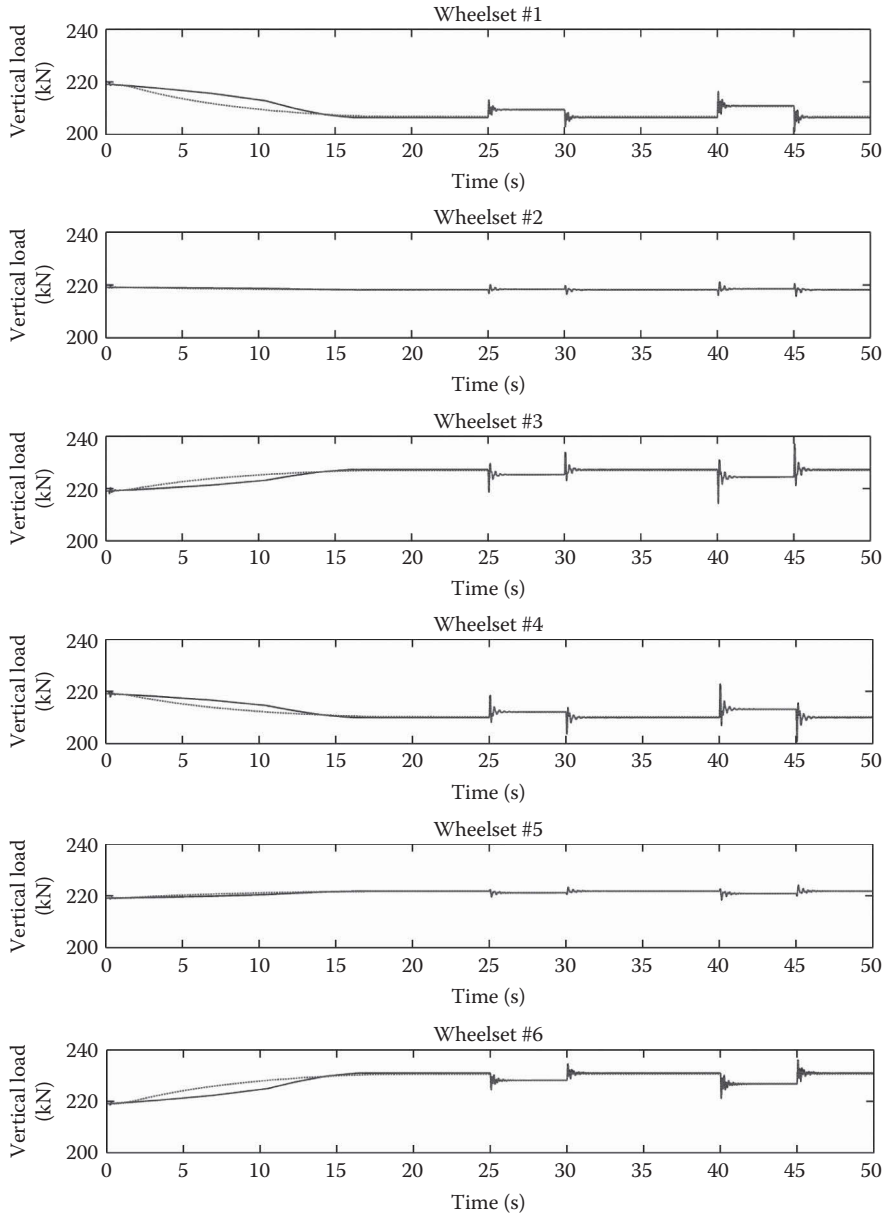

FIGURE 9.18 Comparison of wheelset vertical forces in the time domain (solid line—advanced model, dashed line—simplified model).

equal wheelset slip is that wheelsets with higher vertical reaction forces will develop higher tractive efforts.

The simplified model results in slight differences in the distribution of motor traction torques between wheelsets, as shown in Figure 9.15. This leads to variations in slip values and traction coefficients between wheelsets, as shown in Figures 9.16 and 9.17. These variations are caused by the absence in the simplified model of any induction machine dynamics that may force the equalisation of wheelset slip. The conclusion is that advanced models should be applied for the study of traction slip control systems. The advanced model shows much more stable slip results during switching of friction conditions (Figure 9.16) and much better realisation of traction by each wheelset (Figure 9.17).

The wheelset load distribution, as shown in Figure 9.18, has some high spike values during transients for the advanced model. This leads to the conclusion that the dynamics behaviour of locomotives with an advanced modelling approach for the power subsystems can produce higher contact forces in transients. The outcome is that a simplified model can still be used at the initial stages for the development of slip control algorithms, but an investigation of processes at the wheel-rail interface under traction, as well as vibration dynamics of traction motor suspension, may require the use of an advanced modelling approach. Verification of simplified models for traction control system designs using advanced models is also recommended, because the values of time constants used in low-pass filter equations for power system components must be tuned in order to get results that are most accurate for any given scenario (refer also to Section 6.3).

9.2 LONGITUDINAL TRAIN DYNAMICS IN HEAVY HAUL LOCOMOTIVE DYNAMICS BEHAVIOUR STUDIES

We will now evaluate the effect of lateral coupler forces on locomotives under continuous traction, taking into account their positions in the train configuration. We assume that the multibody locomotive model already exists, and in this case, a simulation methodology consists of only two stages, a flowchart of which is shown in Figure 9.19. A similar methodology has been used in previous studies [33,34].

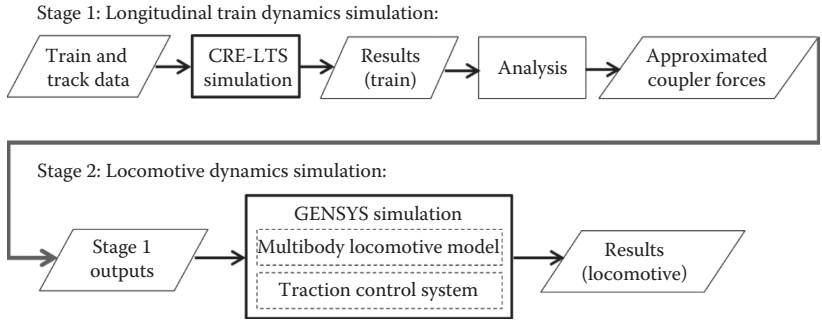

FIGURE 9.19 Simulation methodology stages.

The longitudinal train dynamics modelling approach described in Chapter 5 will be used here to perform longitudinal train dynamics simulations. The objective is to obtain lateral coupler forces for selected locomotives in the train consist that is traversing a given track geometry. However, in order to simplify the following multibody locomotive simulations, approximate expressions for the lateral coupler forces are determined from the longitudinal train simulation data.

Using the locomotive multibody model described in Section 7.7.1, further code is added to allow the simulation of lateral coupler forces by using the approximate expressions developed in Stage 1. The lateral coupler forces, which depend on the locomotive's position in the train, are applied at each locomotive's coupling centres at a nominal coupler height above rail level, and these forces do change continuously with respect to track geometry. All results of the simulations can be stored for further post-processing.

9.2.1 Simulation Scenario Task

The following task commonly arises when it is necessary to investigate a locomotive's dynamic performance in the curve. In this example, we need to compare lateral contact forces between wheels and rails for the leading wheelsets (axles) of the first and third locomotives in the hypothetical train configuration. The hypothetical train configuration is chosen as follows:

- Three locomotives are arranged at the front of the train.
- Fifty five wagons are hauled by these locomotives.

The train runs on a standard (1435 mm) gauge track. The simulation is focused on the study of locomotive behaviour for curves of radius 240 m, with transitions of 55 m on a hypothetical section of track of a total length of 4.5 km, as shown in Figure 9.20. Six reverse curves of decreasing radius are evenly distributed on the constant gradient section, each curve radius being presented in both right- and left-hand geometries with the curve radii of 600, 400, 300, 260, 240 and 220 m, respectively, as shown in Figure 9.20. The train runs on the track that has US Federal Railroad Administration Class 5 track irregularities [35] superimposed over the designed track geometry to model typical track roughness. How do we find a solution? A step-by-step solution is presented.

9.2.2 Longitudinal Train Dynamics Simulation

As defined in the simulation scenario, a hypothetical train set consists of 3 locomotives arranged at the front and hauling 55 identical wagons. Their masses are listed in Table 9.4. While travelling over the curved track sections, the train speed is close to 20 km/h, the maximum speed at which typical Australian AC locomotives develop their maximum continuous tractive effort [36,37]. A standard coupler that is common in Australian mineral trains has been placed between each pair of wagons along the train length [38].

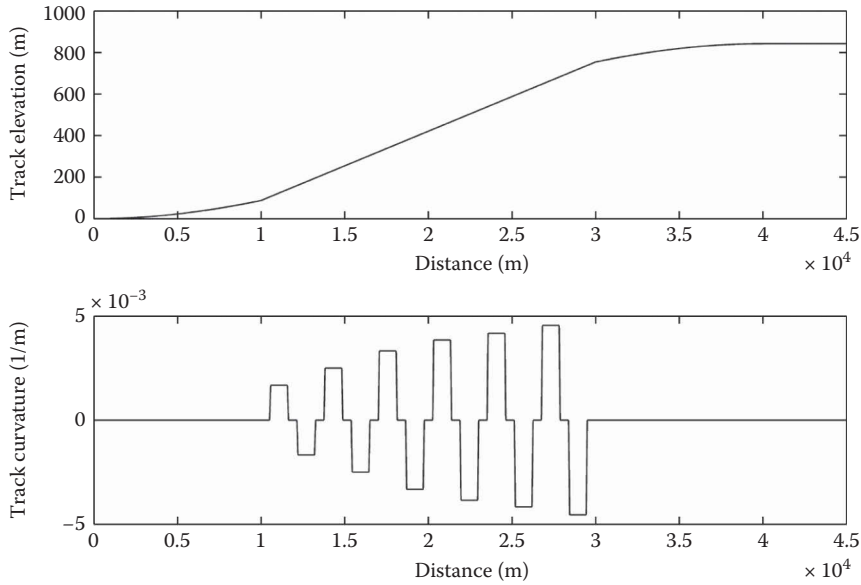

FIGURE 9.20 Hypothetical track geometry profile.

TABLE 9.4
Train Masses (55 Wagons)

Locomotive Type	Number of Locomotives	Locomotive Mass	Wagon Type	Loaded Wagon Mass	Loaded Train Mass
Freight locomotive (Co-Co) with AC traction motors; tractive effort—continuous 420 kN at 20 km/h	3	134 tonnes	Typical 4-axle mineral wagon	80 tonnes	4802 tonnes

The calculation results for lateral coupler forces for the first and third locomotives, obtained from simulation in the longitudinal train dynamics package, are shown in Figure 9.21.

By analysing the lateral coupler force results for the curve of 240 m radius, as shown in Figure 9.22, it can be seen that the lateral coupler force magnitudes for the first locomotives are 0 kN at the front coupler and 24 kN at the rear coupler. In the case of the third locomotive, we have lateral coupler force magnitudes of 48 kN at the front coupler and 124 kN at the rear coupler. This is expected because in-train forces increase along the length of a train when only head-end traction power is in use. These results are used for further locomotive dynamics simulations in the GENSYS multibody software package.

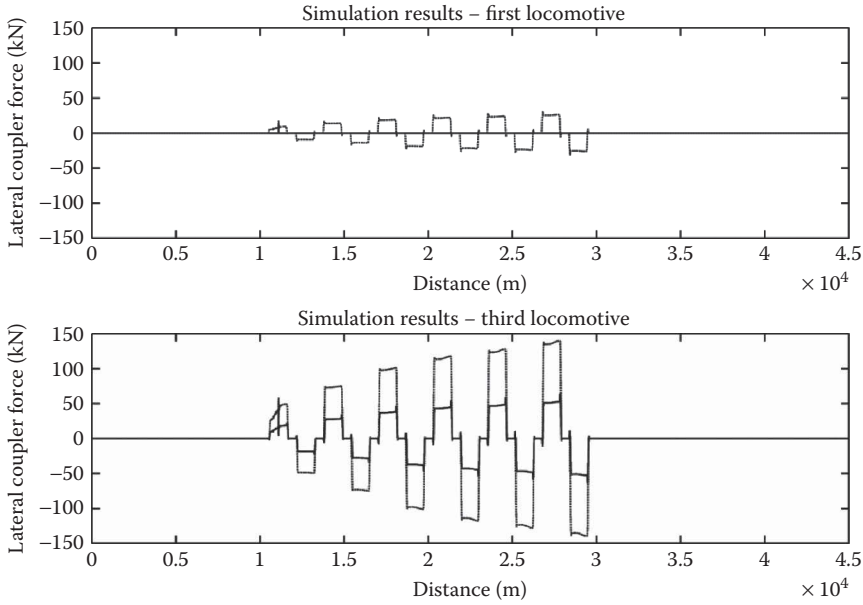

FIGURE 9.21 Lateral coupler forces for first and third locomotives running on the hypothetical track design (solid line—front coupler, dashed line—rear coupler).

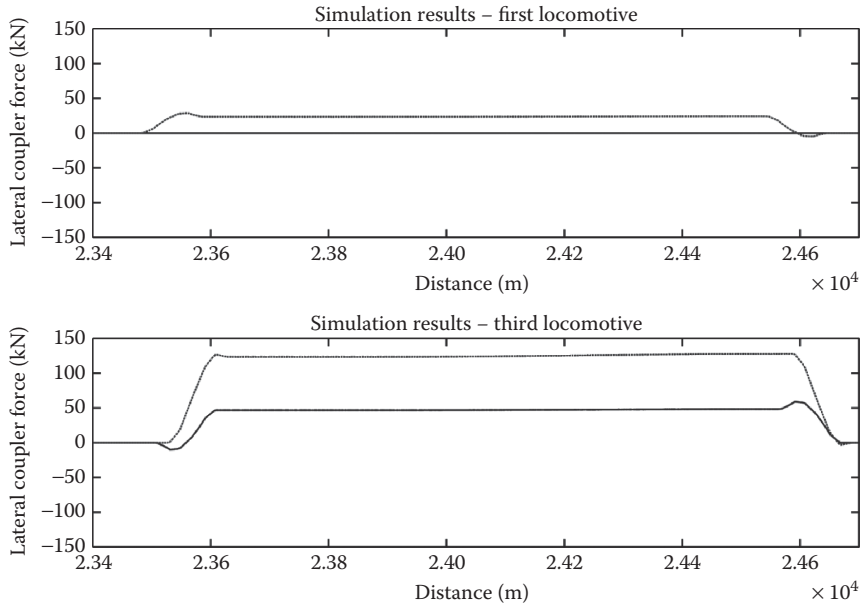

FIGURE 9.22 Zoomed in results of lateral coupler forces for first and third locomotives running on the 240 m radius curve (solid line—front coupler, dashed line—rear coupler).

9.2.3 Locomotive Dynamics Simulation

The locomotive models were run on a standard gauge (1435 mm) track and have a Co-Co wheel arrangement with rigid bogies, as described in Section 7.7.1. For traction control purposes, a simplified traction system has been developed for the locomotive model based on the bogie traction control strategy of one inverter per bogie, implemented as a subroutine in GENSYS, hence no co-simulation is needed in this case. The modified FASTSIM parameters for this study have been taken for dry friction conditions, as presented in Table 9.3 and shown in Figure 9.8. The value of maximum friction coefficient at gauge corner and gauge face contact points needs to be reduced to 0.2 in order to make it close to a real operational scenario.

Two simulation cases (one for each locomotive) with the same wheel and rail profiles have been performed in this study. To do this, the locomotive models were run on a 240 m radius right-hand curved track with the geometry as described in Table 9.5. The applicable track cant of 65 mm for this curve is used in both study cases. As specified previously, the test track has US Federal Railroad Administration Class 5 irregularities, as shown in Figure 9.23. Locomotives run with a constant speed of 20 km/h under the maximum TE possible for such a locomotive. The following assumptions are made:

- The throttle notch is set in the highest position in order to realise the maximum achievable traction for the required speed; that is, the TE is only limited by speed in this case.
- The slip threshold for the traction control system is set to 0.08.

For both locomotives, lateral coupler forces, except the force on the first locomotive's front coupler (which is zero), are directed towards the inside of the curve as determined by means of the longitudinal train dynamics simulation detailed in the previous section.

The models were run with a solver based on the two-step Runge-Kutta method, which makes back steps if the tolerance is not met, with a calculation time step of 0.001 s inside the GENSYS model, and the data were stored with a time step of 0.02 s. The simulation time was set to 65 s for both models.

The approximate lateral coupler force magnitudes applied to the model, based on the results from the longitudinal train simulation test, are shown in Figure 9.24.

TABLE 9.5
Track Geometry for Locomotive Dynamics Simulation

Distance from Start (m)	Track Section
0–45	45 m tangent track
45–100	55 m entry transition
100–300	200 m right curve
300–355	55 m exit transition
355–400	45 m tangent track

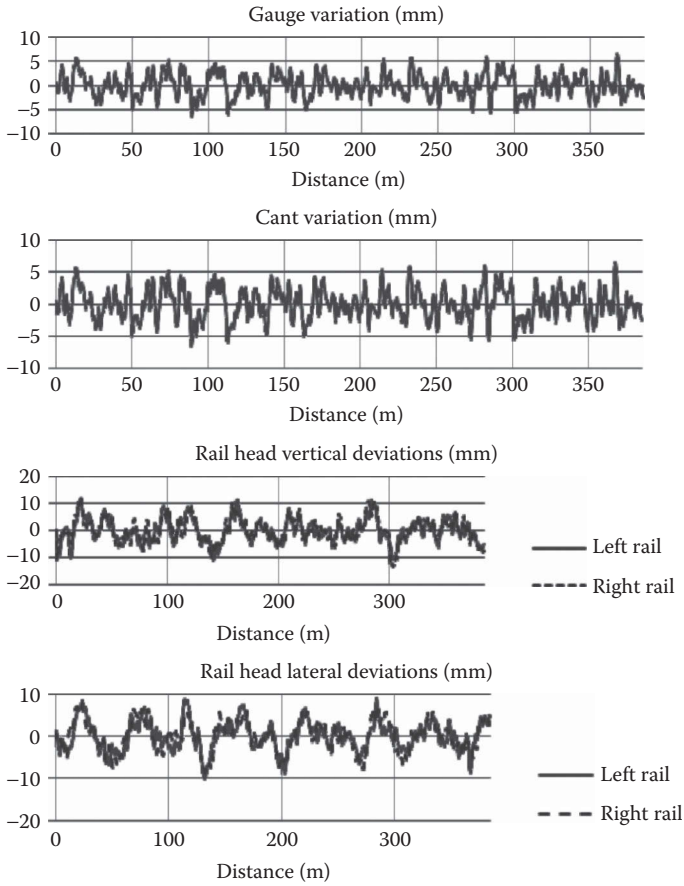

FIGURE 9.23 US Federal Railroad Administration Class 5 track geometry irregularities.

During the simulation process, the wheels and rails establish only two-point contact (wheel tread and wheel flange contacts with the rail head and gauge corner/face, respectively) in both simulation cases, as shown in Figure 9.25. For the first and third locomotives, there is not much difference between the lateral contact patch forces for the wheel tread and/or rail head, as seen in the results shown in Figure 9.25. Most importantly, it can be seen that, for the third locomotive, these lateral 'flanging' forces are reduced. Because the third locomotive is subjected to greater lateral coupler forces within the curve than the first locomotive, the former gets pulled further towards the low (inside of the curve) rail.

This example shows that it is very important to analyse locomotive dynamics accurately to account for the significant variations in coupler forces when transiting a curve. However, this approach does not fully depict the real situation, and further improvement in result accuracy in vehicle dynamics studies can be achieved by means of the application of a co-simulation approach, which allows connecting a longitudinal train dynamics simulator with a multibody dynamics software package.

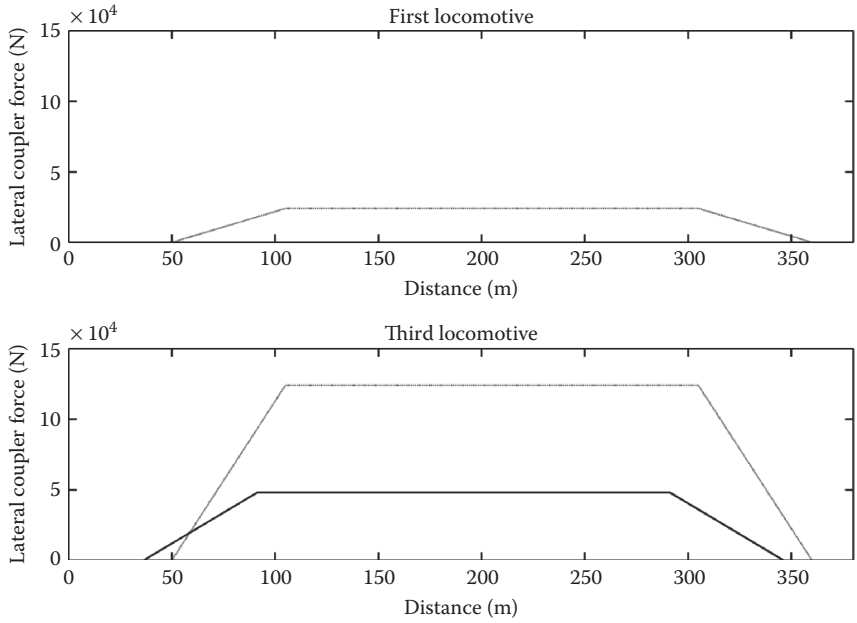

FIGURE 9.24 Approximate lateral coupler forces in the time domain (solid line—front coupler, dashed line—end coupler).

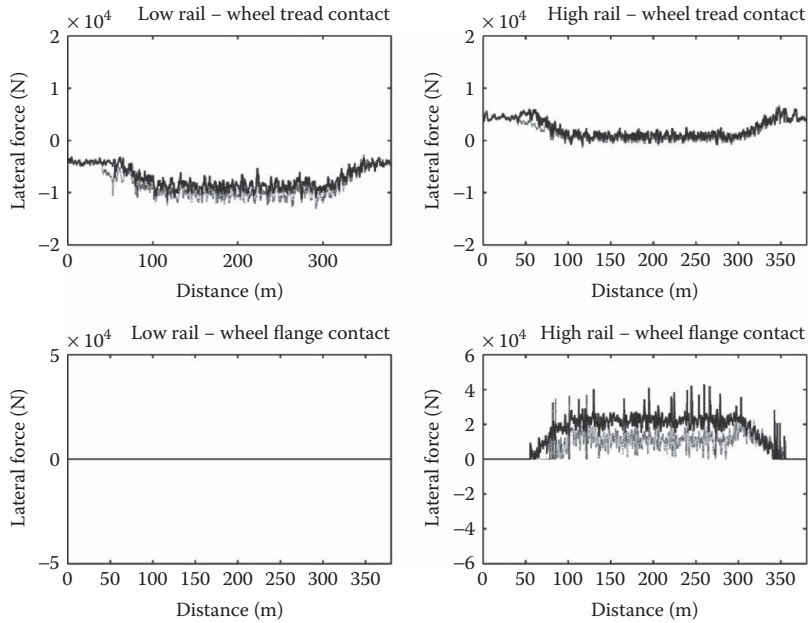

FIGURE 9.25 Lateral contact forces for the leading wheelsets (solid line—first locomotive, dashed line—third locomotive).

REFERENCES

1. S. Iwnicki (ed.), *Handbook of Railway Vehicle Dynamics*, CRC Press, Boca Raton, FL, 2006.
2. M. Spiryagin, C. Cole, Y.Q. Sun, M. McClanachan, V. Spiryagin, T. McSweeney, *Design and Simulation of Rail Vehicles, Ground Vehicle Engineering Series*, CRC Press, Boca Raton, FL. 2014.
3. M. Arnold, A. Carrarini, A. Heckman, G. Hippmann, Simulation techniques for multidisciplinary problems in vehicle system dynamics. In *Computational Mechanics in Vehicle System Dynamics, Supplement to Vehicle System Dynamics*, M. Valášek (ed.), Taylor & Francis Group, London, UK, 2004, vol. 40, pp. 17–36.
4. R.M. Goodall, W. Kortum, Mechatronic developments for railway vehicles of the future, *Control Engineering Practice*, 10(8), 2002, 887–898.
5. M. Spiryagin, P. Wolfs, C. Cole, Modelling of traction in railway vehicles (Editorial), *Vehicle System Dynamics*, 53(5), 2014, 603–604.
6. J.J. Kalker, A fast algorithm for the simplified theory of rolling contact, *Vehicle System Dynamics*, 11, 1982, 1–13.
7. O. Polach, Creep forces in simulations of traction vehicles running on adhesion limit, *Wear*, 258(7–8), 2005, 992–1000.
8. O. Polach, Influence of locomotive tractive effort on the forces between wheel and rail, *Vehicle System Dynamics*, 35(S), 2001, 7–22.
9. M. Spiryagin, K.S. Lee, H.H. Yoo, O. Kashura, O. Kostjukevich, Modeling of adhesion for railway vehicles, *Journal of Adhesion Science Technology*, 22, 2008, 1017–1034.
10. M. Spiryagin, O. Polach, C. Cole, Creep force modelling for rail traction vehicles based on the Fastsim algorithm, *Vehicle System Dynamics*, 51(11), 2013, 1765–1783.
11. E.A.H. Vollebregt, Numerical modeling of measured railway creep versus creep-force curves with CONTACT, *Wear*, 314(1–2), 2014, 87–95.
12. C. Weidemann, State-of-the-art railway vehicle design with multibody simulation, *Journal of Mechanical Systems for Transportation and Logistics*, 3(1), 2010, 12–26.
13. A. Steimel, *Electric Traction — Motive Power and Energy Supply: Basics and Practical Experience*, Oldenbourg Industrieverlag, Essen, 2008.
14. R. Mathew, F. Flinders, W. Oghanna, Locomotive 'total systems' simulation using SIMULINK. In *Proceedings of International Conference on Electric Railways in a United Europe*, Amsterdam, The Netherlands, 27–30 March 1995, pp. 202–206. Institution of Electrical Engineers, UK.
15. M. Ahmadian, On the virtues of steerable locomotive bogies. In *Proceedings of the ASME Rail Transportation Division*, *1997 ASME International Congress and Exposition*, Dallas, TX, 16–21 November 1997.
16. S. Simson, C. Cole, Simulation of curving at low speed under high traction for passive steering hauling locomotives, *Vehicle System Dynamics*, 46(12), 2008, 1107–1121.
17. M. Spiryagin, A. George, Y.Q. Sun, C. Cole, T. McSweeney, S. Simson, Investigation on the locomotive multibody modelling issues and results assessment based on the locomotive model acceptance procedure, *Rail and Rapid Transit*, 227(5), 2013, 453–468.
18. H.P. Kotz, A toolkit for simulating mechatronics in railway vehicles, Simpack User Meeting, Freiburg, Germany, 8–9 April 2003. See: http://www.simpack.com/fileadmin/simpack/doc/usermeeting03/um03-siemens_kotz.pdf.
19. M. Spiryagin, S. Simson, C. Cole, I. Persson, Co-simulation of a mechatronic system using Gensys and Simulink, *Vehicle System Dynamics*, 50(3), 2012, 495–507.
20. O. Polach, A. Böttcher, D. Vannucci, J. Sima, H. Schelle, H. Chollet, G. Götz, M.G. Prada, D. Nicklisch, L. Mazzola, M. Berg, M. Osman, Validation of simulation models in the context of railway vehicle acceptance, *Rail and Rapid Transit*, 229(6), 2015, 729–754.

21. Vampire User Guide – Part S, Simulink Interface, Version 4.32, AEA Technology, Derby, UK, 2004, pp. 453–499.
22. Universal Mechanism, User's manual – UM co-simulation tool – Version 6.0, Bryansk State Technical University, Russia, 2010.
23. Universal Mechanism, Interface with MATLAB/Simulink – Version 6.0, Bryansk State Technical University, Russia, 2010.
24. R.V. Kovalev, G.A. Fedyaeva, V.N. Fedyaev, Modelling of an electro-mechanical system of locomotives, Sbornik Trudov of DIIT, no. 14, 2007, pp. 123–127 (in Russian). See: http://www.universalmechanism.com/index/download/elmechloco.pdf.
25. V.N. Fedyaev, Influence of electrical and mechanical subsystems of a shunting locomotive on the realization limit tractive efforts. PhD Thesis, Bryansk State Technical University, Bryansk, Russia, 2006 (in Russian).
26. G.A. Fedyaeva, Forecasting of dynamic process under transient and emergency mode for traction drives with asynchronous motors. DSc Thesis, Moscow State Railway University, Moscow, Russia, 2008 (in Russian).
27. M. Spiryagin, Y.Q. Sun, C. Cole, T. McSweeney, S. Simson, I. Persson, Development of a real-time bogie test rig model based on railway specialised multibody software, *Vehicle System Dynamics*, 51(2), 2013, 236–250.
28. M. Spiryagin, K.S. Lee, H.H. Yoo, Control system for maximum use of adhesive forces of a railway vehicle in a tractive mode, *Mechanical Systems and Signal Processing*, 22(3), 2008, 709–720.
29. M. Spiryagin, Y.Q. Sun, C. Cole, S. Simson, I. Persson, Development of traction control for hauling locomotives, *Journal of System Design and Dynamics*, 5(6), 2011, 1214–1225.
30. M. Spiryagin, P. Wolfs, F. Szanto, C. Cole, Simplified and advanced modelling of traction control systems of heavy-haul locomotives, *Vehicle System Dynamics*, 53(5), 2014, 672–691.
31. Y. Yao, H.J. Zhang, Y.M. Li, S.H. Luo, The dynamic study of locomotives under saturated adhesion, *Vehicle System Dynamics*, 49(8), 2011, 1321–1338.
32. E. Pfleger, Parameter-excited vibrations in rail vehicle drives. In *Simpack User-Meeting 2007*, Bonn, Germany, 20–22 November 2007.
33. M. Spiryagin, A. George, Y. Sun, C. Cole, S. Simson, I. Persson, Influence of lateral components of coupler forces on the wheel-rail contact forces for hauling locomotives under traction. In *Proceedings of the 13th Mini Conference on Vehicle System Dynamics, Identification and Anomalies*, Budapest, Hungary, 5–7 November 2012.
34. A.L. George, Theoretical and numerical investigation on traction forces for high adhesion locomotives. MEng Thesis, Centre for Railway Engineering, Central Queensland University, Rockhampton, Australia, 2015.
35. Federal Railroad Administration, Track safety standards – Classes 1 through 5, Chapter 1. In *Track and Rail and Infrastructure Integrity Compliance Manual*. Federal Railroad Administration, Washington, DC, January 2014.
36. C. Matthews, Development of the Cv43ACi locomotive. In *Proceedings of Conference on Railway Engineering*, Perth, Australia, 7–10 September 2008, pp. 489–494. Railway Technical Society of Australasia, Australia.
37. N. Ramsey, F. Szanto, P. Hewison, Introducing the next generation locomotive to the Australian rail network. In *Proceedings of Conference on Railway Engineering*, Perth, Australia, 7–10 September 2008, pp. 471–480. Railway Technical Society of Australasia, Australia.
38. C. Cole, M. McClanachan, M. Spiryagin, Y.Q. Sun, Wagon instability in long trains, *Vehicle System Dynamics*, 50(S1), 2012, 303–317.

10 Conclusion

Our intent in writing this book was to make available the knowledge of the highly complex technical subject of locomotive design and performance in heavy haul railways gained throughout our diverse and lengthy careers in the field of railway research and rail industry involvement. We have detailed the main components and the mechanical and electrical systems for both electric and diesel-electric locomotives. General and advanced modelling techniques for individual locomotive dynamics, longitudinal train dynamics, traction control and power systems have been discussed. The text has been structured in such a way that basic issues and terminology are covered before discussing detailed explanations, theories and analysis techniques. Worked examples provide a virtual hands-on approach for those interested in actually carrying out simulations. We hope that readers find the information flow easy to follow and understand. Many references have been provided which will allow readers to further explore the international knowledge base that has developed from experience in operating various types of heavy haul railways and from research to solve problems and improve train safety and performance.

Readers with enquiries regarding the design and simulation of heavy haul locomotives and trains can contact the Centre for Railway Engineering at Central Queensland University, Australia, by email at cre@cqu.edu.au or they can visit the following website to find individual contact details: www.cqu.edu.au/cre.

Glossary

adhesion coefficient: percentage or ratio of the total weight on the driving wheels of a locomotive that is available for traction or braking. The adhesion coefficient is dependent on construction and operational characteristics of rail tracks and railway vehicles, for example, difference between wheel diameters of wheel pairs, conicity and eccentricity of wheels, track curvature, reallocation of loads between wheels, irregular loads of wheels for a wheel pair or a bogie, vibrations and unaccounted for slipping motion. It can vary from as low as 10% (0.1) on wet rail to as high as 40% (0.4) on dry sanded rail.

automatic brake: see **train brake**.

axle: the part of a wheelset on which the two wheels are mounted. Wheels are usually press fitted onto shoulders/seats machined near the ends of the axle.

balance speed: see **equilibrium speed**.

ballast: crushed rock that provides support to the sleepers (ties), transfers the wheel loads to the subgrade and provides longitudinal and lateral support as well as drainage for the track structure.

bogie: an assembly comprising wheels, axles, bearings, sideframes, bolster, brake rigging, springs and connecting components used to support rail vehicles (usually at or near their ends) and capable of rotation in the horizontal plane to provide guidance along the track. A bogie may hold one, two or more wheelsets, and it may also provide support to adjacent ends of an articulated vehicle. A bogie is also referred to as a **truck**.

bogie bolster: the main transverse member of a bogie that transmits rail vehicle body loads to the sideframes through the suspension system/s. The ends of the bolster fit loosely into the sideframes and are retained by the gibs that contact the sideframe column guides. Bogie bolster contact with the vehicle body is through the bogie centre plate, which mates with the body centre plate, and through the side bearings when the vehicle is tilted as in a curve.

bogie centre plate: the circular area centrally placed in the top surface of a bogie bolster that provides the principal bearing support to the vehicle body on the bolster via the vehicle body centre plate. Bogie centre plates are often fitted with a horizontal wear plate and a vertical wear ring to improve wearing characteristics and extend bogie bolster life.

bogie hunting: lateral instability of a bogie (truck), generally occurring at high speed and characterised by wheelsets shifting from side to side with the flanges striking the rail. The resulting motion of the wagon (car) causes excessive wear in wagon and bogie components and creates potentially unsafe operating conditions. For freight vehicles, hunting occurs primarily with empty or lightly loaded wagons having worn wheelsets.

bogies, radial: rail vehicle bogies whose interconnected wheelsets have low yaw constraint links with the bogie frame so as to allow each of the wheelsets to individually align themselves to the radius of a track curve.

broad gauge: railways with running rails spaced at more than 1435 mm (4 ft 8½ in.) standard track gauge.
buff forces: a term used to describe compressive coupler forces in a train caused by run-in of slack from the rear end. The term 'buff' means the opposite of the term 'draft'.
cant (of rail): rail cant involves tilting the tops of running rails in towards each other to assist with rail vehicles self-centring as they move along the track. Rail cant is usually expressed as a rate of inclination (commonly 1 in 20 or 1 in 40).
cant (of track): the cross level of track on a curve used to compensate for lateral forces generated by the train as it passes through the curve. Cant is specified by the vertical difference in height of the outside (high) rail and the inside (low) rail measured at right angles to the centreline of the track. Track cant on a curve is also referred to as **superelevation**. On straight sections of track, the cross level should be zero except near the start and end of non-transitioned curves.
centre beam/sill: the central longitudinal member of a rail vehicle underframe structure that transmits draft and buff shocks from one end of the vehicle to the other.
contact patch: the area of contact between a wheel tread and the railhead.
continuous welded rail (CWR): rail lengths welded into strings providing a track without rail joints.
corrugation (of rails): flaws consisting of wave-like undulations along the top running surface of the head of the rail. Short-wave corrugation, also known as 'roaring rail', has wavelengths of 25–75 mm and is most common on light axle load and high speed operations. Intermediate wave corrugation with wavelengths of 75–600 mm is most common on heavy freight operations. Long-wave corrugation has wavelengths greater than 600 mm and is most common on very high speed operations.
coupler: the device at both ends of a rail vehicle to allow vehicles to be connected together in a train. Modern designs allow vehicles to be attached to each other simply by pushing them together; these are referred to as automatic couplers.
crossing number: the rate at which two tracks separate at a turnout is usually designated by the number of units of centreline length travelled to achieve a divergence of one unit. This is effectively half the cotangent of half the splay angle of the crossing vee and is expressed by way of example as a No. 10 or 1 in 10, also referred to as the **frog number**. The bigger this number, the faster a train can travel through a turnout.
crosstie: see **sleeper**.
cut spike: see **dogspike**.
detail fracture: a rail defect consisting of a progressive fracture of the railhead originating from surface imperfections including shells, head checks and flaking.
dogspike: a steel nail-like device having a square shank and a chisel or pointed end to allow driving of the spike into timber sleepers (ties) to hold the rails in place. The head of the spike hooks over the rail base to restrain the rail. A dogspike is also referred to as a **cut spike**.
draft forces: a term used to describe forces resulting in tension in the couplers of a train. The term 'draft' means the opposite of the term 'buff'.
draft gear: the term is used to describe the energy-absorbing component of the draft system. The draft gear is installed in a yoke that is connected to the coupler shank and is fitted with follower blocks that contact the draft lugs on the rail vehicle

centre sill. The so-called standard draft gear use rubber and/or friction components to provide energy absorption, while 'hydraulic' draft gear use a closed hydraulic system with small ports and a piston to achieve a greater energy-absorbing capability. Hydraulic draft gear assemblies are generally referred to as 'cushioning units'.
draft system: the term is used to describe the arrangement on a rail vehicle for transmitting coupler forces to the centre sill. On a standard draft gear, the draft system includes the coupler, yoke, draft gear, follower, draft key, draft lugs and draft sill. On a vehicle with cushioning units, either hydraulic cushion units replace the draft gear and yoke at each end of the vehicle, or a hydraulically controlled sliding centre sill is an integral part of the vehicle underframe.
drawbar force: the force exerted through the couplers by the locomotive/s on coupled wagons (cars), and by one wagon upon another along the train. This force is usually greatest at the coupler between a locomotive and the first wagon behind it.
equilibrium speed: the speed of a train on a curve at which the wheel loads are evenly divided between the high and low rails. It is dependent on the amount of cant installed on the curve, and is also referred to as **balance speed**.
flange (of wheel): the portion of a wheel rim that protrudes down beside the rail gauge face to guide rolling stock along the track.
flange (of rail): one side of the base/foot of a rail.
flat wheels: rollings stock wheels with flat spots resulting from sliding along the rail, generally found on all wheels on a wheelset or bogie due to severe braking or failure to release handbrakes.
frame: rail vehicle structural unit that either directly supports the body structure or is integrated into a monocoque design as part of a body shell.
friction coefficient: a dimensionless scalar value, often symbolised by the Greek letter μ, that describes the ratio of the force of frictional resistance between two bodies and the force pressing them together. It is a system property that depends upon the materials involved, relative velocity of the bodies and interface issues, including geometric properties, temperature and lubrication state.
frog: see **turnout**.
frog number: see **crossing number**.
gauge corner: see **rail gauge corner**.
gauge, track: distance measured at right angles between the inside running (gauge) faces of the two rails of a track at a specified distance below the top of the rail heads.
gauge, wide: any track gauge greater than a nominal design standard due to installation deficiencies, track component deterioration or wear of the rail.
grade or gradient: the percentage rise or fall of track over the horizontal longitudinal distance or the rate of inclination of track in relation to the horizontal. For example, a rise of one metre in fifty metres equals a grade of 2% and can also be specified as a gradient of 1 in 50.
head check: a rail flaw consisting of shallow surface cracks in the railhead usually found on the gauge corner. Head checks generally run at a 45° angle to the axis of the rail and usually occur on the high rail of curves.
hunting: see **bogie hunting**.
journal bearing: the general term used to describe the load bearing arrangement at the ends of each axle of a rail vehicle bogie (truck). Modern designs involve roller

bearings that are sealed assemblies of hardened steel rollers, races, cups and cones pressed onto axle journals and generally lubricated with grease to reduce rotational friction. Vertical loads are transferred from the journal bearing to the bogie sideframe through a device known as a roller bearing adapter that fits between the bearing outer ring and the sideframe pedestal.

L/V ratio: the L/V ratio is defined as the ratio of the lateral force to the vertical force imposed by a rail vehicle wheel on a rail. When the ratio is greater than 1.0, there is significant potential for the wheel to climb onto the railhead and derail.

MGT: an abbreviation for million gross tonnes, representing the tonnes of traffic load (including the rail vehicles' mass) that have passed over a railway section, expressed in millions and usually calculated on an annual basis.

narrow gauge: railways built to less than 1435 mm (4 ft 8½ in.) standard track gauge.

rail: a rolled steel shape, most commonly a flat-bottom section, designed to be laid end to end in two parallel lines on sleepers (ties) or other suitable supports to form a track for the guidance of railway rolling stock.

rail anchor: a device installed on the rail base/foot against the edge of sleepers (ties) to prevent longitudinal rail movement and the consequent build-up of axial forces.

rail creep: intermittent longitudinal movement of rails in track caused by temperature changes and/or the adhesion forces imposed by trains during acceleration/braking. It is common practice to prevent rail creep by using **rail anchor** or **resilient rail fastener systems**.

rail defect: any surface or internal rail fault that makes it unfit to remain in service.

rail flaw: imperfections in the surface or interior of the rail that are not themselves considered dangerous, but which can propagate into rail defects.

rail gauge corner: the curved transition on the inner (gauge) side of a railhead joining the top surface of the rail and the rail gauge face.

rail gauge face: the side of the railhead that is located immediately below the gauge corner and which contacts the wheel flanges to provide guidance along the track.

rail grinding: the process of removing surface metal using abrasive grinding stones to reshape the railhead to a desired contour to optimise the wheel–rail contact patch while also seeking to eliminate incipient cracks, shells, engine burns and corrugation.

rail, head-hardened: a rail with the railhead heat treated after rolling to increase the surface hardness; usually used at locations of extreme service such as tighter (smaller radius) curves.

rail lubrication: the application of lubricant onto the rail gauge face and/or wheel flange to reduce the friction between them.

rail neutral temperature: the optimum temperature at which continuous welded rail is installed and anchored with no axial force in the rail so as to minimise the stresses that occur at the extreme ends of the ambient temperature range.

rail web: the vertical section of a rail, joining the railhead to the foot, providing beam strength to support rail vehicle loads between adjacent sleepers.

rail, alloy: rail containing small concentrations of silicon, chromium, manganese, nickel, molybdenum, vanadium or other elements for increasing the hardness and wear resistance of rail steel for use in locations of extreme service conditions.

rail, high carbon: a rail with extra carbon added to the steel during manufacturing to increase its hardness.

railhead: the top of the rail on which rolling stock wheels are guided. The railhead also accepts the weight from rolling stock in a very small area at each wheel–rail contact point.
railroad/railway: the entire system of track together with the stations, land, rolling stock and other property used in rail transportation.
regenerative braking: a retardation system on electric-powered rail vehicles that can return power developed by traction motors acting as generators to the third rail or catenary for use by other units.
resilient rail fastener: a type of rail fastener system that maintains a positive holding force on the foot of the rail to restrain its movement relative to sleepers or slab track, and utilising resilient pads under the rail to minimise the dynamic forces transmitted down to the supporting structure.
rolling contact fatigue: the process whereby extreme contact pressures at the wheel–rail interface initiate the development of surface cracks in the railhead and/or the wheel tread that can grow at shallow depths and result in head checks, shelling, spalling, rail squats and so on or that penetrate deeper and can result in crushed railheads, broken rails or severe wheel defects.
rolling radius differential: the different radius contact points between the wheel tread and railhead on the low rail versus the high rail, accomplished by tapered wheels. When in curves, the wheel flange on the high rail is up against the gauge line, with the wheel flange on the low rail pulled away from the low rail gauge line. This action results in a longer radius contact point on the wheel contacting the high rail, thereby inducing a steering effect of wheelsets through curves. In addition, wheel wear and rail wear are minimised due to a reduction in wheel slip.
rolling stock: a general term for any wheeled equipment that operates exclusively on a railway track.
running gear: a general term used to describe the components that facilitate movement of a rail vehicle. Running gear includes the wheels, axles, bearings, suspension system and other components of the bogies (trucks).
side bearing (of wagon): a bearing component, located either on the bogie or wagon bolster, and arranged to absorb vertical loads arising from the rocking motion of the wagon body. Various types of side bearings range from simple flat pads to complex devices, which maintain constant contact between the bogie (truck) bolster and the wagon body.
side bearing (of bogie): a plate or block, roller or elastic unit fastened to the top surface of a bogie (truck) bolster on both sides of the centre plate, and functioning in conjunction with the wagon body side bearing to support the load of a moving rail vehicle when variations in track geometry cause the wagon body to rock transversely on the centre plates.
sideframe: in the conventional three-piece bogie (truck), the heavy cast steel side member that is designed to transmit vertical loads from the wheels through either journal boxes or pedestals to the bogie bolster.
side sill: longitudinal member/s placed along both sides of a rail vehicle load bearing frame structure to provide support for the vehicle body.
slab track: track constructed without sleepers (ties), instead using a concrete base to which the rails are usually connected with direct fixation resilient fasteners.

sleeper: the portion of the track structure generally placed perpendicular to the rails to hold track gauge, distribute the weight of the rails and rolling stock and hold the track to its correct surface and alignment in the ballast. Materials commonly used in the manufacture of sleepers include timber, concrete and steel. Sleepers are also referred to as **ties** or **crossties**.
standard gauge: the standard distance between rails used by about two-thirds of the world's railways, being 1435 mm (4 ft 8½ in.) measured between the inside faces of the rail heads.
superelevation: see **cant (of track)**.
suspension: the resilient system through which a rail vehicle body is supported on its wheels. Suspension systems involve the use of hydraulic devices, friction elements and coil, elliptic, rubber or pneumatic springs.
swing bolster: a bogie (truck) bolster suspended by hangers or links, so that it can swing laterally with relation to the bogie and thus lower the effects of lateral impact received through the sideframes and wheels. Bogies equipped with a swing bolster are known as swing motion bogies.
tamp/tamping: the process of compacting ballast under sleepers (ties) to provide uniform load bearing under the rails and correct horizontal and/or vertical track alignment deficiencies.
thermite welding: welding the ends of two rails together with a foundry-like process. The thermite process involves iron oxide and aluminium powder being ignited with a magnesium charge, creating an exothermic reaction that produces molten steel that is poured between the rail ends, causing fusion.
tie: see **sleeper**.
track buckle: a short length of track that is radically out of its desired alignment. This track defect usually occurs at locations with continuous welded rail and is caused by sub-standard conditions or deficiencies coupled with high rail temperatures, high axial forces and the dynamic loads of moving trains. A track buckle is also referred to as a 'sun kink'.
track defect: an anomaly in any part of the track structure requiring repair, or other action such as an operating speed reduction.
track-train dynamics: the study of the motions and resulting forces that occur during the movement of a train over a track under varying conditions of speed, train makeup, track and equipment conditions, grades, curves and train handling.
track twist: the difference in track cant or cross level measured over a specified distance along the track, also referred to as **warp**.
train brake: the combined brakes on locomotives and wagons (cars) that provide the means of controlling the speed and stopping the entire train, also referred to as **automatic brake**.
train configuration: the composition of the complete train including the locomotive/s.
train resistance: the force that resists or opposes movement of a train. Resistance to motion along the track is attributed to bearings, wind and air resistance, flange contact with rail and so on.
tread: the slightly tapered exterior running surface of the wheel that comes in contact with the top surface of the rail.
truck: see **bogie**.

turnout: the junction where tracks diverge or converge, comprising a pair of switch blades (also called points) and a crossing (also called a frog or vee because of the shape when viewed from above) with guard rails. The frog or crossing vee allows wheels to cross from one track to another and can be either fabricated from rails and blocks or manufactured from a casting.
ultrasonic rail testing: the process of testing for internal defects in rail by passing ultra-high frequency sound through the rail. Sound waves that reflect off a defect are detected and measured to determine its location and size.
vertical bounce: instability at high speed where the vehicle oscillates vertically on the suspension system.
warp: see **track twist**.
wheel: the cast or forged steel cylindrical element that rolls along the rail, carries the weight and provides guidance for rail vehicles. Railway wheels are semi-permanently mounted in pairs on steel axles, and are designed with flanges and a tapered tread to provide for operations on track of a specific gauge.
wheel burn: damage to the rail and/or wheel resulting in metal flow and/or discolouration due to heat from their frictional contact.
wheel creep: an operating condition wherein the wheel is neither purely rolling on the rail nor purely slipping on the rail. The coefficient of friction between wheel and rail is greatest in this transition between purely rolling and purely slipping.
wheel flange: the tapered projection extending completely around the inner rim of a railway wheel, the function of which is to keep wheelsets on the track by limiting their lateral movement between the inside gauge faces of the running rails.
wheel profiling: process of restoring the desired contour of rail vehicle wheels by rotating the wheelsets in a wheel lathe to remove metal under precise control.
wheel slide: where the wheel does not rotate on its axis and motion exists at the area of contact between the wheel and the rail, usually caused by over braking during poor adhesion conditions. It is a common cause of **flat wheels**.
wheel slip: where a wheel rotates on its axis but relative motion occurs between the wheel and rail at their point of contact. Wheel rotation speed during wheel slip is greater than during rolling. This phenomenon is caused on a powered-rail vehicle by over application of power to the drive system relative to the available adhesion. Modern creep control systems using microprocessors permit some limited degree of slip as this has been proven to improve acceleration efficiency.
wheel tread: the slightly tapered or sometimes cylindrical circumferential surface of a railway wheel that bears on the rail and serves as a brake drum on rail vehicles with conventional bogie (truck) brake rigging.
wheelset: a pair of wheels mounted on an axle.